LEABHARLANN CHOLÁISTE NA TRÍONÓIDE, BAILE ÁTHA CLIATH | TRINITY COLLEGE LIBRARY DUBLIN
Ollscoil Átha Cliath | The University of Dublin

Terms and Conditions of Use of Digitised Theses from Trinity College Library Dublin

Copyright statement

All material supplied by Trinity College Library is protected by copyright (under the Copyright and Related Rights Act, 2000 as amended) and other relevant Intellectual Property Rights. By accessing and using a Digitised Thesis from Trinity College Library you acknowledge that all Intellectual Property Rights in any Works supplied are the sole and exclusive property of the copyright and/or other IPR holder. Specific copyright holders may not be explicitly identified. Use of materials from other sources within a thesis should not be construed as a claim over them.

A non-exclusive, non-transferable licence is hereby granted to those using or reproducing, in whole or in part, the material for valid purposes, providing the copyright owners are acknowledged using the normal conventions. Where specific permission to use material is required, this is identified and such permission must be sought from the copyright holder or agency cited.

Liability statement

By using a Digitised Thesis, I accept that Trinity College Dublin bears no legal responsibility for the accuracy, legality or comprehensiveness of materials contained within the thesis, and that Trinity College Dublin accepts no liability for indirect, consequential, or incidental, damages or losses arising from use of the thesis for whatever reason. Information located in a thesis may be subject to specific use constraints, details of which may not be explicitly described. It is the responsibility of potential and actual users to be aware of such constraints and to abide by them. By making use of material from a digitised thesis, you accept these copyright and disclaimer provisions. Where it is brought to the attention of Trinity College Library that there may be a breach of copyright or other restraint, it is the policy to withdraw or take down access to a thesis while the issue is being resolved.

Access Agreement

By using a Digitised Thesis from Trinity College Library you are bound by the following Terms & Conditions. Please read them carefully.

I have read and I understand the following statement: All material supplied via a Digitised Thesis from Trinity College Library is protected by copyright and other intellectual property rights, and duplication or sale of all or part of any of a thesis is not permitted, except that material may be duplicated by you for your research use or for educational purposes in electronic or print form providing the copyright owners are acknowledged using the normal conventions. You must obtain permission for any other use. Electronic or print copies may not be offered, whether for sale or otherwise to anyone. This copy has been supplied on the understanding that it is copyright material and that no quotation from the thesis may be published without proper acknowledgement.

PREDICTION OF GROUND VIBRATIONS DUE TO A TUNNEL BORING MACHINE

By

MUHAMMAD EKHLASUR RAHMAN
B.Sc. Eng. (BUET), M.Eng.Sc. (UCD)

Thesis submitted to the University of Dublin, Trinity College, for the Degree of Doctor of Philosophy

March 2007

TRINITY COLLEGE
05 JUL 2007
LIBRARY DUBLIN
THESIS
8114

DECLERATION

I declare that this Thesis, in whole or in part, has not been submitted to any University as an exercise for a degree. I further declare that, except where reference is given in the text, it is entirely my own work.

I confirm that the library may lend or copy this Thesis upon request, for academic purposes.

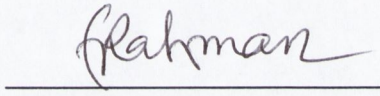

Muhammad Ekhlasur Rahman

SUMMARY

Changing social needs and increases in traffic have led to the demand for increased infrastructure. Due to the limitation of space in urban areas, underground structures, such as tunnels, are becoming more important for potential infrastructure. Tunnelling under city streets has now become a common activity for nearly all types of transportation. The construction of a tunnel induces ground vibration, which may affect the existing surface structures, particularly when the tunnel is constructed in hard ground, such as rock, or is at shallow depth. It is necessary to ensure that historically and economically important structures will not be adversely affected by tunnel construction and that any effects will be within acceptable limits.

This programme of research involved carrying out laboratory tests to determine the dynamic properties, such as the small strain shear stiffness and the damping ratio, of Dublin boulder clay. It also involved predicting, using 3-D finite element modelling (FEM), the vibrations at the ground surface due to construction of the north bound Dublin Port Tunnel and the south bound Dublin Port Tunnel. Further, it also involved the development of a new semi-empirical method for estimating the vibration level at the surface above a tunnel boring machine (TBM). Finally, a comparative study was carried out to compare the vibrations predicted using the 3-D FEM and those predicted using the empirical methods with the measured vibrations.

Several parametric studies were carried out to examine the sensitivity of the predicted vibrations to variations in the various input parameters including variations in the small strain stiffness and the damping ratio of soil.

During construction of Dublin Port Tunnel, field tests were carried out at different locations and in all cases it was found that the measured peak particle velocity (PPV) values were within the acceptable limit with respect to building damage.

3-D finite element analyses of the ground vibrations were found to be very time consuming, but good agreement, in terms of PPV, was obtained between the

measured PPV values and the values calculated using the 3-D finite element analyses. Parametric studies were performed and these showed that the stiffness of the soil had a significant effect on the vibrations at the ground surface.

A comparison study between three empirical methods, the 3-D FEM and the measured results, was carried out which revealed the following important features concerning the prediction of ground vibrations. It was found that all methods had similar attenuation characteristics. The NCC and the Godio et al. equations overpredict the magnitude of the PPV values with large differences between the predicted and measured values. However, good agreement was found between the resultant PPV values predicted by the 3-D FEM analyses, the new semi-empirical model and the measured PPV values. The NCC and the Godio et al. empirical models are crude at best, as they are functions of only the direct distance between the source and the point of interest, while the groundborne vibrations depend also on the soil properties and the tunnel boring machine excitation, which are taken into account in the 3-D FEM analyses and in the new semi-empirical model.

ACKNOWLEDGEMENTS

The author expresses his heartiest gratitude and sincerest indebtedness to his supervisor to Dr. Trevor Orr for his constant encouragement, expert guidance and valuable suggestions at all stages of this project.

The author wishes to thank the University of Dublin: Trinity College, Nishimatsu Construction Company Ltd., and The Geotechnical Thrust Fund of the Institute of Engineers of Ireland whose financial support made this project possible.

The author would like to thank all faculty members especially Dr. Eric Farrell, Dr. Roger West, Prof. Margaret O'Mahony and Prof. Biswajit Basu.

The author would also like to thank Mr. Martin Carney for assisting the author with the soil testing in the soil laboratory and all other technicians and staffs in the Department of Civil Engineering, Trinity College Dublin.

Finally, but most importantly, the author would like to thank his parents, family members and Engr. Sharfuddin for their unending generosity and encouragement.

To my parents and family members

CONTENTS

Declaration		ii
Summary		iii
Acknowledgements		v
Dedication		vi
Contents		vii
List of Figures		xiii
List of Tables		xxi
Chapter 1	**Introduction**	1
1.1	General	1
1.2	Dublin Port Tunnel	3
1.3	Geology	10
	1.3.1 General	10
	1.3.2 Limestone	10
	1.3.3 Glacial Deposits	11
	1.3.3.1 Upper Brown Boulder Clay	12
	1.3.3.2 Upper Black Boulder Clay	12
	1.3.3.3 Lower Brown Boulder Clay	13
	1.3.3.4 Lower Black Boulder Clay	13
	1.3.3.5 Near-Surface Deposits	14
1.4	Geotechnical properties of Dublin boulder clay and limestone	20
1.5	Aims and Objectives	29
1.6	Thesis Outline	30
Chapter 2	**Literature Review**	31
2.1	Introduction	31
2.2	Tunnelling	31
	2.2.1 Cut and Cover Tunnel	31
	2.2.2 Bored Tunnel	32
	2.2.2.1 Bored Tunnels in Soft Tunnel	32
	2.2.2.2 Bored Tunnels in Hard Ground	35

2.3 Ground Vibrations 37
2.3.1 General 37
2.3.2 Types of Vibration 39
2.3.3 Vibration Propagation 41
2.3.3.1 Body Waves 41
2.3.3.2 Surface waves 43
2.3.4 Attenuation of Ground Vibration 44
2.3.5 Reflection and Refraction of Waves 48
2.3.6 Human Response to Vibration 50
2.3.7 Structural Response to Vibration 52
2.3.8 Vibration Control 55
2.4 Geotechnical Studies on Dublin Boulder Clay 63
2.5 Dynamic Ground Properties 65
2.5.1 General 65
2.5.2 Dependency of Deformation Characteristics Upon Strains 66
2.5.3 Shear Moduli 67
2.5.4 Maximum Shear Modulus (G_{max}) 69
2.5.4.1 Factors Affecting the Shear Modulus 74
2.5.5 Damping Ratio 77
2.5.6 Stress-Strain Relations in Cyclically Loaded Soils 81
2.5.6.1 Linear Elastic Model 82
2.5.6.2 Equivalent Linear Model 82
2.5.6.3 Cyclic Non-Linear Models 83
2.5.6.4 Advanced Constitutive Models 86
2.6 Determination of Small Strain Shear Modulus, G_{max} 87
2.6.1 Bender Element Tests 87
2.6.2 Analysis of Bender Element Test Results 91
2.7 Conclusions 109

Chapter 3 Brief Introduction on Finite Element Analysis 111
3.1 Introduction 111
3.2 Finite Element Analysis 111
3.3 Strain Displacement Relations 112

3.4 Stress-Strain Relations 112
3.5 Element Stiffness Matrix 114
3.6 Element Mass and Damping Matrix 114
3.7 Dynamic Equation 115
3.7.1 Direct Time Integration Methods 116
3.7.1.1 The Central Difference Method 118
3.7.1.2 The Newmark Method 119
3.7.1.3 Hilber-Hughes-Taylor Method 119
3.7.2 Modal Analysis 120
3.8 Damping 121
3.8.1 Proportional (Rayleigh) Damping 122
3.9 Discretization Considerations 123
3.10 PLAXIS and ABAQUS 124
3.11 The Typical Finite Element Mesh 124

Chapter 4 Measurement of Dynamic Ground Properties 132
4.1 General 132
4.2 Field Tests 133
4.2.1 Small-Strain Field Tests 134
4.3 Laboratory Tests 136
4.3.1 Small Strain Tests 137
4.3.1.1 Resonant Column Test 137
4.3.1.2 Ultrasonic Pulse Test 140
4.3.1.3 Other Small Strain Stiffness Tests Apparatus 140
4.4 Small Strain Stiffness (G_{max}) 143
4.4.1 Dynamic Finite Element Analysis 144
4.4.1.1 Finite Element Model 144
4.4.1.2 Model Properties 145
4.4.1.3 Comparative Study Between Plane Strain Elements and Axi-Symmetric Element 146
4.4.1.4 The Effects of Mesh Density 147
4.4.1.5 Measurement of G_{max} Using Single Sine Wave 148
4.4.1.6 Measurement of G_{max} Using a Continuous Sine Wave

154
4.4.1.7 Measurement of G_{max} Using a Distorted Sine Wave 159
4.4.2 Laboratory Tests 162
4.4.2.1 Introduction 162
4.4.2.2 Laboratory Test Equipments 162
4.4.2.3 Preparation of Undisturbed Soil Sample 166
4.4.2.4 Calibration 166
4.4.2.5 Measurement Method 167
4.4.2.6 Results and Discussions 168
4.5 Comparison between G_{max} values obtained from Bender Element Tests & a Semi-Empirical method 171
4.6 Determination of Damping Ratio 172
4.6.1 Finite Element Analyses 172
4.6.2 Experimental Work 174
4.6.3 Results and Discussions 174
4.7 Summary 178

Chapter 5 Field Measurement and Analysis of Vibrations 181
5.1 General 181
5.2 Vibration Parameters 181
5.2.1 Amplitude Parameters 182
5.2.2 Frequency Content Parameters 184
5.2.2.1 Fourier Series 184
5.2.2.2 DFT and FFT 185
5.2.2.3 Power Spectra 186
5.3 Measuring Devices 186
5.3.1 Accelerometers 187
5.3.2 Geophones 188
5.4 Test Set-up and Methodology for Field Measurement of Vibration in Dublin Port Tunnel 189
5.5 Results and Analysis of Test Data 193
5.5.1 TBM Excitation 193
5.5.2 Ground Surface Vibrations 194

5.6 Summary 201

Chapter 6 Numerical Analyses 202

6.1 General 202

6.2 Finite Element (FE) Model 202

6.3 Materials Properties 205

6.4 Boundary Conditions 208

6.5 Loading 209

6.6 Numerical Results 210

6.6.1 Results and Discussions of Measuring Section 1 and 2 211

6.6.2 Results and Discussions of Measuring Section 3 and 4 219

6.6.3 Results and Discussions of Measuring Section 5 224

6.6.3.1 The Effects of Existing Tunnel on Surface Vibrations 228

6.7 Parametric Study 229

6.7.1 The Effects of Varying the Stiffness of the Soil 230

6.7.2 The Effects of Varying the Damping of the Soil 233

6.8 Modified 3D Modelling 236

6.8.1 Results and Discussions 237

6.9 2-D Axi-symmetry Model 240

6.10 Summary 241

Chapter 7 Empirical Model 242

7.1 Introduction 242

7.2 Ground Vibrations Predictions 242

7.3 Empirical Model 1 243

7.4 Empirical Model 2 244

7.5 Empirical Model 3: The Rahman-Orr Model 249

7.6 Comparison Between Model Predictions and Measured PPP Values 255

7.7 Vibration Amplification 257

7.8 Summary 259

Chapter 8 Conclusions 260

8.1 Introduction 260

8.2 Conclusions 260

8.3 Recommendations for Further Research 267

References 268

Appendix A presents laboratory test documentations 289

Appendix B presents the TBM excitation at different sections 308

Appendix C presents the predicted Peak Particle Velocity at the surface. 317

Appendix D presents the ABAQUS input file. 322

Appendix E publications 365

LIST OF FIGURES

Figure	Title
1.1	The route of Dublin port tunnel & city map
1.2	Route details of Dublin Port Tunnel
1.3	Bored tunnel section; Whitehall to Fairview
1.4	Cut and Cover Tunnel
1.5	Bored Tunnel Cross Section
1.6	Inside of bored section of Dublin Port Tunnel
1.7	Hard rock TBM 'GRÁINNE'
1.8	Boulder Clay TBM 'MEGHAN'
1.9	Stratigraphy of the geology of the Dublin Port Tunnel
1.10	Detailed geological cross section of Dublin Po
1.11	Typical borehole log in Dublin Port Tunnel area
1.12	Simplified Stratigraphic Sequence for Use on FE Analysis
1.13	Moisture content
1.14	Plasticity chart for brown and black diamictons
1.15	Particle size distribution curves
1.16	Selected grading curves of boulder clays from locations indicated
1.17	Particle size distribution curves of brown and black diamictons
1.18	Comparison of stiffness measured in situ and in the laboratory dynamic tests
2.1	Open shield TBM
2.2	Types of vibration
2.3	Deformations Produced By Body Waves
2.4	Deformations Produced By Surface Waves
2.5	Reflected and Refracted Rays Resulting from Incident
2.6	Co-Ordinate System for Human Sensitivity to Vibration
2.7	Deformation and Inertial Forces Due to Ground Wave Motion
2.8	Transient Vibration Guide Values For Cosmetic Damage
2.9	Amplitude of vertical displacements vs. distance from source for five tests
2.10	Amplitude reduction factor vs normalised trench depth

2.11 Isolation effect of gas-filled cushions in different soils and vibration sources
2.12 Backbone curve showing typical variation of G_{sec} with shear strain
2.13 Variation of stiffness parameters for G_{max} with plasticity index
2.14 Variation of G_{max} as function of confining pressure
2.15 Variation of G_{max} as function of depth
2.16 Shear Modulus Ratio Reduction Curves With Shear Strain For Fine-Grained Soils of Different Plasticity
2.17 Influence of mean effective confining pressure on shear modulus ratio reduction curves for
2.18 Hysteretic Stress-Strain Relationship for Cyclic Loading
2.19 Variation in Damping Ratio with Cyclic Shear Strain Amplitude and Plasticity Index
2.20 Modelling of Soil Behaviour in Compliance with Strain-Dependent Characteristics
2.21 Secant Shear Modulus, G_{sec} and Tangent Shear Modulus, G_{tan}
2.22 Hyperbolic Backbone Asymptotic Curve
2.23 Extended Mashing Rules
2.24 Piezoelectric bender element
2.25 Bender elements in the triaxial apparatus
2.26 Frequency response curve for half-power method
2.27 Relationship Between Travel Time and Sample Length
2.28 Bender Element Trace for a Square Input Wave in Kaolin
2.29 Typical Bender Element Input Output Sine Wave
2.30 Notation For Three-Dimensional Motion of Points
2.31 Analytical Solution of The Motion at the Monitoring Point
2.32 Test Data For Sinusoidal Input Waves in Kaolin
2.33 Cancelling the Near Field Effect with a Distorted Sine Wave
2.34 Resonance of the Receiving Element
2.35 Input Shape and Near Field Effect in Time Domain
2.36 Input shape and near field effect
2.37 Bender element tests results

2.38	Typical Oscilloscope Signals From a Bender Element Test With a Square Wave
2.39	Cross-Correlation of Input to Output Signals
2.40	Input and Output Signals
2.41	FE Solution For the Motion at the Monitoring Point
2.42	Comparison of bender element test results
3.1	Relationship Between Damping Ratio and Frequency for Rayleigh Damping
3.2	A typical finite element mesh
4.1	Modelling of Soil Behaviour in Compliance with Strain-Dependent Deformation Characteristics
4.2	Velocity Logging by Cross-Hole Method
4.3	Velocity Logging by the Down Hole Method
4.4	Seismic Refraction Test Set-Up
4.5	Amplitude Decay of Free Vibration
4.6	Amplitude Versus Cycles
4.7	Compression Transducer
4.8	Shear-Plate Transducer
4.9	Finite Element Mesh
4.10	The Effects of Mesh Density
4.11	Input Single Sine Signal
4.12	Horizontal Deflection at the Tip of the Receiving Bender Element For R_d=1
4.13	Horizontal Deflection at the Tip of the Receiving Bender Element For R_d=2
4.14	Horizontal Deflection at the Tip of the Receiving Bender Element For R_d=3
4.15	Horizontal Deflection at the Tip of the Receiving Bender Element For R_d=4
4.16	Horizontal Deflection at the Tip of the Receiving Bender Element For R_d=5
4.17	Horizontal Deflection at the Tip of the Receiving Bender Element For R_d=6

4.18 Horizontal deflection at the tip of the receiving bender element for R_d=7

4.19 Horizontal deflection at the tip of the receiving bender element for R_d=8

4.20 Percentage of G_{max} Error With R_d (First Inflexion)

4.21 Percentage of G_{max} Error With R_d (First Peak to Peak)

4.22 Percentage of G_{max} Error With R_d (Cross Correlation Method)

4.23 Input Continuous Sine Signal

4.24 Horizontal Deflection at the Tip of the Receiving Bender Element For R_d=1

4.25 Horizontal Deflection at the Tip of the Receiving Bender Element For R_d=2

4.26 Horizontal Deflection at the Tip of the Receiving Bender Element For R_d=3

4.27 Horizontal Deflection at the Tip of the Receiving Bender Element For R_d=4

4.28 Horizontal Deflection at the Tip of the Receiving Bender Element For R_d=5

4.29 Horizontal Deflection At The Tip Of The Receiving Bender Element For R_d=6

4.30 Horizontal Deflection at the Tip of the Receiving Bender Element For R_d=7

4.31 Horizontal Deflection at the Tip of the Receiving Bender Element For R_d=8

4.32 Percentage of G_{max} Error With R_d (First Inflexion)

4.33 Percentage of G_{max} Error With R_d (First Peak to Peak)

4.34 Input Distorted Sine Signal

4.35 Horizontal Deflection at the Tip of the Receiving Bender Element For Amplitude Ratio 1/1.5

4.36 Horizontal Deflection at the Tip of the Receiving Bender Element For Amplitude Ratio ½

4.37 Horizontal Deflection at the Tip of the Receiving Bender Element For Amplitude Ratio 1/3

4.38	Horizontal Deflection at the Tip of the Receiving Bender Element For Amplitude Ratio ¼
4.39	Normalised Initial Deflection Values With Respect to the Initial Deflection Value of 1/3
4.40	Bender Elements
4.41	Function Generator
4.42	ADC-212 Oscilloscope
4.43	Bender Element Calibration Results
4.44	Typical Standard Sine Wave
4.45	Typical Arbitrary Distorted Sine Wave
4.46	The Effects of Cell Pressure on G_{max}
4.47	Comparison of Bender Element Test Results with Empirical Results
4.48	Three-Dimensional Finite Element Model
4.49	Different Mode Shape for Undisturbed Boulder Clay, 100 KPa and $C_A = 0$
4.50	Experimental Frequency Response Spectra
5.1	Acceleration, Velocity and Displacement Time Histories
5.2	Geophone Sensor Operation
5.3	Vibrations measurement area
5.4	Measuring Ground Vibrations
5.5	Geophone arrangements
5.6	Time History Plot of Transverse TBM Vibrations For TBM at Section 1
5.7	Time History Plot of Vertical TBM Vibrations For TBM at Section 1
5.8	Time History Plot of Longitudinal TBM Vibrations For TBM at Section 1
5.9	FFT of Time History Plot of Transverse TBM Vibrations
5.10	FFT Time History Plot of Vertical TBM Vibrations
5.11	FFT of Time History Plot of Longitudinal TBM Vibrations
5.12	Histogram of Measured Ground Surface Vibrations Values, Transverse Direction
5.13	Histogram of Measured Ground Surface Vibrations Values, Vertical Direction

5.14 Histogram of Measured Ground Surface Vibrations Values, Longitudinal Direction
6.1 Finite element model geometry at measuring Sections 1 and 2
6.2 Finite element meshes of ground at measuring Sections 1 and 2.
6.3 Finite element mesh of tunnel (Enlarge figure) at measuring Sections 1 and 2
6.4 Finite element model geometry at measuring Sections 3 and 4
6.5 Finite element model geometry at measuring Section 5
6.6 A short triangular pulse
6.7 Fast Fourier Transform (FFT) of a short triangular pulse
6.8 Predicted time history at the surface at Measurement Section 1;
6.9 FFT of predicted time history at the surface at Measurement Section 1; transverse direction.
6.10 Measured TBM excitation velocity at Measurement Section 1; transverse direction.
6.11 FFT of TBM excitation at Measurement Section 1; transverse direction.
6.12 Predicted transverse vibration velocity (Frequency domain) at the surface at Measurement Section 1 due to transverse load.
6.13 Predicted vibration velocity in the x direction at the surface at Measurement Section 1 due to transverse load.
6.14 Predicted vibration velocity in the y direction at the surface at Measurement Section 1 due to transverse load.
6.15 Predicted vibration velocity in the z direction at the surface at Measurement Section 1 due to transverse load.
6.16 Predicted Transverse Peak Particle Velocity (PPV) at the surface at Section 1
6.17 Predicted time history of the velocity at surface; transverse direction
6.18 FFT of time history at surface; transverse direction
6.19 Measured TBM excitation velocity; transverse direction
6.20 FFT of measured TBM excitation; transverse direction
6.21 Predicted transverse vibration velocity (Frequency domain) at the surface

6.22 Predicted transverse vibration velocity at the surface
6.23 Finite element meshes at Section 5;
6.24 Predicted time history at surface; transverse direction
6.25 FFT of predicted time history at surface; transverse direction.
6.26 Measured TBM excitation velocity; transverse direction
6.27 FFT of predicted TBM excitation; transverse direction
6.28 Predicted transverse vibration velocity (Frequency domain) in surface
6.29 Predicted transverse vibration velocity at the surface
6.30 The effects of existing tunnel on surface vibration
6.31 Output response (frequency domain) at the surface due to short triangular pulse
6.32 FFT of measured TBM excitation at Section 1
6.33 Predicted vibration velocity (Frequency domain) at surface
6.34 Damping ratio of 1% dependent on frequency
6.35 Output response (frequency domain) at the surface at 0m from TBM face due to short triangular pulse
6.36 Output response (frequency domain) at the surface at -10m from TBM face due to short triangular pulse
6.37 Finite element model geometry
6.38 Modified 3-D finite element results at Section 1
6.39 Modified 3-D finite element results at Section 2
6.40 Modified 3-D finite element results at Section 1
6.41 Modified 3-D finite element results at Section 2
6.42 Axi-symmetry model (1)
6.43 Axi-symmetry model (2)
7.1 Definition of The Parameters for the Empirical Equation
7.2 Predicted PPV Values Using Godio et al. Equation for Hard Ground
7.3 Predicted Upper-Bound Vibration Levels Using NCC Equation
7.4 Predicted Lower-Bound Vibration Levels Using NCC Equation
7.5 Absorption coefficient at small strain levels
7.6 Relative vibration amplitude with different absorption coefficient
7.7 Measured TBM excitation; transverse direction

7.8 Measured TBM excitation; vertical direction
7.9 Measured TBM excitation; longitudinal direction
7.10 The flow diagram
7.11 Comparison between Model Predictions and Measured PPP Values; Section 1
7.12 Comparison between Model Predictions and Measured PPP Values; Section 2
7.13 Comparison between Model Predictions and Measured PPP Values; Section 3
7.14 Comparison between Model Predictions and Measured PPP Values; Section 5
7.15 Influence of frequency on steady-state response of a damped, linear elastic layer

LIST OF TABLES

Table	Title
2.1	Proposed Classification of earth materials by attenuation coefficient, α
2.2	Summary of tunnel vibration data sites compared to predictions
2.3	Different wave types with propagation velocity
2.4	Changes in soil behaviour with shear strain and corresponding modelling
2.5	Typical properties of some soils and rocks
2.6	Overconsolidation Ratio Exponent
2.7	Estimation of $K_{2,\,max}$
2.8	Values of G_{max}/c_u
2.9	Effects of environmental and loading conditions on G_{max} and G/G_{max} of normally consolidated and moderately overconsolidated clays
2.10	Field measurements of damping ratios
2.11	Laboratory measurements of damping ratios
2.12	Effects of environmental and loading conditions on damping ratio of NC and moderately OC clays
3.1	Generalised stress-strain matrices for isotropic materials and different design situations
4.1	Material properties
4.2	A comparative study results
4.3	% error in G_{max} calculated from measured shear wave velocity, v_s.
4.4	Values of parameters for Dublin boulder clay and limestone
4.5	Material properties
4.6	Results
4.7	Different mode shape and corresponding deformation type and resonance frequency
4.8	C_M value
4.9	Damping ratio, ξ, values for Dublin boulder clay
5.1	Characteristics of materials at measurement area
5.2	Overview of the measurement points

5.3 Measured PPV Values

6.1 Properties of materials (NCC data)

6.2 Properties of materials (Author's data)

6.3 Predicted and Measured PPV Values at Section 1 and 2

6.4 Predicted and Measured PPV Values at Section 3 & 4

6.5 Predicted and Measured PPV Values at Section 5

6.6 Characteristics of materials

6.7 PPV values for reference model and models with varied upper soil layer stiffness

6.8 Normalised PPV values with reference model results

6.9 Characteristics of materials

6.10 PPV (mm/s) at measuring points for reference model and models with adopted relative damping

6.11 Normalised PPV with respect to reference model results

6.12 Values of ground parameters used in ABAQUS analyses

6.13 Values of ground parameters used in ABAQUS analyses

7.1 Summary of tunnel vibration data sites compared to predictions

7.2 A comparison study

7.3 Coefficient "A" based on shear wave velocity v_s in m/s and frequency *f*, Hz.

7.4 Coefficient "n" based on shear wave velocity v_s in m/s and frequency *f*, Hz.

7.5 Shear wave velocity

CHAPTER 1

INTRODUCTION

1.1 General

Changing social needs and increases in traffic has led to the demand for increased infrastructure. Due to the limitation of space in urban areas, underground structures, such as tunnels, are becoming more important for potential infrastructure. Tunnelling under city streets has now become a common activity for nearly all types of transportation. Long urban tunnels are principally for metros, water supply and sewers while shorter tunnels may be required for highway underpasses and pedestrian subways, most usually constructed in cut-and-cover. Longer highway tunnels are sometimes suggested but problems of access and ventilation add greatly to the difficulty and cost of construction, against which preservation of surface land and gains in environmental amenity may prove a quite inadequate offset (Megaw & Bartlett, 1982).

The construction of a tunnel induces ground vibration, which may affect the existing surface structures, particularly when the tunnel is constructed in hard ground, such as rock. It is necessary to ensure that historically and economically important structures will not be affected and that any effects will be within acceptable limits. It is also necessary to ensure that the vibrations due to tunnelling do not cause a nuisance to those living or working close to the tunnel.

Tunnel construction is a highly complex operation involving many different activities. The complexity of tunnelling activities can take many forms, such as airborne noise, ground vibration, ground deformations, visual intrusion, dust and smoke, etc (Taylor, 1998).

Airborne noise is generated by mechanised tunnelling due to the use of machines that generate high levels of vibration and hence dissipate large amounts of energy, in the form of ground vibrations and noise into the environment (New, 1982).

The interaction of ground vibrations with a structure can induce dynamic strains within the structure. Depending upon the relative dimensions of the structure and the wavelength of the incident vibrations, differential dynamic distortions or whole body accelerations can be induced. These may be of sufficient magnitude to lead to damage, but a more common problem is disturbance to the occupants of the building. This is because the human body is extremely sensitive to vibrations (Hillar & Hope, 1998 and Massarsch, 2000).

Another potential source of intrusion is groundborne noise. This is the audible noise emitted by components of buildings, especially suspended floors and ceilings, when they are caused to vibrate by ground vibration (Hillar & Hope, 1998).

Vibrations can also induce permanent deformations in soils, which result in ground settlement. Structures adjacent to a new tunnel, in particular old masonry buildings, may suffer damage resulting in costly repairs or requiring expensive protective measures, such as compensation grouting (Lee, 2002 and Athanasopoulos & Pelekis, 2000). These expenditures may significantly increase the total project cost of a tunnel project.

Vibrations and noise from tunnelling activities will generally be of a temporary nature, but the disturbance caused may result in permanent damage to property and substantial nuisance to the neighbouring population. Either factor may lead to restraints on the working method that may result in additional costs or even, in extreme circumstances, curtailment of activity (New, 1982 and Hillar & Hope, 1998).

The environmental effects of vibrations also have received considerable attention in recent years owing to the damage they can cause both to buildings and people (Hall, 2003). These consequences of tunnelling activities have prompted recent research into improved methods for predicting the ground vibrations induced by tunnelling on adjacent structures and people.

1.2 Dublin Port Tunnel

The Dublin Port Tunnel project comprises approximately 5.6km of dual carriageway, of which 4.5km are underground, which includes 1.9km of twin cut and cover tunnels and 2.6km of twin-bored tunnels, with associated interchanges and infrastructure. It provides a link from Dublin Port to Santry in the Dublin suburbs and the motorways to the rest of Ireland. The Dublin Port Tunnel is a key element of the National Development Plan's strategy to deliver a more efficient and safer transport system in Dublin City. Its primary purpose is to provide a high quality access route to Dublin Port, as well as relieving traffic congestion in many areas of the city. The route of the Dublin Port Tunnel is shown in Figs.1.1, 1.2 and 1.3.

The first part of the tunnel was constructed in cut and cover tunnel from the portals of Santry to the Whitehall, constructing the tunnel inside the trench, and filling in the trench afterwards. The cut and cover tunnel is shown in Fig.1.4.

The bored tunnels, from Whitehall to Fairview, were driven from a circular working shaft 57m in diameter and 25m deep. This shaft accommodates one of the four vehicle cross passages to be provided in the tunnel. Staged construction of the working shaft, with ring beams and anchoring, followed the construction of deep reinforced concrete perimeter diaphragm walls.

The depth of the bored tunnel section, from existing ground level to the roof of the tunnels, ranges from approximately 19m to 24m under residential areas. The cross sections of a typical bored tunnel using a tunnel-boring machine are shown in Fig.1.5 and the inside of the bored section of Dublin Port Tunnel is shown in Fig.1.6. From the working shaft in Whitehall, two Tunnel Boring Machines (TBM 1 & TBM 2) set off to drill the two-lane, 11.8m-diameter tunnels. The 11.8m-diameter TBM1 (nicknamed Gráinne) that tunnelled from Collins Avenue to Fairview was delivered to the shaft in 103 parts and assembled at the launch pit in May 2002. The 156m-long, 1,600t machine was a hard rock tunnelling machine that advanced at an average rate of 10m per day and by the time it had completed its round-trip of 4.5km, it had excavated more than 500,000m^3 of rock. The hard rock TBM had a rotating cutter head at the front of the machine with 72 and 0.43m disk cutters to

break the hard limestone. The cutting wheel was fitted with hard rock discs which rotated on the working face and notched into it. The notching effect caused large sections of rock to break off and caused vibrations in the ground. Buckets located behind the discs transported the rock away from the cutting wheel. Conveyor equipment then transported the excavated material out of the tunnel. Another source of ground vibrations was the jacks were pushing the TBM forward. The cutter head rotation speed was 4 revolutions per minute. The machine travelled approximately 2.25km from the working shaft to the reception chamber located at Fairview Park at the south end of the bored tunnel section where it U-turned for its return drive towards Collins avenue (Goto et al., 2004).

The other TBM2 (nicknamed Meghan) was an open face machine especially designed to excavate a hard clay stratum, like the Dublin Boulder Clay. This machine travelled the relatively short distance of 330m from the Collins Avenue working shaft to the interface with the northern cut and cover section, where it was also U-turned and returned to Collins Avenue. This machine was equipped with three excavation arms for excavating the Boulder Clay and a screw conveyer for removing it, two intermediate support decks, and various movable face breasting plates for face support forward (Goto et al., 2004). The sources of vibrations in the case of this TBM were the excavators digging the soil and the jacks pushing the TBM forward. The open face machine excavated from Collins Avenue to Whitehall Church in Dublin suburb with very little ground cover (14 to 7m). It was 60m long, weighed 1,100t and travelled at a rate of 5m per day. It required 18 staff per shift to function fully (Goto et al., 2004). Photograph of TBM 1 and TBM 2 are shown in Figs. 1.7 and 1.8 respectively. The vibration measuring area is shown in Fig.1.2.

The geological and geotechnical conditions of the Dublin Port Tunnel area are described in Sections 1.3 and 1.4 respectively. During the construction of Dublin Port Tunnel project, there were a number of complaints from house owners in the area when the boring was through limestone whereas there were no complaints in the area where the boring was through boulder clay and hence boring through limestone was important with regard to this research.

Fig.1.1–The route of Dublin port tunnel & city map

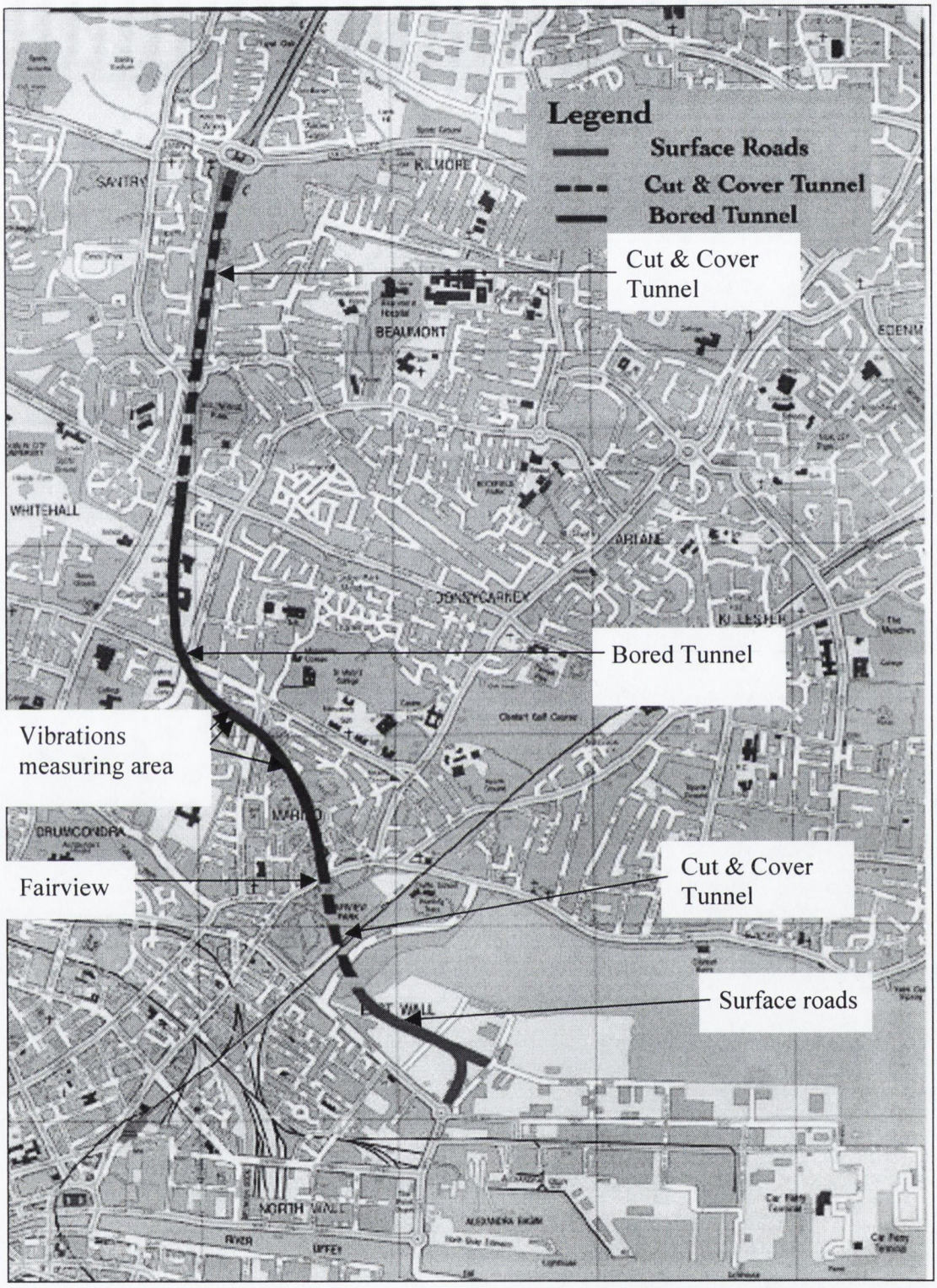

Fig.1.2–Route details of Dublin Port Tunnel

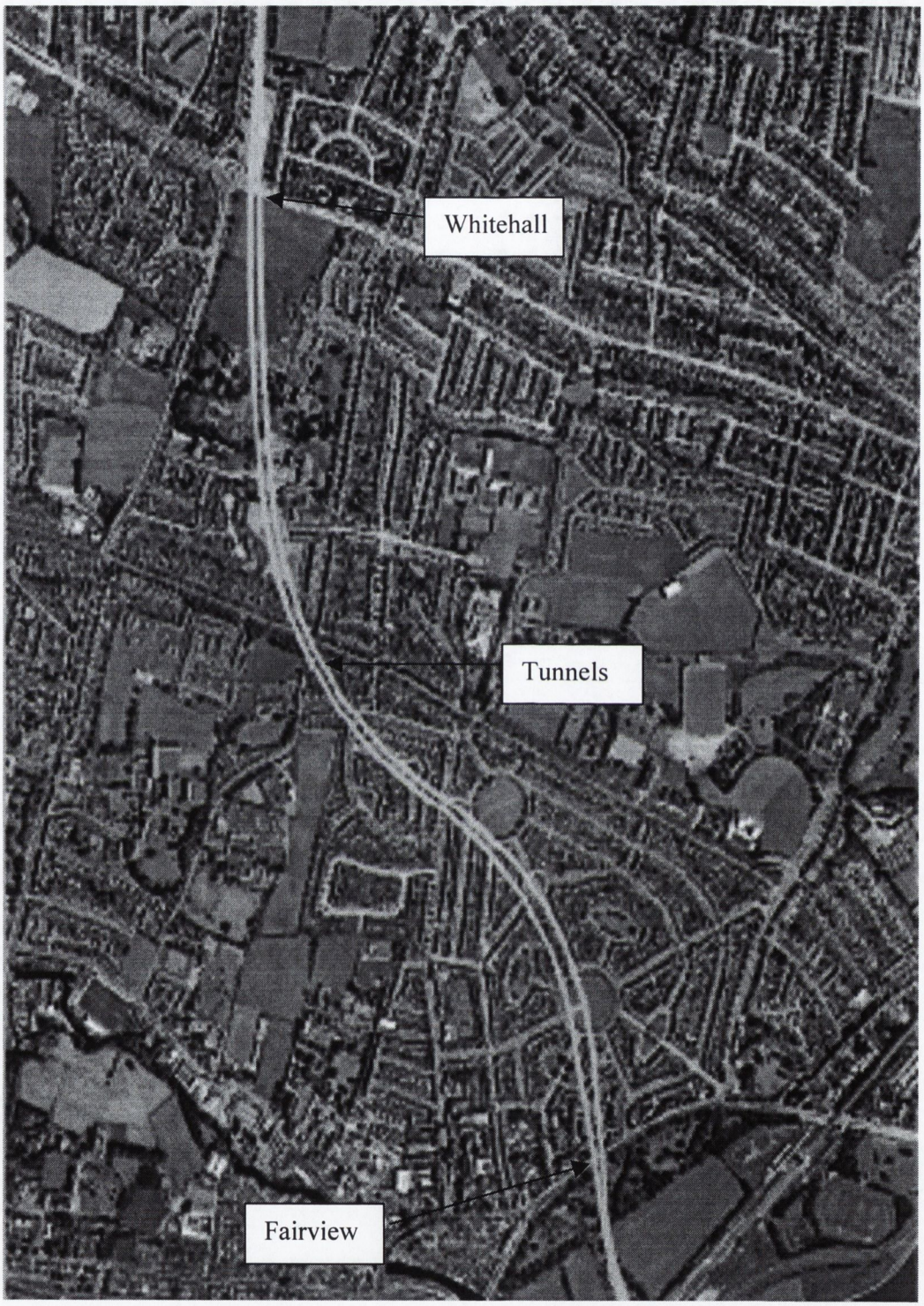

Fig.1.3– Bored tunnel section; Whitehall to Fairview

Fig.1.4–Cut and cover tunnel

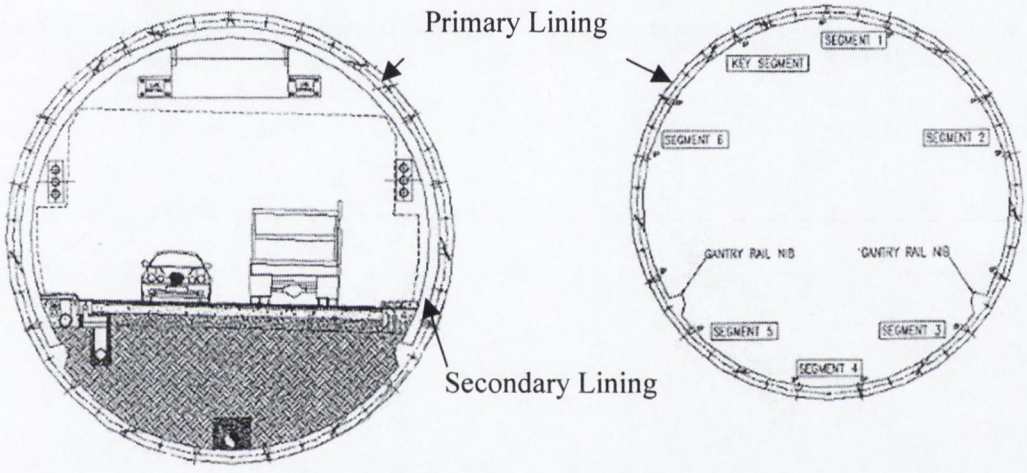

Fig.1.5–Typical bored tunnel cross section

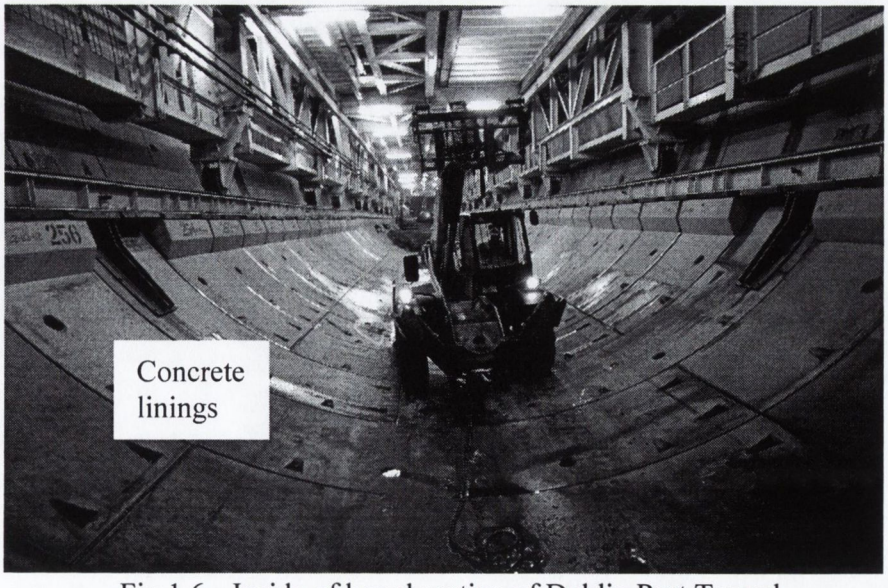

Fig.1.6– Inside of bored section of Dublin Port Tunnel

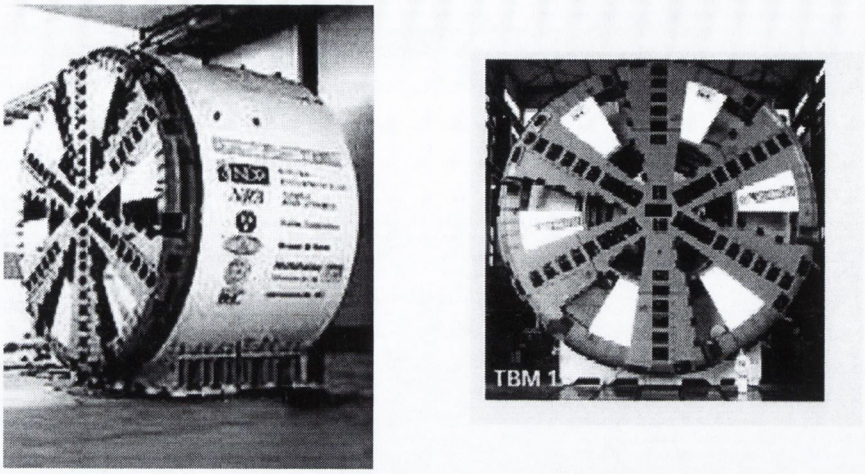

Fig. 1.7– Hard rock TBM 'GRÁINNE'

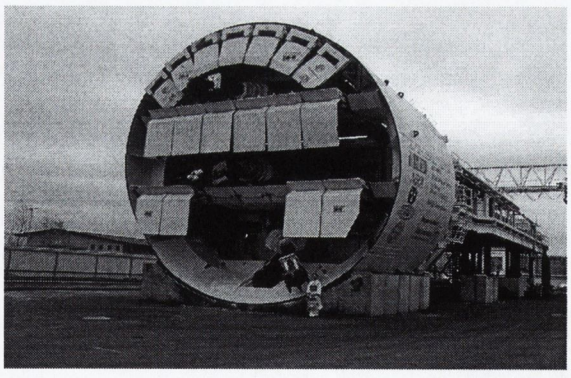

Fig. 1.8–Boulder Clay TBM 'MEGHAN'

1.3 Geology

1.3.1 General

A major underground construction project, such as the Dublin Port Tunnel, needs very comprehensive knowledge of the ground conditions. Many site investigations have been carried out since the beginning of the project along the route of the tunnel. A variable sequence of soil-type materials overlies the bedrock.

The soil within the tunnel area consists primarily of glacial deposits resting on limestone bedrock. The glacial deposits comprise boulder clays, silts, sands and gravels. In many areas within tunnel these deposits are overlain by made ground of varying thickness, which is site specific, generally resulting from abandoned quarries, the filling of streambeds, ponds and valleys, etc. From borehole logs, the strata of the boulder clay and limestone were determined.

1.3.2 Limestone

The Dublin bedrock formation comprises carboniferous limestone and shales of the Fingal group, known as 'Calp' limestone. The limestone can be categorised as a predominant strong to very strong, very thin to medium bedded, dark grey predominantly by medium to coarsely crystalline and fosssiliferous (crinoids approximately 6mm diameter) limestone, with occasional interbedded, moderately strong, very thin to thin, dark grey to black, unweathered shaley mudstones and strong to very strong fine grained argillaceous limestone. Farrell & Wall (1990) stated that the limestone was deposited in a shallow marine environment and that cyclical changes in the water depth and depositional conditions led to marked changes in the rock properties and thickness, variations in the sand and clay content, and inclusions of shale or mudstone layers, occasionally weathered to clay. Discontinuities varied from planar smooth and tight, to open, with little to much clay. Through extensive in-tunnel logging, faulting and folding of the limestone and shales has been observed. The dip of bedding is generally between 5^0 and 30^0, with vertical bedding being recorded within fault zones, and the rock is highly fractured within the fractures generally containing gouges and clay joint infill. The limestone

within the project area lies wholly beneath the water table and water inflows during tunnelling were generally around 250 l/min for the full 11.8m diameter rock face. The bored section tunnel lies almost entirely in the limestone bedrock (Goto et al., 2004 & Skipper et al., 2005).

The shale bands within the limestone formation have given rise to some problems during tunnelling, by way of crushing to a clay/silt consistency and when encountered with a high dip>50^0 led to plucking of boulder size slabs of the surrounding limestone. Some overbreaking occurred along areas on intersection joint and bedding planes, but this rarely extended more than 300mm and had limited effect on surface settlement (Goto et al., 2004). The engineering properties of the limestone are discussed in Section 1.4.

1.3.3 Glacial Deposits

Glacial deposits are found over the limestone bedrock. Farrell & Wall (1990) and Farrell et al. (1995) have comprehensively described the glacial deposits in the Dublin area. The authors made the distinction between the brown boulder clay and black boulder clay and stated that black boulder clay upon weathering produces brown boulder clay 2 to 3 m in thickness. The clays, referred as the Dublin black\brown boulder clays, are glacial tills formed by the deposition of particles at the base of glaciers, and therefore have been subjected to very high vertical pressures. Thus, these boulder clays are generally highly overconsolidated deposits of stiff to very stiff consistency. Although the glacial tills are mainly composed of clay, they also contain some significant quantities of gravels and cobbles (Farrell et al., 1995).

These lodgement tills are the predominant soils in Dublin and its surrounding area. The black boulder clay is usually the lower portion of till, although at the Port Tunnel they have also found brown boulder clay below the black boulder clay. The quaternary glacial deposits are complex and the presence of fluvioglacial and glaciomarine sand and gravel sediments are indicative of either local withdrawals or advances of the ice sheet (Orr & Farrell, 1996).

Skipper et al. (2005) identified four units in the Dublin boulder clays: an upper brown boulder clay (the brown boulder clay of Farrell et al., 1995), an upper black boulder clay (the black boulder clay of Farrell et al., 1995), a lower brown boulder clay and a lower black boulder clay. The authors also stated that average engineering properties of all four boulder clays are very similar. The stratigraphy of the geology of the Dublin Port Tunnel area is shown in Fig. 1.9. The detailed geological cross section of the Dublin Port Tunnel North Cut and Cover Section is shown in Fig. 1.10 and a typical borehole log is shown in Fig. 1.11.

1.3.3.1 Upper Brown Boulder Clay

The upper brown boulder clay (the brown boulder clay of Farrell et al., 1995) was found to have a thickness of up to 3m below ground level and this is the weathered mantle of the upper black boulder clay (Skipper et al., 2005 & Farrell et al., 1995). It is a stiff to very stiff, yellowish brown, slightly sandy slightly gravely silt/clay with some cobbles. Although its mechanical properties are similar to the upper black boulder clay, microscopically, differences are apparent. The upper brown boulder clay contains a small number of higher permeability sand and gravel lenses, which are clearly weathered versions of the small-scale features in the upper black boulder clay (Skipper et al., 2005).

The upper brown boulder clay represents a complex pedogenic horizon, which developed during a period of climate warming and glacial retreat after the deposition of the upper black boulder clay. It is classified as a separate formation from the lower black boulder clay as it is distinct in appearance (Skipper et al., 2005).

1.3.3.2 Upper Black Boulder Clay

The upper black boulder clay is a dense and stiff to very stiff or hard deposit from which it is difficult to obtain relatively undisturbed samples because of its stone content and its high stiffness. Dublin black boulder clay was deposited as a lodgement till during the Midlandian Glaciation. During the maximum extent of this glaciation, ice from a large sheet crossed Dublin in a southeast direction leaving a widespread drape of lodgement till rich in erratic material from the north and

northwest. The composition is typically a heterogeneous mixture of particle sizes ranging from clays to cobbles and boulders (Farrell et al., 1995). A detailed geological profile of Dublin Port Tunnel area is shown in Fig. 1.10. The upper black boulder clay was seen to display consistent characteristics over a distance of 4 km. it is characteristically a very stiff, dark grey to black, slightly gravely, slightly sandy clay with some cobbles, and can be described overall as a diamicton. (Skipper et al., 2005 & Menkiti et al., 2004).

1.3.3.3 Lower Brown Dublin Boulder Clay

Three sub-units were present in the lower brown boulder clay formation. Of these the upper and lower units were diamictons, but the middle subunit proved to be by far the most lithologically variable of all the sediments encountered in the study area. All units in the lower brown boulder clay were discernible as more silty and browner in colour than either the upper or lower black boulder clays. The uppermost lower brown boulder clay unit was generally found to be a very stiff, dark brown, slightly gravely silt or clay silt with a relatively high proportion of gravel to cobble sized particles and rarely boulder-size exotic clasts - certainly more than are usually found within the upper black boulder clay. The unit is usually up to 5m thick. The second sub-unit is only 1-5m in thickness. It varies in consistency from a soft to very stiff, light brown to reddish brown clay, to a loose to dense sand with some gravel. The third sub-unit is at least 2.5m thick and consists of a diamicton, similar to the top sub-unit, but with an apparently lower cobble content than the top sub-unit (Skipper et al., 2005).

1.3.3.4 Lower Black Boulder Clay

The lower black boulder clay, which was seen in the area of the open cut tunnel sections, has a maximum thickness of approximately 4m. The lower black boulder clay was seen to display consistent characteristics over a distance of at least 3 km and therefore qualifies as a formation. It is consists of very stiff, dark grey to black, slightly sandy, slightly gravely silts/clay with some to cobbles. The main difference between the upper and lower black boulder clays is that the lower black boulder clay

is generally blacker and more plastic when wetted in hand specimen than the upper black boulder clay (Skipper et al., 2005 & Menkiti et al., 2004).

Several types of discontinuities and fissures are identified. Fissures are generally rough and tightly closed and did not have an impact on the engineering behaviour of the till for the structures constructed (Skipper et al., 2005).

1.3.3.5 Near-surface deposits

Much of Dublin city is built on made ground. Made ground is the uppermost layer and is composed of clayey sand with man-made materials like rubble, glass and ceramics, deposited on tidal flats or in old streambeds. The Dublin port area has been reclaimed using mainly hydraulic fill. The fill is generally loose to medium dense with pockets of silt (Farrell & Wall, 1990). The relatively high void ratio of the top layer has resulted in permeability higher than that of the Dublin boulder clay beneath.

Fig. 1.12 shows a simple stratigraphic model for Dublin soil and rock based on the discussions outlined in this section.

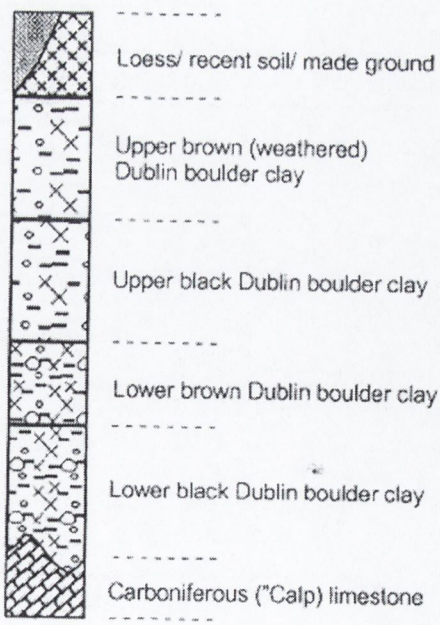

(A)

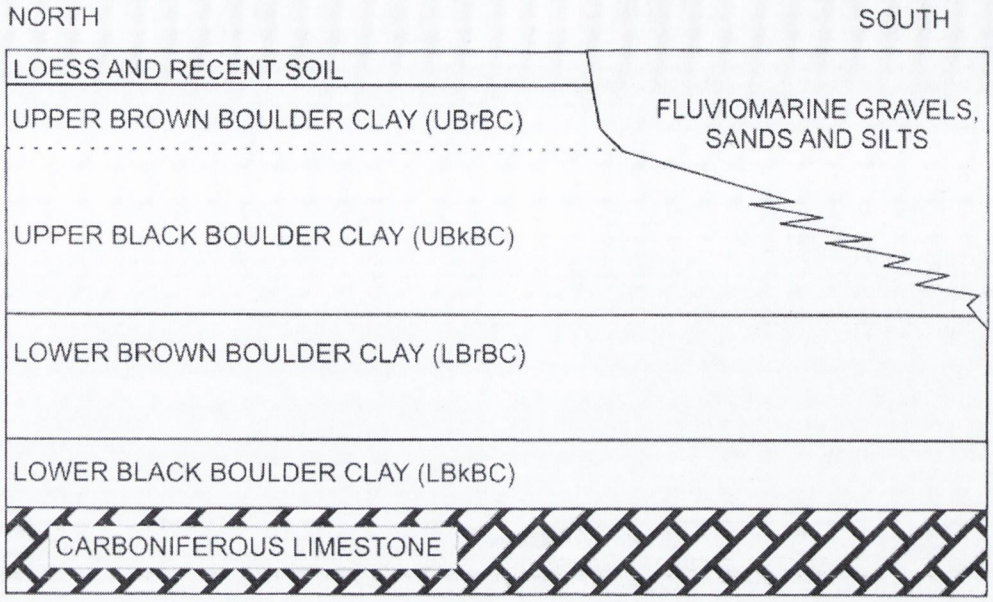

(B)

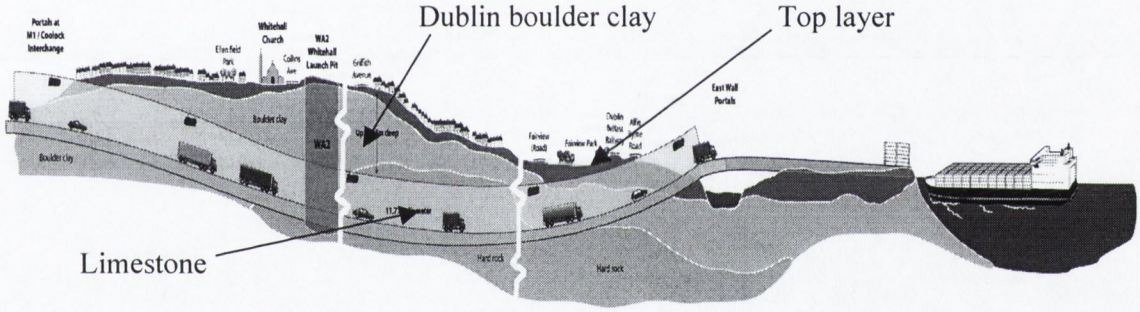

(C)

Fig. 1.9- Stratigraphy of the geology of the Dublin Port Tunnel (A) Menkiti et al., (2005), (B) Skipper et al., (2005). (C) Not in scale

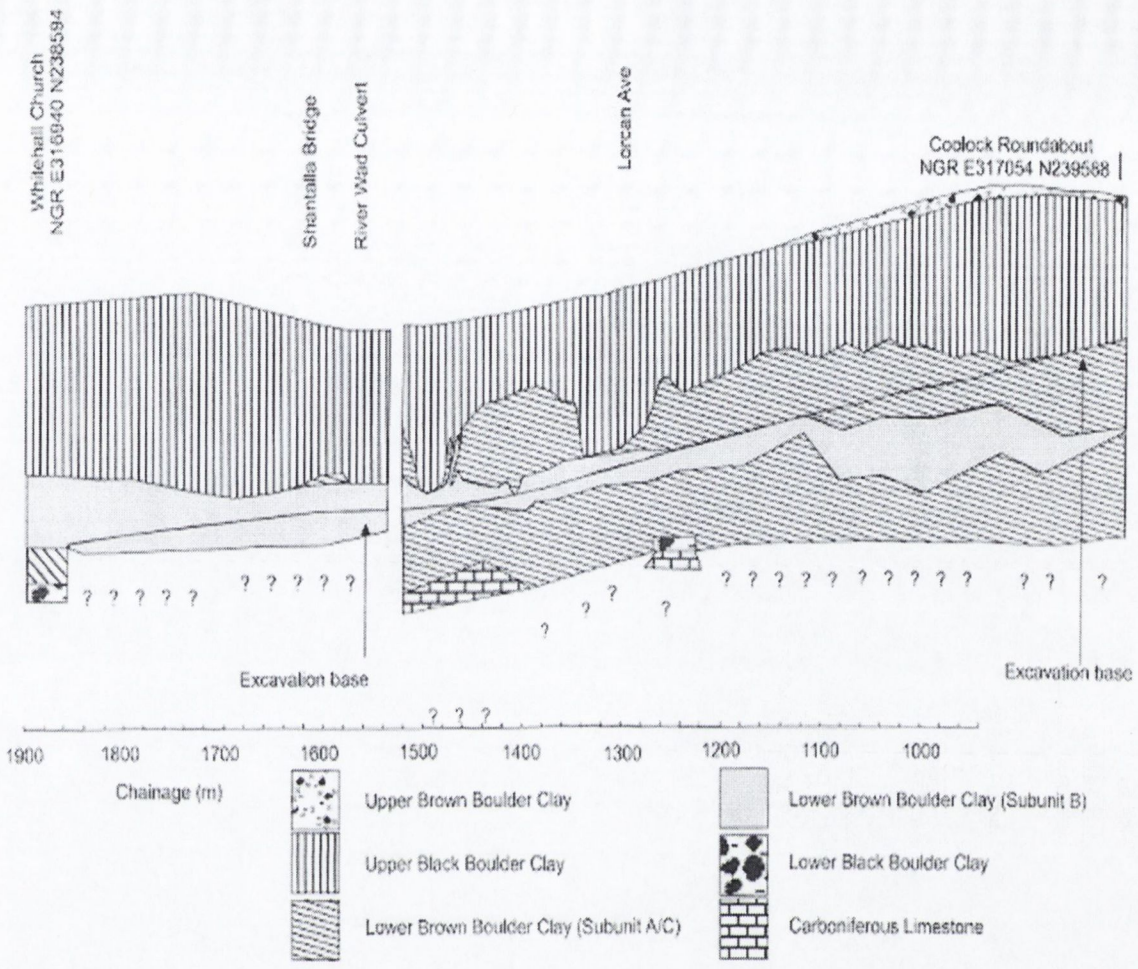

Fig.1.10 – Detailed geological cross section of Dublin Port Tunnel North Cut and Cover Section (Skipper et al., 2005)

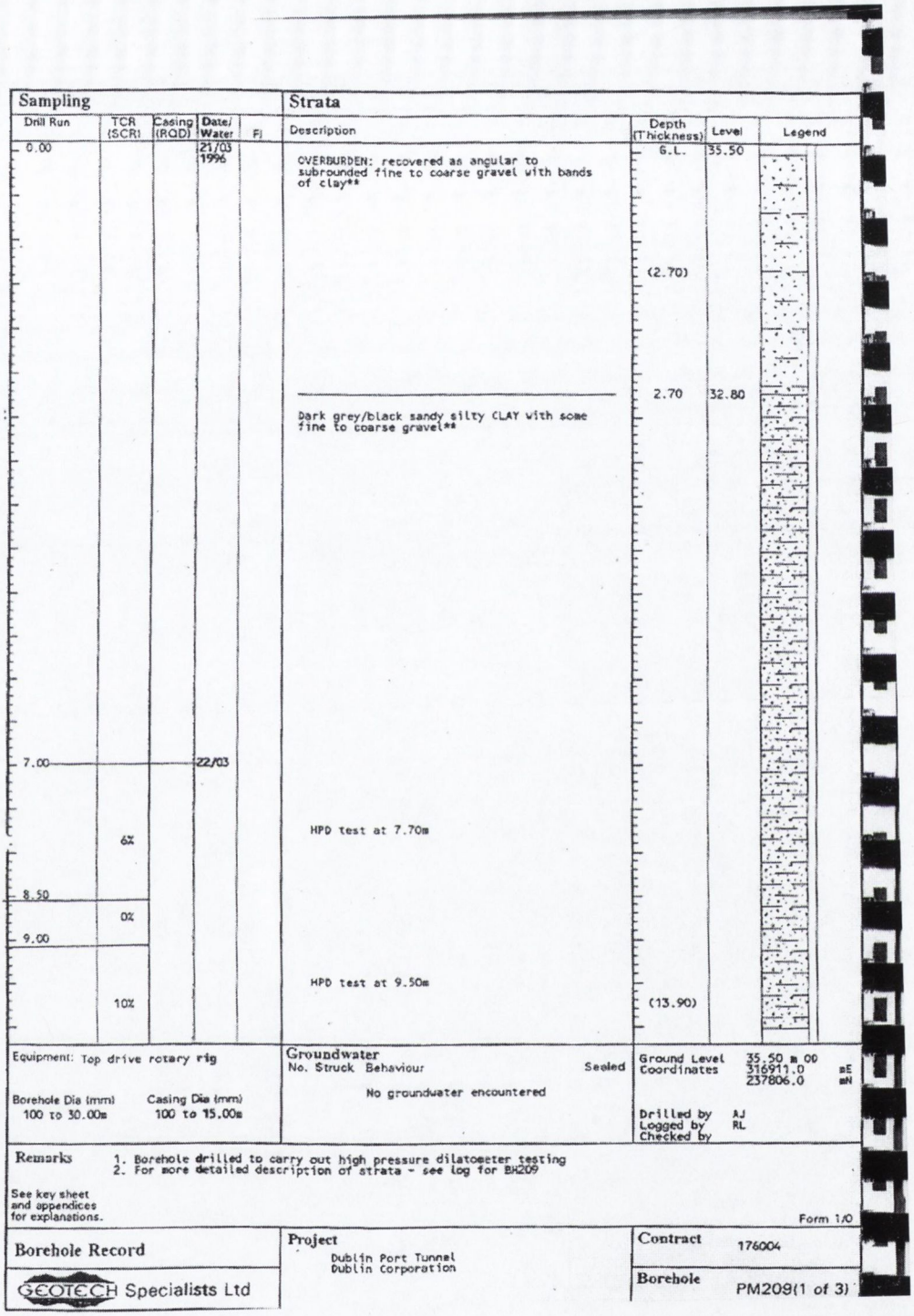

Sampling					Strata			
Drill Run	TCR (SCR)	Casing (RQD)	Date/ Water	Fl	Description	Depth (Thickness)	Level	Legend
0.00			21/03 1996		OVERBURDEN: recovered as angular to subrounded fine to coarse gravel with bands of clay**	G.L.	35.50	
						(2.70)		
					Dark grey/black sandy silty CLAY with some fine to coarse gravel**	2.70	32.80	
7.00			22/03					
	6%				HPD test at 7.70m			
8.50								
	0%							
9.00								
	10%				HPD test at 9.50m	(13.90)		

Equipment: Top drive rotary rig

Borehole Dia (mm): 100 to 30.00m
Casing Dia (mm): 100 to 15.00m

Groundwater
No. Struck: Behaviour: Sealed
No groundwater encountered

Ground Level: 35.50 m OD
Coordinates: 316911.0 mE, 237806.0 mN

Drilled by: AJ
Logged by: RL
Checked by:

Remarks
1. Borehole drilled to carry out high pressure dilatometer testing
2. For more detailed description of strata - see log for BH209

See key sheet and appendices for explanations.

Form 1/0

Borehole Record

GEOTECH Specialists Ltd

Project
Dublin Port Tunnel
Dublin Corporation

Contract 176004

Borehole PM209(1 of 3)

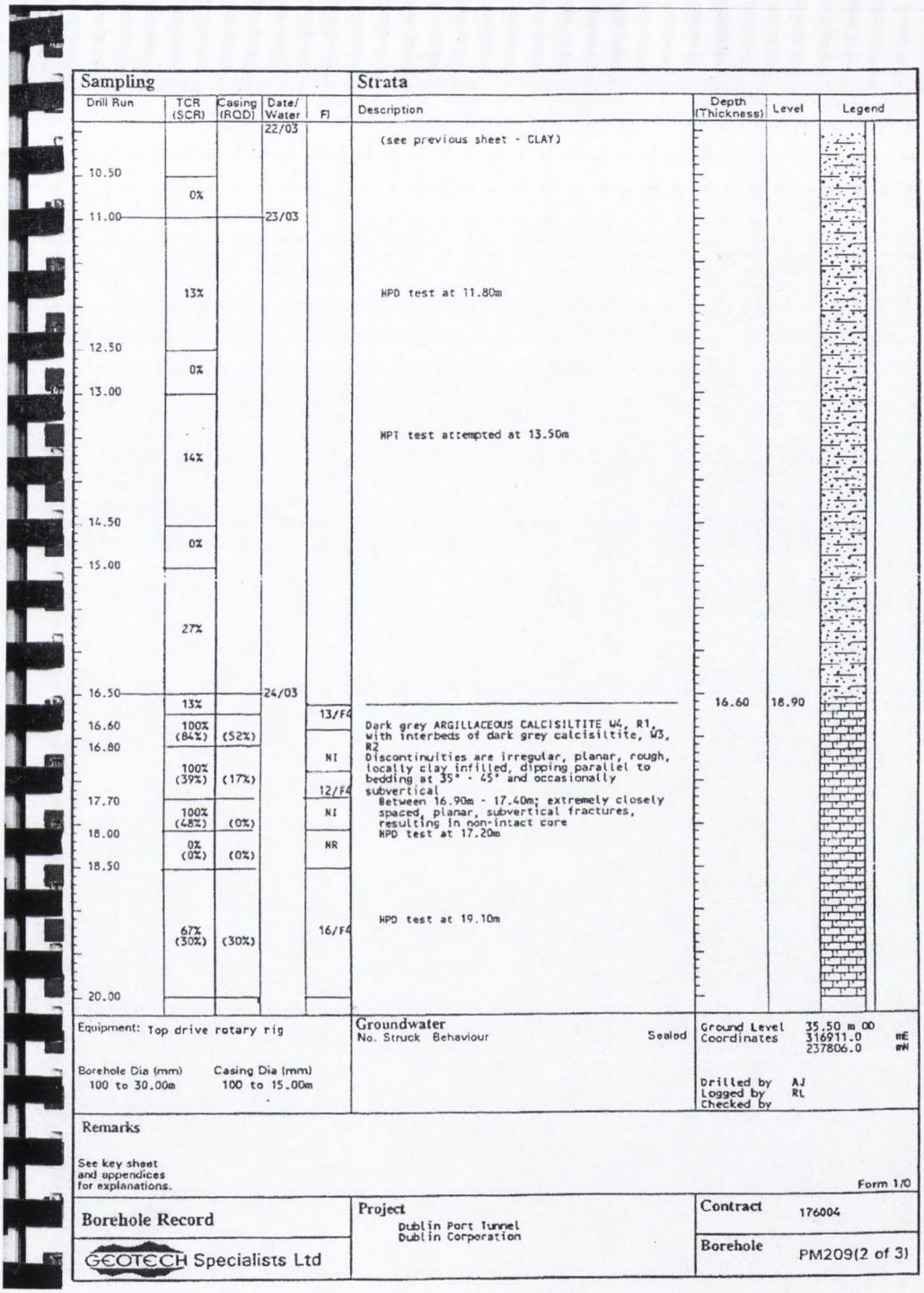

Sampling					Strata			
Drill Run	TCR (SCR)	Casing (RQD)	Date/ Water	FI	Description	Depth (Thickness)	Level	Legend
			22/03		(see previous sheet - CLAY)			
10.50	0%							
11.00			23/03					
	13%				HPD test at 11.80m			
12.50	0%							
13.00					HPT test attempted at 13.50m			
	14%							
14.50	0%							
15.00								
	27%							
16.50	13%		24/03	13/F4		16.60	18.90	
16.60	100% (84%)	(52%)		NI	Dark grey ARGILLACEOUS CALCISILTITE W4, R1, with interbeds of dark grey calcisiltite, W3, R2 Discontinuities are irregular, planar, rough, locally clay infilled, dipping parallel to bedding at 35° - 45° and occasionally subvertical Between 16.90m - 17.40m; extremely closely spaced, planar, subvertical fractures, resulting in non-intact core HPD test at 17.20m			
16.80	100% (39%)	(17%)		12/F4				
17.70	100% (48%)	(0%)		NI				
18.00	0% (0%)	(0%)		NR				
18.50	67% (30%)	(30%)		16/F4	HPD test at 19.10m			
20.00								

Equipment: Top drive rotary rig

Borehole Dia (mm) 100 to 30.00m

Casing Dia (mm) 100 to 15.00m

Groundwater
No. Struck Behaviour Sealed

Ground Level 35.50 m OD
Coordinates 316911.0 mE
237806.0 mN

Drilled by AJ
Logged by RL
Checked by

Remarks

See key sheet and appendices for explanations.

Form 1/0

Borehole Record

GEOTECH Specialists Ltd

Project
Dublin Port Tunnel
Dublin Corporation

Contract 176004

Borehole PM209(2 of 3)

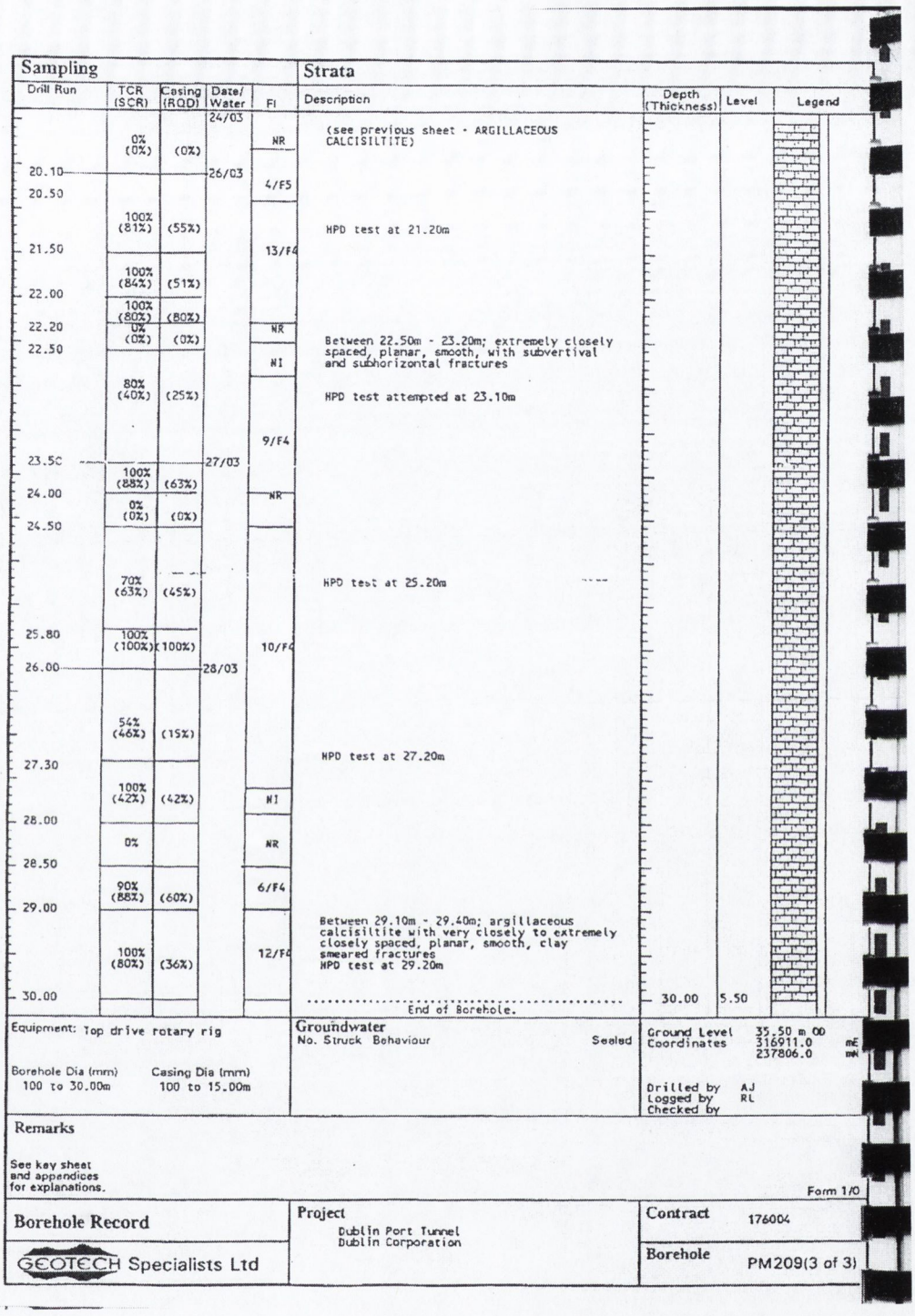

Fig.1.11–Typical borehole log in Dublin Port Tunnel area

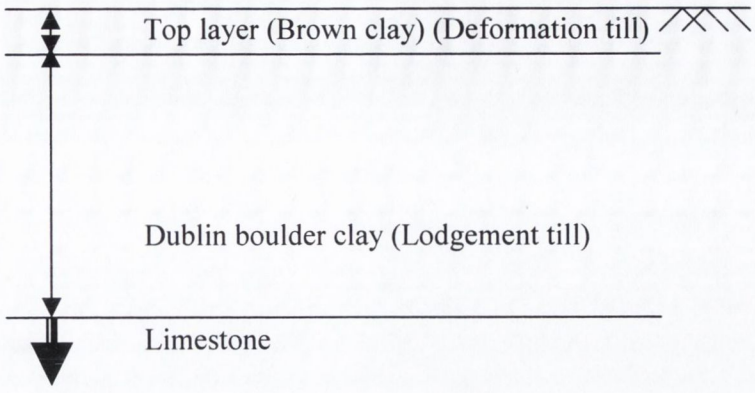

Fig.1.12–Simplified stratigraphic model for use in FE analysis (Lawler 2002)

1.4 Geotechnical properties of Dublin boulder clay and limestone

The following is an overview of the geotechnical properties of the Dublin boulder clay and limestone. In engineering terms, Dublin's boulder clay is separated into brown and black boulder clay. Brown boulder clay is widely considered to be a weathered product of black boulder clay (Farrell et al., 1995). Skipper et al., (2005) identified four units, referred to by them as the upper brown boulder clay, upper black boulder clay, lower brown boulder clay and lower black boulder clay and which discussed in the previous section.

The low permeability in the range of 10^{-9} ms^{-1} to 10^{-11} ms^{-1} and high gravel content of Dublin boulder clay have resulted in the till being referred to as a boulder clay (Lehane & Simpson, 2000 and Skipper et al., 2005). The moisture content and bulk density is shown in Table 1.1 & 1.2. Overall, both moisture content and bulk density values are uniform with depth. The average moisture content in the upper brown boulder clay is somewhat greater than for the other layers, with a corresponding slightly smaller bulk density. The upper black boulder clay has the lowest water content and highest bulk density, while the values of lower two layers are almost identical. The measured water contents and bulk densities for upper black boulder clay fall within the overall range of 11 ± 3% and 2.2 ± 0.05 Mg m^{-3} respectively for Dublin boulder clay as suggested by Farrell & Wall (1990); Lehane & Simpson (2000). A typical water content chart is presented in Fig.1.13 and from Fig.1.13 it can be seen that the typical water contents are of order of 10%. The water content of the soil in the top metre is substantially higher at about 20%. Table 1.1 shows that

the average index values for all four materials are very similar. Plastic limit values fall reasonably close to the natural moisture content, indicating the liquidity index is close to zero. Again, measured values for liquid limit and plasticity index are close to the previously suggested ranges of 25 ±4% and 11 ±2% respectively (Lehane & Simpson, 2000) and around 30% and 10 to 15% respectively (Farrell & Wall, 1990). A typical plasticity chart is shown in Fig. 1.14. In Fig. 1.14, it can be seen that the results lies above the Skempton's A-line and are close to the T-line (Farrell et al., 1995) where T-line is till line suggested by Boulton & Paul (1976 cited by Farrell et al., 1995 & Lawler 2002).

Particle size distribution (PSD) curves for the four formations are shown in Fig. 1.15. The curves are typical of those of a lodgement till (Hanrahan 1977) who carried out PSD tests on Dublin boulder clay found that the PSD curves had straight-line distributions as shown in Fig. 1.16. Farrell et al. (1995) carried out PSD tests on nine samples, including both the brown and black diamictons, and found that the PSD curves fell within a very narrow band characteristic of glacial diamictions and were effectively indistinguishable (Fig.1 .17). The Table 1.1 shows the remarkable consistency with depth observed in terms of index properties of these boulder clays.

Lawler (2002) carried out seismic refraction tests and laboratory dynamic tests to determine the small strain stiffness of Dublin boulder clay and the results are presented in Fig. 1.18. It can be seen from the Fig. 1.18 that the small strain stiffness increases with increasing confining pressure. The author carried out a large number of drained and undrained triaxial compression tests on variable soil samples for determining the strength parameter of black boulder clay and interpreted results from all the tests. The results are $\varphi' = 40^0$ and $c' = 0$ kN/m^2. Farrell et al. (1995) also found $\varphi' = 35^0$ and 37^0 and $c' = 0$ kN/m^2.

Limestone cores were obtained using core barrels equipped with diamond or tungsten carbide tipped bits. There are three basic types of core barrels; single tube, double tube, and triple tube. Use of double and triple tube core barrel systems are preferred since single tube core barrels generally provide poor recovery rates. Laboratory classification tests were carried out to determine density, porosity, absorption and moisture content. The modulus of elasticity, Poisson's ratio and

unconfined compression strength were measured using unconfined compressive strength tests. From stress-strain curves the tangent modulus and secant modulus were measured. The geotechnical properties of limestone in the area of Dublin Port Tunnel are presented in Appendix A3. The data were taken from Dublin Port Tunnel site investigation reports, where tests were commissioned by Geoconsult and ARUP consulting engineering companies. From Appendix A3 it can be seen that the bulk density and dry density are uniform with depth and location and are both around 2.7 Mg/m^3. The average moisture content is less than 1%. The Young's modulus values are different for different locations and the average value is around 29 GPa. This values is lower than the value that is relevant for the small strain levels associated with ground vibrations as it is determined from unconfined axial compression tests. The Poisson's ratio values are also different for different location and the average value is around 0.19.

Table 1.1- Summary of average basic material properties (Skipper et al., 2005)

Parameter	Upper Brown	Upper Black	Lower Brown	Lower Black
Moisture content, %	13.1	9.7	11.5	11.3
Bulk density, Mgm^{-3}	2.228	2.337	2.283	2.284
Liquid limit, %	29.3	28.3	30.0	29.5
Plastic limit, %	15.9	15.1	14.9	17.8
Plasticity index, %	13.4	13.2	15.1	11.8
Clay content, %	11.7	14.8	17.8	17.5
Silt content, %	17.0	24.7	28.3	30.5
Sand content, %	25.0	24.7	25.7	34.0
Gravel content, %	46.3	35.8	28.0	35.5

Table 1.2-Database of the index, state and strength properties of stiff tills

Parameter	Black boulder clay	Brown boulder clay	Reference
Grading curve	Straight line grading curve	Straight line grading curve	Farrell et al., 1995. Hanrahan (1977 cited by Farrell & Wall, 1990)
Plasticity index	10 to 15% 11 ±2%	10 to 15% 11 ±2%	Farrell & Wall, 1990. Lehane & Simpson, 2000
Liquid limit	>30% 26% 25 ±4%	<30% 23 & 30%	Farrell & Wall, 1990 Farrell et al., 1995 Lehane & Simpson, 2000
Plastic limit	14 & 17% 14 ±2%	16 & 17%	Farrell et al. 1995 Lehane & Simpson, 2000
Water content	8.6 & 8.7% 11 ±3%	9.5 & 10.6 %	Farrell et al., 1995 Lehane & Simpson, 2000
Bulk Density, Mg/m^3	2.29 & 2.35 2.2 ±50	2.24 & 2.28	Farrell et al., 1995 Lehane & Simpson, 2000
Void ratio	0.24 & 0.28	0.29 & 0.33	Farrell et al., 1995
Clay fraction	15 ±5%		Lehane & Simpson, 2000
Gravel fraction	30 ±5%		Lehane & Simpson, 2000
Permeability, ms^{-1}	10^{-8} to 10^{-11}		Lehane & Simpson, 2000
Angle of friction	37^0 40^0	35^0	Farrell & Wall, 1990 Lawler, 2002
c'	0	0	Farrell & Wall, 1990 Lawler, 2002
Undrained shear strength, kN/m^2	Around 450		Farrell et al., (1995a)
Preconsolidation stress, MPa	1.3 ±3		Lehane & Simpson, 2000

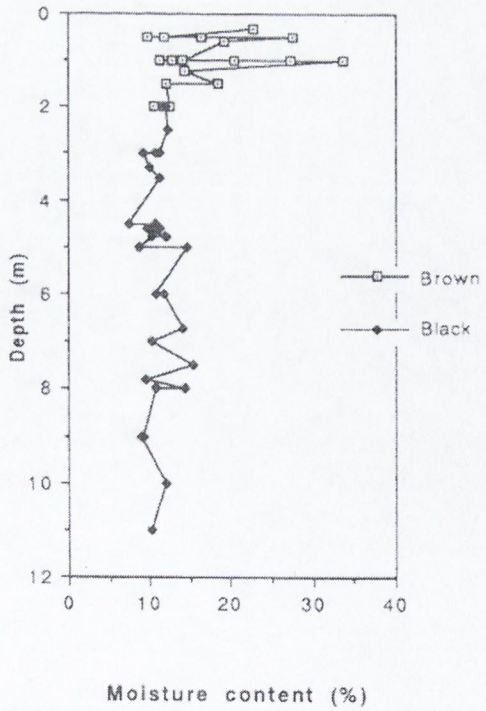

Fig. 1.13-Moisture content (Farrell et al., 1995)

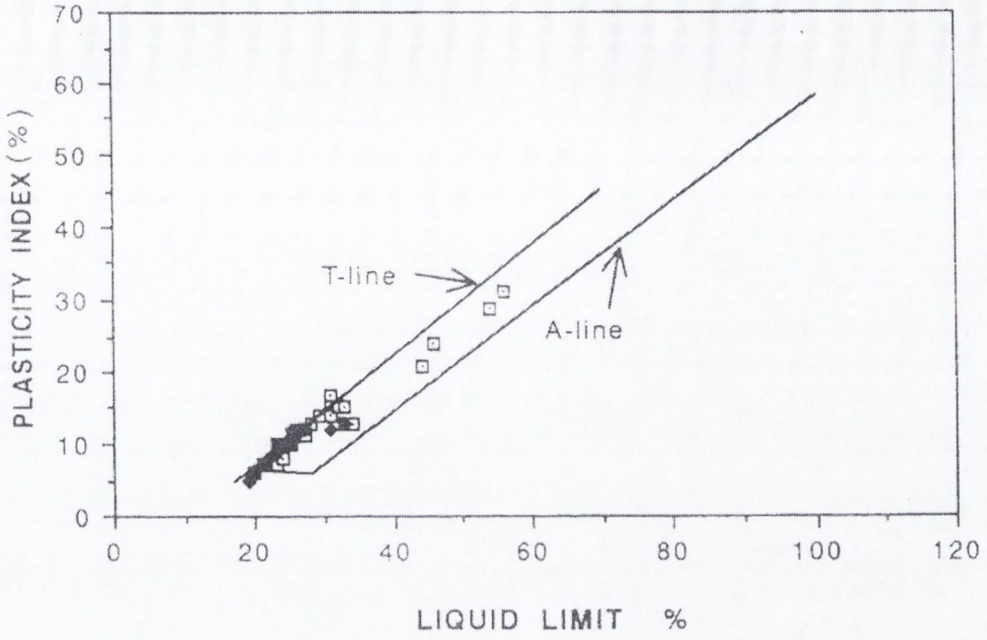

Fig. 1.14 – Plasticity chart for brown and black diamictons (Farrell et al., 1995)

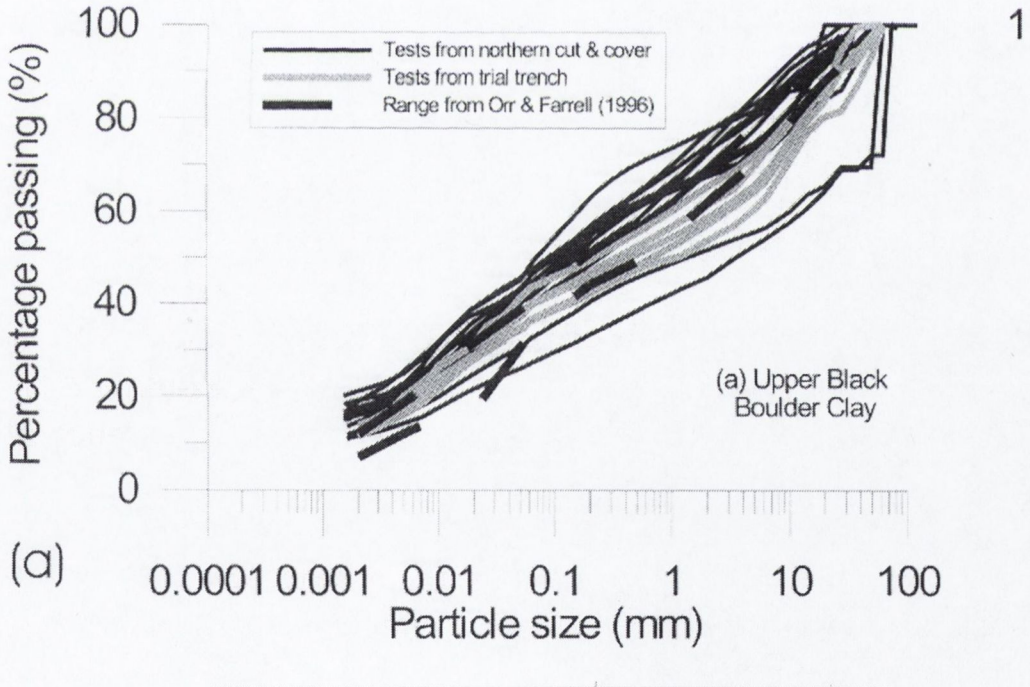

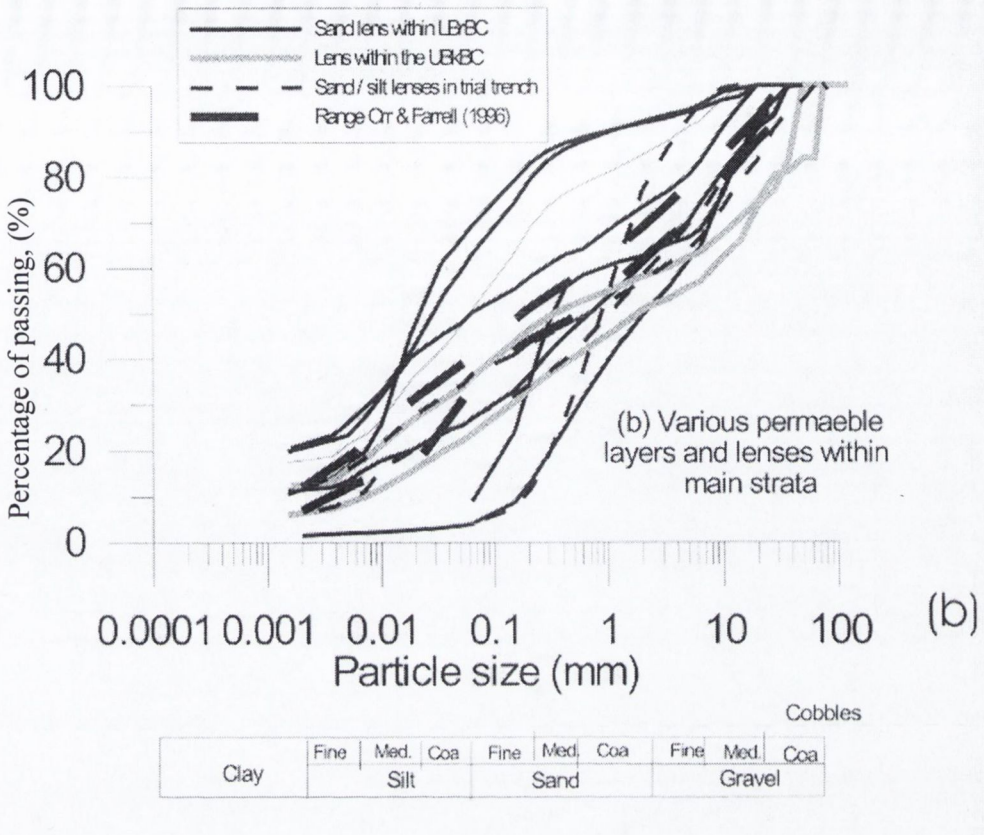
Sand lens within LBrBC
Lens within the UBkBC
Sand / silt lenses in trial trench
Range Orr & Farrell (1996)
Percentage of passing, (%)
100
80
60
40
20
0
(b) Various permaeble layers and lenses within main strata
0.0001 0.001 0.01 0.1 1 10 100
Particle size (mm)
(b)
Cobbles
Clay
Fine Med. Coa Fine Med. Coa Fine Med. Coa
Silt
Sand
Gravel

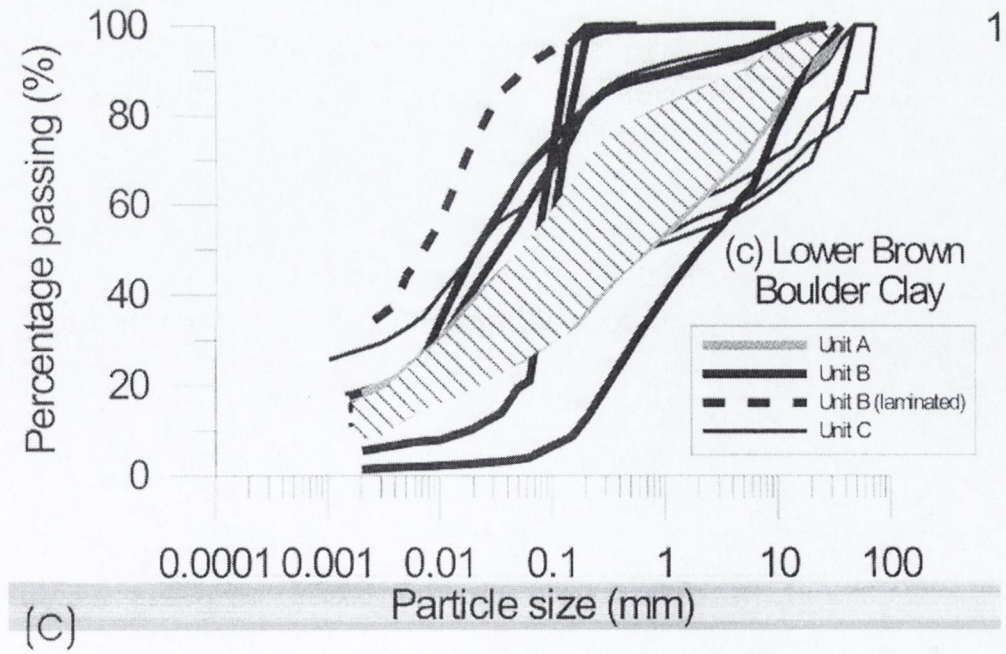
Clay
Fine Med. Coa Fine Med. Coa Fine Med. Coa
Silt
Sand
Gravel
Cobbles
Percentage passing (%)
100
80
60
40
20
0
(c) Lower Brown Boulder Clay
Unit A
Unit B
Unit B (laminated)
Unit C
0.0001 0.001 0.01 0.1 1 10 100
Particle size (mm)
(c)

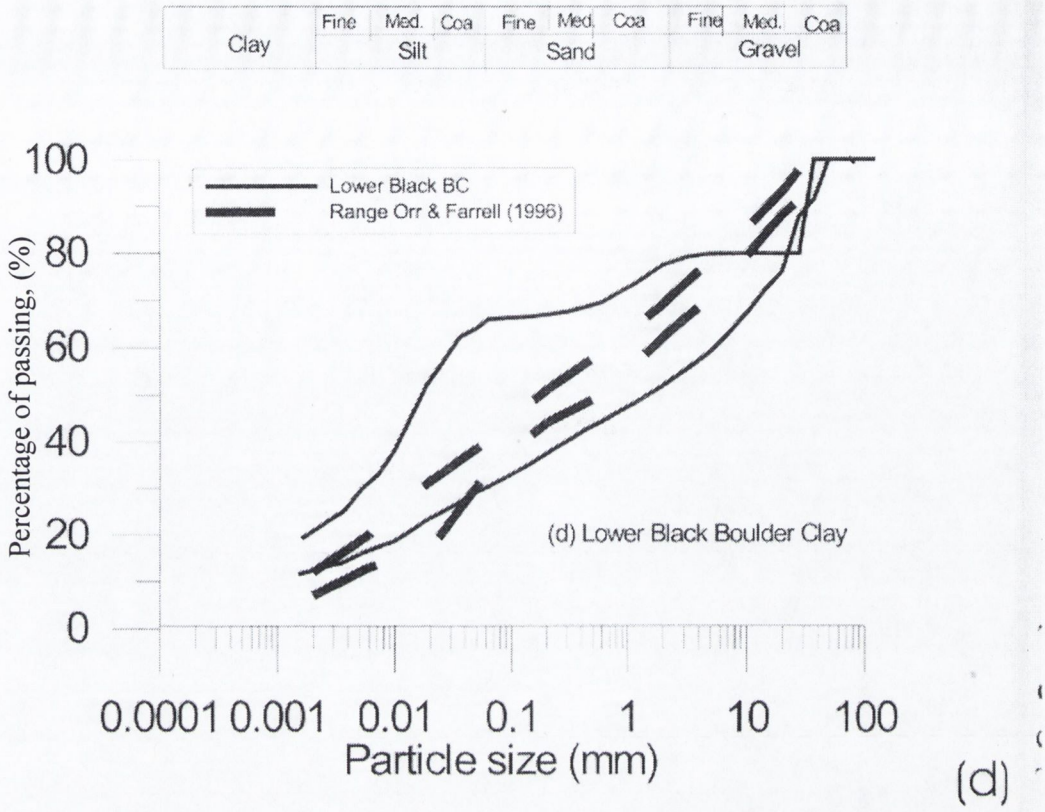

Fig.1.15 – Particle size distribution curves for; (a) upper black boulder clay; (b) For various lenses and layers with the Dublin Boulder Clay formations; (c) For Lower brown boulder clay; and (d) for Lower black boulder clay (Skipper et al., 2005).

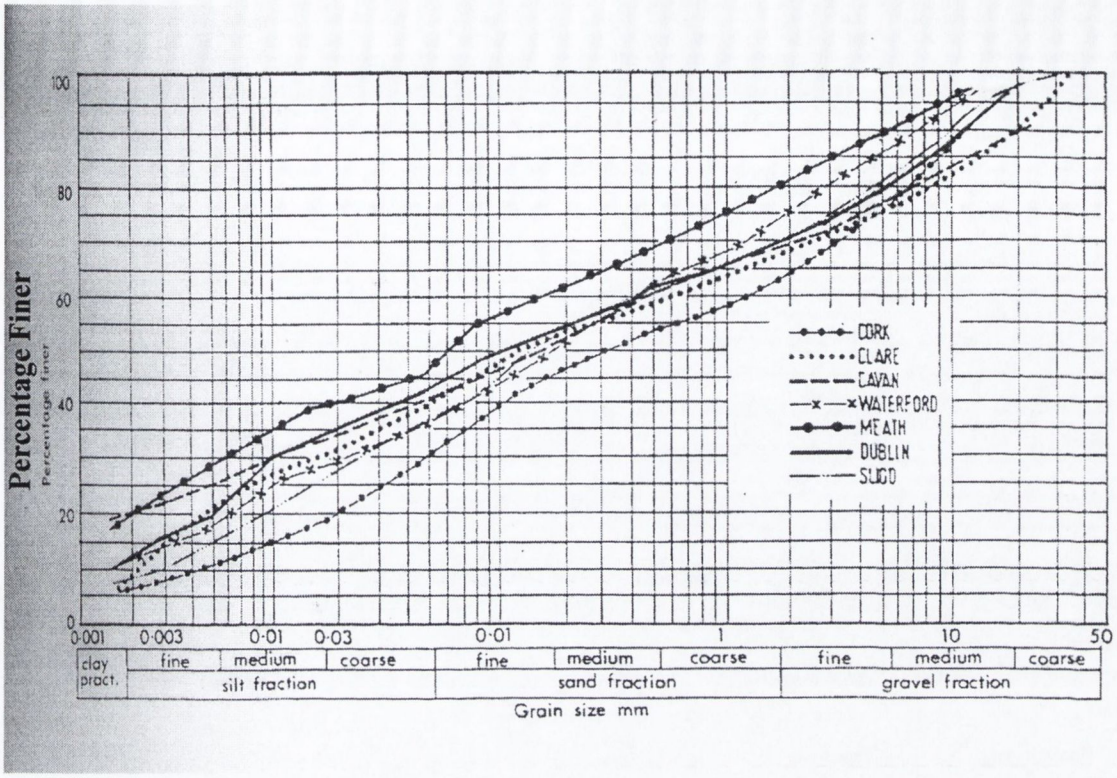

Fig. 1.16–Selected grading curves of boulder clays from locations indicated (Hanrahan 1977)

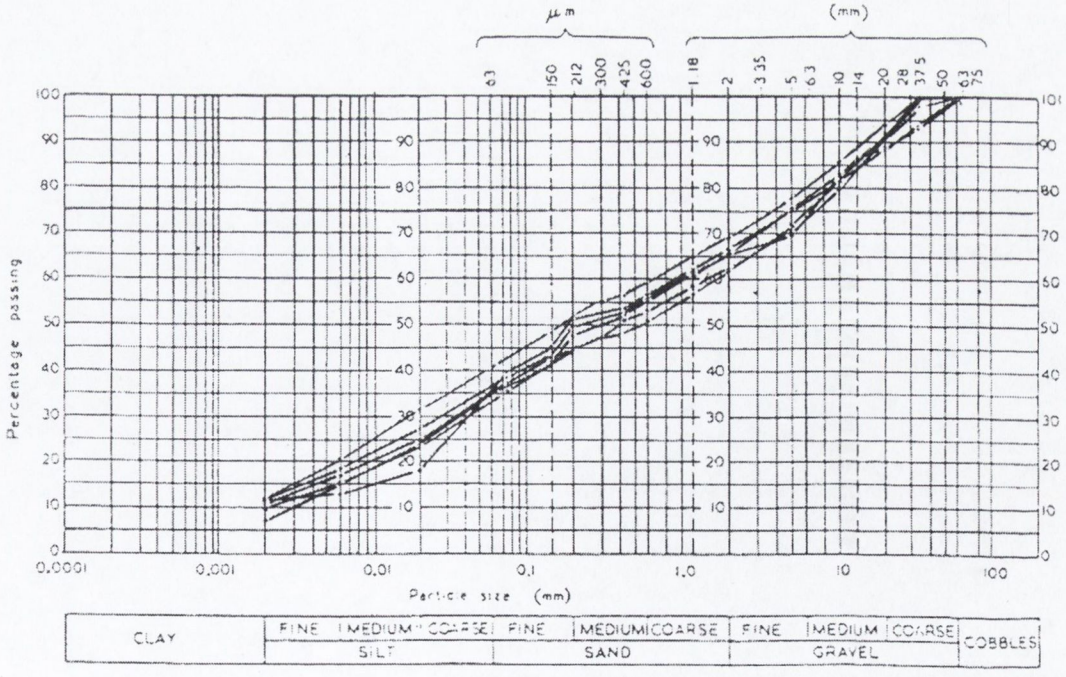

Fig.1.17–Particle size distribution curves of brown and black diamictons (Farrell et al., 1995)

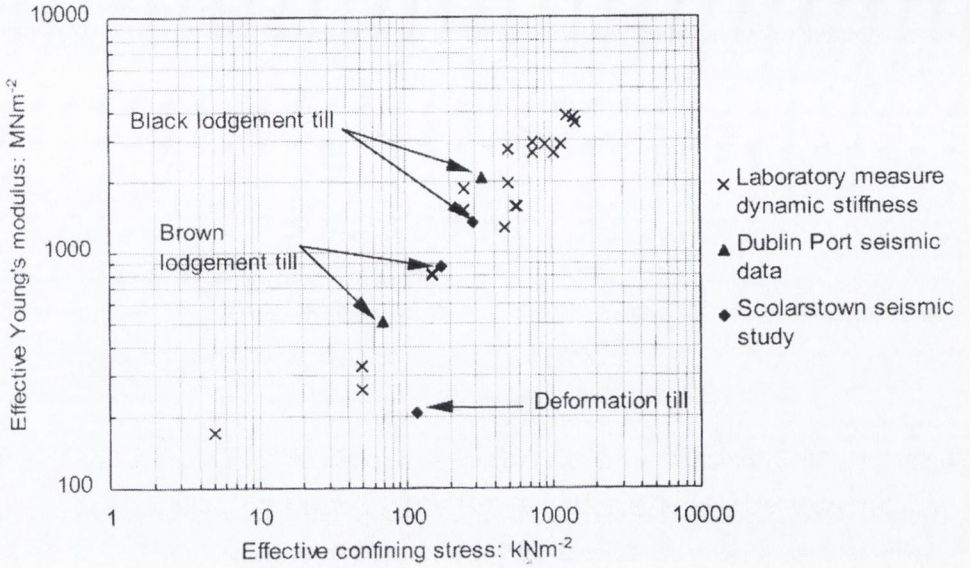

Fig.1.18– Comparison of stiffness measured in situ and in the laboratory dynamic tests (Lawler, 2002)

1.5 Aims and Objectives of research

The main aims and objectives of this research are summarised as follows:

1. To carry out laboratory tests to determine the dynamic properties, such as stiffness and damping ratio, of the Dublin boulder clay.

2. To predict, using 3-D finite elements modelling, the vibrations at the ground surface due to construction of the north bound Dublin Port Tunnel and to make a comparison between the vibrations predicted using finite elements and the measured vibrations.

3. To predict, using 3-D finite element modelling, the vibrations at the ground surface due to construction of the south bound Dublin Port Tunnel while north bound tunnel is existence and to make a comparison between the vibrations predicted using finite elements and the measured vibrations.

4. To carry out several parametric studies to examine the sensitivity of the predicted vibrations to various parameters of input data, which include the stiffness and the damping ratio of soil.

5. To predict the vibrations at the surface above the tunnelling boring machine using existing empirical methods.

6. To develop a new empirical equation, based on the wave attenuation equation, to predict the vibrations at the surface due to the tunnel boring machine and to compare these predicted vibrations with those predicted using the existing empirical models, 3-D FE analyses and the measured vibrations.

1.6 Thesis Outline

The following chapter, Chapter 2, presents a review of the relevant literature in order to provide a background to ground vibrations and to highlight recent research work that has been carried out by researchers working in this area.

Chapter 3 presents the fundamentals of the finite element method regarding its use in the analysis of soil dynamic problems and a brief description of the dynamic features available in the finite element packages PLAXIS and ABAQUS.

In Chapter 4, the results of an investigation using bender elements to measure the small strain stiffness and damping ratio of Dublin boulder clay are presented. The results of this investigation are compared to the parameter values supplied by Nishimatsu Construction Co. Ltd and to the values obtained by Lawler (2002).

Chapter 5 describes the measurement in the field of the tunnel boring machine excitation and the ground vibrations induced at the surface due to the tunnelling.

Chapter 6 presents 3-D finite element analyses of tunnelling induced ground vibrations while Chapter 7 describes the empirical methods used to predict tunnelling induced ground vibrations, including the development of a new empirical equation.

Finally, in Chapter 8, the main conclusions and recommendations for future research of this thesis are presented.

Appendix A presents laboratory test documentations
Appendix B presents the TBM excitation at different sections.
Appendix C presents the predicted Peak Particle Velocity (PPV) at the surface.
Appendix D presents the ABAQUS input file.
Appendix E presents the publications.

CHAPTER 2

LITERATURE REVIEW

2.1 Introduction

In recent years construction works have utilised larger plant as economic pressures have forced greater emphasis on mechanical rather than labour-intensive techniques. Mechanisation of tunnelling methods has resulted in the use of tunnel boring machines (TBM) that dissipate large amounts of energy, in the form of ground vibrations, into the environment (New, 1982 and Hillar & Hope, 1998).

This chapter reviews the literature concerning the different factors that influence the propagation and spreading of TBM induced ground vibrations into the surroundings. In the first section, the types of tunnelling are described. In the second section, the ground vibrations and their effects, the propagation of ground vibrations and their attenuation, the way in which the waves are reflected and refracted and the control of vibrations are all discussed. In the third section, the dynamic ground properties are discussed. Finally, in the fourth section, the bender element test used to determine dynamic ground properties is discussed.

The main purpose of this chapter is to provide from literature a theoretical background that can be useful when analysing TBM induced ground vibrations and other problems of soil dynamics.

2.2 Tunnelling

2.2.1 Cut and Cover Tunnel

Shallow depth tunnels, such as large sewer tunnels, vehicular tunnels, and rapid transit tunnels are frequently designed as structures to be constructed using the cut-and-cover

method. Tunnel construction is characterized as cut-and-cover construction when the tunnel structure is constructed in a braced, trench-type excavation and is subsequently backfilled. For depths up to 10-15m this method is often cheaper and more practical than underground tunnelling (Bickel et al., 1996).

When designing a shoring system for a cut-and-cover excavation, it is important to consider the effects of ground settlements on nearby buildings. Probable amounts of settlement must be determined so that effects on nearby buildings may be analysed. If unacceptable settlements are predicted, then the shoring plan should be re-evaluated or options for ground treatments studied in order to limit damage. Factors influencing ground settlements include excavation dimensions, soil type, construction methods and workmanship quality (Megaw & Bartlett, 1982, O'Reilly et al., 1990 and Fredriksen et al., 1994).

A general guide proposed by Peck (Terzaghi et al., 1996) based on many case histories, summarizes expected settlements adjacent to internally braced or tied-back flexible walls. Peck was the first to propose that settlements at distances from the excavation can be related to the excavation depth.

2.2.2 Bored Tunnel

2.2.2.1 Bored Tunnel in Soft Soil

Tremendous advances have been made since Brunel invented the first soft ground-tunnelling machine in 1818 (Megaw & Bartlett, 1982). Brunel's shields, used to excavate tunnels under the Thames, were the forerunners of today's modern soft ground tunnelling machines. Today's engineers have many tunnelling methods to choose from when seeking an option for a tunnelling project. The selection of the optimal tunnelling method depends on many factors, which include the soil and water conditions, tunnel size and support methods as well as tunnel excavation sequence and other logistical factors. Economics play a deciding role as well as equipment availability and the

experience of the engineer/constructor when selecting one method in preference to another.

The most basic tunnelling machine is the simple shield type that was invented by Brunel and is still in use, with minor modifications, up to the present day. Brunel's shield was designed to provide (Megaw & Bartlett, 1982):

- A skin, supporting the ground on all sides. This was done by means of iron staves sliding forward as the excavation was advanced, and supported by iron frames.
- Means to support the face and yet provide access for excavation. The iron frames carried horizontal oak poling boards, supported by screw jacks which could be moved forward one at a time as the small area of face open was excavated.
- Means to move the shield forward into the excavated space and then to build the permanent lining at the rear. Jacking from the completed arch brickwork propelled the shield forward.

Sutcliffe (1896, cited by Megaw & Bartlett, 1982) gives the following functions of a Tunnel Boring Machine (TBM):

- to excavate the ground
- to remove the material excavated
- to maintain the line and grade of the excavation
- to support the excavated tunnel temporarily until permanent support can be provided
- to handle adverse ground conditions.

Excavation of tunnels in soft ground or with inflowing water is problematic. In order to stem the flow of water, which erodes and weakens the surrounding ground, modern TBMs are equipped with watertight seals, which allow the cutting of the ground to be performed under pressure and which restrain the flow of groundwater into the

excavation. A TBM handles this by several methods. A brief description of these methods follows.

The use of compressed air as a means of ground stabilization and groundwater control in sandy and squeezing clay soils has been used for many years prior to the development of TBMs. The first use of compressed air for tunnelling was in 1879 to excavate a tunnel under the Hudson River in New York. This proved to be an effective way to offset groundwater pressure at the tunnel face, thus controlling the flow of water into the face. In spite of these benefits, there are several major disadvantages of working under compressed air conditions. The first of these is the difficulty in striking a correct balance between the air pressure required at the crown and water pressure at the invert (Megaw & Bartlett, 1982).

The second major disadvantage to tunnelling under compressed air is health related. Working under increased atmospheric pressure conditions may be harmful to a tunneller's health. There are many statutes regulating the exposure time, age and physical condition of the tunneller for working under such conditions. Workers must take precautions similar to deep-sea divers to ensure against suffering from the bends as they re-enter normal atmospheric pressure (Megaw & Bartlett, 1982 and Attewell, 1995).

In 1964 the Robbins Company developed a TBM for the excavation of Metro tunnels in Paris. This TBM relied on pressurized air at the face ahead of an airtight bulkhead. A drawback to this method is the compressible nature of air and its highly explosive nature when highly compressed (Megaw & Bartlett, 1982).

A system preferable to pressurized air was developed by the German construction firm Ways & Freitag A.G. (Megaw & Bartlett, 1982) which used a combination of slurry and air to provide pressure at the face. As the TBM advances, the bentonite slurry carries the excavated material back to a separation plant where the separated spoil is disposed of and the cleaned bentonite is recycled through the slurry back to the TBM. The

cushion of compressed air in the plenum, or excavation chambers, regulates the operating pressure of the slurry in order to compensate for the variations in the surrounding groundwater pressure and effectively limits surface settlement by limiting losses due to the over-excavation volume.

2.2.2.2 Bored Tunnels in Hard Ground

The tunneller has three options for tunnelling in hard ground:

- Drill & Blast
- Road header
- Tunnel Boring Machine (TBM)

Drill and Blast methods are suitable for full or partial face advance and for any cross section geometry. The Drill and Blast method may be an integral part of the New Austrian Tunnelling Method (NATM) method for advancing the tunnel. The potential for overbreak and problems due to noise and vibration make it unsuitable for most urban projects (Deane, 1994).

The use of road headers is suitable for full or partial face advance and for any cross sectional geometry. They are also known as "continuous miners" and are usually generic pieces of equipment not specifically modified for a particular project. When compared to a TBM, they are inexpensive. Road headers are very adaptable and can be quickly modified to perform drilling operations required for fore poling or rock bolting as well as installing steel arches used as primary support members (Megaw & Bartlett, 1982 and Attewell, 1995).

The use of a full face TBM in rock assumes the ability to cut a cylindrical hole, self-supporting for a sufficient time. The machine typically comprises a fixed head, supported by jacks on shoes in the invert and at the sides, containing the drive motors and a rotating cutting head carried in a large and heavy thrust bearing. Behind, and attached to the fixed head, is a chassis on which are mounted electro hydraulic motors,

conveyor, rear jack, and an expanding ring or series of pads which can grip the tunnel walls and against which forward thrust can be made. The whole mechanical system must transmit the torque and thrust necessary for boring, while remaining accurately on the centre line, and steerable (Megaw & Bartlett, 1982). The open shield TBM is shown in Fig.2.1.

When the TBM is driven forward, a precast concrete segmental lining is assembled inside the TBM's steel cylinder and this replaces the cylinder to resist earth and water pressures. Therefore the tunnel face walls are always protected either by the steel cylinder or the concrete lining. Because the thickness of the steel cylinder and the concrete lining are different, there are voids between the excavated surface and concrete lining. These voids are filled with grout to stabilize the excavated surface. For the voids ranging from 0.5m to 2.5m away from the tunnel face, pressurised grouting is performed to fill the voids and loosened parts of soil, to prevent settlement of the ground and buildings above the tunnel.

One of the great advantages of a TBM in rock is that, unless the rock is so cracked and fissured that blocks fall into the tunnel, it cuts a smooth bore of the correct profile which not only gives a useful reduction in the amount of excavation but also makes the best use of the rock strength and facilitates the construction of any tunnel lining whether it be in situ concrete or a precast segmental lining (Whittaker et al., 1990). The disadvantage of a TBM in rock is that the tunnel-boring machines may give rise to vibration problems (New, 1990a).

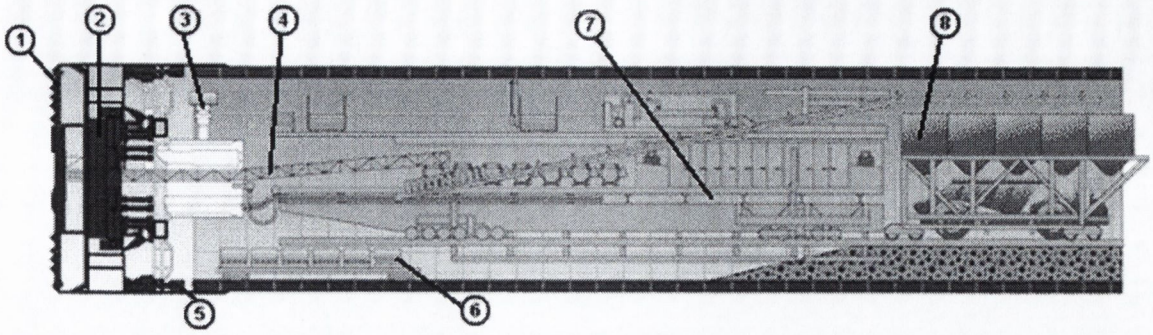

1. cutting head
2. drive
3. erector
4. conveyor belt
5. tunnelling jacks
6. lining segment supply
7. backup system
8. silo car

Fig.2.1– Open shield TBM (http://www.herrenknecht.com)

2.3 Ground Vibrations

2.3.1 General

Vibration can be considered to be the oscillation or repetitive motion of an object around an equilibrium position due to an external force. The equilibrium position is the position the object will attain when the force acting on it is zero.

The environmental effects of noise and ground vibrations have received considerable attention in recent years due to the damage ground vibrations can cause buildings and due to the sensitivity of people to noise and vibration (Hillar & Hope, 1998 and Hall, 2003). Vibrations can be generated by either natural or artificial sources. Natural sources are earthquakes, ocean waves and landslide. In the case of earthquakes, the intensity of ground vibrations may be high enough to result in heavy structural damage or even collapse of structures accompanied by loss of life. Ground vibrations from artificial sources are called man-made vibrations. Sources of man-made vibrations may be classified into the following main categories: (1) operation of machines; (2) road and railways traffic; and (3) construction activities (Athanasopoulos & Pelekis, 2000 and Dobry & Vucetic, 1987).

The magnitude of man-made vibrations is normally much smaller compared to earthquake vibrations and hence these vibrations do not, in most cases, cause serious structural damage to buildings and their effects are limited to the development of cosmetic cracks in the walls and floors of buildings. Structures adjacent to a new tunnel, in particular old masonry buildings, may suffer damage resulting in costly repairs or require expensive protective measures, such as underpinning or compensation grouting (Athanasopoulos & Pelekis, 2000; Liu et al., 2000). Man-made vibrations can also induce densification in sandy soils, resulting in foundation settlement. This settlement has the potential of inducing more serious structural damage than the cosmetic cracking (Athanasopoulos & Pelekis, 2000).

Ground vibrations from the operations of heavy machines are mostly continuous and periodic and have been studied extensively by both analytical and experimental methods. The focus of the relevant studies has been on the development of methods for estimating the magnitude of the expected vibrations from machine foundations. Fewer studies have focused on the establishment of vibration criteria to protect the integrity of the machine and avoid the disturbance of people (Athanasopoulos & Pelekis, 2000).

Ground vibrations caused by road and railway traffic are in most cases random motions and have been the subject of numerous studies in the past 25 years. These studies involved field measurements and focused on developing: (1) methods for empirical prediction of the intensity of ground vibrations generated at a given distance from vehicular traffic; and (2) numerical models encompassing the source of vibration and the transmission path for predicting the vibration level at different distances from the source and for investigating the study of the effects of parameter variability (Athanasopoulos & Pelekis, 2000 and Madshus et al., 1998).

During the past few decades, construction vibrations have become the subjects of intensive study (Dowding, 1996; Skip, 1998; Hillar & Hope, 1998; and Athanasopoulos & Pelekis, 2000). Construction activities resulting in vibrations include blasting operations in rock sites, explosive demolition, pile driving in soils, vibratory or dynamic

compaction of soils, deep excavation and tunnelling activities in either soil or rock (Athanasopoulos & Pelekis, 2000). The effect of vibrations, above the human perception level, may cause disturbance to human comfort and even damage to existing structures. In this chapter, some of the literature considering the effects of vibrations on humans and on structures is reviewed.

2.3.2 Types of Vibrations

Besides the magnitude and frequency of vibrations, the potential for damage and disturbance is also dependent on the nature and duration of the vibrations. The motion of a discrete element of a vibrating material has its simplest form when it is sinusoidal. Ground vibrations can be classified into the following:

- Sinusoidal vibrations: sinusoidal vibrations are the simplest form of vibrations described by sine functions, as shown in Fig. 2.2 (a). Vibratory pile drivers can often generate steady-state sinusoidal vibration (Head & Jardine, 1992).

- Transient vibrations: transient vibrations have a cyclical variation in amplitude, which reaches a peak and then decays towards zero, as shown in Fig. 2.2 (b). Such vibrations can be generated by blasting and impact hammers.

- Periodic vibrations: periodic vibrations have a cyclical variation in amplitude which repeats many times, as shown in Fig. 2.2 (c); vibrations generated from heavy machines are an example of periodic vibration. Sinusoidal vibrations are also periodic vibrations.

- Random vibrations: random vibrations are not predictable and the displacement-time pattern never repeats, as shown in Fig. 2.2 (d). Vibrations from road and railway traffic and seismic activities are random vibrations.

For sinusoidal motion, the displacement (x)-time (t) relation is

$$x = A \sin(\omega t - \varphi) \qquad [2.1]$$

where A is the displacement amplitude; ω is the circular frequency and φ is the phase angle. The particle velocity can be obtained by differentiating Equation 2.1 with respect to time:

$$v = \frac{dx}{dt} = A\omega\cos(\omega t - \varphi) \qquad [2.2]$$

Also, differentiation of Equation (2.1) with respect to time gives the particle acceleration:

$$a = \frac{d^2x}{dt^2} = -A\omega^2\sin(\omega t - \varphi) \qquad [2.3]$$

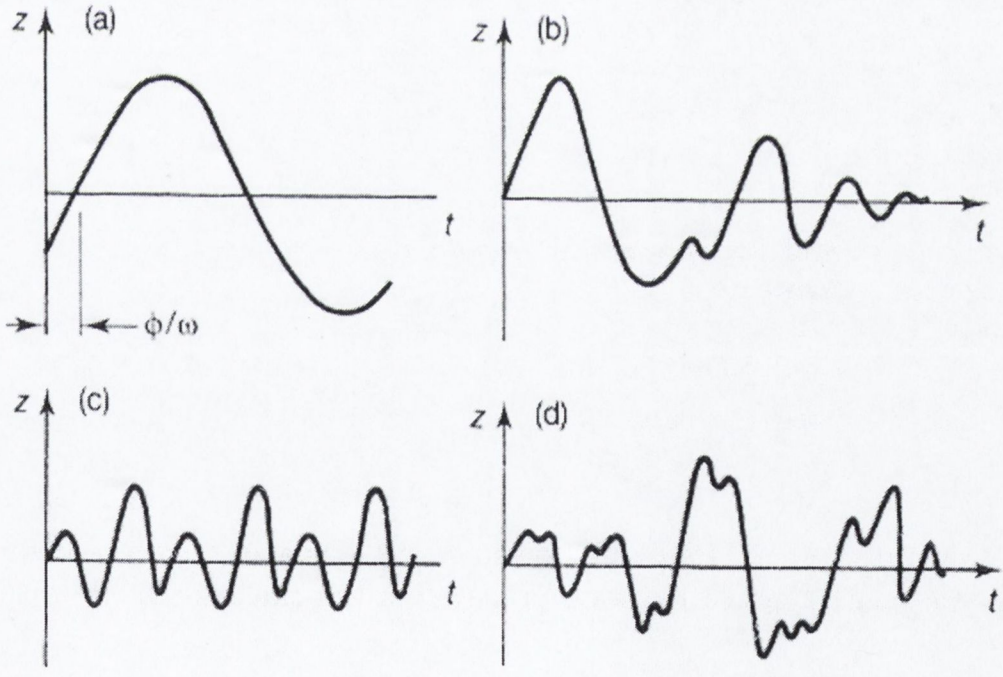

Fig. 2.2–Types of vibration: (a) sinusoidal (b) transient (c) periodic (d) random (from Head and Jardine, 1992)

2.3.3 Vibration Propagation

Vibrations are quantified in terms of the velocity attained by particles in the ground, as they are disturbed from their at-rest position during the passage of a wave. As an individual particle vibrates it transmits its vibration to adjacent ones. Vibration is propagated away from the source in the form of a wave (Hillar & Hope, 1998).

A wave can be defined as a disturbance travelling from one point to another transferring energy but not particles. A wave can be distinguished from particle vibration through the following example. Consider the movement generated in water when a small piece of stone is thrown into the centre of a pond. A single disturbance moves at a constant speed away from the source of the disturbance towards the edges of the pond. The movement of the disturbance is described as wave motion and it has a wave velocity. If a piece of wood lies on the water surface, the up and down movement of the wood as the water wave passes its location is defined as its particle velocity (Hillar & Hope, 1998 and Fahy & Walker, 1998).

In engineering practice, attention is focused on studying ground motion, which is defined as particle velocity. The measurement of the vibration at the ground surface is usually expressed in terms of particle velocity where its form and amplitude is a function of the source, the ground conditions and the radial distance from the source. Vibration is propagated away from the source in the form of body waves and surface waves.

2.3.3.1 Body Waves

Body waves, which can travel through the ground, are of two types: one is a P-wave another is an S-wave. P-waves, also known as primary, compressional, or longitudinal waves (Fig. 2.3a), involve successive compression and rarefaction (Fig.2.3a) of the materials through which the waves pass. P waves are the fastest body waves and arrive before the S waves. The P waves carry energy through the ground as longitudinal

waves, moving particles in the same line as the direction of the wave. They can travel through all layers of the ground. Like sound waves, compression waves can travel through both solids and fluids. P waves are generally felt by humans as a bang or thump (Kramer, 1996 and Santamarina, 2001). The compression waves, v_p, can be calculated using following Equation:

$$v_p = \frac{\sqrt{M}}{\sqrt{\rho}} = \sqrt{\frac{E(1-\nu)}{\rho(1+\nu)(1-2\nu)}} \qquad [2.4]$$

where M = constrained (oedometer) modulus; E = Young's modulus; ρ = bulk density and ν = Poisson's ratio.

S-waves, also known as shear, secondary and transverse waves, cause shearing deformations as they travel through a material. The motion of an individual particle is perpendicular to the direction of the S-wave travel (Fig.2.3 (b)). Shear wave carry energy through the ground in a pattern of transverse (crosswise) waves. These waves move more slowly than P wave. The direction of particle movement can be used to divide the S-waves into two components, SV (vertical plane movement) and SH (horizontal plane movement). Fluids, which have no shearing stiffness, cannot sustain S-waves (Kramer, 1996 and Santamarina, 2001). The shear waves, v_s, can be calculated using following Equation:

$$v_s = \frac{\sqrt{G}}{\sqrt{\rho}} \qquad [2.5]$$

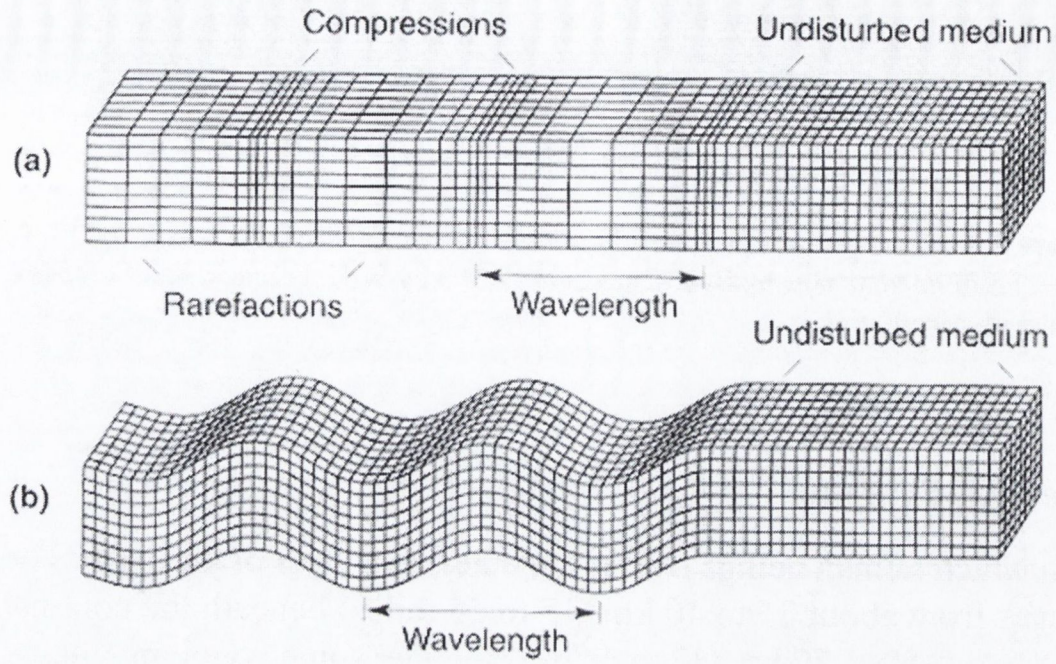

Fig. 2.3–Deformations produced by body waves: (a) P-wave; (b) SV-wave (from Bolt, 1993 cited by Kramer, 2000)

2.3.3.2 Surface Waves

Surface waves result from interaction between body waves and the ground surface. They travel along the earth's surface with amplitudes that decrease roughly exponentially with depth. Because of the nature of the interaction required to produce them, surface waves are more prominent at distance farther from the source. The most important surface waves, for engineering purposes, are Rayleigh waves and Love waves (Fig.2.4). Rayleigh waves are produced by interaction of P-and SV-waves with the ground surface; involve both vertical and horizontal particle motion. They are similar, in some respects, to the waves produced by a rock thrown into a pond. The velocity of Rayleigh waves is slower than that of body waves. The velocity of Rayleigh waves (v_r) can be calculated using following Equation:

$$v_r = \frac{0.87 + 1.12\upsilon}{1+\upsilon} v_s \qquad [2.6]$$

Love waves result from the interaction of SH-waves with a soft surficial layer and have no vertical component of particle motion.

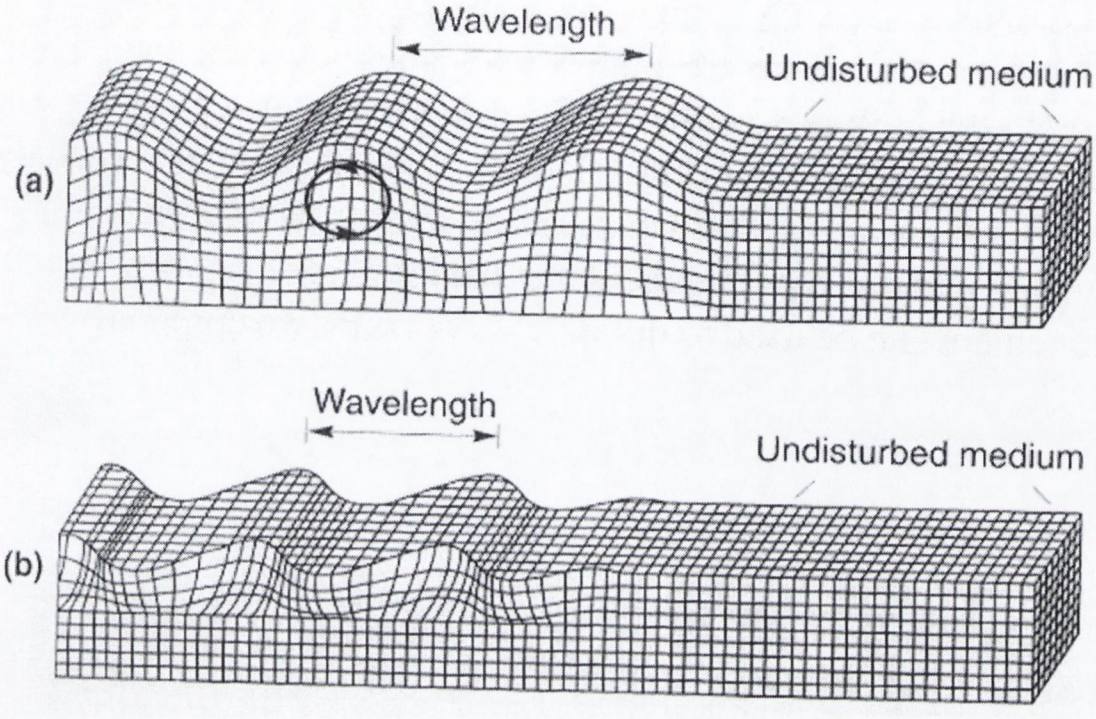

Fig. 2.4–Deformations produced by surface waves: (a) Rayleigh wave (b) Love-wave (from Bolt, 1993 cited by Kramer, 1996)

2.3.4 Attenuation of Ground Vibration

Attenuation describes the processes by which the magnitude of a vibration reduces as it propagates away from the source. Attenuation occurs by geometric spreading and material damping. Attenuation with distance from a source should not be confused with decay with time at a point. The first effect is purely geometrical and occurs because the energy radiated from the source is spread over an increasingly large volume of material as the wave front propagates. So this effect is independent of the material properties of the ground. The second effect, material damping, is a property of the propagating medium and describes the frictional, inelastic, hysteretic energy losses that occur during the passage of a wave, as elements of soil undergo cyclical shearing or compression. It

is affected by the characteristics of the soil and the amplitude of motions (Hillar & Crabb, 2000).

For the decay of both body and surface waves the geometrical damping is an important parameter. The energy attenuates according to $1/r^2$ for the body waves, where r is the distance from the source and the amplitude is proportional to the radial distance (1/r). The amplitude of the Rayleigh waves is proportional to the square root of the radial distance ($1/\sqrt{r}$). Thus, the attenuation of the amplitude of the Rayleigh waves is slower than that for the body waves (Das, 1984). Geometric attenuation is independent of the properties of the material through which the energy propagates.

Richart et al., (1970) found that the attenuation of waves in soils is more rapid than that predicted by elastic theory. The amplitude is attenuated by material damping caused by frictional dissipation of the elastic energy.

The combined effect of material and geometric damping is given by Mintrop's (1911, cited by Hillar & Crabb, 2000), attenuation equation is:

$$A_1 = A_0 [r_0/r_1]^{ß} e^{-\alpha (r_1 - r_o)} \qquad [2.7]$$

where A_1 is the amplitude at distance r_1 from the source; A_o is the amplitude at distance r_o from the source; α is the absorption coefficient; and ß is the geometric spreading term.

In Equation 2.7, $(r_0/r_1)^{ß}$ represents the geometrical damping and the power, ß, is a function of the wave type, with ß = 1 for body waves in the ground that spread spherically, except at the surface where ß = 2, and ß = 0.5 for Rayleigh waves (Dowding, 1996). In Equation 2.7, α (r_1-r_0) is the material damping and the α is the coefficient of attenuation. The α coefficient increases with increase in the dominant frequency, as a higher-frequency wave will pass through more motion cycles than will low-frequency waves when travelling the same distance and hence will undergo attenuation. For material damping, decay is a function of energy loss per cycle of

deformation, not the distance travelled per second. The lower-frequency components have undergone fewer deformational cycles and hence have lost proportionally less energy. As shown in Table 2.1, α has also been found (Woods and Jedele, 1985) to be larger in soil than in rock.

Table 2.1 Proposed Classification of earth materials by attenuation coefficient, α

Classification of Earth Materials	Attenuation Coefficient, α (1/m)		Description of Material
	5 Hz	50 Hz	
I	0.01-0.03	0.1-0.3	Weak or soft soils
II	0.003-0.01	0.03-0.1	Competent soils
III	0.0003-0.003	0.003-0.03	Hard soils
IV	<0.0003	<0.003	Hard, component rock

(from Woods and Jedele, 1985)

Godio et al. (1992 cited by Hillar and Crabb, 2000) proposed an equation for predicting the ground vibrations, through the calculation of the peak particle velocities. This is a useful first estimate for predicting the vibration levels likely to be generated by mechanised bored tunnelling works and is given by the exponential equation:

$$V=Ar^{-1.3} \qquad [2.8]$$

Where,

V is the predicted resultant peak particle velocity (mm/s).

A is a constant whose value depends on the ground condition; for hard ground A=180.

r is the direct distance from the vibration source to the measurement point (m).

Equation 2.8 is for values of r ranging from 10 to 100m.

The direct distance, r, from the source of the vibrations to the point of interest is an important parameter when predicting the vibration level. This direct distance may be calculated from the horizontal and vertical distances between the source and the measurement locations. For tunnelling works, it is clearly important that the depths as well as the lateral distance are recorded in order to calculate the direct distance from the source of the vibrations to the point of interest.

Nishimatsu Construction Co. (NCC) Ltd. has also developed a general equation for predicting the vibrations due to tunnelling from PPV values monitored on other construction sites. This equation provides a correlation between the peak particle velocity, V and the distance from the point source to the point of interest, r of the form $V = Nr^{-m}$ but it was found that the coefficients N and m change with the ground conditions, the diameter of the tunnel boring machine and the thrust force of the machine. The specific equations for obtained by NCC from a number of different tunnelling works, are presented in Table 2.2.

Table 2.2–Summary of tunnel vibration data sites compared to predictions

Project Reference Number	Project Name	Geology	TBM type	Tunnel diameter (m)	Tunnel cover (m)	NCC Equation $V = Nr^{-m}$
No. 1	Rail (JLE)	Sands and clays	Mix shield	5.13	21.2	$V = 0.15r^{-0.66}$
No 2	Rail (Channel Tunnel)	Clay/ Chalk	Full face TBM	8.72	22.6-55	$V = 3.4r^{-0.71}$
No.3	Cable Tunnel	Mudstone	Full face TBM	2.44	11	$V = 133r^{-1.96}$
No. 4	Emergency Tunnel	Nohi rhyolites	Open shield	4.5	100	$V = 0.6r^{-0.27}$
No.5	Road (Pilot Tunnel)	Sandstone	Open shield	5.0	70	$V = 7.6r^{-1.4}$
No. 6	No Information					$V = 48r^{-1.47}$

From the equations for the PPV values in Table 2.2 obtained from previous tunnelling projects, the following upper-bound equation and a lower bound equation were obtained to predict the peak particle velocity in the case of Dublin Port tunnel:

$$V = 176r^{-1.18} \quad \text{upper bound} \quad [2.9]$$

$$V = 7.4r^{-1.07} \quad \text{lower bound} \quad [2.10]$$

The new Rahman-Orr model, Equation 7.6 and 7.8, is developed and based on the wave attenuation Equation 2.7, which considered the combined effects of material and geometric damping. The model takes account the TBM excitation, ground dynamic properties and direct distance between the source and the point of interest. If the source vibration velocities are known, then Equation 7.6 and Table 7.3 and 7.4 can be used as a generalised Equation for any type of soil and rock to predict the ground vibrations. However, if source vibration velocities are unknown, then Equation 7.8, which is a simplified version of Equation 7.6, can be used for limestone boring to predict the ground vibrations.

2.3.5 Reflection and Refraction of Waves

Consider the case of two half-spaces of different elastic materials with one resting on the other. The different types of waves produced by incident P-, SV-, or SH-waves impinging on the boundary of two layers are shown in Fig.2.5. In Fig.2.5, it can be observed that the waves are divided into two new waves one is refracted into the top layer material and the other is reflected back into the original material. Since incident P- and SV-waves involve particle motion perpendicular to the plane of interface; they will each produce both reflected and refracted P-, and SV-waves. An incident SH-waves does not involve particle motion perpendicular to the interface; consequently, only SH-wave are reflected and refracted. The directions and relative amplitudes of the waves produced at the interface depend on both the direction and amplitude of the incident wave to the interface and the propagation velocities and densities of the two materials (Kramer, 1996 and Das, 1984).

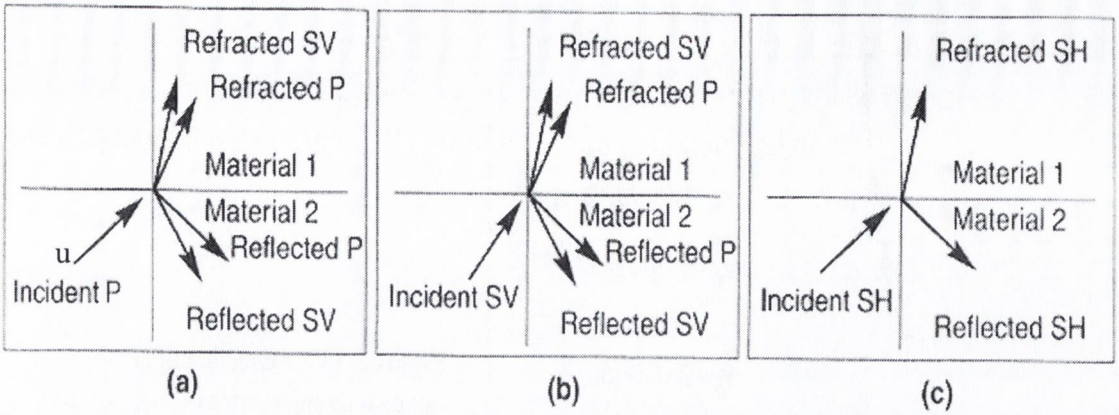

Fig.2.5–Reflected and refracted rays resulting from incident (a) p-wave, (b) SV-wave, and (c) SH-wave (from Kramer, 1996).

Using Snell's law these directions can be determined. Snell showed that

$$\sin(i)/c = \text{constant} \qquad [2.11]$$

where i is the angle between the wave path and the normal to the interface and c is the velocity of the wave of interest (Kramer, 1996 and Das, 1984). Using the velocities u, v, y, z and angles a, b, c, d, e and f defined in Table 2.3 the direction of all waves are easily related to the direction of the incident wave using Snell's law:

Table 2.3 Different wave types with propagation velocity

Wave Type	Velocity	Angle with normal
Incident P	u	a
Incident S	v	b
Reflected P	u	c
Reflected S	v	d
Refracted P	y	e
Refracted S	z	f

$$\frac{\sin a}{u} = \frac{\sin b}{v} = \frac{\sin c}{u} = \frac{\sin d}{v} = \frac{\sin e}{y} = \frac{\sin f}{z} \qquad [2.12]$$

Since incident and reflected waves travel through the same material, a = c and b = d, which shows that the angle of incidence is equal to the angle of reflection for both P-, S-waves. There is also a critical angle of incidence, i_c, where the refracted waves travel parallel to the interface (Kramer, 1986). Therefore,

$$i_c = \sin^{-1}u/y = \sin^{-1}v/z \qquad [2.13]$$

2.3.6 Human Response to Vibrations

Vibrations produced during construction operations normally become of considerable concern before threshold-sized cracking occurs because of the low threshold of human perception. Defining a control limit for vibrations in these conditions can be challenging because it will inevitably depend on the existing vibration environment and human tolerance (Dowding, 1996).

Human reaction is influenced more by previous experience and understanding than by the actual level of vibration itself; a person's state of health, temperament and age will all contribute to this reaction (New, 1990a).

Many controlled experiments have been conducted by researchers, summarized by Griffin (1990), which show that perception thresholds are difficult to establish, and exhibit a great deal of scatter. This is because determination of perception threshold requires many other factors to be considered or isolated, such as frequency and duration of vibration, effect of visual and audible cause, foot vibration of seated subjects (stationary or moving footrest), subject attention (reading or concentrating), presence of background vibration, subject's willingness to guess or wait until they are sure that they could feel the vibration, subject's confusion between a required judgement for perception or comfort, and lack of repeatability of results for a given subject's response. The analytical and statistical methods used for determining thresholds also have a significant bearing on the results.

The British Standard BS 6472 (1992) gives detailed guidance on the evaluation of the effects of vibration exposure on humans in the frequency range of 1 Hz to 80 Hz. It gives guidance on the threshold values for human perception and the higher levels above which complaints become more likely in a variety of environments. Consider the human body coordinate system defined in Fig.2.6. Here, the x-axis defines the back-to-chest direction, the y-axis defines the right side to left side direction, and the z-axis defines the foot -(or-buttocks-) to-head direction.

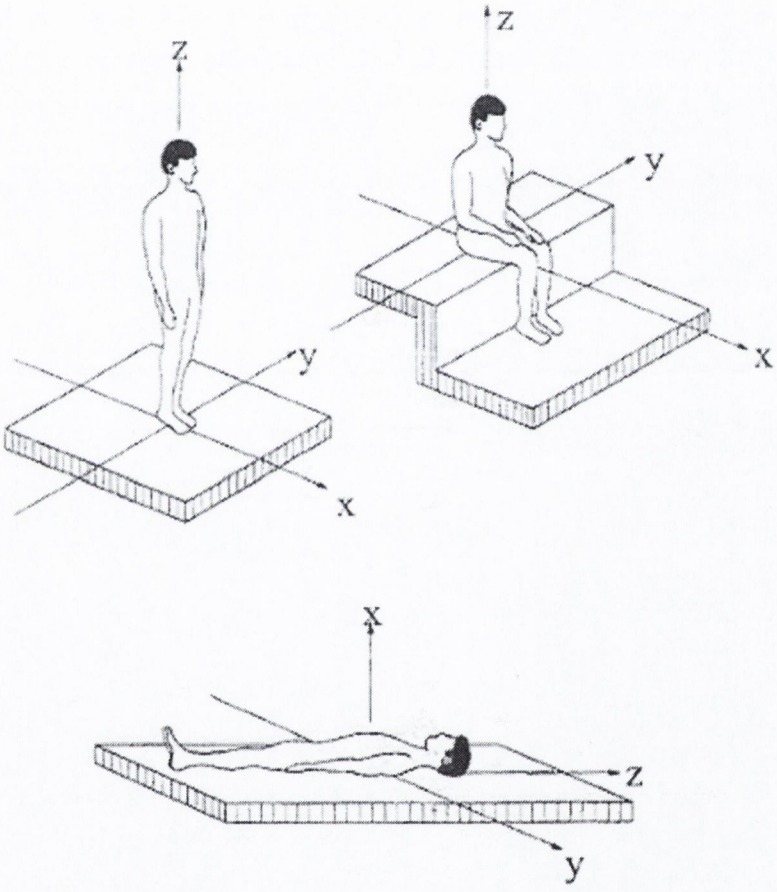

Fig.2.6–Co-ordinate system for human sensitivity to vibration (from BS 6472)

BS recommends that measurements are made in terms of particle accelerations but curves are presented for particle accelerations and velocities, the curves for velocities being calculated assuming sinusoidal motion. For z-axis vibration the threshold level for human perception is 0.141mm/s between 8Hz and 80Hz and higher at lower frequencies, rising to 2.25mm/s at 1Hz and the multiplication factors applicable are 2 &

4 (for residential and day time) giving the threshold limits as 0.282mm/s and 0.564mm/s. For x- or y-axis vibrations, the threshold level is 0.402mm/s between 2Hz and 80Hz, rising to 0.804mm/s at 1Hz. The base curve values without multiplication factor are applicable to the most sensitive situations.

Richart and Woods (1987) focused on the effect of vibrations on humans and found that the amplitude, frequency and duration of vibrations are the important parameters. The authors found that a vibration of 0.25mm/s is hardly detectable to people while a vibration of 2.5mm/s causes people discomfort.

New (1990a) found that when vibration levels from an unusual source exceed the human threshold of perception (PPV, 0.2-0.3mm/s), complaints may occur. In the urban situation, serious complaints are probable when PPV values exceed 3mm/s. Complaints will increase with the duration of the vibration and will be most severe when the intrusion occurs outside normal working hours, particularly at night.

2.3.7 Structural Response to Vibrations

The response of buildings to ground vibrations is governed by the following factors:

- Relationship between natural frequencies of the building and its elements and the characteristic frequency of the ground motion
- Magnitude of vibration
- Stiffness of building and elements
- Damping characteristics of the building
- Other factors such as height and dimensions of the building and the types of materials used in the construction (Head and Jardine, 1992).

When the induced frequencies of the ground vibrations coincide with one of the building's natural frequencies, this may result in large vibrations. This is known as resonance frequency. Damping is the property of a material to absorb vibration energy and every material has some degrees of damping. The vibration energy induced by a

dynamic load decreases with higher damping and vice versa (Clough & Penzien, 1993; Kramer, 1996 and Dowding, 1996).

The growth in instrumentation has led to ever more detailed measurements of vibration, often in terms of velocity, yet very little effort has been directed at carefully monitoring the structures for evidence of damage which can be directly linked to the vibration. Whilst Peak Particle Velocity (PPV) is often used to assess vibration effects on a building, velocity in itself cannot create damaging forces. New (1990b) pictorially showed (Fig.2.7) that such forces are generated by:

- Differential displacements, which give rise to distortion of the structure as it follows movement of the ground.
- Change in ground particle velocity (magnitude or direction), which produces inertial forces upon the structure.

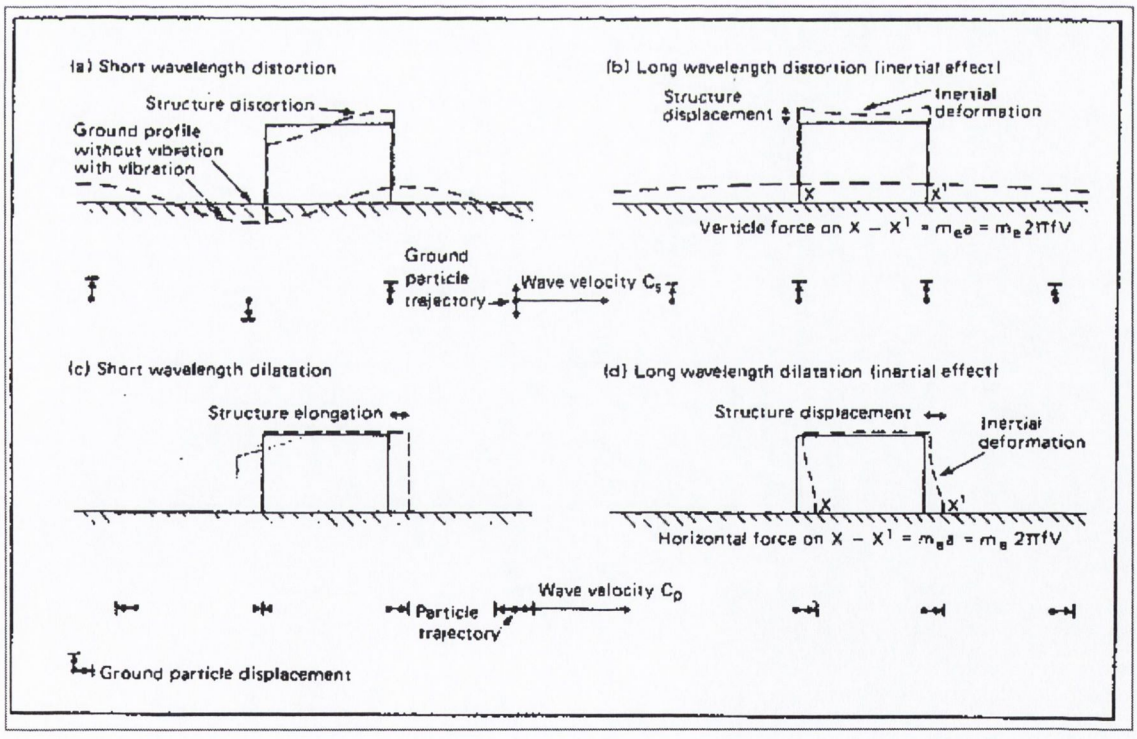

Fig.2.7–Deformation and inertial forces due to ground wave motion (from New, 1990b)

Distortion and inertial mechanisms arise at the same time. These are superimposed upon pre-existing stresses and strains from other causes. Damage occurs when the combined stress exceeds a limiting level, or there may be fatigue failure (New, 1990b).

A review of the possible effect of road traffic vibration on heritage buildings was undertaken by Morton and Fox (1989), who concluded that there are many other plausible reasons for the damage observed, related to factors such as poor ground, weathering effects and decay. Another factor not specifically mentioned relates to the effect that the road surface itself introduces on the moisture content of the soil, such as drainage of storm water from road surfaces.

The problem of structural damage to buildings caused by vibration has been the subject of research in recent years (Dowding, 1996). Because of the frequent construction of high-rise buildings on piled foundations, especially in the urban area, much work has concentrated on the study of vibrations due to piling. The risk of damage to a particular structure depends on its condition and the type of ground on which it is founded. The building may be previously stressed from differential settlement or uneven loading, so that small additional dynamic strain may be sufficient to trigger damage. With respect to the ground conditions, pile driving in loose granular soils or fill may cause settlement, while driving dense soils may cause heave of a temporary or permanent nature.

The British Standard BS 7385 (1993) defines three damage categories: cosmetic, minor and major, and relates vibration levels to these. Cosmetic or threshold damage is the formation of hairline cracks in plaster or drywall surfaces; in addition, the formation of hairline cracks in mortar joints of brick/concrete block construction or the growth of existing cracks in plaster, drywall surfaces or mortar joints. Minor damage is the formation of large cracks or loosening and falling of plaster on drywall surfaces, or cracks through bricks/concrete blocks. Major or structural damage is damage to the structural elements of a building, cracks in support columns, loosening of joints, splaying of masonry cracks, etc.

BS 7385 recommends that the peak particle velocity is used to quantify vibration and specifies damage criteria in terms of PPV for frequencies between 1Hz to 1kHz. In terms of cosmetic damage, the guide value is 15mm/s peak particle velocity at a frequency of 4 Hz, increasing to 20mm/s at 15Hz and 50mm/s at 40Hz and above as shown in Fig. 2.8. Minor damage is possible at vibration magnitudes that are greater than twice those given for the possible onset of cosmetic damage with major damage to a building structure possibly at values greater than four times the cosmetic damage values. The BS's guide values relate to transient vibrations and to low-rise buildings. BS 7385: Part 2: 1993 states that the guide values may need to be reduced by up to 50 percent for continuous vibrations.

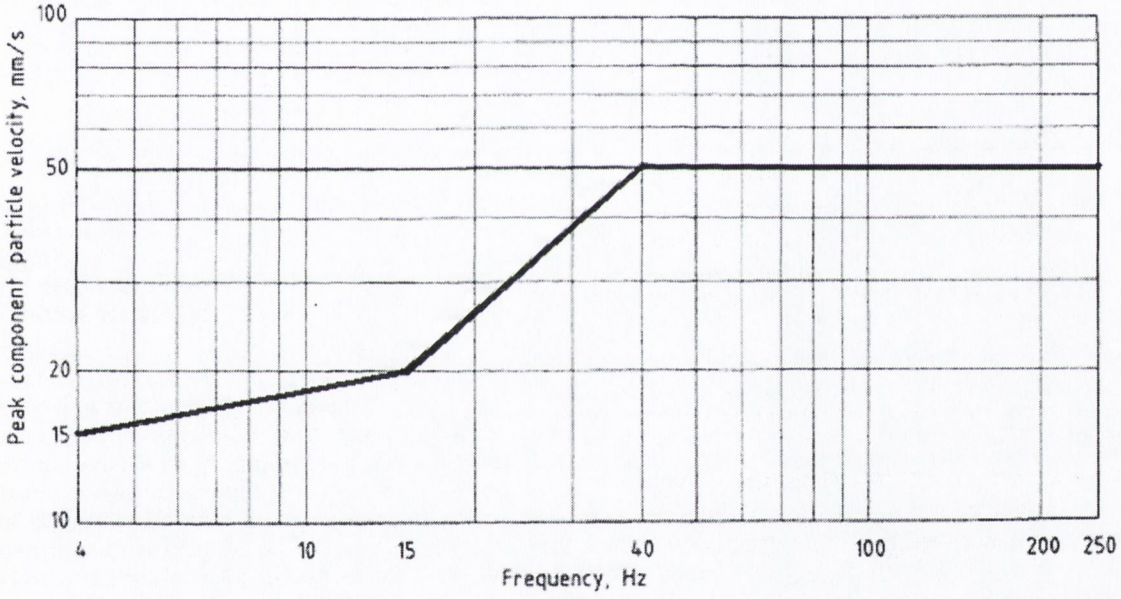

Fig 2.8–Transient vibration guide values for cosmetic damage

2.3.8 Vibration Control

A number of methods have been developed to control ground vibrations. The common countermeasures include floating slab tracks for railway vibration, wave impending barriers and installation of trenches. Another possible method is increasing the tunnel depth.

Floating slabs, which basically consist of concrete slab tracks supported on resilient elements (capable of returning to an original shape or position after having been compressed), have been widely used in modern rail transit systems (Wilson et al., 1983). It is well known that greater effectiveness can be achieved in reducing ground vibrations when the frequencies exceed $\sqrt{2}$ times the resonance frequency of the floating slab system. Resilient pads support the floating slab system. However, when the frequency is equal or close to the resonant frequency, vibrations will be greatly amplified. Designs which employ floating slab tracks assume the existence of a single degree-of-freedom system, in which the lumped mass includes that of the floating slab and the unsprung mass of the train, and in which the spring stiffness is determined by the supporting resilient pads. In order to increase the effectiveness of the floating slab track, that is, to lower the resonant frequency, the mass of the floating slab should be made as large as possible, as the resilient pads have to maintain a minimum level of rigidity to ensure rail stability under full axle loads (Hung and Yang, 2001).

Many devices can be used as resilient elements. These can be rubber or steel springs under the rail, the ballast, a resilient element under the sleepers or the plates that support the rail, or a foam rubber under the ballast. The best results are obtained when the resilient elements are made as soft as safety considerations allow them to be, and when the mass between the rail and the resilient element is made as large as space (Heckl et al., 1996).

Balendra et al. (1989) found that, in the high frequency range, a floating slab track system behaves as an effective vibration isolator. Grootenhuis, (1977) found the effectiveness of the floating track slab system for cut-and-cover type of construction. He proposed a design for a floating track slab inside a bored tunnel without the need to increase the tunnel diameter.

Wagner (2002) found that high vibration attenuation levels can be reliably achieved with well designed, low-tuned floating track beds. Long slabs or troughs, supported on steel springs, provide advantages in terms of construction, installation and performance.

The springs are generally accessible. They allow fast and easy readjustment of deviated track levels.

Wilson et. al., (1983) found that floating slabs were effective in isolating train induced ground vibrations in the frequency range above 20Hz, although floating slabs can be designed to extend the effectiveness to lower frequencies.

A Wave impeding block (WIB) is an artificial stiff plate installed at a certain depth below the source acting as artificial bedrock. Antes & von Estorff (1994) and Takemiya & Fujiwara (1994) found that the WIB could effectively reduce ground vibrations due to a train, but wave propagation into the surrounding area cannot be totally impeded because the artificial bedrock also vibrates. The effectiveness of the artificial bedrock can be improved by increasing its stiffness. The shielding of a building from soil vibrations can also be achieved by installing an artificial bedrock directly beneath the building (Hung and Yang, 2001).

Ground vibrations due to man-made sources, such as traffic and machine foundation, and ground vibrations due to TBMs could be a major problem in densely populated urban areas and for structures, which are housing sensitive equipment. The environmental effects of vibrations have received considerable attention in recent years owing to the damage they can cause to buildings and the disturbance to people and in many countries new rules and regulations have been introduced to control vibrations (Hall, 2003). Therefore, screening of vibrations induced by traffic and construction activities has become an important issue in recent times and it has been shown that it is possible to reduce the ground vibration significantly by placing a suitable wave barrier in the ground. Wave barriers are often installed in the ground to reduce ground vibrations induced by man-made sources such as traffic and machine foundations (Al-Hussaini and Ahmed, 1991).

The problems of vibration isolation for soil-structure interaction systems are classified into two families, that is active isolation and passive isolation. Active isolation is also

known as source isolation refers to the installation of barriers at a distance so close to the wave source that energy transmitted from it can be directly cut off or it can also be installed surrounding the vibration source (Yang and Hung, 1997). Passive isolation is also known as receiver isolation placing suitable barriers in the ground before the structure or surrounding the structure (Ahmed and Al-Hussaini, 1991). An active isolation barrier can effectively isolate stationary sources of vibration, whereas a passive isolation barrier is effective for a wide variety of wave generating sources including moving vibration sources such as train. Different kinds of wave barriers, among them open and backfilled trenches, are the most common in practical application as they are most effective and have low installation costs (Adam & Estorff, 2005 and Klein et al., 1997).

However, to study the effectiveness of wave barriers in reducing ground vibration, much research, both experimental and numerical, has been carried out in the past few decades. An analytical approach has rarely been used because it is extremely difficult to obtain closed-form solutions except for very simple geometries and boundary conditions that hardly exist in practice. While detailed full-scale experimentation is too expensive to be carried out, small-scale model test results could be difficult to extrapolate to prototype situations. An efficient numerical technique, on the other hand, can be an effective alternative for conducting a detailed investigation into the vibration isolation phenomena (Al-Hussaini and Ahmed, 1991 and Ahmed and Al-Hussaini, 1991).

Barkan (1962) investigated the screening of waves by means of a trench and found that the amplitude of the waves decreased with increasing the depth of the trench. Woods (1968) also carried out a series of field model tests on active vibration isolation by installing open trenches very close to the wave source as well as in the far field. The depth of the open trenches was 0.15m to 0.6m and the trenches were located at distances of 0.15m and 0.3m from a 0.1m diameter circular surface footing undergoing periodic vertical vibration. The author investigated the influence of the location and depth of an open trench on its effectiveness as a wave barrier and concluded that a

minimum trench depth of 0.6 times the Rayleigh wave length is needed to achieve a 75% reduction in ground displacement amplitude. To study passive isolation, the depth of the open trenches was 0.3m to 1.2m, the length of the open trenches was 0.3m to 2.4m and the width of the open trenches was 0.1m to 0.3m. The author found that the critical dimension for trench barriers was the ratio between the depths of the trench to the wave length. Amplitude of vertical displacement with distance along a line of symmetry from the vibrator through the trench for five tests are shown in Fig.2.9. The increasing effectiveness of the larger trenches can be seen in region beyond the trench by the relative position of the curves for each test.

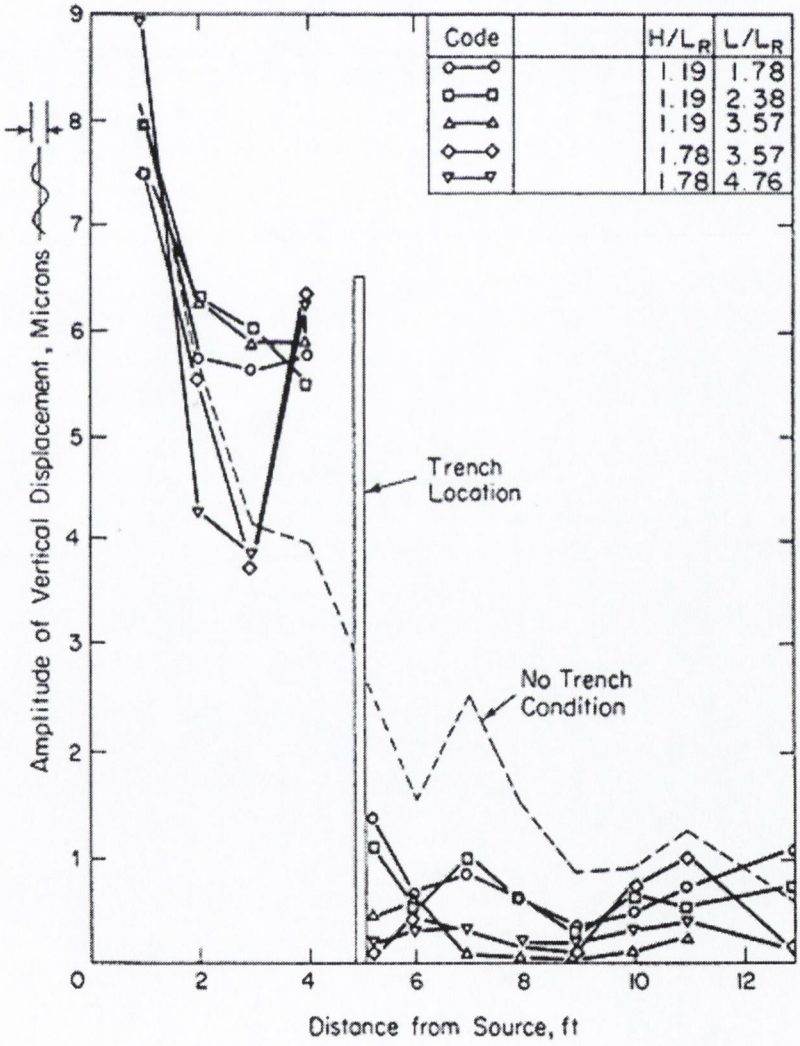

Fig.2.9 – Amplitude of vertical displacements vs. distance from source for five tests (From Woods, 1968).

Haupt (1981) conducted a series of laboratory tests on the vibration isolation effect of various measures in the ground. Solid barriers like concrete core walls as well as rows of boreholes and open trenches are considered. The author found that the screening in the near field is more effective than in the far field. At rows of bore holes stabilised by plastic tubes and increase of the isolated effect with increasing normalised shielded area was found. The screening effect of open trenches is increased with the normalised depth and results are presented in Fig. 2.10.

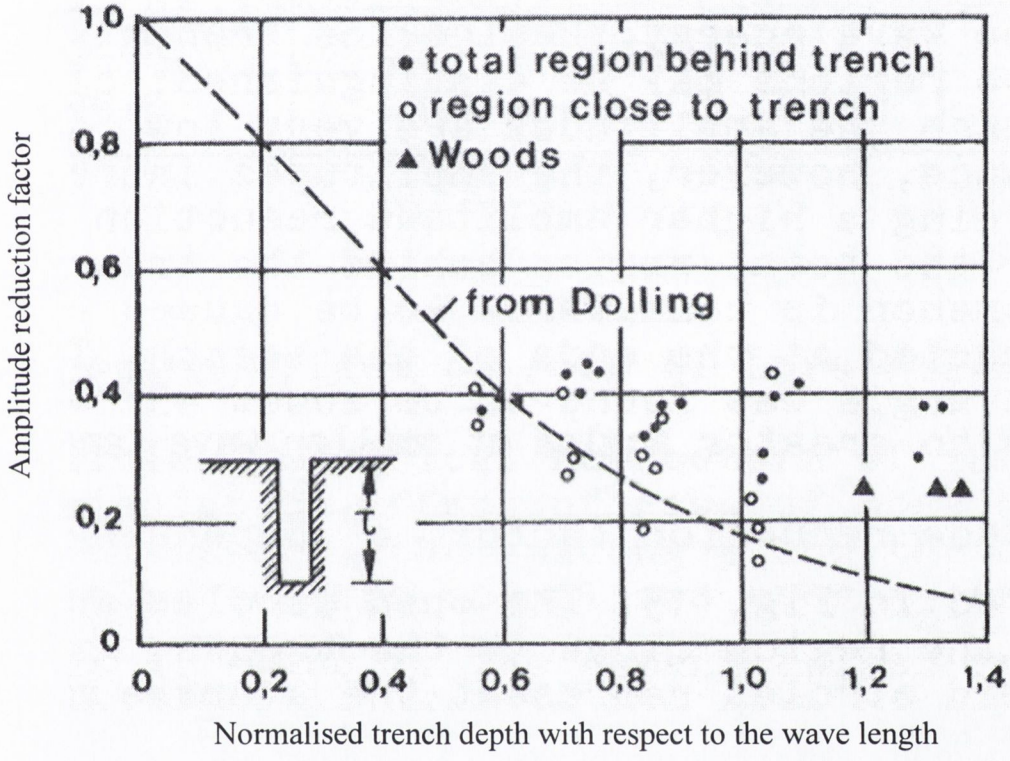

Fig.2.10-Amplitude reduction factor vs normalised trench depth (From Haupt 1981)

Massarsch (2004, 2005) described the gas cushion method which was developed thirty years ago. It is vertical panels of gas-filled flexible cushions with very low impedance can be installed in a trench to great depth without losing its dynamic properties. The author evaluated the effectiveness of the gas cushion method in different soil conditions and recommended the design of the gas cushion method and also described the recent improvements of the gas cushion method. The author concluded that the efficiency of the gas cushion screen in reducing the amplitude of vibrations is comparable to that of open trenches. The results are presented in Fig.2.11 from full-scale projects in different

soil conditions. It can be seen from the Fig.2.11 that there is a good agreement between the results reported by Haupt (1981), while the vibration amplitude reduction is less than that predicted theoretically. Amplitude reductions of 50% to 80% can be obtained if the depth of the trench is equal to the one wavelength. The author also recommended that a separate slot be made at about 2m depths from the ground surface to avoid rigid contact between stiff elements in order to get better efficiency from the gas cushion method at higher frequencies.

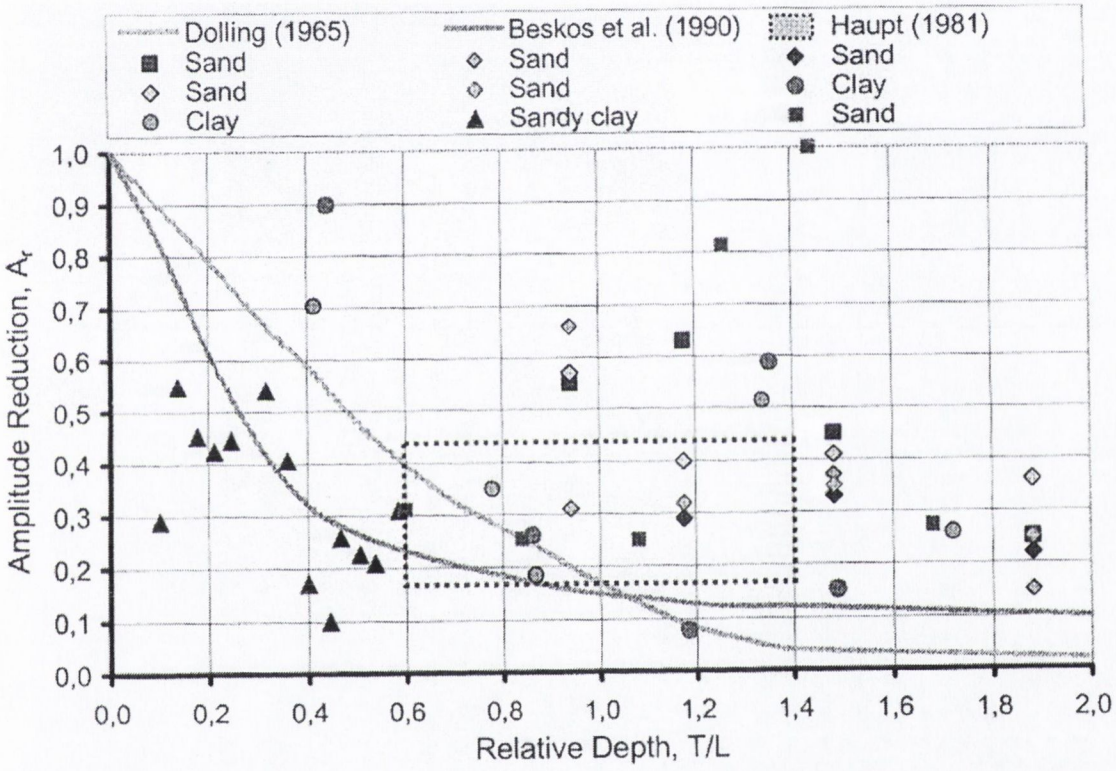

Fig.2.11-Isolation effect of gas-filled cushions in different soils and vibration sources (From Massarsch, 2005)

In the past few decades, many researchers have used several numerical techniques to study the vibration screening problem. Ju (2004) used a three-dimensional finite element analysis with absorbent boundary conditions to investigate the screening of train-induced vibrations by means of an open and two infilled trenches. The dimensions of the open trenches were 25m deep and 3.75m wide and the dimensions of two infilled trenches were 50m and 90m deep and 3.75m wide. The trenches were set 50m from the

centre of the main train line. The author found that the infilled trenches could not efficiently provide a screen against horizontal vibrations lower than 5Hz, however, they were more efficient in providing a screen against vertical vibrations. It was also found that the open trench could not provide a screen against vibrations that were lower than 3.3Hz although it did provide an efficient enough screen against vibrations over 4Hz. This method performed more efficiently than infilled trenches. The author recommended that to improve the screening efficiency, the trenches should be deeper and wider in both cases. However, it is very difficult to make deeper open trench without any lateral support. Yang and Hung (1997) carried out a parametric study of the suitability open and in-filled trenches and elastic foundations for reducing train–induced vibrations and found that all three types of wave barriers are suitable for screening vibrations associated with waves of higher frequencies. Segol et al. (1978) used the FEM along with special non-reflecting boundaries to study vibration isolation by means of open and backfilled trenches in layered soils. They concluded that the width of the trench is insignificant. Aboudi (1973) carried out a combined perturbation, mathematical method to find an approximate solution to a problem which cannot be solved exactly, -finite difference method treatment to the problem of half space by the thin barrier and suggested that open trench barrier will yield the best results for screening purposes.

Ju (2002) applied the 3-D finite element method to simulate soil vibrations due to a high-speed train moving across bridges and investigated the screening of neighbouring structures from these vibrations by means of open and backfilled trenches. The author found that these could not screen the neighbouring buildings totally from the low-frequency waves. Yang and Hung (2001) proposed a 2-D finite/infinite element procedure to model with ground vibrations induced by moving loads. Besides the two in-plane degrees of freedom per node conventionally used for plane strain elements, an extra degree of freedom was introduced to account for out-of-plane wave transmission. The profile of the half-space was divided into a near field and a semi-infinite far field. The near field containing structures was simulated by the finite elements, while far field

covering the soils extending to infinity was modelled by the infinite elements with due to account taken of the radiation effects for moving loads.

In the past few decades, the boundary element method (BEM) has emerged as an efficient numerical technique for solving a wide class of engineering problems. This method is especially well suited for wave propagation problems in soils involving a semi-infinite domain. A number of researchers have carried out 2-D and 3-D numerical analyses for the screening of vibrations by means of open and backfilled trenches and different types foundations due to machine foundation using the BEM (Al-Hussaini & Ahmed, 1991 & 1996; Ahmed & Al-Hussaini, 1991; Ahmed et al., 1996, Klein et al., 1997 and Kattis et al. 1999). Several procedures for coupling finite with boundary elements or finite with infinite elements have been proposed by a number of researchers (Adam & Estorff, 2005).

It can be observed from the above literature review that a number of researchers have carried out a lot of work on systems to provide screening from machine foundation or high-speed train induced vibrations. However, no work has been reported in the published geotechnical literature on the use of wave barriers to provide screening from the ground vibrations due to a TBM. Therefore, it is important to study the performance of wave barriers in reducing the ground vibrations due to a TBM. In this thesis numerical studies, using a 3-D finite element model coupling with infinite elements, are presented which investigate the effectiveness of wave barriers, i.e. open trenches and backfilled trenches, in reducing the ground surface vibration due to tunnelling activities.

2.4 Geotechnical Studies on Dublin Boulder Clay

In this section, geotechnical studies on Dublin boulder clay are presented and findings are presented in Section 1.4.

Farrell et al., (1995) presented the results of a study into the physical, chemical and mineralogical composition of the Dublin boulder clay. The authors carried out

systematic classification tests to a significant depth and obtained geotechnical properties (Moisture content, Specific gravity, Liquid limit, Plastic limit, Bulk density and Void ratio of this soil). The carbonate contents were determined using hydrochloric acid to convert $CaCO_3$ to $CaCl_2$ and then the remaining HCL with NaOH was titrated using phenolphthalein as an indicator. The organic content was determined using the wet oxidizing method. The mineral properties were determined using X-ray diffraction, clast lithological analysis and microscopic analysis.

Farrell & Wall (1990) discussed the distribution of the different soil types that occur in the Dublin City area and their geotechnical properties, principally in regards to foundation design and construction. The authors made the distinction between the brown and black boulder clay and determined index and strength properties of Dublin boulder clay.

Farrell et al., (1995a) presents a study of the stiffness of the Dublin black boulder clay based on the results from a trial footing test and from the load/settlement curves recorded in load tests on precast concrete piles.

Lawler (2002) carried out extensive laboratory and field studies on the Dublin boulder clay. A laboratory study includes: one-dimensional consolidation, triaxial bender element tests, soil suction and microscopic and mineralogical studies. A field study includes: pressuremeter, seismic and pile load tests. The objective of the one dimensional consolidation test was to determine the yield stress, to re-establish the in situ stress-state of the till prior to measuring the soil stiffness and understanding of the behaviour of the intact till. The primary objective of the test was to determine the G_{max} variation for intact boulder clay. Filter paper method was used for the measurement of soil suction. Qualitative and quantitative X-ray diffraction tests and scanning electron microscope tests were conducted for the mineralogical and microscopic studies. The objective of the pressuremeter test was to determine K_0, horizontal shear modulus and undrained shear strength. Seismic tests were carried to determine the very small strain stiffness.

Lehane & Simpson (2000) presents index, state and strength properties of Dublin boulder clay. A laboratory testing programme was put in place with one of its primary aims being to establish the stiffness characteristics of the till at low and intermediate strain levels. These findings are subsequently applied to a new three-dimensional version of the brick soil model to investigate the suitability of this model for the till.

Skipper et al., (2005) presents a detailed description of the stratigraphy and lithology of the boulder clay in Dublin port tunnel area and made the distinction among the upper brown, upper black, lower brown and lower black boulder clay. The author also presents the index and state properties of four layers boulder clay.

London City University (LCU) and Trinity College Dublin (TCD) carried out laboratory tests on boulder clay in Dublin port tunnel area on behalf of Geoconsult-ARUP private company to determine index properties and also carried out classification and triaxial tests. LCU carried out bender element tests to determine small strain stiffness. Geoconsult-ARUP private company also organised to carry out SPT, dynamic probes tests, plate loading tests, high pressure dilatometer tests, variable head permeability tests, pumping tests, geophysical tests, Sieve analyses, CBR, shear strength and consolidation tests.

2.5 Dynamic Ground Properties

2.5.1 General

The propagation of vibration waves is strongly influenced by the response of the ground to dynamic loading. This response is controlled by the dynamic properties of the ground. In order to evaluate the response of ground subjected to vibrations and the manner of vibrations and their transmission through the ground, the dynamic characteristics of soils must be determined. The most important dynamic properties that should be obtained are the shear modulus and damping characteristics at small strains. The measurement of soil shear modulus and damping at small strains assumes greater

importance in the study of soil dynamics and its application to geotechnical design. The shear modulus represents the stiffness of the soil and damping represents the attenuation characteristics of the soil. The changes in stiffness and damping of soil with stress and strain have been the subject of much research over the years (Kramer, 1996) and the dependence of deformation characteristics with strain is discussed in the following section.

2.5.2 Dependency of Deformation Characteristics Upon Strains

The deformation characteristics of soils vary to a large extent depending upon the magnitude of the shear strains to which soils are subjected. Overall changes in soils behaviour with changes in shear strain are illustrated in Table 2.4, in which approximate ranges of the shear strain producing elastic, elasto-plastic, and failure states of stress are indicated. In the infinitesimal strain range below the order of 10^{-5}, the deformations exhibited by most soils are purely elastic and recoverable (Brignoli et al., 1996, Ishihara, 1996, Karl et al., 2003). Strains of this order are associated with the phenomena of vibration or wave propagation through soil. Over the intermediate range of strain between 10^{-4} to 10^{-2}, the behaviour of soils is elastic-plastic and produces irrecoverable permanent deformations. The development of cracks or differential settlements in soil structures appears to be associated with the elasto-plastic behaviour of soils that is exhibited within such a range of strain. When large strains exceeding a few percent are imposed on soils, the strains tend to become considerably large without increase in shear stress and failure takes place in the soils (Ishihara, 1996). From table 2.4, it can be seen that the soil can be modelled as a linear elastic for wave propagation problems.

Table 2.4 Changes in soil behaviour with shear strain and corresponding modelling (from Ishihara, 1996)

Shear strain level	10^{-6} 10^{-5} 10^{-4}	10^{-3} 10^{-2}	10^{-1}
Phenomena	Wave propagation, vibrations	Cracks, differential settlements	Slides, compaction, liquefaction
Soil behaviour	Elastic Recoverable deformations	Elasto-plastic Irrecoverable deformations	Failure Major deformations
Constants	Shear modulus Poisson's ratio and damping		Angle of internal friction, cohesion

2.5.3 Shear Moduli

An elastic modulus, or modulus of elasticity, is the mathematical description of an object or substance's tendency to be deformed when a force is applied to it. The elastic modulus of an object is defined as the slope of its stress-strain curve. The concept of a constant elastic modulus is dependent on the assumption that the stress-strain curve is always linear. In reality, the curve is only linear within certain limits.

The elastic modulus of soil (very small strain stiffness) is an important property and the dynamic loading effects depend on the elastic stiffness of the soil. The elastic soil modulus can be described by its bulk and shear moduli.

The bulk modulus, K, measures the change in relative volume due to a change in pressure, essentially measuring the substance's resistance to uniform compression and is a function of stress level, density and the degree of saturation. For a saturated soil its value is quite high. If soil contains significant air content then there is large reduction in the bulk modulus.

The shear modulus is the elastic stiffness with respect to a change in the shear stress and its values are mainly measured in tests with cyclic stress paths having uniform and constant shear stress or shear strain amplitude. Laboratory tests have shown that the

shear stiffness is influenced by cyclic strain amplitude, void ratio, mean principal effective stress, plasticity index, over consolidation ratio, and number of loading cycles (Pennington et al., 2001, Dano & Hicher, 2003, Lenart, 2004, Kramer, 1996 and Wichtmann et al., 2004). The secant shear modulus, defined as the slope of a line from the origin of the curve to a specific point on the stress-strain curve, of an element of soil varies with cyclic shear strain amplitude. At low strain amplitudes, the secant modulus is high, but it decreases as the strain amplitude increases. The locus of points corresponding to the tips of hysteresis loops of various cyclic strain amplitudes is called a backbone curve and is shown Fig.2.12 (a); its slope at the origin represent the largest value of the shear modulus, G_{max}. At greater cyclic strain amplitudes, the modulus ratio G_{sec}/G_{max} drops to values of less than 1. The variation of the modulus ratio with shear strain is described graphically by a modulus reduction curve as shown in Fig.2.12 (b).

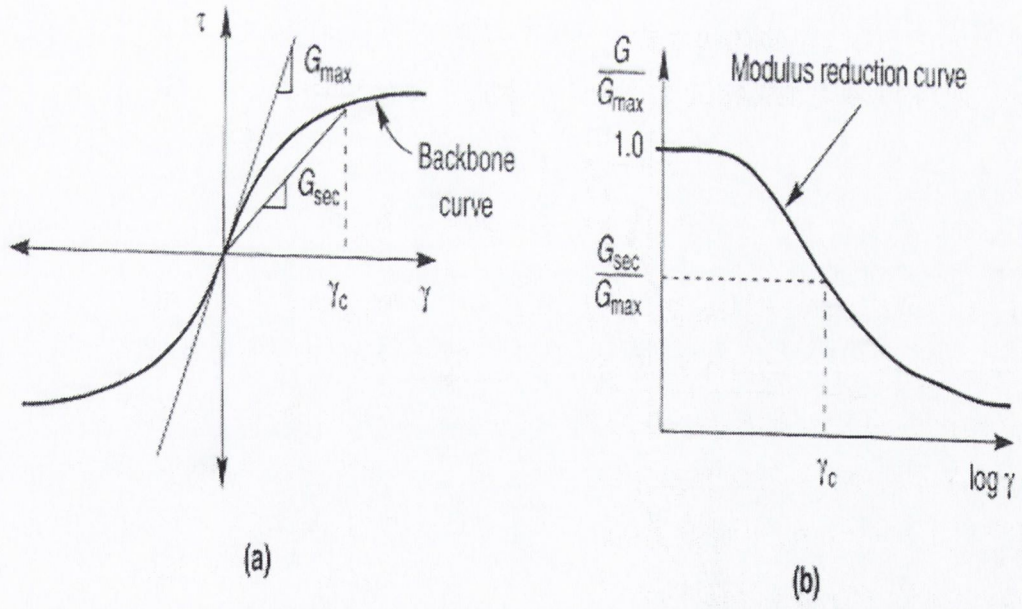

Fig. 2.12–(a) Backbone curve showing typical variation of G_{sec} with shear strain. (b) Modulus reduction curve (from Kramer, 1996).

2.5.4 Maximum Shear Modulus (G_{max})

The maximum shear modulus, G_{max}, is used for describing the waves propagation problems through the soil. Since most seismic geophysical tests induce small shear strains, the measured shear wave velocities can be used to compute G_{max} as

$$G_{max} = \rho v_s^2 \qquad [2.13]$$

where ρ is the soil density and v_s is the shear wave velocity.

The use of measured shear wave velocity is generally the most reliable means of evaluating the in situ value of the G_{max} (Kramer, 1996). Typical values for the G_{max} for Dublin boulder clay and limestone are presented in Table 2.5. Other than in situ seismic geophysical tests, the low strain laboratory tests, which include the resonant column test, the ultrasonic pulse test, and the piezoelectric bender element test, are also used to determine the maximum shear modulus.

Table 2.5 Typical properties of Dublin boulder clay and limestone (from Lawler 2002, & Dublin port tunnel site investigation reports)

Material	Density, ρ (kg/m^3)	Poisson's ratio	G_{max}, (MPa)	E_{max}, (MPa)
Dublin boulder clay	2150-2350	0.37-0.48	134-1103	323-2646
Limestone (Results from very few studies)	2600-2740	0.15-0.35	24000-33000	60000-83000

Care must be taken in the interpretation of the shear wave velocity, particularly at sites with anisotropic stress conditions, which can cause measured shear wave velocities to vary with the direction of wave propagation and particle movement (Roesler, 1979 & Yan and Byrne, 1990, cited by Kramer, 1996).

When shear wave velocity measurements are not available, G_{max} can be estimated in several different ways. The shear modulus can be estimated by empirical relationships based either on laboratory or in situ test parameters.

Hardin (1978) suggested that small strain shear modulus, G_{max}, could be determined from the semi-empirical equation:

$$G_{max} = 625F(e)\,(OCR)^{k}\,P_a^{\,1-n}(\sigma'_m)^n \qquad [2.14]$$

where $F(e) = 1/(0.3+0.7e^2)$, OCR is the overconsolidation ratio, k is the overconsolidation ratio exponent shown in Table 2.6, σ'_m is the mean principal effective stress, n is a stress exponent, P_a is the atmospheric pressure in the same units as σ'_m and G_{max}, and $\sigma'_m = 3(1+2K_0)/\sigma'_v$, where K_0 is the coefficient of lateral earth pressure and σ'_v is the vertical effective stress. The stress exponent is often taken as n = 0.5 but can be computed for individual soils from the results of laboratory tests at different effective confining pressures.

Table 2.6 Overconsolidation Ratio Exponent, k

Plasticity Index	k
0	0.00
20	0.18
40	0.30
60	0.41
80	0.48
≥100	0.50

From Hardin and Drnevich (1972)

Viggiani and Atkinson (1995) proposed another semi-empirical equation for calculation of G_{max} which is as follows:

$$\frac{G_o}{P_a} = A(\frac{p'}{P_a})^n R_o{}^m \qquad [2.15]$$

where, $G_o = G_{max}$, P_a is the atmospheric pressure, p' is the current effective stress and R_o is the overconsolidation ratio defined as p'_m/p' where p'_m is the maximum preconsolidation stress and for Dublin boulder clay and it is 1.3 ± 0.3 MPa (Lehane and Simpson, 2000).

In Equation 2.15, A, n and m are material parameters. As a result of experimental work, Viggiani and Atkinson (1995) found that these parameters vary with soil plasticity and they developed graphs relating these parameters to the plasticity index which are shown in Fig.2.13.

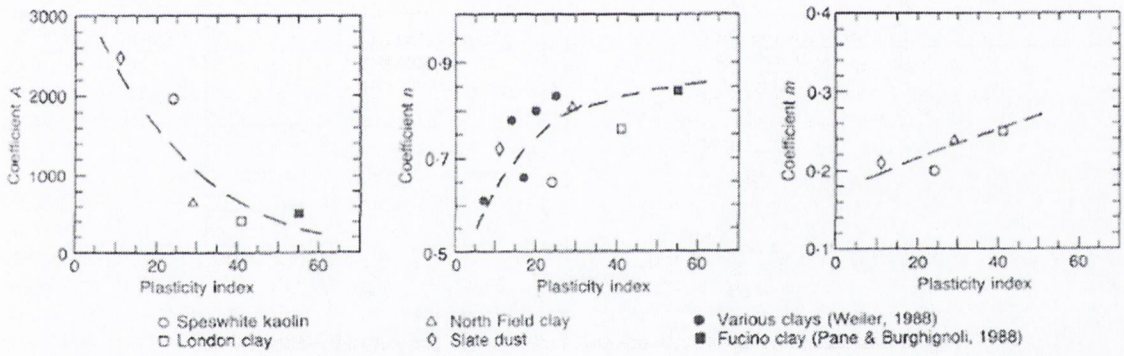

Fig. 2.13– Variation of stiffness parameters for G_{max} with plasticity index (from Viggiani & Atkinson, 1995)

From Equation 2.14 & 2.15, it can be seen that Hardin (1978) considered G_{max} to be a function of the void ratio, effective confining pressure, overconsolidation ratio, atmospheric pressure and plasticity index, while, Viggiani and Atkinson (1995) considered G_{max} to be a function of the current effective stress, overconsolidation ratio, atmospheric pressure and plasticity index.

The variation of the G_{max} as a function of confining pressure and depth for Dublin boulder clay is shown in Figs 2.14 and 2.15 respectively. For Dublin boulder clay, the plasticity index of Dublin boulder clay is (11 ± 2)% (Lehane and Simpson, 2000).

Therefore, assuming the plasticity index is 11%, from Fig. 2.15, A= 2200, n = 0.65 and m = 0.195. The maximum preconsolidation stress is 1.3 MPa, and K_0 is 2.0 (Lawler, 2002 and Lehane and Simpson, 2000). The water table is assumed, for the particular case being considered, to be at 2.5m below the ground level.

It can be seen from Figs.2.14 & 2.15 that the shear modulus increases with increasing the confining pressure and depth and decreases with increasing the void ratio. The confining pressure is also function of depth. Although the G_{max} value is assumed constant with confining pressure/depth in the analysis, it is not constant with confining pressure or depth but changes even with small variation in void ratio. From this study it can be concluded that the G_{max} should be considered to vary with confining pressure and depth in analyses. Figs 2.14 & 2.15 show that the Viggiani and Atkinson (1995) equation gives higher value than the Hardin (1978) equation for same type of Dublin boulder clay due to the multiplying and exponential values being different for the two equations.

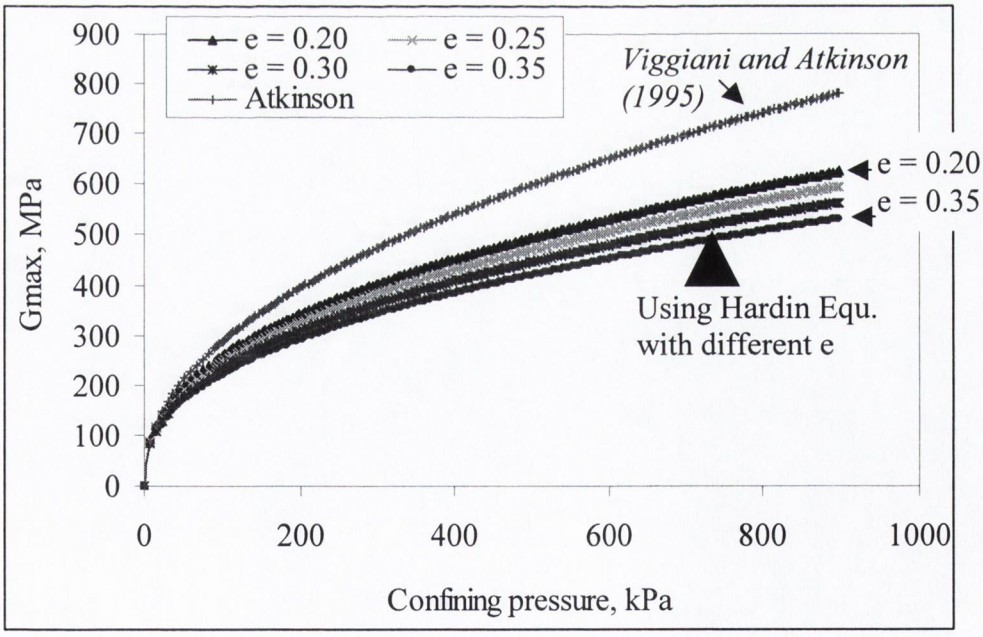

Fig. 2.14- Variation of G_{max} as function of confining pressure

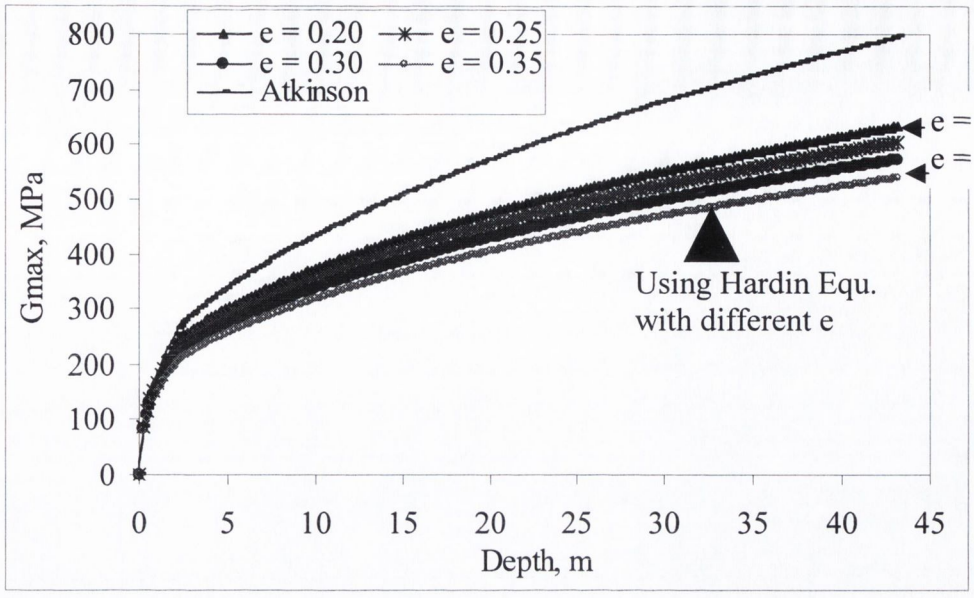

Fig. 2.15- Variation of G_{max} as function of depth

Other empirical relationships have been proposed for specific soil types. The maximum shear modulus of sand, for example, is often estimated using the following equation:

$$G_{max} = 1000\, K_{2,\,max}\, (\sigma'_m)^{0.5} \qquad [2.16]$$

where $K_{2,max}$ is determined from the void ratio e or relative density D_r (Table 2.6) and σ'_m is the mean principal effective stress in lb/ft^2 (Seed and Idriss, 1970, cited by Kramer, 1996) and 1 kPa = 20.89 lb/ft^2.

Table 2.7 Estimation of $K_{2,\,max}$

e	$K_{2,\,max}$ Determined from e	D_r %	$K_{2,\,max}$ Determined from Dr%
0.4	70	30	34
0.5	60	40	40
0.6	51	50	43
0.7	44	60	52
0.8	39	75	59
0.9	34	90	70

For fine-grained soils, preliminary estimates of the maximum shear modulus, expressed as a ratio of the undrained shear strength c_u, can be obtained from the plasticity index PI, and overconsolidation ratio OCR, as shown in Table 2.8 (Weiler, 1988, cited by Kramer, 1996).

Table 2.8 Values of G_{max}/c_u

Plasticity Index PI	G_{max}/c_u		
	OCR = 1	OCR = 2	OCR = 3
15-20	1100	900	600
20-25	700	600	500
25-45	450	380	300

From Weiler (1988, cited by Kramer, 1996)

2.5.4.1 Factors Affecting the Shear Modulus, G

Evaluation of shear modulus can be complicated by the effects of environmental and loading conditions. The brief summary of the effects of environmental and loading conditions on the maximum shear modulus and the shear modulus ratio of normally and moderately overconsolidated soils is shown in Table 2.9.

Table 2.9 Effects of environmental and loading conditions on G_{max} and G/G_{max} of normally consolidated and moderately overconsolidated clays (Dobry & Vucetic, 1987).

Increasing factor	G_{max}	G/G_{max}
Void ratio, e	Decreases with e	Increases with e
Geologic age, t_g	Increases with t_g	May increases with t_g
Cementation, c	Increases with c	May increases with c
OCR	Increases with OCR	Not affected
PI	Increases with PI if OCR>1; remains approximately about constant if OCR=1	Increases with PI
Cyclic strain	———	Decreases with cyclic strain
Number of loading cycles, N	Decreases after N cycles of large strain; but recovers later with time	Decreases after N cycles of large strain
Strain rate	No effect for non plastic soils; increases with strain rate for plastic soils	Not affected
Effective confining pressure, σ'_m	Increases with σ'_m	Increases with σ'_m ; effect decreases with increasing PI

Dobry and Vucetic (1987) concluded that the shape of the modulus reduction curve is influenced more by the plasticity index than by the void ratio and presented curves of the type shown in Fig.2.16. These curve show that the linear cyclic threshold shear strain is greater for highly plastic soils than for soils of low plasticity. This characteristic is extremely important; it can strongly influence the manner in which a soil deposit will amplify or attenuate earthquake or any other motions.

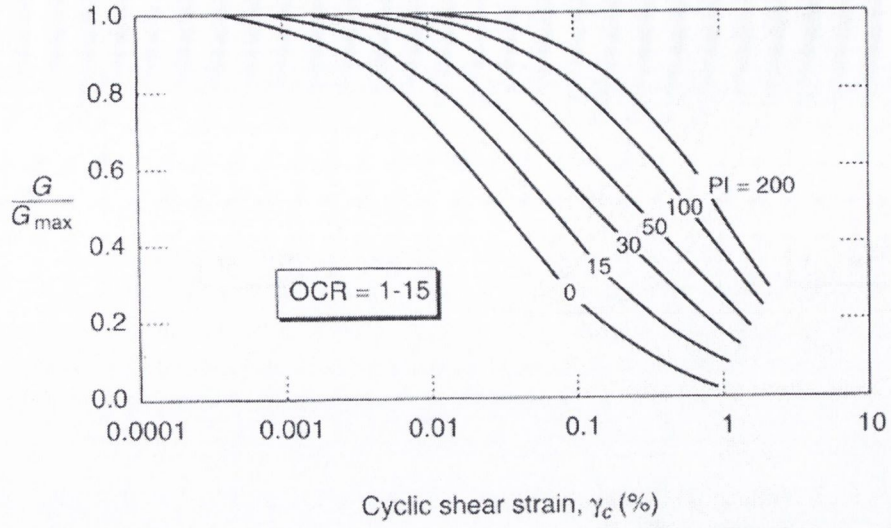

Fig. 2.16 – Shear modulus ratio reduction curves with shear strain for fine-grained soils of different plasticity (from Vucetic and Dobry, 1991)

The modulus reduction behaviour is also influenced by the effective confining pressure σ'_m, particularly for soils at low plasticity. The shear modulus increases with increasing confining pressure and decreases with increasing shear strain and void ratio (Pennington et al., 2001, Dano & Hicher, 2002, Lenart, 2004, Dano et al., 2003, Sharma & Fahey, 2003, Inci et al., 2003, Wichtmann & Triantafyllidis, 2004 and Boulanger et al., 1998). The linear cyclic threshold shear strain is greater for high σ'_m than for soils of low σ'_m. The effects of effective confining pressure and plasticity index on the reduction of shear modulus ratio are combined by Ishibashi & Zhang (1993, cited by Kramer 1996) in the following equation:

$$\frac{G}{G_{max}} = K(\gamma, PI)(\sigma'_m)^{m(\gamma,PI)-m_0} \qquad [2.17]$$

where,

$$K(\gamma, PI) = 0.5\{1 + \tanh[\ln(\frac{0.000102 + n(PI)}{\gamma})^{0.492}]\}$$

$$m(\gamma, PI) - m_0 = 0.272\{1 - \tanh[\ln(\frac{0.000556}{\gamma})^{0.4}]\}\exp(-0.0145PI^{1.3})$$

$n(PI) = 0.0$ for $PI = 0$

$= 3.37 \times 10^{-6}\ PI^{1.404}$ for $0 < PI \leq 15$

= 7.0 X 10-7 PI 1.976 for 15 <PI ≤ 70

=2.7 X 10-5 PI 1.115 for PI > 70

The effects of confining pressures are illustrated in Fig 2.17 using the above equation.

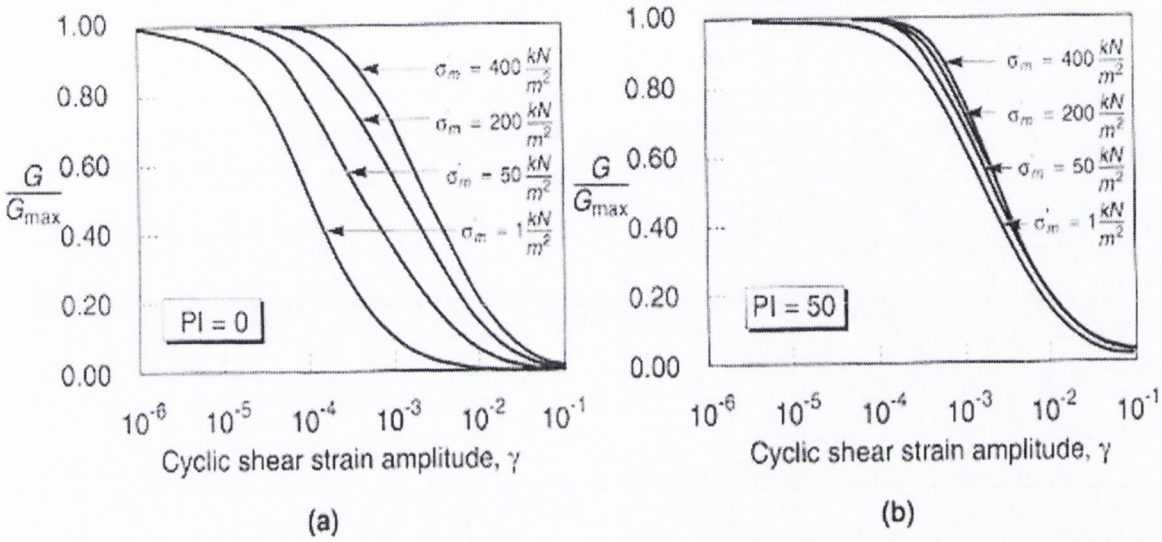

Fig. 2.17–Influence of mean effective confining pressure on shear modulus ratio reduction curves for (a) non plastic soils, (b) plastic soils according to equation 2.17 (from Ishibashi & Zhang, 1992, cited by Kramer, 1996).

2.5.5 Damping Ratio

In practical cases, all vibrations undergo a gradual decrease of amplitude with time. This characteristic of vibration is referred to as damping. Damping is actually the measure of energy dissipation within the system during vibration. It is an effect, either deliberately engendered or inherent to a system that tends to reduce the amplitude of oscillations of an oscillatory system.

Theoretically at strains below the linearly cyclic threshold shear strain, there is no hysteretic dissipation of energy. Experimentally it has been shown that a small amount of energy is dissipated at very low strain levels and the damping ratio is never zero. Above the threshold strain, the breadth of the hysteresis loops exhibited by a cyclically

loaded soil increase with increasing cyclic strain amplitude, which indicates that the damping ratio increases with increasing strain amplitude (Rollins et al., 1998, Lin et al., 1999, Teachavorasinskun et al., 2002, Kramer, 1996 and Al-Hunaidi et al., 1996). The area of the hysteresis loop in Fig. 2.18 is a measure of the energy dissipation and can be described by the damping ratio ξ as follows in Equation 2.18:

$$\xi = \frac{A_L}{4\pi A_T} \qquad [2.18]$$

where, A_L is the area of hysteresis loop and A_T is the area of triangle.

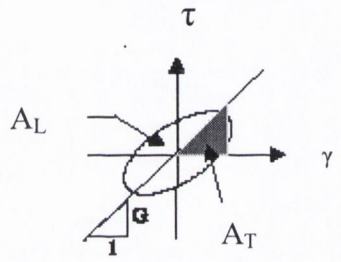

Fig. 2.18– Hysteretic stress-strain relationship for cyclic loading

Whitman (1970, cited in Stewart & Campanella, 1991) noted that the most important factors affecting damping, at least in sands, are shear strain and confining pressure. There was a slight increase in damping when water was introduced to dry sand, and damping in clay appeared to be less than in sand. Typical field measurement and laboratory values of damping at small strains are given in Table 2.10 and Table 2.11 respectively.

Table 2.10 Field measurements of damping ratios (Stewart & Campanella, 1991).

Type of Soil	Damping ratio (%)	Source
Clay	1.7	Tonouchi, Sakayama & Imai (1983)
Fine sand	1.7	Tonouchi, Sakayama & Imai (1983)
Silt	2.5	Kudo & Shima (1970)
Sandy silt	2.5	Tonouchi, Sakayama & Imai (1983)
Sand	2-3	Mok et al. (1988)
Alluvium	3.5	Redpath et al. (1982)
Sand	4	Meissner & Theilen (1986)
Bay mud	4	Redpath & Lee (1986)
Clay	4-7	Mok et al. (1988)
Sandy	5	Tonouchi, Sakayama & Imai (1983)
Sand	6	Kudo & Shima (1981)

Table 2.11 Laboratory measurements of damping ratios (Stewart & Campanella, 1991 and Vucetic & Dubry, 1991)

Type of soil	Strain (%)	Damping ratio (%)	Source
Sand	10^{-3}	0.5-1	Zovoral (1990)
Cohesionless soil	10^{-4}-10^{-3}	0.5-2	Seed, Wong, Idriss & Tokimatsu (1986)
Sand	10^{-3}	1	Sexena & Reddy (1989)
Cohesive soils	10^{-3}	1-2	Kim & Novak (1981)
Saturated sand	10^{-3}	1-3	Seed & Idriss (1970)
Marine clays	10^{-3}	1-4	Andersson et al. (1983)
Soft clay	10^{-3}	1.5	Romo, Jaime & Resendiz, (1988)
Sand	10^{-3}	1.5	Ishihara (1982)
Clay	10^{-3}	1.5-2	Zovoral (1990)
Soft clay	10^{-3}	1.5-2.5	Leon, Jaime & Rabago (1974)
Cohesive	10^{-3}	3	Sun, Golesorkhi & Seed (1988)
Marine clay	10^{-3}	4-5.5	Koutssoftas & Fischer (1980)

Just as modulus reduction behaviour is influenced by plasticity characteristics, so is damping behaviour (Dobry and Vucetic, 1987). Damping ratios of highly plastic soils are lower than those of low plasticity soils at the same cyclic strain amplitude. The effects of plasticity characteristics on damping are shown in Fig.2.19. Damping is also influenced by a number of environmental and loading conditions. The influence of various environmental and loading conditions on the damping ratio of normally consolidated and moderately overconsolidated soils is described in Table 2.12. Damping is also influenced by effective confining pressure, particularly for soils of low plasticity. Ishibashi & Zhang (1993, cited by Kramer, 1996) developed an empirical expression for the damping ratio of plastic and nonplastic soils that is as follows:

$$\xi = 0.33 \frac{\{1 + \exp(-0.0145 PI^{1.3})\}}{2} [0.586 (\frac{G}{G_{max}})^2 - 1.547 (\frac{G}{G_{max}}) + 1] \qquad [2.19]$$

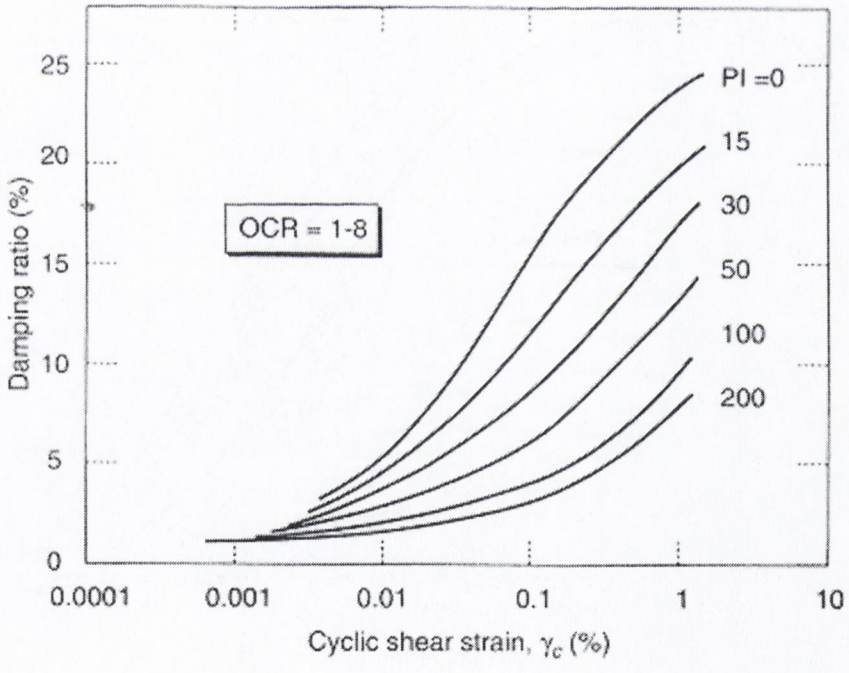

Fig. 2.19–Variation in damping ratio with cyclic shear strain amplitude and plasticity index. (From Vucetic and Dobry, 1991)

Table 2.12 Effects of environmental and loading conditions on the damping ratio of NC and moderately OC clays (Dobry & Vucetic, 1987).

Increasing factor	Damping ratio, ξ
Void ratio, e	Decreases with e
Geologic age, t_g	Decreases with t_g
Cementation, c	May decreases with c
OCR	Not affected
PI	Decreases with PI
Cyclic strain	Increases with cyclic strain
Number of loading cycles, N	Not significant for moderate strain and N
Strain rate	Stays constant or may increases with strain rate
Effective confining pressure, σ'_m	Decreases with σ'_m; effect decreases with increasing PI

2.5.6 Stress-Strain Relations in Cyclically Loaded Soils

The mechanical behaviour of soils can be quite complex under static and cyclic loading conditions. Geotechnical engineers are constantly challenged by the need to characterize the most important aspects of cyclic soil behaviour as accurately as possible with simple, rational models. Modelling of soil behaviour under cyclic or random loading conditions must be made so that the model can represent the deformation characteristics in the ranges of strain under consideration. Soil model can be classified into four categories depending on strain level: linear elastic models, equivalent linear models, cyclic non-linear models and advanced constitutive models (Ishihara 1996 and Kramer 1996). Modelling of soil behaviour with strain-dependent deformation characteristics is shown in Fig.2.20.

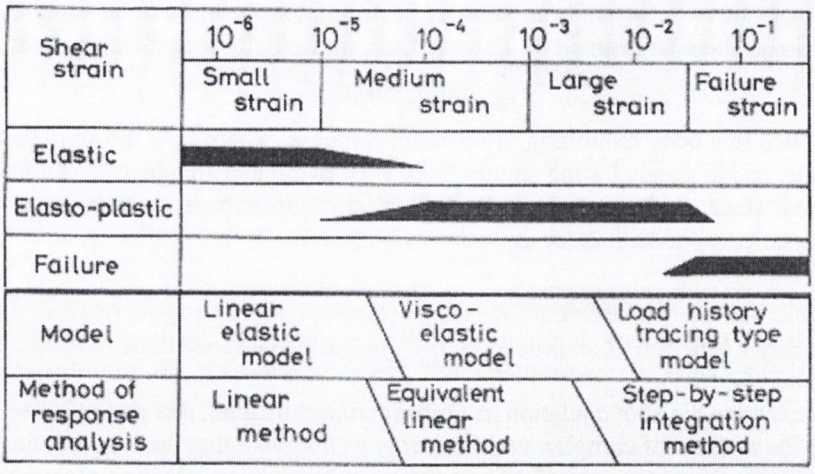

Fig. 2.20–Modelling of soil behaviour in compliance with strain-dependent characteristics. (From Ishihara, 1996)

2.5.6.1 Liner Elastic Models

Linear elastic models are used for describing the vibration behaviour of soil. When soil behaviour is expected to stay within the small strain range, the use of a linear elastic model is justified and the shear modulus is the key parameter to model properly the soil behaviour (Ishihara, 1996 and Kramer, 1996).

2.5.6.2 Equivalent Linear Models

When a given problem is associated with the medium range of strain, as shown in Fig.2.20, the soil behaviour becomes elasto-plastic and the shear modulus tends to decrease as the shear strain increases. At the same time, energy dissipation occurs during cycles of load application. The energy dissipation in soils is mostly rate-dependent and of hysteretic nature, and the damping ratio can be used to represent the energy absorbing properties of soils (Ishihara, 1996). Two important characteristics of the shape of a hysteretic loop are its inclination and its breadth. The inclination of the loop depends on the stiffness of the soil, which can be described at any point during the loading process by the tangent shear modulus, G_{tan}. Obviously, G_{tan} varies throughout a

cycle of loading, but its average value over the entire loop can be approximated by the secant shear modulus G_{sec} as in Equation 2.20 and as shown in Fig.2.21.

$$G_{sec} = \frac{\tau_c}{\gamma_c} \qquad [2.20]$$

where τ_c and γ_c are the shear stress and shear strain amplitude, respectively. The breadth of the hysteresis loop is related to the area, which as a measure of energy dissipation.

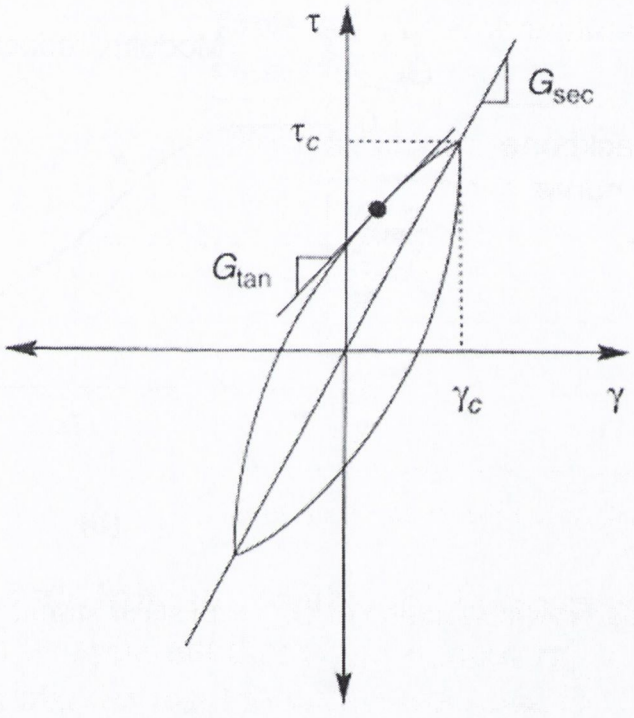

Fig. 2.21–Secant shear modulus, G_{sec} and tangent shear modulus, G_{tan} (from Kramer, 1996)

2.5.6.3 Cyclic Non-Linear Models

For strain levels larger than 10^{-2}, soil properties tend to change appreciably not only with the shear strain but also with the progression of cycles (Ishihara, 1996). This behaviour of soils can be represented more accurately by cyclic non-linear models that follow the actual stress-strain path during cyclic loading. Such models are able to represent the shear strength of the soil and, with an appropriate pore pressure generation

mode, changes in effective stress during undrained cycle loading. A variety of cyclic non-linear models have been developed, all characterized by a backbone curve and a series of "rules" that govern the unloading–reloading behaviour, stiffness degradation, irregular loading, densification and other effects.

The performance of cyclic non-linear models can be illustrated by a very simple example in which the shape of the backbone curve is described by $\tau = F_{bb}(\gamma)$. The shape of any backbone curve is tied to two parameters, the initial (low-strain) stiffness and the (high-strain) shear strength of the soil. For the simple example, the backbone function, $F_{bb}(\gamma)$, can be described by a hyperbola

$$F_{bb}(\gamma) = \frac{G_{max}\gamma}{1 + (G_{max}/\tau_{max})|\gamma|} \qquad [2.22]$$

The shape of the hyperbolic backbone curve is illustrated in Fig.2.22. The simplest of these models have relatively simple backbone curves and only a few basic rules, which described as follows (Kramer, 1996):

1. For initial loading, the stress-strain curve follows the backbone curve.

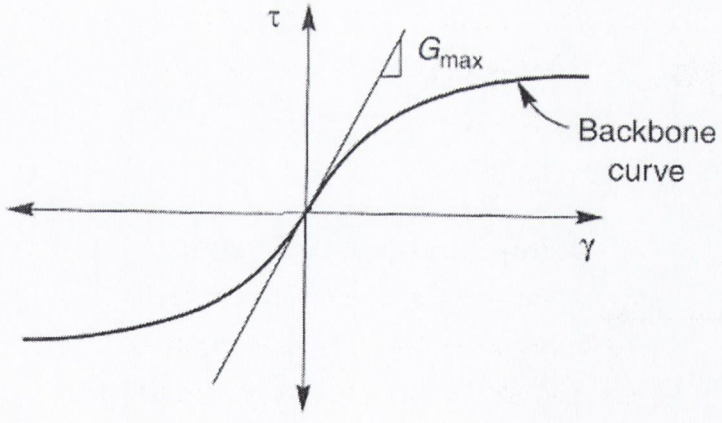

Fig. 2.22–Hyperbolic backbone asymptotic curve (from Kramer, 1996)

2. If a stress reversal occurs at a point defined by (γ_r,τ_r), the stress-strain path follows a path given by $\frac{\tau - \tau_r}{2} = F_{bb}(\frac{\lambda - \gamma_r}{2})$
3. If the unloading or reloading exceeds the maximum past strain and intersects the backbone curve, it follows the backbone curve until the next stress reversal.
4. If an unloading or reloading curve crossed an unloading curve from the previous cycle, the stress-strain curve follows the previous cycle.

Models that follow these four rules are often called extended Mashing model as shown in Fig.2.23. Cyclic loading begins at point A, and the stress-strain curve during initial loading (from A to B) follows the backbone curve as required by rule 1. At point B, the loading is reversed and the unloading portion of the stress-strain curve moves away from B along the path required by rule 2. The initial unloading modulus is equal to G_{max}. The unloading path intersects the backbone curve at points C and, according to rule 3, continue along the backbone curve until the next loading reversal at point D. the reloading curve then moves away from D as required by rule 2, and the process is repeated for the remainder of the applied loading.

The ability to represent the development of permanent strains is one of the most important advantages of cyclic non-linear models over equivalent linear models. Another significant advantage is they enable the computation of changes in pore pressure, hence also changes in effective stress. When incorporated in computational models for the ground response analyses, cyclic non-linear models allow prediction of the generation, redistribution, and eventual dissipation of pore pressure during and after an earthquake.

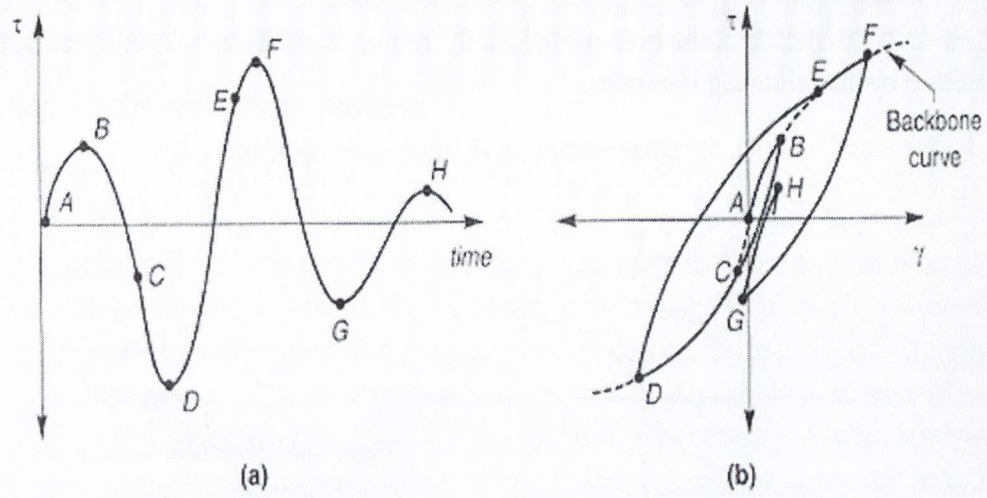

Fig. 2.23– Extended Mashing rules: (a) variation of shear stress with time; (b) resulting stress-strain behaviour (from Kramer, 1996)

2.5.6.4 Advanced Constitutive Models

Advanced constitutive models are the general methods for the representation of soil behaviour that use the basic principles of mechanics to describe observed soil behaviour for (a) general initial conditions, (b) a wide variety of stress paths (c) rotating principal stress axes, (d) cycle or monotonic loading, (e) high or low strain rates and (f) drained or undrained conditions. These models generally require a yield surface that describes the limiting stress conditions for which elastic behaviour is observed, a hardening law that describes changes in the size and shape of the yield surface as plastic deformation occurs, and a flow rule that relates increments of plastic strain to increments of stress (Kramer, 1996).

Although advanced constitutive models allow considerable flexibility and generality in modelling the response of soils to cyclic loading, their description usually requires many more parameters than equivalent linear models or cyclic non-linear models and the evaluation of these parameters can also be difficult (Kramer, 1996).

A hierarchy of advanced constitutive models is available for characterizing the stress-strain behaviour of cyclically loaded soils. The models range considerably in complexity and accuracy; a model that is appropriate for one type of problem may not be appropriate for another. No single stress-strain model is appropriate for all problems.

2.6 Determination of Small Strain Shear Modulus, G_{max}

2.6.1 Bender Element Tests

Bender elements have been used for the measurement of elastic small strain stiffness and damping ratio in a triaxial cell. The bender element technique has undergone ongoing development in the last three decades (Dano and Hicher, 2002). In the early stage, piezoceramics were mainly used to generate and receive compression P-waves. Since little information about the soil structure can be obtained from P-waves and since the P-wave velocities are highly influenced by the pore fluid, the piezoceramics have been combined in different forms to generate and receive shear waves. Such combined forms of piezoceramic are used in gauges for measuring vibrations known as bender elements (Brocanelli & Rinaldi, 1998 and Karl et al., 2003).

Bender elements consist of two thin piezoceramic plates rigidly bonded to a central metallic plate. Two thin conductive layers, which serve as electrodes, are glued externally to the bender element. The polarization of the ceramic material in each plate and the electrical connections are such that when a driving voltage is applied to the element, one plate elongates and the other shortens. The net result is a bending deflection as shown in Fig. 2.24. When the measurement of the shear wave velocity is made using bender elements in the triaxial test apparatus, one bender element is fixed in place in the top cap and the other in the pedestal, as shown in Fig. 2.25. The elements have dimensions of 1 mm in thickness, 12 mm in width and about 15mm in length. In the set-up in the triaxial cell, the bender elements at both ends protrude in the specimen as cantilevers, as shown in Fig. 2.25. When the bender element at the top is set into motion, the soil surrounding it is forced to move back and forth horizontally and its

motion initiates the propagation of a shear wave through the soil sample. When the shear wave reaches the other bender element at the other end of the specimen in the triaxial apparatus, it causes it to bend and thus produce a voltage. This output signal can be captured on an oscilloscope and the travel time determined by measuring the time difference between the input and the output signals. From this the shear wave velocity can be found by dividing the travel distance, L, by the travel time, t where the travel distance of the wave is taken to be equal to the specimen's length minus the protrusion of the two-bender elements at the both ends. The reason for chosen this length is explained in Section 2.6.2. After determining the propagation shear wave velocity, it is possible to calculate the small strain shear modulus, G_{max}, by the elastic continuum mechanics relationship:

$$G_{max} = \rho v_s^2 \qquad [2.23]$$

where ρ is the soil density and v_s is the shear wave velocity.

The damping ratio, D, can be determined from the frequency response curve using the half–power bandwidth method. The half-power bandwidth method is the most common method for measuring damping and uses the relative width of the response spectrum. The frequency response curve is shown in Fig.2.26. Using the quantities indicated on the curve, the logarithmic decrement, δ, can be calculated from following equation (Richart et al., 1970 and Karl et al., 2003):

$$\delta = \frac{2\pi D}{\sqrt{1-D^2}} = \frac{\pi}{2}\frac{f_2^{\,2} - f_1^{\,2}}{f_m^{\,2}}\sqrt{\frac{A^2}{A_{max}^{\,2} - A^2}}\frac{\sqrt{1-2D^2}}{1-D^2} \qquad [2.24]$$

When D is small, the last term and $(1\text{-}D^2)^{0.5}$ can be taken as equal to 1.0. Further simplification is possible, if A is chosen equal to 0.707 A_{max}, so that the equation for D becomes

$$D = \frac{f_2^{\,2} - f_1^{\,2}}{4 f_m^{\,2}} \qquad [2.25]$$

The advantages of bender elements are that they can also be incorporated into the oedometer test apparatus and simple shear test device but normally they are incorporated into the triaxial apparatus (Karl, et al., 2003, Ishihara, 1996 and Kramer, 1996). Anisotropy of the soil stiffness can also be investigated by locating bender elements on two vertical and opposite sides of a sample. The disadvantage of the bender element is that the element must be waterproofed to prevent short circuits, which is often difficult to achieve when testing dense or hard saturated materials. Insertion of the bender element into such hard materials can easily damage the sealing for waterproofing (Ishihara, 1996).

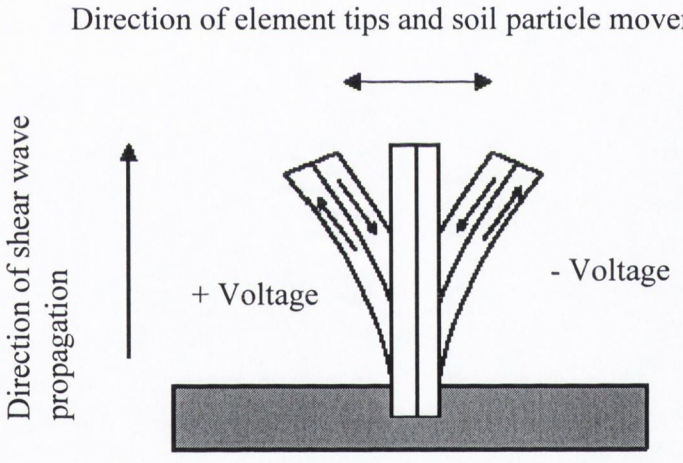

Fig.2.24–Piezoelectric bender element (from Kramer, 1996)

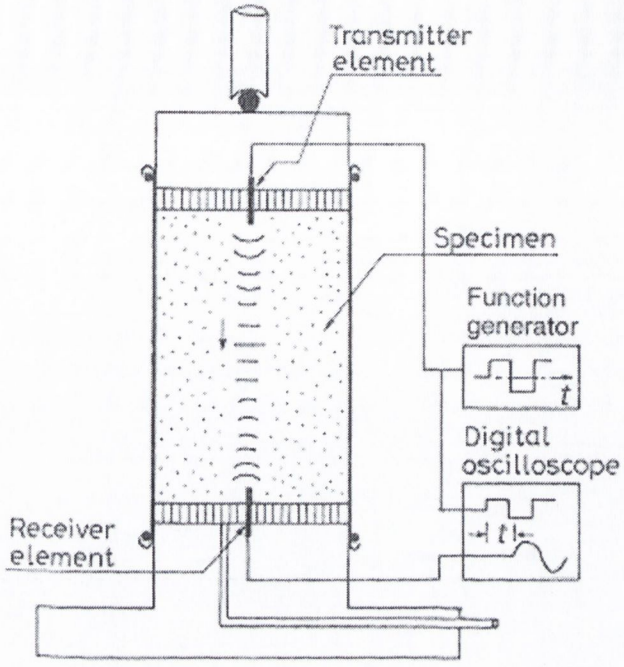

Fig.2.25– Bender elements in the triaxial apparatus (from Ishihara, 1996)

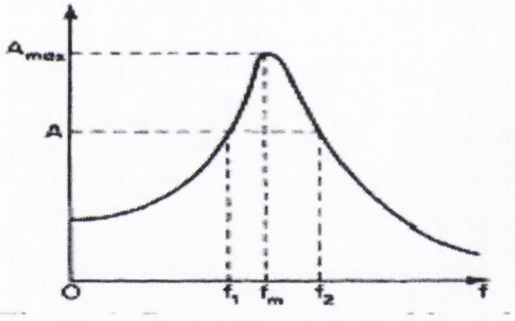

Fig.2.26 – Frequency response curve for half-power method (from Richart et al., 1970)

The application of the bender element test for the measurement of small strain stiffness and the damping ratio is not straightforward as it is difficult to measure the exact travel time between the input and output signals, though the use of the apparatus is simple. Due to the difficulty in measuring the travel time, a major review was undertaken of the stiffness and damping ratios measured by bender element tests reported in the literature.

The shear modulus of soil is simply related to the shear wave velocity determined using a bender element test. The bender element induces very small strains which lie within the elastic limit. Dyvik & Madshus (1985) estimated the maximum shear strain induced

by bender elements to be less than 0.001%, so that the shear modulus determined is G_{max} relevant to very small strain (Brignoli et al., 1996 and Karl et al., 2003). The strain level induced by the bender element test is directly proportional to the displacement at the tip of the bender element so that it is difficult to measure. Jovicic (1997) validated the assumption of elasticity experimentally through finding that there was no volume change in specimens when drained bender element tests were performed, and no pore water pressures were generated when undrained tests were carried out.

2.6.2 Analysis of Bender Element Test Results

Determination of the shear wave velocity is the main work required to calculate the small strain shear modulus in bender element tests. The shear wave velocity is directly related to the shear wave travel distance and the travel time and is simply calculated by dividing the travel distance by the travel time. Initially there was some doubt as to what should be taken as the true travel distance. Intuitively one would take the distance between the bender element tips, although some researchers thought it might be the full height of the sample. Viggiani and Atkinson (1995) carried out some laboratory tests on a set of reconstituted samples of Speswhite kaolin of different lengths to investigate what should be taken as the travel distance. Travel times are plotted against the overall length of the sample for different confining stress state conditions shown in Fig. 2.27. The test data fall on straight lines, each with an intercept of about 6 mm on the vertical axis where the bender elements used for those tests were 3 mm long. From these tests it has been concluded that the travel wave distance should be between the tips of the elements rather than the full length of the sample. This is in agreement with previous experimental work by Brignoli and Gotti (1992) and Dyvik and Madshus (1985).

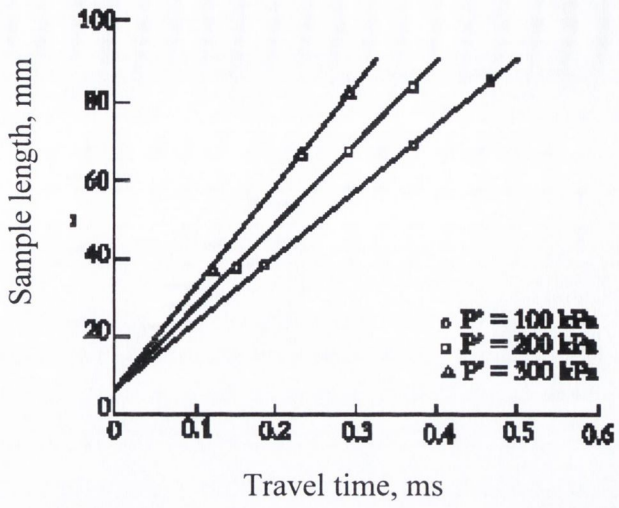

Fig. 2.27–Relationship between travel time and sample length (from Viggiani & Atkinson, 1995)

The most important parameter to be determined in a bender element test is the exact travel time of the shear wave between the transmitter and the receiver. Actually the principal problem with the bender element test has always been the subjectivity of the determination of the arrival time used to calculate shear wave velocity (Jovicic et al., 1996 and Lee & Santamarina, 2004). The travel time is dependent on the shape of the wave transmitted through the soil sample. The procedure commonly used in bender element tests is to generate a square wave and to determine the time of first arrivals (Jovicic et al., 1996 and Viggiani & Atkinson, 1995) although there is considerable distortion of the output signal using a square wave, as shown in Fig. 2.28. The problem with the square wave is that it is composed of a wide spectrum of frequencies (Jovicic et al., 1996). From the received signal of the square wave alone, it is uncertain whether the shear wave arrival is at the point of first deflection (0), the reversal point (1), or some other point.

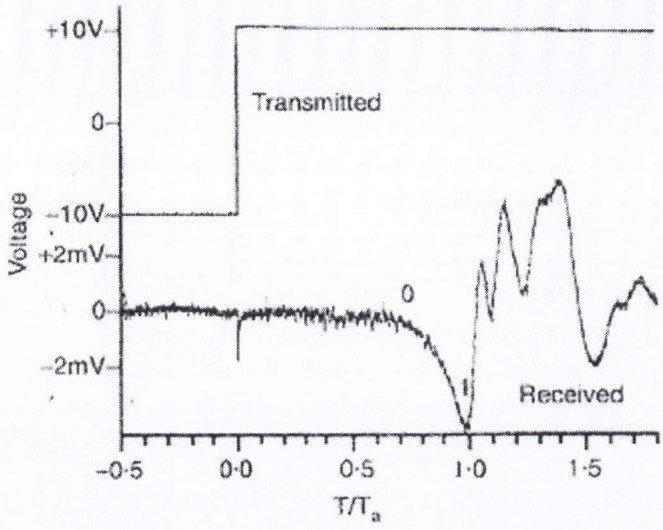

Fig.2.28–Bender element trace for a square input wave in kaolin (from Jovicic et al., 1996)

To reduce the degree of subjectivity in the interpretation, and to avoid the difficulty in interpreting the square wave response, Viggiani and Atkinson, (1995) suggested using a sine pulse as the input signal. Being mainly of one frequency, the output wave was generally of a similar shape to the input signal, but it is still very difficult to determine the travel time as shown in Fig.2.29. The problem arises due to a phenomenon called the near field effect. The near field effect is caused by the very rapid P-waves that mask the first arrivals of the, slower, S-waves. The near field effect may mask the arrival of a shear wave when the distance between the source and the receiver is within the range of 1/4 to 4 wavelengths. This is the situation in bender element tests where the distance between the transmitter and the receiver is relatively small and is about 2 to 3 wavelengths (Viggiani and Atkinson, 1995). Brignoli & Gotti (1992) also found the existence of near field effects in bender element tests and these have been further investigated by Jovicic et al. (1996). The wavelength can be estimated from:

$$\lambda = v_s/f \qquad [2.26]$$

where, f is the frequency of the input signal.

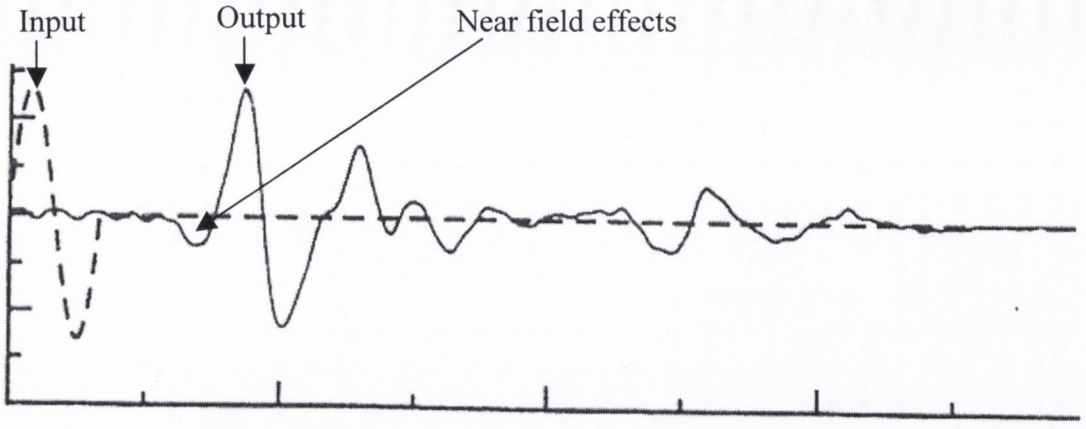

Fig.2.29–Typical bender element input output sine wave. (from Arulnathan et al., 1998)

Jovicic et al., (1996) derived an analytical solution for the time record at a point resulting from the equation for the excitation by a transverse sine pulse of a point source within an infinite isotropic elastic medium, obtained by Sanches-Salinero et al., (1986 cited by Jovicic et al., (1996)). The analysis uses the Cartesian coordinate system and is shown in Fig 2.30. The excitation motion of the source point located at the origin is in the X direction and is given in an exponentional form of a complex number $e^{i\omega t}$ where t is the time and ω the angular velocity. The monitoring point of transverse motion, s, is located at a distance d from the source in the Y direction.

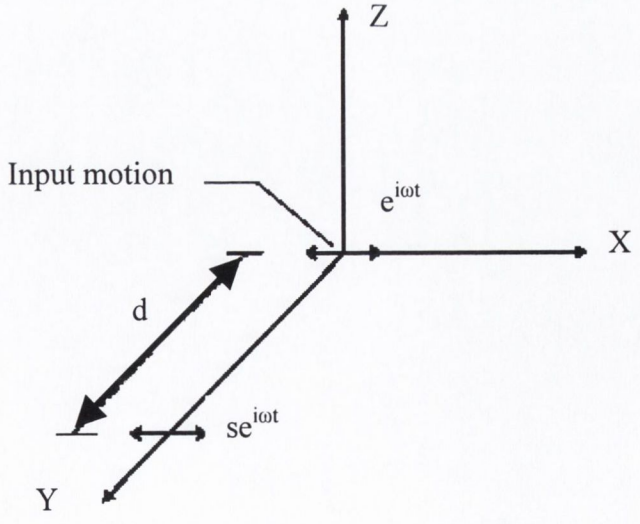

Fig. 2.30–Notation for three-dimensional motion of points (Jovicic et al., (1996))

The set of formulae, which define the motion, are:

$$\lambda = v_s/f, \qquad f = 1/T \tag{2.27}$$

where λ is a wavelength and T is the period.

The fundamental solution for the transverse motion S (Sanches-Salinero et al., (1986 cited by Jovicic et al., (1996))) is given in the form:

$$S = \frac{1}{4\pi\rho v_s^{\,2}}\Gamma \tag{2.28}$$

where the function Γ is given by:

$$\Gamma = \frac{1}{d}e^{-i(\varpi d/v_s)} + \left(\frac{1}{i\frac{\varpi d^2}{v_p}} - \frac{1}{\frac{\varpi^2 d^3}{v_p^{\,2}}}\right)e^{-i(\varpi d/v_s)} - \left(\frac{v_s}{v_p}\right)^2\left(\frac{1}{i\frac{\varpi d^2}{v_p}} - \frac{1}{\frac{\varpi^2 d^3}{v_p^{\,2}}}\right)e^{-i(\varpi d/v_p)} \tag{2.29}$$

From Equation 2.29, it can be seen that there are three coupled components to the transverse motion, which comprise both the near field and far field effects. This is because the motions of the elements are not pure compressive or shear motions (Brignoli et al. cited) and generally some compressive or shear motion occurs. All three terms represent transverse motion; while they propagate with different velocities; the first two travel with the velocity of a shear wave, and the third travels with the velocity of a compression wave. The attenuation occurs at different rates with geometrical damping for the three components, the second and third terms attenuating at a rate an order of magnitude faster than the first term. The coefficient of first term is proportional to the inverse of the distance and the coefficients of second and third terms are proportional to the inverse of square of the distance and the cubic of the distance, which implies that the last two terms are only significant for small distances and are called near field terms and first term is significant for larger distances and is called the far field

term. In bender element tests, the effect is amplified by the S-wave source and substantial P-wave energy that is often developed.

Sanches-Salinero et al. (1986 cited by Jovicic et al. (1996)) expressed their results in terms of the ratio d/λ, where d is the distance between the transmitter and receiver of bender element and λ is the wavelength of the input signal; later Jovicic et al. (1996) denoted this ratio as R_d. The value of R_d represents the number of wave lengths that occur between the bender element transmitter and receiver and which control the shape of the received signal through the degree of attenuation of each term of Equation 2.29 that occurs as the wave travels through the sample. R_d is calculated from:

$$R_d = d/\lambda = df/v_s \qquad [2.30]$$

For low values of R_d there is an initial downward deflection of the trace before the shear wave arrives, representing the near field effect given by the third component of Equation 2.29. For high values of R_d the near field effect is almost absent, as shown in Fig. 2.31 where the displacement of the monitoring point is plotted against normalised time T/T_a, where the time T is normalised with respect to the true arrival time of the shear wave T_a.

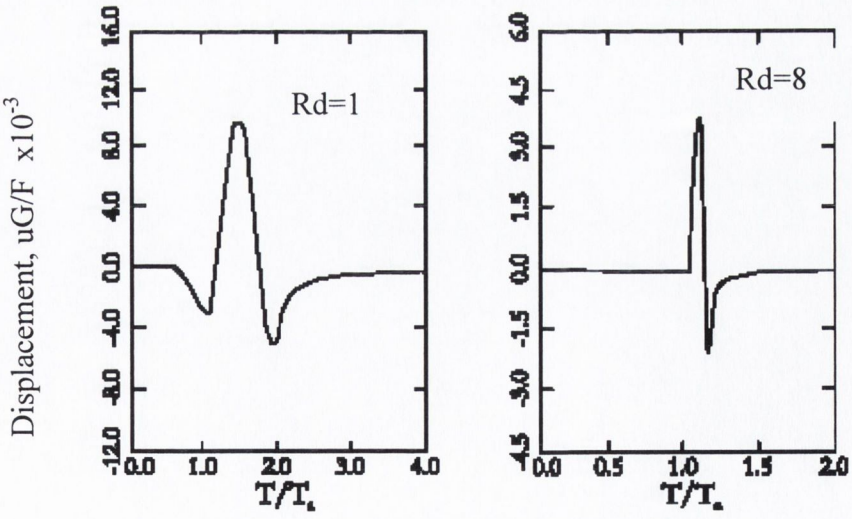

Fig.2.31–Analytical solution of the motion at the monitoring point (from Sanches-Salinero et al. (1986 cited by Jovicic et al., (1996))) (u = particle displacement, F = amplitude of loading force)

Jovicic et al. (1996) carried out series of experiments using bender elements on Speswhite kaolin specimens with an isotropic effective stress of 200 kPa and values of R_d of 1.1 and 8.1. The results shown in Fig. 2.32 confirmed that for low R_d values the near field effect dominates, while for high R_d values the near field effect is almost insignificant. The authors recommended selecting a high, enough frequency so that the soil being tested has a high R_d ratio. In practice this cannot be always achieved, because at the high frequency required for stiffer materials, overshooting, to shoot or pass over or beyond, of the transmitting element can occur. The authors carried out experimental work on cemented granular soft rock, with G_{max} of 2.5 GPa at an effective stress of 200 kPa. At 2.96 kHz the element follows perfectly the input wave, while at 29.6 kHz it does not and overshooting occurs. The limiting frequency at which overshooting starts to occur depends on the relative impedances of the soil and the element and overshooting is found to be severe for stiffer soil as well as being pronounced for square waves.

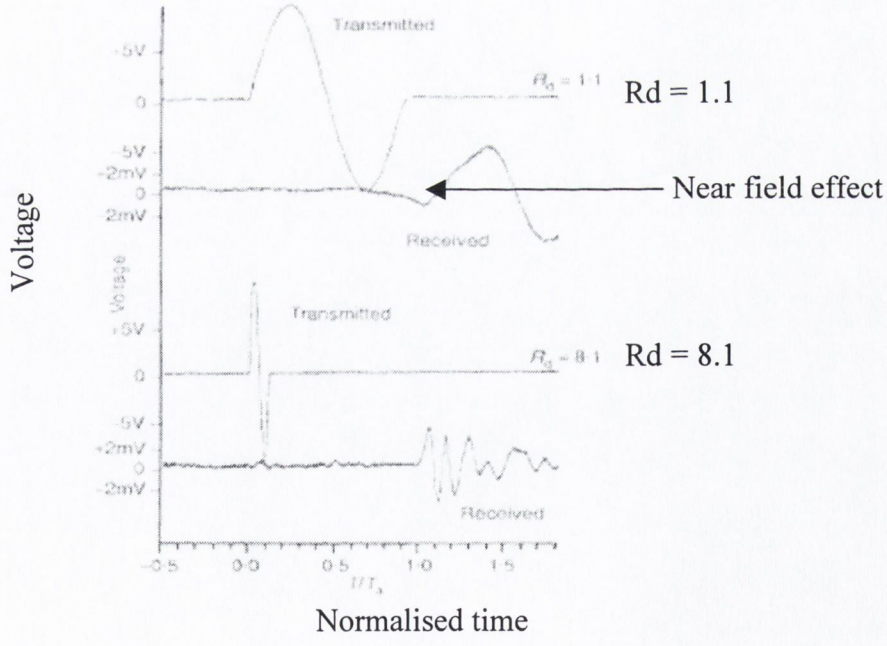

Fig.2.32–Test data for sinusoidal input waves in kaolin (from Jovicic et al., 1996)

To overcome the problem of overshooting the authors recommended two methods. The first method is to use a distorted sine wave where the amplitude of first upward cycle of

the wave may be reduced so as to cancel out the near field effect as shown in Fig.2.33. In second method, the frequency of the input wave may be adjusted so as to give forced oscillation of the receiver at one of its natural frequencies, in which case resonance occurs as shown in Fig. 2.34. The arrival time may be simply taken from one of the peaks or troughs of the input wave and the corresponding point on the output.

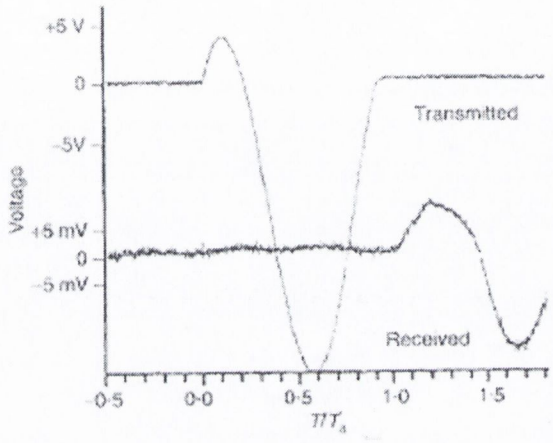

Fig.2.33–Cancelling the near field effect with a distorted sine wave (from Jovicic et al., 1996)

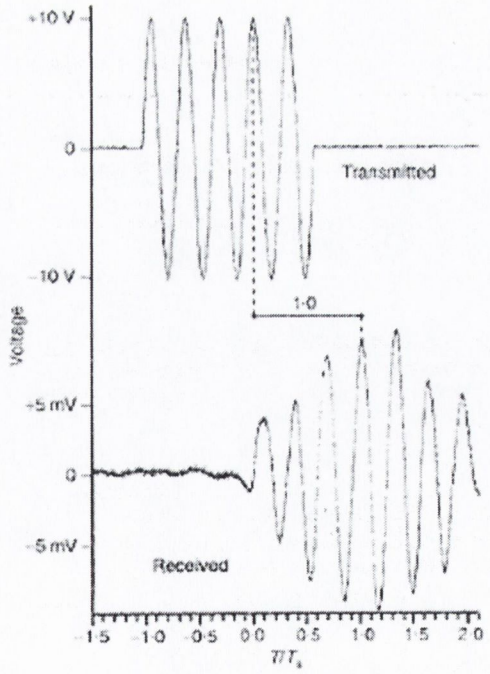

Fig.2.34–Resonance of the receiving element (from Jovicic et al., 1996)

Arroyo et al. (2003) focussed on the effects of the input wave on near-field effects as shown in Fig.2.35. The authors found that the square shaped signal is the least favourable shape because it is the most affected signal and the distorted sine the most favourable shape as it is the least affected signal. However, the result is strongly dependent on the amount of distortion introduced. The distorted sine signal is given by the following Equation:

$$I = A \{\sin [\pi (2tf + d_i/2)] - \sin (\pi d_i/2)\} \quad [2.31]$$

where A is the amplitude, f is the frequency and d_i is the distortion factor. The behaviour of sine and sine-burst signals are almost similar.

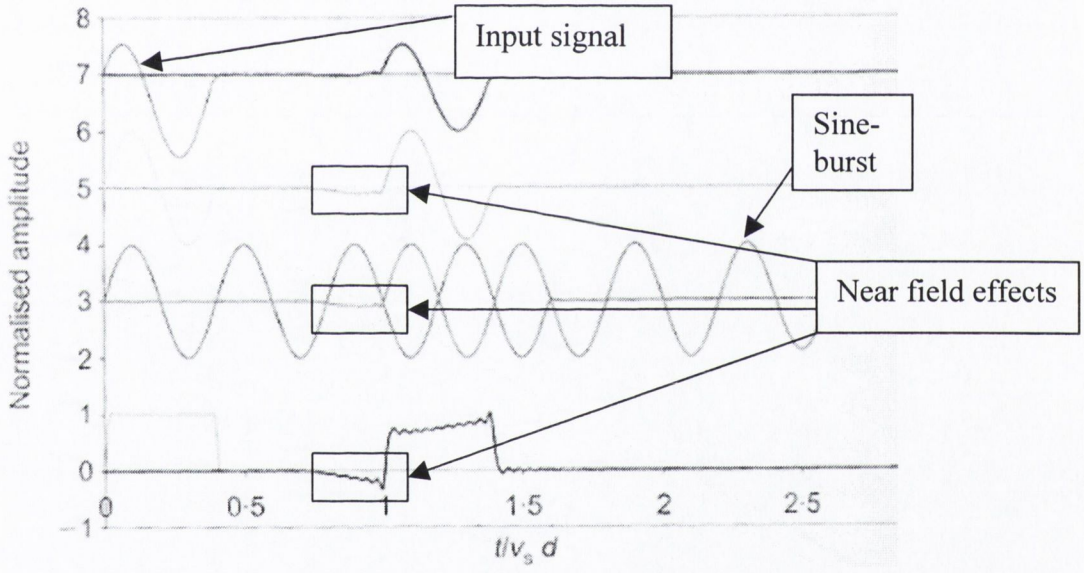

Fig.2.35–Input shape and near field effect in time domain (from Arroyo et al., 2003)

Lawler (2002) carried out laboratory tests on Dublin boulder clay using bender elements with isotropic and anisotropic consolidation condition and found that the stiffness of the Dublin boulder clay increased with increasing confining pressure. The author also carried out a study of the effects of the input wave on the near-field effects as shown in Fig.2.36. He found that the square shaped signal is the least favourable shape because it is the most affected signal and the distorted sine the most favourable shape as it is the

least affected signal. The G_{max} values obtained from laboratory tests are presented in Fig. 2.37.

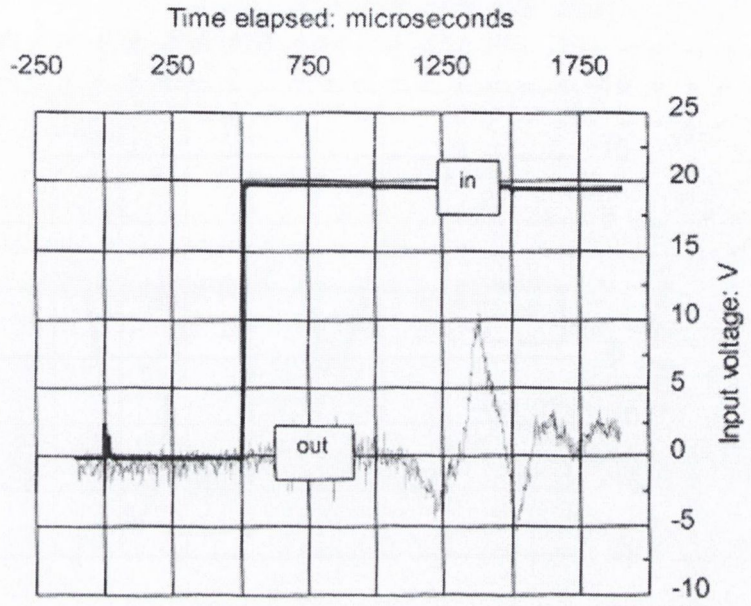

(a)

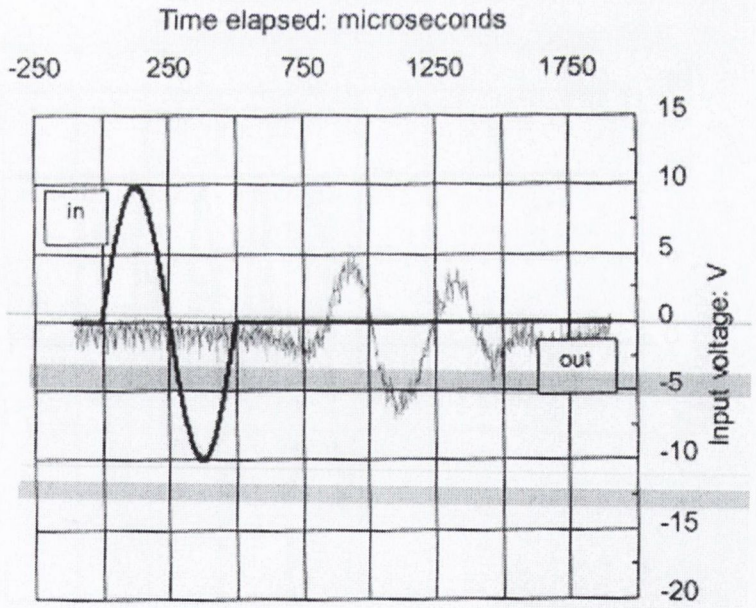

(b)

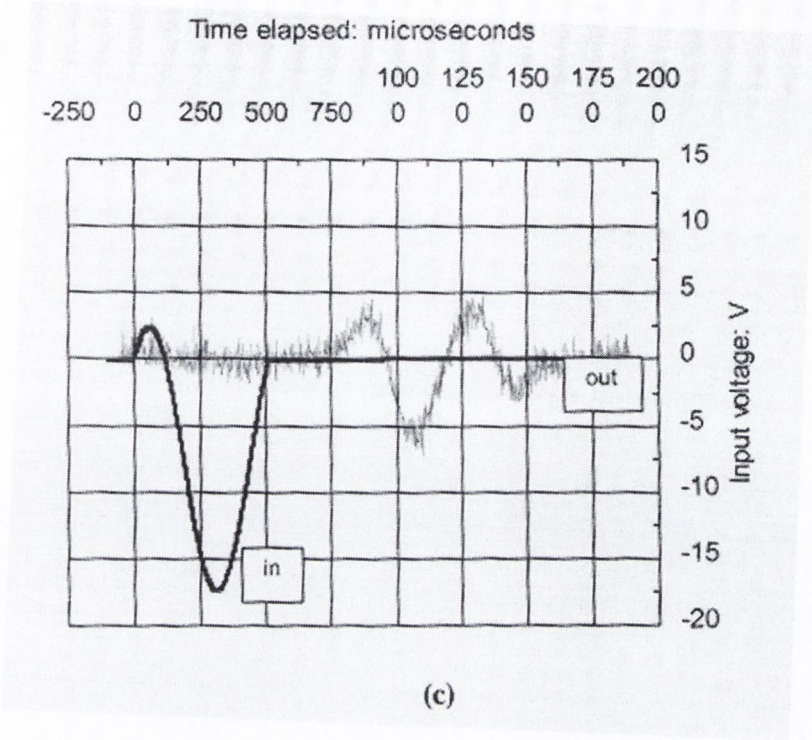

(c)

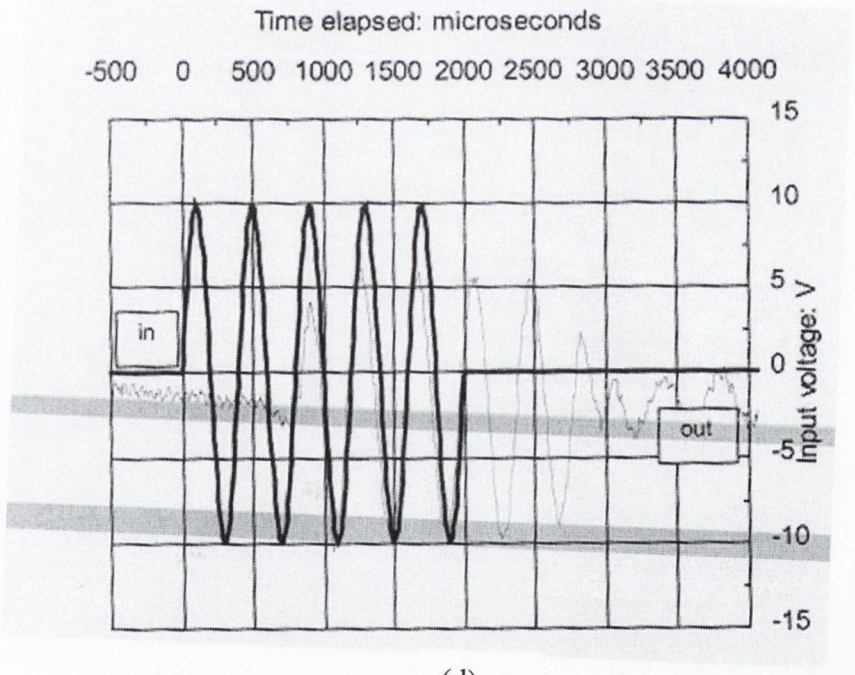

(d)

Fig.2.36–Input shape and near field effect (a) Typical square wave; (b) typical sine wave; (c) arbitrary sine wave (no near filed effect); (d) typical resonance test (from Lawler 2002)

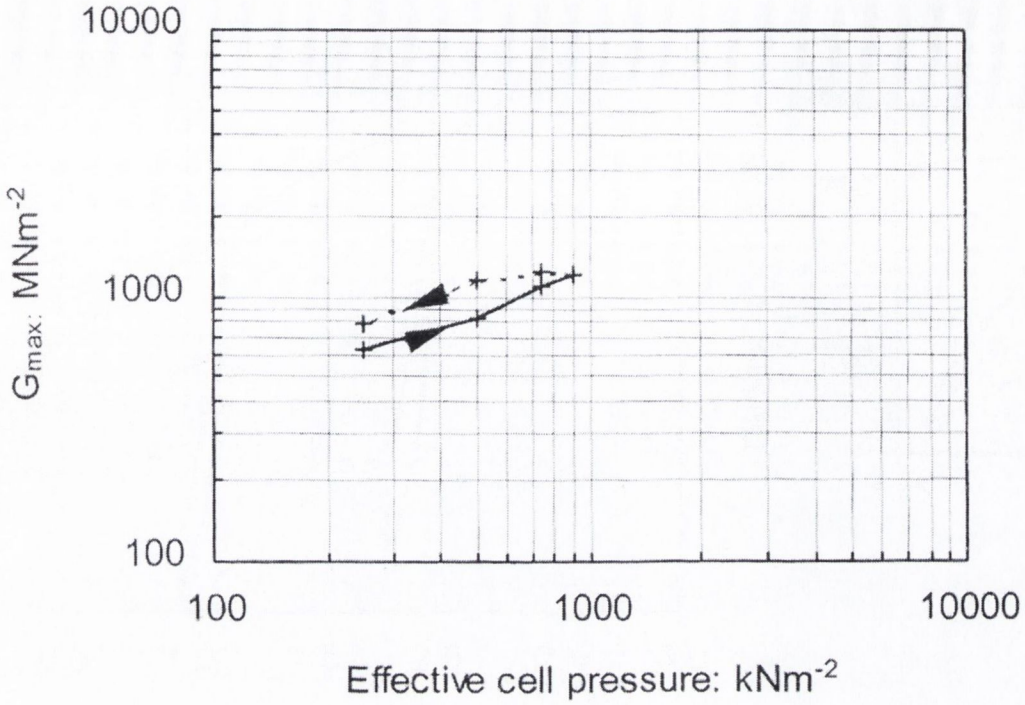

(A)

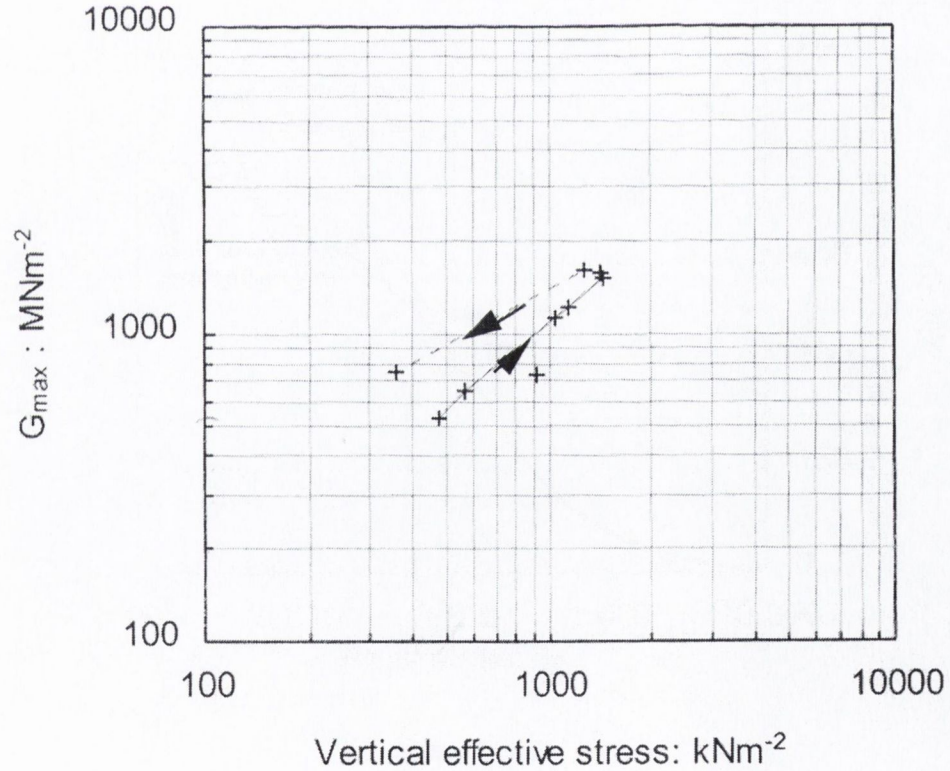

(B)

Fig.2.37-Bender element tests results: (A) isotropic condition (B) anisotropic condition (from Lawler 2002)

The error in the measured stiffness is particularly affected by errors in the estimation of first arrivals produced by the near-field effects (NFE). Errors in G_{max} estimated from the measured shear wave velocity are amplified due to the square of the shear wave velocity in the formula that is used:

$$G_{max} = \rho v_s^2 = \rho (L/t)^2 \qquad [2.32]$$

where ρ is the density of the soil, L is the length between the transmitter and the receiver and t is the travel time.

The potential error in the shear modulus is given by (Viggiani and Atkinson, (1995)):

$$\frac{\Delta G_{max}}{G_{max}} = \frac{\Delta \rho}{\rho} + \frac{2\Delta L}{L} + \frac{2\Delta t}{t} \qquad [2.33]$$

where $\Delta\rho$, ΔL and Δt are the errors in ρ, L and t respectively.

$\Delta\rho$ is low, as the density of a cylindrical soil sample can be determined precisely by direct measurements. The error in the measurement of the distance between the elements could potentially cause a large error in G_{max}, due to the square in the formula. However, Viggiani & Atkinson (1995) and Brignoli et al. (1996) have shown that the effective length, L_e, which a wave travels, is the distance between the ends of the elements. It is not so difficult to determine the travel distance. So the main reason behind the potential error in the measurement of G_{max} due to near field effects falls largely on the estimate of travel time. From Fig.2.38 it can be seen how difficult it is to measure the travel time between the transmitter to the receiver due to near field effects. The first arrival of the shear wave could correspond to any of the points 0, 1 and 2. Using these arrival times for these points in Equation 2.33, the potential error due to the near field effects is about 60% in G_{max}.

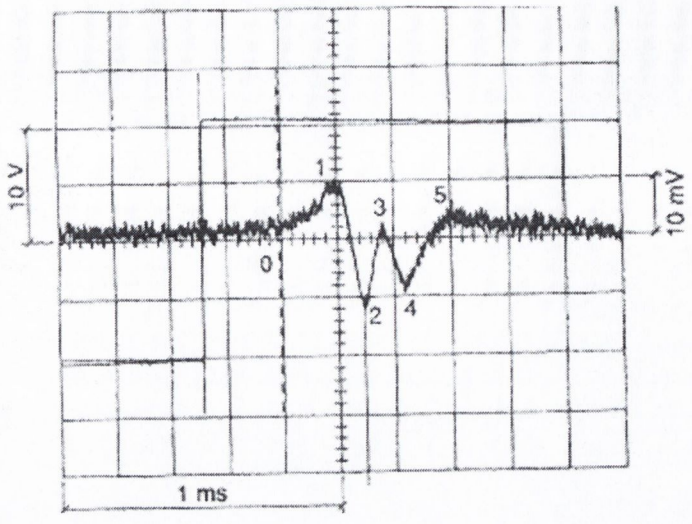

Fig.2.38–Typical oscilloscope signals from a bender element test with a square wave (from Viggiani & Atkinson, 1995)

Viggiani & Atkinson (1995) carried out complex numerical analyses to overcome the near field effect on a sinusoidal wave to calculate the travel time. The travel time of an impulse wave between two points can be taken as the time shift that produces the peak cross-correlation between the signals recorded at these two points, based on the assumption of plane wave fronts and the absence of any reflected or refracted waves (Arulnathan et al., 1998). In this method the time domain record can be decomposed into a group of harmonic waves of known frequency and amplitude.

The cross-correlation function CC_{xy} (t) is a measure of the degree of correlation of two signals $S_1(T)$ and $S_2(T)$. The analytical expression of the cross-correlation function is given by:

$$CC_{xy}(t) = \lim_{T \to \infty} \frac{1}{T} \int_T S_1(T) S_2(T+t) dT \qquad [2.34]$$

where T is the total time length of the signal and t is the time shift between the two signals.

It is convenient to calculate the cross-correlation in the frequency domain using the following steps. A fast Fourier transform (FFT) transforms the time domain records to the frequency domain, as shown in the following equation:

$$L_{s1}(f) = FFT(S_1(t)) \quad [2.35]$$

$$L_{s2}(f) = FFT(S_2(t)) \quad [2.36]$$

where $L_{s1}(f)$ and $L_{s2}(f)$ are the linear spectra of signals S_1 and S_2 respectively. The linear spectra are a vector in the complex field; its magnitude and phases are the amplitude and the phase shift respectively of each of the harmonic components of the signal (Viggiani and Atkinson, 1995).

The cross power spectrum ($G_{s1\text{-}s2}(f)$) of the input and output is then calculated as follows:

$$G_{s1\text{-}s2}(f) = L_{s1}^{*}(f)\, L_{s2}(f) \quad [2.37]$$

Where $L_{s1}^{*}(f)$ is the complex conjugate of $L_{s1}(f)$. The cross-correlation can now be calculated as follows

$$CC_{s1\text{-}s2}(t) = IFFT(G_{s1\text{-}s2}(f)) \quad [2.38]$$

where IFFT is the inverse fast Fourier transform. Fig.2.39 shows the cross-correlation of the signals in Fig.2.40.

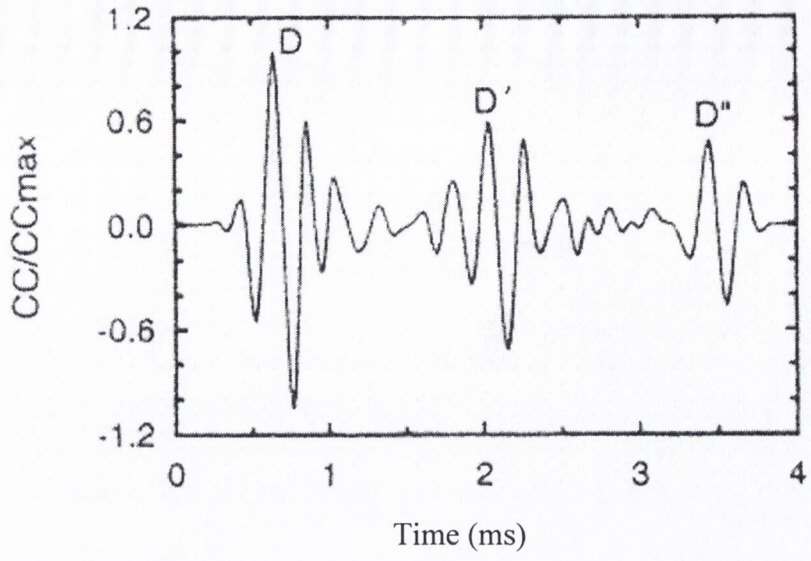

Fig. 2.39–Cross-correlation of input to output signals (from Arulnathan et al., 1998)

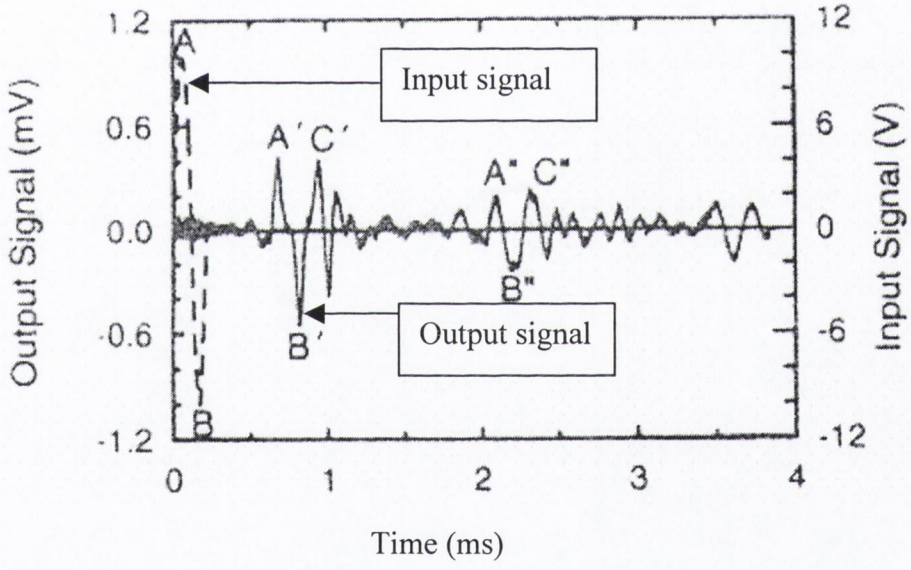

Fig.2.40 – Input and output signals (from Arulnathan et al., 1998)

Jovicic et al. (1996) carried out dynamic finite element analysis using the SOLVIA 90 package to check the influence of the boundary conditions on the applicability of the analytical solution to the bender element test when carried out in a triaxial apparatus. In this analysis the soil was modelled as isotropic, elastic and undrained with stiffness E of 118 MPa and density of 2000 kg/m^3, representing normally consolidated Speswhite kaolin at an effective confining stress of 200 kPa. The analysis was carried out using

plane strain elements (the shear wave propagation and the bender element motion are not axi-symmetric boundary conditions) with a fine mesh of 2000 elements. The authors mentioned that full 3-D modelling of the problem gave qualitatively similar results. Transverse sinusoidal motion was applied at a tip of the transmitter as an input dynamic loading and the output signal was determined in the transverse direction at the tip of the receiver. The analysis was performed using R_d (which represents the number of wave lengths that occur between the bender element transmitter and receiver) values of 1.1 and 8.1 and the displacement-time traces obtained for transverse motion at the point representing the source and at the point representing the receiver are shown in Fig. 2.41. For the value of R_d = 1.1, the near field effects is again clearly present as a significant initial downward deflection occurs before the true shear wave arrives at a T/Ta of 1.0. The authors mentioned that the near field effects are responsible for the initial deflection of the output signal. For the value of R_d = 8.1, there is no initial deflection of output signal.

Finite element analyses were carried out by Arulnathan et al. (1998) to identify the travel time errors associated with several techniques used to calculate the shear wave velocity. 2-D linear elastic finite element analyses were carried out using GeoFEAP, a finite element package with plane strain elements for the soil and bender elements to evaluate the combined errors resulting from wave interference at the caps and non-one-dimensional wave travel and near field effects. The 36 mm wide by 72 mm long specimen was modelled using 1818 four-noded quadrilateral elements. Fixed-end boundary conditions were applied at the top and bottom boundaries and the side boundaries were considered as stress free conditions. In the FE analyses, the input voltage signal applied to the transmitting bender element was modelled as an in-phase bending moment uniformly distributed along the length of the bender element. The shear wave velocities were calculated using (1) the time difference between the first peak of the input and output signals, (2) the difference between the first trough of the input and output signals, (3) the time difference between the first shear wave arrival and the second shear wave arrival, (4) the cross co-relation method between input and output signals and (5) the first and second maximums in the cross correlation plot.

The example given by the Arulnathan et al. (1998) was for a bender element length of 4.0 mm. The correct shear wave velocity was 80 m/s and the excitation frequency was 2.5 kHz. The travel time was calculated using all the five methods above and the percentage errors were +2.6, +6, -1.25, +3.79 and –3.1 respectively.

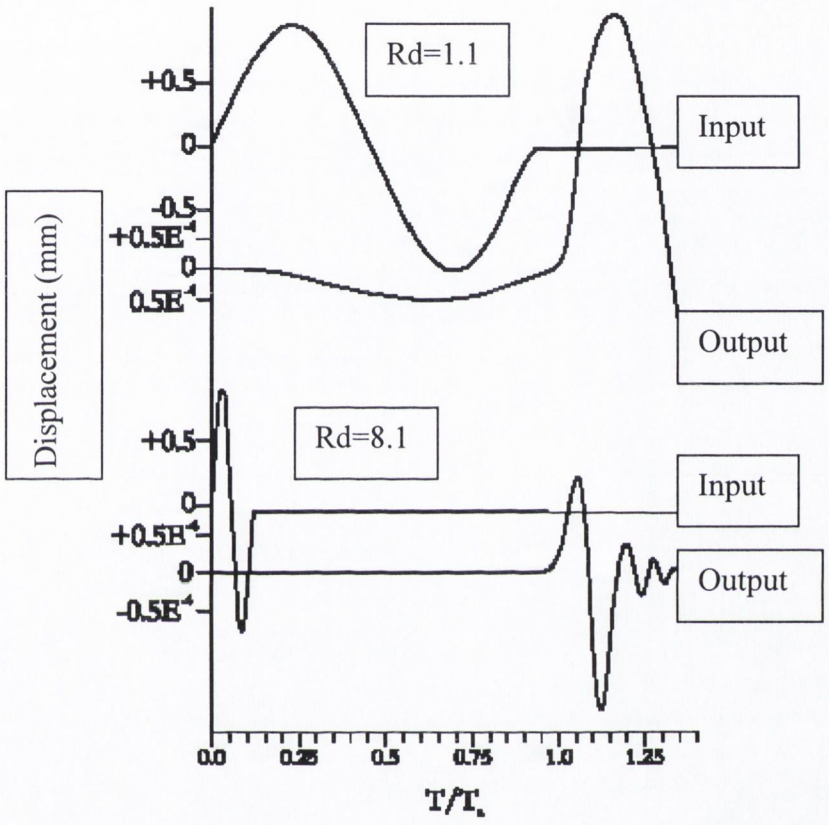

Fig.2.41–FE solution for the motion at the monitoring point (from Jovicic et al, 1996)

The results of bender element tests, carried out by Lawler 2002 on Dublin boulder clay and London City University (LCU, 1996) on behalf of Geoconsult-Arup private consulting company on boulder clay in Dublin Port Tunnel area, are presented in Fig. 2.42. It is found that the bender element results by Lawler (2002) and LCU (1996) are similar and reasonable agreements were found between them. In every case the G_{max} increases with increasing confining pressure.

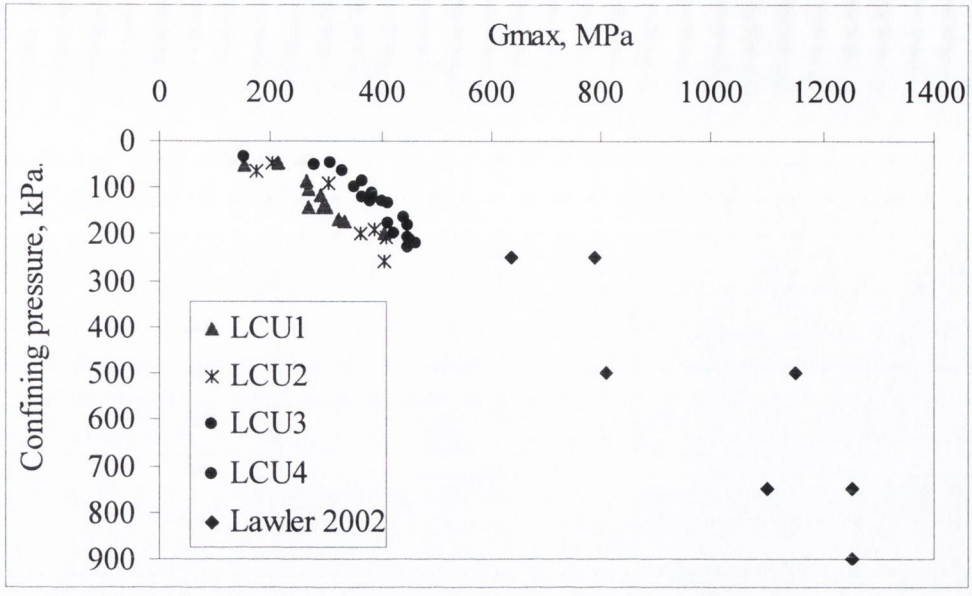

Fig.2.42–Comparison of bender element test results

2.7 Conclusions

A brief discussion is presented in this chapter on tunnelling, the ground vibrations due to a TBM and their effects on humans and buildings, the propagation characteristics and parameters of ground vibration waves and recent research that has been carried out on these. More emphasis was given to discussing in detail those topics which are directly or indirectly related to the finite element modelling of the project.

The literature review covered the definition of ground vibrations, first for underground construction works in general, but especially for mechanised tunnelling works. These vibration travel in the ground in different forms as body waves and surface waves, with their wave propagation velocities dependent upon the ground characteristics and the TBM excitation.

Standards have been reviewed which cover the criteria against which the predicted ground vibrations need to assessed; these are structural damage and perceptible intrusion.

It has been seen that the shear modulus increases with increasing confining pressure/depth and decreases with void ratio. Confining pressure is also function of depth. Although the G_{max} value has been assumed constant with confining pressure/depth for theoretical analyses however, it is not constant with confining pressure/depth even it changes with small variations in void ratio.

Bender element tests are normally used to determine the G_{max}. In a bender element test, the travel time is determined by measuring the time difference between the input and the output signals. From this the shear wave velocity can be found by dividing the travel distance by the travel time. The travel distance of the wave is taken to be equal to the specimen's length minus the protrusion of the two-bender elements at the both ends. After determining the propagation shear wave velocity, it is possible to calculate the small strain shear modulus, $G_{max,}$ by the elastic continuum mechanics relationship. However, it is very difficult to determine the exact travel time due to near field effects, which are dependent on wave type and frequency of waves. It is found that the distorted sine wave is more favourable than other wave.

The environmental effects of vibrations also have received considerable attention in recent years owing to the damage they can cause to buildings and the disturbance to people. These consequences of tunnelling activities have prompted recent research into improved methods for predicting the ground vibrations induced by a TBM. The main objective of this project is to predict the vibration at the surface above a tunnel boring machine using finite element modelling.

CHAPTER 3

BRIEF INTRODUCTION ON FINITE ELEMENT ANALYSIS

3.1 Introduction

The objective of this chapter is to provide a basic theoretical outline of the finite element method used to solve the problems described in later chapters. This chapter is not intended as a text on the finite element method, rather as a brief description of how the method was utilised here.

3.2 Finite Element Analysis

Finite element analysis (FEA), also called the finite element method (FEM), is a method for numerical solution of field problems. Mathematically, a field problem is described by differential equations or integral expression. Finite element formulations, in ready-to-use form, are contained in general-purpose FEA programs. It is possible to use FEA programs while having little knowledge of the analysis method or the problems to which they are applied.

Individual finite elements can be visualized as small pieces of a body. Elements are connected at points called nodes. The assemblage of elements is called a finite element body. The particular arrangement of elements is called mesh. Numerically, an FE mesh is represented by a system of algebraic equations to be solved for unknowns at nodes. The basic steps of an FEA are as follows (Stasa, 1985; Bathe, 1982 and Cook et. al., 2002):

- Problem identification and discretization: that subdivide the problem into nodes and elements.
- Selection of an interpolation function to represent the physical behaviour of an element; that is an approximate continuous function as assumed to represent the behaviour of an element.
- Development of the displacement equation for each element.
- Assembly of the elements to represent the entire problem and construction of the global stiffness matrix.
- Application of the boundary conditions, initial conditions and loading.

- Solution of a set of linear or non-linear algebraic equations simultaneously to obtain nodal results, such as displacement values at different nodes.
- Use of the nodal values and interpolation functions to determine other parameters such as stress, strain and velocity etc. inside each element.

3.3 Strain-Displacement Relations

A displacement field describes how a body deforms as well as how it displaces. Strain-displacement relations extract the strain field contained in a displacement field and play a prominent role in formulating commonly used elements. The relation between the strain and displacement of the nodes is obtained using a shape function. The displacement of the soil at any point within an element, {u} can be related to the nodal point displacements vector, {d} from the following equation (Stasa, 1985; Bathe, 1982, Kramer 1986 and Cook et. al., 2002):

$$\{u\} = [N]\{d\} \qquad [3.1]$$

where, matrix [N] is the shape function.
The strains within each element {ε} are then given by:

$$\{\varepsilon\} = [\partial]\{u\}$$
$$= [\partial][N]\{d\}$$
$$\{\varepsilon\} = [B]\{d\} \qquad [3.2]$$

where, matrix [B] is called the strain-displacement matrix.

3.4 Stress-Strain Relations

If deformations are small, the material is assumed to remain within the elastic limits of Hooke's law so that the stress (σ) is proportional to the strain (ε). The linear stress-strain relation can be expressed as:

$$\{\sigma\}=[C]\{\varepsilon\} \qquad [3.3]$$

where [C] is the stress-strain matrix. Stress-strain matrices for different problems are shown in Table3.1. If strains are large, considerable non-linear effects occur in the material.

Table 3.1–Generalised stress-strain matrices for isotropic materials and different design situations (after Bathe, 1982).

Problem	Material Matrix C
Bar in tension/compression	E
Beam in bending	EI
Plane stress	$\frac{E}{1-\nu^2}\begin{bmatrix} 1 & \nu & \\ \nu & 1 & \\ & & \frac{1-\nu}{2} \end{bmatrix}$
Plane strain	$\frac{E(1-\nu)}{(1+\nu)(1-2\nu)}\begin{bmatrix} 1 & \frac{\nu}{1-\nu} & \\ \frac{\nu}{1-\nu} & 1 & \\ & & \frac{1-2\nu}{2(1-\nu)} \end{bmatrix}$
Axisymmetric	$\frac{E(1-\nu)}{(1+\nu)(1-2\nu)}\begin{bmatrix} 1 & \frac{\nu}{1-\nu} & & \frac{\nu}{1-\nu} \\ \frac{\nu}{1-\nu} & 1 & & \frac{\nu}{1-\nu} \\ & & \frac{1-2\nu}{2(1-\nu)} & \\ \frac{\nu}{1-\nu} & \frac{\nu}{1-\nu} & & 1 \end{bmatrix}$

Three-dimensional	$\frac{E(1-\nu)}{(1+\nu)(1-2\nu)}\begin{bmatrix} 1 & \frac{\nu}{1-\nu} & \frac{\nu}{1-\nu} & & & \\ \frac{\nu}{1-\nu} & 1 & \frac{\nu}{1-\nu} & & & \\ \frac{\nu}{1-\nu} & \frac{\nu}{1-\nu} & 1 & & & \\ & & & \frac{1-2\nu}{2(1-\nu)} & & \\ & & & & \frac{1-2\nu}{2(1-\nu)} & \\ & & & & & \frac{1-2\nu}{2(1-\nu)} \end{bmatrix}$
Notation: E = Young's Modulus, ν = Poisson's ratio, I = 2nd moment of area	

3.5 Element Stiffness Matrix

In the finite element formulation, it is assumed that the displacements of the finite element assemblage are assumed to be infinitesimally small and that the material is linearly elastic. In addition, the nature of the boundary conditions remains unchanged during the application of the loads on the finite element assemblage. With these assumptions, the finite element equations derived were for static analysis:

$$\{F_e\} = [K_e]\{d\} \qquad [3.4]$$

where, $[K_e]$ is the element stiffness matrix, $\{d\}$ is the nodal point displacement vestor and $\{F_e\}$ is the matrix of the nodal point forces. $[K_e]$ can be found using following equation (Bathe, 1982 and Cook et. al., 2002):

$$[K_e] = \int [B]^T.[C].[B]dV \qquad [3.5]$$

3.6 Element Mass and Damping Matrix

In a dynamic analysis, the inertia forces and damping are the extra parameters making the difference between static and dynamic analyses. Inertia forces can be calculated from the

following equation:

$$\{F_{Ie}(t)\} = -[M_e].\{\ddot{d}\}, \quad [3.6]$$

where, $\{F_{Ie}(t)\}$ is the inertia forces matrix, $[M_e]$ is the element mass matrix and $\{\ddot{d}\}$ is the nodal point acceleration vector. The mass matrix can be written as follows:

$$[M_e] = \int \rho [N]^T [N] dV \quad [3.7]$$

where, ρ is the density, assumed constant within the element. This is called the consistent element mass matrix, because its shape function, [N] is the same as for the element stiffness matrix.

During the vibration of ground and structures some energy is being attenuated. This attenuation is included in the dynamic equation as damping forces. The damping forces on a single element are:

$$\{F_{De}\} = -[C_e]\{\dot{d}\} \quad [3.8]$$

where, $\{F_{De}\}$ is the damping force, $\{\dot{d}\}$ is the nodal point velocity vector and $[C_e]$ is the elemental damping matrix. The damping matrix can be written as:

$$[C_e] = \int c_e [N]^T [N] dV \quad [3.9]$$

where, c_e is a damping parameter analogous to viscosity

3.7 Dynamic Equation

The dynamic equation of equilibrium for each element can be written as follows:

$$[M_e]\{\ddot{d}\} + [C_e]\{\dot{d}\} + [K_e]\{d\} = \{r\} \quad [3.10]$$

where, $[M_e]$, $[C_e]$ and $[K_e]$ are the mass, damping and stiffness matrices; $\{r\}$ is the external load vector; and $\{\overset{oo}{d}\}$, $\{\overset{o}{d}\}$ and $\{d\}$ are the nodal acceleration, velocity and displacement vectors.

Once the dynamic equations for each element are obtained, they are combined in a way that satisfies compatibility of displacements to obtain the global dynamic equilibrium equations:

$$[M]\{\overset{oo}{D}\} + [C]\{\overset{o}{D}\} + [K]\{D\} = \{R\} \qquad [3.11]$$

where, $\overset{oo}{D}$, $\overset{o}{D}$ and D are the global point acceleration, velocity and displacement vectors. [M], [C] and [K] are the global mass, damping and stiffness matrices and {R} is the global load vector. Equation 3.11 can be written as follows:

$$F_I(t) + F_D(t) + F_E(t) = R(t) \qquad [3.12]$$

where, F_I, F_D, F_E matrices of the are the inertia forces, damping forces and elastic forces respectively, all of them being time-dependent. Therefore, in dynamic analyses the effects of acceleration-dependent inertia forces and velocity-dependent damping forces are considered.

Mathematically, Equation 3.11 represents a system of linear differential equations of the second order and, in principle, the solution to the equations can be obtained by standard procedures for the solution of differential equations with constant coefficients. However, the procedures proposed for the solution of general systems of differential equations can become very expensive if the order of the matrices is large. In practical finite element analyses, a few effective methods are used. The procedures considered are divided into two methods of solution. The main procedures are: (a) the direct time integration methods, (b) the modal analysis method (Bathe, 1982).

3.7.1 Direct Time Integration Methods

The most general approach for solving the dynamic response of structural systems is by direct numerical integration of the dynamic equilibrium equations. This involves, after the solution is defined at time zero, attempts to satisfy dynamic equilibrium at discrete points in time.

Most methods use equal time intervals giving time stages of Δt, $2\Delta t$, $3\Delta t$,---,$n\Delta t$, and so on. At the nth time stage, the equilibrium equation, Equation 3.11, is

$$[M]\{\overset{oo}{D}\}_n + [C]\{\overset{o}{D}\}_n + [K]\{D\}_n = \{R\}_n \qquad [3.13]$$

Many different numerical solution techniques are available; however, the algorithms adopted can fundamentally be classified as either explicit or implicit integration methods and these are explained below.

Explicit methods do not involve the solution of a set of linear equations at each step. Basically, these methods use the differential equation at time "t" to predict a solution at time "t+Δt". An explicit algorithm uses following expression in the general form (Cook et. al., 2002)

$$\{D\}_{t+\Delta t} = f(\{D\}_t, \{\overset{o}{D}\}_t, \{\overset{oo}{D}\}_t, \{D\}_{t-\Delta t} \ldots\ldots) \qquad [3.14]$$

which contains only previously calculated information on its right hand side. For most real problems, which contain stiff elements, a very small time step is required in order to obtain a stable solution. Therefore, all explicit methods are conditionally stable with respect to the size of the time step. This condition is shown as follows (ABAQUS, 2004):

$$\Delta t = \min (L/v_p) \qquad [3.15]$$

where, L is the element dimension and v_p is the P-wave propagation velocity of the material. This method is suited to wave propagation problems and when computer storage requirements are low (Cook et. al., 2002).

In the implicit methods to solve the differential equation at time "t+Δt", the values are required values not only at time 't' but also at time "t+Δt". An implicit algorithm uses following expression in the general form

$$\{D\}_{t+\Delta t} = f(\{D\}_t, \{\overset{o}{D}\}_{t+\Delta t}, \{\overset{oo}{D}\}_{t+\Delta t}, \{D\}_{t-\Delta t} \ldots\ldots) \qquad [3.16]$$

which is combined with the equation of motion at time stage t+Δt. These methods require the solution of a set of linear equations at each time stage; however, larger time intervals may be used. Implicit methods can be unconditionally stable; they are suited to structural dynamics problems. In the following sections a few commonly used direct integration methods are presented (Cook et. al., 2002).

3.7.1.1 The Central Difference Method

In ABAQUS, the explicit dynamics analysis method is based on the implementation of an explicit integration rule together with the use of diagonal ("lumped") element mass matrices. The equations of motion for the body are integrated using the explicit central-difference integration rule:

$$\{D_{i+1}\} = \{D_i\} + \Delta t_{i+1}\{\overset{o}{D}_{i+1/2}\} \qquad [3.17]$$

$$\{\overset{o}{D}_{i+1/2}\} = \{\overset{o}{D}_{i-1/2}\} + \frac{\Delta t(i+1) + \Delta t(i)}{2}\{\overset{oo}{D}_i\} \qquad [3.18]$$

where D is a degree of freedom and the subscript, i refer to the increment number in an explicit dynamics step. The central difference method is explicit in the sense that the kinematic state is advanced from the previous increment using known values of $\overset{o}{D}_{i-1/2}$ and $\overset{oo}{D}_i$.

The explicit integration rule is quite simple but it does not provide the computational efficiency associated with the explicit dynamics procedure. The key to the computational efficiency of the explicit procedure is the use of diagonal element mass matrices because, following ABAQUS (2004), the accelerations at the beginning of the increment are computed by:

$$\{\overset{oo}{D}_i\} = [M]^{-1}\{\{R_i\} - \{I_i\}\} \qquad [3.19]$$

where, M is the mass matrix, R is the applied load vector and I is the internal force vector. A lumped mass matrix is used because its inverse is simple to compute and because the vector multiplication of the inverse mass matrix by the inertial force requires only n operations, where n is the number of degrees of freedom in the model.

3.7.1.2 The Newmark Method

The Newmark analysis procedure used in PLAXIS is based on the implementation of an implicit integration method. In 1959 Newmark presented a family of single-step integration methods for the solution of dynamic problems. During the past 45 years Newmark's method has been applied to the dynamic analysis of many practical engineering problems. It is based on the assumption that the acceleration varies linearly from time t to time $t+\Delta t$. The equation of motion becomes as follows:

$$[\mathrm{M}]\{\overset{oo}{D}\}_{t+\Delta t} + [\mathrm{C}]\{\overset{o}{D}\}_{t+\Delta t} + [\mathrm{K}]\{D\}_{t+\Delta t} = \{\mathrm{R}\}_{t+\Delta t} \qquad [3.20]$$

in which the displacements and the velocities are defined as follows:

$$\{D_{t+\Delta t}\} = \{D_t\} + \Delta t(\overset{o}{D}_t) + \Delta t^2((1/2-\beta)\{\overset{oo}{D}_t\} + \beta(\overset{oo}{D}_{t+\Delta t})) \qquad [3.21]$$

$$\{\overset{o}{D}_{t+\Delta t}\} = \{\overset{o}{D}_t\} + \Delta t((1-\delta)\{\overset{oo}{D}_t\} + \delta\{\overset{oo}{D}_{t+\Delta t}\}) \qquad [3.22]$$

where β and δ are parameters controlling the stability and accuracy of the integration process. When $\beta = 1/6$ and $\delta = 1/2$, equations [3.21] and [3.22] correspond to the linear acceleration method. Newmark originally proposed as an unconditionally stable scheme the constant-average-acceleration method in which case $\beta = 1/4$ and $\delta = 1/2$.

3.7.1.3 Hilber-Hughes-Taylor Method

The general direct-integration method provided in ABAQUS/Standard is called the Hilber-Hughes-Taylor method. The method is implicit: the integration operator matrix must be inverted, and the set of simultaneous dynamic equilibrium equations must be solved at each time increment. This solution is done iteratively using Newton's method. A parameter, α, is

used in this method to introduce artificial damping to minimise high frequency noise. This damping is purely numerical-material damping. The equation of motion in this method becomes:

$$[M]\{\overset{oo}{D}_{t+\Delta t}\} + (1+\alpha)[C]\{\overset{o}{D}_{t+\Delta t}\} - \alpha[C]\{\overset{o}{D}_t\} + (1+\alpha)[K]\{D_t\} - \alpha[K]\{D_t\} = \{R_{t+\Delta t}\} \qquad [3.23]$$

in which the displacements and the velocities are defined as follows:

$$\{D_{t+\Delta t}\} = \{D_t\} + \Delta t(\overset{o}{D}_t) + \Delta t^2((1/2-\beta)\{\overset{oo}{D}_t\} + \beta\{\overset{oo}{D}_{t+\Delta t}\}\} \qquad [3.24]$$

$$\{\overset{o}{D}_{t+\Delta t}\} = \{\overset{o}{D}_t\} + \Delta t((1-\delta)\{\overset{oo}{D}_t\} + \delta\{\overset{oo}{D}_{t+\Delta t}\}\} \qquad [3.25]$$

where, $\beta = 1/4(1-\alpha)^2$; $\delta = 1/2-\alpha$; $-1/3 \leq \alpha \leq 0$.

The parameter α can take any value from $\alpha = 0$, which gives no artificial damping and is exactly the trapezoidal rule, to $\alpha = -1/3$, which provides the maximum artificial damping available from this operator. A value of $\alpha = -0.05$ is used by default because this provides just enough artificial damping in the system to allow the automatic time stepping procedure to work smoothly (Bathe, 1982).

3.7.2 Modal Analysis

The modal dynamic procedure provides time history analysis of linear systems. The excitation is given as a function of time: it is assumed that the amplitude curve is specified so that the magnitude of the excitation varies linearly within each increment. The method is much less expensive computationally than the direct integration method and is also very accurate because the integration operator used is exact whenever the forcing functions vary piecewise linearly with time. Initially it neglects the damping properties when solving the eigenvalue problem:

$$([K]-\varpi^2[M]).\{\Phi\} = \{0\} \qquad [3.26]$$

where ω is the natural frequency and Φ is the matrix of the mode shapes.

When the model is projected onto the eigenmodes used for its dynamic representation, a set of uncoupled one degree of freedom systems is obtained, for any of which the equilibrium equation at time t is

$$\overset{oo}{\{u\}} + 2\xi\{\varpi\}.\overset{o}{\{u\}} + \{\varpi\}^2\{u\} = \{r_t\} = \{r_{t-\Delta t} + \frac{\Delta r}{\Delta t}\Delta t\} \qquad [3.27]$$

where, ξ is the critical damping ratio; u is the "generalized coordinate" of the mode (the amplitude of the response in this mode); r is the magnitude of the loading projected onto this mode (the "generalized load" for the mode); and Δr is the change in r over the time increment, which is Δt. The actual finite element nodal displacements {d} can be obtained by linear transformation using following equation(Cook et. al., 2002):

$$\{d\} = [\Phi].\{u\} \qquad [3.28]$$

3.8 Damping

Damping is the decrease in amplitude with time due to the dissipation of energy. The types of damping that influence soil and structural dynamics can be categorized as follows.

- Viscous damping that exerts a force, which is proportional to the velocity.
- Hysteresis damping that is inherent in the material and may result from plastic action on a small scale.
- Coulomb damping that resembles hysteresis damping but is associated with dry friction.
- Radiation damping that refers to energy loss to a practically unbounded medium, such as soil that supports a structure.

Viscous damping is easy to represent in dynamic equations. Damping forces are less than 10% of the other forces (Cook et. al., 2002). Proportional damping, where the damping force is proportional to the velocity, is commonly used to represent the viscous damping and is to type of damping considered in this thesis.

3.8.1 Proportional (Rayleigh) Damping

Proportional damping, which is also known as Rayleigh damping, defines the global damping matrix [C] as a linear combination of the global mass and stiffness matrices.

$$[C] = \alpha [M] + \beta [K] \qquad [3.29]$$

where, α, β are damping factors and constants. The relationship between the damping ratio and frequency is as follows (Cook et al., 2002 and Clough & Penzien, 1993).

$$\xi = \frac{1}{2}(\frac{\alpha}{\varpi} + \beta\varpi) \qquad [3.30]$$

where, ξ is the damping ratio and ϖ is the frequency.

It is now possible to evaluate the two Rayleigh damping factors, α and β, by the solution of a pair of simultaneous equations if the damping ratios ξ_1 and ξ_2 associated with two specific frequencies ϖ_1 and ϖ_2 are known. Writing Equation (3.30) for each of these two cases leads to

$$\xi_1 = \frac{1}{2}(\frac{\alpha}{\varpi_1} + \beta\varpi_1) \text{ and } \xi_2 = \frac{1}{2}(\frac{\alpha}{\varpi_2} + \beta\varpi_2) \qquad [3.31]$$

$$\alpha = 2\varpi_1\varpi_2[\frac{\xi_1\varpi_2 - \xi_2\varpi_1}{\varpi_2^{\,2} - \varpi_1^{\,2}}] \text{ and } \beta = 2[\frac{\xi_2\varpi_2 - \xi_1\varpi_1}{\varpi_2^{\,2} - \varpi_1^{\,2}}] \qquad [3.32]$$

The evaluation of desired damping ratio at frequencies ϖ_1 and ϖ_2 gives a damping ratio-frequency relationship of the form as shown in Fig.3.1.

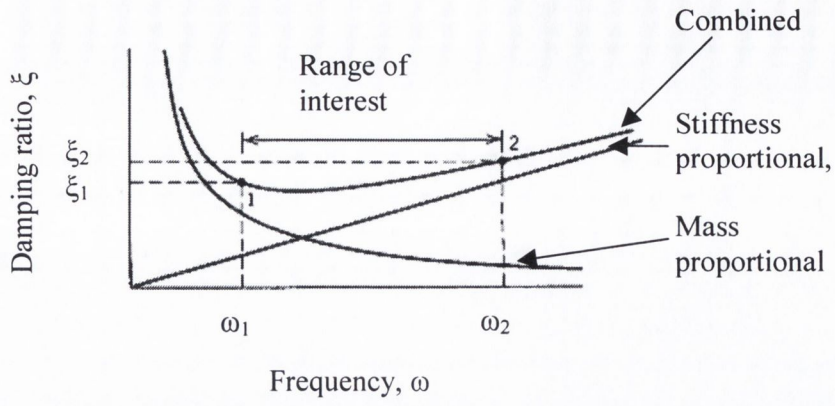

Fig.3.1–Relationship between damping ratio and frequency for Rayleigh damping

Due to detailed information about the variation of damping ratio with frequency seldom being available, it usually is assumed that the same damping ratio applies to both control frequencies; i.e., $\xi_1 = \xi_2 = \xi$ (Clough & Penzien, 1993). In this case, the proportional factors are given by a simplified version of Equation (3.33).

$$\alpha = 2\xi[\frac{\varpi_2 \varpi_1}{\varpi_2 + \varpi_1}] \text{ and } \beta = 2\xi[\frac{1}{\varpi_2 + \omega_1}] \qquad [3.33]$$

The Rayleigh α is the parameter that determines the influences of the mass in the damping of the system. The higher the α value, the more the lower frequencies are damped. Rayleigh β is the parameter that determines the influence of the stiffness in the damping of the system. The higher the β value, the more the higher frequencies are damped.

3.9 Discretization Considerations

The element size is the important parameter in finite element model in terms of computational time and accuracy of the solution. The results of the finite element model can be seriously influenced by the discretization. In case of 3-D model it is necessary to select as large as possible element size without compromising the accuracy of the solution in order to save computing time. The equation of shortest wavelength is as follows:

$$\lambda = \frac{v_s}{f_{\max}} \qquad [3.34]$$

where, f_{max} is the highest frequency of interest and v_s is the shear-wave velocity. The maximum dimension of any element should be limited to one-eighth (Kuhlemeyer and Lysmer, 1973 cited in Kramer, 1996) to one-fifth (Lysmer et. al., 1975 cited in Kramer, 1996) of the shortest wavelength considered in the analysis.

3.10 PLAXIS and ABAQUS

PLAXIS is a finite element package specially intended for the analysis of deformation, stability and dynamics in geotechnical engineering projects. However, its dynamic model is limited to 2-D problems. It is also stated in the PLAXIS Manual that it is not possible to fully absorb shear waves at the boundary and hence, when shear waves are present, a boundary effect is noticeable (PLAXIS v7). ABAQUS is a general-purpose 3-D simulations package, based on the finite element method. ABAQUS Explicit is a special-purpose analysis product in the ABAQUS packages that uses an explicit dynamic finite element formulation. It is suitable for modelling dynamic events (ABAQUS 2004) as it has infinite elements that can disappear waves without reflection to the original model. As TBM induced ground vibrations are 3-D in nature, ABAQUS was used to carry on the studies although it is very difficult to make model for combination of finite elements and infinite elements, as ABAQUS is a general-purpose finite element package. After using ABAQUS, the 3-D TBM induced ground vibrations were predicted and details results are presented in chapter 6.

3.11 The Typical Finite Element Mesh

A typical finite element mesh of limestone and soil with a tunnel is presented in Fig.3.2. In the mesh, three-dimensional eight-noded linear brick and reduced integration elements were employed for the limestone and soil and the tunnel lining. Reduced-integration elements use fewer integration points in each direction than the fully integrated elements. They reduce running time, especially in the analysis of a three-dimensional finite element model. To stop movement or sliding of the tunnel lining relative to the limestone, three-dimensional rough contact surface elements were included at the interface between the limestone and the tunnel lining. Infinite boundary conditions were specified at the four sides of the vertical section and on the bottom to account for the fact that in reality the soil is a semi-infinite medium (Fig. 3.2) (ABAQUS, 2004). A linear elastic isotropic material law was used to define the material properties for the limestone and soil and the tunnel concrete lining. When soil and limestone behaviour is expected to stay within the small strain range, the use of a linear elastic model is

justified and the shear modulus is a key parameter to properly model the soil behaviour (Ishihara, 1996 and Kramer, 1996).

The basic assumption of elastic behaviour, that is common to all the elastic models discussed here, is that the directions of principal incremental stress and incremental strain coincide (Potts & Zdravkovic, 1999). The general constitutive matrix relates increments of total stress to increments of strain:

$$\begin{Bmatrix} \Delta\sigma_x \\ \Delta\sigma_y \\ \Delta\sigma_z \\ \Delta\tau_{xz} \\ \Delta\tau_{yz} \\ \Delta\tau_{xy} \end{Bmatrix} = \begin{bmatrix} D_{11} & D_{12} & D_{13} & D_{14} & D_{15} & D_{16} \\ D_{21} & D_{22} & D_{23} & D_{24} & D_{25} & D_{26} \\ D_{31} & D_{32} & D_{33} & D_{34} & D_{35} & D_{36} \\ D_{41} & D_{42} & D_{43} & D_{44} & D_{45} & D_{46} \\ D_{51} & D_{52} & D_{53} & D_{54} & D_{55} & D_{56} \\ D_{61} & D_{62} & D_{63} & D_{64} & D_{65} & D_{66} \end{bmatrix} \begin{Bmatrix} \Delta\varepsilon_x \\ \Delta\varepsilon_y \\ \Delta\varepsilon_z \\ \Delta\gamma_{xz} \\ \Delta\gamma_{yz} \\ \Delta\gamma_{xy} \end{Bmatrix} \quad [3.35]$$

Elastic constitutive models can take many forms: isotropic, anisotropic, linear and nonlinear, with parameters dependent on stress and/ or strain level. In this FEM mesh, a linear elastic isotropic model is assumed. An isotropic material is one that has point symmetry, i.e. every plane in the body is a plane of symmetry for material behaviour. In such a situation it can be shown that only two independent elastic constants are necessary to represent the behaviour and that the constitutive matrix becomes symmetrical. In structural engineering it is common to use Young's modulus, E, and Poisson's ratio, μ, for these parameters. Equation (3.35) then takes the form shown in Equation (3.36)

If the material behaviour is linear then E and μ are constants and the constitutive matrix expressed as a relationship between accumulated effective stresses $\{\sigma'\}$ and strains $\{\varepsilon'\}$ is the same as that given in Equation (3.36).

$$\begin{Bmatrix} \Delta\sigma'_x \\ \Delta\sigma'_y \\ \Delta\sigma'_z \\ \Delta\tau_{xz} \\ \Delta\tau_{yz} \\ \Delta\tau_{xy} \end{Bmatrix} = \frac{E}{(1+\mu)(1-2\mu)} \begin{bmatrix} 1-\mu & \mu & \mu & 0 & 0 & 0 \\ & 1-\mu & \mu & 0 & 0 & 0 \\ & & 1-\mu & 0 & 0 & 0 \\ & & & \frac{1-2\mu}{2} & 0 & 0 \\ & & sym & & \frac{1-2\mu}{2} & 0 \\ & & & & & \frac{1-2\mu}{2} \end{bmatrix} \begin{Bmatrix} \Delta\varepsilon_x \\ \Delta\varepsilon_y \\ \Delta\varepsilon_z \\ \Delta\gamma_{xz} \\ \Delta\gamma_{yz} \\ \Delta\gamma_{xy} \end{Bmatrix}$$

[3.36]

For geotechnical purposes, it is often more convenient to characterise soil behaviour in terms of the elastic shear modulus, G, and effective bulk modulus, K'. Equation 3.36 then becomes:

$$\begin{Bmatrix} \Delta\sigma'_x \\ \Delta\sigma'_y \\ \Delta\sigma'_z \\ \Delta\tau_{xz} \\ \Delta\tau_{yz} \\ \Delta\tau_{xy} \end{Bmatrix} = \begin{bmatrix} K'+4/3G & K'-2/3G & K'-2/3G & 0 & 0 & 0 \\ & K'+4/3G & K'-2/3G & 0 & 0 & 0 \\ & & K'+4/3G & 0 & 0 & 0 \\ & & & G & 0 & 0 \\ & sym & & & G & 0 \\ & & & & & G \end{bmatrix} \begin{Bmatrix} \Delta\varepsilon_x \\ \Delta\varepsilon_y \\ \Delta\varepsilon_z \\ \Delta\gamma_{xz} \\ \Delta\gamma_{yz} \\ \Delta\gamma_{xy} \end{Bmatrix}$$

$$G = \frac{E}{2(1+\mu)} \quad ; \quad K' = \frac{E}{3(1-2\mu)}$$

[3.37]

Many engineering problems involve contact between two or more components such as underground tunnelling, retaining wall and masonry arch bridges etc. In a finite element analysis, contact conditions are a special class of discontinuous constraint, allowing forces to be transmitted from one part of the model to another. The constraint is discontinuous because it is applied only when the two surfaces are in contact. ABAQUS /Explicit provide two

algorithms for modelling contact interactions. The general contact algorithm allows very simple definitions of contact with very few restrictions on the types of surface involved. The contact pair algorithm has more restrictions on the types of surfaces involved and often requires careful definition of contact; however, it allows for some interaction behaviours that currently are not available with the general contact algorithm

Contact definitions are not entirely automatic with the general contact algorithm but are greatly simplified. The generality of this algorithm is primarily in the relaxed restrictions on the surfaces that can be used in contact. To stop the movement or the sliding of the tunnel lining relative to the ground, three-dimensional rough general contact surface elements were included at the interface between the limestone and the tunnel lining. The general contact algorithm generates contact forces to resist node-into-face and edge-into-edge contact penetrations (ABAQUS, 2004).

Infinite elements are used in boundary value problems defined in unbounded domains or problems in which the region of interest is small in size compared to the surrounding medium. Infinite elements are intended to be used for such cases in conjunction with first- and second-order planar, axisymmetric, and three-dimensional finite elements. Standard finite elements should be used to model the region of interest, with the infinite elements modelling the far field region. These infinite elements allow the wave to disappear from the model without reflections, so that the model behaves like an infinite layered half space.

The node numbering for infinite elements must be defined such that the first face is the face that is connected to the finite element part of the mesh. It is important to choose the position of the nodes in the infinite direction appropriately with respect to the loading position. The second node along each edge pointing in the infinite direction must be positioned so that it is twice as far from the applied loading point as the node on the same edge at the boundary between the finite and the infinite elements. However, the location of these nodes is not meaningful for explicit analysis.

In direct-integration implicit dynamic response analyses, direct-solution steady-state dynamic analyses and explicit dynamic analyses, infinite elements provide quiet boundaries to the finite element model. They also maintain the static force that was present on this boundary at the start of the dynamic response analysis; as a consequence, the far-field nodes in the infinite

elements will not displace during the dynamic response. The infinite elements do not provide any contribution to analysis procedures that are based on the eigenmodes of the system.

Unlike a dashpot element (another type of wave absorbing element), an infinite element does not require calculations of absorbent coefficients, which require knowledge of detailed soil properties and mesh geometry. For 3-D problems, one infinite element can replace up to twelve dashpot elements, which reduces the total number of elements in the model achieving significant economy in the case of large models, such as the one shown in Fig.3.2. Unlike a dashpot, the infinite element is more manageable and accessible. In addition to the convenience and economy of use, the infinite element offers a slight improvement in the regularity of the wave absorbing characteristics (ABAQUS 2004). Now the formulations of infinite element are as follows:

The infinite elements are based on consideration of plane body waves travelling orthogonally to the boundary. The response adjacent to the boundary is of small enough amplitude so that the medium responds in a linear elastic manner. The equilibrium equation is

$$-\rho \ddot{u} + \frac{\partial}{\partial x}\sigma = 0 \qquad [3.38]$$

where ρ is the material's density, $\ddot{u}$ is the material particle acceleration, σ is the stress, and x is position.

The material's response is assumed isotropic, linear elastic, and thus it can be written as

$$\sigma = \lambda(\varepsilon + 2G\varepsilon) \qquad [3.39]$$

where ε is the strain and

$$\lambda = \frac{E\nu}{(1+\nu)(1-2\nu)}$$

and

$$G = \frac{E}{2(1+\nu)}$$

Introducing this material response in the equilibrium equation, and assuming small strain:

$$\varepsilon = \frac{1}{2}\{\frac{\partial u}{\partial x} + [\frac{\partial u}{\partial x}]^T\} \qquad [3.40]$$

The governing equation for the motion is

$$\rho \ddot{u}_i = G\frac{\partial^2 u_i}{\partial x_j \partial x_j} + (\lambda + G)\frac{\partial^2 u_j}{\partial x_i \partial x_j} \qquad [3.41]$$

where index notation has been used for simplicity.

Now considering plane waves travelling along the x-axis. Two body wave solutions of this form exist for this equation. One describes plane, longitudinal ("push") waves, which have the form

$$u_x = f(x \pm v_p t), u_y = u_z = 0 \qquad [3.42]$$

where, by substitution in the governing equation above, the wave speed, v_p, is

$$v_p = \sqrt{\frac{\lambda + 2G}{\rho}} \qquad [3.43]$$

The other solution of this form is the "shear" wave solution

$$u_y = f(x \pm v_s t), u_x = u_z = 0$$

or

$$u_z = f(x \pm v_s t), u_x = u_y = 0$$

where v_s is shear wave velocity and again by substitution in the governing equation

$$v_s = \sqrt{\frac{G}{\rho}} \qquad [3.44]$$

In each case the solution $f(x\text{-}vt)$ represents waves moving in the direction of increasing x, while $f(x+ vt)$ represents waves moving in the direction of decreasing x. Now consider a boundary at $x = L$ of a medium modelled by finite elements in $x < L$. Introducing distributed damping on this boundary, such that

$$\sigma_{xx} = -d_p \dot{u}_x$$

and

$$\sigma_{xy} = -d_s \dot{u}_y$$

$$\sigma_{xz} = -d_s \dot{u}_z$$

where now choosing the damping constants d_p and d_s to avoid reflection of longitudinal and shear wave energy back into the medium in $x < L$. Plane, longitudinal waves approaching the boundary have the form $u_x = f_1(x - v_p t), u_z = u_y = 0$,. If they are reflected at all as plane, longitudinal waves, their reflection will travel away from the boundary in some form $u_x = f_2(x + v_p t), u_z = u_y = 0$. Since the problem is linear, superposition provides the total displacement $f_1 + f_2$, with corresponding stresses $\sigma_{xx} = (\lambda + 2G)(f_1' + f_2')$, all other $\sigma_{ij} = 0$, and velocity $\dot{u}_x = -v_p(f_1' - f_2')$. For this solution to satisfy the damping behaviour introduced on the boundary at $x = L$ requires

$$(\lambda + 2G - d_p v_p) f_1' + (\lambda + 2G + d_p v_p) f_2' = 0 \qquad [3.45]$$

Therefore, it is necessary to ensure that $f_2 = 0$ (so that $f_2' = 0$) for any f_1 by choosing

$$d_p = \frac{\lambda + 2G}{v_p} = \rho v_p \qquad [3.46]$$

A similar argument for shear waves provides

$$d_s = \rho v_s \qquad [3.47]$$

These values of boundary damping constants d_p and d_s are built into the infinite elements in ABAQUS. From the above discussion, it can be seen that they transmit all normally impinging plane body waves exactly. General problems involve non-plane body waves that do not impinge on the boundary from an orthogonal direction and may involve Rayleigh surface waves and Love waves. Nevertheless, these "quiet" boundaries work quite well even for such general cases, provided they are arranged so that the dominant direction of wave propagation is orthogonal to the boundary or, at free surfaces and interfaces where Rayleigh

or Love waves are of concern, is orthogonal to the surface. As the boundaries are "quiet" rather than silent (perfect transmitters of all waveforms), and because the boundaries rely on the solution adjacent to them being linear elastic, they should be placed some reasonable distance from the region of main interest (ABAQUS 2004).

By advancing in the ground, the tunnel-boring machine is a vibrating source from which vibrations are transmitted into the ground. Therefore, the impacts of the TBM on the ground during boring have been modelled by a dynamic loading system. The finite elements representing the TBM cutter disc have been loaded by a short triangular pulse. Due to this pulse, waves propagate through the soil and the response at the surface is determined. The main reason is to use input pulse in the FE model that it ensures parsimonious handling of the FE model rather than a direct application of the actual TBM source excitation. Due to use of an input pulse, it reduced the FE modelling time by several days for one FE analysis and hence by several months for entire project, which is very significant. A short triangular pulse has a wide power spectrum and it is suitable for analysing wave ranging from low to high frequency waves. In FEM analyses, the pulse was applied at the beginning of the calculations, and the vibration energy was damped out during the rest of the calculation. As a result, there is no also possibility of reflection of waves in the model due to this short triangular pulse.

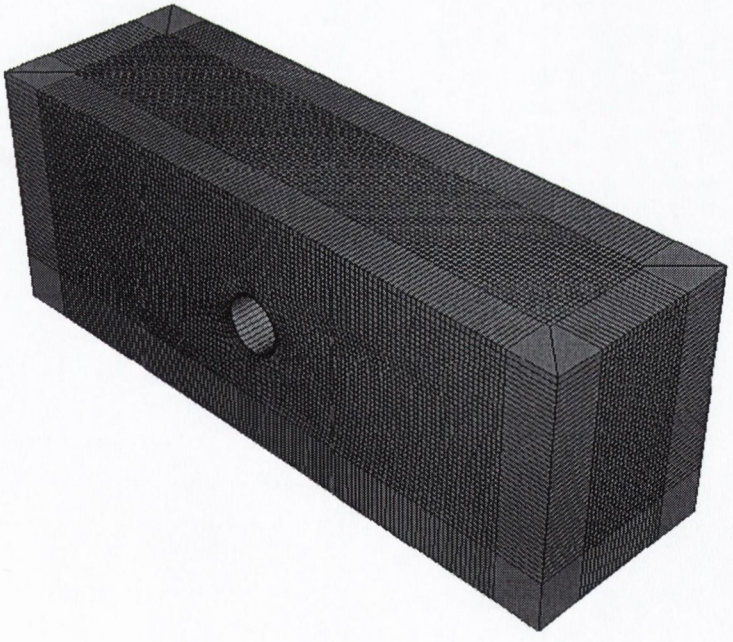

Fig.3.2- A typical finite element mesh

CHAPTER 4

MEASUREMENT OF DYNAMIC GROUND PROPERTIES

4.1 General

Dynamic analyses to evaluate the response of earth structures to dynamic stress applications, such as those produced by earthquakes, blasting, tunnelling construction, wind loading or machine vibrations, are finding increased applications in civil engineering practice. Various idealised models and analytical techniques may be used to represent a soil deposit and its response, but whatever procedure is followed; it is first necessary to evaluate the appropriate dynamic properties of the materials in the deposit. Precise measurement of dynamic soil properties is a somewhat difficult task when analysing dynamic geotechnical engineering problems (Sitharam & Raju, 2003 and Kramer, 1996).

Several field and laboratory techniques are available to measure the dynamic properties, many of which involve measurements at small-strain and many others involve measurements at large strain levels. However, the choice of a particular technique depends on the specific problem to be solved. Fig. 4.1 shows the changes in the types of soil behaviour with shear strain.

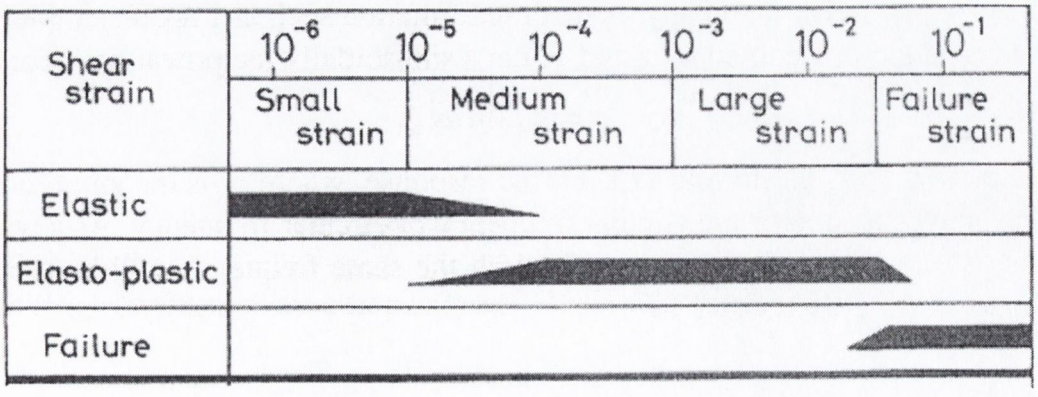

Fig.4.1– Modelling of soil behaviour in compliance with strain-dependent deformation characteristics (from Ishihara, 1996).

Soil properties that influence wave propagation and other low-strain phenomena include stiffness, damping, Poisson's ratio and density. Of these, stiffness and damping are the most important; the others have less influence and tend to fall within relatively narrow ranges. At high level of strain, the influence of strain rate, number of cycles and volume change characteristics may also be of importance. Volume change characteristics are also important at large strain levels (Kramer, 1996).

4.2 Field Tests

In field tests, the soil properties are measured in situ. The evaluation of dynamic soil properties by field tests has a number of advantages, as these tests do not require sampling that can alter the stress, chemical, thermal, and structural conditions in soil specimens. Further, the tests measure the response of relatively large volumes of soil, which also minimizes the effects due to evaluating small, unrepresentative specimens. In field tests, it is also possible to induce soil deformations that are similar to those of the problem of interest.

On the other hand, field tests do not allow the effects of conditions other than in situ conditions to be investigated easily, nor do they allow pore water drainage to be controlled. Some field tests can be performed from the ground surface, while others require the drilling of boreholes or the insertion of probes into the soil. Field tests involving boreholes and probes are expensive and time consuming while surface tests are often less expensive and can be performed relatively quickly. In many field tests, the specific soil property of interest is not measured but must be determined indirectly, by theoretical analysis or empirical correlation. However, these field tests can be further classified, based on the range of magnitude of strain, as small-strain and large-strain tests (Kramer, 1986) and small-strain field tests are described in the following section.

4.2.1 Small-Strain Field Tests

Dynamic soil properties depend much on the shear strain level. In the strain range below the order of 10^{-5} (0.001%), the deformations shown by most soils are purely elastic and recoverable and the damping is negligible. Small strain tests operate below the strain specified above and are based on the theory of wave propagation in the materials.

Seismic geophysical tests represent an important class of field tests for the determination of dynamic soil properties. The three types of seismic geophysical test are: cross-hole tests, down-hole tests and surface refraction tests and these give the three different methods for determining the dynamic soil properties described in the following paragraphs.

In the cross-hole method, a shear wave or a compressional wave is generated in a source borehole and its propagation in the horizontal direction is detected by means of receivers placed in two or three other adjacent boreholes in a linear array. The layout of the test is shown in Fig. 4.2. The advantage of this method is that it may be used to detect the modulus values of individual soil strata in a horizontally layered structure. However, the cost of the test is usually high, because it requires at least three holes (Ishihara, 1996).

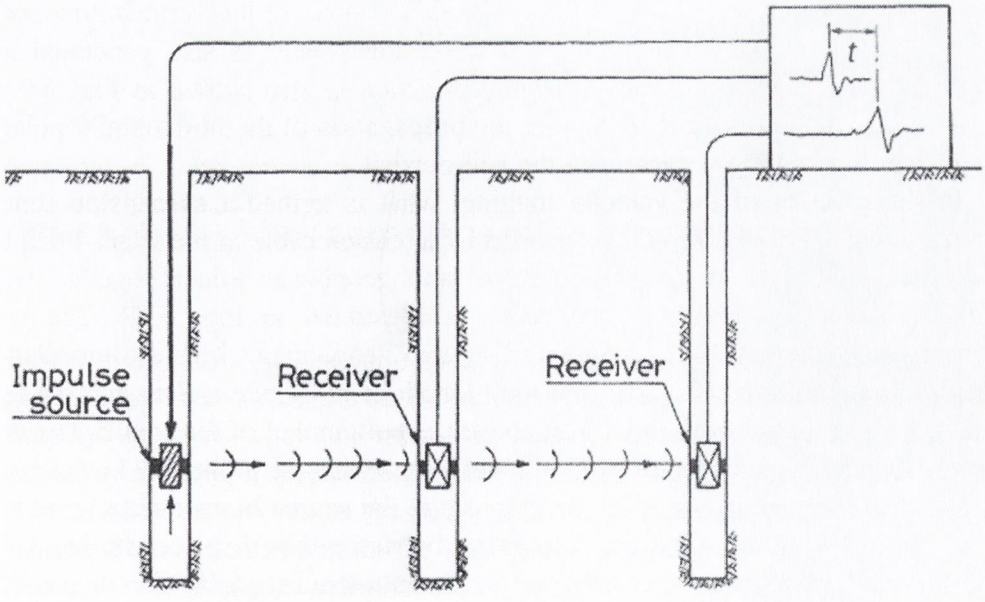

Fig. 4.2–Velocity logging by cross-hole method (from Ishihara, 1996)

In the case of the down hole logging, a geophone is clamped to the wall of a borehole, as illustrated in Fig. 4.3, to monitor the arrival of the wave front propagating downward from the source on the ground surface. Potential difficulties with down-hole tests and their interpretation can result from disturbance of the soil during boring excavation of the borehole (Kramer, 1996).

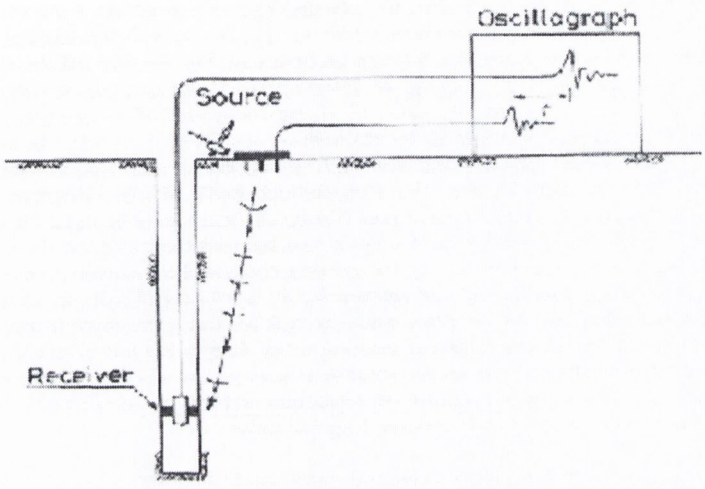

Fig. 4.3–Velocity logging by the down hole method (from Ishihara, 1996)

The refraction method is the simplest and most conventionally used procedure to obtain an overall picture of the soil and rock profiles over a wide area. In this method, an impact or explosive energy is applied on the ground surface and the wave front propagation is captured at a point some distance from the source. The distance and time of arrival make it possible to calculate the velocity of wave propagation. After calculating the wave velocity, the shear modulus may be calculated. The layout of the test is shown in Fig. 4.4.

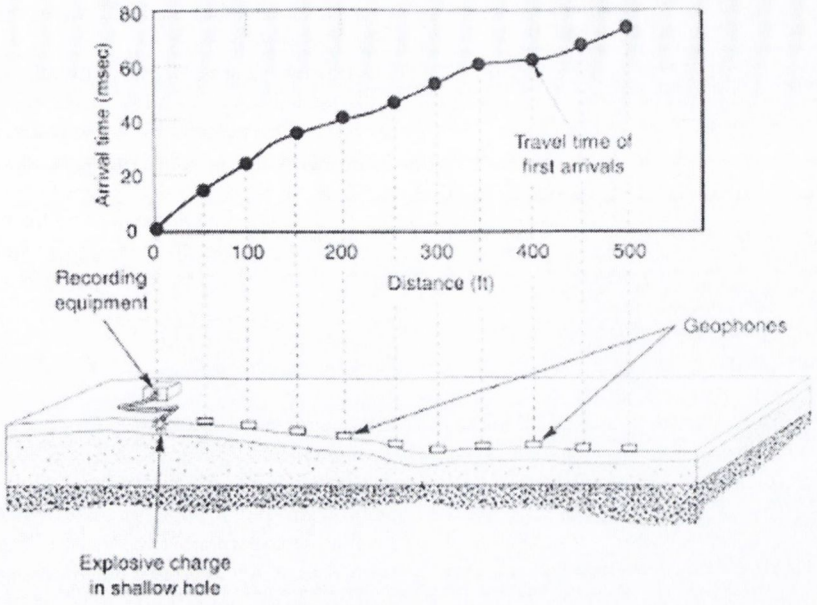

Fig.4.4–Seismic refraction test set-up. (from Redpath, 1973 cited by Kramer, 1996)

4.3 Laboratory Tests

In the laboratory, the tests to determine the dynamic properties of soil are carried out on relatively small specimens that are assumed to be representative of a larger body of soil. The specimens are tested as elements. The ability of laboratory tests to provide accurate measurements of soil properties depends on their ability to replicate the initial conditions and loading conditions of the problem of interest.

Dynamic soil properties are influenced by many factors, including density and stress conditions, and other factors, such as soil fabric or structure, age, stress and strain history and cementation. While the void ratio and stress conditions can be recreated in a reconstituted specimen, the effects of the other factors cannot. Since the effects of these other factors are manifested primarily at low strain levels, they are easily destroyed by sample disturbance. For the results of laboratory tests to reflect the actual behaviour of the in situ soil as closely as possible, high-quality undisturbed sample must be obtained. Like field tests, laboratory tests can be classified based on the range of strain as small-strain and large-strain tests and small-strain laboratory tests are described in the following section.

4.3.1 Small Strain Laboratory Tests

Laboratory tests are available to measure the dynamic properties of soils at small strain levels. The resonant column test, ultrasonic pulse test, and bender element test are the commonly employed techniques to measure small strain dynamic properties. The bender element test is described in Chapter 2.

4.3.1.1 Resonant Column Test

The resonant column test is the most generally used in the laboratory test for measuring the low-strain properties of soils such as stiffness and damping of soils. In this test, a solid or hollow cylindrical sample is subjected to harmonic excitation by an electromagnetic driving system (Drnevich, 1985). The soil specimen can be excited in either the torsional or the longitudinal modes of vibration by means of an electromagnetic loading system. The frequency is initially set to a small value, and gradually increased. The frequency of input vibration can be changed until the first resonant frequency mode of the soil sample is found. The resonant frequency is a function of the small strain stiffness of the soil, the geometry of the specimen and certain characteristics of the resonant column apparatus. Shear modulus values are then calculated from values of the shear velocities and the density of the soil (Richart, Hall & Woods, 1970). Consider a resonant column sample of height h, with polar moment of inertia J, subjected to a harmonic torsional loading. The torque T at the top of the sample is given by:

$$T = GJ\frac{\partial\theta}{\partial z} = G\frac{I}{\rho}\frac{\partial\theta}{\partial z} \qquad [4.1]$$

where, G is the shear modulus, θ is the angular rotation of the soil sample, J is the polar 2nd moment of area, I is the 2nd moment of area, z is the height above the base of the sample and ρ is the material density of the soil sample. This torque must be equal to the inertial torque of the loading system. If the 2nd moment of area for the loading system is I_o, inertial torque is given by:

$$T = I_o h \frac{\partial^2 \theta}{\partial t^2} \qquad [4.2]$$

Assuming that the rotations of the sample are harmonic, the equation 4.1 and 4.2 can be solved to calculate the θ and can be expressed using the following Equation 4.3 (Kramer, 1996), where w_n and v_s in Equation 4.3 are the natural frequency and the shear wave velocity respectively. The details of the derivation of the equation are found in Kramer (1996).

$$\frac{I}{I_o} = \frac{w_n h}{v_s} \tan \frac{w_n h}{v_s} \qquad [4.3]$$

For a given sample, I_o, h and I are generally known at the time of testing. The natural frequency is then obtained experimentally, and Equation 4.3 is used to calculate v_s. The shear modulus is then obtained from following equation:

$$G_o = \rho v_s^2. \qquad [4.4]$$

The damping ratio of the soil sample is determined from the amplitude-decay curve obtained by placing the specimen in free vibration. Free vibration is the periodic motion occurring when an elastic system is displaced from its equilibrium position. Free vibration occurs without forcing the vibration of a string after it has been plucked. The amplitude-decay curve and graph of amplitude versus cycles are shown in Fig. 4.5 and Fig. 4.6. The slope of the straight line can be taken as being equal to the value of the logarithmic decrement δ. From the theory of vibrations, the damping ratio D is correlated with the logarithmic decrement (Ishihara, 1996):

$$D = \frac{\delta}{2\pi} \qquad [4.5]$$

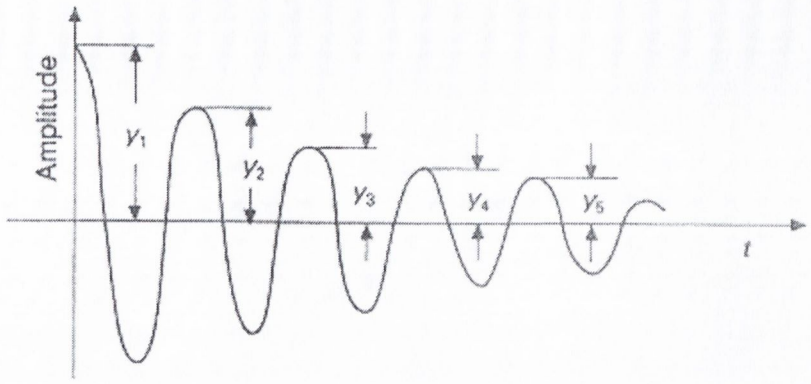

Fig. 4.5– Amplitude decay of free vibration (from Ishihara, 1996)

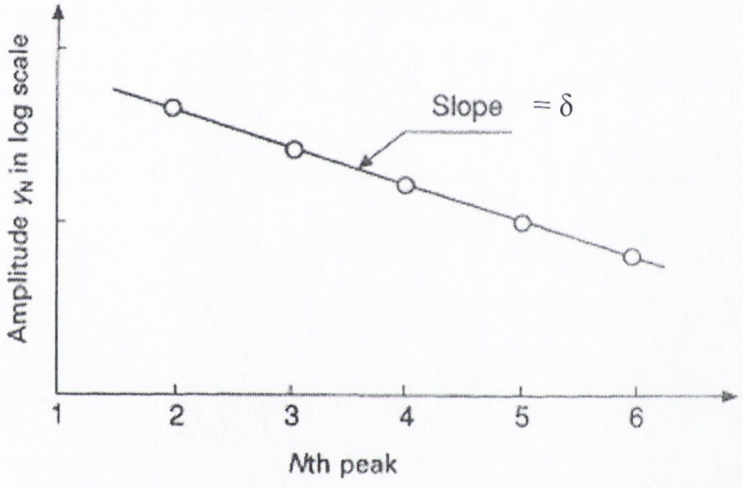

Fig.4.6– Amplitude versus cycles (from Ishihara, 1996)

The resonant column test is a useful tool for obtaining the strain-dependent modulus and damping properties of soils, but there are some drawbacks. The main drawbacks are that the test is relatively expensive and the equipment is complex. The output is not the response of the soil specimen itself but is the combined effect of the soil and its attached apparatus. Thus great caution must be exercised in order to obtain reliable data when using the resonant column test (Ishihara, 1996).

4.3.1.2 Ultrasonic Pulse Test

In the laboratory, the ultrasonic pulse test can be used to measure the wave propagation velocity through the soil sample. In this test, ultrasonic transmitters and receivers are placed at each end of a soil sample. The transmitters and receivers are made of piezoelectric materials. The advantage of piezoelectric materials is that when an electric pulse is applied to the transmitter, it causes it to deform rapidly and produce a stress wave that travels through the specimen toward the receiver. When the stress wave reaches the receiver, it generates a voltage pulse that is measured. The distance between the transmitter and receiver is divided by the time difference between the voltage pulses to obtain the wave propagation velocity (Woods, 1978, cited by Kramer, 1996).

4.3.1.3 Other small strain stiffness tests apparatus

Brignoli et al. (1996) focused on different types of piezoelectric devices used to measure the small strain stiffness of soils and made a comparative study between them. The piezoelectric devices studied were a compression transducer, a bender transducer and a shear-plate transducer. The bender transducer is eventually bender element.

A compression transducer is used to generate compression waves and propagate then through a soil specimen. A compression transducer is placed like a bender element at one end of a specimen and the compression waves are received at the other end of the soil specimen by another transducer. For the generation of compression waves, ceramic elements are polarised in the direction of the thickness of the transducer, and electrodes are placed on the ceramic element faces normal to the polarization direction (Fig.4.7). The transducer is ceramic with a cylindrical shape and a thickness of 2 mm and a diameter of 8 mm. The element expands and contracts in the direction of the thickness is shown in Fig. 4.7. The distance between the two transducers, L, and the time required by the wave to cover this distance, t, are used to calculate the propagation velocity, v, defined by:

$$v = L/t \quad [4.9]$$

There are two types of compression waves for all materials. One type is constrained compression waves, which involve no lateral deformation perpendicular to the direction of the wave propagation. The constrained compression wave velocity, v_p, is related to the small-strain constrained modulus, M_{max}, by equation:

$$M_{max} = \rho v_p^2 \quad [4.10]$$

The other type of compression wave is unconstrained compression waves where the unconstrained compression wave velocity, v_c is related to the small-strain Young's modulus, E_{max}, of the material by equation:

$$E_{max} = \rho v_c^2 \quad [4.11]$$

Brignoli et al., (1996) also mentioned that Vaghela and Stokoe (1995) had shown using the arrangement of compression wave sources and receivers in the centre of each end of the specimen, that only constrained compression waves were measured. However, they also showed that this source-receiver arrangement could be used to measure unconstrained compression waves in the same specimen simply by exciting longitudinal resonance and accounting for added masses attached to the ends of the specimen.

The shear plate transducer is used to generate shear waves that propagate through a soil specimen. A shear plate transducer is placed on one end of the sample and the generated shear wave is received at the other end of the soil sample by another transducer. For the generation of shear waves, ceramic elements are polarised in the width direction and the electrodes are applied to two faces that are parallel to the polarization direction as shown in Fig. 4.8. The ceramic used for the shear-plate transducers is a lead zirconate titanate with the dimensions of length 12.7 mm, width 12.7 mm and thickness 6.3 mm. Shear plate transducers distort in the direction of their width. The principles of shear plate transducers are similar to those of bender element and compression transducers. The

application of a sinusoidal signal to the transmitting transducer initiates a shear wave to propagate through the soil sample. The arrival of this shear wave then excites the receiving transducer and an output voltage is recorded. The G_{max} can then be calculated in the same way as described in Section 2.6. The author found that Lawrence (1963, 1965) first described the use of a shear-plate transducer to measure the shear wave velocity through soil samples.

Shear plate transducers provide shear waveforms similar to those generated by the more widely used bender element transducers. The main advantages of shear plate transducers is that they are better suited than bender elements for testing undisturbed stiff soils with high aggregate contents since shear-plate transducers do not penetrate into the soil sample.

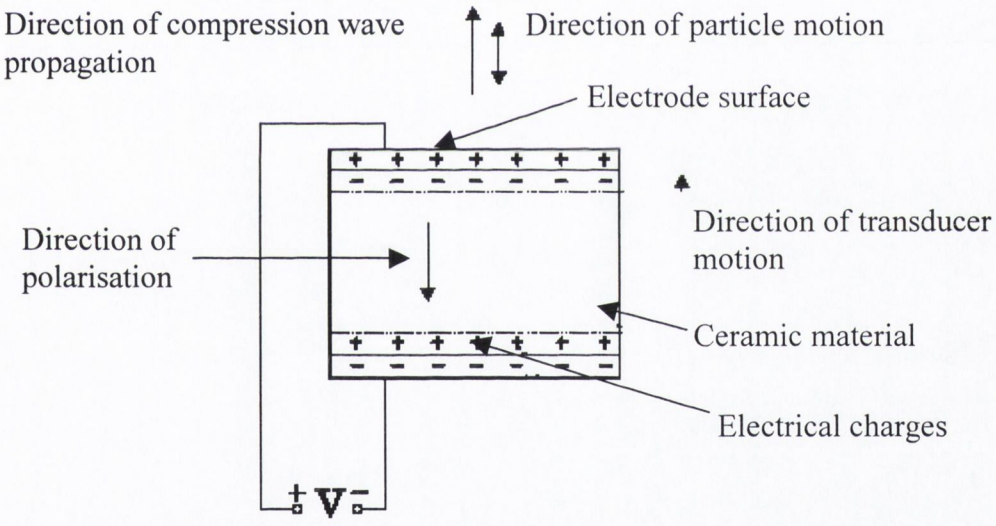

Fig. 4.7–Compression transducer (from Brignoli et al., (1996))

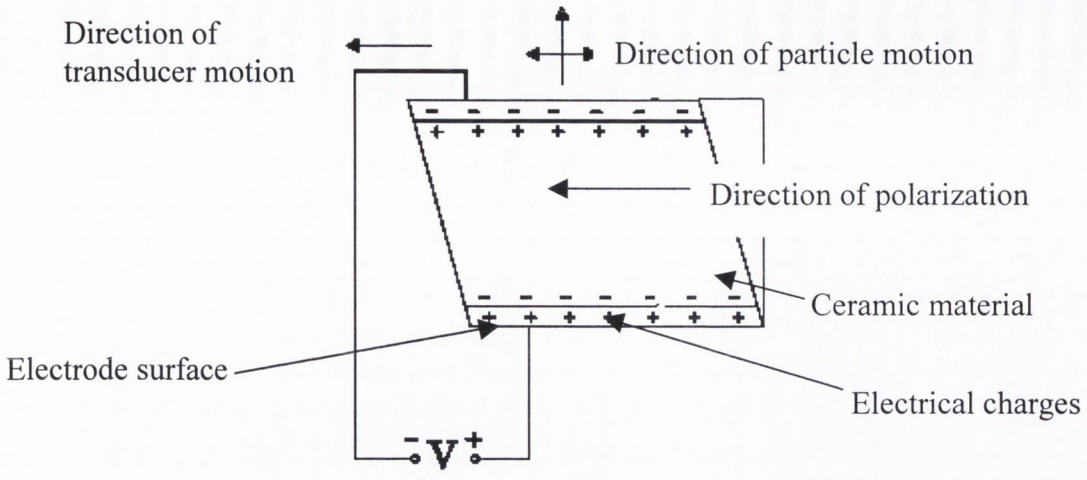

Fig. 4.8–Shear-plate transducer (from Brignoli et al., (1996))

4.4 Small Strain Stiffness (G_{max})

Extensive research on bender elements test has been carried out by many researchers in last two decades however precise guidelines for the carrying out such tests have not been published so far. It is recommended that, when using a particular test for the first time on a particular soil to determine its small strain dynamic properties, several of the methods should be tried and the results compared, in order to improve confidence in the results obtained (Jovicic et. al., 1996 and Arulnathan et. al., 1998).

In the first part of this section, a description is presented of a series of dynamic finite element analyses were carried out to investigate the accuracy of the distorted sine wave signal, which is used in bender element tests in the laboratory to calculate the G_{max}. The time gap between the transmitted and received signals from the analyses was used to back calculate the soil stiffness and this was compared with the known input stiffness which were calculated from the known input soil parameters used in finite element models. The error percentages were calculated and the different input signals were compared.

In the second section, the G_{max} values obtained from bender element tests carried out by author were compared to the G_{max} values obtained from bender element tests carried out

by Lawler (2002) and London City University (1996) and also to the values obtained from using two semi-empirical Equations 2.14 & 2.15.

4.4.1 Dynamic Finite Element Analysis

4.4.1.1 Finite Element Model

Finite element model was developed to calculate the time gap between the transmitted wave and the received wave in the cylindrical triaxial cell sample. The problem is three-dimensional in nature but to make a simplified model, two-dimensional plane strain, linear-elastic finite element analyses were carried out using the commercially available general-purpose finite element package PLAXIS. The soil was replicated using a 15-noded plane strain triangular element. For a 15-node triangle the order of interpolation for deflections is four and the integration involves 12 stress points. The dimensions of the finite element mesh (Fig. 4.9) used to model the bender element were 225mm high and 100mm wide. The behaviour of the bender elements is retroflexed by use of a 5 noded beam element that represents real plates in the out-of-plane direction and the interface between the soil and the bender elements was characterized as an interface element. The beam elements are based on Mindlin's beam theory, which allows for beam deflections due to shearing as well as bending. The bender element top cap was modelled by use of a 15-noded triangular element and the interface between the soil and the top cap was characterized as an interface element.

The boundary conditions were applied by selecting the standard fixities, which were that the horizontal top and bottom boundaries (Fig. 4.9) were fully fixed and the side boundaries were kept stress free to replicate the actual test condition (Arulnathan et. al., 1998).

In the analyses, the input voltage signal applied to the transmitting bender element was modelled by means of a transverse sinusoidal motion with an amplitude of 1.0×10^{-3} mm, which acted at a point representing the tip of the transmitter. The output voltage signal

from the receiving bender element was taken from the tip of the receiver and the travel time of a shear wave between the transmitter and the receiver were taken as the time between characteristic points in the signals recorded at these two points, based on the assumption of plane wave fronts and the absence of any reflected or refracted waves. The most commonly used characteristic points are the first peak, first trough or zero crossing of the input and output signals. The travel time between two points can be taken as the time shift that produces the peak cross-correlation between signals recorded at these two points, again based on the above same assumption (Arulnathan et. al., 1998). The load and boundary conditions and triangular mesh are shown in Fig. 4.9.

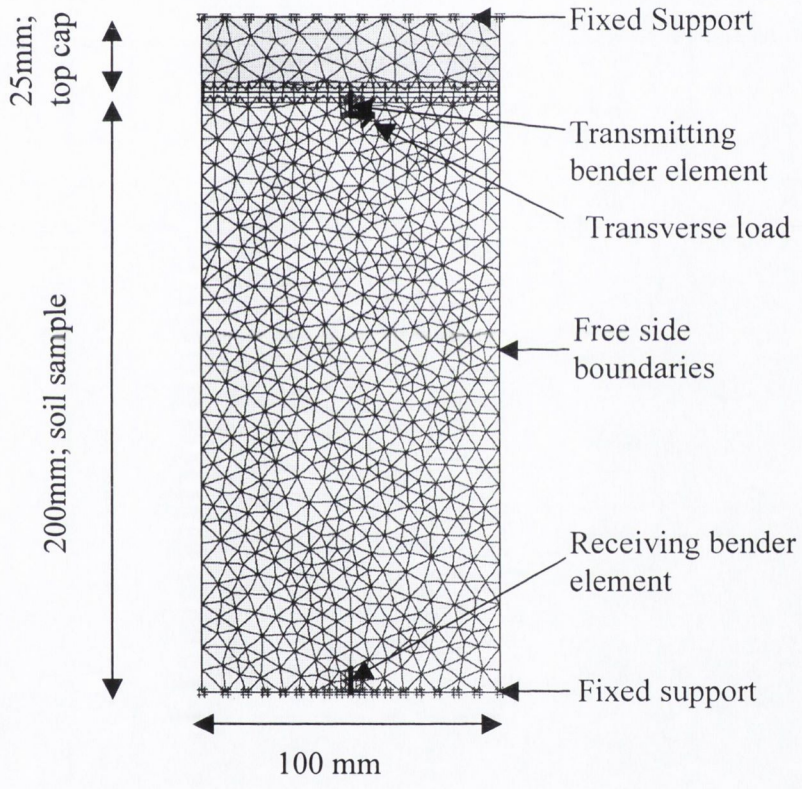

Fig.4.9–Finite element mesh

4.4.1.2 Model Properties

The material properties used in the finite element analyses are summarised in Table 4.1. The Poisson's ratio for the soil was assumed to be 0.495 to replicate the undrained

condition of the soil. The shear wave velocity of soil was 386.2 m/s which was calculated using Equation 4.12. The bender elements and top cap were made of lead zirconate and aluminium respectively.

$$v_s = \frac{\sqrt{E_{\max}}}{\sqrt{2\rho(1+\nu)}} \qquad [4.12]$$

where ρ is the soil density, E_{max} is the small strain Young's modulus, ν is the soil Poisson's ratio and v_s is the shear wave velocity.

Table-4.1 Material properties

Material	Component	Small strain Young's modulus (E_{max}), GPa	Density (ρ), kg/m^3	Poisson's ratio (ν)	G_{max}, MPa	Shear wave velocity (v_s), m/s
Soil	Specimen	1.0	2242	0.495	334.45	386.2
Aluminium	Top cap	70	2700	0.33		-
Lead Zirconate	Bender element	65	7500	0.30		-

4.4.1.3 Comparative Study Between Plane Strain Elements and Axi-Symmetric Element

A comparative study was carried out between the results obtained using plane strain elements and axi-symmetric elements to determine which elements yielded better results as model neither purely plane strain problem nor an axi-symmetry problem. The studies were carried out using 2098 Hz and 10489 Hz single sine waves. The input G_{max} was 334.45 MPa. From the model the time gap between the transmitted wave and received wave were determined and using this time gap the shear wave velocity and G_{max} were calculated. Percentages of G_{max} error were calculated with respect to the input G_{max} value. The results are presented in Table 4.2. It can be seen from the Table 4.2 that the plane strain element yielded better results.

Table 4.2– A Comparative Study Results

Frequency, Hz	% G_{max} error	
	Plane strain element	Axi-symmetry element
2098	+4.57	-19.5
10489	+1.32	-25.2

4.4.1.4 The Effects of Mesh Density

Initially a parametric study, to examine the sensitivity of the calculated of G_{max} to the mesh density, was performed. The response of both equivalent linear and non-linear finite-element models can be influenced by the mesh density. The mesh density in the wave propagation model is based on the wavelength of the shear wave. A minimum number of elements per wavelength are needed to model the shear wave propagations; in particular, the use of too coarse a finite element mesh can result in the filtering of high frequency components whose short wavelengths cannot be modelled by widely spaced nodal points. The results of the parametric study on the effects of the mesh density are presented in Fig. 4.10.

It is clearly evident from Fig. 4.10 that the mesh density has a significant effect on the propagation of waves in dynamic finite element analyses and the error in the predicted wave velocities increases exponentially with mesh density. The percentage of error due to very fine, fine, medium and coarse mesh are 0.55%, 0.97%, 2.7% and 5.5% respectively. Although the percentage errors due to the use of both very fine and fine meshes are both less than 1%, for the subsequent finite element analyses, very fine mesh densities were selected to achieve the best performance.

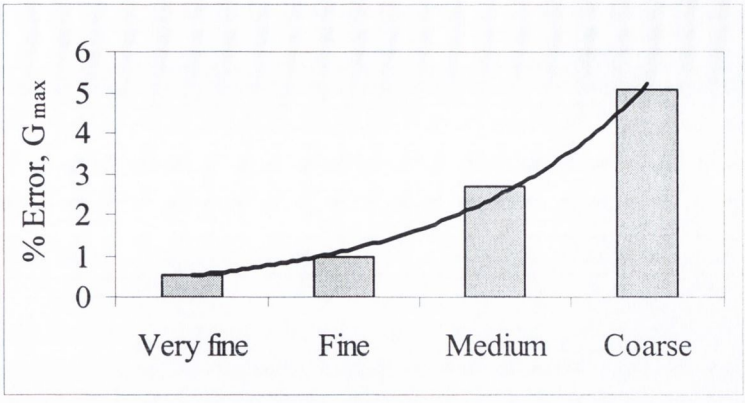

Fig. 4.10–The effects of mesh density

4.4.1.5 Measurement of G_{max} Using Single Sine Wave

In order to calculate G_{max} from the bender element tests, a single sine wave was used in the transverse direction at the tip of the transmitter bender element (Fig. 4.9) as an input signal to cause a deflection of the bender elements and to generate a wave, which went through the soil specimen to the receiving bender element. The input single sine wave is shown in Fig. 4.11.

A series of finite element analyses were carried out for different R_d ($= d/\lambda = df/v_s$, where, d is the distance between the tip of the transmitter and the receiver, λ is the wavelength, f is the frequency and v_s is the shear wave velocity) values between 1 and 8 to examine the effect of wave frequency on the output of the receiving bender element. The frequency range was 2.1 kHz to 16.78 kHz. The outputs of the receiving bender element are presented in Figs. 4.12 to 4.19 for different analyses and the percentages of G_{max} error with different R_d values are shown in Figs. 4.20 to 4.22.

The distance between the tips of the transmitter and the receiver was 0.184m and the input shear wave velocity in Table 4.1 was 386.2 m/s, as shown in Table 4.1, the measured shear wave arrival time should be 4.76×10^{-4} s. The exact arrival time was not shown by the output from the receiving bender element because there was initial downward deflection of the output signal due to the near field effect. The near field effect

is caused by very rapid compression waves that mask the first arrivals of the, slower, shear waves.

From the numerical analyses, it has been found that the input frequency has a significant influence on the near field effect and this effect is not discernible when frequency is increased. Jovicic et al. (1996) has also found similar trends. The existence of significant near field effects on the output signal can lead to errors in calculating the G_{max}. These results demonstrate the need to carry out a series of tests with different input frequencies in order to eliminate the near field effects.

The percentage errors in G_{max} obtained by comparing the calculated G_{max} values obtained from the calculated shear wave velocity values, v_s at the different R_d values with the theoretical G_{max} value of 334.45 MPa. The results of the calculation of the percentage errors in G_{max} are presented in Table 4.3. Different interpretation methods, first inflexion of the output wave, first peak to peak input and output waves, and cross correlation method, were used to calculate the arrival time from the time history plots in Figs. 4.12 to 4.19. The percentage of G_{max} error is shown in Figs. 4.20 to 4.22. Viggiani and Atkinson (1995) suggested that G_{max} should be calculated using the first inflexion of the output signal. The results shown in Figs. 4.20, 4.21 and 4.22 are the percentage errors in G_{max} based on first inflexion interpretation method, first peak-to-peak input and output waves and the cross correlation method respectively. In Fig. 4.20, the percentage error in the calculated G_{max} values obtained using the first inflexion method are 4.57%, 3.8% and 2.6% for the R_d ratios of 1, 2 and 3 respectively, while for the remaining R_d values the percentage errors are less than 2%. In Fig. 4.21, the percentage errors obtained using the first peak-to-peak input and output waves method are 6.2% and 3.89% for the R_d ratios of 1, and 2 respectively, while for remaining R_d values the percentage errors are less than or around 3%. In Fig. 4.22, the percentage errors obtained using the cross correlation method are 5% and 9% for the R_d ratios of 1, and 2 respectively, while for the remaining R_d values the percentage errors are less than or around 2%. In summary, therefore, Figs. 4.20 to 4.22 show that there is a significant similarity among the three interpretation methods and that when R_d values are 1 and 2 the percentage of error is higher than 3.5%

while it is less than 3.5% for R_d values of 3 to 8. These results suggest that the true shear wave arrival time is masked by errors due to near-field effects, as the measured arrival time and theoretical arrival time are not the same. It can also be seen from the following Figs. 4.12 to 4.19 that there is a clear initial downward deflection of the output wave at the receiver bender element for low R_d values. This downward deflection decreases and hence the potential sources of error reduce as the input frequency, i.e. R_d, increases.

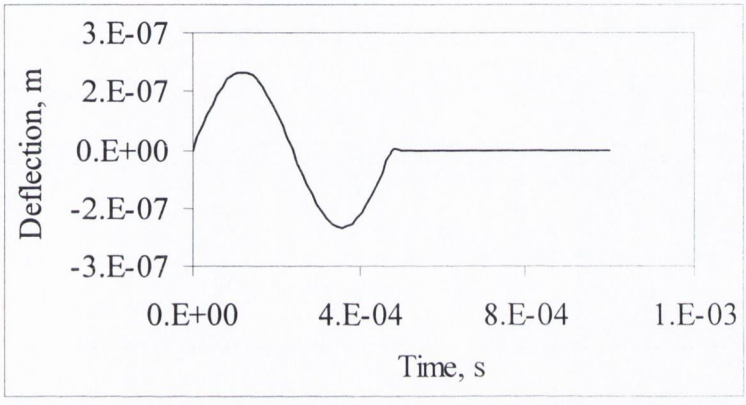

Fig. 4.11– Input single sine signal

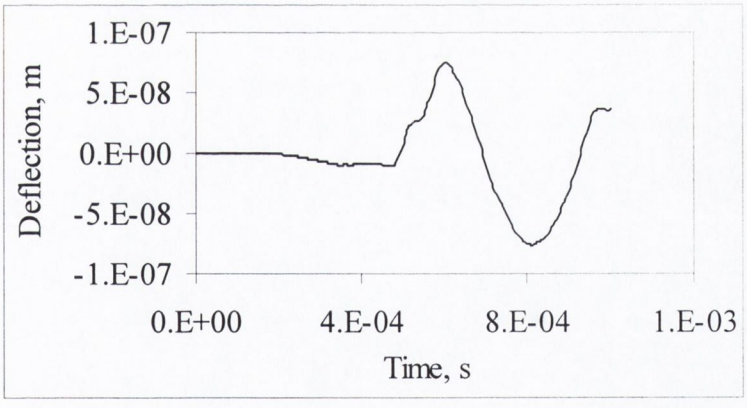

Fig.4.12–Horizontal deflection at the tip of the receiving bender element for R_d=1

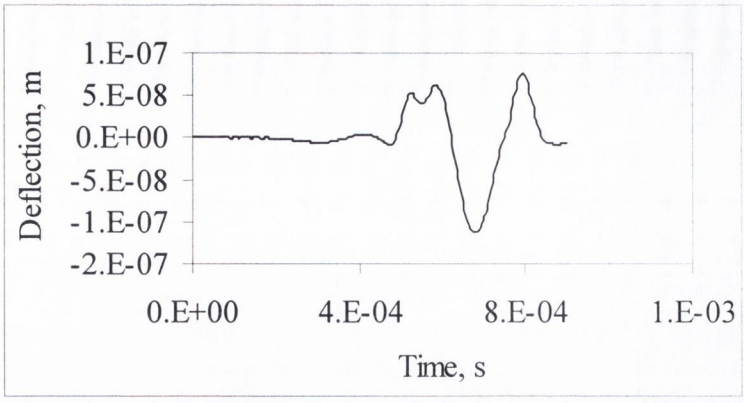

Fig.4.13–Horizontal deflection at the tip of the receiving bender element for R_d=2

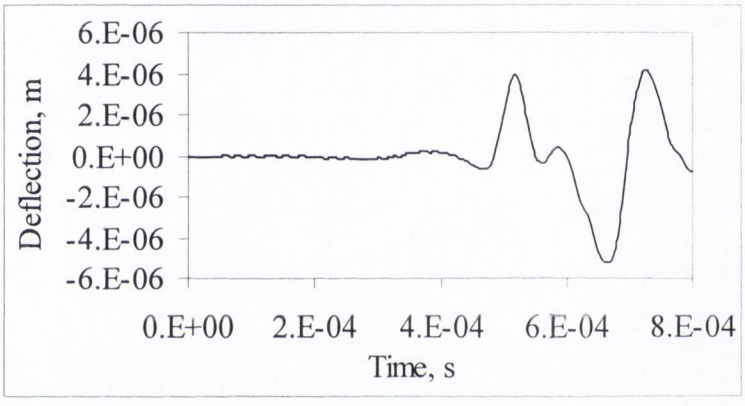

Fig.4.14–Horizontal deflection at the tip of the receiving bender element for R_d=3

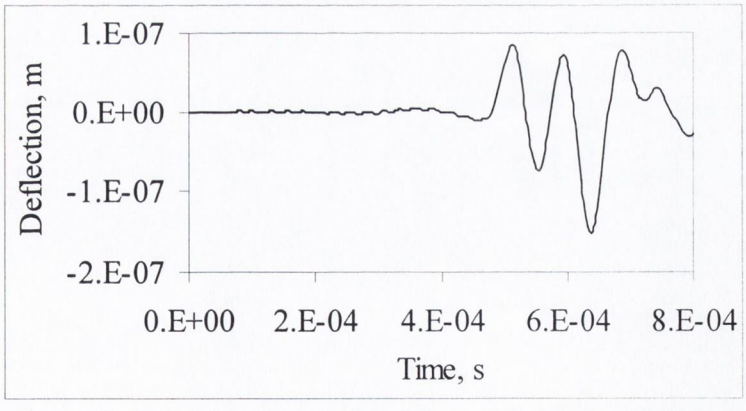

Fig.4.15–Horizontal deflection at the tip of the receiving bender element for R_d=4

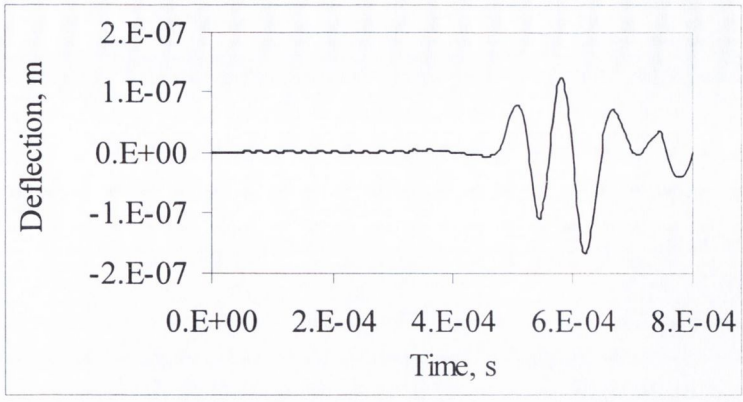

Fig.4.16–Horizontal deflection at the tip of the receiving bender element for R_d=5

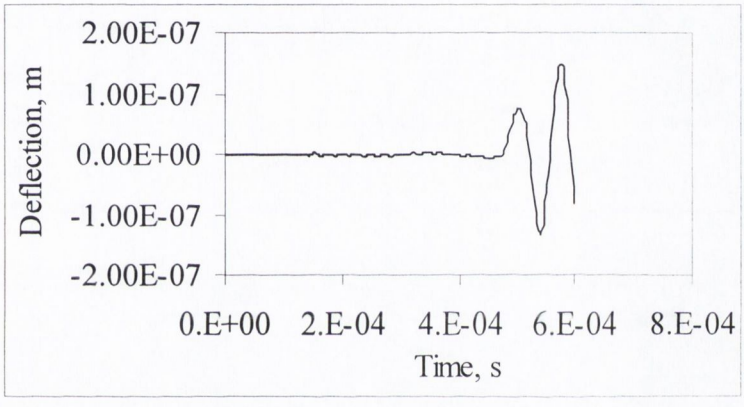

Fig.4.17–Horizontal deflection at the tip of the receiving bender element for R_d=6

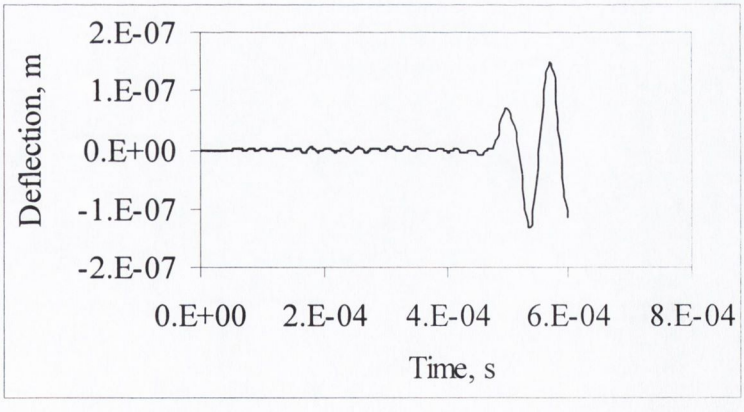

Fig.4.18–Horizontal deflection at the tip of the receiving bender element for R_d=7

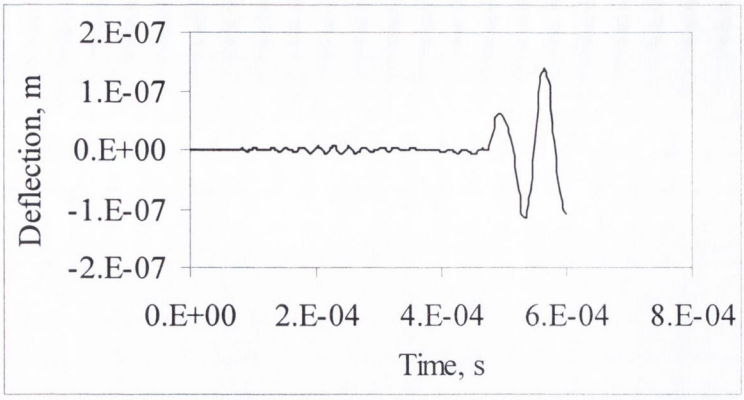

Fig.4.19–Horizontal deflection at the tip of the receiving bender element for R_d=8

Table 4.3 – % error in G_{max} calculated from shear wave velocity, v_s.

Frequency, kHz	R_d	Arrival time, s	v_s, m/s	G_{max}, MPa Measured	G_{max}, MPa Theoretical	% error
2.1	1	0.000492	373.98	313.66	334.45	6.22
4.2	2	0.000486	378.60	321.45	334.45	3.89
6.3	3	0.00048	383.33	329.54	334.45	1.47
8.4	4	0.000483	380.95	325.46	334.45	2.69
10.5	5	0.000483	380.95	325.46	334.45	2.69
12.6	6	0.000484	380.17	324.11	334.45	3.09
14.7	7	0.00048	383.33	329.54	334.45	1.47
16.8	8	0.00047893	384.19	331.01	334.45	1.03

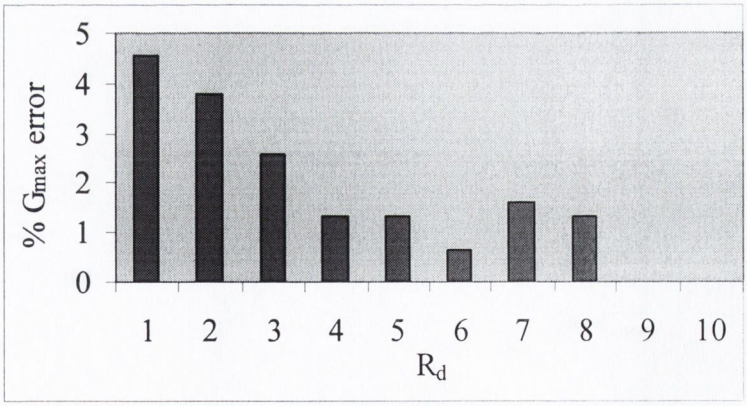

Fig.4.20–Percentage of G_{max} error with R_d (first inflexion)

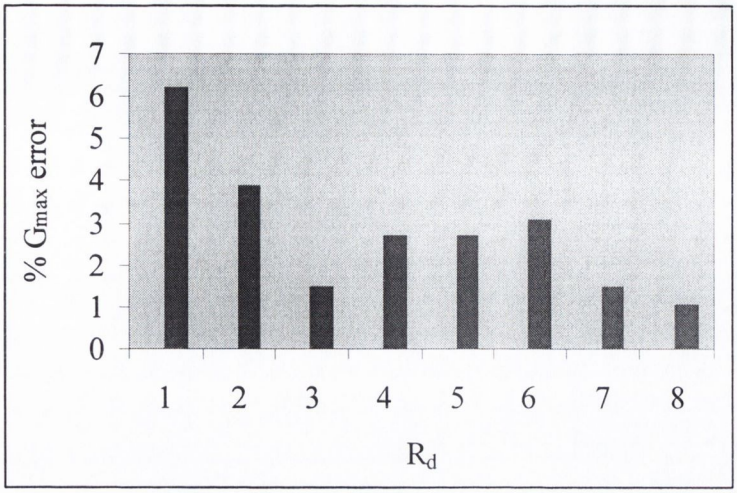

Fig.4.21–Percentage of G_{max} error with R_d (First peak to peak)

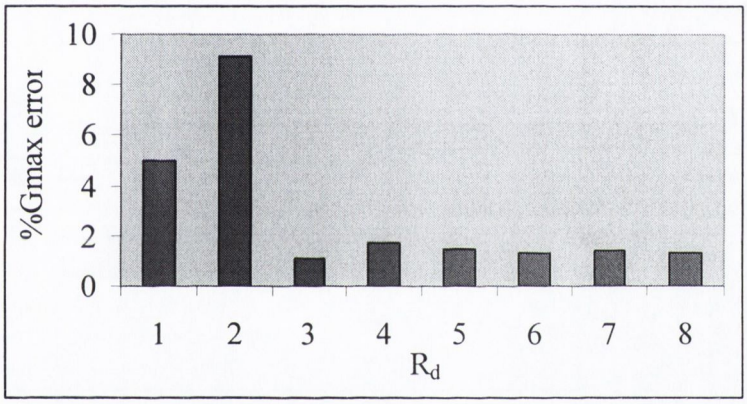

Fig.4.22–Percentage of G_{max} error with R_d (cross correlation method)

4.4.1.5 Measurement of G_{max} Using a Continuous Sine Wave

The FE analyses were carried out to study the effect of continuous sine wave on bender element test. In this section, the use of a continuous sine wave instead of a single sine wave in the transverse direction at the tip of the transmitter bender element (Fig. 4.9) as the input signal to cause a deflection of the bender and to generate a wave, which goes through the soil sample to the receiver bender is presented. The input continuous sine wave is shown in Fig. 4.23.

A similar series of finite element analyses were carried out for different R_d values between 1 and 8 to examine the effect of frequency on the output of the receiving bender element. The mesh, boundary conditions and material properties are the same as those used for the single sine wave analyses. The outputs of the receiving bender element are shown in Fig.4.24 to Fig.4.31 for the FE analysis with different R_d values and the percentage of G_{max} error with different R_d values are shown in Fig.4.32 to 4.33. It is also interesting to note that single sine and continuous sine signals behave very similarly with respect to the initial downward deflection.

The results shown in Fig.4.32 and 4.33 are based on the first inflexion interpretation method and the first peak-to-peak input and output wave method. In Fig.4.32, the percentage errors in the calculated G_{max} values using the first inflexion interpretation method are 17.4%, 4.6%, 3.74% and 3.3% for the R_d ratios of 1, 2, 3 and 4 respectively while for remaining R_d values the percentage errors are less than 2%. In Fig.4.33, the results of the analyses using first peak-to-peak input and output wave method with an R_d ratio of 1 give higher percentage errors while the remaining results give a reasonably consistent errors of between 1.37 and 2.6 percent for the calculated G_{max}. As in the case of the results using the single sine wave, the results obtained using the continuous sine wave indicate that errors due to wave interference at the boundary, the near field effect and non-one-dimensional wave travel totally mask the true shear wave arrival. The second and third potential sources of error reduce as the input frequency, i.e. R_d, increases.

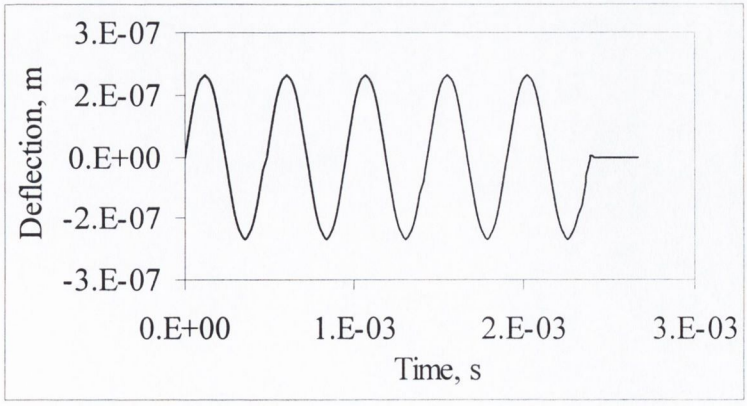

Fig. 4.23– Input continuous sine signal

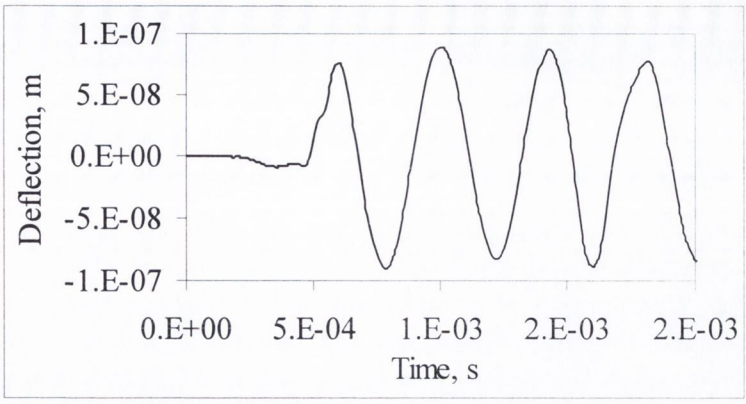

Fig.4.24–Horizontal deflection at the tip of the receiving bender element for R_d=1

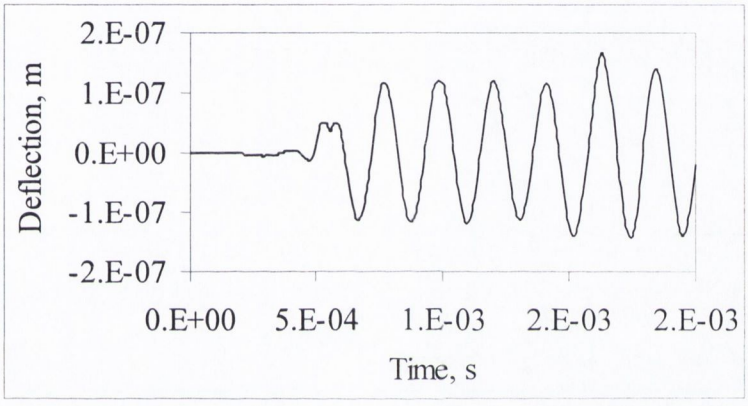

Fig.4.25–Horizontal deflection at the tip of the receiving bender element for R_d=2

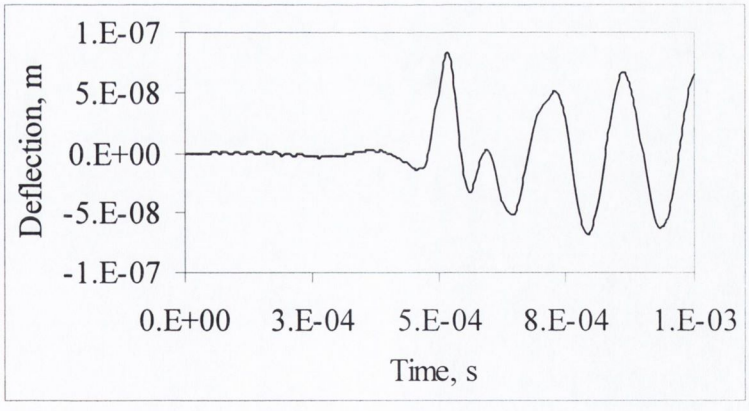

Fig.4.26–Horizontal deflection at the tip of the receiving bender element for R_d=3

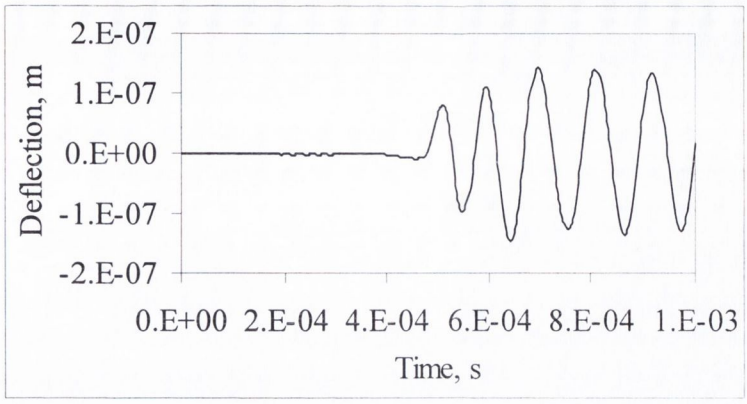

Fig.4.27–Horizontal deflection at the tip of the receiving bender element for R_d=4

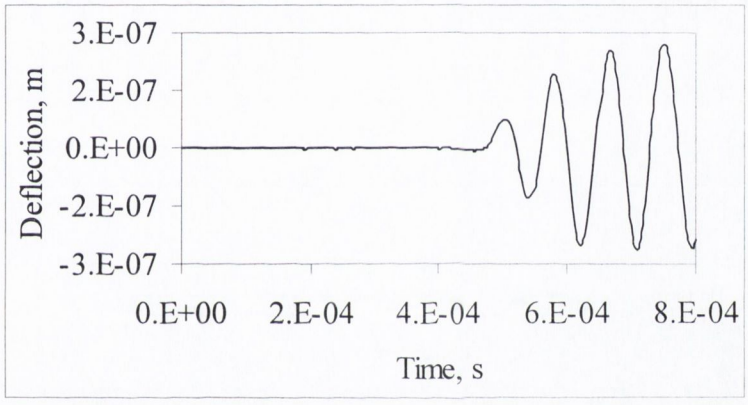

Fig.4.28–Horizontal deflection at the tip of the receiving bender element for R_d=5

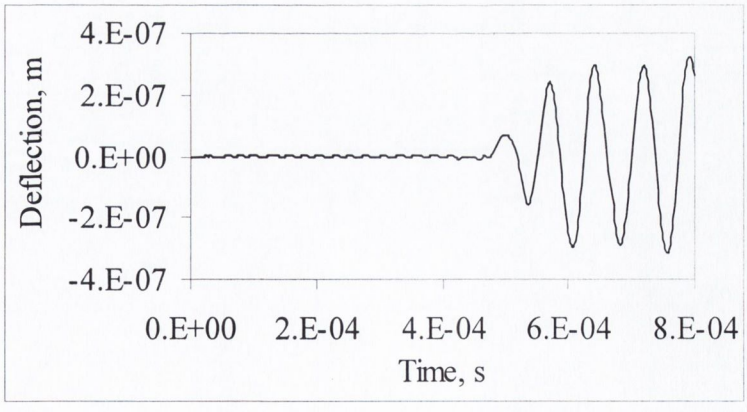

Fig.4.29–Horizontal deflection at the tip of the receiving bender element for R_d=6

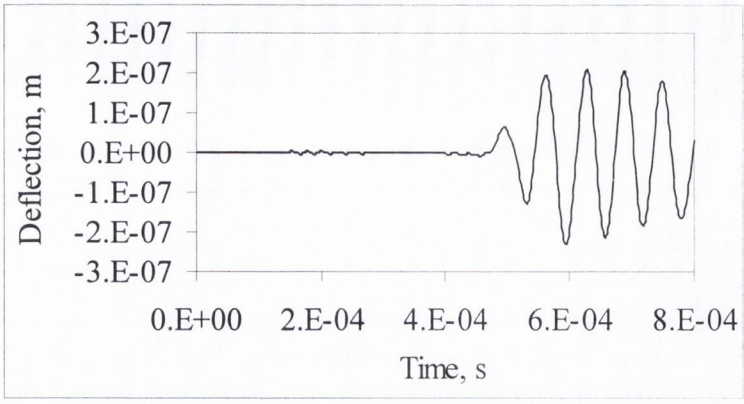

Fig.4.30–Horizontal deflection at the tip of the receiving bender element for R_d=7

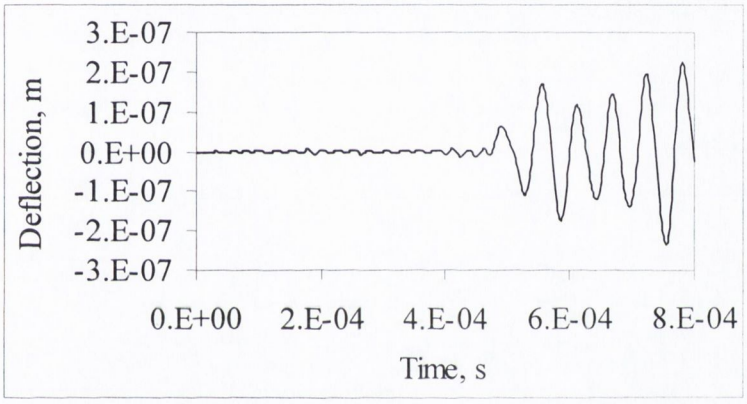

Fig.4.31–Horizontal deflection at the tip of the receiving bender element for R_d=8

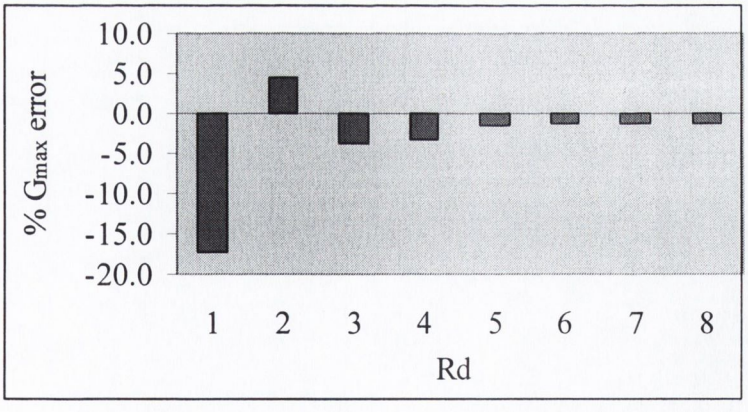

Fig.4.32–Percentage of G_{max} error with R_d (first inflexion)

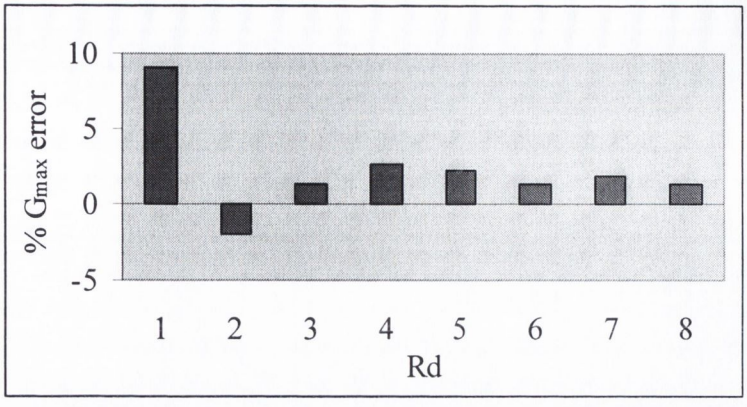

Fig.4.33–Percentage of G_{max} error with R_d (First peak to peak)

4.4.1.6 Measurement of G_{max} Using a Distorted Sine Wave

In this section, the use of a distorted sine wave instead of a single sine wave in the transverse direction at the tip of the transmitter bender element (Fig. 4.9) as an input signal to cause a deflection of the bender element and to generate a wave, which goes through the soil sample to the receiver bender element, is presented. The input distorted sine wave is shown in Fig. 4.34. The result is strongly dependent on the amplitude ratio, which is the ratio between the amplitude of the first upward cycle to the amplitude of the second downward cycle. Jovicic et. al. (1996) recommended that the amplitude of the first upward cycle of the wave should be reduced so as to cancel out the near field effect. A parametric study, to examine the effect of this ratio on the initial deflection, was performed. The analyses were carried out using amplitude ratios of 1/1.5 (0.66), 1/2 (0.5), 1/3 (0.33), and 1/4 (0.25) and the initial deflection value were normalised with respect to the initial deflection value for an amplitude ratios of 1/3. The outputs of the receiving bender element are shown in Figs.4.35 to 4.38 and the normalised result is presented in Fig. 4.39.

The initial deflection of the traces before the true shear waves arrive in Figs. 4.35 and 4.36 show that the near field is clearly present. However, this near field effect reduces as the amplitude of the first upward cycle of the wave decreases and cancels out at the cycle ratio of 1/3. Figs.4.39 compares the initial deflections for different amplitude ratios

normalised with respect to the initial deflection for a cycle ratio of 1/3. It can be seen that the normalised deflection decreases with reducing cycle ratio up to 0.33 and then it increases.

It is clearly evident from the graphs in Figs. 4.35 to 4.38 that the amplitude ratios of first upward cycle to the first downward cycle of the waves have significant effects in cancel out the near field effect. From these studies it can be concluded that the distorted sine wave is more favourable than single sine wave and continuous sine wave.

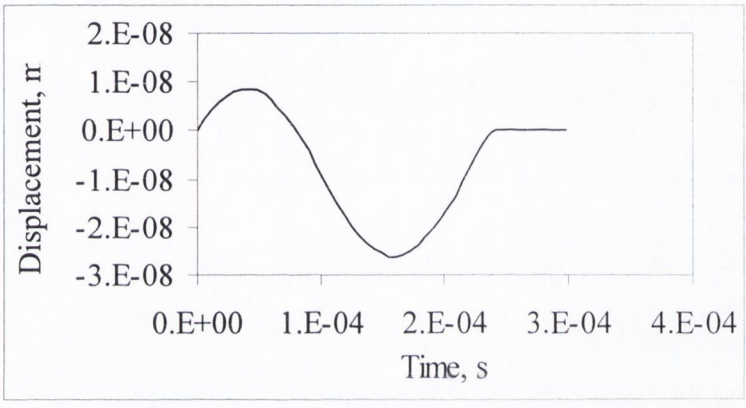

Fig. 4.34– Input distorted sine signal

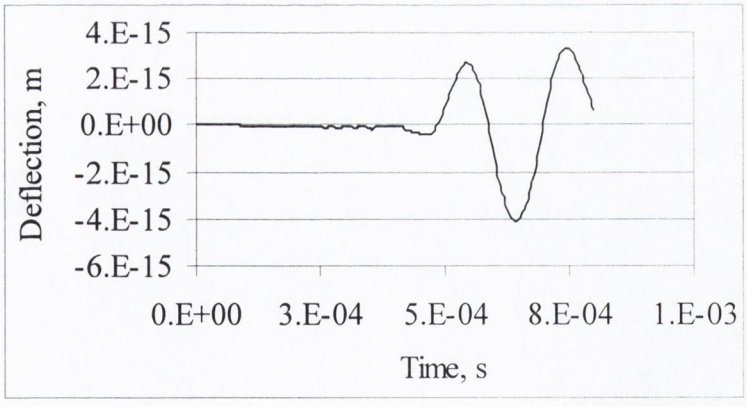

Fig.4.35–Horizontal deflection at the tip of the receiving bender element for amplitude ratio 1/1.5

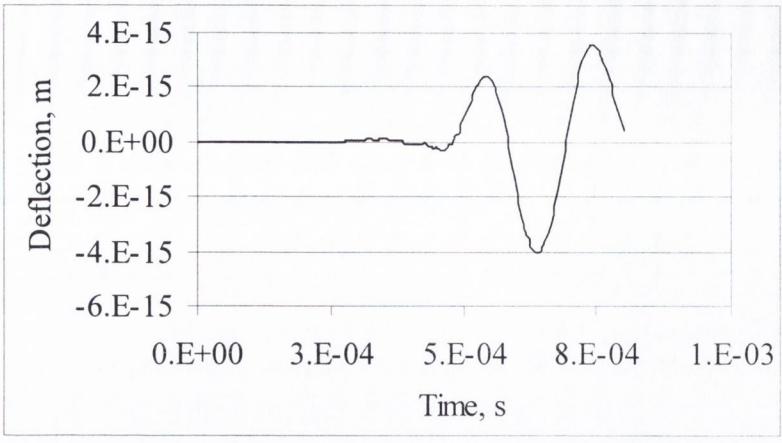

Fig.4.36–Horizontal deflection at the tip of the receiving bender element for amplitude ratio ½

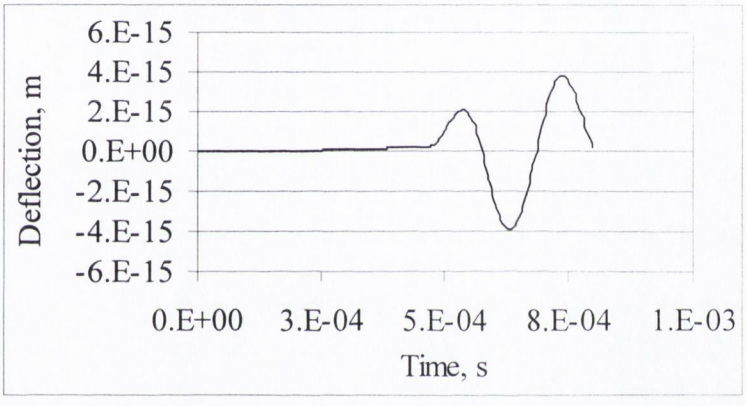

Fig.4.37–Horizontal deflection at the tip of the receiving bender element for amplitude ratio 1/3

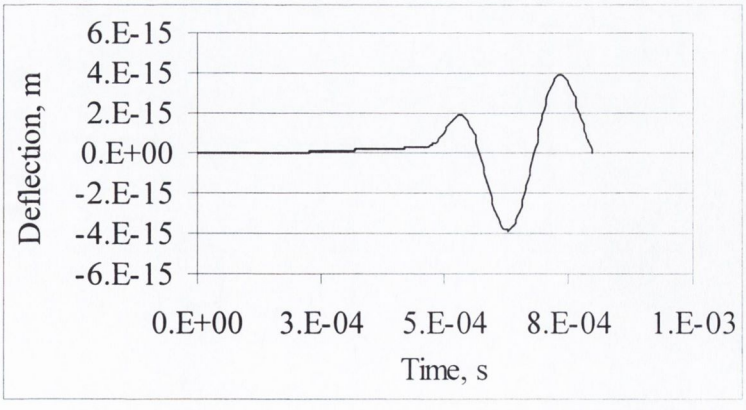

Fig.4.38–Horizontal deflection at the tip of the receiving bender element for amplitude ratio 1/4

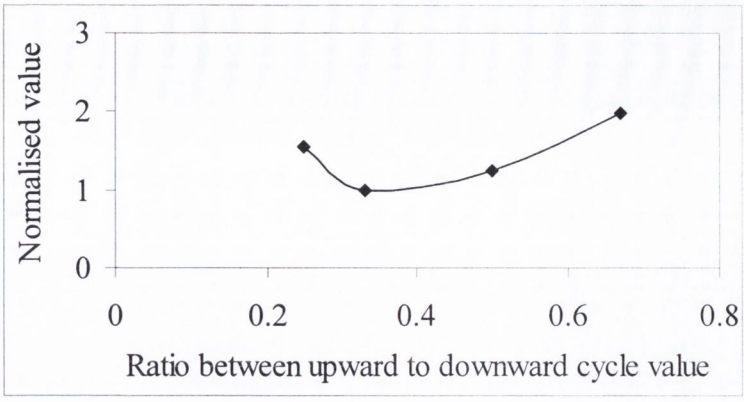

Fig.4.39–Normalised initial deflection values with respect to the initial deflection value of 1/3

4.4.2 Laboratory Tests

4.4.2.1 Introduction

The bender element tests were carried out to determine the small strain stiffness (G_{max}) for undisturbed and disturbed Dublin boulder clay with specimen of 200mm long and 100mm in diameter. The sample was isotropically consolidated under an effective stress increasing from100 kPa to 400 kPa and again unconsolidated down to the 100 kPa.

4.4.2.2 Laboratory Test Equipments

The following equipment was used with the Wykeham-Farrance 100 mm triaxial cell to carry out the bender element tests:

- Bender elements in top and base pedestals.
- A Thurlby Thander TGA 1240 function generator.
- A Pico ADC-212 high-resolution oscilloscope.
- Pico Scope software.
- Shielded output cables.

Bender elements are usually available in two versions that differ simply in the electrical connection to the two polarized plates, which is either a series or a parallel connection. The receiver bender element is normally connected in series as it gives a higher voltage output response for a given distortion. This response occurs because the voltage is equal to the sum of the potentials available to the electrodes of each ceramic element. The transmitter bender element was connected in parallel as it gives the largest distortion for a given input. This performance is helpful in the case of a low intensity supply source. With this connection, the available voltage was applied to each ceramic plate and is not divided between the two plates as in the series connection (Brignoli et al., 1996). The transducers were coated with a waterproofing material and insulated. The electrical cables used for connections with external devices were coaxial.

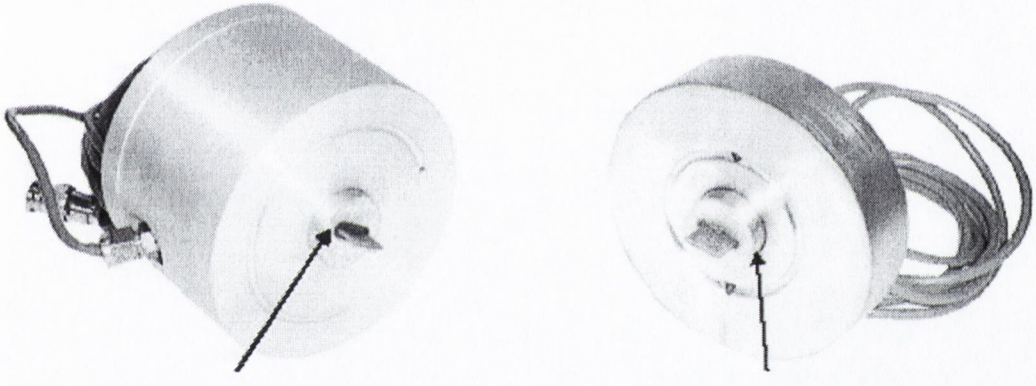

Top cap with bender element transmitter

Base pedestal with bender element receiver

Fig.4.40–Bender elements

The excitation signal, produced by a function generator (Fig.4.41), was amplified and sent to the piezoelectric transmitter transducers in the top cap. Signals were generated by a function generator with maximum peak-to-peak amplitude of 20 V. The function generator, a Thurlby Thander TGA 1240 arbitrary wave generator, allowed, in addition to the standard waveforms, user defined waves. This was necessary to allow the advanced analysis applied in the test series. Waves transmitted through the soil specimen were recorded at the other end by the receiver transducer. The excitation signal and amplified

receiver signals were converted to a digital signal by an ADC and displayed on an oscilloscope. Since the times necessary for the waves to propagate through the specimen were very short and small magnitude deformation/voltage involved, the oscilloscope needed to be of very high resolution.

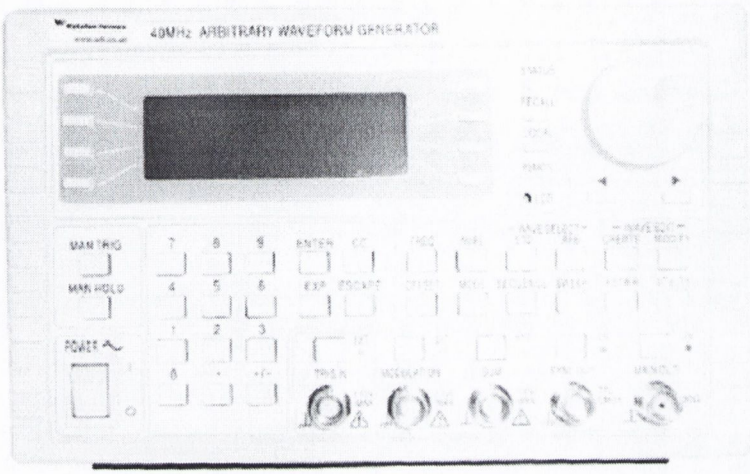

Fig.4.41–Function generator

The important aspects of an oscilloscope for the study of shear waves through soils include the sampling rate, resolution, and storage capabilities. Brignoli et al. (1996) suggest that a minimum sampling rate of 20 x 10^6 samples per second is necessary for accurate shear wave velocity measurements. Typical sampling rates for new digital oscilloscopes are 100 x 10^6 samples per second.

The resolution of the oscilloscope, meaning the smallest voltage signal that can be accurately observed, is extremely important. The received signal of the shear wave velocity is very small, usually between 0.1 and 5 mV. Using an oscilloscope with good resolution can remove the need for complicated post-processing techniques such as stacking (adding signals to increase the voltage of the received signal) or using amplifiers on the received signal.

The Pico ADC-212 computer based oscilloscope (Fig.4.42) was used for this study. The computer was a high speed Pentium 3 processor of 750 MHz speed. The traces obtained

were converted to spreadsheet cells to allow extensive analysis. The characteristics of the Pico ADC-212 PC Oscilloscope are following:

- 12 bit resolution
- ±1% accuracy.
- 3 MS/s sampling rate
- 32k waveform buffer
- Simply plugs into any desktop or laptop PC.

The 3 MS/s sampling speed and 32 KB waveform buffer made the ADC-212 an ideal solution for high speed data acquisition. The 12-bit resolution in the Y-axis gives the ADC-212 the ability to detect changes as small as 0.024 per cent (Pico, 2001).

Fig.4.42–ADC-212 Oscilloscope

4.4.2.3 Preparation of Undisturbed Soil Sample

The undisturbed sample was not obtained from the same area as where the vibration studies were carried out; however it was black boulder clay from Dublin and its wet density was 2200kg/m^3. Two holes, the size of a bender element, were made in the top and bottom surfaces of the cylindrical soil specimen and filled with remoulded boulder clay, from which the coarse fraction had been removed. This allowed the bender elements to protrude into the soil and ensured that the elements were surrounded by the soil (Lawler, 2002).

4.4.2.4 Calibration

Calibration of the complete system was necessary so that any delay time introduced in the measurements by the electronics, ceramics, and coating materials could be determined. Calibration was carried out by placing the two platens in direct contact and measuring the time interval between the initiation of the electrical impulse sent to the transmitter and the initial arrival of the waveform recorded at the receiver. The top platen was marked with respect to the base platen in order to avoid any ambiguity in test interpretation (Lawler, 2002). The measured waveforms and calibration times for bender elements obtained are shown in Fig. 4.43 and show that there was not any time lag.

In the calibration process, the absence of wave transmission paths other than through the soil specimen was checked. In this case, the calibration was carried out by placing the two platens without contact in the triaxial cell and then pulses were generated by the transmitter; no wave arrivals were recorded by the receiver. The only meaningful transmission path during the soil testing was, therefore, represented by the path through the specimen (Lawler, 2002).

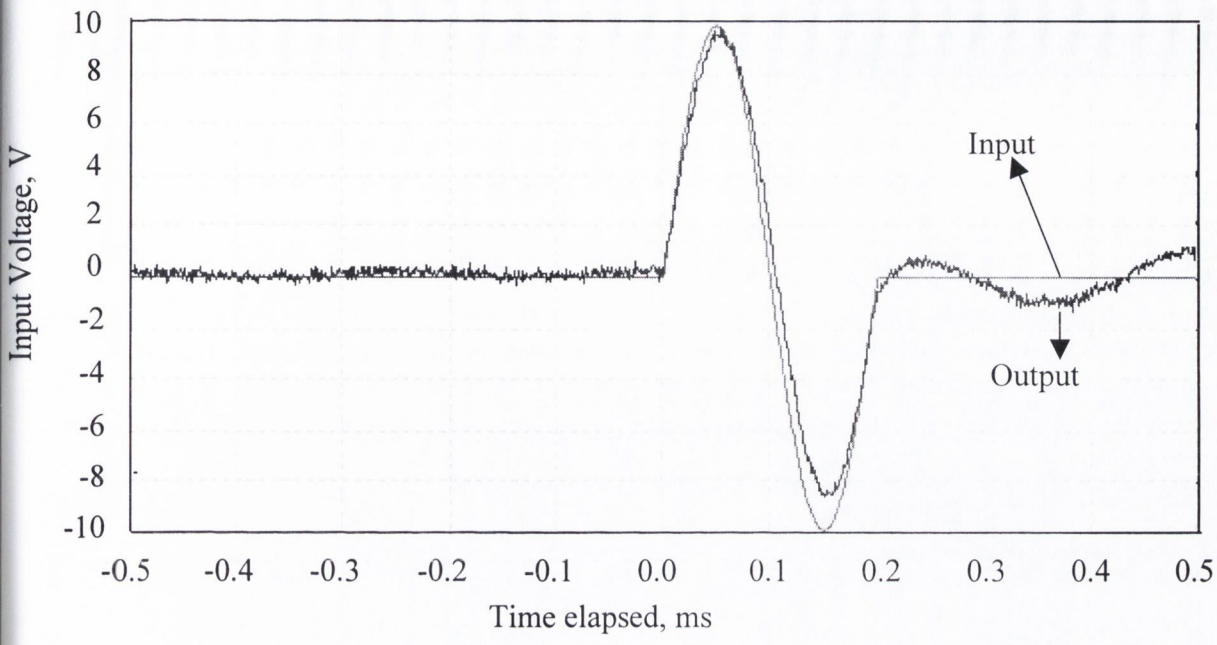

Fig.4.43–Bender element calibration results

4.4.2.5 Measurement Method

Measurements were carried out by exciting the transmitter with a single pulse of the standard or arbitrary waveform and detecting the first arrival of the wave at the receiver. Signals were sent top down, from the top cap to the bottom base. Lings and Greening, (2001) found that there was no difference between when signals are sent top down or bottom up. The function generator was programmed with a manual trigger. Initially bender element tests were performed on homogeneous clay using a standard sine wave and arbitrary distorted sine waves. Input and output traces of a standard sine wave are shown in Fig. 4.44. Fig. 4.44 shows the presence of a near-field effect. Following the tests on homogeneous clay, tests were carried out on undisturbed Dublin boulder clay using only an arbitrary distorted sine wave and typical input and output traces are presented in Fig. 4.45 which show no near-field effect.

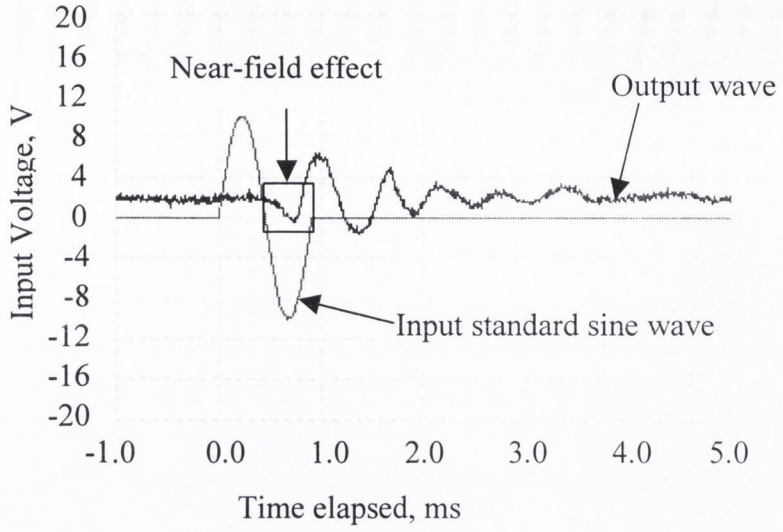

Fig.4.44–Typical standard sine wave

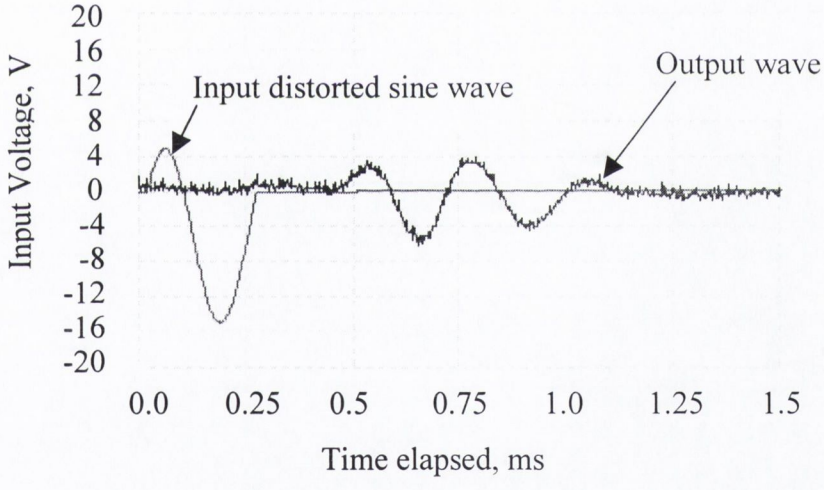

Fig.4.45–Typical arbitrary distorted sine wave

4.4.2.6 Results and Discussions

The values of G_{max} calculated from the bender element tests on the Dublin boulder clay are presented in Fig. 4.46. The tests were carried out using the distorted sine wave developed by Jovicic et al. (1996) at different confining pressures under isotropic compression and swelling conditions. The frequency of the input signal was selected by

manually varying it to visually optimise the strength and clarity of the output signal. The shear modulus interpreted from these tests represents the elastic modulus of the soil at very small strains. Fig. 4.46 shows the shear modulus increasing as the confining pressure increases, therefore, the stiffness is positively related to the confining pressure. To assess the performance of the bender element tests, the G_{max} results obtained from the bender element tests carried out by the author are compared with the bender element results obtained by Lawler (2002) and London City University (LCU) on boulder clay in Dublin Port Tunnel area. It can be seen from the Fig. 4.46 that a reasonably agreement was obtained between the author's results and the Lawler's (2002) results although the samples were not taken from the same location and LCU results are bit lower than the author's results. The results confirm the remarkable consistency with location in the Dublin Port Tunnel area observed in terms of small strain stiffness (G_{max}). Although the soil samples were not taken from the vibration studies area, the G_{max} values obtained by the author were relevant for use in the FE analyses. The boulder clay parameter values given by NCC are presented in Table 4.4. The G_{max} value of the Dublin boulder clay given by NCC was 330 MPa. It can be seen from the Fig. 4.46 that the average G_{max} value obtained by LCU is around 350 MPa. It should be noted that Fig. 4.46 is drawn with increasing confining pressures plotted downwards. This is to reflect the fact that the confining pressure increases with depth in the ground and hence G_{max} increases with increasing depth.

The Ultrasonic pulse velocity method was used to determine the dynamic elastic modulus (E) of limestone. Two samples were obtained from County Meath and one sample was from Portlaoise in Ireland. The velocity of an ultrasonic pulse travelling in a limestone depends on the density and elastic properties of the limestone. The distance between the transmitter and the receiver is divided by the time difference between the voltage pulses to obtain the pulse wave propagation velocity. After getting the pulse wave velocity, V, the following equation can be used to determine the dynamic elastic modulus (E) of limestone.

$$V^2 = \frac{E(1-\nu)}{\rho(1+\nu)(1-2\nu)} \qquad [4.13]$$

where ρ is the density and ν is Poisson's ratio.

The experimental results are presented with NCC parameter values in Table 4.4. The values in Table 4.4 shows that the author's stiffness values are a bit higher than the values given by NCC, however there is no significant difference between them.

The documentation of geotechnical parameters values of Dublin boulder clay and rock were presented in Appendix A. Due to lack of more details of NCC data and documentation, these all documentation were obtained from Dr. Eric Ferrall, Senior Lecturer, Dept.of Civil Engineering, TCD.

Table 4.4- Values of parameters for Dublin boulder clay and limestone

Parameter	Dublin boulder clay (NCC)	Limestone	
		Author (3 samples)	NCC
Density, kg/m^3	2240	2670, 2664 & 2686	2710
Young's modulus, E_{max}, GPa	1.0	83.4, 73.9 & 82.6	60
G_{max}, GPa	0.33	33.4, 29.6 & 33	24
Damping ratio, %	1.75	--	1

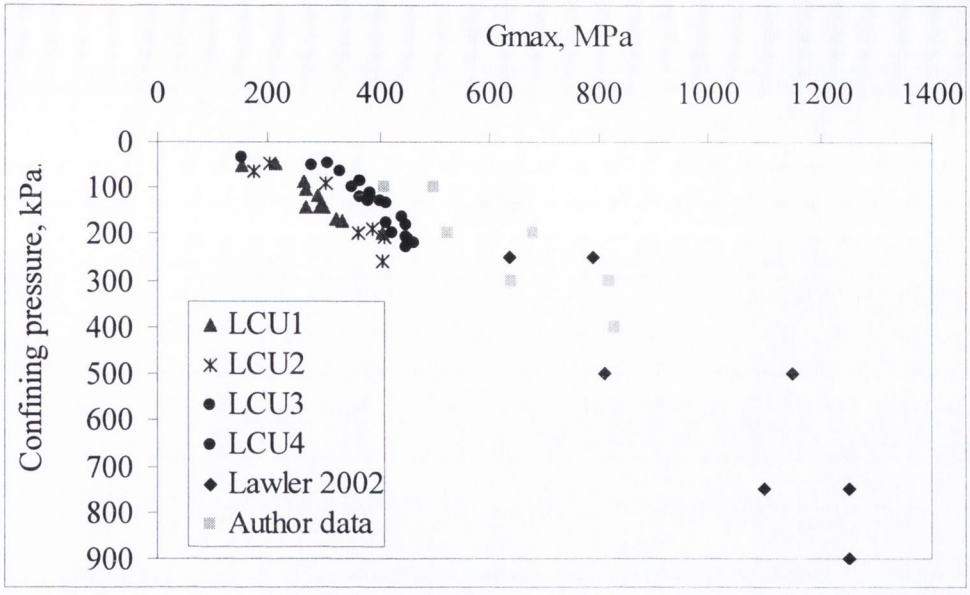

Fig.4.46–The effects of confining pressure on G_{max}

4.5 Comparison between G_{max} values obtained from Bender Element Tests & a Semi-Empirical method

A comparison study was carried out between G_{max} values obtained from bender element tests and from two semi-empirical Equations 2.14 and 2.15. Two semi-empirical equations, which are taken from Hardin (1978) and Viggiani & Atkinson (1995), were discussed in Section 2.5.4 in Chapter 2. The G_{max} values obtained from the bender element tests and the semi-empirical equations are shown in Fig. 4.47. Good agreement was found between the G_{max} values obtained from the bender element tests carried out by London City University and the semi-empirical equations. While the G_{max} values obtained from the bender element tests carried out by the Author's and the Lawler (2002) were bit higher than those obtain from the semi-empirical equations, as shown by the values and graphs in Fig. 4.47. In the absence of measured G_{max} from laboratory or field tests, Viggiani & Atkinson (1995) semi-empirical equation can be used to obtain G_{max} value for Dublin boulder clay.

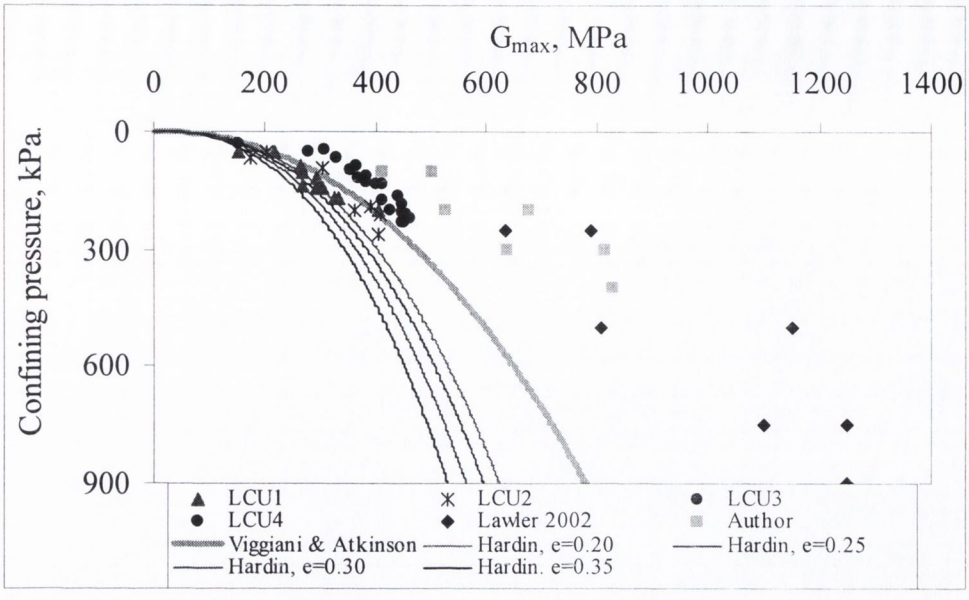

Fig. 4.47–Comparison of bender element test results with empirical results

4.6 Determination of Damping Ratio

The purpose of this part of the research was to determine the damping ratio from the bender element tests. Finite element analyses were carried out to estimate the natural frequency of the soil. Based on this natural frequency, further experimental work was carried out to obtain response spectrum. The damping ratio is estimated using the half bandwidth method at points on the response spectrum curve around the natural frequency.

4.6.1 Finite Element Analyses

Three-dimensional finite element analyses were carried out using a commercially available general-purpose finite element package ABAQUS to extract the natural frequencies of the sample. The natural frequency was used to select the starting for the bender element tests which was chosen to be less than the natural frequency. The soil sample and top cap were cylindrical in shape and replicated by the use of an 8-nodded linear brick element. The interface between the soil and the top cap was characterized as

a rough contact element. All the nodes on the bottom surface of the sample were fixed while the top and side surfaces of the sample were free so that it acted as a cantilever beam as shown in Fig.4.48. The diameter of the top cap and soil sample was 100mm and heights of the top cap and soil sample were 25mm and 200mm respectively, giving a length to diameter ratio of 2.0. The modelling of the bender elements themselves was not important and was neglected as the modelling focused on determining the natural frequencies and mode shapes of the soil sample.

The material properties of the top cap and soil sample were assumed to be linearly elastic and are shown in Table. 4.5.

Table 4.5–Material properties

Material	Stiffness (E), GPa	Density, kg/m^3	Poisson's ratio
Soil	1.36	2242	0.495
Top cap	70	2700	0.33

The FE analyses were performed at 100 kPa and 200 kPa confining stress and for length to diameter ratio of 2.0. The results are presented in Table 4.6 and the mode shapes are shown in Fig. 4.49. Different mode shape and corresponding deformation type and resonance frequency are shown in Table 4.7. From Fig. 4.49 it can be seen that the first mode is a flexural mode dominated by shear deformation. For long samples or very large top cap masses, the first mode of the cantilever beam will be predominately of flexure (Brocanelli & Rinaldi, 1998).

A parametric study was also carried out to examine the effect of the water mass on the natural frequency of the sample. In any types of triaxial testing, the water is used to apply the confining pressure. The water is considered as an incompressible and inviscid fluid. In a bender element test, the effect of the water on the natural frequency of an elastic cylinder can be taken in to account by introducing an additional mass to the system. The additional mass per unit length is estimated using following equation (Wilson, 2003):

$$m_a = C_A \rho \pi \frac{d^2}{4} \quad [4.15]$$

$$C_A = C_M - 1 \quad [4.16]$$

Where, m_a is the added mass per unit length, C_A is the non-dimensional added mass coefficient, ρ is the water density, d is the diameter of the cylinder and C_M is the inertia coefficient. The value of C_M is based on the cylinder length to diameter ratio (Wilson, 2003) as shown by the C_M values in Table 4.8. Hence resonance frequency calculations, including the effects of the confining water, can be easily performed using a virtual mass composed of the actual body mass and the added mass given above.

4.6.2 Experimental Work

Bender element tests were performed on Dublin boulder clay with different effective confining stresses. In these tests, the top bender element was excited with a sine signal of constant voltage and the amplitude was measured at the receiver bender element. This process was repeated at different frequencies until the whole spectrum of the sample response was defined. As noted in Section 4.6.1, the selection of frequency was based on the results of the finite element analyses.

4.6.3 Results and Discussions

Fig. 4.50 shows the frequency response obtained for the sample tested using confining stresses of 100 kPa and 200 kPa. The identified experimented resonant frequencies are indicated in Fig. 4.50. The experimented damping ratios were calculated as 5.66% and 5.23% for these confining stresses using the half power method, described in section 2.6 at the points on the curves around the resonant frequency. The finite element calculated resonance frequency, the experimentally determined resonant frequencies and the estimated damping ratio are presented in Table 4.6. The finite element analyses for the resonant frequency of first mode were carried out both without added mass ($C_A = 0$) and with an added mass coefficient of $C_A = 0.76$, which corresponds to a length to diameter

ratio of 2.25, to allow comparisons. The resonant frequencies obtained with no added mass were found to be higher than those obtained with added additional mass.

The finite element and experimental results show that the resonant frequencies increase with increasing confining pressure. The graphs in Fig. 4.50 shows that the input and output waves amplitude ratios of the observed peaks decrease with increasing stress level. In all cases the experimental resonance frequencies are larger than the predicted frequencies. The finite element analyses do not model the boundaries perfectly: i.e. the influences of the rubber membrane and the not fully rigid mounting of the bottom cap are not taken in to account. Additionally the modelling of the effects of water in the cell by an additional mass might not be sufficiently correct. A more correct finite element analysis could help predict the resonant frequencies more accurately but the results from these finite element analyses are not important as they are only used to select the starting point for the frequencies in the bender element tests.

The damping ratio, ξ, values are presented in Table 4.9. In Table 4.9 it can be seen that the damping ratio obtained from the laboratory tests is higher than data given by NCC. A possible reason for this is the dependence of the damping ratio on the frequency.

Lin et al. (1996) carried out cyclic torsional shear tests on Ottawa sand and I-lan River sand under different confining pressure and frequency and found that the damping ratio increased significantly with increasing excitation frequency. With a strain amplitude of 4 x 10^{-5}, the damping ratio was about 2.5% when cycled under a frequency of 0.1 Hz. When the frequency increased to 20Hz, the damping ratio became about 6%, which is 2.4 times the damping ratio at the frequency of 0.1 Hz. This phenomenon was for Ottawa sand but a similar trend was also found for the I-lan river sand. Lin et al. concluded that the damping ratios for both sands increased with increasing shear strain and frequency and with decreasing confining pressure.

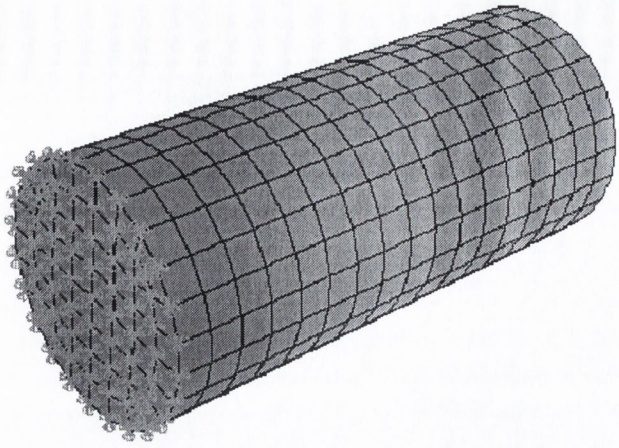

Fig.4.48–Three-dimensional finite element model

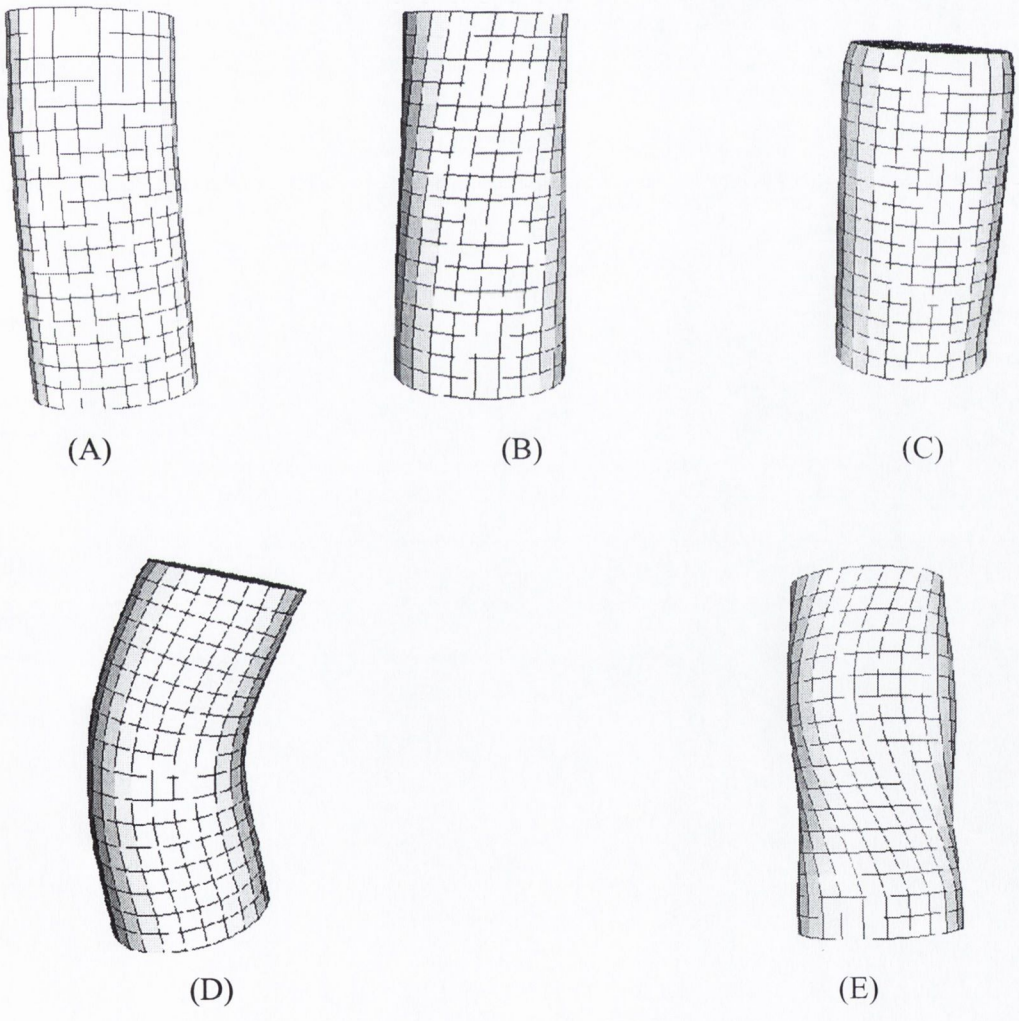

Fig.4.49–Different mode shapes for undisturbed boulder clay, cell pressure 100 kPa and $C_A = 0$; (A) first (B) second (C) third (D) fourth and (E) fifth mode.

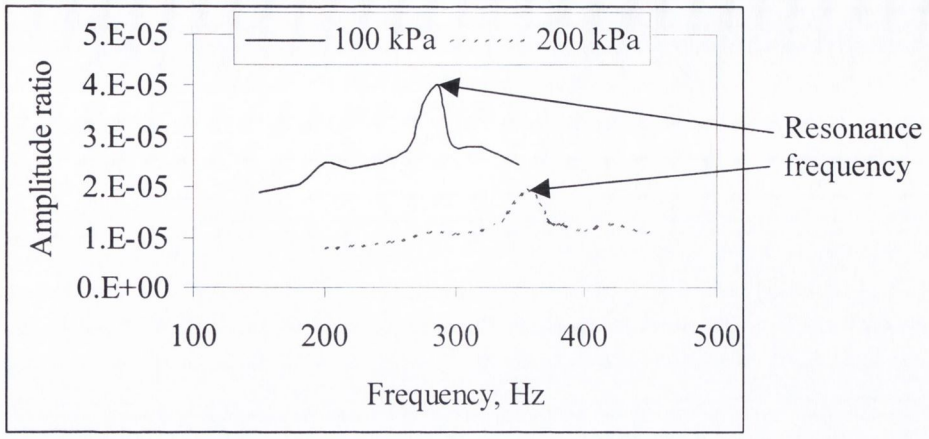

Fig.4.50–Experimental frequency response spectra

Table 4.6–Results

Effective confining stress, kPa	Resonant frequency, Hz			Experimental Damping ratio, %
	Calculated Finite element method		Determined from laboratory tests	
	$C_A = 0$	$C_A = 0.76$		
100	197.19	170.57	285	5.66
200	222.26	192.26	355	5.23

Table 4.7–Different mode shapes and corresponding deformation types and resonant frequency

Mode shape	Deformation type	Resonance frequency, Hz
1	Flexural	197.2
2	Torsional	486.2
3	Longitudinal	833.0
4	Flexural	1472.0
5	Torsional	1798.5

Table 4.8–C_M value

Length/Diameter	C_M
1.2	1.62
2.5	1.78
5	1.90
9	1.96
∞	2

Table 4.9–Damping ratio, ξ, values for Dublin boulder clay

Material Parameter	NCC results	Laboratory results at 100 kPa	Laboratory results at 200 kPa
ξ	1.75	5.66	5.23

4.7 Summary

The analytical results suggest that the choice of input signal is important when carrying out bender element tests to determine the G_{max} values. It is found from the FE analyses that a distorted sine wave is most favourable than single sine wave or a continuous sine wave, as also experimentally observed by Jovicic et al., (1996). The distorted sine wave is better at cancelling out the near field effect than a single sine wave or a continuous sine wave. However, this result is strongly dependent on the ratio between the amplitudes of the first upward wave to the first downward wave of the input signal.

The G_{max} values obtained from single sine and continuous sine waves presented in this study suggest that if the ratio R_d is three or above, the near field effect does not significantly affect the measured travel time. The value of R_d represents the number of wave lengths that occur between the bender element transmitter and the receiver, and which controls the shape of the received signal through the degree of attenuation of each term of Equation 4.17 that occurs as the wave travels through the sample. The Equation 4.17 was described in Section 2.62 in Chapter 2. For low values of R_d there is an initial

downward deflection of the trace before the shear wave arrives, representing the near field effect given by the third component of Equation 4.17. For high values of R_d the last two terms of Equation 4.17 are not significant and initial downward deflection of the trace before the shear wave arrives are almost absent.

$$\Gamma = \frac{1}{d} e^{-i(\varpi d / v_s)} + \left(\frac{1}{i\frac{\varpi d^2}{v_p}} - \frac{1}{\frac{\varpi^2 d^3}{v_p^2}}\right) e^{-i(\varpi d / v_s)} - \left(\frac{v_s}{v_p}\right)^2 \left(\frac{1}{i\frac{\varpi d^2}{v_p}} - \frac{1}{\frac{\varpi^2 d^3}{v_p^2}}\right) e^{-i(\varpi d / v_p)} \qquad [4.17]$$

A reasonably agreement was found between the G_{max} values obtained from the author's bender element tests and the Lawler's (2002) bender element tests. Good agreement was found between the G_{max} values obtained from the London City University bender element tests and the semi-empirical equations. While the G_{max} values obtained from the Author's and the Lawler's (2002) bender element tests were bit higher than those obtain from the semi-empirical equations. In the absence of measured G_{max} from laboratory or field tests, Viggiani & Atkinson (1995) semi-empirical equation can be used to obtain G_{max} value for Dublin boulder clay. Bender element test results are important for theoretical studies. The small strain stiffness is dependent on confining pressure and it increases with increasing the confining pressure. From bender element tests it is able to measure the small strain stiffness with different confining pressure and can use for theoretical studies.

A bender element resonant test was used to measure the damping ratio of Dublin boulder clay. First a finite element analysis was carried out to determine the resonant frequency of first mode to be used in the laboratory tests. The influence of the confining water was modelled by adding an extra mass to the total mass. In the laboratory, the tests were carried out at different frequencies to obtain the response spectra and a half power method was used to calculate the damping ratio from the vibration amplitudes at the resonant frequency.

The damping ratio values determined from the laboratory tests were found to be higher than those supplied by the Nishimatshu Construction Company Ltd. The reason for

obtaining higher damping ratios from the laboratory bender element tests could be the frequency dependency of the damping ratio. The tests were carried out under a range of frequencies to obtain the response spectrum and the damping ratio was determined from the vibration amplitudes at the resonant frequency. It can be concluded that the bender element tests give different range of damping ratio due to the frequency dependence of the damping ratio.

CHAPTER 5

FIELD MEASUREMENT AND ANALYSIS OF VIBRATIONS

5.1 General

In this chapter the results of the TBM excitation and ground vibration measurements are presented and discussed. The objective of the TBM programme was to monitor the TBM excitation for use as an input in the finite element analyses. The monitored vibration levels at the surface area were compared with finite element results and their magnitude was examined to assess if structural damage would be caused by the TBM. Of secondary concern was the annoyance that could be caused if the TBM vibrations were perceptible to humans and animals residing above the tunnel alignment.

The measurement of ground vibrations induced by any natural or man-made sources is difficult as a very large amount of data can be obtained from a small number of measurements. The processing of all these data has formally been a difficult task. However, due to the availability of improved computer capacity and software, the processing of data and the acquisition, analysis and storage stages has been improved (Hall, 2000).

The three components representing vibration characteristics that are commonly measured are the displacement amplitude, the particle velocity and the particle acceleration. Each of these is measured as peak values in three orthogonal directions to produce the resultant vector sum. Conversions between the three parameters may be made by electronic instruments using an integration or differentiation process (Head & Jardine, 1992).

5.2 Vibration Parameters

A comprehensive description of vibrations requires details of the amplitude and frequency of the vibration, together with an indication of how these parameters change with time (Kramer, 1996). Vibrations of physical systems can be decomposed by means of Fourier analysis into harmonic components (Hillar & Crabb, 2000).

5.2.1 Amplitude Parameters

The most common way of describing a ground vibration is with a time-history graph. The vibrations parameters that may be used are the acceleration, velocity and displacement time-history graphs are shown in Fig. 5.1. Typically, only one of these parameters is measured directly, with the others computed from it by integration and/or differentiation. The acceleration time-history graph shows a significant proportion of relatively high frequencies and the velocity time-history shows substantially less high-frequency motion than the acceleration time-history graph. The displacement time-history graph, obtained by another round of integration, is dominated by relatively low frequency motion (Kramer, 1996).

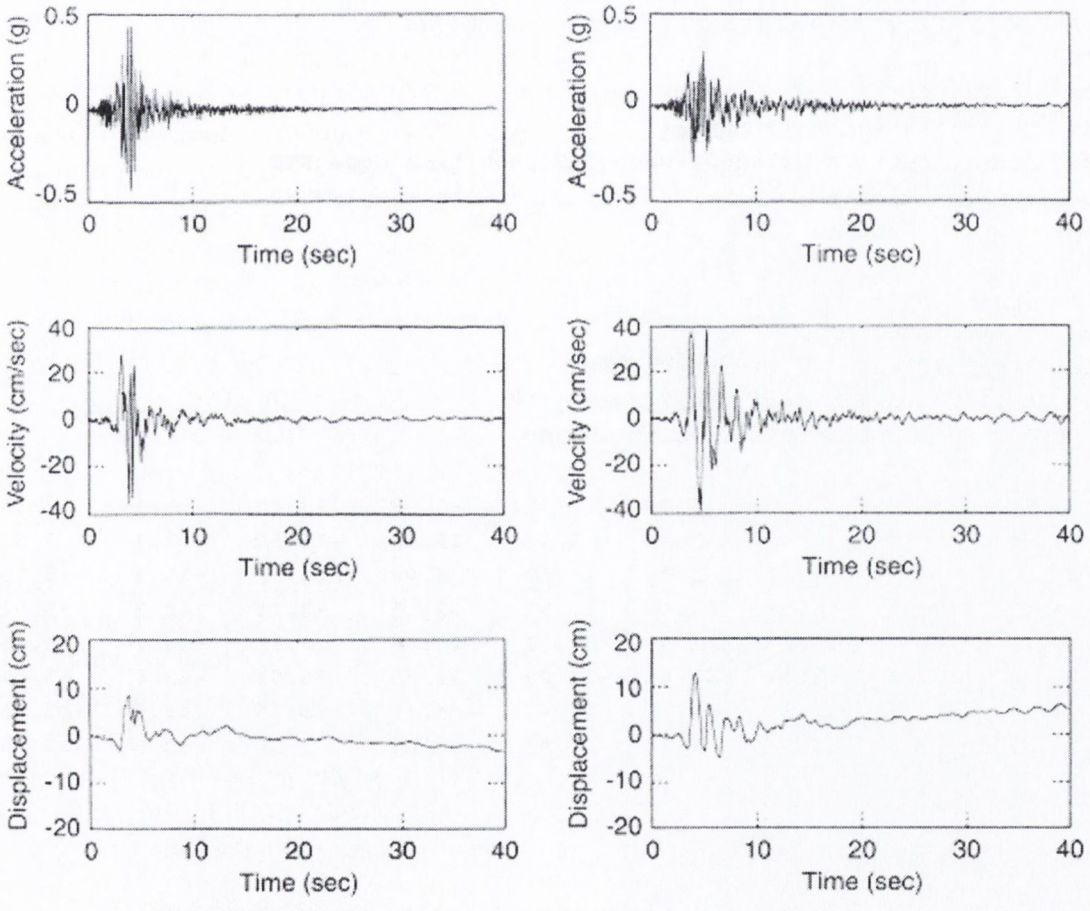

Fig.5.1–Acceleration, velocity and displacement time histories (from Kramer, 1996)

Ground vibrations can be described, analysed and reported using a variety of harmonic vibration parameters such as: peak particle displacement, peak particle velocity, peak particle acceleration and frequency (Flanagan, 1993). The peak particle parameters are the maximum values associated with the motion of a particle at the point in the ground being considered.

For analysing the lower frequency components of earthquake motion, the peak particle displacements are generally used. These are, however, often difficult to determine accurately in the case of the higher frequency vibrations due to construction activities, such as those produced by a TBM, due to signal processing errors in the filtering and integration of the measured accelerations or velocities. As a result, peak particle displacement is less commonly used as a measure of ground motion than peak particle velocity or acceleration (Kramer, 1996) in construction projects.

In the context of structural damage, ground vibrations are commonly described in terms of peak particle velocity (PPV) and frequency. The reason for this choice is the well-established correlation between peak particle velocity and observed cosmetic damage which is explained theoretically by the fact that the strain induced in the ground during vibration is proportional to the peak particle velocity (New, 1990a and Athanasopoulos & Pelekis, 2000). The PPV is also easy to measure, using a geophone, which has an output proportional to the particle velocity (Hillar & Crabb, 2000).

The particle velocity at a point of interest is usually measured in three mutually perpendicular directions, one of them always coinciding with the vertical direction (V-direction). The resultant intensity of vibrations is expressed either as the maximum single value of the three directional components (peak component) or by the true vector sum (TVS) of the three components. In some circumstances the vibration intensity is simply described by the peak vertical component of particle velocity. The square root of the sum of the squares (SRSS) of maximum values of the three components (irrespective of the time of occurrence) has also been used in the past. This latter approach is now considered as conservative. The SRSS could theoretically exceed the true resultant by a factor of $\sqrt{3}$, but is typically 20% higher than the true resultant, although this depends on the characteristics of the wave form (Dowding, 1996; New, 1990a, Hillar & Crabb, 2000, Hillar & Hope, 1998 and Athanasopoulos & Pelekis, 2000).

The peak particle horizontal acceleration (PHA) is more commonly used in earthquake engineering as a measure of the amplitude of the vibration in a particular direction. The PHA in a particular direction is simply the largest value of the horizontal acceleration obtained from the accelerogram in that direction. By taking the vector sum of two orthogonal horizontal components, the maximum resultant PHA can be obtained. Vertical particle accelerations have received less attention in earthquake engineering than horizontal accelerations, primarily because the margin of safety against gravity-induced static vertical forces in structures usually provides adequate resistance to dynamic forces induced by vertical accelerations during earthquakes (Kramer, 1996).

5.2.2 Frequency Content Parameters

The frequency content describes how the amplitude of a ground motion is distributed among different frequencies. Since the frequency content of an earthquake motion or any other vibration will strongly influence the effects of that motion, characterization of the motion can not be complete without consideration of its frequency content.

5.2.2.1 Fourier Series

Any periodic function that repeats itself at constant intervals can be expressed using Fourier analysis as the sum of a series of simple harmonic terms of different frequency, amplitude and phase. Since a Fourier series is simply a summation of simple harmonic functions, it can be expressed using either trigonometric function or exponential function (Kramer, 1996):

$$x(t) = a_o + \sum_{n=1}^{\infty} [a_n \cos \omega_n t + b_n \sin \omega_n t]$$

$$= c_o + \sum_{n=1}^{\infty} c_n \sin (\omega_n t + \Phi_n) \qquad [5.1]$$

where the Fourier coefficients are

$$a_o = \frac{1}{T} \int_0^T x(t) dt$$

$$a_n = \frac{2}{T}\int_0^T x(t)\cos\varpi_n t dt$$

$$b_n = \frac{2}{T}\int_0^T x(t)\sin\varpi_n t dt$$

and

$$c_o = a_o$$

$$c_n = \sqrt{a_n{}^2 + b_n{}^2}$$

$$\Phi_n = \tan^{-1}(a_n / b_n)$$

c_n and Φ_n are the amplitude and phase respectively. A plot of Fourier amplitude versus frequency is known as a Fourier amplitude spectrum; a plot of Fourier phase angle gives the Fourier phase spectrum. The Fourier amplitude spectrum of ground motion shows how the amplitude of the motion is distributed with respect to frequency. It expresses the frequency content of a motion very clearly. The Fourier amplitude spectrum may be narrow or broad. A narrow spectrum implies that the motion has a dominant frequency, which can produce a smooth, almost sinusoidal time history. A broad spectrum corresponds to a motion that contains a variety of frequencies that produce a jagged, irregular time history.

5.2.2.2 Discrete Fourier Transform (DFT) and Fast Fourier Transform (FFT)

In geotechnical engineering applications, loading or motion parameters are described by a finite number of data points. In such cases the Fourier coefficients are obtained by summation rather than integration and can be determined either by the discrete Fourier transform (DFT) or the fast Fourier transforms (FFT). For a variable $x(t_k)$, where k = 1, N, and $t_k = k\Delta t$, the DFT is given by:

$$X(\varpi_n) = \Delta t \sum_{k=1}^{N} x(t_k) e^{-i\varpi_n t_k} \qquad [5.2]$$

where, $\varpi_n = n\Delta\omega = 2\pi n/N\Delta t$. Using Euler's law, the DFT can also be written as

$$X(\varpi_n) = \Delta t \sum_{k=1}^{N} [x(t_k)\cos\varpi_n t_k - ix(t_k)\sin\varpi_n t_k] \qquad [5.3]$$

The DFT was developed long before computers were available, and its use, for even modest values of N, was extremely labour intensive. As early as 1805, the beginning of a more efficient approach to the DFT was described (Brigham 1974 cited by Kramer, 1996). As digital computers were developed in the 1960s, a computational algorithm, for the case where N is a power of 2, was also developed. This algorithm decreased the computing time tremendously and has become known as the fast Fourier transform (FFT). By performing repeated operations on groups that start with a single number and increase in size by a factor of 2 at each stage, the time required to complete a transform with the FFT is proportional to $N\log_2(N)$ and the time required for computation of a DFT is proportional to N^2. The disadvantage with the FFT is that the sampled signal must have a power of 2, while the DFT is independent of the number of samples. So, for example, a transform on 1024 points using the FFT is 10 times quicker than using the DFT, a significant speed increase (Hall, 2000, Kramer, 1996 and Newland, 1993).

5.2.2.3 Power Spectra

The Fourier amplitude spectrum illustrates how the strength of a quantity varies with the frequency. This information can also be expressed in terms of power. The power spectrum, also called the power spectral density function (PSD), (Kramer, 1996 and Hall, 2000) is defined as:

$$P_{xx}(\omega_n) = X^*(\omega_n).\, X(\omega_n) \qquad [5.4]$$

where, $X^*(\omega_n)$ is the complex conjugate of $X(\omega_n)$.

5.3 Measuring Devices

In the broad field of ground vibrations, it is common to use transducers that measure the ground motion. Transducers convert physical motion into electrical energy. Accelerometers, which produce a voltage output that is proportional to the acceleration, are the most common transducers to measure the ground vibrations. For general use they are smaller than velocity

transducers (geophones), and their frequency and dynamic ranges are wider. However, in the range of frequencies normally under consideration for piling (Head & Jardine, 1992) and tunnelling, geophones give more consistent direct results; and velocity measurements provide the best single-parameter that reflects response of both people and structures. Geophones give a voltage output that is proportional to the velocity (Hall, 2003), which is the most appropriate vibration parameter for the evaluating the impact of environmental vibration (Hillar & Grab, 2000).

5.3.1 Accelerometers

Acceleration may be derived by time-differentiating velocity or by doubly differentiating displacement, either electronically on the signals or numerically on the recorded data. Obtaining reliable acceleration data from displacement or velocity readings is hardly feasible. A large number of accelerometers are available such as resistance strain gauges, piezoresistive and piezoelectric accelerometers, the most common being the piezoelectric type (Gatti & Ferrari, 1999).

A resistance strain gauge consists of fine wire, which exhibits a change in resistance proportional to any mechanical strain imposed on it. It is not self-generating and requires external DC power and is suitable for low frequency vibrations.

A piezoresistive accelerometer consists of semiconductor material and is also not self-generating and needs an external DC power source. It is suitable for low frequency, steady state vibrations or motions of long duration (Gatti & Ferrari, 1999).

A piezoelectric accelerometer utilizes a piezoelectric element, which generates an electrical charge when compressive (or tensile), shear, or flexural forces are applied to the element. Typically quartz and polycrystalline ceramics are used in piezoelectric accelerometers, with quartz being the more desirable choice because of its stability over time. Traditionally, piezoelectric accelerometers are a poor choice for testing of low frequencies because they do not respond well at low frequencies. However, newer designs have been developed to take advantage of the quartz stability and durability while providing low frequency capabilities.

All accelerometers have a sensitivity associated with them. The sensitivity is defined as the ratio of electrical output to mechanical input. Accelerometer sensitivities are typically expressed in terms of voltage (mV) per unit of acceleration (g).

5.3.2 Geophones

Functionally a geophone is a coil of wire suspended around a magnet as shown in Fig.5.2. The magnet is free to move in a field of magnetic flux lines. By Lenz's law, induced voltage due to ground motion is proportional to the speed at which flux lines are traversed. Induced coil voltage is therefore proportional to the relative velocity of the coil to the magnet. In practice, it does not matter whether the coil or the magnet moves. Only the motion and speed relative to each other are important.

The sensor responds well to the geophone's case velocity when the frequency of the ground vibration is higher than the geophone coil resonance frequency, typically 4 Hz for large and 30 Hz for small geophones. When the ground vibration frequency is lower than the coil's resonance frequency the vibrations are depressed. Normally traffic induced ground vibrations contain low frequencies and 1-2 Hz geophones may be necessary which are more expensive than above geophones.

Geophones are widely used in the oil and gas exploration industry and are considered as being very reliable. The measurements of TBM excitation and ground vibrations throughout the construction of the Dublin port tunnel were carried out using Geophones.

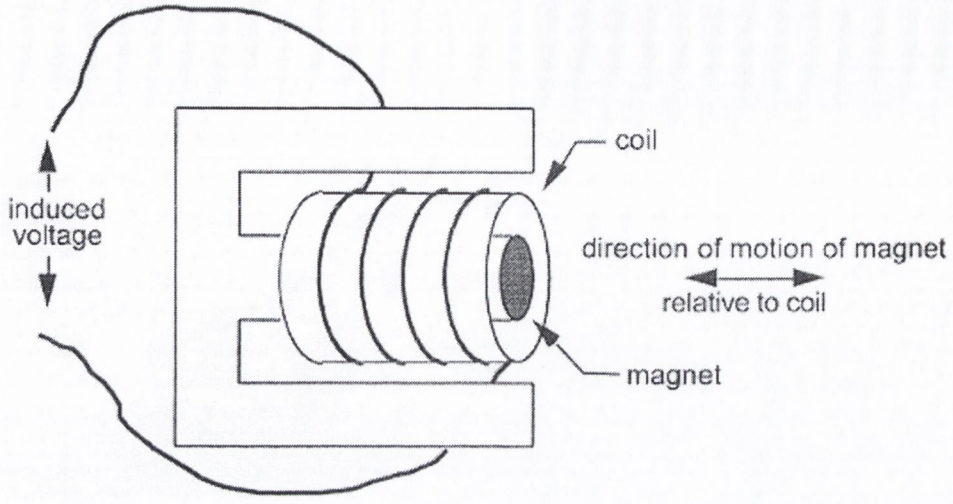

Fig.5.2–Geophone sensor operation

5.4 Test Set-up and Methodology for Field Measurement of Vibration in Dublin Port Tunnel

Three orthogonal components of the TBM excitation and the ground surface vibration at measurement Sections 1, 2, 3 and 4 were recorded during the construction of northbound Dublin Port Tunnel and at measurement Section 5 during the construction of south bound Dublin Port Tunnel using Geophones. The vibrations measurement area indicates in Fig.5.3 and the geotechnical properties are presented in Table 5.1.

The TBM excitation and ground surface vibration measurements reported in this study were conducted using vertical and horizontal geophones. The measurements at each measuring point were conducted using of a set of three geophones positioned in such a way as to measure particle velocities in the transverse, longitudinal and vertical directions. The geophones were connected to a laptop computer equipped with data acquisition software. A photograph of the system and the author is shown in Fig. 5.4. The Geophone arrangements for the different measuring points on ground surface along the northbound tunnel and the southbound tunnel are shown in Fig. 5.5 and an overview of the locations of the measurement points at the test site is given in Table 5.2. The ground surface vibration measurements at Section 1 are presented and discussed in section 5.5.

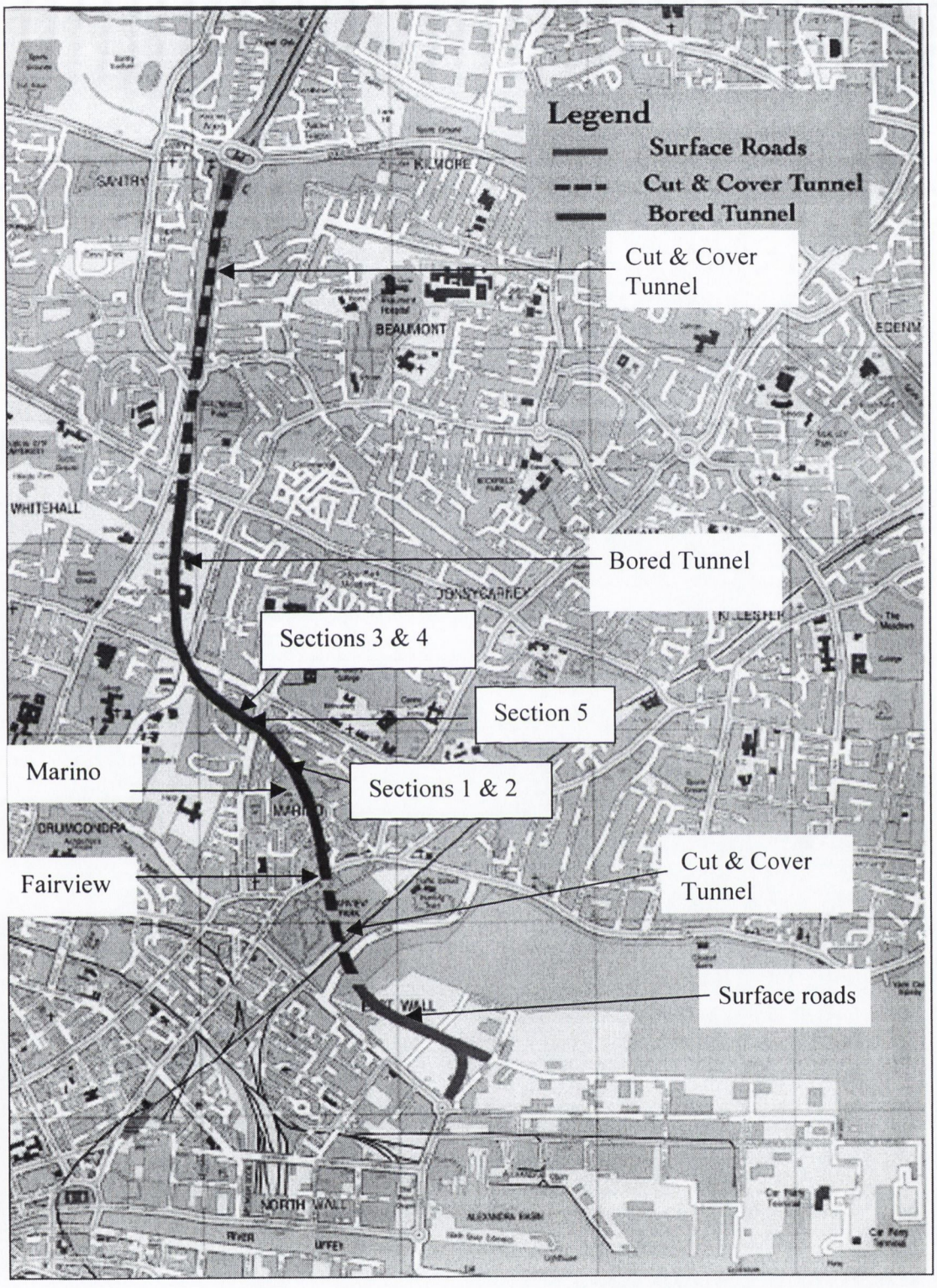

Fig.5.3-Vibrations measurement area

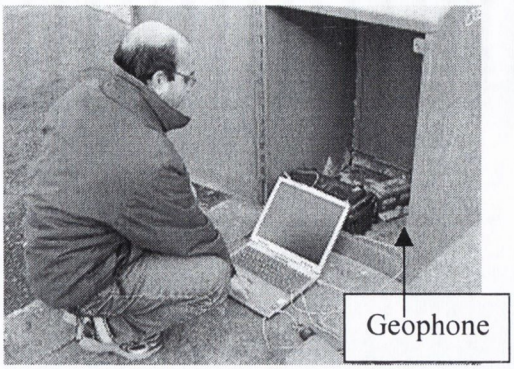

Fig.5.4–Measuring ground vibrations

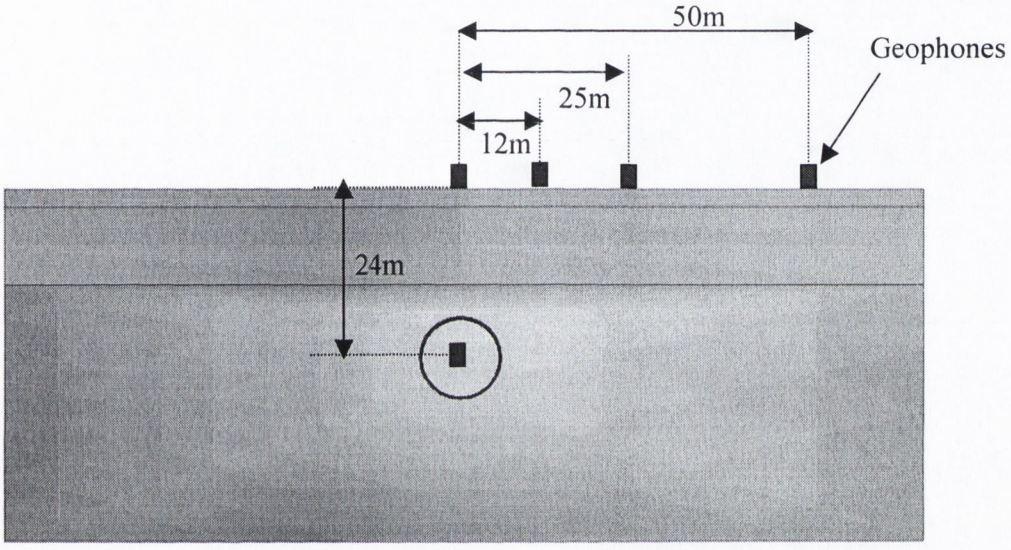

Fig.5.5 (a)–Geophone arrangements; Sections 1& 2

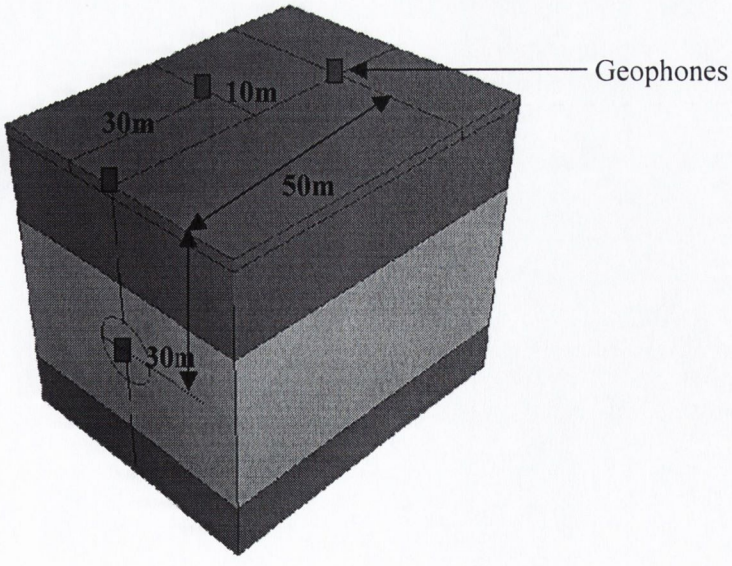

Fig.5.5 (b)–Geophone arrangements; Sections 3& 4

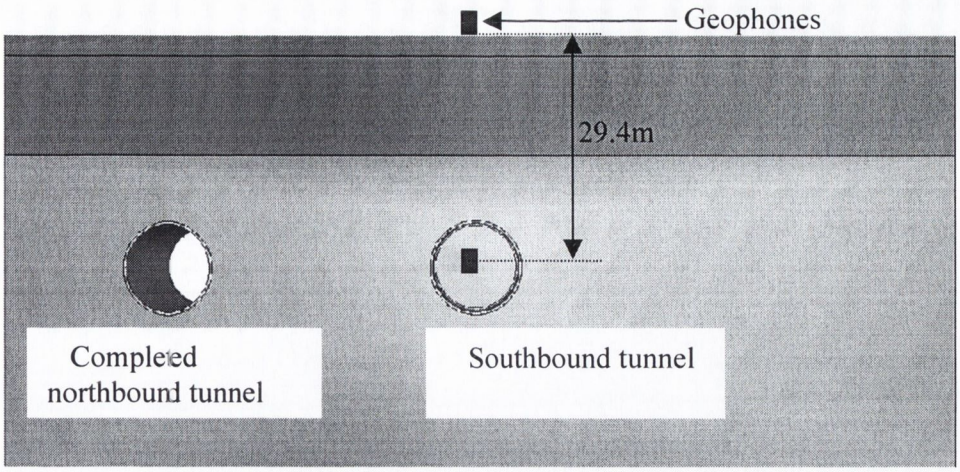

Fig.5.5 (c)–Geophone arrangements; Section 5

Table 5.1: Characteristics of materials at measurement area

Parameter	Top layer, (brown clay)	Dublin boulder clay	Limestone
Density, kg/m^3	2000	2240	2710
Young's modulus, E_{max}, GPa	0.2	1.0	60
G_{max}, GPa	0.067	0.33	24
Poisson's ratio	0.495	0.495	0.25
Damping, %	2.85	1.75	1.0

Table 5.2–Overview of the measurement points

Section	Measurement Point	Distance from TBM along tunnel axis (m)	Cross distance (m)
1	1	0	0
2	1	0	0
	2	0	12
	3	0	25
	4	0	50
3	1	0	0
	2	50	0
4	1	0	0
	2	30	10
5	1	0	0

5.5 Results and Analysis of Test Data

5.5.1 TBM Excitation

Geophones were used to record hard rock TBM excitation. The cutter head rotation speed was 4 revolutions per minutes and the cutting rate of the hard rock TBM was 10m/day. The cutting wheel was fitted with hard rock discs which rotated on the working face and notched into it. The notching effect caused large sections of rock to break off and was the main sources of the vibrations in the ground. Buckets located behind the discs transported the rock behind the cutting wheel. Conveyor equipment then transported the excavated material out of the tunnel. Another source of ground vibrations were when the jacks were pushing the TBM forward. The TBM exciting vibrations presented in this section were obtained when the TBM was at measuring Section 1 in Dublin Port Tunnel. The measured TBM vibrations at Section 1, plotted as particle velocity versus time, are presented in Fig. 5.6 to Fig. 5.8. The remaining vibration measurements, when the TBM was at other sections, are presented in Appendix B. The presentation of the vibration records as a function of time is known as a time history plot. By comparing the peak component particle velocities in the three orthogonal directions it is found that the maximum TBM velocity did not exceed 15 mm/s at Section 1.

Matlab was used to calculate the frequencies of the measured vibrations from the time history plot. In Matlab, the Fast Fourier Transform (FFT) algorithm was applied to convert the time history signal to the frequency domain. The FFT analysis was carried out using the particle velocity data recorded on the TBM frame. Fig. 5.9 to Fig. 5.11 show the vibrations of the TBM in the frequency domain. The main purpose of the FFT analysis was to determine at which frequency the TBM was delivering most energy. According to the frequency analysis of the TBM vibrations, it is observed from Fig. Fig. 5.9 to Fig. 5.11 that the energy is mainly in the frequency range 4 - 26 Hz with a peak near 14 Hz in transverse direction. The frequency ranges and peaks for the vertical and longitudinal TBM vibration velocities are 7 - 48 Hz and 1- 42 Hz, and 18 Hz and 12 Hz respectively.

5.5.2 *Ground Surface Vibrations*

In this section, the results of the ground surface vibrations obtained at Measuring Point 1 with the TBM at Section 1 in the Dublin Port Tunnel are presented. The installation of the geophones to measure the ground vibrations and the recording of the vibrations during construction of the Dublin Port Tunnel were carried out by the contractor Nishimatsu Construction Company's engineers. During the construction of Dublin Port Tunnel project there were a number of significant complaints from house owner in the area of limestone boring. The maximum capacity of the geophone used by NCC for recording the surface vibrations in time history mode was 10 second. As a result, the vibrations at the surface were monitored continuously in a histogram mode rather than in a time history mode. The histogram record mode is often used for recording long-term vibrations, such as ground vibrations due to pile driving or a TBM. The monitor samples the vibration data continuously at the chosen sample rate but only stores the relevant peaks for the interval. This reduces the data recorded and greatly increases the monitor's recording time. For each interval, it calculates the maximum peak particle velocity rather than RSM value. As NCC controlled all the field tests some information was not obtained such as the frequency range of the geophones and the filtering method. Histograms were prepared of the recorded peak particle velocities and examples of these are shown in Fig. 5.12 to Fig. 5.14.

Fig. 5.12, Fig. 5.13 and Fig. 5.14 show the measured maximum ground surface vibrations at, Measurement Point 1, Section 1 in transverse, vertical and longitudinal directions respectively. The results show the ground surface vibrations due to two different TBM activities which were: a) the TBM installing segments and b) boring. From 0 to 17 minutes and 50 to 64 minutes, the TBM is installing segments and vibration level is very low. Between 17 and 50 minutes, there is a higher almost constant vibration level. The period with a constant higher level of the vibration is when the TBM is actually boring and the jacks are pushing the TBM forward. The measured vibrations at, Measurement Point 1, Section 1 during this period in Figs. 5.12 to 5.14 show that the vibrations in the transverse direction, with an average velocity of 1.04mm/s, are higher than those in the longitudinal direction, with an average velocity of 0.77mm/s, and that these are higher than those in the vertical direction, with an average velocity of 0.70mm/s. However, at measuring points at other measuring sections, it was found that the measured vibration velocities in the longitudinal direction were

higher than those in the transverse direction and those in the transverse direction are higher than those in the vertical direction as shown in Table 5.3.

The maximum measured ground surface vibrations in transverse, vertical and longitudinal directions at measuring point 1 are 1.21, 0.84 and 0.91 mm/s and the averages are 1.04, 0.70 and 0.77mm/s respectively. BS 7385 recommends that the peak particle velocity is used to assess vibrations and specifies damage criteria for frequencies between 1Hz to 1 kHz. In terms of avoiding cosmetic damage, at a frequency of 4Hz, the recommended maximum value is 15mm/s peak particle velocity, increasing to 20mm/s at 15Hz and 50mm/s at 40 Hz and above.

BS 6472 states that the threshold levels at which vertical vibrations become perceptible to humans are 0.141mm/s for frequencies between 8Hz and 80Hz for vertical vibrations and is greater at lower frequencies, for example increasing to 2.25mm/s at 1Hz. Multiplication factors of 2 and 4 (for residential and day time) may be applied to the threshold levels giving increased threshold limits of 0.282mm/s and 0.564mm/s for frequencies between 8Hz and 80Hz. For longitudinal or transverse vibrations, the threshold level is 0.402mm/s between 2Hz and 80 Hz, rising to 0.804mm/s at 1Hz.

It can be seen from Table 5.3 that the maximum resultant PPV 2.10 mm/s was obtained at Section 3 and minimum resultant PPV 1.73 mm/s was obtained at Section 1. Points were considered just above TBM. It is possible to make correlation with resonance frequency of TBM and ground deposits; it is also one of the main reasons for higher PPV. The resonance frequency of the TBM was 14 Hz however, the resonance frequency of the ground deposits at Section 1 is 18 Hz and at Section 3 is 15 Hz which are shown in Chapter 6. The resonance frequencies of the TBM and ground deposit at Section 3 are very close and yielded higher PPV. Because when the resonance frequency of the ground deposit and the TBM excitation coincide or are very close, this results in a maximum PPV. On the basis of the maximum peak particle velocity it is concluded that the measured values were high enough to be noticeable to humans.

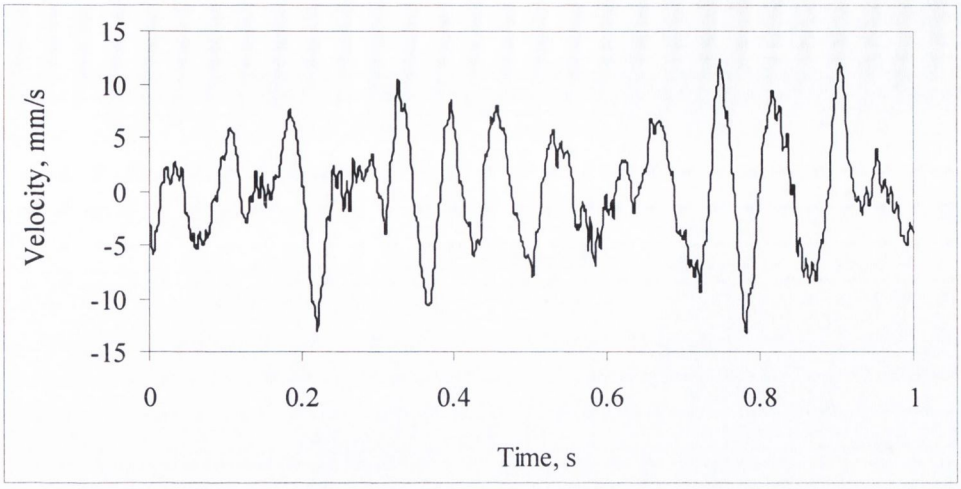

Fig.5.6–Time history plot of transverse TBM vibrations for TBM at Section 1

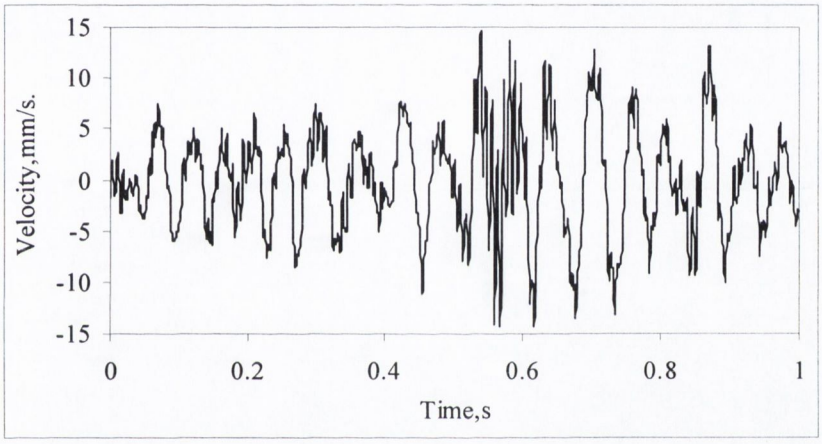

Fig.5.7– Time history plot of vertical TBM vibrations for TBM at Section 1

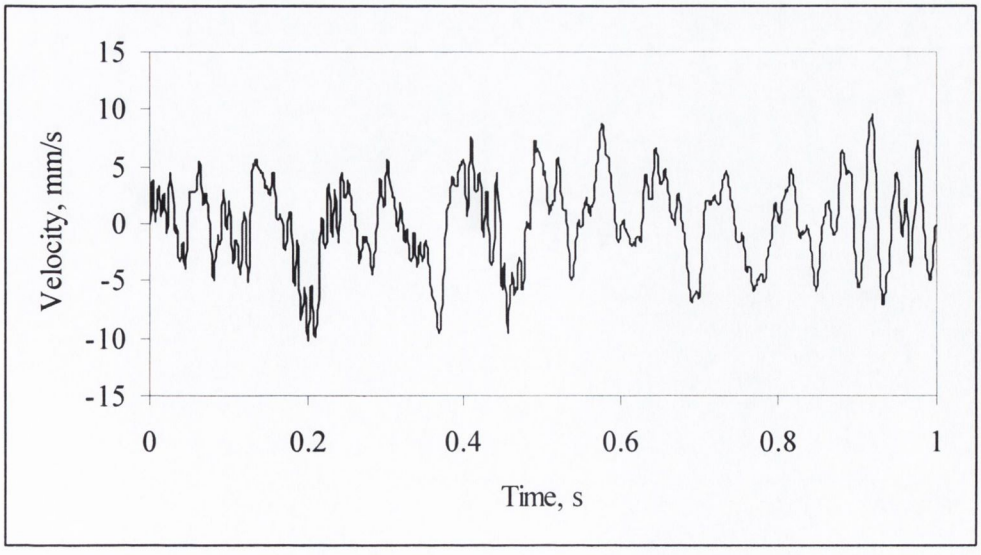

Fig.5.8– Time history plot of longitudinal TBM vibrations for TBM at Section 1

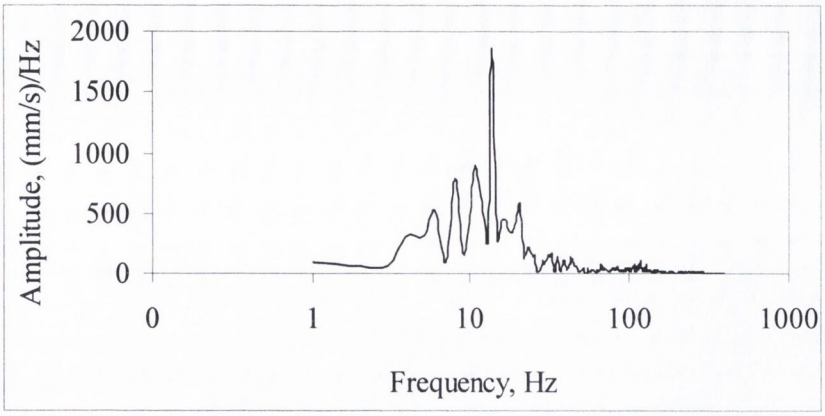

Fig.5.9–FFT of time history plot of transverse TBM vibrations

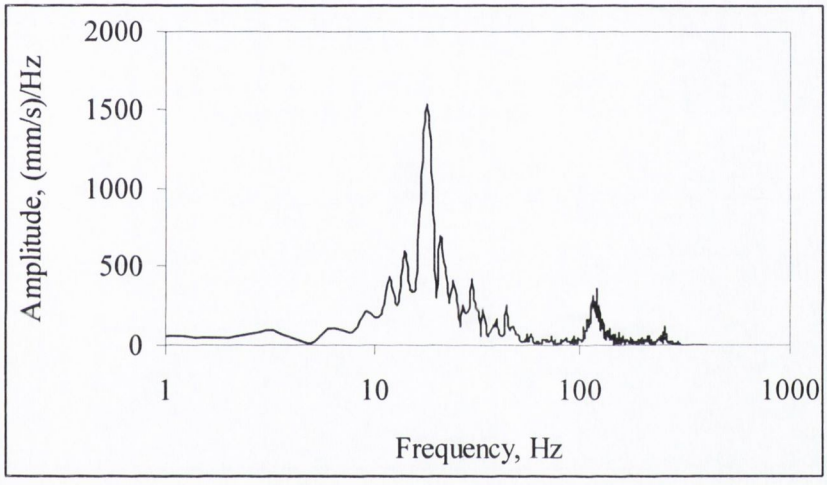

Fig.5.10– FFT of time history plot of vertical TBM vibrations

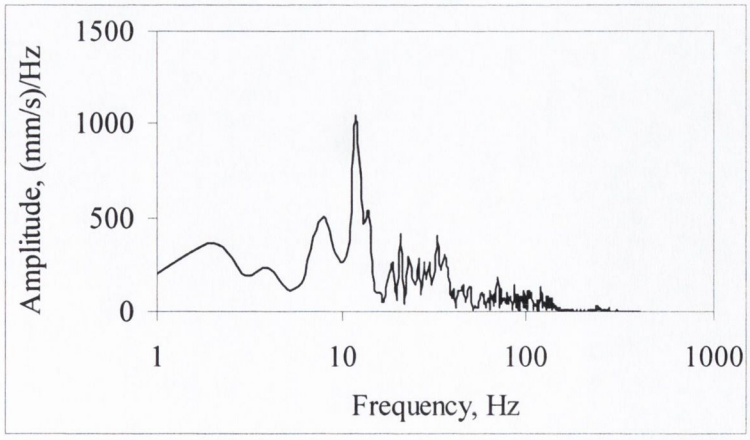

Fig.5.11– FFT of time history plot of longitudinal TBM vibrations

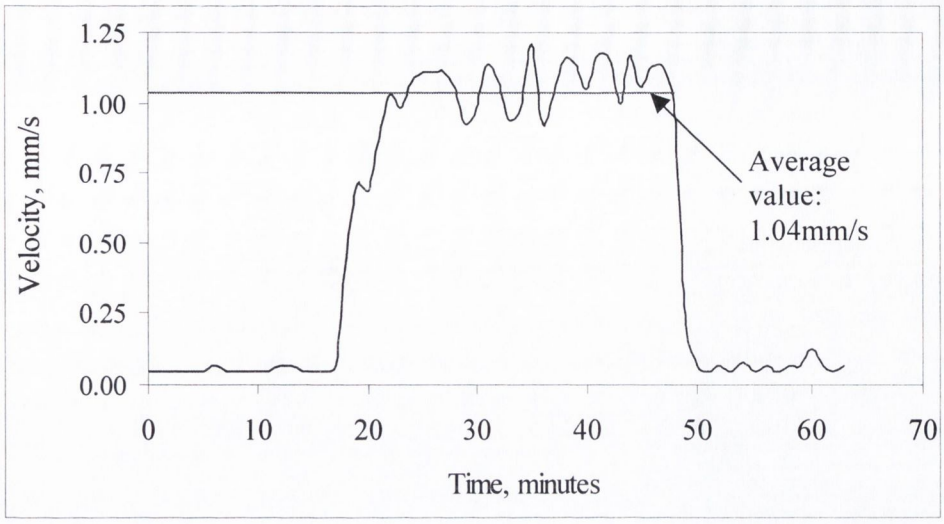

Fig.5.12– Histogram of measured Peak Particle Velocity at the ground surface at Measurement Point 1 and at Section 1, transverse direction

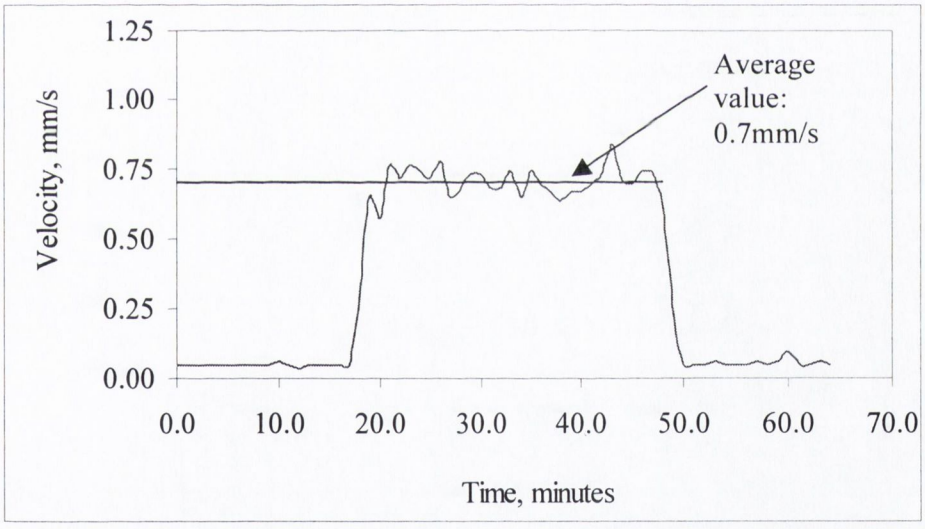

Fig.5.13– Histogram of measured Peak Particle Velocity at the ground surface at Measurement Point 1 and at Section 1, vertical direction

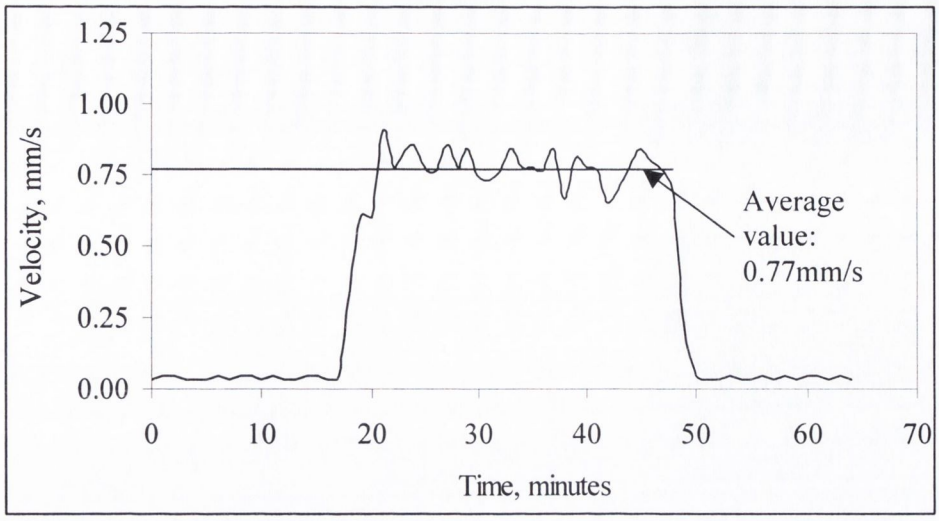

Fig.5.14 – Histogram of measured Peak Particle Velocity at the ground surface at Measurement Point 1 and at Section 1, longitudinal direction

Table 5.3–Measured PPV Values

Section	Measurement Points on Surface	Direction	Measured PPV values, mm/s
1	Just above the TBM axis	Transverse	1.21
		Vertical	0.84
		Longitudinal	0.91
		Resultant	**1.73**
2	Just above the TBM axis	Transverse	1.24
		Vertical	0.51
		Longitudinal	1.58
		Resultant	**2.07**
	12 m away from TBM in transverse direction	Transverse	0.71
		Vertical	0.33
		Longitudinal	1.02
		Resultant	**1.29**
	25 m away from TBM in transverse direction	Transverse	0.52
		Vertical	0.24
		Longitudinal	0.67
		Resultant	**0.88**
	50 m away from TBM in transverse direction	Transverse	0.29
		Vertical	0.17
		Longitudinal	0.35
		Resultant	**0.49**
3	Just above TBM	Transverse	0.91
		Vertical	0.42
		Longitudinal	1.84
		Resultant	**2.10**
	50 m away from TBM face in tunnel direction	Transverse	0.43
		Vertical	0.22
		Longitudinal	0.84
		Resultant	**0.96**
4	Just above TBM	Transverse	0.82
		Vertical	0.30
		Longitudinal	1.68
		Resultant	**1.89**
	30 m in tunnel direction & 20 m in transverse direction	Transverse	0.36
		Vertical	0.16
		Longitudinal	0.79
		Resultant	**0.88**
5	Just above TBM	Transverse	1.0
		Vertical	0.38
		Longitudinal	1.5
		Resultant	**1.84**

5.6 Summary

Vibration-induced damage thresholds are usually expressed in terms of peak particle displacement, velocity or acceleration and sometimes include a frequency dependent factor. It is most usual to use the peak particle velocity (PPV) in the case of man-made ground vibration studies and geophones are normally used to measure the ground vibrations. In this project the vibration are expressed in terms of PPV.

Field measurements of the TBM excitation vibrations and the ground surface vibrations produced by the TBM were made in an urban environment and provided values of the TBM vibrations velocities and the PPV of the soil particles at the ground surface at varying distances (up to 50 m) from the source of the vibrations, in a variety of ground conditions. The cutting rate of the TBM was 1.7m/hour.

The intensities of the ground surface vibrations were measured in this study and found that it was high enough to be noticeable to humans. As a result complaints about vibrations were reported during the construction of limestone boring Dublin Port Tunnel, apparently due to the steady state nature of the vibrations. TBM vibrations may be uncomfortable to humans when the tunnel boring is relatively close, for example 25m as in the case of Sections 1 and 2 for the Dublin Port Tunnel.

CHAPTER 6

NUMERICAL ANALYSES

6.1 General

In this chapter the use of a three-dimensional finite element model to investigate the ground vibrations at the surface level in terms of the peak particle velocity (PPV) due to the construction of the Dublin Port tunnel is discussed. This situation is analysed using a commercially available general-purpose finite element package ABAQUS and a comparative study is carried out between the three-dimensional finite element results, the empirical results and the measured results. A series of parametric studies to examine the sensitivity of the predicted vibrations to variations in various input parameters required by finite element method, including the stiffness and the damping of the soil, is carried out.

During the construction of Dublin Port Tunnel project, there were a number of complaints from house owners in the area when the boring was through limestone whereas there were no complaints in the area where the boring was through boulder clay and hence boring through limestone was important with regard to this research. How ground parameters obtained were discussed in Chapters 1 and 4.

6.2 Finite Element (FE) Model

The FE analyses were carried out to evaluate the levels of the ground vibrations at the surface level. Three-dimensional finite element models allow the analyst to account accurately for the extent and geometry of each of these constituents in constructing a representative numerical model of ground vibrations due to a tunnel boring machine (TBM). The ABAQUS V6.4 finite element software was used to construct the model and three-dimensional eight-noded linear brick and reduced integration elements, C3D8R, were employed for the ground and the tunnel lining. Reduced-integration elements use fewer integration points in each direction than the fully integrated elements. They reduce running time, especially in the analysis of a three-dimensional finite element model. To prevent movement or sliding of the tunnel lining relative to the ground, three-dimensional rough

contact surface elements were included at the interface between the soil and the tunnel lining. In the model, the top layer was brown clay, the middle layer was Dublin boulder clay and the bottom layer was limestone.

The dimensions of the finite element model at measuring Sections 1 and 2 were 132m in transverse direction, 50m in vertical direction and 40m in along the tunnel direction. The thickness of the top layer was 2.5m, the middle layer was 11m and the bottom layer was 36.5m. The diameter of the tunnel was 12m. The finite element model geometry and mesh are shown in Figs. 6.1, 6.2 and 6.3.

At measuring Section 3 and 4, the dimensions of the finite element model were 52m in transverse direction, 56m in vertical direction and 85m in along the tunnel direction. The thickness of the top layer was 2m, the middle layer was 15m and the bottom layer was 39m. The diameter of the tunnel was 12m. The geometry of finite element model is shown in Fig. 6.4.

The dimensions of the finite element model at measuring Section 5 were 122m in transverse direction, 55.4m in vertical direction and 40m in along the tunnel direction. The thickness of the top layer was 2.5m, the middle layer was 12.7m and the bottom layer was 40.2m. The diameter of the tunnel was 12m. The geometry of finite element model is shown in Fig. 6.5.

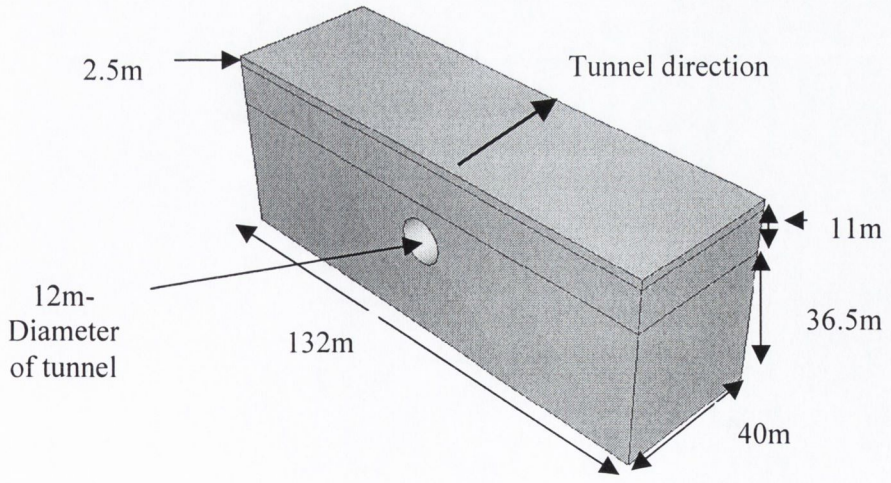

Fig.6.1–Finite element model geometry at measuring Sections 1 and 2

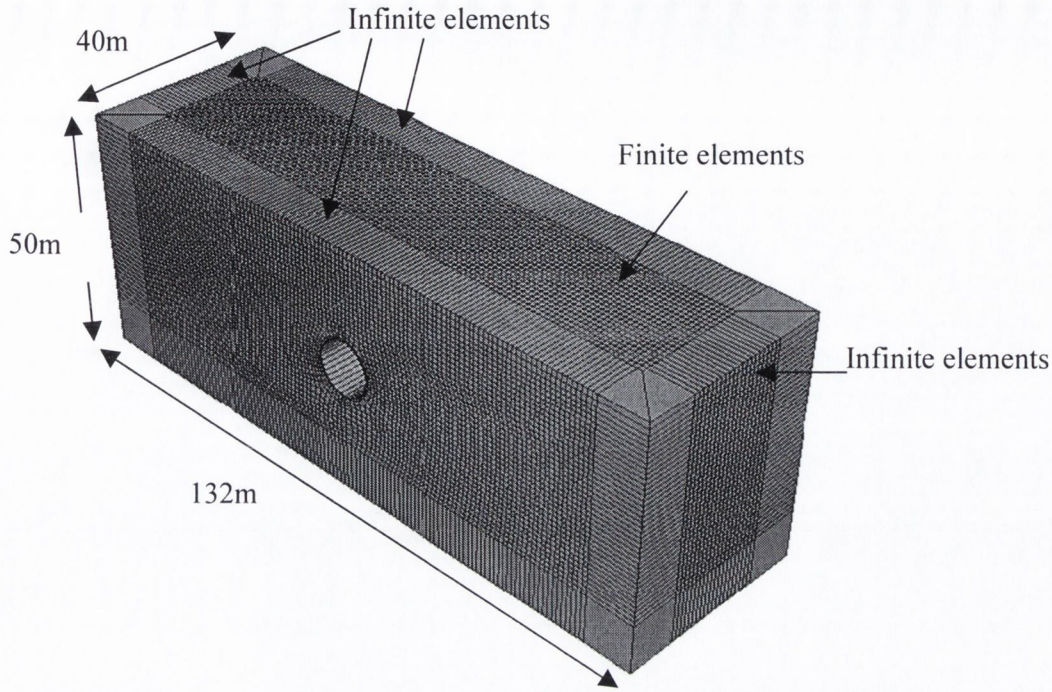

Fig.6.2–Finite element meshes of ground at measuring Sections 1 and 2.

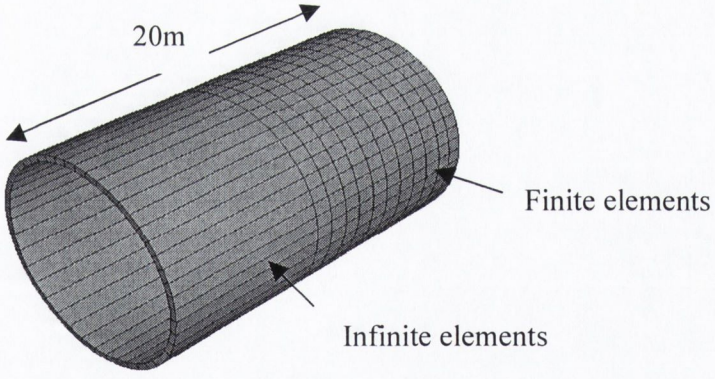

Fig.6.3–Finite element mesh of tunnel (Enlarge figure) at measuring Sections 1 and 2

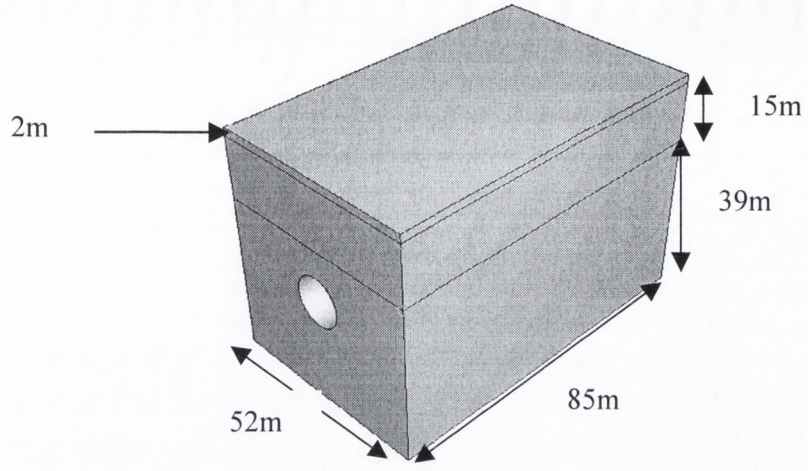

Fig.6.4–Finite element model geometry at measuring Sections 3 and 4

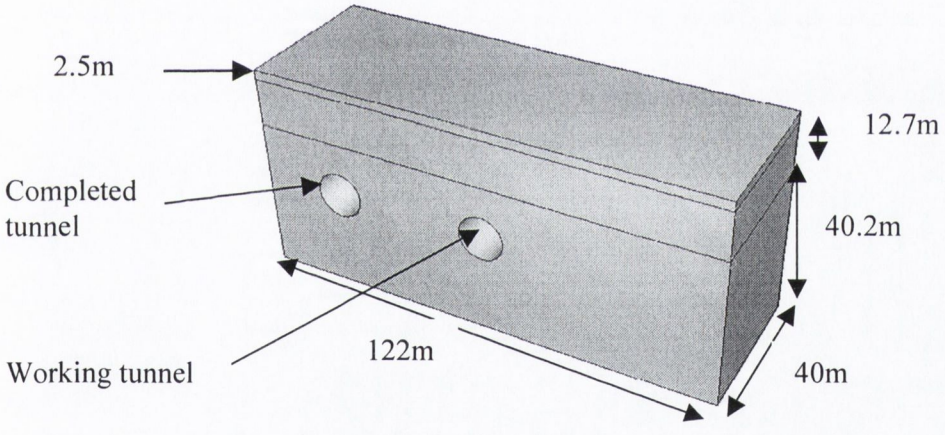

Fig.6.5–Finite element model geometry at measuring Section 5

6.3 Materials Properties

There were three different layers of soil strata and the material properties for the each layer were based on the results of ground investigations. A linear elastic material law was used to define the material properties for the ground, the tunnel concrete lining and the TBM steel frame. Linear elasticity was assumed to be valid because the displacements and strain due to vibrations are very small. The values used for these parameters in the finite element

analyses are given in Table 6.1. The relationship between G_{max}, E_{max} and the shear wave velocity, v_s, are as follows:

$$G_{\max} = \frac{E_{\max}}{2(1+\upsilon)} \quad [6.1]$$

$$v_s = \sqrt{\frac{G_{\max}}{\rho}} \quad [6.2]$$

Where υ is the Poisson's ratio and ρ is the density.

Although the linear elastic material law requires only density, stiffness, Poisson's ratio and damping ratio, it is also important to discuss some other parameters of soil and limestone.

Skipper et al. (2005) distinguished four sub-division of the Dublin boulder clay: an upper brown boulder clay, an upper black boulder clay, a lower brown boulder clay and a lower black boulder clay. Farrell et al. (1995) made the distinction between the brown and the black boulder clay. In each sub-division overall density values are uniform with depth (Skipper et al., 2005). Skipper et al. (2005) found that the densities of the upper brown boulder clay, upper black boulder clay, lower brown boulder clay and lower black boulder clay are 2228 kg/m^3, 2337 kg/m^3, 2283 kg/m^3 and 2284 kg/m^3 respectively. Farrell et al. (1995) found the density of the brown boulder clay is 2240 kg/m^3 and 2280 kg/m^3 and for black boulder clay is 2290 kg/m^3 and 2350kg/m^3. Lawler (2002) found that the density of brown boulder clay is 2150 kg/m^3 and the density of the black boulder clay is 2250 kg/m^3.

Lawler (2002) carried out seismic refraction tests and laboratory dynamic tests to determine the stiffness of Dublin boulder clay and the results are presented in Fig. 1.18 in Chapter 1. The parameters obtained from the NCC study and those obtained from the author's bender element test are presented in Table 6.1 and Table 6.2 respectively.

Lawler (2002) carried out a large number of triaxial, drained and undrained, compression tests on a variety of soil samples with very high deviator stresses associated with failure to determine the strength parameter of black boulder clay and interpreted the results from all

the tests. The results are $\varphi' = 40^0$ and $c' = 0$ kN/m^2. Farrell et al. (1995) also found $\varphi' = 35^0$ and $c' = 0$ kN/m^2.

Skipper et al. (2005) found that, in each soil type, the moisture content are uniform with depth and it was 13.1% for upper brown boulder clay, 9.7% for upper black boulder clay, 11.5% for lower brown boulder clay and 11.3% for lower black boulder clay. This measured values fall within the overall range of 11 ±3% for Dublin boulder clay as suggested by Farrell & Wall (1990) and Lehane & Simpson (2000). The plasticity index and liquid limit are 11 ±2% and 25 ±4% respectively (Farrell & Wall, 1990; Lehane & Simpson, 2000 and Skipper et al. 2005).

Few of studies have been carried out by different authors to investigate the properties of limestone. To investigate the dynamic properties of limestone ultrasonic pulse tests were carried out by the author and the results are presented in Table 6.2. The NCC supplied data are presented in Table 6.1. Farrell & Wall (1990) found that the unconfined compressive strength of Calp limestone was 80 MPa to 161 MPa and O'Donoghue & White (1975 cited by Farrell & Wall 1990) found that it was 58 MPa to 220 MPa. The results of Geotechnical laboratory tests (density, water content, UCS, porosity, Void ratio, Young's modulus, Poisson's ratio) for limestone in the Dublin Port Tunnel area were presented in Appendix A. The results were taken from the Dublin Port Tunnel site investigation reports which were organised by the consulting engineering companies Geoconsult and Arup.

If the dynamic properties (stiffness and damping), density and Poisson's ratio of the boulder clay and if the measured TBM excitations are available, the 3D FE model is developed for modelling the vibrations due to boring in limestone can be used to predict the TBM induced ground surface vibrations when boring in boulder clay.

Table 6.1: Properties of materials (NCC data)

Parameter	Top layer, (brown clay)	Dublin boulder clay	Limestone	Concrete	Steel
Density, kg/m^3	2000	2240	2710	2400	7800
Young's modulus, E_{max}, GPa	0.2	1.0	60	40	200
G_{max}, GPa	0.067	0.33	24	16.67	76.92
Poisson's ratio	0.495	0.495	0.25	0.2	0.3
Damping, %	2.85	1.75	1.0	1.0	0.5

Table 6.2: Properties of materials (Author's data)

	Cell pressure (kPa)	G_{max}, GPa	Density, kg/m^3	Damping ratio
Dublin boulder clay	80.0	0.42	2200	5.65 (100 kPa cell pressure) 5.23 (200 kPa)
	136.4	0.51		
	194.3	0.59		
	248.0	0.66		
Limestone (sample 1)		33.4	2670	
Limestone (sample 2)		33.0	2686	
Limestone (sample 3)		29.6	2660	

6.4 Boundary Conditions

Infinite boundary conditions were specified at the four sides of the vertical section and on the bottom to account for the fact that in reality the soil is a semi-infinite medium (Fig. 6.2). These boundary conditions allow the wave to disappear from the model without reflections, so that the model behaves like an infinite layered half space. Without these infinite boundary conditions, the waves would be reflected on the model boundaries, returning into the model and disturbing the results. The elementary boundary conditions are applied on the four sides of the vertical section to obtain horizontal fixities, which allow only vertical movement, and these boundaries are also applied on the bottom to obtain a full fixity.

6.5 Loading

By advancing in the ground, the tunnel-boring machine is a vibrating source from which vibrations are transmitted into the ground. Therefore, the impacts of the TBM on the ground during boring have been modelled by a dynamic loading system. The finite elements representing the TBM cutter have been loaded by a short triangular pulse. Loads were applied directly on limestone just in front of TBM. Due to this pulse, waves propagated through the soil and the response at the surface was determined. The analyses were carried out in the time domain and models of a dynamic loading in the time domain and in the frequency domain are shown in Figs.6.6 and 6.7 respectively. The main reason for using an input pulse in the FE model rather than a direct application of the actual TBM excitation is because it ensures parsimonious handling of the FE model. Due to use of an input pulse, it saved the FE modelling time of couple of days for one model run while for the entire project, it saved a couple of months which is very significant. A short triangular pulse has a wide power spectrum (Fig.6.7) and it is able to analyse waves ranging from low to high frequency. In FEM analyses, the pulse is applied at the beginning of the calculation, and the vibration energy is damped out during the rest of the calculation. As a result, there is no possibility of reflection of waves in the model due to this short triangular pulse. Due to the short input pulse, it is able to calculate the transfer function. The transfer function is the ratio between the output wave and the input wave (Equation 6.3) and hence the magnitude of the input wave is not an important factor. The input wave has a larger high frequency component than the measured signal. High frequencies are filtered out in the soil of the model.

$$H(\varpi) = \frac{Y(\varpi)}{X(\varpi)} \qquad [6.3]$$

where $H(\varpi)$ is a transfer function in the frequency domain, $Y(\varpi)$ is an output wave in a frequency domain and $X(\varpi)$ is an input wave in a frequency domain.

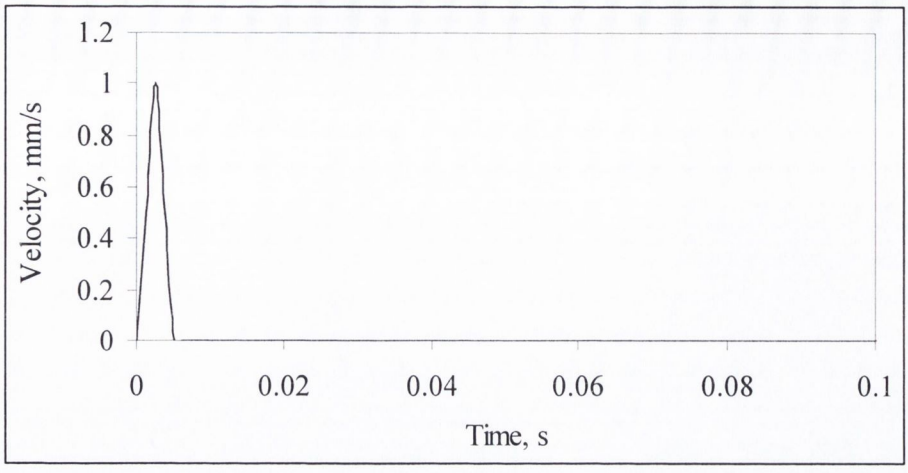

Fig.6.6–A short triangular pulse

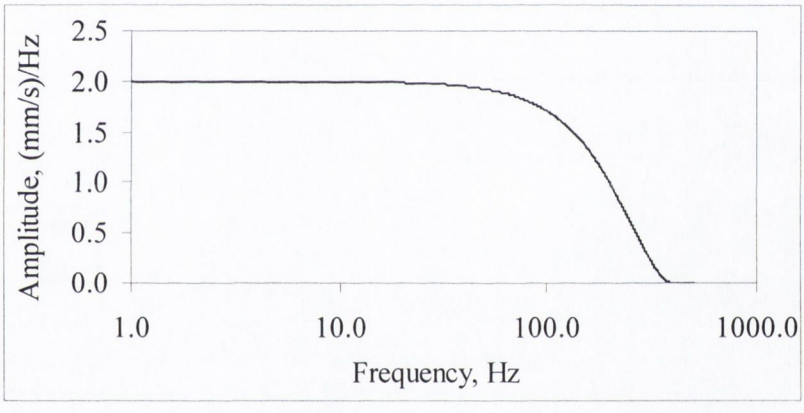

Fig.6.7–Fast Fourier Transform (FFT) of a short triangular pulse

6.6 Numerical Results

Finite element models were constructed of the ground, tunnel lining and the TBM frame at different sections along the tunnel bore. Consistent modelling techniques were used for each section points with material properties for the ground at these sections based on ground investigations.

The choice of element to be used for the ground, the tunnel lining and the TBM frame was limited in ABAQUS V6.4 because the three-dimensional eight-noded linear brick and reduced integration element, C3D8R, was the only element available both in the continuum

solid element and the infinite element family. Eight-noded linear brick elements with a linear material model have been used to define the ground, the tunnel lining and the TBM shutter frame.

In each case, the thicknesses of the different layers of ground were selected from the ground investigation information and extended in the tunnel direction to generate the solid model. For simplification, the material properties in each layer were assumed to be constant in the tunnel direction and in the transverse direction in the three-dimensional finite element model.

The boundary conditions applied to the finite element mesh were the same for each of the models. The ABAQUS/Explicit dynamics method was used to carry out the analyses of ground vibrations due to tunnelling. This method was originally developed to analyse high-speed dynamic events that can be extremely costly to analyse using implicit programs, such as ABAQUS/Standard. The ABAQUS/Explicit method is suitable for wave propagation problems or short-duration blast loading, etc. Contact conditions (between soil and structure) are formulated more easily using an explicit dynamics method than using an implicit method. An implicit method has difficulty converging because of the contact element, resulting in a large number of iterations. Such analyses are expensive in ABAQUS/Standard (implicit method) because each iteration requires a large set of linear equations to be solved. Contact conditions are readily formulated in the explicit method and can be enforced on a node-by-node basis without iteration. Another advantage of ABAQUS/Explicit is that it requires much less disk space and memory than ABAQUS/Standard for the same simulation.

6.6.1 Results and Discussions of Measuring Sections 1 and 2

The dimensions of the different layers of ground at Measurement Sections 1 and 2 are same and the same 3-Dimensional finite element model, which is shown in Fig.6.1, was used for both sections. The total length of the model was 132m and the depth was 40m. The thickness of the model was 20m and the length of the infinite element in each side of the model was 10m.

The vibrations were generated in the finite element model by applying a unit triangular pulse (Fig.6.6) to the ground in front of TBM frame. The duration of the analyses was 48hours. The output results presented in Figs.6.8 and 6.9 are the ground response in the transverse direction on the surface just above the TBM in the time domain and the frequency domain respectively at Measurement Section 1 due to the unit triangular pulse. In Figure 6.8, it can be seen that the finite element predicted ground vibrations are free from any reflections and this indicates that the infinite elements in ABAQUS are working effectively. In Fig. 6.9 it can be seen that the frequency band of greatest vibration amplitudes is in the range of 8 to 30Hz and the peak amplitude occurs at 18Hz. Fig.6.10 shows the measured TBM excitation in the transverse direction at Measurement Section 1 in the time domain and Fig. 6.11 is the Fast Fourier Transform (FFT) of Fig.6.10 and shows that most of the energy is concentrated in the frequency range of 3 to 30Hz; these are also called the source function.

Fig.6.12 shows the predicted vibration velocity $V(\omega)$ in the transverse direction due to transverse input load plotted against frequency, which is derived from the following equation:

$$V(\varpi) = F(\varpi) * \frac{Output(\varpi)}{Input(\varpi)} \qquad [6.4]$$

where $V(\omega)$ is vibration velocity at the surface and $F(\omega)$ is the source function, i.e. the TBM excitation.

Fig. 6.13, Fig. 6.14 and Fig.6.15 show the predicted vibration velocity in the time domain at the surface level just above TBM at measuring Section 1 in the three orthogonal directions (x, y and z respectively) due to the transverse TBM input load. The peak particle velocity due to a transverse load and the resultant peak particle velocity are calculated using Equations 6.5 and 6.6 respectively (Head and Jardine, 1992).

Peak Particle Velocity (PPV) due to a transverse load (T_{PPV}) $= \sqrt{T_x^{\,2} + T_y^{\,2} + T_z^{\,2}}$ [6.5]

Resultant PPV $= \sqrt{T_{PPV}^{\,2} + V_{PPV}^{\,2} + L_{PPV}^{\,2}}$ [6.6]

where T_x = Vibration velocity in the x direction (transverse) due to a transverse input load

T_y = Vibration velocity in the y direction (vertical) due to a transverse input load

T_z = Vibration velocity in the z direction (longitudinal) due to a transverse input load

T_{PPV} = Peak Particle Velocity (PPV) due to a transverse input load

V_{PPV} = Peak Particle Velocity (PPV) due to a vertical input load

L_{PPV} = Peak Particle Velocity (PPV) due to a longitudinal input load

The predicted transverse peak particle velocity with time at Section 1 is shown in Fig.6.16. The FE predicted peak particle velocity values are tabulated in Table 6.3 together with the measured values at different points at Sections 1 and 2 and the predicted values normalised with respect to the measured values. The predicted vertical and longitudinal peak particle velocity with time at Sections 1and 2 are shown in Appendix C.

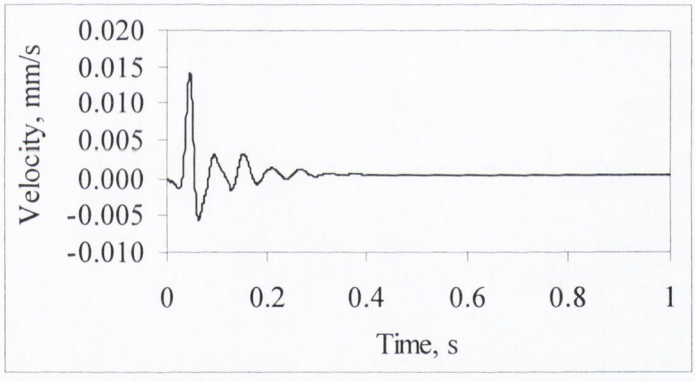

Fig.6.8–Predicted time history at the surface at Measurement Section 1; transverse direction

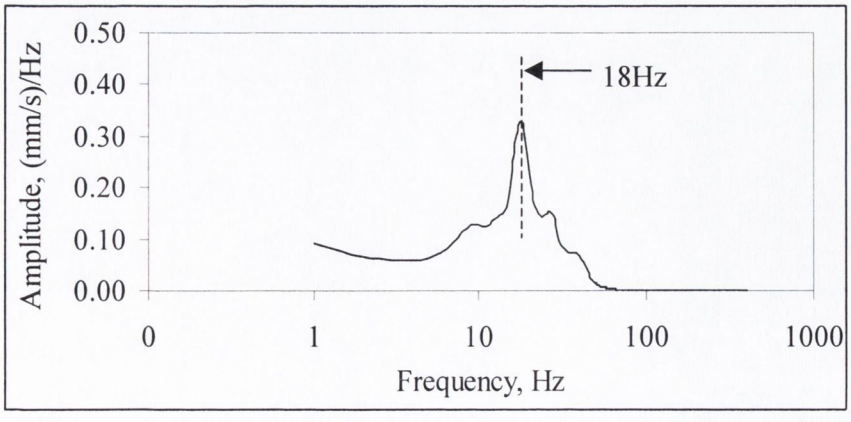

Fig.6.9–FFT of predicted time history at the surface at Measurement Section 1; transverse direction.

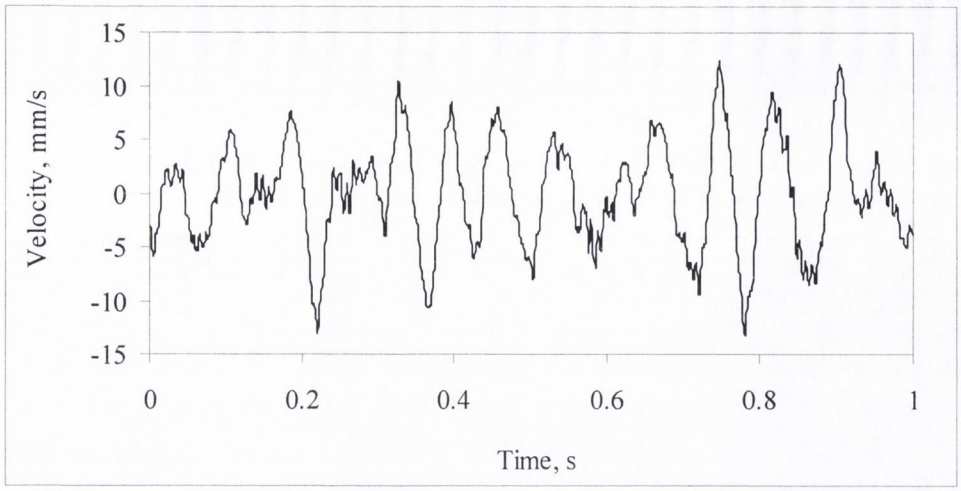

Fig.6.10–Measured TBM excitation velocity at Measurement Section 1; transverse direction.

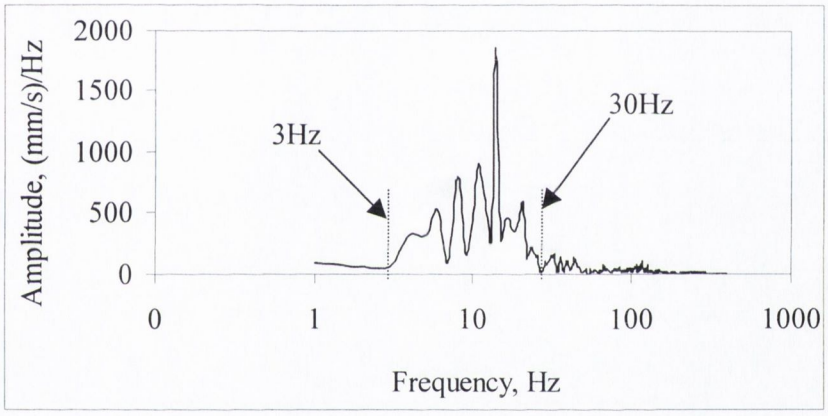

Fig.6.11–FFT of TBM excitation at Measurement Section 1; transverse direction.

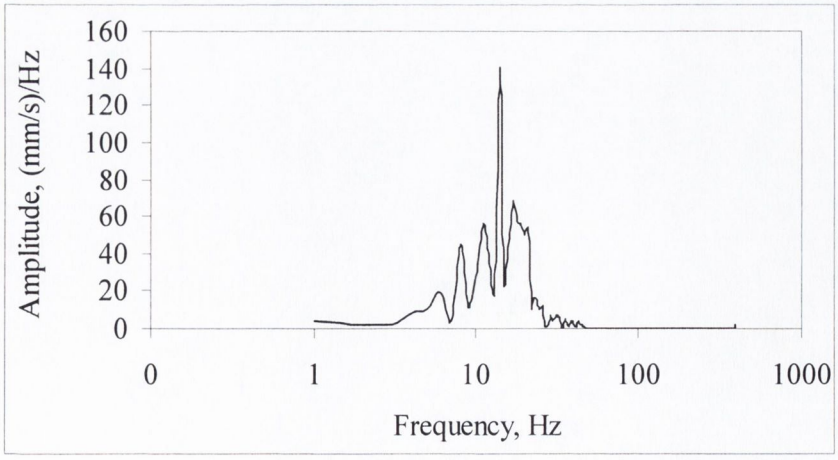

Fig.6.12– Predicted transverse vibration velocity (Frequency domain) at the surface at Measurement Section 1 due to transverse load.

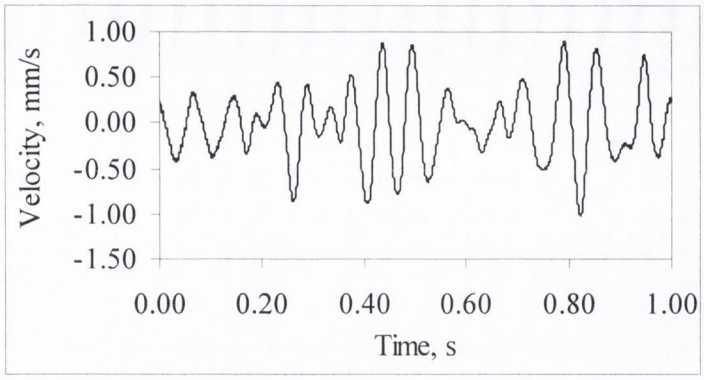

Fig.6.13–Predicted vibration velocity in the x direction at the surface at Measurement Section 1 due to transverse load.

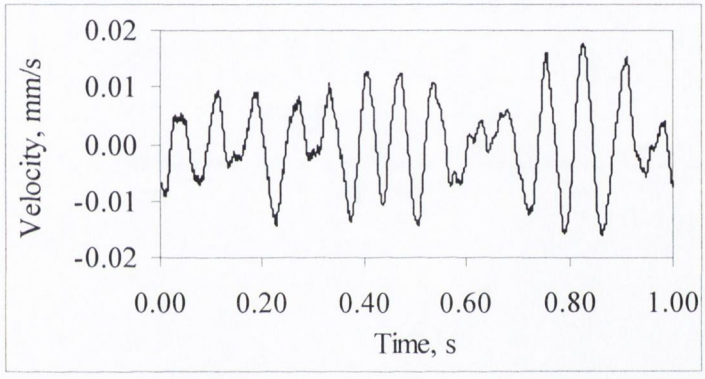

Fig.6.14– Predicted vibration velocity in the y direction at the surface at Measurement Section 1 due to transverse load.

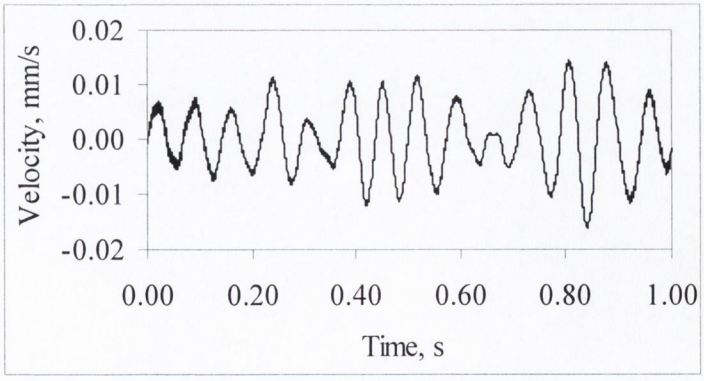

Fig.6.15– Predicted vibration velocity in the z direction at the surface at Measurement Section 1 due to transverse load.

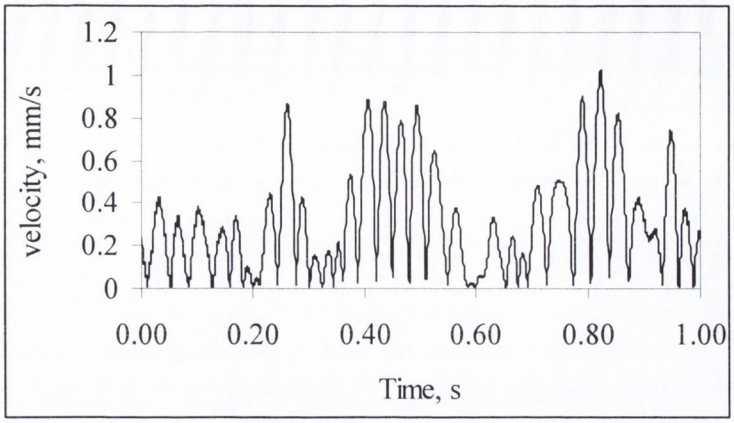

Fig.6.16–Predicted Transverse Peak Particle Velocity (PPV) at the surface at Section 1

Table 6.3– Predicted and Measured PPV Values at Section 1 and 2

Measurement Section	Measuring Points on Surface	Direction	FE Predicted PPV values, mm/s	Measured PPV values, mm/s	FE Predicted results normalised with respect to the measured values	% of Difference
1	Directly above TBM axis	Transverse	1.02	1.21	0.84	-16
		Vertical	0.45	0.84	0.54	-46
		Longitudinal	1.29	0.91	1.42	+42
		Resultant	1.69	1.73	0.98	-2
2	Directly above TBM axis	Transverse	0.76	1.24	0.61	-39
		Vertical	0.33	0.51	0.65	-35
		Longitudinal	1.82	1.58	1.15	+15
		Resultant	2.00	2.07	0.97	-3
2	+ 12 m away from TBM axis in transverse direction	Transverse	0.56	0.71	0.79	-21
		Vertical	0.21	0.33	0.64	-36
		Longitudinal	1.50	1.02	1.47	+47
		Resultant	1.61	1.29	1.25	+25
2	+ 25 m away from TBM axis in transverse direction	Transverse	0.4	0.52	0.77	-23
		Vertical	0.17	0.24	0.71	-29
		Longitudinal	0.80	0.67	1.19	+19
		Resultant	0.90	0.88	1.02	+2
2	+ 50 m away from TBM axis in transverse direction	Transverse	0.23	0.29	0.79	-21
		Vertical	0.16	0.17	0.94	-6
		Longitudinal	0.42	0.35	1.2	+20
		Resultant	0.50	0.49	1.02	+2

The percentage differences between the predicted and measured PPV values at Section 1 of the transverse, vertical and longitudinal vibrations at a point just above TBM on the surface are given in Table 6.3 with the FE values normalised with respect to the measured values which are found to be -16%, -46% and +42% respectively. Although the percentage differences between the FE predicted and the measured PPV values in the vertical and longitudinal directions are high but there is not a great difference between the FE predicted and measured vertical velocities which are 0.45 mm/s and 0.84 mm/s and the FE predicted and measured longitudinal velocities which are 0.91 mm/s and 1.29 mm/s. The percentage difference between the predicted and the measured resultant PPV is very small, being 2%.

At Section 2, the vibration velocities at the surface were measured and predicted at four different points: the first point directly above the TBM, the second 12m, the third 25m and the forth 50m in transverse directions from the tunnel centre line. The percentage differences between the predicted and the measured PPV values in the transverse, vertical and longitudinal directions, normalised with respect to the measured values, are -39%, -35% and +15% respectively, and given in Table 6.3. At the second point, the normalised differences between the predicted and measured PPV values in the transverse, vertical and longitudinal directions are -21%, -36% and +47% respectively. At the third point, the normalised differences between the predicted and measured PPV values in the transverse, vertical and longitudinal directions are -23%, -29% and +19% respectively. Finally at the forth point, the normalised differences between the predicted and measured PPV values in the transverse, vertical and longitudinal directions are -21%, -6% and +20% respectively. The percentage differences between the predicted and the measured resultant PPV values are small at the third and fourth points and which is 2%. The maximum percentage difference is 25% at the second point.

One of the reasons for the differences between the predicted and measured PPV values is because of the simplification of the ground profile, which has been modelled as three horizontal layers, and the assumption that the soil is a homogeneous and elastic material throughout the section.

6.6.2 Results and Discussions of Measuring Sections 3 and 4

The dimensions of the different layers of ground at Sections 3 and 4 are similar and the same 3-Dimensional finite element model, which is shown in Fig.6.4, was used. The total length of the model is 65m and the depth is 46m. The width of the model is 32m and the length of the infinite element in each side of the model is 10m.

The vibrations are generated in the finite element model by applying the unit triangular pulse (Fig.6.6) on the ground in front of the TBM frame and the analyses time was 46 hours. The results presented in Fig. 6.17 and Fig.6.18 are the output of the ground response at the surface just above TBM in the time domain and frequency domain respectively at Section 3 due to the unit triangular pulse. In Fig.6.17, it can be seen that there are no reflected vibrations, which indicates that the infinite elements in ABAQUS are working effectively. In Fig.6.18 it can be seen that the frequency band is 7-48 Hz. with a peak at 15 Hz. Fig.6.19 shows the measured transverse TBM excitation at Section 3 in the time domain and Fig.6.20 shows the FFT of the TBM excitation with a frequency band of 8-20Hz and a peak at 14Hz; this is called also source function.

Fig.6.21 shows the horizontal vibration velocity in the frequency domain in the transverse direction of the surface, which is derived from the Equation 6.4. Fig.6.22 shows the horizontal transverse vibration velocity at the surface level just above the TBM at Section 3 in time domain due to the transverse input load. The horizontal peak particle velocity and resultant horizontal peak particle velocity in transverse direction are calculated using Equation 6.5 and Equation 6.6 respectively. The FE predicted peak particle velocity values are tabulated in Table 6.4 together with the measured values at different points at Section 3 and 4 and the predicted values normalised with respect to the measured values. The predicted transverse, vertical and longitudinal peak particle velocity with time at Sections 3 and 4 are shown in Appendix C.

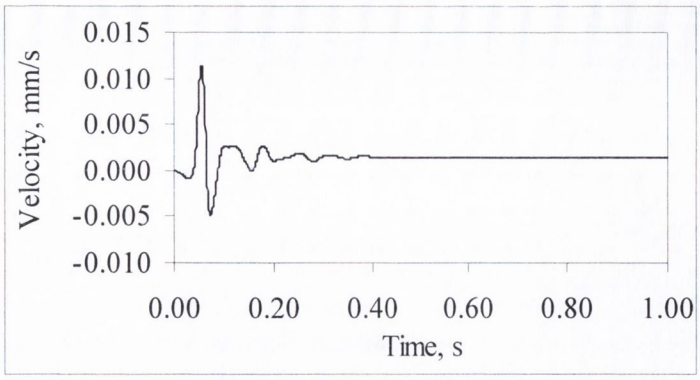

Fig.6.17–Predicted time history of the velocity at surface; transverse direction

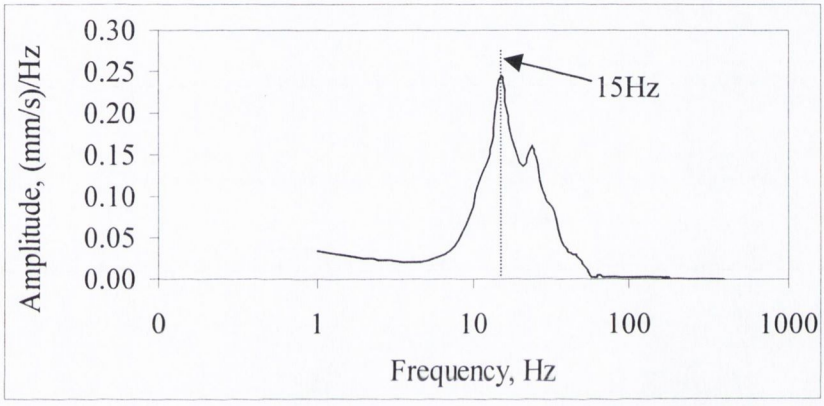

Fig.6.18–FFT of time history at surface; transverse direction

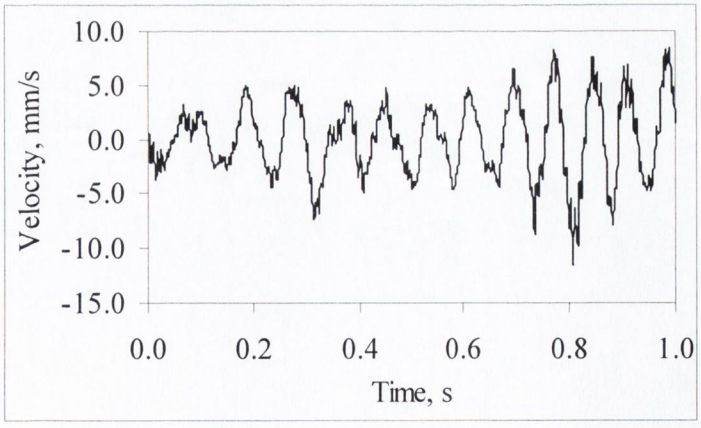

Fig.6.19–Measured TBM excitation velocity; transverse direction

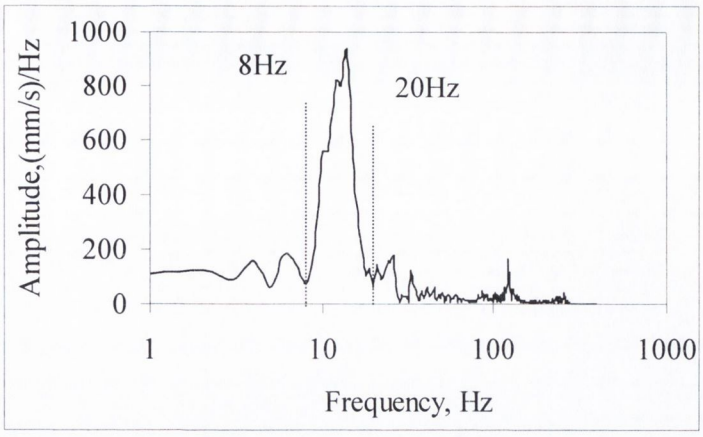

Fig.6.20–FFT of measured TBM excitation; transverse direction

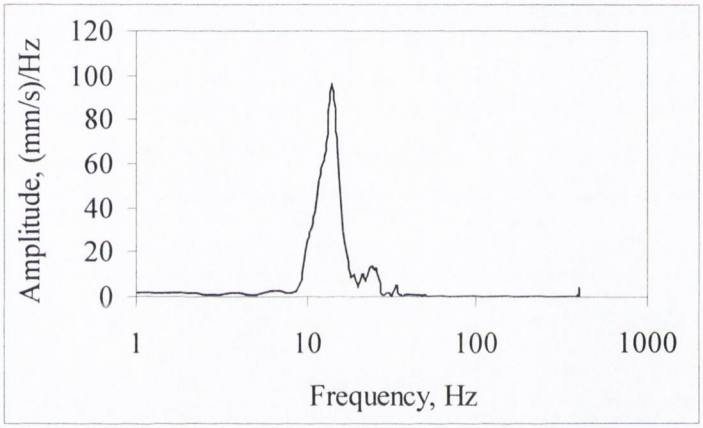

Fig.6.21–Predicted transverse vibration velocity (Frequency domain) at the surface

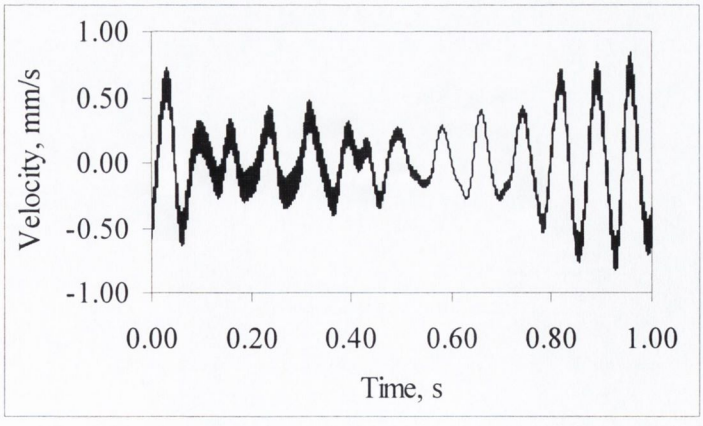

Fig.6.22– Predicted transverse vibration velocity at the surface

Table 6.4– Predicted and Measured PPV Values at Sections 3 and 4

Measuring Section	Measuring Points on Surface	Direction	FE Predicted PPV values, mm/s	Measured PPV values, mm/s	FE Predicted results normalised with respect to the measured values	% of Difference
3	Directly above TBM axis	Transverse	0.84	0.91	0.92	-8
		Vertical	0.52	0.42	1.24	+24
		Longitudinal	1.69	1.84	0.92	-8
		Resultant	1.96	2.10	0.93	-7
3	50m away from TBM axis in tunnel direction	Transverse	0.2	0.43	0.47	-53
		Vertical	0.15	0.22	0.68	-32
		Longitudinal	0.62	0.84	0.74	-26
		Resultant	0.67	0.96	0.70	-30
4	Directly above TBM axis	Transverse	0.64	0.82	0.78	-22
		Vertical	0.23	0.30	0.77	-23
		Longitudinal	1.38	1.68	0.82	-18
		Resultant	1.54	1.89	0.81	-19
4	30m in tunnel direction & 10m in transverse direction	Transverse	0.25	0.36	0.69	-31
		Vertical	0.091	0.16	0.57	-43
		Longitudinal	1.23	0.79	1.56	+56
		Resultant	1.26	0.88	1.43	+43

The percentage differences between the predicted and measured PPV values at Section 3 of the transverse, vertical and longitudinal vibrations at a point just above TBM on the surface are given in Table 6.4 with the FE values normalised with respect to the measured values and are -8%, +24% and -8% respectively. Although the percentage differences between the predicted and the measured PPV values in the vertical direction at 23% is higher than in the other directions, there is not a great difference between the FE predicted and measured vertical velocities which are 0.52 mm/s and 0.42 mm/s. The percentage differences between the predicted and the measured resultant PPV is small, being -7%. The percentage differences between the predicted and the measured PPV values in the transverse, vertical and longitudinal directions for the point on the surface 50m away from the TBM are -53%, -32% and -26% respectively. The percentage differences between the predicted and the measured resultant PPV values is -30%. Thus the percentage of difference between the predicted and measured PPV values at a point just above TBM is smaller than at the point 50m away from the TBM.

At Section 4, the vibration velocities at the surface were measured and predicted at 2 different points: the first point directly above the TBM and the second 30m in advance of TBM face and 20m in the transverse direction. The percentage differences between the measured and predicted PPV values in the transverse, vertical and longitudinal directions, normalised with respect to the measured values, are -22%, -23% and -18% respectively, and are given in Table 6.4. At the second point, the normalised differences between the measured and predicted PPV values in the transverse, vertical and longitudinal directions, are -31%, -43% and +56% respectively. The percentage differences between the predicted and the measured resultant PPV values at the 2 points at Section 4 are -19% and +43% respectively. This is due to the simplification of ground profile, which has been modelled as three horizontal layers, and assumption that the soil is a homogeneous and elastic material throughout the section.

It can be seen from the Table 6.4 that the predicted and measured velocities at Section 3 are greater than the corresponding predicted and measured values at Section 4 due to the difference of TBM excitation which are presented in Appendix B.

6.6.3 Results and Discussions of Measuring Section 5

The geometry of the 3-D finite element model at Section 5 is shown in Fig.6.5. The total length of the model is 122m and the depth is 45.4m. The centre-to-centre distance between the two tunnels is 40m. The 3-D finite element mesh is shown in Fig. 6.23.

The vibrations are generated in the finite element model by applying the unit triangular pulse (Fig.6.6) to the ground in front of the TBM frame. The analyses time was 7 days. The results presented in Fig. 6.24 and Fig.6.25 are the output of the ground response at the surface just above TBM in the time domain and frequency domain respectively at Section 5 due to the unit triangular pulse. In Fig.6.24, it can be seen that there are no reflected vibrations, which indicates that the infinite elements in ABAQUS are working effectively. In Fig.6.25 it can be seen that the frequency band is 6-38 Hz. with the peak vibration amplitude at 17 Hz. Fig.6.26 shows the measured transverse TBM excitation at Section 5 in the time domain and Fig.6.27 shows the FFT of TBM excitation and the frequency band 1-30Hz and peak vibration amplitude at 12Hz; this is called also source function.

Fig.6.28 shows the transverse surface vibration velocity in frequency domain directly above the TBM at Section 5, which is derived from the Equation 6.4. Fig.6.29 shows the predicted vibration velocity at the surface level just above TBM at Section 5 in time domain due to the transverse input load. The peak particle velocity in transverse direction and the resultant peak particle velocity are calculated using Equation 6.5 and Equation 6.6 respectively. The FE predicted peak particle velocity values at Section 5 are tabulated in Table 6.5 together with the measured values and the predicted values are normalised with respect to the measured values. The predicted transverse, vertical and longitudinal peak particle velocity with time at Section 5 are shown in Appendix C.

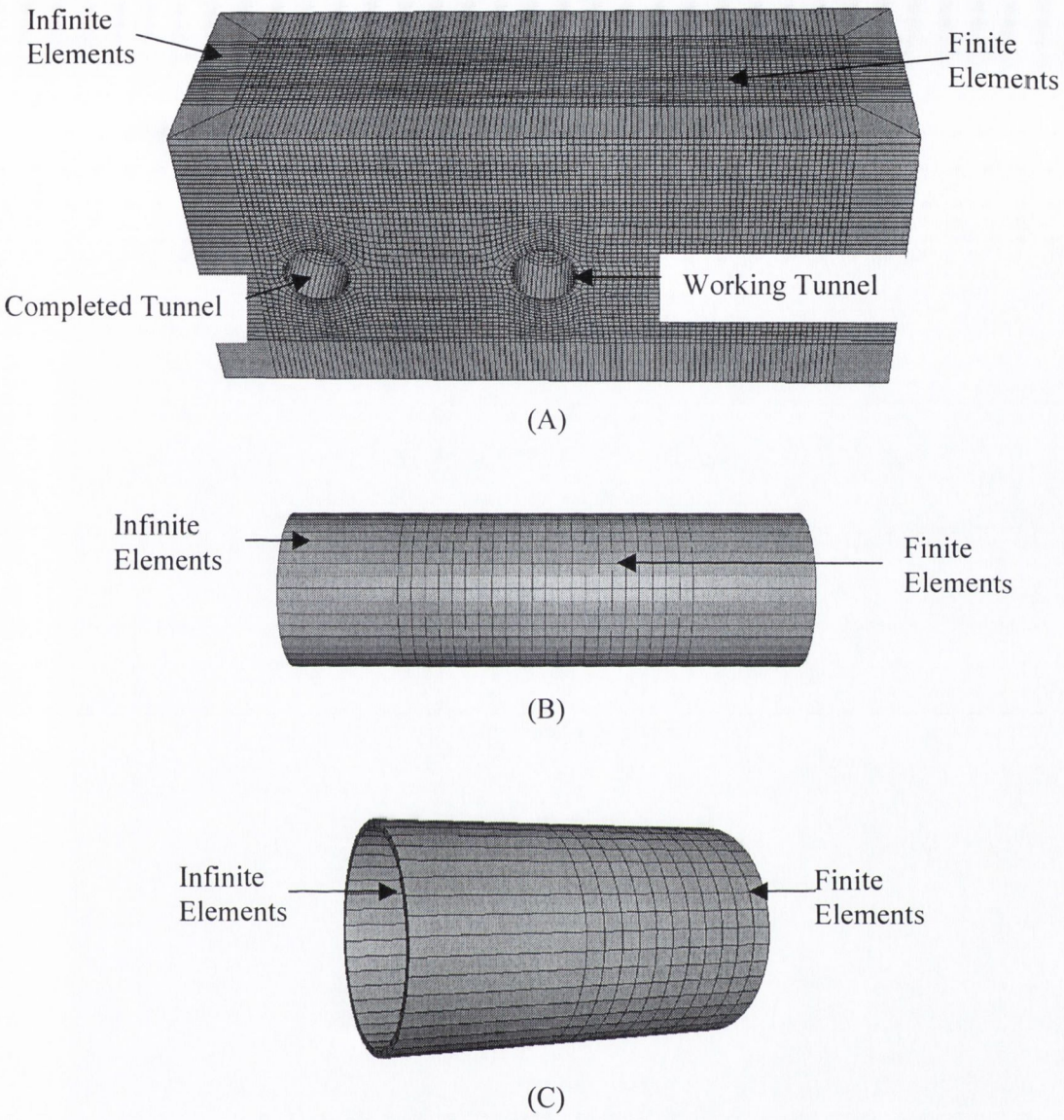

Fig.6.23–Finite element meshes at Section 5; (A) Ground, (B) Completed tunnel (C) Working tunnel

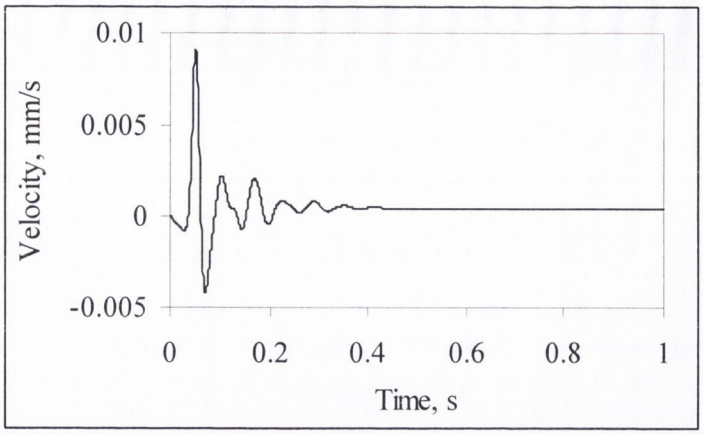

Fig.6.24–Predicted time history at surface; transverse direction

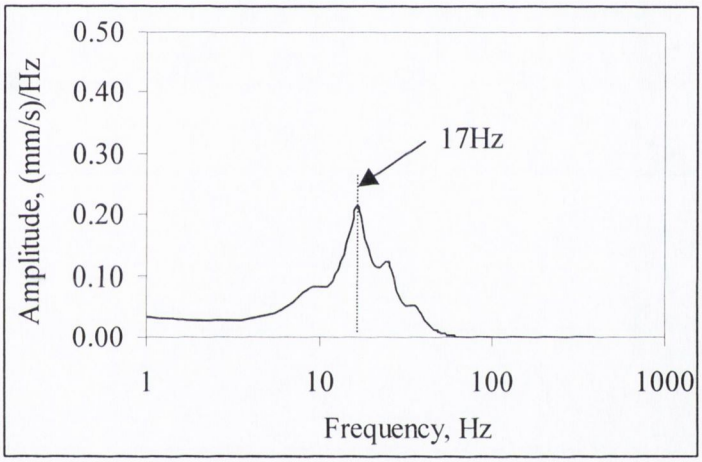

Fig.6.25–FFT of predicted time history at surface; transverse direction.

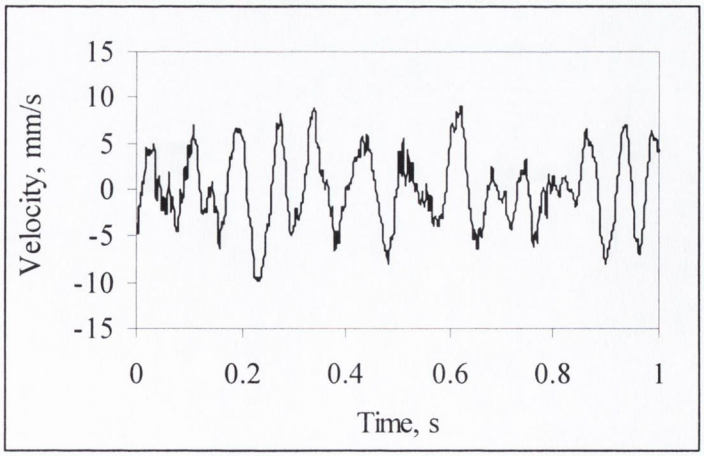

Fig.6.26–Measured TBM excitation velocity; transverse direction

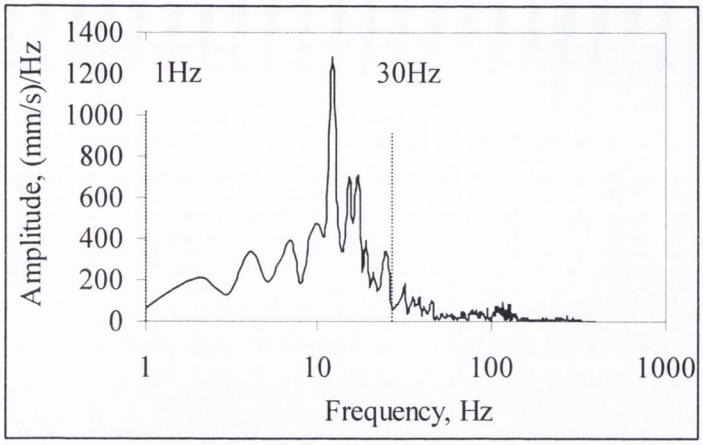

Fig.6.27–FFT of predicted TBM excitation; transverse direction

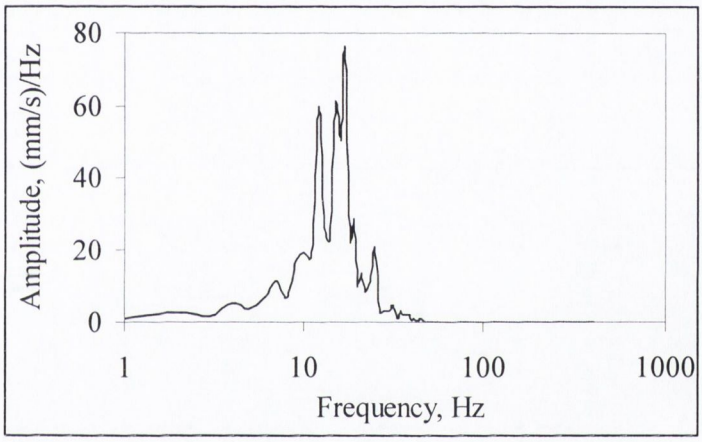

Fig.6.28– Predicted transverse vibration velocity (Frequency domain) in surface

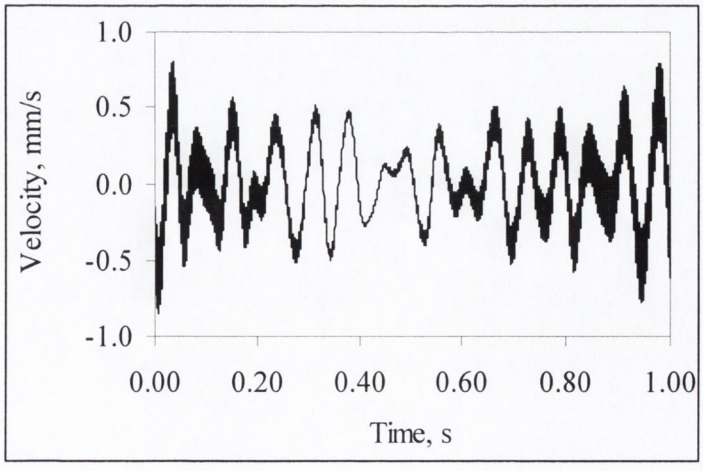

Fig.6.29– Predicted transverse vibration velocity at the surface

Table 6.5– Predicted and Measured PPV Values

Measuring Section	Measuring Points on Surface	Direction	FE Predicted PPV values, mm/s	Measured PPV values, mm/s	FE Predicted results normalised with respect to the measured values	% of Difference
5	Directly above TBM axis	Transverse	0.81	1.0	0.81	-19
		Vertical	0.48	0.38	1.26	+26
		Longitudinal	1.27	1.5	0.85	-15
		Resultant	1.58	1.84	0.86	-14

The percentage differences between the FE predicted and the measured PPV values in the transverse, vertical and longitudinal directions at a point on the surface just above the TBM are –19%, + 26% and –15% respectively, as shown in Table 6.5. The percentage difference between the predicted and the measured resultant PPV is also close, being equal to –14%.

One of the reasons for the differences between the predicted and measured PPV values is because of the simplification of the ground profile, which has been modelled as three horizontal layers, and the assumption that the soil is a homogeneous and elastic material throughout the section. Since the predicted resultant PPV value is within 14% of the measured value it is concluded that the model is good enough to predict the surface vibrations due to TBM.

6.6.3.1 The Effects of Existing Tunnel on Surface Vibrations

A study has also been carried out to investigate how the surface vibrations are affected by the presence of an existing tunnel during the construction of a second tunnel. The separation, i.e. the clear distance between the tunnel, S = 28.2m so that S/D = 2.39, where

D=11.8m is the tunnel diameter, and the cover, i.e. thickness of ground above the tunnels, C = 18m, so that C/D = 1.53. The 3-D finite element model is presented in Fig.6.23 and the results of the resultant PPVs that includes the existing tunnel are presented in Fig. 6.30 as the resultant PPV on the surface plotted against the direct distance from the centre of the TBM. It can be seen from Fig. 6.30 that the resultant PPV on the surface in the direction of the existing tunnel, at distances between about around 30m to 40m, is slightly higher than the resultant PPV at the same distance but is in the opposite direction away from the existing tunnel. A possible reason for this is the reflection of vibrations from the existing tunnel. However, the differences between these two results are very small indicating that, for the separation and depth of the particular diameter tunnels in this study, the effect of the existing tunnel on the surface vibrations is insignificant.

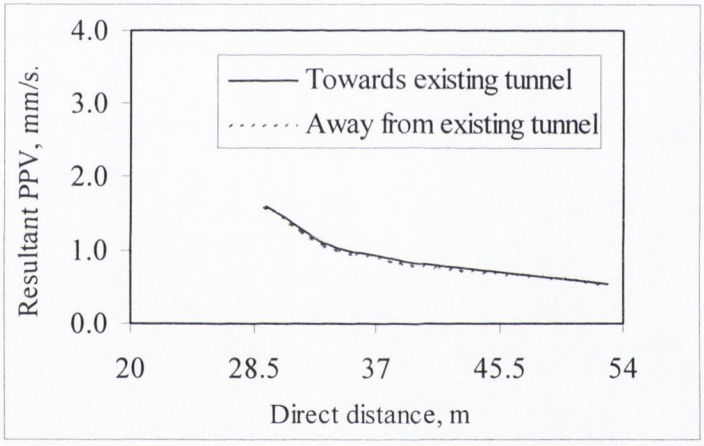

Fig. 6.30– The effects of existing tunnel on surface vibration

6.7 Parametric Study

The level of vibration observed at any point depends on the energy transmitted into the ground at the source and its subsequent attenuation within the ground. In this section, the results of a series of parametric studies to examine the sensitivity of the vibration predictions to variations in the various input parameters, which include the stiffness and the damping properties of the soil, are discussed.

The Nishimatsu Construction Company supplied the values of the material parameters used for the finite element modelling of the strata. The samples of soil were collected at different

locations and different depths along the tunnel line for testing in the laboratory.

6.7.1 The Effects of Varying the Stiffness of the Soil

A reference model of the ground was selected in which the soil parameter values were based on the results of the soil tests. The parameters required for the dynamic analyses were the weight density, dynamic Young's modulus, Poisson's ratio and the damping ratio and the values of these parameters are given in Table 6.1.

In order to investigate the effect of variations in the material parameters on the produced vibrations, the stiffness of the upper soil layer of the reference model was changed. The values used in this parametric study for the soil parameters in the upper soil layer are summarised in Table 6.6.

Table 6.6: Characteristics of materials

Parameter	Upper layer, (brown clay)	Dublin boulder clay	Limestone	Concrete	Steel
Density, kg/m^3	2000	2240	2710	2400	7800
Young's modulus, GPa	*0.10, 0.15, 0.20 & 0.25*	1.0	60	40	200
Poisson's ratio [v]	0.495	0.495	0.25	0.2	0.3
Damping, %	2.85	1.75	1.0	1.0	0.5

The results of the parametric study into the effects of variation in the upper layer's modulus of elasticity are presented in Fig. 6.31, Fig. 6.32 and Table 6.7. These are normalised with respect to the reference model (stiffness 0.2 GPa) results in Table 6.8.

As can be seen in Fig. 6.31, the resonance frequency increases with increasing stiffness of the upper soil layer. The resonance frequency is dependent on the stiffness of the soil layer. When the resonance frequency of the soil layer and the TBM excitation coincide or are very close, this results in a maximum vibration velocity. In Fig. 6.31, it can be seen that the resonance frequency of the soil layer at stiffnesses of upper soil layer of 0.1GPa, 0.15GPa, 0.20GPa and 0.25GPa are 15Hz, 17Hz, 18Hz and 19Hz respectively and in Fig.6.32 the

resonance frequency of the TBM excitation is 14Hz. Since the resonance frequency of 15Hz of the soil layers at stiffness 0.1GPa of upper soil layer is very close to the resonance frequency of 14Hz of the TBM excitation, the maximum vibration velocity at the surface is obtained at this stiffness as is shown by the graph in Fig. 6.33. The minimum vibration velocity is obtained at stiffness of upper soil layer of 0.25 GPa, since at this stiffness there is the greatest difference between the resonance frequency of the soil layers and the resonance frequency of the TBM excitation. Tables 6.7 and 6.8 show the dependence of the resultant PPV values on the upper soil layer parameters. The vibrations at points on the ground surface directly above the tunnel axis and up to 50m an either side are most sensitive to variations in the stiffness of the upper soil layer. After 50m from the tunnel axis the influence of the material parameters on the surface vibrations is relatively small.

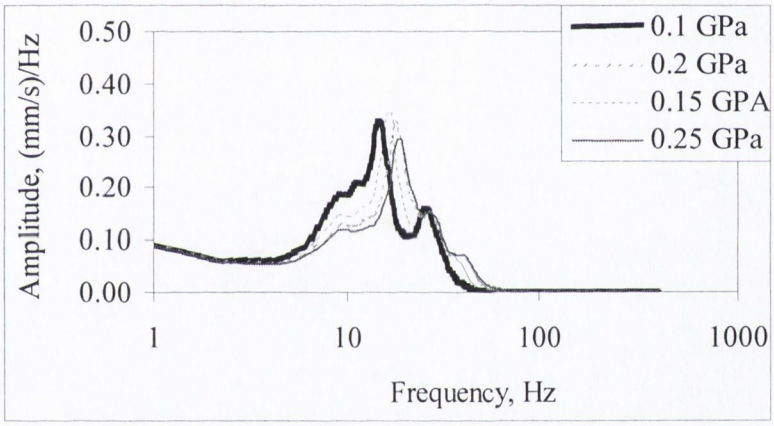

Fig.6.31–Output response (frequency domain) at the surface due to short triangular pulse

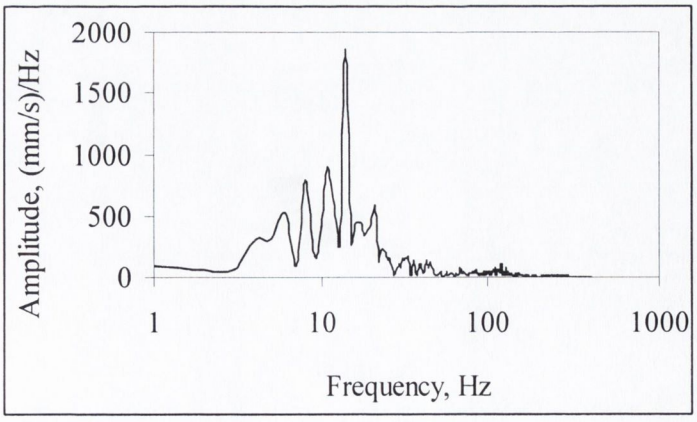

Fig.6.32–FFT of measured TBM excitation at Section 1

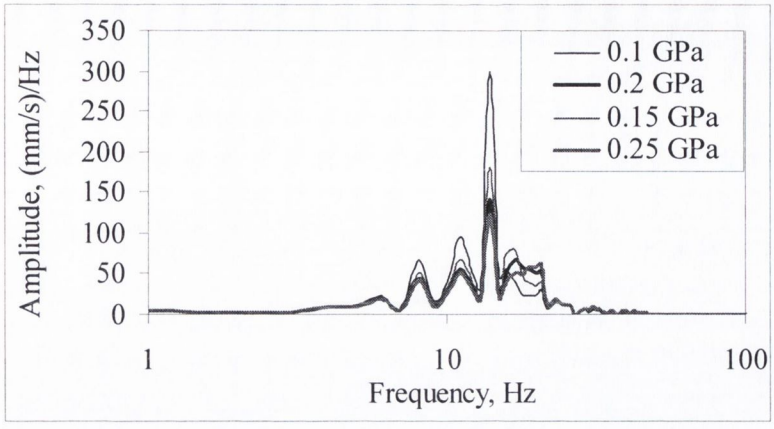

Fig. 6.33– Predicted vibration velocity (Frequency domain) at surface

Table 6.7–PPV values for reference model and models with varied upper soil layer stiffness

Location from the TBM face	PPV values (mm/s)			
	Reference model	Varied upper soil layer stiffness		
	0.20 GPa	0.10 GPa	0.15 GPa	0.25 GPa
0 m	1.02	1.32	1.15	0.93
12 m	0.62	0.88	0.74	0.60
25 m	0.34	0.49	0.39	0.32
50 m	0.14	0.15	0.14	0.16

Table 6.8–Normalised PPV values with reference model results

Location from the TBM face	PPV values (mm/s)			
	Reference model	Varied upper soil layer stiffness		
	0.20 GPa	0.10 GPa	0.15 GPa	0.25 GPa
0 m	1.00	1.29	1.13	0.91
12 m	1.00	1.42	1.19	0.97
25 m	1.00	1.44	1.15	0.94
50 m	1.00	1.07	1.00	1.14

6.7.2 The Effects of Varying the Damping of the Soil

Damping is the property of material to absorb vibration energy. The ratio between the damping of the material to the critical damping is called damping ratio. Critical damping is the smallest amount of damping for which no oscillation occurs in the vibration system. The damping ratio of the soil is a parameter that is difficult to determine. Often the damping ratio is assumed to be 1-6% of the critical damping. In the ABAQUS finite element program, the damping matrix, C is defined as a having two components, one proportional to the mass and the other proportional to the stiffness (ABAQUS, 2004):

$$[C] = \alpha [M] + \beta [K] \qquad [6.7]$$

where [K] is the stiffness matrix, [M] is the mass matrix, [C] is the damping matrix, α is the coefficient of mass damping and β is the coefficient of stiffness damping.

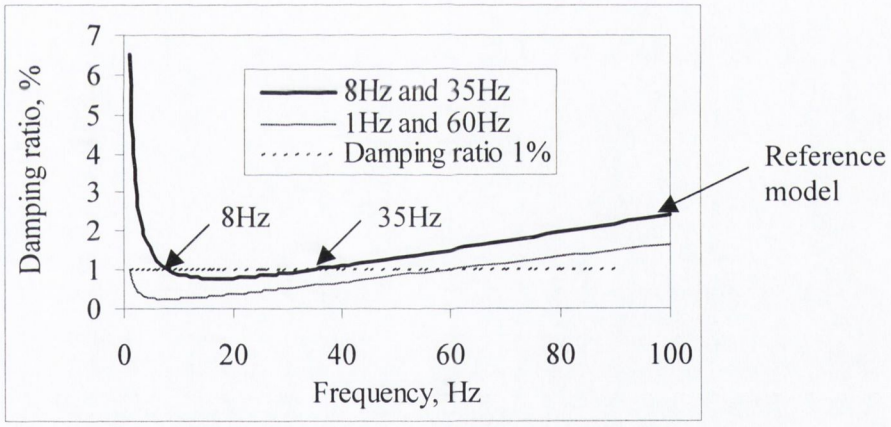

Fig.6.34–Damping ratio of 1% dependent on frequency

In this formulation of the damping, two frequencies can be chosen at which a given proportional damping applies. At other frequencies, the damping ratio will be different. Fig. 6.34 shows two cases. In the reference model, the frequency is chosen so that it is exactly 1.0% at 8 and 35 Hz. In that case, the damping ratio is close to 1.0% between 8 and 35 Hz. However, at lower and larger frequencies, the damping ratio is considerably larger. The two frequencies values at which the damping ratio matches should not be far away from each other. In Fig. 6.34, it can be seen that the damping ratio will drop to 0.28% if the lower and

upper bounds are 1 and 60 Hz; i.e. if the chosen frequency range is wide, the damping will be small between the lower and upper bound frequencies.

In order to investigate the effect of the material parameters on the results, the frequency range to calculate the α and β values for the reference model have been changed. The data used in this study are summarised in Table 6.9.

Table 6.9: Characteristics of materials

Parameter	Top layer, (brown clay)	Dublin boulder clay	Limestone	Concrete	Steel
Density, kg/m^3	2000	2240	2710	2400	7800
Young's modulus, GPa	0.2	1.0	60	40	200
Poisson's ratio [ν]	0.495	0.495	0.25	0.2	0.3
Damping, %	2.85	1.75	1.0	1.0	0.5
Frequencies ranges	*8 and 35 Hz*	*8 and 35 Hz*	*8 and 35 Hz*	*8 and 35 Hz*	*8 and 35 Hz*
	1 and 60 Hz	*1 and 60 Hz*	*1 and 60 Hz*	*1 and 60 Hz*	*1 and 60 Hz*

Over the whole frequency range, the response function, which is the vibration amplitude at the surface level due to input load in front of the TBM face, will increase if the chosen frequency range is wide. It can be seen from Figs. 6.35 and 6.36 that the response function increased with increase in the chosen frequency range. With increase in the chosen frequency range, the damping ratio values decrease (Fig.6.34) and yield larger response function. The results of the parametric study on the effects of the damping are presented in Table 6.10. These are normalised with respect to the reference model results in Table 6.11. In Table 6.10, it can be seen that the vibration velocity increases with increasing frequency range i.e. with decreasing damping value. However, the increase in the vibration velocity is the highest on the surface directly above the TBM and decreases with distance from the tunnel face (Table 6.11).

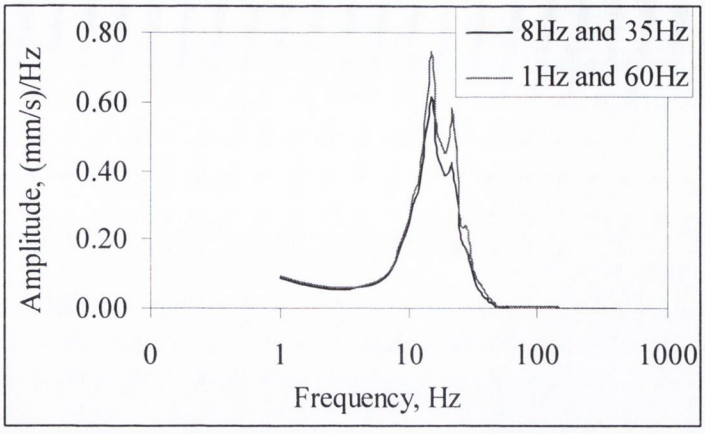

Fig.6.35– Output response (frequency domain) at the surface at 0m from TBM face due to short triangular pulse

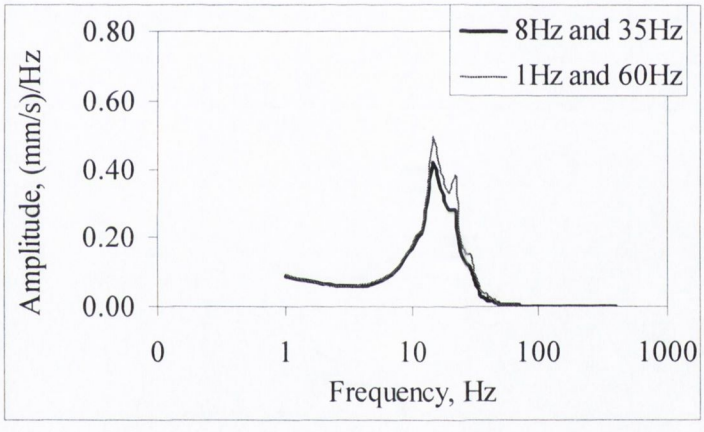

Fig.6.36– Output response (frequency domain) at the surface at -10m from TBM face due to short triangular pulse

Table 6.10: PPV (mm/s) at measuring points for reference model and models with adopted relative damping

Frequency ranges	PPV at measuring points on surface		
	-10 m from TBM face	0 m from TBM face	+50 m from TBM face
8 and 35 Hz [Reference]	0.50	0.84	0.20
1 and 60 Hz	0.55	0.99	0.21

Table 6.11–Normalised PPV with respect to reference model results

Frequency ranges	PPV at measuring points on surface		
	-10 m from TBM face	0 m from TBM face	+50 m from TBM face
8 to 35 Hz [Reference]	1.00	1.00	1.00
1 to 60 Hz	1.10	1.18	1.05

6.8 Modified 3-D Modelling

In this section, the results of analyses using a modified 3D finite element program are presented. The ABAQUS V6.5 finite element software was used to construct the model and three-dimensional eight-noded linear brick and reduced integration elements, C3D8R, were employed for the ground and the tunnel lining. In this model the middle layer, the Dublin black boulder clay, was divided in to four layers instead of one layer as in the previous analyses.

The dimensions of the finite element model were 132m in transverse direction, 50m in vertical direction and 40m in along the tunnel direction. The thickness of the top layer was 2.5m, the middle layer was 11m and the bottom layer was 36.5m. The diameter of the tunnel was 12m. The finite element model geometry is shown in Fig. 6.37. The material properties for the four layers of Dublin boulder clay were based on the results of the author's laboratory bender element tests. The values of the ground parameters used in these finite element analyses are given in Table 6.12. It can be seen by comparing Tables 6.1 and 6.12 that the stiffness and damping parameters for the mid layer (Dublin boulder clay) are higher for the second study (new) than for the first (old).

Another study was carried out in which the limestone properties were varied. The limestone properties were determined by ultrasonic pulse velocity tests. In this study the bolder clay properties were kept constant and number of layer was one. The main purpose of this study was to determine the effect on the surface vibrations of varying only the limestone properties. The material properties of the limestone samples are presented in Table 6.13.

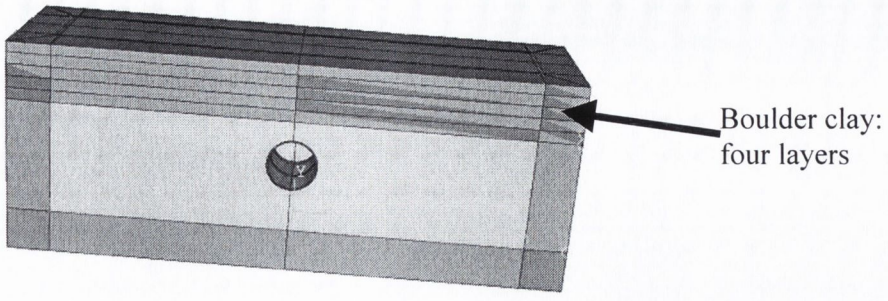

Fig.6.37– Finite element model geometry

Table 6.12- Values of ground parameters used in ABAQUS analyses

Layer/Parameter		Density, kg/m^3	G_{max}, GPa	E_{max}, GPa	Damping ratio, %	Poisson's ratio [ν]
Top layer, (brown clay)		2000	0.067	0.2	2.85	0.495
Dublin boulder clay	Layer 1	*2200*	*0.42*	*1.26*	*5.65*	0.495
	Layer 2	*2200*	*0.51*	*1.52*	*5.65*	0.495
	Layer 3	*2200*	*0.59*	*1.76*	*5.23*	0.495
	Layer 4	*2200*	*0.66*	*1.97*	*5.23*	0.495
Limestone		2710	24	60	1	0.25

Table 6.13- Values of ground parameters used in ABAQUS analyses

Layer/Parameter	Density, kg/m^3	G_{max}, GPa	E_{max}, GPa	Damping ratio, %	Poisson's ratio [ν]
Top layer, (brown clay)	2000	0.067	0.2	2.85	0.495
Dublin boulder clay	2240	0.33	1.0	1.75	0.495
Limestone	*2673*	*32*	*80*	1.0	0.25

6.8.1 Results and Discussions

The vibrations were generated in the finite element model by applying a unit triangular pulse (Fig.6.6) to the ground in front of TBM frame. The analysis time for the original one layer of Dublin boulder clay model was 2 days while the analyses time for second modified model (new) was 8 days due to increase in the number of layers for the Dublin boulder clay and stiffness which increase the global matrix size. The results of the new analyses using

the author's bender element data are presented in Figs. 6.38 and 6.39 where they are compared with the results of the first study.

The results of the second modified model (new) are presented in Figs.6.40 and 6.41. In this model the material properties were based on Table 6.13. The average shear modulus of the three limestone samples was 32 GPa (Table 6.13) whereas in the original old model it was 24 GPa (Table 6.1).

Figs. 6.38 to 6.41 show that the second study (new), using the author's data, gives higher vibration velocities at the surface than first study while there is no significant difference between the two studies. It can be concluded that the NCC stiffness and damping data and author's stiffness data are relevant whereas the author's damping data is bit higher for like stiff Dublin boulder clay. However, it was found from the parametric studies that the effects of the damping on the surface vibrations are insignificant compared to the effect of variations in the stiffness of the material, which was modelled as being linear elastic.

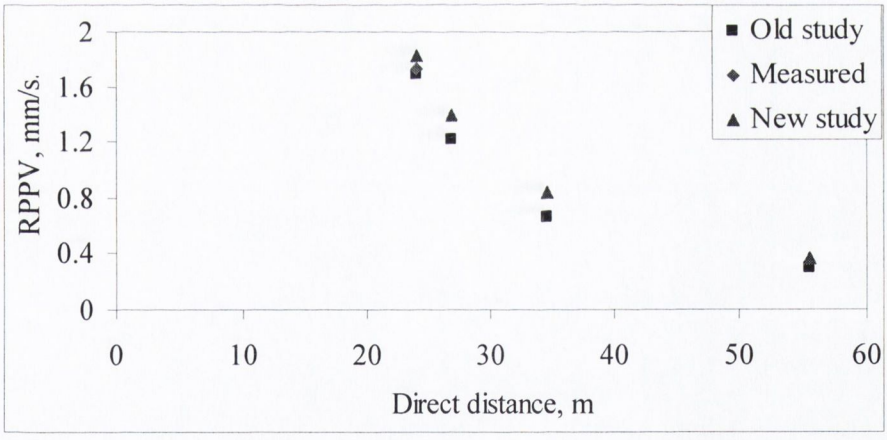

Fig. 6.38 – Modified 3-D finite element results at Section 1

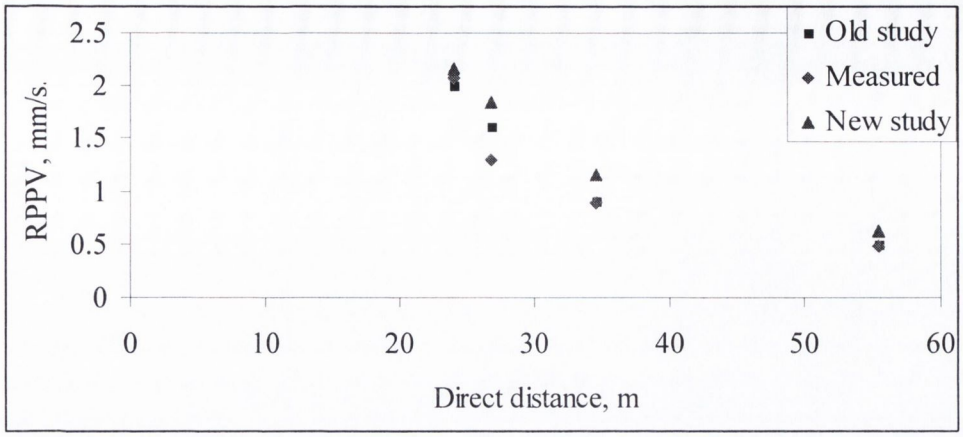

Fig. 6.39 – Modified 3-D finite element results at Section 2

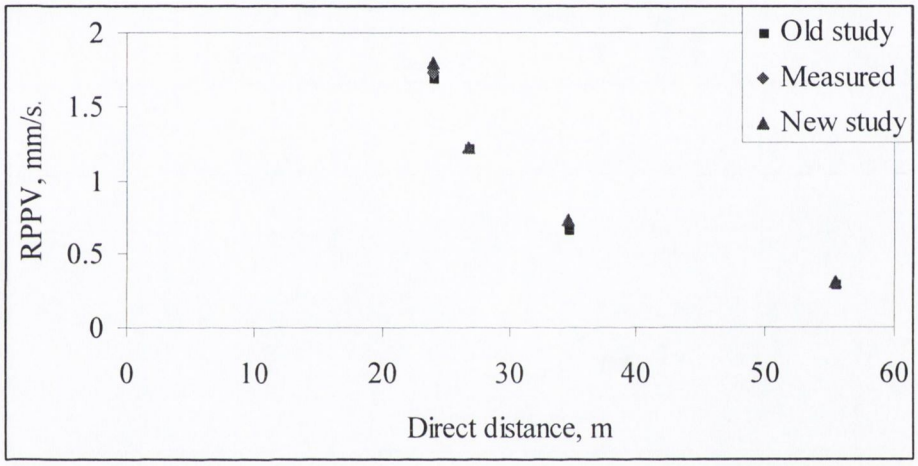

Fig. 6.40 – Modified 3-D finite element results at Section 1

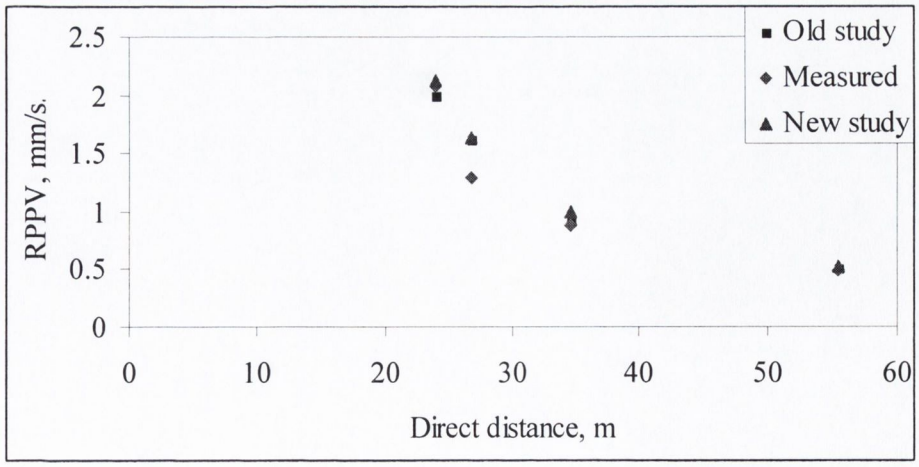

Fig. 6.41 – Modified 3-D finite element results at Section 2

6.9 2-D Axi-symmetry Model

An Axi-symmetry element type can be used to model a solid of revolution but this can only be used when the geometry, material properties, constraints, and loads are all axisymmetric. In this section, two ways that were used to try to develop an axi-symmetry finite element model are described and the geometry of these models is shown in Figs. 6.42 and 6.43. Fig.6.42 shows the first way with a vertical axis of symmetry where the geometry and soil layers are symmetrical while vibration from the TBM in the direction of the tunnel axis is not symmetrical because it is not in the direction of the vertical axis of symmetry. Fig.6.43 shows the second way, with a horizontal axis of symmetry along the tunnel axis. In this case the soil layers are not symmetrical although it is possible to apply vibration in the direction of tunnel axis. From this discussion it can be concluded that axi-symmetry analyses can not be used to predict of TBM induced ground vibrations.

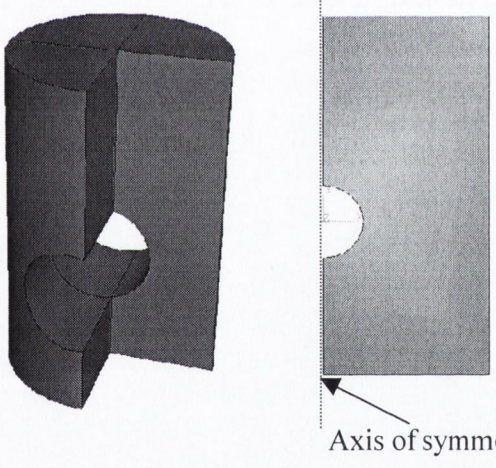

Fig.6.42– Axi-symmetry model (1)

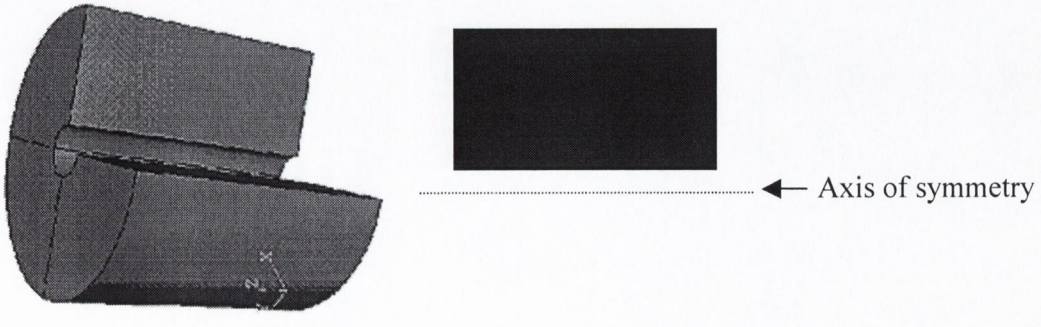

Fig.6.43– Axi-symmetry model (2)

6.10 Conclusion

3D finite element analyses of TBM induced ground vibrations have been used to model the ground response at the surface and it has been found that it is possible to simulate and analyse the ground vibrations. The finite element method is a numerical method for obtaining approximate solutions to engineering problems. Good agreement, in terms of PPV, has been found between the measured PPV values and the values calculated using 3-D finite element analyses. Although good agreement has been found and the FE method widely applicable, there are some limitations for practical applications regarding the time for the analyses and the input data required. The minimum analyses time was 48 hours which is very time consuming for practical applications. In order to carry out 3D FE analyses, the dynamic soil parameters, such as small strain stiffness, the damping ratio, Poisson's ratio, density and TBM excitation are required. Although it is possible to obtain the soil parameters before the start of tunnel construction, however it is not possible to obtain the TBM excitation before the start of tunnel construction and analyses will not be carried out. An axi-symmetry model cannot be used for FE analyses as there is no axis about which both the soil layers and the TBM vibrations are symmetrical.

The stiffness of the ground was found to be the most important parameter affecting the resonance frequency of the ground. If the resonance frequency of the ground coincides with the resonance frequency of the TBM excitation or is very close to it, it will lead to larger vibration levels and vice versa. Variations in the stiffness of the ground close to the tunnel have a significant influence on the magnitude of the vibrations at the surface while variations in the stiffness of the ground at distances 50m from the tunnel have little influence on the surface vibrations. The effects of the damping ratio on the surface vibrations are insignificant compared to the effect of the stiffness on the vibrations.

CHAPTER 7

EMPIRICAL MODEL

7.1 Introduction

In this chapter the use of empirical models to predict the ground vibrations at the surface due to construction of the Dublin Port Tunnel, which are based on experience and a limited number of case studies, are discussed. The prediction of the vibrations at the ground surface due to a TBM is complex as the vibrations are a function of the vibrational excitation provided by the TBM, the ground properties and the distance between the vibration source and the points of interest. As so many variables are involved in the determination of the vibration levels in the ground due to tunnelling, no explicit relationships exist which allow accurate predictions of the vibration magnitudes to be made for any given source and ground conditions. Approximate empirical relations have been developed based on experience and a limited number of case studies, relating the resultant peak particle velocity at the ground surface to the distance from the TBM for different ground conditions.

7.2 Ground Vibrations Predictions

Any method for predicting ground vibrations should be appropriate for both the activity and the site. Although mechanised tunnelling generates groundborne levels vibration that are unlikely to cause damage to most structures, these vibration levels may cause disturbance to people at quite considerable distances from the works. While many published relationships can be found for predicting the vibrations due to piling and blasting, there are few published reports that provide relationships for predicting the vibrations due to tunnelling.

7.3 Empirical Model 1

Godio et al. (1992 cited by Hillar and Crabb, 2000) proposed an equation for predicting the ground vibrations at the surface due to tunnelling, in the form of an equation for the peak particle velocity. This is a useful first estimate for predicting the vibration levels likely to be generated by mechanised bored tunnelling works and is given by the exponential equation:

$$V=Ar^{-1.3} \qquad [7.1]$$

Where,

V is the predicted resultant peak particle velocity (mm/s).

A is a constant whose value depends on the ground condition; for hard ground A=180.

r is the direct distance from the vibration source to the measurement point (m).

Equation 7.1 is suitable for values of *r* ranging from 10 to 100m.

The direct distance r, (Fig. 7.1) from the source of the vibrations to the point of interest is an important parameter when predicting the vibration level at the surface due to tunnelling. This direct distance may be calculated from the horizontal and vertical distances between the TBM as the source and the measurement locations. For tunnelling works, it is clearly important that the TBM depth as well as the lateral distance are recorded in order to calculate the direct distance from the source of the vibrations to the point of interest.

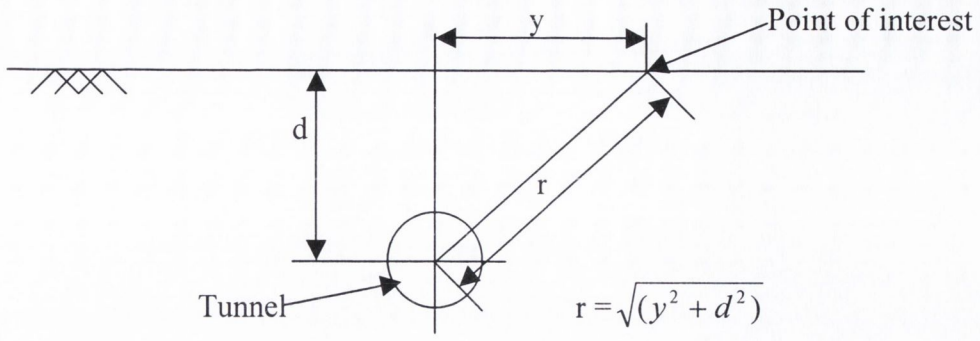

Fig. 7.1– Definition of the parameters for the empirical equation

Using Godio et al.'s equation, several cross sections along the line of the bored tunnel have been studied in order to determine the influence of the TBM operation on the surface vibrations at these cross sections. The cross sections chosen along the tunnel alignment are at every 200m between the sections at chainage 2000m and 4500m. For each cross section, the depth to the tunnel axis, d, is determined. The calculations have been carried out for the vibrations on the surface at each cross section directly above the centreline of the tunnel and at different distances, y, of 15, 30, 45, 60, 75 and 90m from this centreline. The results of the calculations for the vibrations at the surface along the centre line of the tunnel are presented in the Fig. 7.2.

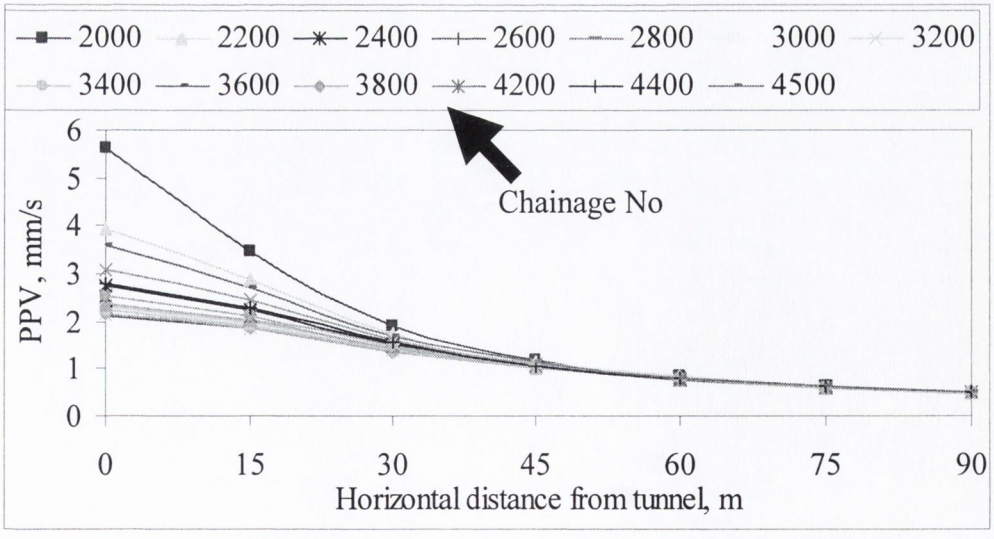

Fig.7.2–Predicted PPV values using the Godio et al. equation for hard ground

For a 90m wide corridor along the bored tunnel between chainages 2000m and 4500m, the maximum estimated peak particle velocities using the Godio et al. equation for hard ground with A = 180, are between 0.49mm/s and 5.62mm/s. BS 7385 recommends that the peak particle velocity is used to assess the impact of the vibrations and specifies damage criteria for frequencies between 1Hz to 1 kHz. In terms of avoiding cosmetic damage, at a frequency of 4Hz, the recommended maximum value is 15mm/s peak particle velocity, increasing to 20mm/s at 15Hz and 50mm/s at 40 Hz and above. However, these maximum PPV values are much higher than the published acceptable limits of 0.28mm/s to 0.56mm/s for avoiding disturbance & humans. The maximum predicted PPV value is at chainage 2000, at the start of the bored tunnel, where the tunnel is at depth of 14.4m and hence closest to the ground level. The minimum predicted PPV value is at chainages 2800m and 3200m where the depth of the tunnel is 29.9m. It is concluded that the estimated values were high enough to be noticeable to humans.

7.4 Empirical Model 2

Nishimatsu Construction Co. (NCC) Ltd. has also developed an equation for predicting the vibrations due to tunnelling from PPV values monitored on other construction sites. Correlations between the peak particle velocity, V and the distance from the point source to the point of interest, r of the form $V = Nr^{-m}$ but it was found that the coefficients N and m change with the ground conditions, the diameter of the tunnel boring machine and the thrust force of the machine. The equations obtained from a number of different tunnelling works, are presented in Table 7.1.

Table 7.1–Summary of tunnel vibration data sites compared to predictions

Project No	Project	Geology	TBM type	Tunnel diameter (m)	Tunnel cover (m)	NCC Equation $V = Nr^{-m}$
No. 1	Rail (JLE)	Sands and clays	Mix shield	5.13	21.2	$V = 0.15r^{-0.66}$
No 2	Rail (Channel Tunnel)	Clay/ Chalk	Full face TBM	8.72	22.6-55	$V = 3.4r^{-0.71}$
No.3	Cable Tunnel	Mudstone	Full face TBM	2.44	11	$V = 133r^{-1.96}$
No. 4	Emergency Tunnel	Nohi rhyolites	Open shield	4.5	100	$V = 0.6r^{-0.27}$
No.5	Road (Pilot Tunnel)	Sandstone	Open shield	5.0	70	$V = 7.6r^{-1.4}$
No. 6	No Information					$V = 48r^{-1.47}$
No. 7	Dublin Port Tunnel	Limestone	Open shield	11.8	14.4-29.9	Upper bound $V = 176r^{-1.18}$
No. 8						Lower bound $V = 7.4r^{-1.07}$

From the equations for the PPV values in Table 7.1 obtained from previous tunnelling projects, the following upper- and lower bound equations were obtained to predict the peak particle velocity in the case of Dublin Port tunnel:

$$V = 176r^{-1.18} \quad \text{upper bound} \qquad [7.2]$$

$$V = 7.4r^{-1.07} \quad \text{lower bound} \qquad [7.3]$$

Using the NCC upper and lower bound equations, several cross sections along the line of the bored tunnel have been studied in order to predict the vibrations at the surface due to the TBM. The cross sections chosen along the tunnel alignment are the same as those chosen for the Godio et al. equation, i.e. every 200m along the tunnel, between chainages 2000m and 4500m. The calculations have been carried out for the vibrations on the surface at each cross section at a point directly above the tunnel centreline and at distances, y, of 15, 30, 45, 60, 75 and 90m from this centreline. The results of the calculations of upper and lower bounds for the vibrations at the surface along the centre line of the tunnel are presented in the Fig. 7.3 and 7.4.

For a 90m wide corridor along the bored tunnel, the maximum predicted upper bound peak particle velocities using the NCC Equation are between 0.84mm/s and 7.56mm/s, while the minimum predicted lower bound PPV values are between 0.058mm/s and 0.426mm/s. The highest value is again predicted at the start of the bored tunnel, where the tunnel is the closest to the ground level.

In every case the ground surface vibrations predicted using the NCC equation are different at the different chainage points up to horizontal distances of 50-60m from directly above the tunnel centreline while after 50-60m the values are almost same. This is because the equations are function of only the direct distance between the sources of vibration to the point of interest and the direct distance is a combination of the depth of tunnel and the horizontal distance from the tunnel centre to the point of interest r = $\sqrt{(d^2 + y^2)}$. Close to the tunnel centreline the depth of tunnel, d, is greater than the horizontal distance, y, and d is different for each chainage section and hence different PPV values are predicted for each point using NCC equation. With increasing transverse distance from the tunnel centreline the value of y is increasing and d is constant. y is same for every chainage point and hence PPV values are almost same for every chainage point which is shown in Table 7.2.

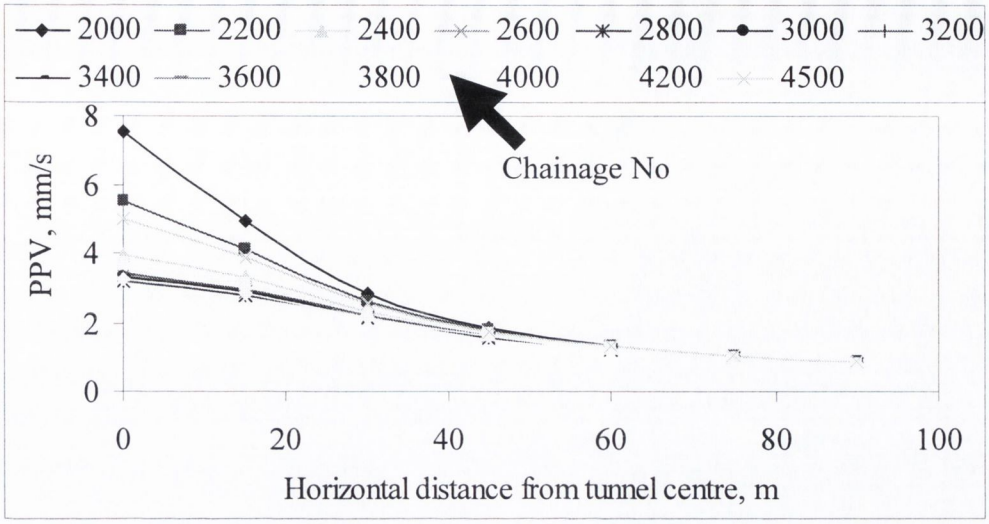

Fig.7.3–Predicted upper-bound vibration levels using NCC equation

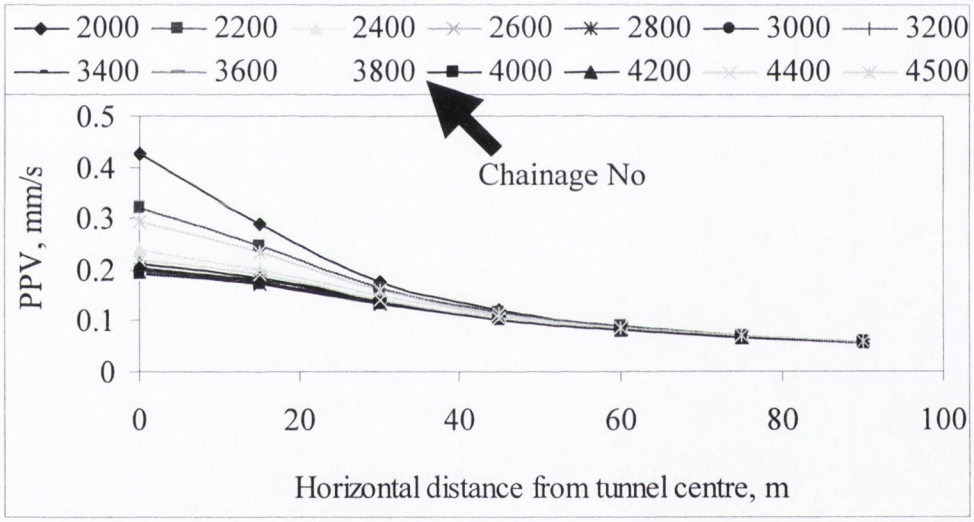

Fig.7.4–Predicted lower-bound vibration levels using NCC equation

Table 7.2–A comparison study

Depth	Location	d (m)	y (m)	r (m)	$176r^{-1.18}$
Shallow depth	Above tunnel centre line	14.4	0	14.40	7.56
	90m from tunnel centre line	14.4	90	91.14	0.86
Deep depth	Above tunnel centre line	29.9	0	29.90	3.19
	90m from tunnel centre line	29.9	90	94.84	0.82

7.5 Empirical Model 3: The Rahman-Orr Model

The author has developed a more general equation than the Godio et al and Nishimatsu equations for predicting the surface vibrations due to tunnelling. This equation referred to as the Rahman-Orr semi-empirical model, take account of the magnitude of the source vibrations at TBM and also the effects of both material and geometric damping on the ground vibrations. The Rahman-Orr model is based on following Mintrop (1911, cited by Hillar & Crabb, 2000) attenuation equation:

$$A_1 = A_0 [r_o/r_1]^{ß} e^{-\alpha (r_1 - r_o)} \qquad [7.4]$$

where A_1 is the amplitude at distance r_1 from the source; A_o is the amplitude at distance r_o from the source which is known; α is the absorption coefficient; and ß is the geometric spreading term. The most frequently mentioned limitation of using the Equation 7.4 is the fact that, in order to predict the vibration intensity at a given distance from the source, the intensity of vibrations at a distance close to the source must be known (Athanasopoulos et al., 2000).

In Equation 7.4, the term $(r_0/r_1)^{ß}$ represents the geometrical damping and the power, ß, is a function of the wave type, with ß = 1 for body waves in the ground that spread spherically, except at the surface where ß = 2, and ß = 0.5 for Rayleigh waves (Dowding, 1996).

In Equation 7.4, the term $\alpha(r_1-r_0)$ represent the material damping. The α coefficient increases with dominant frequency, as a higher frequency wave will pass through more motion cycles than a lower frequency wave when travelling the same distance. For material damping, decay is a function of energy loss per cycle of deformation, not distance travelled per second. Lower frequency components experience fewer deformational cycles and hence lose proportionally less energy than higher frequency components. The coefficient α can be calculated using following Equation (Massarsch, 1992):

$$\alpha = \frac{2\pi Df}{v_s} \qquad [7.5]$$

where D is material damping, f is the predominant vibration frequency and v_s is the shear wave velocity. The absorption coefficient α is calculated using Equation 7.5 and presented in Fig.7.5. α decreases with increasing wave velocity and with decreasing vibration frequency.

At small strain levels the shear modulus, which is a function of shear wave velocity, is the key parameter for modelling the soil behaviour. The relative vibration amplitude (A_1/A_0) is calculated using Equation 7.4 with different absorption coefficient α and presented in Fig. 7.6. The most satisfactory and most manageable relation that was found is presented in Equation 7.6, based on Figs. 7.5 and 7.6.

$$RPPV_s = RPPV_o * Ar^{-n} \qquad [7.6]$$

where, $RPPV_s$ = Resultant Peak Particle Velocity at surface

$RPPV_o$ = Resultant Peak Particle Velocity at source

r is the direct distance between the source to the measurement point (m)

A and n (A and n are a function of α and α is a function of shear wave velocity and vibration frequency and hence A and n are a function of shear wave velocity and vibration frequency) are the coefficient. A and n are calculated using different shear wave velocity and vibration frequency and presented in Table 7.3 and 7.4.

For Dublin condition,

The average shear wave velocity, v_s = 1566m/s (from Table 7.5).

The average vibration frequency f = 15Hz

$RPPV_o$ = 29.60mm/s [from Figs. 7.7 to 7.9].

The coefficient A and n are 1.1853 and 1.0578 from Table 7.3 and 7.4 respectively. The Equations become as follows:

$$RPPV_s = 29.60 * 1.1853\ r^{-1.0578}$$
$$RPPV_s = 35.087\ r^{-1.0578} \qquad [7.7]$$

$$RPPVs = 35r^{-1} \text{ [more simplified]} \qquad [7.8]$$

If the source vibration velocities are known the Equation 7.6 and Table 7.3 and 7.4 can be used for any types of soil and rock. However if the source vibration velocities are unknown, then Equation 7.8 can be used as a generalised equation for boring in limestone. The flow diagram indicating how to calculate the PPV at the surface is shown in Fig. 7.10.

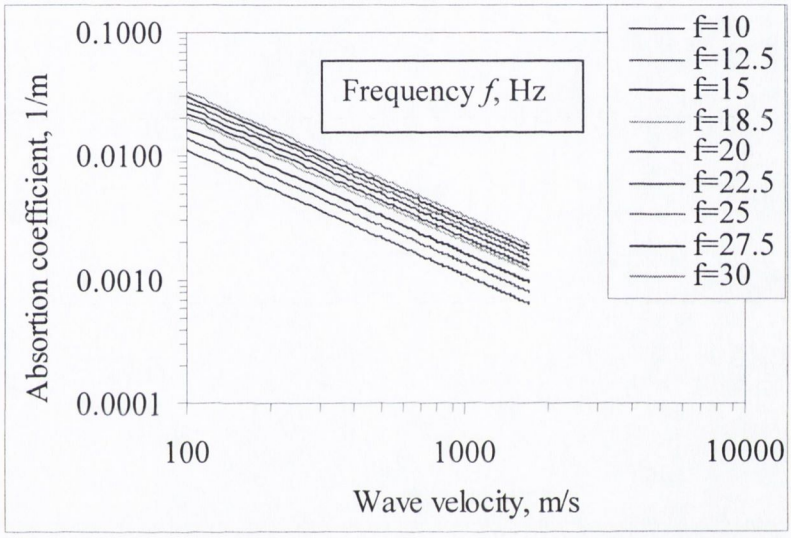

Fig.7.5– Absorption coefficient at small strain levels

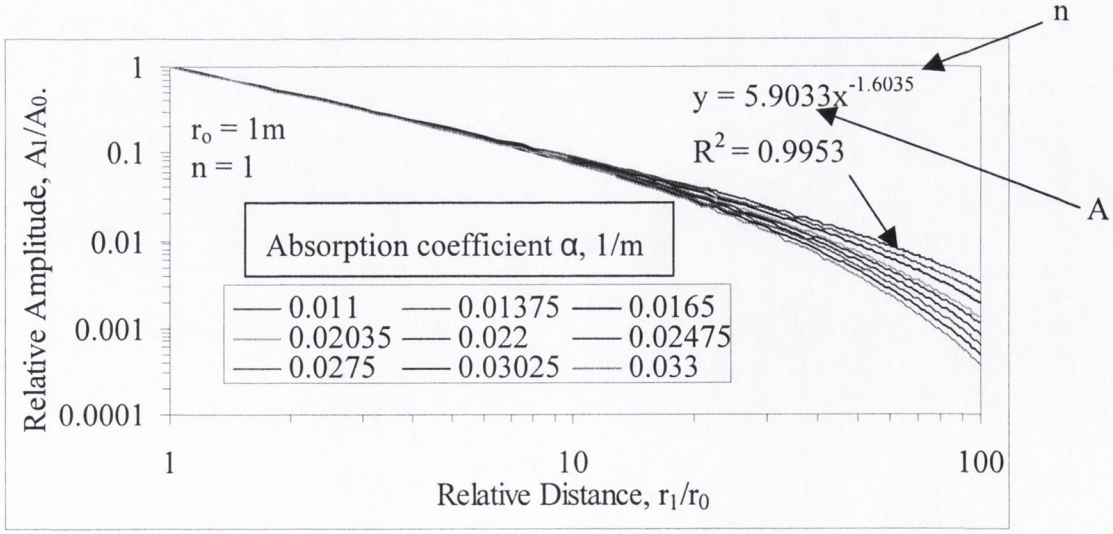

Fig.7.6–Relative vibration amplitude with different absorption coefficient

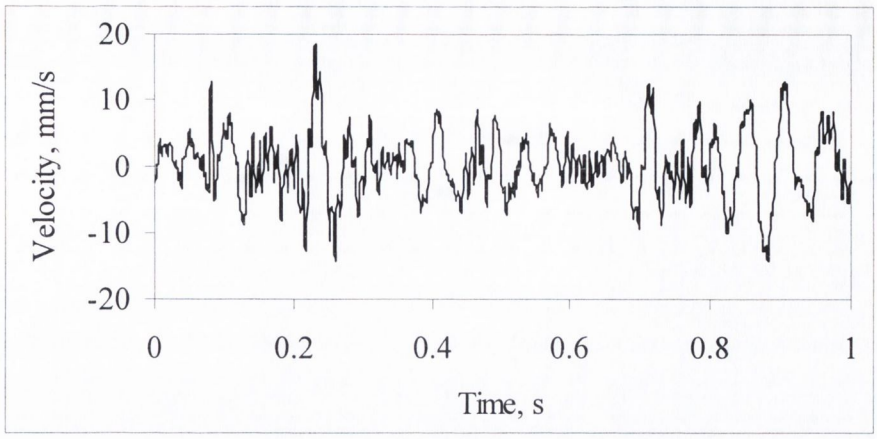

Fig.7.7–Measured TBM excitation; transverse direction

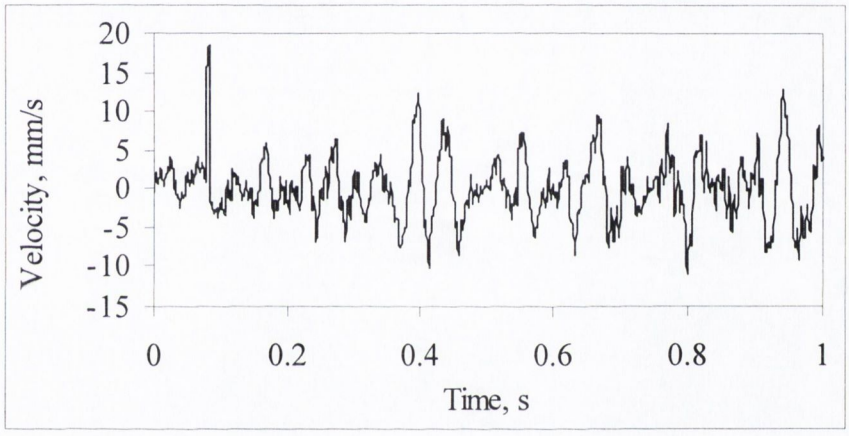

Fig.7.8–Measured TBM excitation; vertical direction

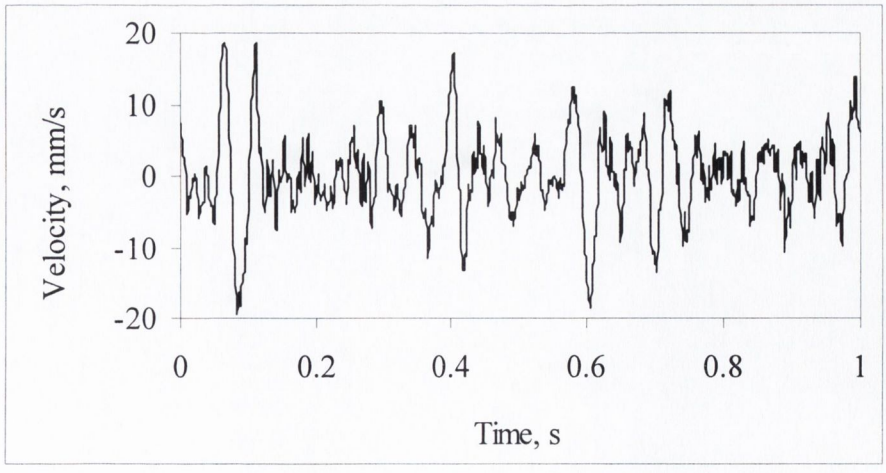

Fig.7.9–Measured TBM excitation; longitudinal direction

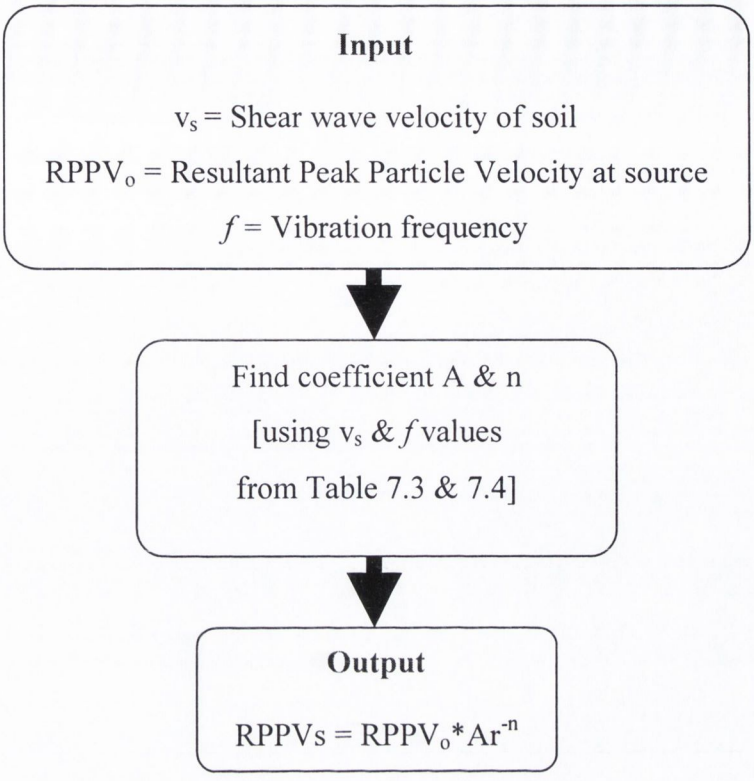

Fig. 7.10 – The flow diagram

Table 7.3 – Coefficient "A" based on shear wave velocity v_s in m/s and frequency *f*, Hz.

v_s/f	10.0	12.5	15.0	18.5	20.0	22.5	25.0	27.5	30.0
100	5.903	9.202	14.34	26.7	34.85	54.32	84.7	132	205.72
130	3.918	5.514	7.758	12.5	15.36	21.61	30.4	42.77	60.179
160	3.033	4.003	5.283	7.79	9.202	12.14	16	21.15	27.91
200	2.43	3.033	3.787	5.17	5.9	7.367	9.2	11.49	14.343
250	2.034	2.43	2.901	3.72	4.139	4.943	5.9	7.05	8.42
300	1.807	2.096	2.43	2.99	3.266	3.787	4.39	5.091	5.9033
400	1.559	1.742	1.946	2.27	2.43	2.715	3.3	3.389	3.787
500	1.426	1.559	1.703	1.93	2.034	2.223	2.43	2.655	2.9017
600	1.344	1.448	1.559	1.73	1.807	1.946	2.1	2.256	2.4297
700	1.289	1.373	1.463	1.6	1.661	1.77	1.89	2.009	2.1403
800	1.249	1.32	1.395	1.51	1.559	1.648	1.74	1.841	1.9461
900	1.218	1.28	1.344	1.44	1.484	1.559	1.64	1.72	1.8073
1000	1.194	1.249	1.305	1.39	1.426	1.491	1.56	1.63	1.7034
1100	1.175	1.224	1.274	1.35	1.381	1.438	1.5	1.559	1.6229
1200	1.16	1.203	1.249	1.31	1.344	1.395	1.45	1.502	1.5587
1300	1.146	1.186	1.227	1.29	1.314	1.36	1.41	1.456	1.5064
1400	1.135	1.171	1.21	1.26	1.289	1.33	1.37	1.417	1.463
1500	1.126	1.16	1.194	1.24	1.267	1.305	1.34	1.385	1.4263
1600	1.117	1.149	1.181	1.23	1.249	1.284	1.32	1.357	1.395
1700	1.11	1.14	1.17	1.21	1.232	1.265	1.3	1.333	1.368
1800	1.104	1.131	1.16	1.2	1.218	1.249	1.28	1.311	1.3444
1900	1.098	1.124	1.151	1.19	1.206	1.234	1.26	1.293	1.3236
2000	1.093	1.117	1.142	1.18	1.194	1.221	1.25	1.277	1.3052

Table 7.4– Coefficient "n" based on shear wave velocity v_s in m/s and frequency *f*, Hz.

v_s/f	10.0	12.5	15.0	18.5	20.0	22.5	25.0	27.5	30.0
100	1.604	1.754	1.905	2.12	2.207	2.358	2.51	2.66	2.8106
130	1.464	1.58	1.696	1.86	1.929	2.045	2.16	2.277	2.3928
160	1.377	1.472	1.566	1.7	1.754	1.849	1.94	2.037	2.1316
200	1.302	1.377	1.453	1.56	1.604	1.679	1.75	1.83	1.9053
250	1.241	1.302	1.362	1.45	1.483	1.543	1.6	1.664	1.7242
300	1.201	1.252	1.302	1.37	1.402	1.453	1.5	1.553	1.6035
400	1.151	1.189	1.226	1.28	1.302	1.34	1.38	1.415	1.4526
500	1.121	1.151	1.181	1.22	1.241	1.272	1.3	1.332	1.3621
600	1.101	1.126	1.151	1.19	1.201	1.226	1.25	1.277	1.3018
700	1.086	1.108	1.129	1.16	1.172	1.194	1.22	1.237	1.2587
800	1.075	1.094	1.113	1.14	1.151	1.17	1.19	1.208	1.2263
900	1.067	1.084	1.101	1.12	1.134	1.151	1.17	1.184	1.2012
1000	1.06	1.075	1.091	1.11	1.121	1.136	1.15	1.166	1.1811
1100	1.05	1.069	1.082	1.1	1.11	1.123	1.14	1.151	1.1646
1200	1.05	1.063	1.075	1.09	1.101	1.113	1.13	1.138	1.1509
1300	1.046	1.058	1.07	1.09	1.093	1.105	1.12	1.128	1.1393
1400	1.043	1.054	1.065	1.08	1.086	1.097	1.11	1.119	1.1293

1500	1.04	1.05	1.06	1.07	1.081	1.091	1.1	1.111	1.1207
1600	1.038	1.047	1.057	1.07	1.075	1.085	1.09	1.104	1.1132
1700	1.036	1.044	1.053	1.07	1.071	1.08	1.09	1.098	1.1065
1800	1.034	1.042	1.05	1.06	1.067	1.075	1.08	1.092	1.1006
1900	1.032	1.04	1.048	1.06	1.064	1.072	1.08	1.087	1.0953
2000	1.03	1.038	1.045	1.06	1.06	1.068	1.08	1.083	1.0905

Table7.5 Shear wave velocity

	Thickness, m	Shear wave velocity, v_s, m/s
Top layer	2.5	183.00
Dublin boulder clay	2.75	438.61
	2.75	481.82
	2.75	519.46
	2.75	549.00
	11 (total)	
Limestone	2.63	2981.00
	2.63	2981.00
	2.63	2981.00
	2.63	2981.00
	10.5 (total)	*Average 1566*

7.6 Comparison Between Model Predictions and Measured PPP Values

To assess suitability of the 3D- FE model and the Rahman-Orr semi-empirical model for predicting PPV values, the PPV values at measuring Sections 1, 2, 3 and 5 are plotted in Figs. 7.11 to 7.14 together with the PPV values predicted using the Godio, Nishimatsu (NCC) upper and lower bound model and the measured PPV values at these section. The PPV values plotted in Figs. 7.11 to 7.14 show that there is reasonably good agreement between the 3D-FE predicted values, the Rahman-Orr semi-empirical model and the measured values. It can be seen from the results plotted for each section that the FE, the Rahman-Orr semi-empirical model and measured values all lie between the Nishimatsu upper and lower bounds models. However, the results in Fig. 7.13 show that at Section 3, the measured values lie on the Godio model line while at every other section the PPV

values predicted by the Godio model are closer to the measured values than the values predicted by the Nishimatsu upper model. It can also be seen from Figs. 7.11 to 7.14 that all the models have similar attenuation characteristics. Although good agreement is found between the resultant PPV values predicted by the 3D-FE analyses, the Rahman-Orr semi-empirical model and the measured values, there is a large difference between the measured values and the NCC and Godio empirical model results. The NCC and Godio empirical models are crude at best, as they are functions of only the direct distance between the source and the point of interest, while the groundborne vibrations also depend on the soil properties, particularly on the stiffness and the resonance frequency of the soil layer, and on the tunnel boring machine excitation.

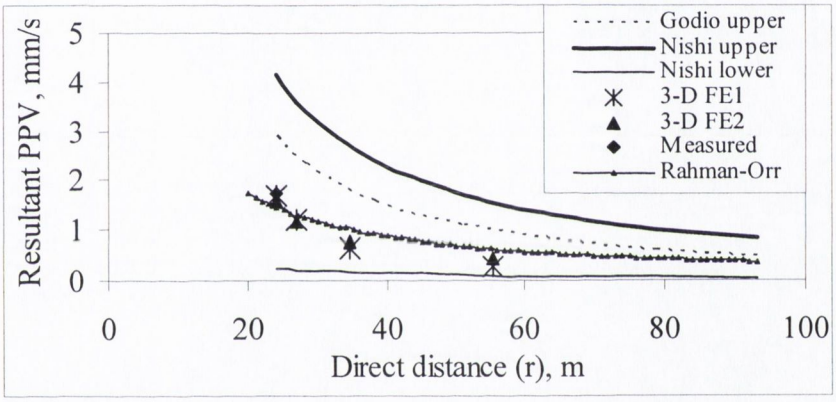

Fig.7.11–Comparison between Model Predictions and Measured PPP Values; Section 1

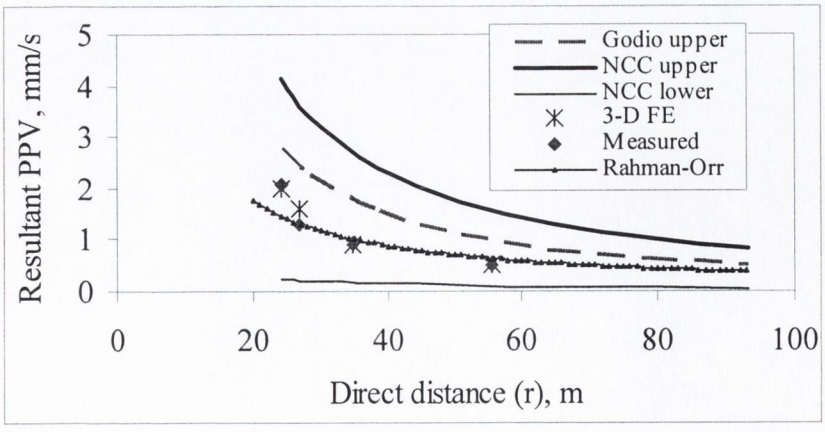

Fig.7.12–Comparison between Model Predictions and Measured PPP Values; Section 2

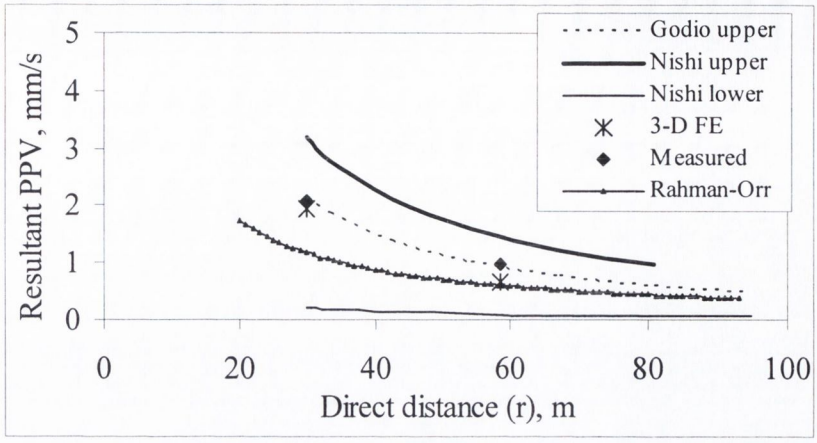

Fig.7.13–Comparison between Model Predictions and Measured PPP Values; Section 3

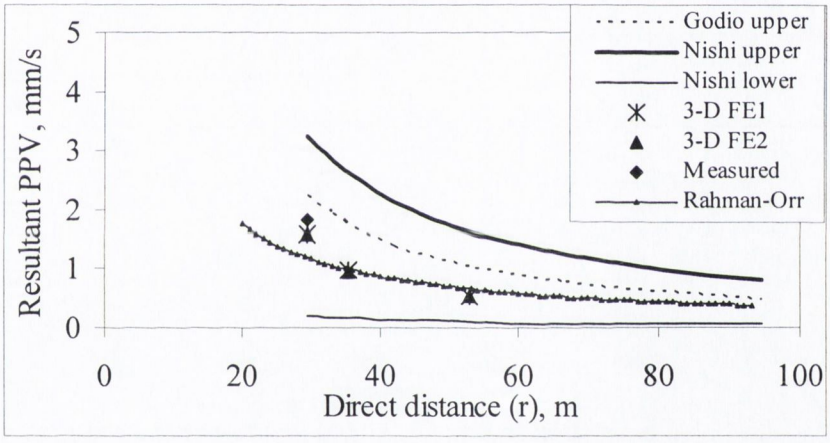

Fig.7.14–Comparison between Model Predictions and Measured PPP Values; Section 5

7.7 Vibration Amplification

Vibration amplification due to resonance depends on the dominating frequency of the TBM excitation wave that propagate through the soil deposit and the natural frequencies of the soil deposit. The natural frequencies of the soil deposit are a function of geometry (thickness) and material properties (s-wave velocity/stiffness) of the soil deposit. When the natural frequency of the soil deposit and the dominant frequency of the vibration source wave (TBM excitation) coincide or are very close, this results in a vibration amplification (Massarsch, 1992 & Kramer, 1996).

Another soil parameter that influences the vibration amplification is damping. The amplification by a damped soil layer also varies with frequency. The frequencies that correspond to the local maxima are the natural frequencies of the soil deposit. The variation of the amplification factor with frequency is shown for different levels of damping in Fig. 7.15. This amplification factor is equal to the ratio of the free surface motion amplitude to the bedrock motion amplitude. The n^{th} natural frequency of the soil deposit is given by:

$$\omega_n \cong \frac{v_s}{H}\left(\frac{\pi}{2} + n\pi\right) \quad n = 0, 1, 2, \ldots\ldots, \infty \qquad [7.9]$$

Fig.7.15 shows that the peak amplification factor decreases with increasing natural frequency, the greatest amplification factor will occur approximately at the lowest natural frequency, also known as the fundamental frequency:

$$\omega_n = \frac{\pi v_s}{2H} \qquad [7.10]$$

The period of vibration amplification corresponding to the fundamental frequency is called the characteristic site period,

$$T_s = \frac{2\pi}{\omega_o} = \frac{4H}{v_s} \qquad [7.11]$$

The characteristic site period, which depends only on the thickness and shear wave velocity of the soil, provides a very useful indication of the period of vibration at which the most significant amplification can be expected (Kramer, 1996).

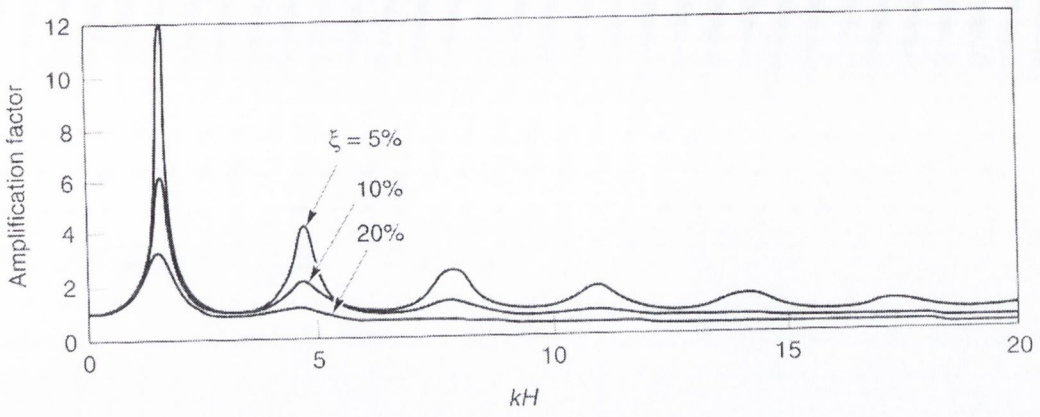

Fig. 7.15 – Influence of frequency on steady-state response of a damped, linear elastic layer (From Kramer, 1996)

7.8 Summary

The Rahman-Orr model is based on the wave attenuation equation, which considered the combined effects of material and geometric damping. The model takes account the TBM excitation, the ground dynamic properties and the direct distance between the source and the point of interest. If the source vibration velocities are known, the Equation 7.6 and Tables 7.3 and 7.4 can be used to provide a generalised Equation for any types of soil and rock. However if source vibration velocities are unknown, then Equation 7.8 can be used to predict the surface vibrations due to tunnel boring in limestone.

Good agreement is found between the resultant peak particle velocity values predicted by the 3D FE analyses, the Rahman-Orr model and the measured results. The NCC and Godio et al. empirical models are crude at best for predicting these, as they are a function of only the direct distance between the source of the vibrations and the point of interest, while the groundborne vibrations depend also on the soil properties and the tunnel boring machine excitation energy.

CHAPTER 8

CONCLUSIONS

8.1 Introduction

This thesis has described the measuring, analysing and control of ground vibrations caused by tunnelling construction. The research carried out has involved investigating the published research on ground vibrations due to tunnelling. This investigation has found that previous research into the vibrations due to tunnelling has been largely empirical and has resulted in upper and lower bound equations being proposed for predicting the range of magnitude of the expected vibrations at the surface. The author has not been able to find any report of previous research where a more theoretical approach, based on the properties of the ground between a TBM and the surface, has been used to relate the vibrations at the ground surface to the actual vibrations produced by a TBM.

8.2 Conclusions

Tunnel construction is a highly complex operation involving many different events. The impact of tunnel construction on the environment and people can take many forms, such as ground vibrations, ground deformation, airborne noise, visual intrusion, dust and smoke etc. The highest levels of vibrations and noise generated from mechanised tunnelling methods have resulted due to the use of plants that dissipate large amounts of energy, in the form of ground vibrations and noise, into the environment.

Vibrations from tunnelling activities are generally of a temporary nature, but the disturbance caused may result in permanent damage to property and substantial nuisance to the neighbouring population. The need to avoid vibrations causing either permanent damage to property or substantial nuisance to people may lead to restraints on the working method that result in additional costs or even, in extreme circumstances, curtailment of the activity.

Vibrations due to construction activities travel in the ground in different forms, as body waves and surface waves, with their wave propagation velocities dependent upon the ground characteristics. These waves shake the ground particles, causing vibrations; this is the mechanism of the ground vibrations. The vibrations move upwards until the ground surface is reached and may induce vibrations in structures at the surface. The elements of these structures re-radiate these vibrations, and these re-radiated vibrations in the air are groundborne noise.

Vibration-induced damage thresholds are usually expressed in terms of peak particle displacement, velocity or acceleration but it is most usual to use peak particle velocity (PPV) in the field of man-made ground vibration studies as the strain induced in the ground is proportional to the particle velocity and geophones, are normally used to measure the ground vibrations.

Standards have been reviewed which cover the criteria against which assessment of ground vibrations prediction can be made. These criteria are for the structural damage and for perceptible intrusion.

The British Standard BS 7385 (1993) defines three damage categories: cosmetic, minor and major, and relates vibration levels to these. Cosmetic or threshold damage is the formation of hairline cracks or the growth of existing cracks in plaster, drywall surfaces or mortar joints. Minor damage is the formation of large cracks or loosening and falling of plaster on drywall surfaces, or cracks through bricks/concrete blocks. Major or structural damage is damage to the structural elements of a building.

The British Standard BS 6472 (1992) gives detailed guidance on the evaluation of the effects of vibration exposure on humans in the frequency range of 1 Hz to 80 Hz. It gives guidance on the threshold values for human perception and the higher levels above which complaints become more likely in a variety of environments.

The environmental effects of vibrations have received considerable attention in recent years owing to the use of more powerful construction equipments, such as pile drives and TBMs, in urban areas that cause ground vibrations and can cause damage to buildings and disturbance to people. These consequences of tunnelling activities have prompted recent research into improved methods for predicting the ground vibrations induced by tunnelling.

Many site investigations have been carried out and some reports about previous studies in Dublin have been collected to determine the characteristics of the Dublin Brown Boulder clay, the Dublin Black Boulder clay and the limestone bedrock. These soils and this rock form the ground conditions along the line of the Dublin Port Tunnel. Hence, the values of the parameters for these materials are necessary for all the calculations and modelling of the ground vibrations.

The finite element analyses require the ground properties and TBM excitation. The relevant ground properties are its stiffness, damping, bulk density and Poisson's ratio. The stiffness and damping can be determined from seismic geophysical tests and represent an important class of field tests for the determination of dynamic soil properties. The seismic geophysical tests are: the down-hole test, the cross-hole test and the surface refraction test. Laboratory tests are also available to measure the dynamic properties of the ground (stiffness, damping) at small strain levels. The resonant column test, ultrasonic pulse test, and bender element test are the commonly employed techniques to measure the small strain dynamic properties. The TBM excitation can be measured using geophones and the geophone data should be recorded in time history mode in order to carry on vibrations analyses.

The types of waves are P-, SV-, and SH-waves. Since incident P-and SV-waves involve particle motion perpendicular to the plane of interface, they will each produce both reflected and refracted P-, and SV-waves. An incident SH-waves does not involve particle motion perpendicular to the interface; consequently, only SH-waves are reflected and refracted. The directions and relative amplitudes of the waves produced at the

interface depend on both the direction and amplitude of the incident wave to the interface and the propagation velocities and densities of the two materials. Using Snell's law the angles of reflection and refraction directions can be determined. There is also a critical angle of incidence, i_c, where the refracted waves travel parallel to the interface.

Laboratory triaxial tests with bender elements were carried out to determine the dynamic stiffness of the soil. Initially numerical analyses were carried out to determine the most favourable input signal to be used for the bender elements in the laboratory tests. It was found that the distorted sine wave was most favourable input signal, as experimentally observed by Jovicic et al., (1996). However, this result was strongly dependent on the ratio between the first upward amplitude to the first downward amplitude of the input signal. Using a distorted sine wave as the input signal, a reasonably agreement was found between the G_{max} values obtained from the author's bender element tests and the Lawler's (2002) bender element tests. Good agreement was found between the G_{max} values obtained from the London City University bender element tests and the semi-empirical equations. While the G_{max} values obtained from the Author's and the Lawler's (2002) bender element tests were bit higher than those obtain from the semi-empirical equations. In the absence of measured G_{max} from laboratory or field tests, Viggiani & Atkinson (1995) semi-empirical equation can be used to obtain G_{max} value for Dublin boulder clay.

The Bender element resonant method was also used for measuring the damping ratio of undisturbed Dublin boulder clay. First, a finite element analysis was carried out to determine the resonant frequency of first mode to be used in the laboratory tests. The influences of the confining water were accounted for by adding an extra mass to the total mass of the test specimen. In the laboratory, the tests were carried out with different frequencies to obtain the response spectra and a half power method was used to calculate the damping ratio.

Field measurements are important in order to validate numerical models and semi-empirical models. Peak particle velocity, frequency and/or time history should be recorded by a geophone during the field measurement. The data from the field

measurements can be recorded in histogram mode and time history mode. In histogram mode, the geophone monitor samples data continuously at the chosen sample rate but only stores the relevant peaks for the interval. For each interval, the geophone calculates the maximum positive and negative peaks and the frequency of the largest peak. In time history mode, the geophone records the vibration data continuously at the chosen sample rate and it is possible to convert the data into frequency domain using the Fast Fourier Transform algorithm. From frequency domain, the vibrations frequency range and the resonance frequency can be found which are important parameters for vibrations studies. Measurements should be made of the vibration which affects people and these should be made inside and outside of buildings. Vibration should usually be measured in three perpendicular directions, so that the results can be combined and compared to the criteria. The resultant PPV at the source due to a TBM is around 30mm/s and frequencies range at around 1 to 100Hz with resonance frequency at around 15 Hz.

The finite element method (FEM) is a suitable tool for predicting the vibrations generated by a tunnel boring machine (TBM) during the construction of a tunnel. Vibrations generated by a TBM are a truly 3-D phenomenon, therefore 3-D finite element analyses of TBM induced ground vibrations have been used to model the ground response at the surface. A good agreement was found, in terms of PPV, between the measured PPV values and the values calculated using 3-D finite element analyses. Although good agreement is found and the FEM is widely applicable, there are some limitations for practical applications regarding to the analyses time and input data. The minimum analyses time was 48 hours, which is very time consuming for practical applications. To carry out 3-D FE analyses, the dynamic soil parameters like the small strain stiffness, damping, Poisson's ratio and density and TBM excitation are very important. Although it is possible to get the soil parameters before the start of tunnel construction, it is not possible to get the TBM excitation before the start of tunnel construction and analyses will not be carried out. Axi-symmetry analyses can only be carried out when the geometry and loading are both symmetrical about an axis. However, a simple 2-D axi-symmetry model cannot be used in place of 3-D FE analyses, in the case of a TBM

excavating a tunnel as neither the loading nor the geometry are symmetrical about the tunnel axis.

More sophisticated numerical model should be used to solve problems that have no analytic solution, or for which the analytic solution is prohibitively difficult to find. From field measurement or empirical model it is not possible to carry out parametric studies however, from numerical model it is possible to carry out several parametric studies to examine the sensitivity of vibration predictions to the values of various parameters input data.

Parametric studies were performed and some important information was obtained about the prediction of ground vibrations. The stiffness of the ground was found to be the most important parameter, because changing its value has a significant effect on the vibrations at the surface level and affects the resonance frequency of the ground. The resonance frequency of the ground was found to increase with increasing stiffness of the ground. If the resonance frequency of the ground coincides with the resonance frequency of the TBM excitation or is very close to it, then large vibration levels occur and vice versa.

In the finite element formulation, the damping ratio is defined as a combination of mass proportional and stiffness proportional. It was found that the frequency at which the damping ratio applies needs to be chosen with care. If the chosen frequency range is wide, it was found that the damping ratio was small between the lower and upper bound frequencies and this results in a high vibration level at the surface.

The author has examined the use of and limitations of the existing empirical models for the vibrations due to tunnelling, which are functions of the distance from the source and an empirical parameter to represent all the other factors, such as the properties of the ground and the TBM excitation, affecting the vibration levels. As part of this research, an empirical model, the Rahman-Orr model, that takes account of both the ground properties and TBM excitation has been developed to predict the vibrations due to TBM. This model, given by the semi-empirical Equations 7.6 and 7.8, is based on the wave

attenuation equation, which considered the combined effects of material and geometric damping. If the source vibration velocities are known, then Equation 7.6 and Table 7.3 and 7.4 can be used as a generalised equation to predict the ground vibrations for boring in any types of soil or rock. However if source vibration velocities are unknown, then Equation 7.8 can be used for boring in limestone.

A comparative study of the vibrations predicted using three empirical methods, and the 3-D FE method with the measured vibrations was carried out and the following important findings were made concerning the prediction of ground vibrations. It was found that all the methods predict similar attenuation of the vibrations. The NCC and the Godio et al. equations overpredict the magnitude of the PPV values with large differences between the predicted and measured values. However, good agreement was found between the resultant PPV values predicted by the 3-D FEM analyses, the Rahman-Orr model and the measured PPV values. The NCC and the Godio et al. empirical models are crude at best, as they are functions of only the direct distance between the source and the point of interest, while the groundborne vibrations depend also on the soil properties and the tunnel boring machine excitation, which are taken into account in the 3D-FEM analyses and in the Rahman-Orr model. The results of this study have been applied to predict the surface vibrations in the case of the Dublin Port Tunnel and to develop a semi-empirical equation. The results of study can also be applied in other projects, like proposed metro tunnel in Dublin, by means of 3-D FE model and the Rahman-Orr semi-empirical model. The proposed metro tunnel is an example of a practical application of these methods to predict TBM induced ground vibrations.

Finally, it can be concluded that the 3-D FE analyses and the Rahman-Orr semi-empirical model provide satisfactory predictions of the surface vibrations due to a TBM.

8.3 Recommendations for Further Research

Some suggestions for further research in this area are as follows:

- Although Ireland/Dublin is an area of very low seismic activity so that there is little risk of ground vibrations due to earthquakes, plenty of different types of construction activity is in progress or is being planned (i.e. a metro tunnel in Dublin) that could produce ground vibrations which could cause public annoyance. In order to predict the likely level of vibrations due to these activities, extensive field and laboratory research works should be carried out throughout Dublin to determine the dynamic properties of the soil and rock; especially its stiffness and damping ratio.

- Numerical analyses should be carried out to determine the effects of vibrations on different types and heights of building and to investigate the effectiveness of open trenches and filled trenches in reducing the impacts of the vibrations.

- Extensive research works should be carried out to predict, using field measurement and 3-D finite element modelling, the vibrations at the ground surface as well as in the buildings due to traffic flow through the Dublin Port Tunnel and due to the proposed metro tunnel in Dublin.

REFERENCES

ABAQUS, (2004), "Analysis User's Manual", Hibbit, Karlsson & Sorensen, ABAQUS Europe BV, Maastricht, The Netherlands.

ABAQUS, (2004), "ABAQUS/CAE User's Manual", Hibbit, Karlsson & Sorensen, ABAQUS Europe BV, Maastricht, The Netherlands.

ABAQUS, (2004), "Getting Started with ABAQUS/Standard", Hibbit, Karlsson & Sorensen, ABAQUS Europe BV, Maastricht, The Netherlands.

ABAQUS, (2004), "Keywords Reference Manual", Hibbit, Karlsson & Sorensen, ABAQUS Europe BV, Maastricht, The Netherlands.

Aboudi, J. (1973), "Elastic waves in half-space with thin barrier", ASCE Journal of Engineering Mechanics, 99(1), 69-83.

Adam, M and Estorff, O. V., (2005), "Reduction of train-induced vibrations by using open and filled trenches", Computers and Structures, 83(1), 11-24.

Ahmad, S. and Al-Hussaini, T.M., (1991), "Simplified design for vibration screening by open and in-filled trenches", Journal of Geotechnical Engineering ASCE, 117(1), 67-88.

Ahmed, S., Al-Hussaini, T.M. and Fisherman, K.L., (1996), "An Investigation on active isolation of machine foundation by open trenches", ASCE Journal of Geotechnical Engineering, 122(6), 454-464.

Al-Hunaidi, M.O., Chen, P.A., Rainer, J.H. and Tremblay, M., (1996), "Shear moduli and damping in frozen and unfrozen clay by resonant column tests", Canadian Geotechnical Journal, 33(3), 510-514.

Al-Hussaini, TM. and Ahmad, S., (1991), "Design of wave barriers for reduction of horizontal ground vibration", ASCE Journal of Geotechnical Engineering, 117(4), 616-636.

Al-Hussaini, TM. and Ahmad, S., (1996), "Active isolation of machine foundations by in-filled trench barriers", ASCE Journal of Geotechnical Engineering, 122(4), 288-294.

Amick, H. and Gendreau, M., (2000), "Construction vibration and their impact on vibration-sensitive facilities", Presented at ASCE Construction Congress 6, Orlando, Florida, Feb. 22, 2000, 1-10.

Amick, H., (1999), "A frequency-dependent soil propagation model", Proceedings of SPIE Conference on Current Developments in Vibration Control for Optomechanical Systems, Denver, Colorado, 71-85.

Antes, H. and O. von Estorff, (1994), "Dynamic response of 2D and 3D block foundations on a half space with inclusions", International Journal of Soil Dynamics and Earthquake Engineering, 13(5), 305-311.

Arroyo, M., Wood, D.M., and Greening, P.D., (2003), "Source near field effects and pulse tests in soil samples", Geotechnique, 53(3), 337-345.

Arulnathan, R., Boulanger and Riemer, M. F, (1998), "Analysis of bender element tests", ASTM Geotechnical Testing Journal, 21(2), 120-131.

Arulnathan, R., Boulanger, R.W., Kutter, B.L. and Sluis, W.K., (2000), "New tool for shear wave velocity measurements in model tests", ASTM Geotechnical Testing Journal, 23(4), 444-453.

Athanasopoulos, G.A. and Pelekis, P.C., (2000), Ground vibrations from sheet pile driving in urban environment: measurements, analysis and effects on buildings and

occupants, International Journal of Soil Dynamics and Earthquake Engineering, 19(5), 371-387.

Atkinson, J.H., (2000), "Fortieth Rankine lecture: Non-linear soil stiffness in routine design, Geotechnique, 50(5), 487-508

Attewell, P.B. & Woodman, J.P., (1982), "Predicting the dynamics of ground settlement and its derivatives caused by tunnelling in soil", Ground Engineering, 15,8,13-22.

Attewell, P.B., (1986), Noise and vibration in civil engineering, Municipal Engineering Journal, 3, 139-158.

Attewell, P.B., (1995), Tunnelling Contracts and Site Investigation, E & F.N. Spon, London.

Augarde, C.E., Burd, H.J. and Houlsby, G.T. (1995) "A Three Dimensional Finite Element Model of Tunnelling", Proceedings of the Fourth International Symposium on Numerical Models in Geomechanics - NUMOG V, Davos, Switzerland, 457-462.

Augarde, C.E., Burd, H.J. and Houlsby, G.T. (1998) "Some Experiences of Modelling Tunnelling in Soft Ground Using Three-Dimensional Finite Elements", Proc. 4th European Conference on Numerical Methods in Geotechnical Engineering, Udine, Springer-Verlag, 603-612.

Balendra, T. K. H., Chua, K. W. Lo, and Lee, S. L., (1989), "Steady-state vibration of subway-soil-building system", ASCE Journal of Engineering Mechanics, 115(1), 145-162.

Baranski, M., (2003), "Laboratory measurements of the stiffness of normally consolidated till polluted by benzene with bender element tests", Geological Quarterly, 47(2), 211-214.

Barkan, D. D. (1962), "Dynamics of bases and foundations", McGraw-Hill, New York.

Basu, B. and Gupta, V.K., (2000), "Stochastic seismic response of single-degree-of-freedom systems through wavelets", Engineering Structures, 22, 12, 1714-1722.

Bathe, K. J. (1982.), "Finite Element Procedures In Engineering Analysis", Englewood Cliffs; London, Prentice-Hall.

Beatty, J.G., Ganey, R. J., and Killingsworth, J.E., (1994), "Increased productivity in construction of civil and mining tunnels through the use of high-capacity tunnel-boring machines and continuous belt conveyer muck haulage", Tunnelling' 94-Instituition of Mining and Metallurgy and the British Tunnelling Society, Chapman & Hall, 799-819.

Bickel, J., Kuesel, T., and King, E., (1996), "Tunnel engineering handbook", New York ; London : Chapman & Hall.

Blewett, J., Blewett, I.J. and Woodward, P.K., (1999), "Measurement of shear-wave velocity using phase-sensitive detection techniques", Canadian Geotechnical Journal, 36(5), 934-939.

Blewett, J., Blewett, I.J. and Woodward, P.K., (2000), "Phase and amplitude responses associated with the measurement of shear-wave velocity in sand by bender elements", Canadian Geotechnical Journal, 37(6), 1348-1357.

Bloodworth, A.G., Houlsby, G.T., Burd, H.J. and Augarde, C.E. (2001) "Three Dimensional Modelling of the Interaction Between Buildings and Tunnelling Operations", Proc. Conference on Response of Buildings to Excavation-Induced Ground Movements, 1-10.

Bloodworth, A.G. and Houlsby, G.T., (1999), "Three Dimensional Analysis of Building Settlement Caused by Shaft Construction", Proc. Int. Symp. on Geotechnical Aspects of Underground Construction in Soft Ground, Tokyo.

Boulanger, R.W., Arulnathan, R., Harder, L.F., Torres, R.A. and Driller, M. W., (1998), "Dynamic properties of sherman island peat", ASCE Journal of Geotechnical and Geoenvironmental Engineering, 124(1), 12-20.

Brignoli, E.G.M., Gotti, M., and Stokoe, K. H., (1996), "Measurement of shear waves in laboratory specimens by means of piezoelectric transducers", ASTM Geotechnical Testing Journal, 19(4), 384-397.

British Standard Institution (1992), BS 6472, "Evaluation of human exposure to vibration in buildings".

British Standard Institution (1993), BS 7385, Part 2, "Evaluation and measurement for vibration in buildings, guide to damage levels from groundborne vibration".

Brocanelli, D. and Rinaldi, V., (1998), "Measurement of low-strain material damping and wave velocity with bender elements in the frequency domain", Canadian Geotechnical Journal, 35(6), 1032-1040.

Burd, H.J., Houlsby, G.T., Chow, L,. Augarde, C.E. and Liu, G. (1994) "Analysis of Settlement Damage to Masonry Structures", Proceedings of the 3rd European Conference on Numerical Methods in Geomechanics, Manchester, 203-208.

Burd, H.J., Houlsby, G.T., Augarde, C.E. and Liu, G. (2000), "Modelling the Effects on Masonry Buildings of Tunnelling-Induced Settlement", Proceedings Institution of Civil Engineers: Geotechnical Engineering, 143, 1, 17-29.

Carnevale, M., Young, G., Hager, J. & Carnevale, M.C., (2000), "Monitoring of TBM-induced ground vibrations", North American Tunnelling'00, eds. Ozdemir, Balkema, Rotterdam, 1-9.

Chatterjee, P., Degrande, G., Jacobs, S., Charlier, J., Bouvet, P. and Brassenx, D., (2003), "Experimental results of free field and structural vibrations due to underground railway traffic", Tenth International Congress on Sound and Vibration, Stockholm, Sweden.

Chowdhury, I. and Dasgoptha, S., (2003), Computation of Rayleigh damping coefficient for large systems", http://www.ejge.com/2003/Ppr0318/Ppr0318.pdf.

Clough, R. W. and Penzien, J., (1975), "Dynamics of Structures", 2nd ed., McGraw-Hill.

Cook, R. D., Malkus, D. S., Plesha, M.E. and Witt, R. J., (2002), "Concepts and applications of finite element analysis", 4th ed, New York, John Wiley and Sons.

Crockett, J.H.A., (1980), Piling vibrations and structural fatigue. Recent Developments in the Design and Construction of Piles, The Institution of Civil Engineers, 305-320.

Dano, C. and Hicher, P., (2002), "Evaluation of elastic shear modulus in granular materials along isotropic and deviatoric stress paths", 15th ASCE Engineering Mechanics Conference, New York, 1-8.

Dano, C., Hareb, H. and Hicher, P., (2003), "Characterization of loire river sand in the small strain domain using new bender-extender elements", 16th ASCE Engineering Mechanics Conference, Seattle, 1-9.

Das, B. M., (2002), "Principle of Geotechnical Engineering", 5th ed., California, Brooks/Cole Thomson Learning.

Das, B. M., (1984), "Fundamentals of soil dynamics", New York; Oxford: Elsevier.

Davis, J.V., (1970), Ground vibrations from tunnel blasting, Tunnels and Tunnelling, 141-144.

Deane, A. P., (1994), "Application of NATM to design of underground stations in London clay", Tunnelling' 94-Instituition of Mining and Metallurgy and the British Tunnelling Society, Chapman & Hall, 87-97.

Dobry, R. and Vucetic, M., (1987), "Dynamic properties and seismic response of soft clay deposits", Proceedings of the International Symposium on Geotechnical Engineering of Soft soils", Mexico.

Dowding, C. H., (1996), "Construction Vibrations", USA, Prentice Hall.

Fahy, F. and Walker, J. (1998), "Fundamentals of Noise and Vibration", London, E & FN Spon.

Farrell, E. R., Coxon, P., Doff, D.H. and Priedhomme, L., (1995), "The genesis of the brown boulder clay of Dublin", Quarterly Journal of Engineering Geology, 28, 143-152.

Farrell, E. & Wall, D., (1990), "Soils of Dublin", Trans. Inst. Engngs. Ireland, 44-96.

Farrell, E.R., O'Brien, S, Lehane, B. and Orr, T., (1995), "Stiffness of Dublin Black Boulder Clay" Proceedings XI ECSMFE, Copenhagen, pp 1-6.

Flanagan, R.F., (1993), "Ground Vibration from TBMs and shields, Tunnels & Tunnelling", 25, 10, 30-33.

Fredriksen, F. J., (1994), "Design, construction and performance of a 700-m 'Cover and cut' tunnel in soft clay, Norway", Tunnelling' 94-Instituition of Mining and Metallurgy and the British Tunnelling Society, Chapman & Hall, 491-512.

Gatti, P.L. and Ferrari, V., (1999), "Applied Structural and Mechanical Vibrations", London, E & FN Spon.

Gardien, W. and Stuit, H.G., (2003), "Modelling of soil vibrations from railway tunnels", Journal of Sound and Vibration, 267(3), 605-619.

GEOCONSULT–ARUP, (1996), "Site Investigation Report, Dublin Port Tunnel". Volume 5, part 2,5.

GEOCONSULT–ARUP, (1999), "Site Investigation Report (General Information), Dublin Port Tunnel". Part 1.

Goto J., Thompson S., Squires S. and Mizuno S. Excavation of 11.8m diameter hard rock TBM in urban area. Nishimatsu Construction Co., Ltd., Dublin Port Tunnel Project Office, Dublin, Ireland, 2004.

Griffin, M. J., (1998), "A comparison of standardized methods for predicting the hazards of whole-body vibration and repeated shocks", Journal of Sound & Vibration, 215 (4), 883-914.

Griffin, M. J., (1990), "Handbook of Human Vibration", London: Academic Press.

Griffin, M.J. & Whitham, E.M., (1988), Discomfort produced by impulsive whole-body vibration, Journal of Acoust. Soc. Amer., 68 (5) 1277-1284.

Grootenhuis, P., (1977), "Floating track slab isolation for railways", Journal of Sound and Vibration, 51(3), 443-448.

Gupta, I.D. and Trifunac, M.D., (1998), "A note on the statistics of ordered peaks in stationary stochastic processes" International Journal of Soil Dynamics and Earthquake Engineering, 17, 5, 317-328.

Grant, R.J. and Taylor, R.N., (2000), "Tunnelling-induced ground movements in clay", Proceedings Institution of Civil Engineers: Geotechnical Engineering, 143, 1, 43-55.

Hajduk, E. L., Ledford, D.L. and Wright, W.B., (2004), "Construction Vibrations Monitoring in the Charleston, South Carolina Area", Proceedings: Fifth International Conference on Case Histories in Geotechnical Engineering", New York, 1-8.

Hardin, B.O. and Drnevich, V.P., (1972), "Shear modulus and damping in soils: measurement and parameter effects", Journal of Soil Mechanics & Foundation Division, 98, 603–24.

Hardin, B.O., (1978), "The nature of stress-strain behaviour of soils", Proceedings of the ASCE Geotechnical Engineering Division Specialty Conference: Earthquake Engineering and Soil Dynamics, Vol. 1, Pasadena, California, USA.

Hall L., (2000), "Simulations and analyses of train-induced ground vibrations; a comparative study of two- and three-dimensional calculations with actual measurements", PhD Dissertation. Department of Civil and Environmental Engineering, Royal Institute of Technology, Stockholm, Sweden.

Hall, L., (2003), "Simulations and analyses of train-induced ground vibrations in finite element models", International Journal of Soil Dynamics and Earthquake Engineering, 23, 5, 403-413.

Hall, L. and Bodare, A., (2000), "Analyses of the cross-hole method for determining shear wave velocities and damping ratios", International Journal of Soil Dynamics and Earthquake Engineering, 20(1-4), 167-175.

Hashash, Y. M. A and Park, D., (2002), "Viscous damping formulation and high frequency motion propagation in non-linear site response analysis", Soil Dynamics and Earthquake Engineering, 22(7), 611-624.

Hashash, Y. M. A and Park, D., (2002), "Non-linear one-dimensional seismic ground motion propagation in the Mississippi embayment", Engineering Geology, 62, 185-206.

Haupt, W. A., (1981), "Model tests on screening of surface waves", Procee. of the Tenth International Conference in Soil Mecahnics and Foundation Engineering, Stockholm, Vol 3, 215-222.

Head, K.H., (1992), "Manual of Soil Laboratory Testing", London, Pentech Press.

Head, J.M. and Jardine, F.M., (1992), "Ground-borne vibrations arising from piling", CIRIA Technical Note 142.

Heckl, M., Hauck, G. and Wettschureck, R., (1996), "Structure-borne sound abd vibration from rail traffic", Journal of Sound and Vibration, 193(1), 175-184.

Hillar, D.M. & Hope, V.S., (1998), "Groundborne vibration generated by mechanised construction activities", Proceedings Institution of Civil Engineers: Geotechnical Engineering, 131, 4, 223-232.

Hillar, D. M. and Crabb, G.I., (2000), "Groundborne vibration caused by mechanised construction works", Report TRL, No-429, 1-79.

Hope, V.S. & Hiller, D.M., (2000), "The prediction of groundborne vibrations from percussive piling", Canadian Geotechnical Journal, 37, 3, 700-711.

Houlsby, G.T., Burd, H.J. & Augarde, C.E., (1999), "Analysis of Tunnel-Induced Settlement Damage to Surface Structures" XII European Conference on Soil Mechanics and Geotechnical Engineering, Amsterdam, 1, 147-152.

Hung, H.H. and Yang, Y.B., (2001), "A review of researches on ground-borne vibrations with emphasis on those induced by trains", Proc. National Science Council, 25(1), 1-16.

Hwang J.H. and Tu, T.Y., (2006), "Ground vibration due to dynamic compaction", Soil Dynamics and Earthquake Engineering, 26(5), 337-346.

Inci, G., Yesiller, N. and Kagawa, T., (2003), "Experimental investigation of dynamic response of compacted clayey soils", ASCE Geotechnical Testing Journal, 26(2), 125-141.

Ishihara, K., (1996), "Soil Behaviour in Earthquake Geotechnics", Oxford, Oxford science publications.

Ismail I.M, and Mullen, C., (2000), "Soil-structure interaction issues for three dimensional computational simulations of non-linear seismic response", www.ce.utexas.edu/em2000/papers/IIsmail.pdf.

Jafari, M. K., Shafiee, A. and Razmkhah, A., (2002), "Dynamic properties of fine grained soils in South of Tehran", JSEE, 4(1), 25-35.

Jovicic, V., Coop, M.R. and Simic, M., (1996), "Objective criteria for determining Gmax from bender element tests", Geotechnique, 46(2), 357-362.

Ju, S.H., (2004), "Three-dimensional analyses of wave barriers for reduction of train-induced vibrations", Journal of Geotechnical and Geoenvironmental Engineering", 130(7), 740-748.

Ju, S.H., (2002), "Finite element analyses of wave propagations due to high-speed train across bridges", International Journal for Numerical Methods in Engineering, 54, 1391-1408.

Karl, L., Haegeman, W., Pyl, L. & Degrande, G., (2003). "Measurement of material damping with bender elements in triaxial cell", In Proceedings of the Third

International Symposium on Deformation Characteristics of Geomaterials, Lyon, 1, 3-11.

Kattis, S.E., Polyzos, D. and Beskos, D.E., (1999), "Modelling of pile wave barriers by effective trenches and their screening effectiveness", Soil Dynamics and Earthquake Engineering, 18(1), 1-10.

Kim, D.S and Lee, J.S., (2000), "Propagation and attenuation characteristics of various ground vibrations", Soil Dynamics and Earthquake Engineering, 19, 115-126.

Kirzhner, F., Rosenhouse, G. and Zimmels, Y., (2006), "Attenuation of noise and vibration caused by underground trains, using soil replacement", Tunnelling and Underground Space Technology, 21(5), 561-567.

Klein, R., Antes, H. and Houedec, D. Le., (1997), "Efficient 3D modelling of vibration isolation by open trenches", Computers & Structures, 64(1-4), 809-817.

Kogut, J., Lombaert, G., Francois, S., Degrande, G., Haegeman, W. and Karl, L., (2003), "High speed train induced vibrations in situ measurements and numerical modelling", Tenth International Congress on Sound and Vibration, Stockholm, Sweden.

Kramer, S.L., (1996), "Geotechnical Earthquake Engineering", New Jersey, Prentice Hall.

Lawler, M., (2002), "Estimating the ground deformations associated with earthworks and foundations in boulder clay", Ph.D Thesis, Dept. of Civil, Structural & Environmental Engg., Trinity College Dublin, Ireland.

Lehane, B.M. and Simpson, B., (2000), "Modelling glacial till under triaxial conditions using a brick model", Canadian Geotechnical Journal, 37(5), 1078-1088.

Lee, J.S. and Santamarina, C., (2005), "Bender elements: performance and signal interpretation", Journal of Geotechnical and Geoenvironmental Engineering", 131(9), 1063-1070.

Lee, S.W., (2002), "The use of compensation grouting in tunnelling: a case study", Proceedings Institution of Civil Engineers: Geotechnical Engineering, 155, 2, 101-109.

Lenart, S., (2004), "The effect of density and water content upon the dynamic properties of reconstituted moraine samples in the small strain range", www.acadjournal. com.

Lin, M.L. and Huang, T.H., (1996), "The effects of frequency on damping properties of sand", Soil Dynamics and Earthquake Engineering, 15(4), 269-278.

Lin, S. Y., Lin, P.S, Lue, H. and Juang, C.H., (2000), "Shear modulus and damping ratio characteristics of gravely deposits", Canadian Geotechnical Journal, 37(3), 638-651.

Lings, M.L. and Greening, P.D., (2001), "A novel bender/extender element for soil testing", Geotechnique, 51(8), 713-718.

Liu, G., Houlsby, G.T. and Augarde, C.E., (2000), "Two-dimensional analysis of settlement damage to masonry buildings due to tunnelling", The Structural Engineer, 79,1, 19-25.

Lysmer, J. and Wass, G., (1972), "Shear waves in plane infinite structures", ASCE Journal of Engineering Mechanics, 98(1), 85-105.

Madshus, C., Kaynia, A.M. and Holme, J.K., (1998), "A numerical ground model for railway-induced vibration", Ground dynamics and man made processes, London, Thomas Telford.

Massarsch, K. R. (1992), "Static and Dynamic Soil Displacements Caused by Pile Driving", Keynote Lecture, Proceedings, 4th International Conference on the Application of Stress Wave Theory to Piles, the Hague, pp. 77 - 84.

Massarsch, K.R., (2000), "Settlement and damage caused by construction-induced vibrations", Proceedings, International Workshop Wave 2000, Bochum, Germany, 299-315.

Massarsch, K.R., (2004), "Mitigation of Traffic-induced Ground Vibrations", Keynote Lecture, 11th Intern. Conf. on Soil Dynamics and Earthquake Engineering and 3rd on Earthquake Geotechnical Engineering, Berkeley.

Massarsch, K.R., (2005), "Vibration Isolation using Gas-filled Cushions", Keynote Lecture, GEOFRONTIES 2005 - International Conference, American Society of Civil Engineers, Austin, Texas.

Massel, A., (1999), "Power spectrum analysis-modern tool in the study of rail surface corrugations", NDT & E International, 32, 8, 429-436.

Megaw, T.M. & Bartlett, J.V., (1983), Tunnels-Planning, Design, Construction, Chichester, Ellis Horwood Limited.

Menkiti, C. O., Long, M., Kovacevis, N., Edmonds, H.E., Milligan, G.W.E. & Potts, D.M., (2004), "Trial excavation for cut and cover tunnel in glacial till-a case study from Dublin", Proceedings of the Skempton Memorial Conference, Imperial College, 2, Thomas Telford, London, 1090-1104.

Moran, S., (1999), "Effect of the LRT tunnelling project on buildings in Dublin", M.Sc. Thesis, Dept. of Civil, Structural & Environmental Engg., Trinity College Dublin, Ireland.

Mroueh, H. and Shahrour, I., (2003), "A full 3-D finite element analysis of tunnelling-adjacent structures interaction", Computers and Geotechniques, 30, 3, 245-253.

Naggar, M.H., (2003), "Performance evaluation of vibration –sensitive equipment foundations under ground-transmitted excitation", Canadian Geotechnical Journal, 40, 3, 598-615.

New, B.M., (1990a), "Ground vibration caused by construction works", Tunnelling and Underground Space Technology, 5,3, 179-190.

New, B.M., (1990b), "Ground vibration associated with tunnel construction", Tunnel Construction'90-The Institution of Mining and Metallurgy, London, 67-76.

New, B.M., (1982), "Vibration caused by underground construction", Tunnelling '82-The Institution of Mining and Metallurgy, London, 217-229.

Newland, D.E., (1993), An Introduction to Random Vibrations, Spectral and Wavelet Analysis, 3rd ed., Harlow, Longman Scientific & Technical.

O'Reilly, M.P., Symonds, I.F and Carder D.R., (1990), "Instrumentation and monitoring on two cut-and-cover tunnel projects", Tunnel Construction'90-The Institution of Mining and Metallurgy, London, 91-108.

Orr, T.L.L. and Farrell, E.R., (1996), "Geotechnical aspects of tunneling in soft ground in Ireland", Proceedings of the International Symposium on Geotechnical Aspects of Underground Construction in Soft Ground, Eds. Mair and Taylor, A.A. Balkema, Rotterdam, 301-306.

Park, D and Hashash, Y., (2004), "Soil damping formulation in nonlinear time domain site response analysis", Journal of Earthquake Engineering", 8(2), 249-274.

Pak, R. Y.S., (2003), "In-situ soil modulus determination for sand by foundation vibration", 16th ASCE Engineering Mechanics Conference, Seattle.

Paolucci, R., Maffeis, A., Scandella, L., Stupazzini, M. and Vanini, M., (2003), "Numerical prediction of low-frequency ground vibrations induced by high-speed trains at Ledsgaard, Sweden", Soil Dynamics and Earthquake Engineering, 23(6), 425-433.

Peck, R. B., (1969), "Deep excavations and tunnelling in soft ground", 7th International Conference on Soil Mechanics and Foundation Engineering, Mexico City, State of the art Volume, 225-290.

Pennington, D.S., Nash, D.F.T. and Lings, M.L., (2001), "Horizontally mounted bender elements for measuring anisotropic shear moduli in triaxial clay specimens", ASCE Geotechnical Testing Journal, 24(2), 133-144.

PLAXIS, (2002), "Finite element code for soil and rock analyses", Delft, The Netherlands.

Potts, D.M. and Addenbrooke, T.I., (1997), "A structure's influence on tunnelling-induced ground movements", Proceedings Institution of Civil Engineers: Geotechnical Engineering, 125, 2, 109-125.

Potts, D.M, Axelsson, K., Grande, L., Schweiger, H. and Long. M., (2002), "Guidelines for the use of advanced numerical analysis", London, Thomas Telford.

Preisig, M. and Wolf, J.P., (2004), "Dynamic stiffness of foundation embedded in layered halfspace based on wave propagation in cones", 12th European Conference on Earthquake Engineering.

Rahman, M. & Orr, T., (2006), "A Review of Strategies to Control Manmade Induced Ground Vibrations", 13th International Congress on Sound and Vibration, Vienna, Austria.

Rahman, M. & Orr, T., (2006), "A Parametric study of backfill trench for reduction of TBM induced ground vibrations", 13th International Congress on Sound and Vibration, Vienna, Austria.

Rahman, M. & Orr, T., (2006), "An examination of effectiveness of wave barriers for reduction of TBM induced ground vibrations", Under Review, Proceedings Institution of Civil Engineers: Geotechnical Engineering.

Rahman, M. & Orr, T., (2006), "Finite element modelling of ground vibration due to tunnelling in Dublin", Under Review, International Journal of Tunnelling and Underground Space Technology.

Rahman, M. & Orr, T., (2006), "A study of the effects of an existing tunnel on surface vibrations due to a TBM", 9th young Geotechnical Engineers Conference, Queens University, Belfast.

Remington, R., (1994), "Development and performance of tunnel-boring machines on phase II of the London Water-Ring Main", Tunnelling' 94-Instituition of Mining and Metallurgy and the British Tunnelling Society, Chapman & Hall, 211-224.

Ribay, E.D., Maigre, I.D., Cabrillac, R. and Gouvenot, D., (2004), "Shear modulus and damping ratio of grouted sand", Soil Dynamics and Earthquake Engineering, 24(6), 461-471.

Richart, F.E. and Woods, R.D. (1987), "Vibrations. In: Ground Engineer's Reference Book, F.G. Bell, London.

Richart, F.E., Hall, J.R. and Woods, R.D., (1970), "Vibration of soils and foundations", Englewood Cliffs, N.J., Prentice-Hall.

Rollins, K.M., Evans, M.D., Diehl, N.B. and Daily, W.D., (1998)"Shear modulus and damping relationships for gravels", ASCE Journal of Geotechnical and Geoenvironmental Engineering, 124(5), 397-405.

Santamarina, J. C., (2001), "Soils and Waves", Chichester : Wiley.

Segol, G., Lee, P.C. and Abel, J.F., (1978), "Amplitude reduction of surface waves by trenches", ASCE Journal of Engineering Mechanics, 104(EM3), 621-638.

Sharma, S. S. and Fahey, M., (2003), "Degradation of stiffness of cemented calcareous soil in cyclic triaxial tests", ASCE Journal of Geotechnical and Geoenvironmental Engineering, 129(7), 619-629.

Sitharam, T.G. and Raju, L.G., (2003), "Evaluation of dynamic properties of sandy soils at large strain levels", http://civil.iisc.ernet.in/~cpftege/proceedings.html.

Skipp, B.O., (1998), "Ground vibration-codes and standards", Proceedings of the Conference on Ground Dynamics and Man-made Processes, Institution of Civil Engineers, London, 1, 29-41.

Skipper, J., Follett, B., Menkiti, C.O., Long, M. and Clark-Hughes, J., (2005), "The engineering geology and characterization of Dublin Boulder Clay", Quarterly Journal of Engineering Geology and Hydrogeology, 38, 171-187.

Sridharan, A., (2003), "Dynamic properties of soils including layered systems", http://civil.iisc.ernet.in/~cpftege/proceedings.html.

Stasa, F. L., (1985), "Applied Finite Element Analysis for Engineers", New York, CBS College Publishing.

Stewart, W.P. and Campanella, (1991), "Insitu measurement of damping of soils", Proceedings Second International Conference On Recent Advances In Geotechnical Earthquake Engineering and Soil Dynamics", St. Louis, Missouri.

Sutcliffe, H., (1996), Tunnel Boring Machines, Tunnel Engineering Handbook, Chapman & Hall.

Taka, D., Berry, Y. and Rammah, K., (2000) "Measurement of soil stiffness using bender element test in the triaxial apparatus", www.youth.technion.ac.il/scitech2002/civil_eng2.pdf.

Takemiya, H. and Fujiwara, A., (1994), "Wave propagation/impediment in a stratum and wave impeding block measured for SSI response reduction", International Journal of Soil Dynamics and Earthquake Engineering, 13(1), 49-61.

Taylor, R.N., (1998), "Modelling of tunnel behaviour" Proceedings Institution of Civil Engineers: Geotechnical Engineering, 131, 2, 127-132.

Teachavorasinskun, S., Thongchim, P. and Lukkunaprasit, P., (2002), "Shear modulus and damping of soft Bangkok clays", Canadian Geotechnical Journal, 39(5), 1201-1208.

Terzaghi, K., Peck, R.B. and Mesri, (1996), "Soil mechanics in Engineering Practice" New York, John Wiley & Sons.

Thusyanthan, N.I. and Madabhushi, S.P.G., (2003), "Experimental study of vibrations in underground structures", Proceedings Institution of Civil Engineers: Geotechnical Engineering, 156, 2, 75-81.

Treacy, P., (1996), "Deformations around a deep excavation in boulder clay" M.Sc. Thesis. Dept. of Civil, Structural & Environmental Engg., Trinity College Dublin, Ireland.

Ventura, C.E., Liam Finn, W.D., Lord, J-F. and Fujita, N., (2003), "Dynamic characteristics of a base isolated building from ambient vibration measurements and low level earthquake shaking", Soil Dynamics and Earthquake Engineering, 23(4), 313-322.

Viggiani, G. and Atkinson, J.H., (1995), "Interpretation of bender element tests", Geotechnique, 45(1), 149-154.

Viggiani, G. and Atkinson, J.H., (1995), "Stiffness of fine-grained soil at very small strains", Geotechnique, 45(2), 249-266.

Wagner, H., (2002), "attenuation of transmission of vibrations and ground-borne noise by means of steel spring supported low-tuned floating track beds" http://gerb.com/en/bibliothek/downloads/dokumente/WagnerTaiwan.pdf

Wichtmann, T. and Triantafyllidis, T., (2004), "Influence of a cycle and dynamic loading history on dynamic properties of dry sand, part II: cyclic axial preloading", Soil Dynamics and Earthquake Engineering, 24(11), 789-803.

Whittaker, B.N., Smith, S.F. and Chen, H, (1990), "Fracture development around tunnels", Tunnel Construction'90-The Institution of Mining and Metallurgy, London, 187-194.

Whyley, P.J. and Sarsby, R.W., (1992), "Ground borne vibration from piling", Ground Engineering, 26, 4, 32-37.

Wilson, G. P., Saurenman, H. J. and Nelson, J. T., (1983), "Control of ground-borne noise and vibration", Journal of Sound and Vibration, 87(2), 339-350.

Wilson, J.F., (2003), "Dynamics of offshore structures", New York, John Wiley & Sons.

Woods, R. D., (1968), "Screening of surface waves in soils", ASCE J. Soil Mechanics Foundation Engineering Division, 94(4), 951-979.

Yang, Y.B., and Hung, H.H., (1997), "A parametric study of wave barriers for reduction of train-induced vibrations", International Journal for Numerical Methods in Engineering, 40, 3729-3747.

Yang, Y.B., and Hung, H.H., (2001), "A 2.5-D finite/infinite element approach for modelling viscoelastic bodies subjected to moving loads", International Journal for Numerical Methods in Engineering, 51, 1317-1336.

Zhou, J. and Gong, X., (2001), "Strain degradation of saturated clay under cyclic loading", Canadian Geotechnical Journal, 38(1), 208-212.

Zhang, J, Andrus, R. D and Juang, C. H., (2005), "Normalised shear modulus and material damping ration relationships", ASCE Journal of Geotechnical and Geoenvironmental Engineering, 131(4), 453-464.

Zhang, L., McVay, M. and Ng, C., (2001), "A Possible physical meaning of case damping in pile dynamics", Canadian Geotechnical Journal, 38(1), 83-94.

City University

Geotechnical Engineering Research Centre

Results of Bender Element Tests

Client Exploration Associates Limited
Operator Laurentiu Jianu
Dates 22.03.96 - 11.04.96
Apparatus 2

Sample	Soil	boulder clay
	Type	core
	Size	Dia: 100mm, L: 400mm

Drains	all round

Stage	t1 (mins)
2	120

Test Specimen

Initial	Dia (mm)	105.93
	L (mm)	206.87
final	Dia (mm)	110.96
	L (mm)	189.45

Weight (g)	4225.8	
MC of trimmings (%)		10.65
Weight (g)	4237.3	
MC of split sample (%)		11.55

Mass density (Mg/m^3)	2.318
Mass density (Mg/m^3)	2.312

Test Results

Stage	Stresses (kPa)			p'	q'	ε_v	v	G_0'
	σ_a	σ_r	u	(kPa)	(kPa)	(%)		(MPa)
1	236	236	184	52	0	0.00	1.314	153
1	235	235	132	103	0	0.00	1.314	267
2	235	235	95	140	0	0.00	1.314	267
2	237	237	95	142	0	0.18	1.290	292
3	237	237	95	142	0	0.18	1.290	292
3	265	265	95	170	0	0.24	1.283	323
3	294	294	96	198	0	0.34	1.270	405
4	294	294	96	198	0	0.34	1.270	405
4	266	266	95	171	0	0.33	1.272	332
4	237	237	95	142	0	0.30	1.275	302
4	211	211	95	116	0	0.25	1.282	291
4	183	183	95	88	0	0.21	1.287	263
4	144	144	95	49	0	0.02	1.312	215
5	145	145	96	49	0	undr	undr	202
5	155	145	99	49	10	undr	undr	186
5	427	145	68	151	282	undr	undr	313
5	505	145	68	198	360	undr	undr	314
5	534	145	54	220	389	undr	undr	329

City University

Geotechnical Engineering Research Centre

Results of Bender Element Tests

Client Exploration Associates Limited
Operator Laurentiu Jianu
Dates 12.04.96 - 22.04.96
Apparatus 2

Drains	all round

Stage	t1 (mins)
2	120

Sample

Soil	boulder clay
Type	core
Size	Dia: 100mm, L: 400mm

Test Specimen

Initial	Dia (mm)	100.97
	L (mm)	203.56
final	Dia (mm)	102.52
	L (mm)	197.47

Mass (g)	3787.25
MC of trimmings (%)	11.66
Mass (g)	3789.4
MC of split sample (%)	11.33

Mass density (Mg/m^3)	2.324
Mass density (Mg/m^3)	2.325

Test Results

Stage	Stresses (kPa)			p'	q'	ε_v	v	G_0'
	σ_a	σ_r	u	(kPa)	(kPa)	(%)		(MPa)
1	350	350	285	65	0	0.00	1.369	172
1	350	350	293	57	-1	0.00	1.369	164
2	350	350	150	200	-1	0.00	1.369	360
2	350	350	150	200	0	0.63	1.287	360
2	350	350	150	200	0	0.75	1.272	362
3	350	350	150	200	0	0.75	1.272	362
3	412	412	152	260	0	0.86	1.257	405
3	450	450	150	300	-1	0.98	1.242	434
4	450	450	150	300	-1	0.98	1.242	434
4	357	357	149	208	0	0.92	1.250	407
4	336	336	148	188	0	0.90	1.253	388
4	240	240	150	90	0	0.73	1.275	304
4	198	199	150	49	0	0.49	1.306	203

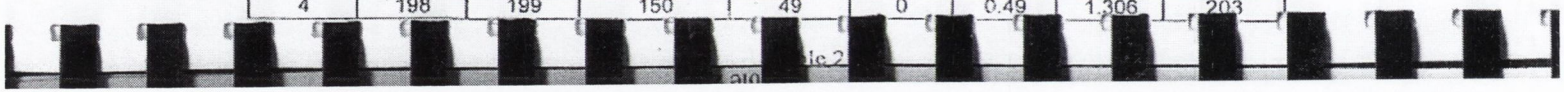

City University

Geotechnical Engineering Research Centre

Results of Bender Element Tests

Client Exploration Associates Limited
Operator Laurentiu Jianu
Dates 07.05.96 - 13.05.96
Apparatus 2

Drains	all round

Stage	t1 (mins)
2	60

Sample

Soil	boulder clay
Type	core
Size	Dia: 100mm, L: 400mm

Test Specimen

Initial	Dia (mm)	101.12	Mass (g)	3546.38		Mass density (Mg/m^3)	2.342
	L (mm)	188.55	MC of trimmings (%)		12.69		
final	Dia (mm)	102.53	Mass (g)	3525.48		Mass density (Mg/m^3)	2.356
	L (mm)	181.21	MC of split sample (%)		9.71		

Test Results

Stage	Stresses (kPa)			p' (kPa)	q' (kPa)	G_o' (MPa)
	σ_a	σ_r	u			
1	320	320	283	37	0	109
1	320	320	287	33	0	151
2	320	320	287	33	0	151
2	320	320	201	119	0	367
3	320	320	201	119	0	367
3	409	409	202	207	-1	422
3	420	420	200	220	0	462
4	420	420	200	220	0	462
4	405	405	200	205	0	448
4	335	335	204	131	0	402
4	317	317	202	115	0	384
4	302	302	203	99	0	352
4	250	250	202	48	0	308
5	250	250	202	48	0	308
5	336	250	217	62	86	328
5	436	250	217	95	186	386

City University

Geotechnical Engineering Research Centre

Results of Bender Element Tests

Client Exploration Associates Limited

Operator Laurentiu Jianu

Dates 03.06.96 - 20.06.96

Apparatus 2

Drains	all round

Stage	t1 (mins)
2	330

Sample

Soil	boulder clay
Type	core
Size	Dia: 100mm, L: 400mm

Test Specimen

Initial	Dia (mm)	101.55	Mass (g)	3658.58		Mass density (Mg/m^3)	2.342
	L (mm)	192.88	MC of trimmings (%)		11.16		
final	Dia (mm)	102.45	Mass (g)	3619.42		Mass density (Mg/m3)	2.344
	L (mm)	187.3	MC of split sample (%)		10.31		

Test Results

Stage	Stresses (kPa)			p' (kPa)	q' (kPa)	ε_v (%)	v	G_0' (MPa)
	σ_a	σ_r	u					
1	329	330	314	16	-1	0.00	1.518	47
2	330	330	201	129	0	1.69	1.301	281
3	417	365	202	181	52	1.84	1.282	358
3	457	380	202	204	77	1.94	1.270	389
3	496	396	203	227	100	2.03	1.258	441
4	496	396	200	229	100	2.07	1.252	443
4	425	368	202	185	57	2.06	1.254	416
4	330	330	202	128	0	1.99	1.262	378
5	330	330	202	128	0	1.98	1.264	381
5	377	377	202	175	0	2.01	1.260	411
5	399	399	201	198	0	2.06	1.255	424
5	430	430	202	228	0	2.10	1.248	449
6	430	430	200	230	0	2.13	1.245	450
6	412	412	200	212	0	2.1247	1.245	453
6	383	382	200	182	0	2.1103	1.247	448
6	363	363	200	164	0	2.0878	1.250	440
6	334	334	199	135	0	2.0609	1.253	413
6	314	314	199	114	0	2.0348	1.257	384
6	285	285	199	86	0	1.98	1.264	366
6	265	265	199	66	0	1.9216	1.271	328
6	250	250	199	51	0	1.8668	1.278	279
7	324	250	203	72	75	undr	undr	313
7	456	250	175	144	206	undr	undr	387
7	477	250	170	155	227	undr	undr	408
7	539	250	156	191	289	undr	undr	421

Summary Sheet of Geotechnical Laboratory Test Results - Soil

Borehole or pit no.	Depth of sample (m)	Type of sample	Lithology	Density γ_d (Mg/m³)	Density γ (Mg/m³)	Density γ_s (Mg/m³)	Water cont. w (%)	Particle size distribution (mm) 75 (% passed)	20 (% passed)	2 (% passed)	0.063 (% passed)	0.002 (% passed)	Atterberg limits LL (%)	Atterberg limits PL (%)	Atterberg limits IP (%)	Shear strength c' (kPa)	Shear strength φ' (°)	CBR top	CBR base	Permeability k (m/s)	Cons	Sstr	Bend
Feasibility Study (1991 - 1992)																							
TP-1	1.70	B	6b				12.80	100	65	50	33	18	28	17	11								
TP-2	4.60	B	6b				8.10	100	87	70	43	27	27	16	11								
TP-3	3.20	B	6b				8.80						25	14	11								
Initial Site Investigation (October to December 1995)																							
TP-7	4.80	B	1					100	87	48	12												
TP-8	4.70	B	1					100	88	50	12												
TP-8	3.80	B	1					100	87	48	12												
TP-10	2.80	B	1					100	81	45	15												
TP-11	2.30	B	1					100	78	50	14												
TP-12	2.30	B	1					100	83	42	14												
BH-101	2.00	B	6a					100	99	84	61	26											
	4.00	B	6b					100	96	85	70	31											
	9.50	B	6b				11.31	100	96	84	65	32	25	18	7								
BH-102	2.50	B	6a				17.55	100	80	61	38	12	29	19	10								
	9.00	B	6b					100	48	35	22	8											
	10.50	B	6b				9.22	100	84	64	40	14	26	19	7								
BH-103	5.60	B	6b					100	86	49	32	19											
	13.00	B	7				10.38	100	95	90	63	34	26	17	9								
	15.00	B	8				18.60	83	34	14	8		31	20	11								
	20.00	B	8				8.74	100	97	69	39	12	26	19	7								
BH-105	13.00	B	6b					100	64	49	30	9											
	16.50	B	6b					100	83	57	29												
	18.50	B	6b					100	46	35	22	7											
BH-107	16.50	B	7					100	97	91	63	15											
	18.50	B	7				16.75	100	100	89	41	14	27	19	8								
BH-108	17.50	B	7				18.40	100	100	92	75	8	39	22	17								
	18.50	B	8					85	28	6	3												
BH-109	10.00	B	8				14.28	100	77	47	31	11	30	17	13								
BH-110	10.00	B	8				11.07	100	54	27	17	4	17	9	8								
BH-111	5.60	B	8				12.94	100	99	77	59	26	18	10	8								
	9.60	B	8					100	90	56	34												
BH-114	4.50	B	2				38.37	100	100	77	40												

Borehole or pit no.	Depth of sample (m)	Type of sample	Lithology	Density γd (Mg/m³)	Density γ (Mg/m³)	Density γs (Mg/m³)	Water cont. w (%)	Particle size distribution (mm) 75 (% passed)	20 (% passed)	2 (% passed)	0.063 (% passed)	0.002 (% passed)	Atterberg limits LL (%)	Atterberg limits PL (%)	Atterberg limits IP (%)	Shear strength c ' (kPa)	Shear strength φ ' (°)	CBR top	CBR base	Permeability k (m/s)	Cons	Sstr	Bend
	5.70	B	3					83	22	8	5												
	8.00	B	8				13.31	100	51	26	13	3											
	12.80	B	8					100	77	50	25	5											
BH-115	12.30	B	4				36.20	100	100	89	49												
	16.00	B	4				9.26	100	100	100	92	23	27	20	7								
	17.50	B	4					100	83	66	57	21											
	18.00	B	3					87	30	2	1												
	21.00	B	8					100	60	41	23	7											
BH-117	12.00	B	4				12.88	100	100	99	71	14	30	19	11								
	18.70	B	8				9.35	100	97	68	39	15	28	21	7								
	21.00	B	5					100	43	14	2												
BH-118	10.00	B	3					100	43	4	1												
	14.50	B	4				22.15	100	80	78	62	10	25	18	7								
	23.00	B	8				8.86	100	94	76	57	31	28	20	8								
BH-120	13.00	B	4				22.14	100	100	97	92	24	28	17	11								
	16.00	B	8				10.70	100	54	41	24	7	24	14	10								
	19.50	B	8					100	92	80	50	10											
DPT Site Investigation (February to May 1995)																							
TP-202	0.70	B	6a		2.23		14.00											6.5	21.0				
	0.70	SB	6a		2.23		15.00											6.5	21.0				
TP-203	0.50	B	1		1.62		36.00											8.5	17.0				
	0.50	SB	1		1.62		35.00											9.4	17.0				
TP-208	0.60	B	1		2.09		13.00											23.0	39.0				
	0.60	SB	1		2.06		16.00											13.0	33.0				
TP-209	0.60	B	1		1.92		23.00											1.7	2.8				
	0.60	SB	1		1.93		23.00											2.1	2.6				
TP-210	0.50	B	1		1.76		27.00											8.3	14.0				
	0.50	SB	1		1.73		30.00											8.0	12.0				
TP-211	0.50	B	1		1.99		18.00											8.9	17.0				
	0.50	SB	1		1.98		20.00											12.0	14.0				
TP-212	0.80	B	1		1.70		28.00											4.9	14.0				
	0.80	SB	1		1.68		29.00											8.6	13.0				
TP-213	0.50	B	1		1.38		20.00											23.0	50.0				
	0.50	SB	1		1.39		33.00											18.0	39.0				
TP-214	0.70	B	1		1.40		22.00											24.0	49.0				
	0.70	SB	1		1.39		31.00											20.0	45.0				
TP-215	0.50	B	1		1.46		21.00											24.0	42.0				
	0.50	SB	1		1.43		33.00											22.0	44.0				
TP-216	0.50	B	1		1.71		20.00											34.0	44.0				
	0.50	SB	1		1.71		25.00											28.0	42.0				
TP-217	0.90	B	1		1.50		19.00											15.0	39.0				

Borehole	Depth	Type	Lithology	Density			Water	Particle size distribution (mm)					Atterberg limits			Shear strength		CBR		Permea-	Cons	Sstr	Bend
or pit	of sample	of		γd	γ	γs	cont. w	75	20	2	0.063	0.002	LL	PL	IP	c '	φ '	top	base	bility			
no.	(m)	sample		(Mg/m³)			(%)	(% passed)					(%)			(kPa)	(°)			k (m/s)			
	0.90	SB	1		1.47		30.00											12.0	29.0				
TP-218	0.50	B	1		1.72		34.00											2.1	2.6				
	0.50	SB	1		1.73		35.00											0.7	1.4				
TT-204	1.00	B	1		2.46		25.00											1.4	1.5				
	1.00	SB	1		1.86		27.00											0.7	1.4				
BH-201	6.50-7.50	CS	6b	2.11	2.34	2.67	11.00	100	93	73	42	15	27	14	13								
	10.50-11.50	CS	6b	2.21	2.40	2.67	8.80	100	92	69	40	16	26	12	14								
	10.50-11.50**	CS	6b	2.20	2.40		9.30									7	36.0						
	**	CS	6b	2.10	2.28		8.60																
	**	CS	6b	2.15	2.33		8.40																
	16.50-17.00	CS	7	1.73	2.07	2.65	20.00	100	100	95	64	18	30	15	15								
	*	CS	7	1.83	2.15	2.65	17.26														✓		
	17.60-18.50	CS	7	1.98	2.22	2.69	12.00	100	99	89	58	26											
	17.60-17.90**	CS	7	2.00	2.22		11.00									39	26.0						
	**	CS	7	2.04	2.26		11.00																
	**	CS	7	1.99	2.25		13.00																
BH-202	5.00-6.00	CS	6b	1.95	2.30	2.66	18.00	100	79	59	33		28	15	13								
	9.50	CS	7	2.09	2.31		10.00													2.48E-11			
	9.50-11.50	CS	7	2.10	2.31	2.68	10.00	100	99	94	66	25										✓(2)	✓
	9.50-10.50**	CS	7	2.10	2.33		11.00									19	35.0						
	**	CS	7	2.15	2.38		11.00																
	**	CS	7	2.10	2.32		10.00																
	10.50-11.50	CS	7		2.36																		
	15.50-16.50	CS	6b	2.12	2.29	2.68	8.00	100	82	59	35	13	29	15	14								
	18.00-19.00	CS	6b	2.15	2.36	2.55	9.80	100	96	66	45	19	30	16	14							✓	✓
BH-203	0.50	B	1				36.00																
BH-204	5.40-6.40	CS	6b	2.10	2.33	(2.40)	11.00	100	82	60	34	14	28	15	13								
	9.00-10.00	CS	7		2.31																	✓	✓
	10.00-11.00	CS	7	2.15	2.36	2.67	10.00	100	100	86	47	15	25	12	13								
	10.00-10.30**	CS	7	2.02	2.26		12.00									5	31.5						
	**	CS	7	1.94	2.19		13.00																
	**	CS	7	2.05	2.25		10.00																
	11.00-12.00	CS	7			2.62	12.00	100	97	88	60	26	26	12	14								
	11.00-12.00**	CS	7	1.89	2.11		12.00									13	33.5						
	**	CS	7	1.96	2.21		13.00																
	**	CS	7	1.88	2.16		15.00																
	19.00-19.40	CS	7	1.97	2.26	2.64	15.00						27	14	13								
	*	CS	7	1.94	2.20	2.64	13.17														✓		
	21.00-22.00	CS	8			2.63	8.00	100	89	43	20	9	30	16	14								
	22.50-24.00	CS	8	2.04	2.19	2.69	7.40	100	98	72	54	22											✓
	23.00-23.50**	CS	8	1.96	2.19		12.00									0	33.0						
	23.00	CS	8		2.31																		
BH-205	6.10-7.00	CS	6b	2.19	2.36	2.69	8.00	100	86	68	38	14	27	15	12								
	9.05-10.05	CS	7	2.19	2.41	2.73	10.00	100	91	73	46	19	27	16	11								
	9.05-10.05**	CS	7	2.19	2.41		10.00									0	32.5						

Borehole	Depth	Type	Lithology	Density			Water	Particle size distribution (mm)					Atterberg limits			Shear strength		CBR		Permea-	Cons	Sstr	Bend
or pit	of sample	of		γd	γ	γs	cont. w	75	20	2	0.063	0.002	LL	PL	IP	c '	φ '	top	base	bility			
no.	(m)	sample		(Mg/m³)			(%)	(% passed)					(%)			(kPa)	(°)			k (m/s)			
	**	CS	7	2.23	2.41		8.20																
	**	CS	7	2.24	2.46		10.00																
	11.60-11.90	CS	7		2.31																		✓
	12.00-12.95	CS	7	2.05	2.32	2.69	13.00	100	99	90	62	23	31	14	17								
	12.00-12.75**	CS	7	2.05	2.32		13.00									0	31.5						
	**	CS	7	2.08	2.35		13.00																
	**	CS	7	2.13	2.38		12.00																
	16.00-16.60	CS	7	1.95	2.22	2.70	14.00	100	100	91	60	20	30	15	15								
BH-206	*5.00*	*B*	***	*1.78*	*2.10*		*18.00*	*100*	*100*	*48*	*12*	*3*	*31*	*14*	*17*	*0*	*33.5*						
	5.00	*B*	***	*1.79*	*2.11*		*18.00*	*100*	*100*	*48*	*11*	*3*	*31*	*14*	*17*	*0*	*32.5*						
	10.00-10.50	B	6b				16.00	100	80	62	38	13	29	15	14								
	14.00-14.50	U	7	1.92	2.19	2.74	14.00	100	100	94	65	15	28	14	14								
	21.00-21.50	U	7	1.90	2.19	2.68	15.00	100	99	91	69	20	28	15	13								
BH-207	4.50-5.50	CS	6b	2.15	2.31	2.70	7.60	100	100	66	40	16	29	15	14								
	4.50-4.80**	CS	6b	2.13	2.31		8.30									62.5	26.0						
	**	CS	6b	2.18	2.32		6.50																
	**	CS	6b	2.09	2.26		8.10																
	5.50-6.50	CS	6b	2.10	2.31	2.67	10.00	100	88	66	40	15	28	15	13								
	11.50-12.50	CS	6b	2.05	2.26	2.68	10.00	100	81	64	41	16	27	14	13								
	13.50-14.50	CS	7	2.05	2.28	2.68	11.00	100	100	93	63	18	27	13	14								
	13.50-14.50**	CS	7	2.04	2.28		12.00									0	31.0						
	**	CS	7	2.04	2.31		13.00																
	**	CS	7	2.04	2.26		11.00																
	14.60-15.50	CS	7	2.04	2.29	2.69	12.00	100	100	94	59	17	26	13	13							✓	✓(2)
	16.90-17.50	CS	7	1.52	1.98	2.69	30.00	100	99	95	70	30	57	25	32						✓		
	*	CS	7	1.53	1.97	2.69	28.64																
	17.50-18.50	CS	7	1.96	2.23	2.70	14.00	100	100	90	52	21	28	14	14								
	20.50-21.50	CS	7	1.96	2.22	2.69	13.00	100	95	88	59	16	28	13	15								
	20.50-21.50**	CS	7	1.96	2.22		13.00									0	30.5						
	**	CS	7	2.01	2.25		12.00																
	**	CS	7	2.00	2.26		13.00																
	23.00-23.50	CS	7	2.04	2.28	2.70	12.00	100	99	93	70	19	27	15	12								
	*	*CS*	*7*	*1.86*	*2.16*	*2.70*	*15.89*														✓		
	23.50-24.50	CS	7	1.78	2.06	2.67	16.00	100	100	92	68	15	30	14	16								
	23.50-23.80**	CS	7	1.76	2.06		17.00									0	30.5						
	**	CS	7	1.88	2.16		15.00																
	**	CS	7	1.90	2.20		16.00																
	26.20-26.80	CS	8	2.13	2.32	2.68	9.00	100	62	44	30	12	31	16	15								
BH-208	11.50-12.50	CS	6b	2.06	2.27	2.63	10.00	100	80	59	35	11	28	15	13								
	14.00-15.00	CS	6b	2.11	2.32	2.67	9.80	100	93	71	44	19	27	14	13								
	14.00-14.35**	CS	6b	2.11	2.32		9.80									0	33.5						
	16.85-17.85	CS	7	2.09	2.32	2.70	11.00	100	96	89	59	21	26	13	13							✓	✓(2)
	18.00-18.85	CS	7	2.09	2.32	2.67	11.00	100	99	93	63	17	28	13	15								
	18.00-18.35**	CS	7	2.09	2.32		11.00									0	34.0						
	**	CS	7	2.13	2.36		11.00																

Borehole	Depth	Type	Lithology	Density			Water	Particle size distribution (mm)					Atterberg limits			Shear strength		CBR		Permea-	Cons	Sstr	Bend
or pit	of sample	of		γd	γ	γs	cont. w	75	20	2	0.063	0.002	LL	PL	IP	c '	φ '	top	base	bility			
no.	(m)	sample		(Mg/m³)			(%)	(% passed)					(%)			(kPa)	(°)			k (m/s)			
	**	CS	7	2.05	2.28		11.00																
	*	CS	7	1.96	2.20	2.67	12.70														✓		
	19.90-20.50	CS	7	2.03	2.27	2.69	12.00	100	100	93	61	19	26	14	12								
	*	CS	7	1.94	2.18	2.69	12.50														✓		
	21.50-22.50	CS	7	1.99	2.27	2.66	14.00	100	100	93	66	23	25	14	11								
	21.50-22.20**	CS	7	2.01	2.27		13.00									0	33.5						
	**	CS	7	1.99	2.25		13.00																
	**	CS	7	1.91	2.22		16.00																
	24.00-24.90	CS	8	2.10	2.29	2.69	9.00	100	74	55	38	15	32	17	15								
	25.40-26.40	CS	8	2.03	2.25	2.69	11.00						33	17	16								
BH-209	6.80-7.50	CS	6b	2.19	2.37	2.65	8.00	100	83	59	33	11	27	14	13								
	12.80-13.60	CS	7	2.02	2.30	2.69	14.00	100	99	88	55	19	26	15	11								
BH-210	0.50	B	1				27.00																
BH-211	9.10-10.00	CS	6b		2.34																		
	10.00-10.50	CS	6b																				✓
	12.50-13.50	CS	7	2.16	2.36	2.67	9.10	100	78	63	30	12	29	13	16								
	12.50-13.50**	CS	7	2.17	2.36		8.80									12.5	31.0						
	**	CS	7	2.17	2.35		8.50																
	**	CS	7	2.01	2.21		10.00																
	13.50-14.50	CS	7	2.05	2.30	2.63	12.00	100	100	93	64	24	30	15	15							✓	✓
	14.50-15.50	CS	7	2.15	2.37	2.64	10.00	100	90	70	44	17	19	12	7								
	14.50-14.95*2	CS	7	2.15	2.37		10.00									0	30.5						
	**	CS	7	2.08	2.29		10.00																
	**	CS	7	2.03	2.25		11.00																
BH-212	4.00	B	***	2.21	2.10		17.00	100	100	93	53	9	27	14	13	0	34.0						
	9.00-9.50	BD	6b				15.00	100	88	68	40	14	29	15	14								
	12.00-12.45	U	7				14.00	100	98	89	60	20	28	14	14								
	15.00-15.50	BD	8				11.00	100	78	57	33	12	29	15	14								
	17.00-17.50	BD	8				16.00						38	21	17								
BH-213	17.80-18.20	CS	8			2.70	10.00						32	18	14								
BH-213/2	10.50-10.80	CS	7				8.00	100	95	77	47	18	27	15	12								
	11.00	CS	7		2.34																		
	11.30-12.30	CS	7																				✓
	17.80-18.20*	CS	8	1.94	2.19	2.70	12.57														✓		
BH-214	6.00-6.50	U	6b				9.00																
	9.00-9.50	B	6b				10.00	100	66	46	21	7	33	16	17								
	12.00-12.50	B	7				19.00	100	92	78	52	18	26	14	12								
	13.00-13.30	B	8				8.00	100	79	30	7		non plastic										
BH-215	5.82	B	8				9.00	100	73	48	29	10	26	15	11								
	6.90	B	8				7.00	100	68	52	30	10	26	15	11								
	7.70	B	8				12.00	100	85	62	33	12	29	16	13								
BH-218	3.00	B	***	1.74	2.09		20.00	100	100	94	50	9	27	13	14	0	31.5						
	8.00-9.50	B	5					100	49	16	2		non plastic										
	10.00-10.90	BD	5				5.00	100	67	35	7		non plastic										
BH-220	4.00-4.50	B	5					100	82	50	5		non plastic										

Borehole or pit no.	Depth of sample (m)	Type of sample	Lithology	Density γd (Mg/m³)	Density γ (Mg/m³)	Density γs (Mg/m³)	Water cont. w (%)	Particle size distribution (mm) 75 (% passed)	20 (% passed)	2 (% passed)	0.063 (% passed)	0.002 (% passed)	Atterberg limits LL (%)	Atterberg limits PL (%)	Atterberg limits IP (%)	Shear strength c ' (kPa)	Shear strength φ ' (°)	CBR top	CBR base	Permeability k (m/s)	Cons	Sstr	Bend
	6.00-6.50	B	8				14.00	100	79	58	28	11	28	15	13								
	7.00	B	5				8.00	100	74	50	17		25	15	10								
BH-222	6.00-6.50	BD	6b				12.00	100	86	60	32	11	28	16	12								
	7.00-7.50	BD	5				4.00	100	63	33	9		non plastic										
BH-223	3.50-4.50	BD	6b				14.00	100	79	48	25	8	25	14	11								
	5.50-6.00	BD	7				14.00	100	98	82	50	20	31	15	16								
	7.50-8.00	BD	8				13.00	100	75	48	21	9	27	15	12								
BH-224	8.80-9.50	CS	8	2.14	2.33	2.67	9.00	100	84	58	21	5											
	9.50-10.00	CS	8			2.64	9.50	100	68	45	36	8	27	16	11								
	*	*CS*	*8*	*1.86*	*2.12*	*2.64*	*13.74*														✓		
BH-225	2.00-2.50	B	3				6.00	100	77	30	3												
	4.00-4.50	B	3					100	81	41	8												
	5.00-5.50	B	3				6.00	100	78	40	11												
	6.00	B	8					100	78	47	18	7											
	8.00	BD	8				8.50	100	85	67	39	8	25	14	11								
	9.00	B	8					100	85	66	37	9											
	9.50	*B*	***	*1.85*	*2.17*		*17.00*						*25*	*13*	*12*	*0*	*34.0*						
	13.50-14.00	B	8				10.00	100	88	68	39	12	26	15	11								
BH-226	5.00-5.50	B	3					100	51	12	2												
	6.00-6.45	U	2	1.94	2.23	2.68	15.00	100	100	100	82	30	26	14	12								
	6.00-6.45**	U	2	1.94	2.23		15.00									0	33.0						
	**	U	2	1.93	2.22		15.00																
	**	U	2	1.97	2.25		14.00																
	7.00-7.50	B	3					100	71	23	6		non plastic										
	9.00-9.50	B	3					100	82	45	2		non plastic										
	13.00-13.50	B	3					100	68	35	3		non plastic										
BH-227	8.00-8.50	B	3				4.00	100	63	15	1		non plastic										
	9.00-9.50	B	4				22.00	100	99	94	88	22	29	18	11								
	10.00-10.50	B	3					100	57	13	1		non plastic										
	14.00-14.50	B	3					100	79	55	25		non plastic										
BH-229	9.00-9.50	B	3					100	74	25	1		non plastic										
BH-230	*18.00-20.00*	*B*	***	*1.83*	*2.12*		*16.00*	*100*	*100*	*88*	*47*	*8*	*26*	*15*	*11*	*0*	*34.0*						
	19.00-19.50	B	3				9.00	100	69	27	4		non plastic										
	21.00-21.50	B	3				8.00	100	61	29	4		non plastic										
BH-232	9.00-9.50	B	3					100	79	28	2		non plastic										
	10.00-10.50	B	3					100	75	20	1		non plastic										
	12.00-12.50	B	4				21.00						23	16	7								
BH-235	8.00-9.50	B	3					100	88	46	15		non plastic										
	11.00-11.50	B	3					100	86	30	2		non plastic										
BH-236	12.00-12.50	B	3					100	58	28	5		non plastic										
	15.00-15.45	U	4	1.66	2.02	2.66	22.00	100	100	100	17	4	23	non plast.									
	15.00-15.45**	U	4	1.58	2.02		28.00									81.5	33.0						
	**	U	4	1.39	1.84		32.00																
	**	U	4	1.48	1.86		26.00																
BH-238	12.00-12.50	BD	3					100	34	8	1		non plastic										

Borehole	Depth	Type	Lithology	Density			Water	Particle size distribution (mm)					Atterberg limits			Shear strength		CBR		Permea-	Cons	Sstr	Bend
or pit	of sample	of		γd	γ	γs	cont. w	75	20	2	0.063	0.002	LL	PL	IP	c '	φ '	top	base	bility			
no.	(m)	sample		(Mg/m³)			(%)	(% passed)					(%)			(kPa)	(°)			k (m/s)			
	14.00-14.45	U	4	1.89	2.19	2.66	16.00	100	100	100	40	11	26	non plast.									
	14.00-14.45**	U	4	1.86	2.18		17.00									75	35.5						
	**	U	4	1.81	2.14		18.00																
	**	U	4	1.84	2.15		17.00																
	16.00-16.45	U	4	1.61	1.97	2.68	22.00	100	100	100	8		26	non plast.									
	16.00-16.45**	U	4	1.43	1.87		31.00									0	41.0						
	**	U	4	1.56	2.00		28.00																
	**	U	4	1.52	2.02		33.00																
	18.00-18.45	U	4	1.60	1.95	2.69	22.00	100	100	100	99	30	34	17	17								
	*	*U*	*4*	*1.73*	*2.12*	*2.69*	*22.79*														✓		
	20.00-20.50	BD	5					100	58	16	7		non plastic										
BH-239	*8.00-8.20*	*B*	*3*					*100*	*46*	*16*	*1*												
	11.00-11.30	*B*	*4*				*18.00*						*24*	*17*	*7*								
	13.10-13.40	*B*	*4*					*100*	*100*	*95*	*67*												
BH-240	*3.20-3.40*	*B*	*3*					*100*	*83*	*41*	*1*												
	7.00-7.20	*B*	*4*				*25.00*	*100*	*100*	*100*	*86*		*29*	*17*	*12*								
	9.30-9.50	*B*	*5*					*100*	*70*	*31*	*2*												
	12.80	*B*	*5*					*100*	*82*	*39*	*2*												
BH-241	*0.90-1.10*	*B*	*3*					*100*	*76*	*39*	*4*												
	4.70-4.90	*B*	*3*					*100*	*74*	*36*	*1*												
	6.80-7.10	*B*	*4*				*20.00*						*22*	*14*	*8*								
BH-244	*2.00-2.45*	*B*	*2*				*26.00*	*100*	*83*	*56*	*23*		*58*	*34*	*24*								
	6.00-6.45	*B*	*3*					*100*	*48*	*17*	*4*												
	12.00-12.45	U	4	1.86	2.19	2.65	18.00	100	100	100	69	17	25	non plast.									
	*	U	4	1.89	2.22	2.65	17.72														✓		
	13.00	U	4	1.82	2.11		16.00													6.70E-10			
	14.00-14.45	U	4	1.71	2.07		21.00													4.07E-10			
	14.00-14.45	U	4	1.66	2.07	2.67	25.00	100	100	100	64	17	22	non plast.									
	15.00-15.45	*U*	*4*				*22.00*																
	17.00	U	4					100	100	100	99	34	34	17	17								
	17.50-17.85	U	4	1.68	2.07	2.67	23.00																
	*	U	4	1.88	2.20	2.67	16.83														✓		
	18.50-18.85	U	4	1.75	2.15	2.68	23.00	100	100	100	97	38	37	17	20								
	18.50-18.95**	U	4	1.72	2.15		25.00									26.5	27.0						
	**	U	4	1.60	2.00		25.00																
	**	U	4	1.58	1.97		25.00																
	19.50-19.95**	U	4	1.58	1.98		25.00									1	31.0						
	**	U	4	1.57	1.96		24.00																
	**	U	4	1.58	1.96		24.00																
BH-245/B	10.00-10.45	U	4	1.90	2.18	2.66	15.00	100	98	95	40	11	24	non plast.									
	10.00-10.45	U	4	1.89	2.18		16.00													5.68E-09			
	12.00-12.45	U	4	1.72	2.06	2.68	20.00	100	100	100	65	23	26	non plast.									
	12.00-12.45**	U	4	1.69	2.06		22.00									0	36.5						
	**	U	4	1.69	2.06		22.00																
	**	U	4	1.71	2.05		20.00																

Borehole	Depth	Type	Lithology	Density			Water	Particle size distribution (mm)					Atterberg limits			Shear strength		CBR		Permea-	Cons	Sstr	Bend
or pit	of sample	of		γd	γ	γs	cont. w	75	20	2	0.063	0.002	LL	PL	IP	c '	φ '	top	base	bility			
no.	(m)	sample		(Mg/m³)			(%)	(% passed)					(%)			(kPa)	(°)			k (m/s)			
	15.00-15.45	U	4	1.62	2.01	2.66	24.00	100	100	100	19	6	non plastic										
	15.00-15.50	U	4	1.59	2.01		26.00													1.84E-10			
	17.00-17.45	*B*	*4*					*100*	*100*	*100*	*31*												
	18.00-18.45	U	4			2.69	20.00	100	100	100	97	33	31	16	15								
	18.00-18.50**	U	4	1.76	2.13		21.00									31	25.0						
	**	U	4	1.73	2.11		22.00																
	**	U	4	1.79	2.16		21.00																
	19.50-19.95	U	4			2.66	20.00	100	100	100	94	31	30	16	14								
	19.50-19.95	U	4	1.64	2.03		24.00													3.96E-10			
BH-246	*1.00*	*D*	*1*				*9.00*																
	2.00	*D*	*1*				*18.00*																
	2.00-2.45	*B*	*1*					*100*	*92*	*74*	*3*												
	3.00	*D*	*1*				*18.00*																
BH-247/A	*1.00*	*D*	*1*				*50.00*																
	3.00	*D*	*1*				*47.00*																
	4.50-4.95	*U*	*2*				*41.00*						*53*	*27*	*26*								
BH-248	*1.00-1.45*	*B*	*1*				*23.00*																
	2.00-2.50	*B*	*1*					*100*	*52*	*13*	*1*		*non plastic*										
	3.00-3.45	*B*	*1*				*35.00*																
	4.00-4.45 #	*B*	*2*				*49.00*																
	5.00-5.45	*U*	*2*				*19.00*						*33*	*non plastic*									
	8.00-8.45	*B*	*3*					*100*	*34*	*10*	*0*												
	10.00-10.50	B	3					100	64	19	1		non plastic										
BH-249	*1.00-1.45*	*B*	*1*				*42.00*																
	3.00-3.45 #	*B*	*1*				*68.00*																
	4.00-4.45	*B*	*1*				*38.00*																
	8.00-8.50	B	3					100	43	14	0		non plastic										
BH-250	*1.50-1.80*	*B*	*1*				*24.00*																
	2.35-2.65	*B*	*1*					*100*	*81*	*54*	*15*												
	4.40-4.65	*B*	*1*				*57.00*																
	7.70-8.00	*B*	*3*					*100*	*78*	*44*	*2*												
BH-251	*1.10-1.30 #*	*B*	*1*				*25.00*																
	1.70-2.00	*B*	*1*				*37.00*																
	4.40-4.60	*B*	*2*				*33.00*	*100*	*92*	*61*	*12*												
	7.60-7.90	*B*	*3*					*100*	*81*	*45*	*2*												
BH-252	*1.10-1.40*	*B*	*1*				*26.00*																
	2.30-2.50 #	*B*	*1*					*100*	*78*	*54*	*16*												
	7.80-8.00	*B*	*3*					*100*	*99*	*66*	*5*												
	7.82-8.88	B	3					100	90	39	3		non plastic										
	11.58-12.85	B	3					100	75	37	2		non plastic										
	14.68-14.80	B	4				10.00	100	99	97	61	19	23	15	8								
BH-253	*1.15-1.30 #*	*B*	*1*					*100*	*94*	*63*	*18*												
	2.05-2.30	*B*	*1*				*44.00*																
	8.30-8.50	*B*	*3*					*100*	*99*	*81*	*7*												
	8.80-9.20	B	3					100	63	33	1		non plastic										

Borehole or pit no.	Depth of sample (m)	Type of sample	Lithology	Density			Water	Particle size distribution (mm)					Atterberg limits			Shear strength		CBR		Permea-	Cons	Sstr	Bend
				γd	γ	γs	cont. w	75	20	2	0.063	0.002	LL	PL	IP	c '	φ '	top	base	bility			
				(Mg/m³)			(%)	(% passed)					(%)			(kPa)	(°)			k (m/s)			
	11.70-12.93	B	3					100	90	39	1		non plastic										
BH-254	*1.20-1.40*	*B*	*1*					*100*	*89*	*61*	*21*												
	2.15-2.35 #	*B*	*1*				*43.00*																
	7.50-7.80	*B*	*3*					*100*	*98*	*79*	*16*												
	9.60-10.78	B	3					100	69	30	1		non plastic										
	13.55-15.00	B	3					100	60	18	1		non plastic										
BH-256	6.00-6.50	BD	6b				10.00	100	90	72	44	18	29	15	14								
	13.00-13.50	BD	6b				13.00	100	94	76	46	16	28	14	14								
BH-257	4.50-5.50	CS	6b	2.02	2.20	2.65	9.00	100	96	71	44	18	34	16	18								
	4.50-5.50**	CS	6b	2.01	2.20		9.30									4.5	31.5						
	**	CS	6b	1.95	2.13		9.10																
	**	CS	6b	2.07	2.25		8.70																
	6.50	CS	6b	2.03	2.24		9.90													1.07E-10			
	6.50-7.50	CS	6b	2.00	2.15	2.68	7.70	100	89	65	41	17	31	14	17								
	13.00-13.30	CS	7	1.80	2.00	2.63	11.00	100	98	84	61	12	24	non plast.									
	*		7	1.75	2.11	2.62	20.57														✓		
	14.50-15.30	CS	7	2.05	2.28	2.61	11.00	100	99	91	55	20	26	non plast.									
	*	*CS*	*7*	*1.96*	*2.20*	*2.61*	*12.06*														✓		
BH-258	2.00-2.50	BD	6a				12.00	100	98	55	20	7	26	14	12								
	6.00-6.50	BD	6b				9.0	100	92	69	40	15	29	15	14								
BH-259	3.00-3.15	U	6a	1.91	2.18	2.69	14.0	100	93	70	41	14	35	19	16								
	5.00-5.45	U	6a	1.94	2.11	2.69	9.0																
	13.00-13.50	BD	7				18.0	100	100	97	65	20	36	18	18								
BH-260	7.00-7.50	BD	6b				18.0	100	95	82	44	17	27	13	14								
	11.50-12.00	BD	6b				17.0	100	98	74	44	17	28	15	13								
BH-261	6.00-6.50	BD	6b				9.0	100	90	70	41	16	28	16	12								
	10.00-10.50	BD	6b				9.0	100	97	72	42	17	29	16	13								
	19.00-19.50	BD	7				15.0	100	99	93	56	19	29	14	15								
BH-262	5.20-6.50	CS	6b	2.06	2.23	2.72	8.0	100	86	64	39		32	15	17								
	5.20-5.60**	CS	6b	2.06	2.23		8.0									10	32.5						
	**	CS	6b	2.04	2.21		8.3																
	**	CS	6b	2.16	2.32		7.4																
	15.50	CS	7		2.24																		
	19.20-20.20	CS	8	2.13	2.32	2.59	9.0	100	84	54	38	15	33	15	18								
	19.20-20.20**	CS	8	2.16	2.32		7.7									100	28.0						
	**	CS	8	2.07	2.24		8.2																
	**	CS	8	2.06	2.24		8.4																
	22.20-23.65	CS	8	2.13	2.34	2.70	10.0	83	69	49	34	15	33	14	19								
	22.20-23.25**	CS	8	2.20	2.34		6.3									76	26.0						
	**	CS	8	2.08	2.27		9.1																
	**	CS	8	1.95	2.13		9.2																
BH-263	15.00-15.45	U	4																				
	18.00-18.50	BD	8				10.0	100	94	77	49	9	21	13	8								
	20.50-21.00	BD	8				13.0						22	14	8								
	21.40-22.50	BD	5				5.0	100	60	29	5		non plastic										

Borehole or pit no.	Depth of sample (m)	Type of sample	Lithology	Density γd (Mg/m³)	Density γ (Mg/m³)	Density γs (Mg/m³)	Water cont. w (%)	Particle size distribution (mm) 75 (% passed)	20 (% passed)	2 (% passed)	0.063 (% passed)	0.002 (% passed)	Atterberg limits LL (%)	Atterberg limits PL (%)	Atterberg limits IP (%)	Shear strength c ' (kPa)	Shear strength φ ' (°)	CBR top	CBR base	Permea-bility k (m/s)	Cons	Sstr	Bend
BH-265	6.00-6.50	BD	8				11.0	100	89	68	32	9	21	13	8								
	8.00-8.50	BD	8				12.0	100	83	58	28	9	22	13	9								
	11.00-11.50	B	5				16.0	100	80	47	12		non plastic										

Key:

Type of sample	CS...core sample, U...undisturbed sample, D...disturbed jar sample, B...disturbed bulk sample, SB...soaked bulk sample, BD...B and D
Density	γd...dry density, γ...bulk density, γs...particle density
Atterberg limits	LL...liquid limit, PL...plastic limit, IP...plasticity index
Cons	consolidation test, for results refer to relevant report sheets
Sstr	small strain triaxial test, for results refer to relevant report sheets
Bend	bender element test, for results refer to relevant report sheets
✓	performed; for results refer to relevant report sheets
(...)	values excluded from statistical evaluation
*	from consolidation test
**	from CU test
***	reconstituted sample
#	organic content and/or loss on ignition tested (ref. Contractor's summary sheets)

Lithology	
1	made ground
2	estuarine/alluvial silts & sands
3	estuarine/alluvial gravels
4	glaciomarine clays & silts & sands
5	glacial gravels & sands
6a	weathered brown boulder clay
6b	upper black boulder clay
7	sandy brown boulder clay
8	lower black boulder clay

Notes:

1. samples and values in *italic* not included in overall statistical analysis (report no. 4-09-R-002) because of late submission by Contractor

Summary Sheet on Geotechnical Laboratory Test Results for Rock

Borehole No.	Depth of sample (m)	Lithology	Bulk density γ (Mg/m³)	Dry density γd (Mg/m³)	Porosity n (%)	Void index Iv (%)	Water content w (%)	UCS (MPa)	Tensile strength (Brazilian) (MPa)	Young's modulus E (GPa)	Poisson ratio v	Slake durability index (%)	Abrasivity (0.1mm)	Fracture energy Wf (Nm)	Fracture energy specific wf (Nm/MPa)	Petro-graphic analysis	Clay mineral analysis	Vitrinite reflect. analysis
1	not known	A							9.0				1.36			✓		
2	14.30	A						200.3	8.3				1.67			✓		
2	18.80	A						165.1	10.4				1.03			✓		
2	20.30	A						127.0	8.7				1.87			✓		
4	10.20	A							11.1				1.57			✓		
6	not known	A						161.1	6.6				1.01			✓		
BH-207	22.70	A														✓		
BH-207	28.00-28.30	B	2.67	2.67	0.31	0.30	0.1	*1)										
BH-207	32.50-33.20	B	2.70	2.69	0.04	0.04	0.1	182	22.9	42.4	0.232							
BH-207	34.70	A														✓		
BH-207	35.00	A														✓		
BH-209	19.10	A														✓		
BH-209	24.10	A/B														✓		
BH-209	24.70-25.00	B	2.67	2.69	0.11	0.02	0.2	181		31.4	0.235							
BH-209	27.70-28.05	B	2.66	2.67	0.19	0.34	0.2	121		28.6	0.189							
BH-209	28.90-29.10	B	2.66	2.71	0.04	0.17	0.1	87.8	10.6	19.6	0.258							
BH-209	29.80	C																✓
BH-211	24.00	A														✓		
BH-211	25.50	C															✓	
BH-211	25.70	A														✓		
BH-211	26.10	FG															✓	
BH-211	26.30	A														✓		
BH-212	19.10-19.50	C					1.7	*1)										
BH-212	21.10-21.30	C					1.9		*1)									
BH-212	21.80	A														✓		
BH-212	21.80-22.50	C	2.42	2.40	1.38		0.8											
BH-212	23.50-23.75	C				0.19												
BH-212	26.40-26.55	A	2.65	2.65	0.04		0.1											
BH-212	26.40-26.55	A	2.69					(225)		*1)				42	0.18			
BH-212	27.50-27.80	A	2.71	2.58	0.35	0.16	0.2	123		34.8	0.344							
BH-212	30.00	C															✓	
BH-212	30.50	A														✓		
BH-213	26.70	A														✓		
BH-213/2	21.50-22.00	A	2.68	2.67	0.08	*1)	0.2	210		29.5	0.155							
BH-213/2	21.50-22.00	A	2.59					(161)		(51.4)				24	0.15			
BH-213/2	23.30-23.70	A	2.68	2.68	0.05	0.28	0.3	161	11.6	36.5	0.236							
BH-213/2	26.20-26.60	A	2.68	2.68	0.12	0.17	0.3	168	25.1	34.6	0.277							
BH-213/2	28.30	A/B														✓		
BH-214	19.90-20.10	B		2.66	0.19	0.34		*1)										

Borehole No.	Depth of sample	Lithology	Bulk density	Dry density	Porosity	Void index	Water content	UCS	Tensile strength	Young's modulus	Poisson ratio	Slake durability index	Abrasivity	Fracture energy		Petro-graphic analysis	Clay mineral analysis	Vitrinite reflect. analysis
			γ	γd	n	Iv	w		(Brazilian)	E	ν			Wf	wf			
	(m)		(Mg/m³)	(Mg/m³)	(%)	(%)	(%)	(MPa)	(MPa)	(GPa)		(%)	(0.1mm)	(Nm)	(Nm/MPa)			
BH-214	21.70	B										99.4						
BH-214	25.00	FG															✓	
BH-214	25.20	A/B														✓		
BH-214	27.60	B										99.3						
BH-214	29.30-29.60	B	2.64	2.63	0.18	0.25	0.3	65.4	9.5	16.3	0.136							
BH-214	31.10-31.30	A	2.70					(238)		(79.3)			0.61	45.7	0.19			
BH-218	17.30	C																✓
BH-218	18.00-18.20	A	2.71	2.61	0.30	0.50	0.7	129		15.1	0.227							
BH-218	18.60-18.80	A	2.68	2.58	0.39		0.1	122	*1)	26.0	0.178							
BH-218	19.00	A/B														✓		
BH-218	20.90	A										99.1						
BH-218	22.10-22.60	A	2.66	2.81	0.45	0.51	0.4	154	7.2	20.1	0.149		0.16					
BH-218	23.85-24.00	A		2.56	0.35	0.35	0.7	*1)										
BH-218	25.10-25.40	A	2.71	2.65	0.05	0.12	0.1	189		37.3	0.181							
BH-218	28.20-28.50	A	2.62	2.62	0.17	*1)	0.1	130	*1)	26.5	0.0759							
BH-218	28.80	C																✓
BH-221	8.80-9.30	A	2.69	2.75	0.05	0.15	0.1	87.5		33.1	0.164							
BH-221	12.20	C															✓	
BH-221	15.00-15.60	A	2.68	2.67	0.13	0.22	0.3	183	*1)	35.8	0.200							
BH-221	15.00-15.60	A	2.69					(206)		(74.7)			1.36	36.4	0.18			
BH-221	17.80-18.00	A		*1)	*1)	0.32	0.3	117		22.6	0.148							
BH-221	18.00-18.40	A	2.72	2.69	0.07	0.16	0.1	106	9.6	36.9	0.179							
BH-221	18.70-18.95	A	2.68	2.68	0.09	0.24	0.1	169		35.5	0.204							
BH-221	18.95-19.30	A		2.62	0.34	0.17	0.4	*1)	13.5									
BH-221	18.95-19.10	A	2.67					(150)		(34.5)			0.45	36.0	0.24			
BH-221	21.20	A/B														✓		
BH-221	21.90-22.15	A	2.70	2.70	0.05	0.27	0.1	146		34.5	0.124							
BH-221	22.70	A										99.6						
BH-221	23.55-23.90	A	2.68	2.68	0.04	0.16	0.1	224		35.0	0.129		1.61					
BH-221	26.40	C										99.2					✓	
BH-221	26.50-26.70	B		*1)	*1)	0.20	0.2	139		21.2	0.151							
BH-222	9.30	A/B														✓		
BH-222	9.40	A/B														✓		
BH-222	10.80-11.10	B	2.65	2.64	0.09	0.16	0.2	209		30.6	0.143							
BH-222	12.80-13.20	B	2.68	2.68	0.19	0.29	0.1	175	18.3	38.1	0.155		1.96					
BH-222	15.50	C																✓
BH-222	16.00	A														✓		
BH-222	16.30-16.80	B	*1)	*1)	*1)	0.61	0.5	*1)										
BH-222	19.10-19.30	B	2.69	2.72	0.03	0.20	0.1	134		32.1	0.218							
BH-222	19.30-19.50	B	2.64	2.63	0.16	0.19	0.2	133		23.5	0.149							
BH-222	20.90-21.20	A	2.68	2.67	0.14	0.22	0.3	59.1	14.3	15.4	0.145		0.82					
BH-222	22.55-22.80	B	2.63	2.61	0.34	0.22	0.6	52.9		11.4	0.199							
BH-222	23.10-23.30	B	2.62	2.60	0.23	0.15	0.6		12.6									
BH-222	24.80	A/B/C														✓		
BH-222	25.00	C															✓	
BH-222	25.10	C										98.9						
BH-222	29.30	C															✓	

Borehole No.	Depth of sample (m)	Lithology	Bulk density γ (Mg/m³)	Dry density γd (Mg/m³)	Porosity n (%)	Void index Iv (%)	Water content w (%)	UCS (MPa)	Tensile strength (Brazilian) (MPa)	Young's modulus E (GPa)	Poisson ratio v	Slake durability index (%)	Abrasivity (0.1mm)	Fracture energy Wf (Nm)	Fracture energy specific wi (Nm/MPa)	Petro-graphic analysis	Clay mineral analysis	Vitrinite reflect. analysis
BH-222	25.00	C															✓	
BH-222	25.10	C										98.9						
BH-222	29.30	C															✓	
BH-222	29.20-30.00	B	2.71	2.71	0.13	0.09	0.1	186		39.7	0.154		1.59					
BH-222	29.70-30.00	B				0.14												
BH-222	30.70-31.10	B	2.72	2.72	0.63	0.19	0.1	132	12.9	38.2	0.145							
BH-223	8.50	A					/									✓		
BH-223	8.80	C										99.0						
BH-223	13.35-13.80	A		2.65	0.10	0.19	0.1											
BH-223	13.35-13.55	A	2.71					(287)		(75.0)			0.50	64.5	0.22			
BH-223	14.20-14.40	A	2.72	2.66	0.17	0.13	0.2	211		38.2	0.222							
BH-223	17.20-17.60	A	2.71	2.70	0.05	0.26	0.4											
BH-223	17.20-17.60	A	2.74					(310)		(66.6)			2.02	54.4	0.18			
BH-223	20.00	A														✓		
BH-223	21.00	A										90.0						
BH-223	22.90-23.30	A	2.63	2.60	0.23	0.29	0.6	84.1	14.3	22.5	0.250							
BH-225	19.10-19.30	B	2.62	2.61	0.11		0.4	140		17.7	0.213							
BH-225	20.10	A														✓		
BH-225	21.20	B/C														✓		
BH-225	23.20-23.45	A	2.69	2.67	0.02	*1)	0.9		13.2									
BH-225	23.20-23.45	A	2.67					(235)		(52.3)				54.3	0.23			
BH-225	24.70-24.95	B	2.60	2.58	0.19		0.6	*1)										
BH-226	27.50	A														✓		
BH-226	30.00	C																✓
BH-257	25.70	C																✓
BH-257	26.50	A														✓		
BH-262	25.50	C															✓	
BH-262	25.70-26.05	A	2.67	2.67	0.04		0.1	92.4		26.0	0.349							
BH-262	27.40-27.70	A	2.63	2.63	0.09		0.1	98.6		28.8	0.268							
BH-262	29.30-29.40	A	2.62	2.61	0.13		0.4		*1)									

Key:

Lithology	A-calcisiltite, B-argillaceous calcisiltite, C-calcareous shale, FG-fault gouge material
UCS	UCS...uniaxial compressive strength
*1)	scheduled test not performed, because sample to weak, unsufficient or broken during preparation
✓	performed, for results refer to test report sheets

Notes:

1. Non-bold density values are calculated from dry density and porosity
2. Bold density values were determined as part of UCS tests
3. (UCS) and (E) determined from samples with diameter/height=1

APPENDIX– B

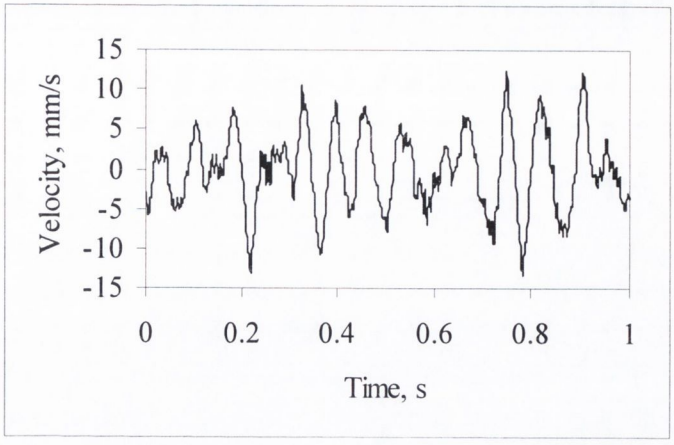

Fig.B.1–Measured TBM excitation at measuring Section 1; transverse direction

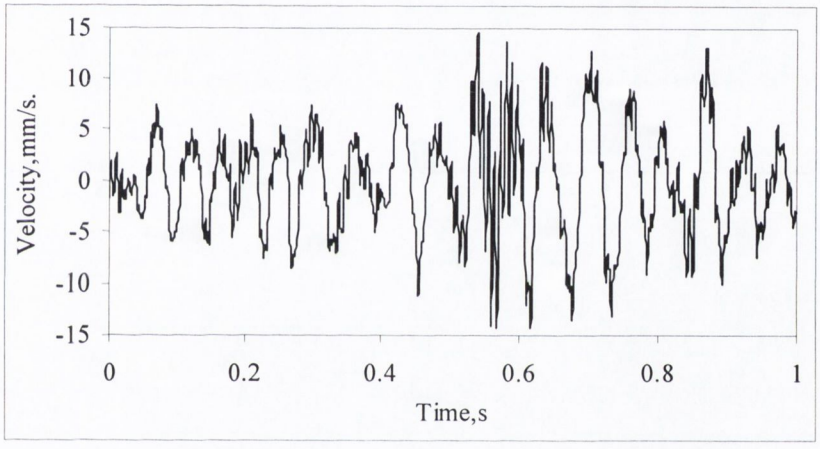

Fig.B.2–Measured TBM excitation at measuring Section 1; vertical direction

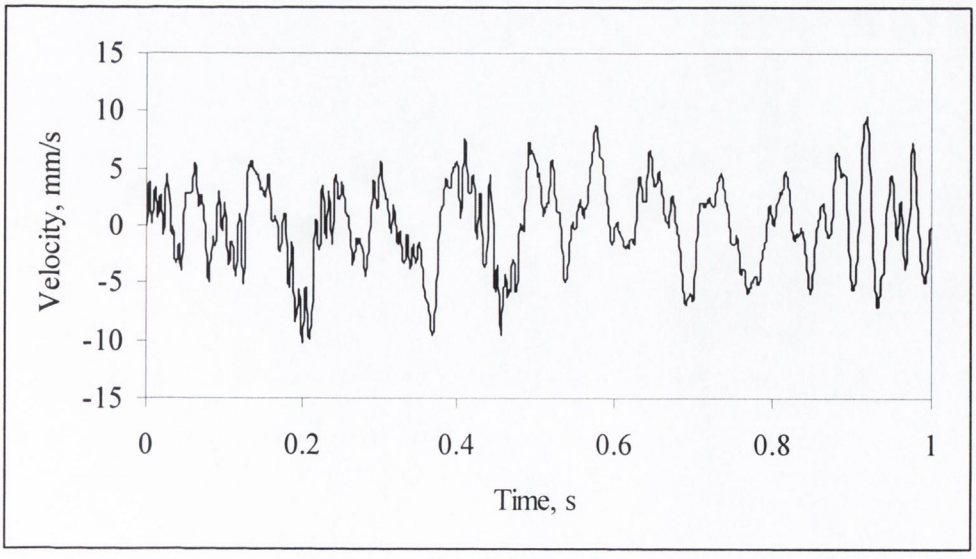

Fig.B.3–Measured TBM excitation at measuring Section 1; longitudinal direction.

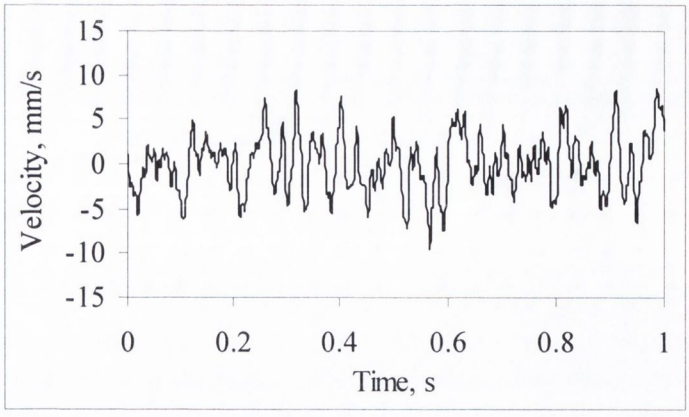

Fig.B.4–Measured TBM excitation at measuring Section 2; transverse direction

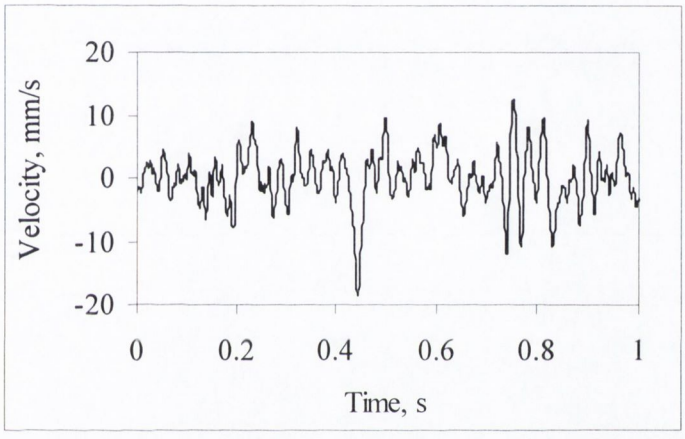

Fig.B.5–Measured TBM excitation at measuring Section 2; vertical direction

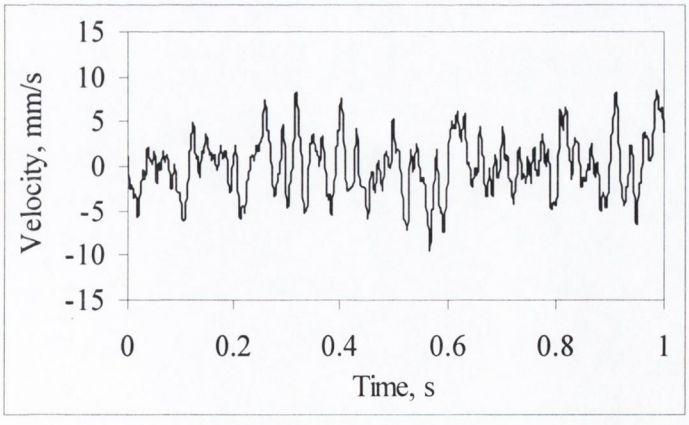

Fig.B.6–Measured TBM excitation at measuring Section 2; longitudinal direction.

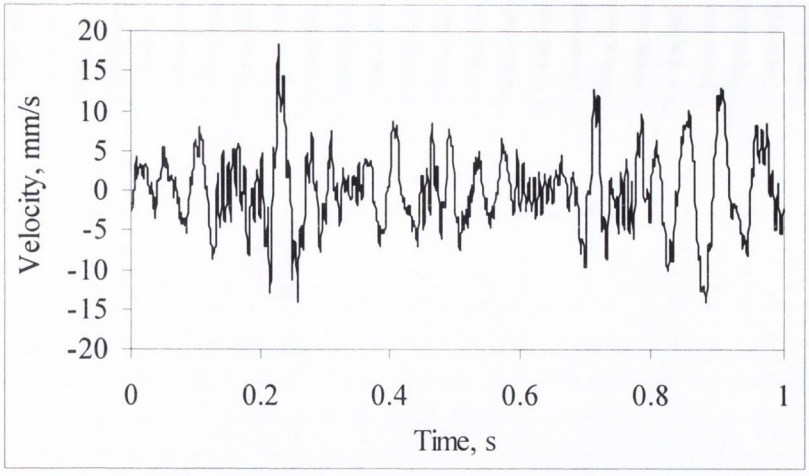

Fig.B.7–Measured TBM excitation at measuring Section 3; transverse direction

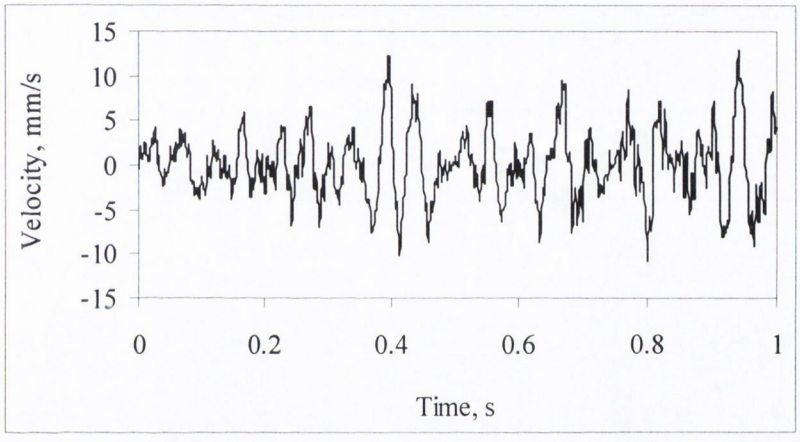

Fig.B.8–Measured TBM excitation at measuring Section 3; vertical direction

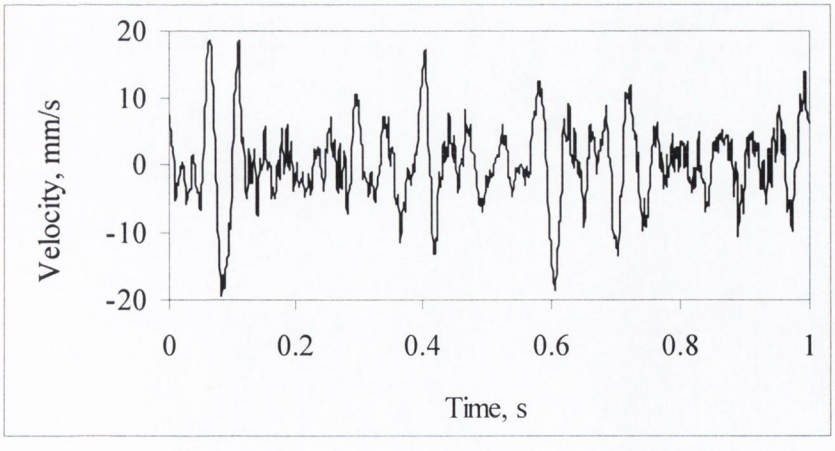

Fig.B.9–Measured TBM excitation at measuring Section 3; longitudinal direction

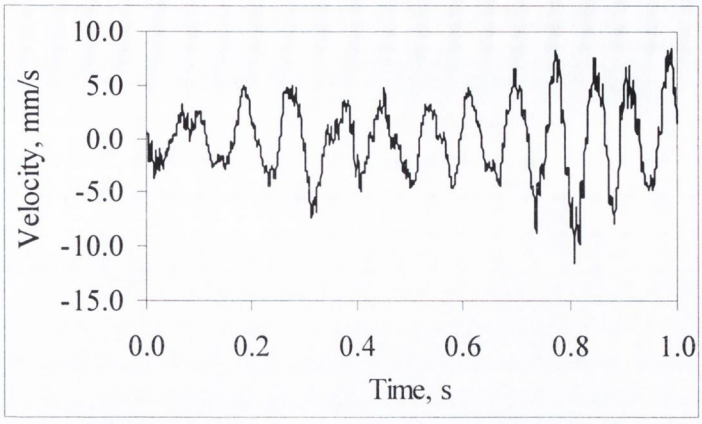

Fig.B.10–Measured TBM excitation at measuring Section 4; transverse direction

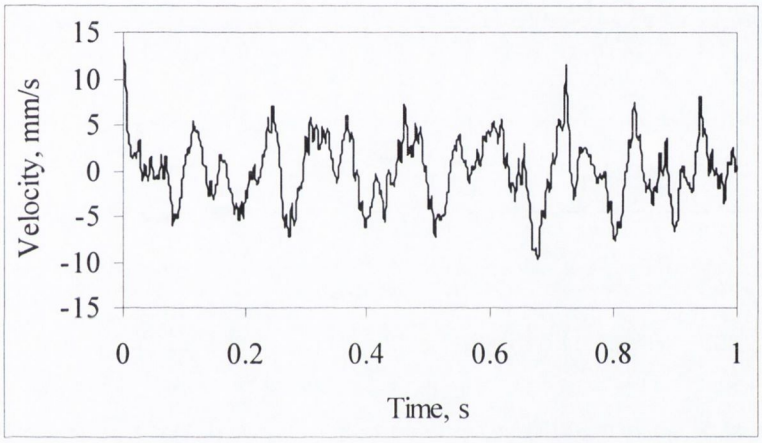

Fig.B.11–Measured TBM excitation at measuring Section 4; vertical direction

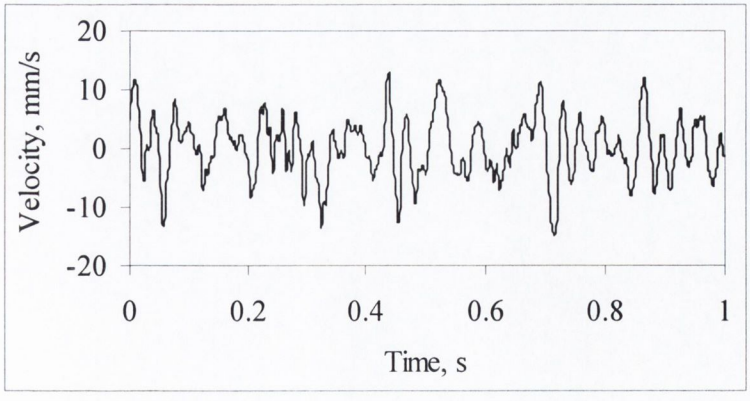

Fig.B.12–Measured TBM excitation at measuring Section 4; longitudinal direction.

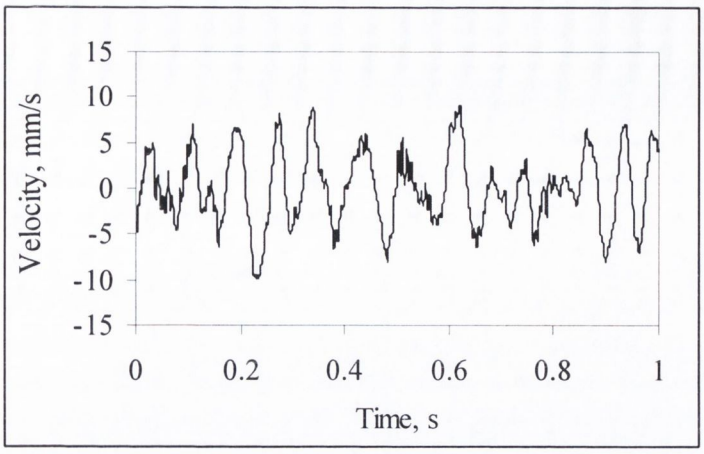

Fig.B.13–Measured TBM excitation at measuring Section 5; transverse direction

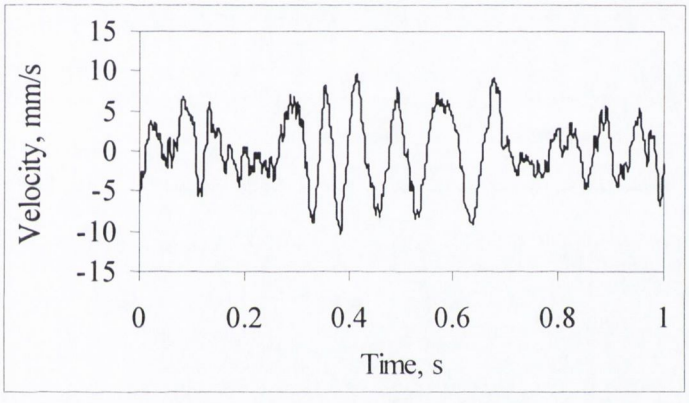

Fig.B.14–Measured TBM excitation at measuring Section 5; vertical direction

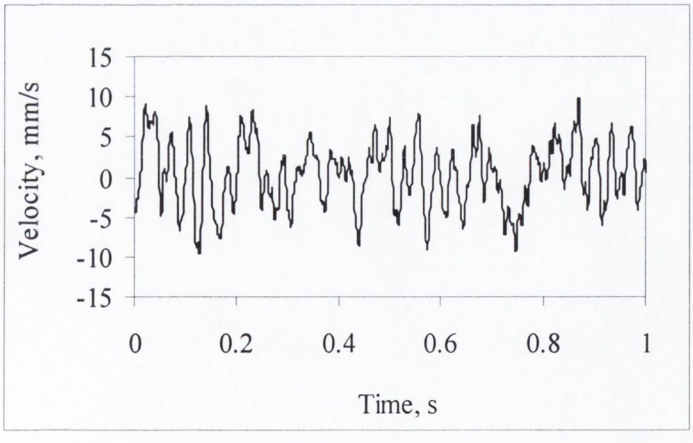

Fig.B.15–Measured TBM excitation at measuring Section 5; longitudinal direction.

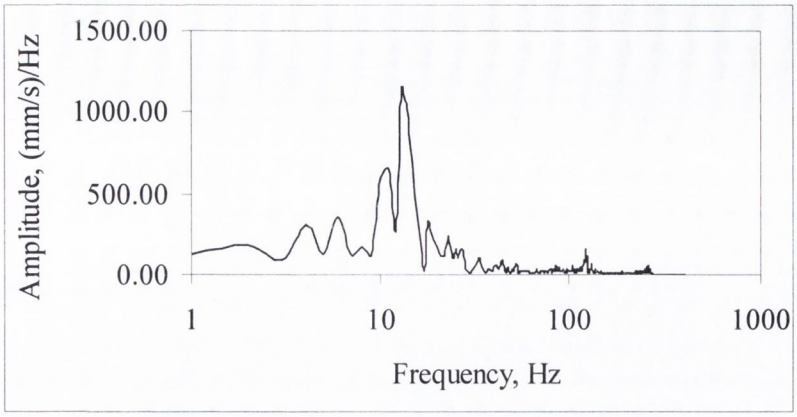

Fig.B.16–FFT of time history plot of transverse TBM vibrations at Section 2; peak frequency at 13Hz

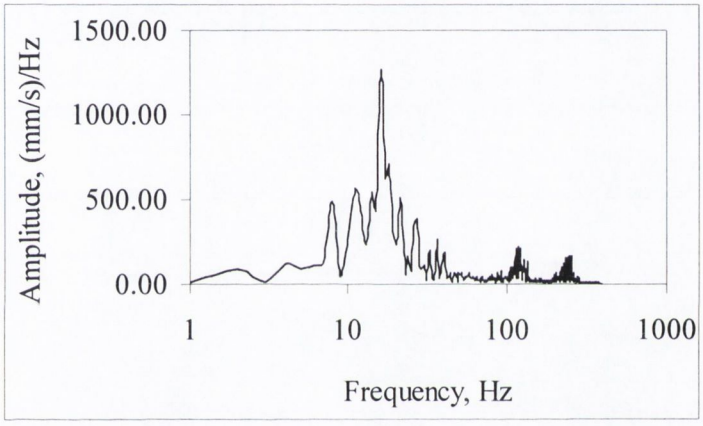

Fig.B.17– FFT of time history plot of vertical TBM vibrations at Section 2; peak frequency at 16Hz

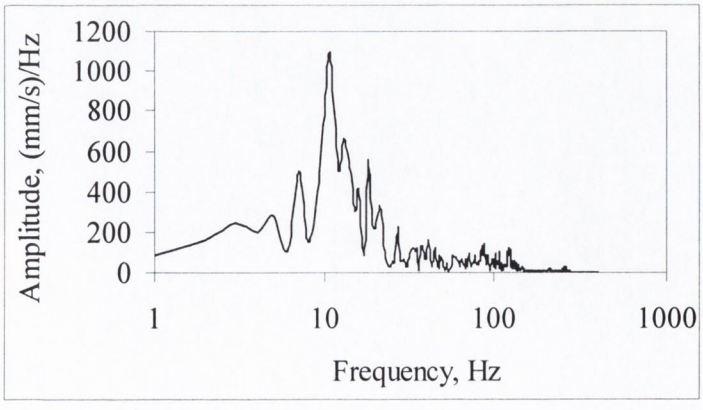

Fig.B.18– FFT of time history plot of longitudinal TBM vibrations at Section 2; peak frequency at 11Hz

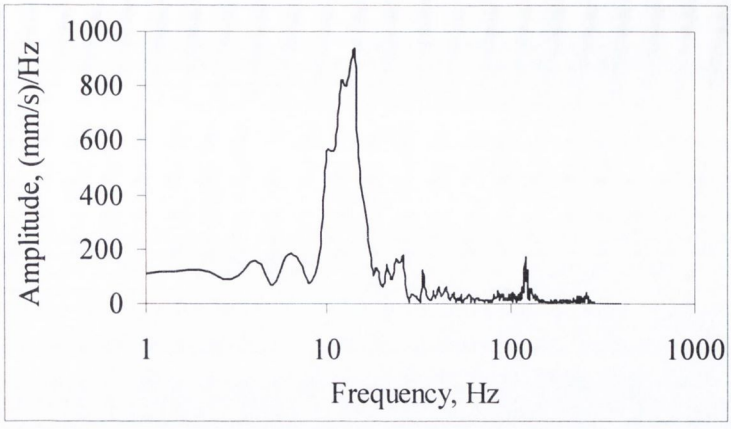

Fig.B.19–FFT of time history plot of transverse TBM vibrations at Section 3; peak frequency at 14Hz

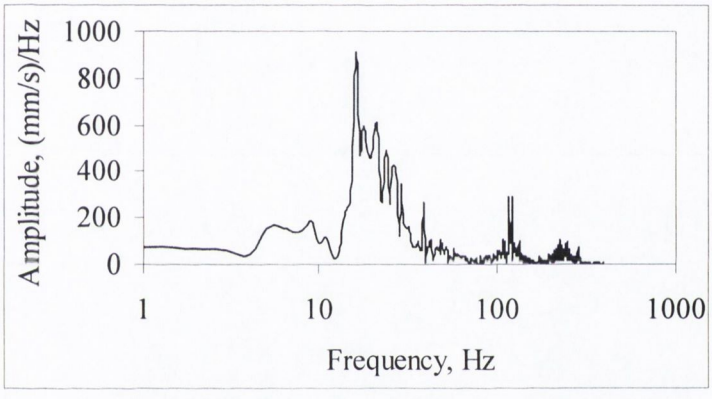

Fig.B.20– FFT of time history plot of vertical TBM vibrations at Section 3; peak frequency at 16Hz

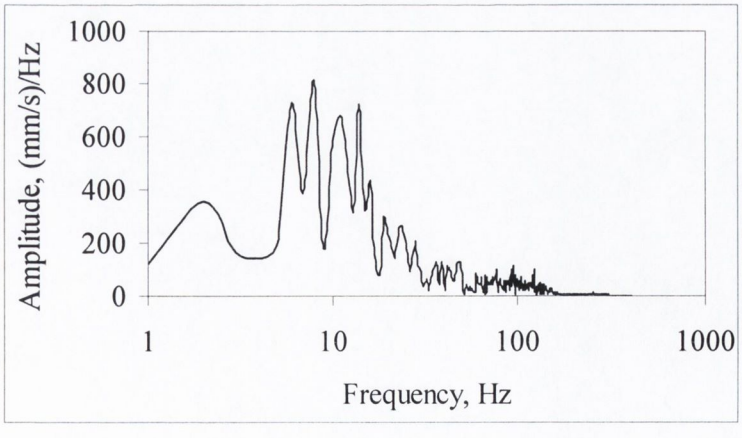

Fig.B.21– FFT of time history plot of longitudinal TBM vibrations at Section 3; peak frequency at 8Hz

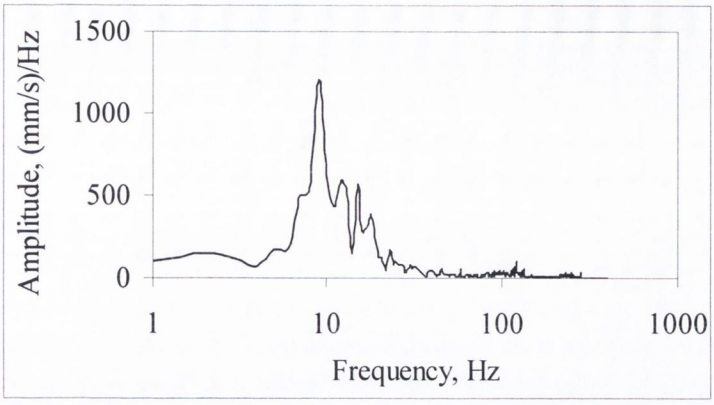

Fig.B.22–FFT of time history plot of transverse TBM vibrations at Section 4; peak frequency at 9Hz

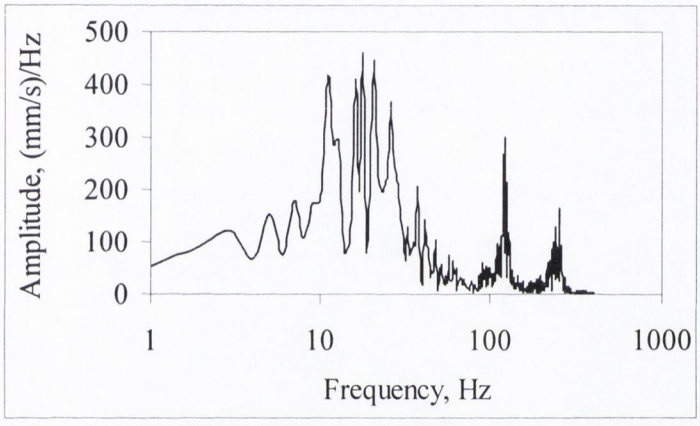

Fig.B.23– FFT of time history plot of vertical TBM vibrations at Section 4; peak frequency at 18Hz

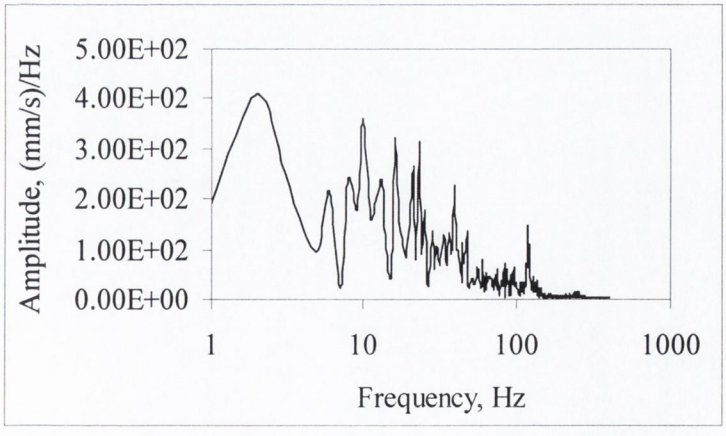

Fig.B.24– FFT of time history plot of longitudinal TBM vibrations at Section 4; peak frequency at 2 & 10Hz

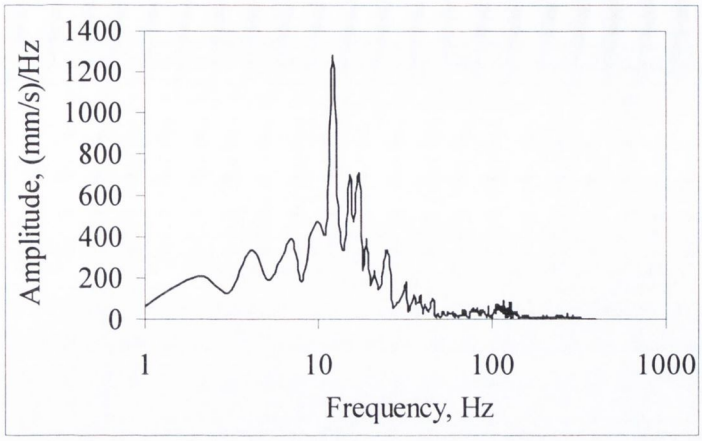

Fig.B.25–FFT of time history plot of transverse TBM vibrations at Section 5; peak frequency at 12Hz

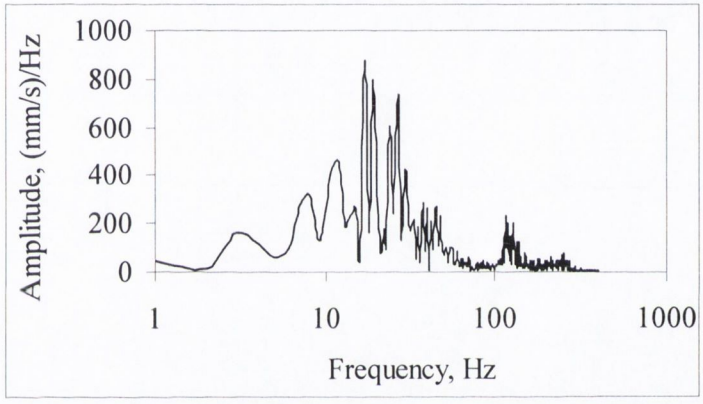

Fig.B.26– FFT of time history plot of vertical TBM vibrations at Section 5; peak frequency at 17Hz

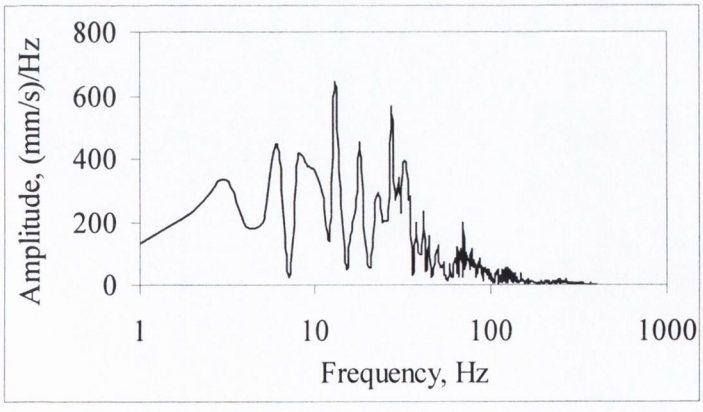

Fig.B.27– FFT of time history plot of longitudinal TBM vibrations at Section 5; peak frequency at 13Hz

City University

Geotechnical Engineering Research Centre

Results of Bender Element Tests

Client Exploration Associates Limited
Operator Laurentiu Jianu
Dates 22.03.96 - 11.04.96
Apparatus 2

Sample	Soil	boulder clay
	Type	core
	Size	Dia: 100mm, L: 400mm

Drains	all round

Stage	t1 (mins)
2	120

Test Specimen

Initial	Dia (mm)	105.93	Weight (g)	4225.8		Mass density (Mg/m^3)	2.318
	L (mm)	206.87	MC of trimmings (%)		10.65		
final	Dia (mm)	110.98	Weight (g)	4237.3		Mass density (Mg/m^3)	2.312
	L (mm)	189.45	MC of split sample (%)		11.55		

Test Results

Stage	Stresses (kPa)			p' (kPa)	q' (kPa)	ε_v (%)	v	G_0' (MPa)
	σ_a	σ_r	u					
1	236	236	184	52	0	0.00	1.314	153
1	235	235	132	103	0	0.00	1.314	267
2	235	235	95	140	0	0.00	1.314	267
2	237	237	95	142	0	0.18	1.290	292
3	237	237	95	142	0	0.18	1.290	292
3	265	265	95	170	0	0.24	1.283	323
3	294	294	96	198	0	0.34	1.270	405
4	294	294	96	198	0	0.34	1.270	405
4	266	266	95	171	0	0.33	1.272	332
4	237	237	95	142	0	0.30	1.275	302
4	211	211	95	116	0	0.25	1.282	291
4	183	183	95	88	0	0.21	1.287	263
4	144	144	95	49	0	0.02	1.312	215
5	145	145	96	49	0	undr	undr	202
5	155	145	99	49	10	undr	undr	196
5	427	145	88	151	282	undr	undr	313
5	505	145	68	198	360	undr	undr	314
5	534	145	54	220	389	undr	undr	329

City University

Geotechnical Engineering Research Centre

Results of Bender Element Tests

Client Exploration Associates Limited
Operator Laurentiu Jianu
Dates 12.04.96 - 22.04.96
Apparatus 2

Drains	all round

Stage	t1 (mins)
2	120

Sample

Soil	boulder clay
Type	core
Size	Dia: 100mm, L: 400mm

Test Specimen

Initial	Dia (mm)	100.97	Mass (g)	3787.25		Mass density (Mg/m^3)	2.324
	L (mm)	203.56	MC of trimmings (%)		11.66		
final	Dia (mm)	102.52	Mass (g)	3789.4		Mass density (Mg/m^3)	2.325
	L (mm)	197.47	MC of split sample (%)		11.33		

Test Results

Stage	Stresses (kPa)			p'	q'	ε_v	v	G_0'
	σ_a	σ_r	u	(kPa)	(kPa)	(%)		(MPa)
1	350	350	285	65	0	0.00	1.369	172
1	350	350	293	57	-1	0.00	1.369	164
2	350	350	150	200	-1	0.00	1.369	360
2	350	350	150	200	0	0.63	1.287	360
2	350	350	150	200	0	0.75	1.272	362
3	350	350	150	200	0	0.75	1.272	362
3	412	412	152	260	0	0.86	1.257	405
3	450	450	150	300	-1	0.98	1.242	434
4	450	450	150	300	-1	0.98	1.242	434
4	357	357	149	208	0	0.92	1.250	407
4	336	336	148	188	0	0.90	1.253	388
4	240	240	150	90	0	0.73	1.275	304
4	198	199	150	49	0	0.49	1.306	203

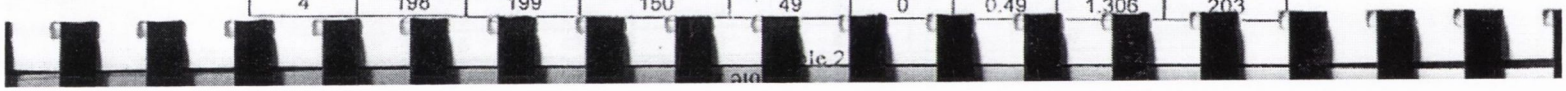

City University
Geotechnical Engineering Research Centre

Results of Bender Element Tests

Client Exploration Associates Limited
Operator Laurentiu Jianu
Dates 07.05.96 - 13.05.96
Apparatus 2

Drains	all round

Stage	t1 (mins)
2	60

Sample

Soil	boulder clay
Type	core
Size	Dia: 100mm, L: 400mm

Test Specimen

Initial	Dia (mm)	101.12
	L (mm)	188.55
final	Dia (mm)	102.53
	L (mm)	181.21

Mass (g)	3546.38	
MC of trimmings (%)		12.69
Mass (g)	3525.48	
MC of split sample (%)		9.71

Mass density (Mg/m^3)	2.342
Mass density (Mg/m^3)	2.356

Test Results

Stage	Stresses (kPa)			p' (kPa)	q' (kPa)	G_o' (MPa)
	σ_a	σ_r	u			
1	320	320	283	37	0	109
1	320	320	287	33	0	151
2	320	320	287	33	0	151
2	320	320	201	119	0	367
3	320	320	201	119	0	367
3	409	409	202	207	-1	422
3	420	420	200	220	0	462
4	420	420	200	220	0	462
4	405	405	200	205	0	448
4	335	335	204	131	0	402
4	317	317	202	115	0	384
4	302	302	203	99	0	352
4	250	250	202	48	0	308
5	250	250	202	48	0	308
5	336	250	217	62	86	328
5	436	250	217	95	186	386

City University

Geotechnical Engineering Research Centre

Results of Bender Element Tests

Client Exploration Associates Limited

Operator Laurentiu Jianu

Dates 03.06.96 - 20.06.96

Apparatus 2

Drains	all round

Stage	t1 (mins)
2	330

Sample

Soil	boulder clay
Type	core
Size	Dia: 100mm, L: 400mm

Test Specimen

Initial	Dia (mm)	101.55	Mass (g)	3658.58		Mass density (Mg/m^3)	2.342
	L (mm)	192.88	MC of trimmings (%)		11.16		
final	Dia (mm)	102.45	Mass (g)	3619.42		Mass density (Mg/m3)	2.344
	L (mm)	187.3	MC of split sample (%)		10.31		

Test Results

Stage	Stresses (kPa)			p' (kPa)	q' (kPa)	ε_v (%)	v	G_0' (MPa)
	σ_a	σ_r	u					
1	329	330	314	16	-1	0.00	1.518	47
2	330	330	201	129	0	1.69	1.301	281
3	417	365	202	181	52	1.84	1.282	358
3	457	380	202	204	77	1.94	1.270	389
3	496	396	203	227	100	2.03	1.258	441
4	496	396	200	229	100	2.07	1.252	443
4	425	368	202	185	57	2.06	1.254	416
4	330	330	202	128	0	1.99	1.262	378
5	330	330	202	128	0	1.98	1.264	381
5	377	377	202	175	0	2.01	1.260	411
5	399	399	201	198	0	2.05	1.255	424
5	430	430	202	228	0	2.10	1.248	449
6	430	430	200	230	0	2.13	1.245	450
6	412	412	200	212	0	2.1247	1.245	453
6	383	382	200	182	0	2.1103	1.247	448
6	363	363	200	164	0	2.0878	1.250	440
6	334	334	199	135	0	2.0609	1.253	413
6	314	314	199	114	0	2.0348	1.257	384
6	285	285	199	86	0	1.98	1.264	366
6	265	265	199	66	0	1.9216	1.271	328
6	250	250	199	51	0	1.8668	1.278	279
7	324	250	203	72	75	undr	undr	313
7	456	250	175	144	206	undr	undr	387
7	477	250	170	155	227	undr	undr	408
7	539	250	155	191	289	undr	undr	421

Summary Sheet of Geotechnical Laboratory Test Results - Soil

Borehole	Depth	Type	Lithology	Density			Water	Particle size distribution (mm)					Atterberg limits			Shear strength		CBR		Permea-	Cons	Sstr	Bend
or pit	of sample	of		γ_d	γ	γ_s	cont. w	75	20	2	0.063	0.002	LL	PL	IP	c '	ϕ '	top	base	bility			
no.	(m)	sample		(Mg/m³)			(%)	(% passed)					(%)			(kPa)	(°)			k (m/s)			
Feasibility Study (1991 - 1992)																							
TP-1	1.70	B	6b				12.80	100	65	50	33	18	28	17	11								
TP-2	4.60	B	6b				8.10	100	87	70	43	27	27	16	11								
TP-3	3.20	B	6b				8.80						25	14	11								
Initial Site Investigation (October to December 1995)																							
TP-7	4.80	B	1					100	87	48	12												
TP-8	4.70	B	1					100	88	50	12												
TP-9	3.80	B	1					100	87	48	12												
TP-10	2.80	B	1					100	81	45	15												
TP-11	2.30	B	1					100	78	50	14												
TP-12	2.30	B	1					100	83	42	14												
BH-101	2.00	B	6a					100	99	84	61	26											
	4.00	B	6b					100	96	85	70	31											
	9.50	B	6b				11.31	100	96	84	65	32	25	18	7								
BH-102	2.50	B	6a				17.55	100	80	61	38	12	29	19	10								
	9.00	B	6b					100	48	35	22	8											
	10.50	B	6b				9.22	100	84	64	40	14	26	19	7								
BH-103	5.60	B	6b					100	86	49	32	19											
	13.00	B	7				10.38	100	95	80	63	34	26	17	9								
	15.00	B	8				18.60	83	34	14	8		31	20	11								
	20.00	B	8				8.74	100	97	69	39	12	26	19	7								
BH-105	13.00	B	6b					100	64	49	30	9											
	16.50	B	6b					100	83	57	29												
	18.50	B	6b					100	46	35	22	7											
BH-107	18.50	B	7					100	97	91	63	15											
	18.50	B	7				16.75	100	100	89	41	14	27	19	8								
BH-108	17.50	B	7				18.40	100	100	92	75	8	39	22	17								
	18.50	B	8					85	28	6	3												
BH-109	10.00	B	8				14.28	100	77	47	31	11	30	17	13								
BH-110	10.00	B	8				11.07	100	54	27	17	4	17	9	8								
BH-111	5.80	B	8				12.94	100	99	77	59	26	18	10	8								
	9.60	B	8					100	90	56	34												
BH-114	4.50	B	2				38.37	100	100	77	40												

Borehole or pit no.	Depth of sample (m)	Type of sample	Lithology	Density γ_d (Mg/m³)	Density γ (Mg/m³)	Density γ_s	Water cont. w (%)	Particle size distribution (mm) (% passed) 75	20	2	0.063	0.002	Atterberg limits (%) LL	PL	IP	Shear strength c ' (kPa)	Shear strength φ ' (°)	CBR top	CBR base	Permeability k (m/s)	Cons	Satr	Bend
	5.70	B	3					83	22	8	5												
	8.00	B	8				13.31	100	51	26	13	3											
	12.80	B	8					100	77	50	25	5											
BH-115	12.30	B	4				36.20	100	100	89	49												
	16.00	B	4				9.26	100	100	100	92	23	27	20	7								
	17.50	B	4					100	83	66	57	21											
	18.00	B	3					87	30	2	1												
	21.00	B	8					100	60	41	23	7											
BH-117	12.00	B	4				12.88	100	100	99	71	14	30	19	11								
	18.70	B	8				9.35	100	97	68	39	15	28	21	7								
	21.00	B	5					100	43	14	2												
BH-118	10.00	B	3					100	43	4	1												
	14.50	B	4				22.15	100	80	78	62	10	25	18	7								
	23.00	B	8				8.86	100	94	76	57	31	28	20	8								
BH-120	13.00	B	4				22.14	100	100	97	92	24	28	17	11								
	16.00	B	8				10.70	100	54	41	24	7	24	14	10								
	19.50	B	8					100	92	80	50	10											
DPT Site Investigation (February to May 1996)																							
TP-202	0.70	B	6a		2.23		14.00											6.5	21.0				
	0.70	SB	6a		2.23		15.00											6.5	21.0				
TP-203	0.50	B	1		1.62		36.00											8.5	17.0				
	0.50	SB	1		1.62		35.00											9.4	17.0				
TP-208	0.60	B	1		2.09		13.00											23.0	39.0				
	0.60	SB	1		2.06		16.00											13.0	33.0				
TP-209	0.60	B	1		1.92		23.00											1.7	2.8				
	0.60	SB	1		1.93		23.00											2.1	2.6				
TP-210	0.50	B	1		1.76		27.00											8.3	14.0				
	0.50	SB	1		1.73		30.00											8.0	12.0				
TP-211	0.50	B	1		1.99		18.00											8.9	17.0				
	0.50	SB	1		1.98		20.00											12.0	14.0				
TP-212	0.80	B	1		1.70		28.00											4.9	14.0				
	0.80	SB	1		1.68		29.00											8.6	13.0				
TP-213	0.50	B	1		1.38		20.00											23.0	50.0				
	0.50	SB	1		1.39		33.00											18.0	39.0				
TP-214	0.70	B	1		1.40		22.00											24.0	49.0				
	0.70	SB	1		1.39		31.00											20.0	45.0				
TP-215	0.50	B	1		1.46		21.00											24.0	42.0				
	0.50	SB	1		1.43		33.00											22.0	44.0				
TP-216	0.50	B	1		1.71		20.00											34.0	44.0				
	0.50	SB	1		1.71		25.00							-				28.0	42.0				
TP-217	0.90	B	1		1.50		19.00											15.0	39.0				

Borehole or pit no.	Depth of sample (m)	Type of sample	Lithology	Density γd (Mg/m³)	Density γ (Mg/m³)	Density γs	Water cont. w (%)	Particle size distribution (mm) 75 (% passed)	20	2	0.063	0.002	Atterberg limits LL (%)	PL	IP	Shear strength c ' (kPa)	φ ' (°)	CBR top	CBR base	Permeability k (m/s)	Cons	Sstr	Bend
	0.90	SB	1		1.47		30.00											12.0	29.0				
TP-218	0.50	B	1		1.72		34.00											2.1	2.6				
	0.50	SB	1		1.73		35.00											0.7	1.4				
TT-204	1.00	B	1		2.46		25.00											1.4	1.5				
	1.00	SB	1		1.86		27.00											0.7	1.4				
BH-201	6.50-7.50	CS	6b	2.11	2.34	2.67	11.00	100	93	73	42	15	27	14	13								
	10.50-11.50	CS	6b	2.21	2.40	2.67	8.80	100	92	69	40	16	26	12	14								
	10.50-11.50**	CS	6b	2.20	2.40		9.30									7	36.0						
	**	CS	6b	2.10	2.28		8.60																
	**	CS	6b	2.15	2.33		8.40																
	16.50-17.00	CS	7	1.73	2.07	2.65	20.00	100	100	95	64	18	30	15	15								
	*	CS	7	1.83	2.15	2.65	17.26														✓		
	17.60-18.50	CS	7	1.98	2.22	2.69	12.00	100	99	89	58	26											
	17.60-17.90**	CS	7	2.00	2.22		11.00									39	26.0						
	**	CS	7	2.04	2.26		11.00																
	**	CS	7	1.99	2.25		13.00																
BH-202	5.00-6.00	CS	6b	1.95	2.30	2.66	18.00	100	79	59	33		28	15	13								
	9.50	CS	7	2.09	2.31		10.00													2.48E-11			
	9.50-11.50	CS	7	2.10	2.31	2.68	10.00	100	99	94	66	25										✓(2)	✓
	9.50-10.50**	CS	7	2.10	2.33		11.00									19	35.0						
	**	CS	7	2.15	2.38		11.00																
	**	CS	7	2.10	2.32		10.00																
	10.50-11.50	CS	7		2.36																		
	15.50-16.50	CS	6b	2.12	2.29	2.68	8.00	100	82	59	35	13	29	15	14								
	18.00-19.00	CS	6b	2.15	2.36	2.55	9.80	100	96	66	45	19	30	16	14							✓	✓
BH-203	0.50	B	1				36.00																
BH-204	5.40-6.40	CS	6b	2.10	2.33	(2.40)	11.00	100	82	60	34	14	28	15	13								
	9.00-10.00	CS	7		2.31																	✓	✓
	10.00-11.00	CS	7	2.15	2.36	2.67	10.00	100	100	86	47	15	25	12	13								
	10.00-10.30**	CS	7	2.02	2.26		12.00									5	31.5						
	**	CS	7	1.94	2.19		13.00																
	**	CS	7	2.05	2.25		10.00																
	11.00-12.00	CS	7			2.62	12.00	100	97	88	60	26	26	12	14								
	11.00-12.00**	CS	7	1.89	2.11		12.00									13	33.5						
	**	CS	7	1.96	2.21		13.00																
	**	CS	7	1.88	2.16		15.00																
	19.00-19.40	CS	7	1.97	2.26	2.64	15.00						27	14	13								
	*	CS	7	1.94	2.20	2.64	13.17														✓		
	21.00-22.00	CS	8			2.63	8.00	100	89	43	20	9	30	16	14								
	22.50-24.00	CS	8	2.04	2.19	2.69	7.40	100	98	72	54	22											✓
	23.00-23.50**	CS	8	1.96	2.19		12.00									0	33.0						
	23.00	CS	8		2.31																		
BH-205	6.10-7.00	CS	6b	2.19	2.36	2.69	8.00	100	86	68	38	14	27	15	12								
	9.05-10.05	CS	7	2.19	2.41	2.73	10.00	100	91	73	46	19	27	16	11								
	9.05-10.05**	CS	7	2.19	2.41		10.00									0	32.5						

Borehole or pit no.	Depth of sample (m)	Type of sample	Lithology	Density γ_d (Mg/m³)	Density γ (Mg/m³)	Density γ_s (Mg/m³)	Water cont. w (%)	Particle size distribution (mm) (% passed) 75	20	2	0.063	0.002	Atterberg limits (%) LL	PL	IP	Shear strength c' (kPa)	Shear strength φ' (°)	CBR top	CBR base	Permeability k (m/s)	Cons	Setr	Bend
	**	CS	7	2.23	2.41		8.20																
	**	CS	7	2.24	2.46		10.00																
	11.60-11.90	CS	7		2.31																		✓
	12.00-12.95	CS	7	2.05	2.32	2.69	13.00	100	99	90	62	23	31	14	17								
	12.00-12.75**	CS	7	2.05	2.32		13.00									0	31.5						
	**	CS	7	2.08	2.35		13.00																
	**	CS	7	2.13	2.38		12.00																
	16.00-16.60	CS	7	1.95	2.22	2.70	14.00	100	100	91	60	20	30	15	15								
BH-206	*5.00*	*B*	***	*1.78*	*2.10*		*18.00*	*100*	*100*	*48*	*12*	*3*	*31*	*14*	*17*	*0*	*33.5*						
	5.00	*B*	***	*1.79*	*2.11*		*18.00*	*100*	*100*	*48*	*11*	*3*	*31*	*14*	*17*	*0*	*32.5*						
	10.00-10.50	B	6b				16.00	100	80	62	38	13	29	15	14								
	14.00-14.50	U	7	1.92	2.19	2.74	14.00	100	100	94	65	15	28	14	14								
	21.00-21.50	U	7	1.90	2.19	2.68	15.00	100	99	91	69	20	28	15	13								
BH-207	4.50-5.50	CS	6b	2.15	2.31	2.70	7.60	100	100	66	40	16	29	15	14								
	4.50-4.80**	CS	6b	2.13	2.31		8.30									62.5	26.0						
	**	CS	6b	2.18	2.32		6.50																
	**	CS	6b	2.09	2.26		8.10																
	5.50-6.50	CS	6b	2.10	2.31	2.67	10.00	100	88	66	40	15	28	15	13								
	11.50-12.50	CS	6b	2.05	2.26	2.68	10.00	100	81	64	41	16	27	14	13								
	13.50-14.50	CS	7	2.05	2.28	2.68	11.00	100	100	93	63	18	27	13	14								
	13.50-14.50**	CS	7	2.04	2.28		12.00									0	31.0						
	**	CS	7	2.04	2.31		13.00																
	**	CS	7	2.04	2.26		11.00																
	14.60-15.50	CS	7	2.04	2.29	2.69	12.00	100	100	94	59	17	26	13	13							✓	✓(2)
	16.90-17.50	CS	7	1.52	1.98	2.69	30.00	100	99	95	70	30	57	25	32								
	*	CS	7	1.53	1.97	2.69	28.64														✓		
	17.50-18.50	CS	7	1.96	2.23	2.70	14.00	100	100	90	52	21	28	14	14								
	20.50-21.50	CS	7	1.96	2.22	2.69	13.00	100	95	88	59	16	28	13	15								
	20.50-21.50**	CS	7	1.96	2.22		13.00									0	30.5						
	**	CS	7	2.01	2.25		12.00																
	**	CS	7	2.00	2.26		13.00																
	23.00-23.50	CS	7	2.04	2.28	2.70	12.00	100	99	93	70	19	27	15	12								
	*	*CS*	*7*	*1.86*	*2.16*	*2.70*	*15.89*														✓		
	23.50-24.50	CS	7	1.78	2.06	2.67	16.00	100	100	92	68	15	30	14	16								
	23.50-23.80**	CS	7	1.76	2.06		17.00									0	30.5						
	**	CS	7	1.88	2.16		15.00																
	**	CS	7	1.90	2.20		16.00																
	26.20-26.80	CS	8	2.13	2.32	2.68	9.00	100	62	44	30	12	31	16	15								
BH-208	11.50-12.50	CS	6b	2.06	2.27	2.63	10.00	100	80	59	35	11	28	15	13								
	14.00-15.00	CS	6b	2.11	2.32	2.67	9.80	100	93	71	44	19	27	14	13								
	14.00-14.35**	CS	6b	2.11	2.32		9.80									0	33.5						
	16.85-17.85	CS	7	2.09	2.32	2.70	11.00	100	96	89	59	21	26	13	13							✓	✓(2)
	18.00-18.85	CS	7	2.09	2.32	2.67	11.00	100	99	93	63	17	28	13	15								
	18.00-18.35**	CS	7	2.09	2.32		11.00									0	34.0						
	**	CS	7	2.13	2.36		11.00																

Borehole or pit no.	Depth of sample (m)	Type of sample	Lithology	Density γd (Mg/m³)	Density γ (Mg/m³)	Density γs (Mg/m³)	Water cont. w (%)	Particle size distribution (% passed) 75	20	2	0.063	0.002	Atterberg limits LL (%)	PL (%)	IP (%)	Shear strength c' (kPa)	Shear strength φ' (°)	CBR top	CBR base	Permeability k (m/s)	Cons	Sstr	Bend
	**	CS	7	2.05	2.28		11.00																
	*	*CS*	*7*	*1.96*	*2.20*	*2.67*	*12.70*														✓		
	19.90-20.50	CS	7	2.03	2.27	2.69	12.00	100	100	93	61	19	26	14	12								
	*	CS	7	1.94	2.18	2.69	12.50														✓		
	21.50-22.50	CS	7	1.99	2.27	2.66	14.00	100	100	93	66	23	25	14	11								
	21.50-22.20**	CS	7	2.01	2.27		13.00									0	33.5						
	**	CS	7	1.99	2.25		13.00																
	**	CS	7	1.91	2.22		16.00																
	24.00-24.90	CS	8	2.10	2.29	2.69	9.00	100	74	55	38	15	32	17	15								
	25.40-26.40	CS	8	2.03	2.25	2.69	11.00						33	17	16								
BH-209	6.80-7.50	CS	6b	2.19	2.37	2.65	8.00	100	83	59	33	11	27	14	13								
	12.80-13.60	CS	7	2.02	2.30	2.69	14.00	100	99	88	55	19	26	15	11								
BH-210	0.50	B	1				27.00																
BH-211	9.10-10.00	CS	6b		2.34																		
	10.00-10.50	CS	6b																				✓
	12.50-13.50	CS	7	2.16	2.36	2.67	9.10	100	78	63	30	12	29	13	16								
	12.50-13.50**	CS	7	2.17	2.36		8.80									12.5	31.0						
	**	CS	7	2.17	2.35		8.50																
	**	CS	7	2.01	2.21		10.00																
	13.50-14.50	CS	7	2.05	2.30	2.63	12.00	100	100	93	64	24	30	15	15							✓	✓
	14.50-15.50	CS	7	2.15	2.37	2.64	10.00	100	90	70	44	17	19	12	7								
	14.50-14.95*2	CS	7	2.15	2.37		10.00									0	30.5						
	**	CS	7	2.08	2.29		10.00																
	**	CS	7	2.03	2.25		11.00																
BH-212	*4.00*	*B*	***	*2.21*	*2.10*		*17.00*	*100*	*100*	*93*	*53*	*9*	*27*	*14*	*13*	*0*	*34.0*						
	9.00-9.50	BD	6b				15.00	100	88	68	40	14	29	15	14								
	12.00-12.45	U	7				14.00	100	98	89	60	20	28	14	14								
	15.00-15.50	BD	8				11.00	100	78	57	33	12	29	15	14								
	17.00-17.50	BD	8				16.00						38	21	17								
BH-213	17.80-18.20	CS	8			2.70	10.00						32	18	14								
BH-213/2	10.50-10.80	CS	7				8.00	100	95	77	47	18	27	15	12								
	11.00	CS	7		2.34																		
	11.30-12.30	CS	7																				✓
	*17.80-18.20**	*CS*	*8*	*1.94*	*2.19*	*2.70*	*12.57*														✓		
BH-214	6.00-6.50	U	6b				9.00																
	9.00-9.50	B	6b				10.00	100	66	46	21	7	33	16	17								
	12.00-12.50	B	7				19.00	100	92	78	52	18	26	14	12								
	13.00-13.30	B	8				8.00	100	79	30	7		non plastic										
BH-215	5.82	B	8				9.00	100	73	48	29	10	26	15	11								
	6.90	B	8				7.00	100	68	52	30	10	26	15	11								
	7.70	B	8				12.00	100	85	62	33	12	29	16	13								
BH-218	*3.00*	*B*	***	*1.74*	*2.09*		*20.00*	*100*	*100*	*94*	*50*	*9*	*27*	*13*	*14*	*0*	*31.5*						
	8.00-9.50	B	5					100	49	16	2		non plastic										
	10.00-10.90	BD	5				5.00	100	67	35	7		non plastic										
BH-220	4.00-4.50	B	5					100	82	50	5		non plastic										

Appendix C3-Geotechnical test results for rock

Borehole or pit no.	Depth of sample (m)	Type of sample	Lithology	Density γd (Mg/m³)	Density γ (Mg/m³)	Density γs	Water cont. w (%)	Particle size distribution (mm) 75 (% passed)	20	2	0.063	0.002	Atterberg limits LL (%)	PL	IP	Shear strength c ' (kPa)	Shear strength φ ' (°)	CBR top	CBR base	Permeability k (m/s)	Cons	Sstr	Bend
	6.00-6.50	B	8				14.00	100	79	58	28	11	28	15	13								
	7.00	B	5				8.00	100	74	50	17		25	15	10								
BH-222	6.00-6.50	BD	6b				12.00	100	86	60	32	11	28	16	12								
	7.00-7.50	BD	5				4.00	100	63	33	9		non plastic										
BH-223	3.50-4.50	BD	6b				14.00	100	79	48	25	8	25	14	11								
	5.50-6.00	BD	7				14.00	100	98	82	50	20	31	15	16								
	7.50-8.00	BD	8				13.00	100	75	48	21	9	27	15	12								
BH-224	8.80-9.50	CS	8	2.14	2.33	2.67	9.00	100	84	58	21	5											
	9.50-10.00	CS	8			2.64	9.50	100	68	45	36	8	27	16	11								
	*	*CS*	*8*	*1.86*	*2.12*	*2.64*	*13.74*														✓		
BH-225	2.00-2.50	B	3				6.00	100	77	30	3												
	4.00-4.50	B	3					100	81	41	8												
	5.00-5.50	B	3				6.00	100	78	40	11												
	6.00	B	8					100	78	47	18	7											
	8.00	BD	8				8.50	100	85	67	39	8	25	14	11								
	9.00	B	8					100	85	66	37	9											
	9.50	*B*	***	*1.85*	*2.17*		*17.00*						*25*	*13*	*12*	*0*	*34.0*						
	13.50-14.00	B	8				10.00	100	88	68	39	12	26	15	11								
BH-226	5.00-5.50	B	3					100	51	12	2												
	6.00-6.45	U	2	1.94	2.23	2.68	15.00	100	100	100	82	30	26	14	12								
	6.00-6.45**	U	2	1.94	2.23		15.00									0	33.0						
	**	U	2	1.93	2.22		15.00																
	**	U	2	1.97	2.25		14.00																
	7.00-7.50	B	3					100	71	23	6		non plastic										
	9.00-9.50	B	3					100	82	45	2		non plastic										
	13.00-13.50	B	3					100	68	35	3		non plastic										
BH-227	8.00-8.50	B	3				4.00	100	63	15	1		non plastic										
	9.00-9.50	B	4				22.00	100	99	94	88	22	29	18	11								
	10.00-10.50	B	3					100	57	13	1		non plastic										
	14.00-14.50	B	3					100	79	55	25		non plastic										
BH-229	9.00-9.50	B	3					100	74	25	1		non plastic										
BH-230	*18.00-20.00*	*B*	***	*1.83*	*2.12*		*16.00*	*100*	*100*	*88*	*47*	*8*	*26*	*15*	*11*	*0*	*34.0*						
	19.00-19.50	B	3				9.00	100	69	27	4		non plastic										
	21.00-21.50	B	3				8.00	100	61	29	4		non plastic										
BH-232	9.00-9.50	B	3					100	79	28	2		non plastic										
	10.00-10.50	B	3					100	75	20	1		non plastic										
	12.00-12.50	B	4				21.00						23	16	7								
BH-235	8.00-9.50	B	3					100	88	46	15		non plastic										
	11.00-11.50	B	3					100	86	30	2		non plastic										
BH-236	12.00-12.50	B	3					100	58	28	5		non plastic										
	15.00-15.45	U	4	1.66	2.02	2.66	22.00	100	100	100	17	4	23	non plast.									
	15.00-15.45**	U	4	1.58	2.02		28.00									81.5	33.0						
	**	U	4	1.39	1.84		32.00																
	**	U	4	1.48	1.86		26.00																
BH-238	12.00-12.50	BD	3					100	34	8	1		non plastic										

Borehole or pit no.	Depth of sample (m)	Type of sample	Lithology	Density			Water	Particle size distribution (mm)					Atterberg limits			Shear strength		CBR		Permea-bility	Cons	Sstr	Bend
				γd	γ	γs	cont. w	75	20	2	0.063	0.002	LL	PL	IP	c '	φ '	top	base	k (m/s)			
				(Mg/m³)			(%)	(% passed)					(%)			(kPa)	(°)						
	14.00-14.45	U	4	1.89	2.19	2.66	16.00	100	100	100	40	11	26	non plast.									
	14.00-14.45**	U	4	1.86	2.18		17.00									75	35.5						
	**	U	4	1.81	2.14		18.00																
	**	U	4	1.84	2.15		17.00																
	16.00-16.45	U	4	1.61	1.97	2.68	22.00	100	100	100	8		26	non plast.									
	16.00-16.45**	U	4	1.43	1.87		31.00									0	41.0						
	**	U	4	1.56	2.00		28.00																
	**	U	4	1.52	2.02		33.00																
	18.00-18.45	U	4	1.60	1.95	2.69	22.00	100	100	100	99	30	34	17	17								
	*	*U*	*4*	*1.73*	*2.12*	*2.69*	*22.79*														✓		
	20.00-20.50	BD	5					100	58	16	7		non plastic										
BH-239	*8.00-8.20*	*B*	*3*					*100*	*46*	*16*	*1*												
	11.00-11.30	*B*	*4*				*18.00*						*24*	*17*	*7*								
	13.10-13.40	*B*	*4*					*100*	*100*	*95*	*67*												
BH-240	*3.20-3.40*	*B*	*3*					*100*	*83*	*41*	*1*												
	7.00-7.20	*B*	*4*				*25.00*	*100*	*100*	*100*	*86*		*29*	*17*	*12*								
	9.30-9.50	*B*	*5*					*100*	*70*	*31*	*2*												
	12.80	*B*	*5*					*100*	*82*	*39*	*2*												
BH-241	*0.90-1.10*	*B*	*3*					*100*	*76*	*39*	*4*												
	4.70-4.90	*B*	*3*					*100*	*74*	*36*	*1*												
	6.80-7.10	*B*	*4*				*20.00*						*22*	*14*	*8*								
BH-244	*2.00-2.45*	*B*	*2*				*26.00*	*100*	*83*	*56*	*23*		*58*	*34*	*24*								
	6.00-6.45	*B*	*3*					*100*	*48*	*17*	*4*												
	12.00-12.45	U	4	1.86	2.19	2.65	18.00	100	100	100	69	17	25	non plast.									
	*	U	4	1.89	2.22	2.65	17.72														✓		
	13.00	U	4	1.82	2.11		16.00													6.70E-10			
	14.00-14.45	U	4	1.71	2.07		21.00													4.07E-10			
	14.00-14.45	U	4	1.66	2.07	2.67	25.00	100	100	100	64	17	22	non plast.									
	15.00-15.45	*U*	*4*				*22.00*																
	17.00	U	4					100	100	100	99	34	34	17	17								
	17.50-17.85	U	4	1.68	2.07	2.67	23.00																
	*	U	4	1.88	2.20	2.67	16.83														✓		
	18.50-18.85	U	4	1.75	2.15	2.68	23.00	100	100	100	97	38	37	17	20								
	18.50-18.95**	U	4	1.72	2.15		25.00									26.5	27.0						
	**	U	4	1.60	2.00		25.00																
	**	U	4	1.58	1.97		25.00																
	19.50-19.95**	U	4	1.58	1.98		25.00									1	31.0						
	**	U	4	1.57	1.96		24.00																
	**	U	4	1.58	1.96		24.00																
BH-245/B	10.00-10.45	U	4	1.90	2.18	2.66	15.00	*100*	*98*	*95*	40	11	24	non plast.									
	10.00-10.45	U	4	1.89	2.18		16.00													5.68E-09			
	12.00-12.45	U	4	1.72	2.06	2.68	20.00	100	100	100	65	23	26	non plast.									
	12.00-12.45**	U	4	1.69	2.06		22.00									0	36.5						
	**	U	4	1.69	2.06		22.00																
	**	U	4	1.71	2.05		20.00																

Borehole or pit no.	Depth of sample (m)	Type of sample	Lithology	Density γd (Mg/m³)	Density γ (Mg/m³)	Density γs	Water cont. w (%)	Particle size distribution (mm) 75 (% passed)	20 (% passed)	2 (% passed)	0.063 (% passed)	0.002 (% passed)	Atterberg limits LL (%)	Atterberg limits PL (%)	Atterberg limits IP (%)	Shear strength c ' (kPa)	Shear strength φ ' (°)	CBR top	CBR base	Permeability k (m/s)	Cons	Sstr	Bend
	15.00-15.45	U	4	1.62	2.01	2.66	24.00	100	100	100	19	6	non plastic										
	15.00-15.50	U	4	1.59	2.01		26.00													1.84E-10			
	17.00-17.45	*B*	*4*					*100*	*100*	*100*	*31*												
	18.00-18.45	U	4			2.69	20.00	100	100	100	97	33	31	16	15								
	18.00-18.50**	U	4	1.76	2.13		21.00									31	25.0						
	**	U	4	1.73	2.11		22.00																
	**	U	4	1.79	2.16		21.00																
	19.50-19.95	U	4			2.66	20.00	100	100	100	94	31	30	16	14								
	19.50-19.95	U	4	1.64	2.03		24.00													3.96E-10			
BH-246	*1.00*	*D*	*1*				*9.00*																
	2.00	*D*	*1*				*18.00*																
	2.00-2.45	*B*	*1*					*100*	*92*	*74*	*3*												
	3.00	*D*	*1*				*18.00*																
BH-247/A	*1.00*	*D*	*1*				*50.00*																
	3.00	*D*	*1*				*47.00*																
	4.50-4.95	*U*	*2*				*41.00*						*53*	*27*	*26*								
BH-248	*1.00-1.45*	*B*	*1*				*23.00*																
	2.00-2.50	*B*	*1*					*100*	*52*	*13*	*1*		*non plastic*										
	3.00-3.45	*B*	*1*				*35.00*																
	4.00-4.45 #	*B*	*2*				*49.00*																
	5.00-5.45	*U*	*2*				*19.00*						*33*	*non plastic*									
	8.00-8.45	*B*	*3*					*100*	*34*	*10*	*0*												
	10.00-10.50	B	3					100	64	19	1		non plastic										
BH-249	*1.00-1.45*	*B*	*1*				*42.00*																
	3.00-3.45 #	*B*	*1*				*68.00*																
	4.00-4.45	*B*	*1*				*38.00*																
	8.00-8.50	B	3					100	43	14	0		non plastic										
BH-250	*1.50-1.80*	*B*	*1*				*24.00*																
	2.35-2.65	*B*	*1*					*100*	*81*	*54*	*15*												
	4.40-4.65	*B*	*1*				*57.00*																
	7.70-8.00	*B*	*3*					*100*	*78*	*44*	*2*												
BH-251	*1.10-1.30 #*	*B*	*1*				*25.00*																
	1.70-2.00	*B*	*1*				*37.00*																
	4.40-4.60	*B*	*2*				*33.00*	*100*	*92*	*61*	*12*												
	7.60-7.90	*B*	*3*					*100*	*81*	*45*	*2*												
BH-252	*1.10-1.40*	*B*	*1*				*26.00*																
	2.30-2.50 #	*B*	*1*					*100*	*78*	*54*	*16*												
	7.80-8.00	*B*	*3*					*100*	*99*	*66*	*5*												
	7.82-8.88	B	3					100	90	39	3		non plastic										
	11.58-12.85	B	3					100	75	37	2		non plastic										
	14.68-14.80	B	4				10.00	100	99	97	61	19	23	15	8								
BH-253	*1.15-1.30 #*	*B*	*1*					*100*	*94*	*63*	*18*												
	2.05-2.30	*B*	*1*				*44.00*																
	8.30-8.50	*B*	*3*					*100*	*99*	*81*	*7*												
	8.80-9.20	B	3					100	63	33	1		non plastic										

Borehole or pit no.	Depth of sample (m)	Type of sample	Lithology	Density γd (Mg/m³)	Density γ (Mg/m³)	Density γs (Mg/m³)	Water cont. w (%)	Particle size distribution (mm) 75 (% passed)	20 (% passed)	2 (% passed)	0.063 (% passed)	0.002 (% passed)	Atterberg limits LL (%)	Atterberg limits PL (%)	Atterberg limits IP (%)	Shear strength c ' (kPa)	Shear strength φ ' (°)	CBR top	CBR base	Permeability k (m/s)	Cons	Sstr	Bend
	11.70-12.93	B	3					100	90	39	1		non plastic										
BH-254	*1.20-1.40*	*B*	*1*					*100*	*89*	*61*	*21*												
	2.15-2.35 #	*B*	*1*				*43.00*																
	7.50-7.80	*B*	*3*					*100*	*98*	*79*	*16*												
	9.60-10.78	B	3					100	69	30	1		non plastic										
	13.55-15.00	B	3					100	60	18	1		non plastic										
BH-256	6.00-6.50	BD	6b				10.00	100	90	72	44	18	29	15	14								
	13.00-13.50	BD	6b				13.00	100	94	76	46	16	28	14	14								
BH-257	4.50-5.50	CS	6b	2.02	2.20	2.65	9.00	100	96	71	44	18	34	16	18								
	4.50-5.50**	CS	6b	2.01	2.20		9.30									4.5	31.5						
	**	CS	6b	1.95	2.13		9.10																
	**	CS	6b	2.07	2.25		8.70																
	6.50	CS	6b	2.03	2.24		9.90													1.07E-10			
	6.50-7.50	CS	6b	2.00	2.15	2.68	7.70	100	89	65	41	17	31	14	17								
	13.00-13.30	CS	7	1.80	2.00	2.63	11.00	100	98	84	61	12	24	non plast.									
	*		7	1.75	2.11	2.62	20.57														✓		
	14.50-15.30	CS	7	2.05	2.28	2.61	11.00	100	99	91	55	20	26	non plast.									
	*	*CS*	*7*	*1.96*	*2.20*	*2.61*	*12.06*														✓		
BH-258	2.00-2.50	BD	6a				12.00	100	98	55	20	7	26	14	12								
	6.00-6.50	BD	6b				9.0	100	92	69	40	15	29	15	14								
BH-259	3.00-3.15	U	6a	1.91	2.18	2.69	14.0	100	93	70	41	14	35	19	16								
	5.00-5.45	U	6a	1.94	2.11	2.69	9.0																
	13.00-13.50	BD	7				18.0	100	100	97	65	20	36	18	18								
BH-260	7.00-7.50	BD	6b				18.0	100	95	82	44	17	27	13	14								
	11.50-12.00	BD	6b				17.0	100	98	74	44	17	28	15	13								
BH-261	6.00-6.50	BD	6b				9.0	100	90	70	41	16	28	16	12								
	10.00-10.50	BD	6b				9.0	100	97	72	42	17	29	16	13								
	19.00-19.50	BD	7				15.0	100	99	93	56	19	29	14	15								
BH-262	5.20-6.50	CS	6b	2.06	2.23	2.72	8.0	100	86	64	39		32	15	17								
	5.20-5.60**	CS	6b	2.06	2.23		8.0									10	32.5						
	**	CS	6b	2.04	2.21		8.3																
	**	CS	6b	2.16	2.32		7.4																
	15.50	CS	7		2.24																		
	19.20-20.20	CS	8	2.13	2.32	2.59	9.0	100	84	54	38	15	33	15	18								
	19.20-20.20**	CS	8	2.16	2.32		7.7									100	28.0						
	**	CS	8	2.07	2.24		8.2																
	**	CS	8	2.06	2.24		8.4																
	22.20-23.65	CS	8	2.13	2.34	2.70	10.0	83	69	49	34	15	33	14	19								
	22.20-23.25**	CS	8	2.20	2.34		6.3									76	26.0						
	**	CS	8	2.08	2.27		9.1																
	**	CS	8	1.95	2.13		9.2																
BH-263	15.00-15.45	U	4																				
	18.00-18.50	BD	8				10.0	100	94	77	49	9	21	13	8								
	20.50-21.00	BD	8				13.0						22	14	8								
	21.40-22.50	BD	5				5.0	100	60	29	5		non plastic										

Borehole or pit no.	Depth of sample (m)	Type of sample	Lithology	Density γ_d (Mg/m³)	Density γ (Mg/m³)	Density γ_s (Mg/m³)	Water cont. w (%)	Particle size distribution (mm) 75 (% passed)	20 (% passed)	2 (% passed)	0.063 (% passed)	0.002 (% passed)	Atterberg limits LL (%)	PL (%)	IP (%)	Shear strength c ' (kPa)	Shear strength φ ' (°)	CBR top	CBR base	Permeability k (m/s)	Cons	Sstr	Bend
BH-265	6.00-6.50	BD	8				11.0	100	89	68	32	9	21	13	8								
	8.00-8.50	BD	8				12.0	100	83	58	28	9	22	13	9								
	11.00-11.50	B	5				16.0	100	80	47	12		non plastic										

Key:

Type of sample	CS...core sample, U...undisturbed sample, D...disturbed jar sample, B...disturbed bulk sample, SB...soaked bulk sample, BD...B and D
Density	γ_d...dry density, γ...bulk density, γ_s...particle density
Atterberg limits	LL...liquid limit, PL...plastic limit, IP...plasticity index
Cons	consolidation test, for results refer to relevant report sheets
Sstr	small strain triaxial test, for results refer to relevant report sheets
Bend	bender element test, for results refer to relevant report sheets
✓	performed; for results refer to relevant report sheets
(...)	values excluded from statistical evaluation
*	from consolidation test
**	from CU test
***	reconstituted sample
#	organic content and/or loss on ignition tested (ref. Contractor's summary sheets)

Lithology	
1	made ground
2	estuarine/alluvial silts & sands
3	estuarine/alluvial gravels
4	glaciomarine clays & silts & sands
5	glacial gravels & sands
6a	weathered brown boulder clay
6b	upper black boulder clay
7	sandy brown boulder clay
8	lower black boulder clay

Notes:

1. samples and values in *italic* not included in overall statistical analysis (report no. 4-09-R-002) because of late submission by Contractor

Summary Sheet on Geotechnical Laboratory Test Results for Rock

Borehole No.	Depth of sample (m)	Lithology	Bulk density γ (Mg/m³)	Dry density γd (Mg/m³)	Porosity n (%)	Void index Iv (%)	Water content w (%)	UCS (MPa)	Tensile strength (Brazilian) (MPa)	Young's modulus E (GPa)	Poisson ratio ν	Slake durability index (%)	Abrasivity (0.1mm)	Fracture energy Wf (Nm)	Fracture energy specific wf (Nm/MPa)	Petro-graphic analysis	Clay mineral analysis	Vitrinite reflect. analysis
1	not known	A							9.0				1.36			✓		
2	14.30	A						200.3	8.3				1.67			✓		
2	18.80	A						195.1	10.4				1.03			✓		
2	20.30	A						127.0	8.7				1.87			✓		
4	10.20	A							11.1				1.57			✓		
6	not known	A						161.1	6.6				1.01			✓		
BH-207	22.70	A														✓		
BH-207	28.00-28.30	B	2.67	2.67	0.31	0.30	0.1	*1)										
BH-207	32.50-33.20	B	2.70	2.69	0.04	0.04	0.1	182	22.9	42.4	0.232							
BH-207	34.70	A														✓		
BH-207	35.00	A														✓		
BH-209	19.10	A														✓		
BH-209	24.10	A/B														✓		
BH-209	24.70-25.00	B	**2.67**	**2.69**	0.11	0.02	0.2	181		31.4	0.235							
BH-209	27.70-28.05	B	**2.66**	**2.67**	0.19	0.34	0.2	121		28.6	0.189							
BH-209	28.90-29.10	B	**2.66**	**2.71**	0.04	0.17	0.1	87.8	10.6	19.6	0.258							
BH-209	29.80	C																✓
BH-211	24.00	A														✓		
BH-211	25.50	C															✓	
BH-211	25.70	A														✓		
BH-211	26.10	FG															✓	
BH-211	29.30	A														✓		
BH-212	19.10-19.50	C					1.7	*1)										
BH-212	21.10-21.30	C					1.9		*1)									
BH-212	21.80	A														✓		
BH-212	21.80-22.50	C	2.42	2.40	1.38		0.8											
BH-212	23.50-23.75	C				0.19												
BH-212	26.40-26.55	A	2.65	2.65	0.04		0.1											
BH-212	26.40-26.55	A	**2.69**					(229)		*1)				42	0.18			
BH-212	27.50-27.60	A	**2.71**	2.58	0.35	0.16	0.2	123		34.8	0.344							
BH-212	30.00	C															✓	
BH-212	30.50	A														✓		
BH-213	26.70	A														✓		
BH-213/2	21.50-22.00	A	2.68	2.67	0.08	*1)	0.2	210		29.5	0.155							
BH-213/2	21.50-22.00	A	**2.59**					(161)		(51.4)				24	0.15			
BH-213/2	23.30-23.70	A	**2.68**	2.68	0.05	0.28	0.3	161	11.6	36.5	0.236							
BH-213/2	26.20-26.60	A	**2.68**	2.68	0.12	0.17	0.3	168	25.1	34.6	0.277							
BH-213/2	28.80	A/B														✓		
BH-214	19.90-20.10	B		2.66	0.19	0.34		*1)										

Borehole No.	Depth of sample	Lithology	Bulk density	Dry density	Porosity	Void index	Water content	UCS	Tensile strength	Young's modulus	Poisson ratio	Slake durability	Abrasivity	Fracture energy		Petro-graphic	Clay mineral	Vitrinite reflect.
			γ	γd	n	Iv	w		(Brazilian)	E	ν	index		Wf	specific wf	analysis	analysis	analysis
	(m)		(Mg/m³)	(Mg/m³)	(%)	(%)	(%)	(MPa)	(MPa)	(GPa)		(%)	(0.1mm)	(Nm)	(Nm/MPa)			
BH-214	21.70	B										99.4						
BH-214	25.00	FG															✓	
BH-214	25.20	A/B														✓		
BH-214	27.60	B										99.3						
BH-214	29.30-29.60	B	2.64	2.63	0.18	0.25	0.3	65.4	9.5	16.3	0.136							
BH-214	31.10-31.30	A	**2.70**					(238)		(79.3)			0.61	45.7	0.19			
BH-218	17.30	C																✓
BH-218	18.00-18.20	A	**2.71**	2.61	0.30	0.50	0.7	129		15.1	0.227							
BH-218	18.60-18.80	A	**2.68**	2.58	0.39		0.1	122	*1)	26.0	0.178							
BH-218	19.00	A/B														✓		
BH-218	20.90	A										99.1						
BH-218	22.10-22.60	A	**2.66**	2.61	0.45	0.51	0.4	154	7.2	20.1	0.149		0.16					
BH-218	23.85-24.00	A		2.56	0.35	0.35	0.7	*1)										
BH-218	25.10-25.40	A	**2.71**	2.65	0.05	0.12	0.1	189		37.3	0.181							
BH-218	28.20-28.50	A	2.62	2.62	0.17	*1)	0.1	130	*1)	26.5	0.0759							
BH-218	28.80	C																✓
BH-221	8.80-9.30	A	**2.69**	2.75	0.05	0.15	0.1	87.5		33.1	0.164							
BH-221	12.20	C															✓	
BH-221	15.00-15.60	A	**2.68**	2.67	0.13	0.22	0.3	183	*1)	35.8	0.200							
BH-221	15.00-15.60	A	**2.69**					(206)		(74.7)			1.36	36.4	0.18			
BH-221	17.80-18.00	A		*1)	*1)	0.32	0.3	117		22.6	0.148							
BH-221	18.00-18.40	A	**2.72**	2.69	0.07	0.16	0.1	106	9.6	36.9	0.179							
BH-221	18.70-18.95	A	2.68	2.68	0.09	0.24	0.1	169		35.5	0.204							
BH-221	18.95-19.30	A		2.62	0.34	0.17	0.4	*1)	13.5									
BH-221	18.95-19.10	A	**2.67**					(150)		(34.5)			0.45	36.0	0.24			
BH-221	21.20	A/B														✓		
BH-221	21.90-22.15	A	2.70	2.70	0.05	0.27	0.1	146		34.5	0.124							
BH-221	22.70	A										99.6						
BH-221	23.55-23.90	A	2.68	2.68	0.04	0.16	0.1	224		35.0	0.129		1.61					
BH-221	26.40	C										99.2					✓	
BH-221	26.50-26.70	B		*1)	*1)	0.20	0.2	139		21.2	0.151							
BH-222	9.30	A/B														✓		
BH-222	9.40	A/B														✓		
BH-222	10.80-11.10	B	2.65	2.64	0.09	0.16	0.2	209		30.6	0.143							
BH-222	12.80-13.20	B	2.68	2.68	0.19	0.29	0.1	175	18.3	38.1	0.155		1.96					
BH-222	15.50	C																✓
BH-222	16.00	A														✓		
BH-222	16.30-16.80	B	*1)	*1)	*1)	0.61	0.5	*1)										
BH-222	19.10-19.30	B	**2.69**	2.72	0.03	0.20	0.1	134		32.1	0.218							
BH-222	19.30-19.50	B	2.64	2.63	0.16	0.19	0.2	133		23.5	0.149							
BH-222	20.90-21.20	A	2.68	2.67	0.14	0.22	0.3	59.1	14.3	15.4	0.145		0.82					
BH-222	22.55-22.80	B	2.63	2.61	0.34	0.22	0.6	52.9		11.4	0.199							
BH-222	23.10-23.30	B	2.62	2.60	0.23	0.15	0.6		12.6									
BH-222	24.80	A/B/C														✓		
BH-222	25.00	C															✓	
BH-222	25.10	C										98.9						
BH-222	29.30	C															✓	

Borehole No.	Depth of sample (m)	Lithology	Bulk density γ (Mg/m³)	Dry density γd (Mg/m³)	Porosity n (%)	Void index Iv (%)	Water content w (%)	UCS (MPa)	Tensile strength (Brazilian) (MPa)	Young's modulus E (GPa)	Poisson ratio ν	Slake durability index (%)	Abrasivity (0.1mm)	Fracture energy Wf (Nm)	Fracture energy specific wi (Nm/MPa)	Petro-graphic analysis	Clay mineral analysis	Vitrinite reflect. analysis
BH-222	25.00	C															✓	
BH-222	25.10	C										98.9						
BH-222	29.30	C															✓	
BH-222	29.20-30.00	B	2.71	2.71	0.13	0.09	0.1	186		39.7	0.154		1.59					
BH-222	29.70-30.00	B				0.14												
BH-222	30.70-31.10	B	2.72	2.72	0.63	0.19	0.1	132	12.9	38.2	0.145							
BH-223	8.50	A					1									✓		
BH-223	8.80	C										99.0						
BH-223	13.35-13.60	A		2.65	0.10	0.19	0.1											
BH-223	13.35-13.55	A	2.71					(287)		(75.0)			0.50	64.5	0.22			
BH-223	14.20-14.40	A	2.72	2.66	0.17	0.13	0.2	211		38.2	0.222							
BH-223	17.20-17.60	A	2.71	2.70	0.05	0.26	0.4											
BH-223	17.20-17.60	A	2.74					(310)		(66.6)			2.02	54.4	0.18			
BH-223	20.00	A														✓		
BH-223	21.00	A										90.0						
BH-223	22.90-23.30	A	2.63	2.60	0.23	0.29	0.6	84.1	14.3	22.5	0.250							
BH-225	19.10-19.30	B	2.62	2.61	0.11		0.4	140		17.7	0.213							
BH-225	20.10	A														✓		
BH-225	21.20	B/C														✓		
BH-225	23.20-23.45	A	2.69	2.67	0.02	*1)	0.9		13.2									
BH-225	23.20-23.45	A	2.67					(235)		(52.3)				54.3	0.23			
BH-225	24.70-24.95	B	2.60	2.58	0.19		0.6	*1)										
BH-226	27.50	A														✓		
BH-226	30.00	C																✓
BH-257	25.70	C																✓
BH-257	26.50	A														✓		
BH-262	25.50	C															✓	
BH-262	25.70-26.05	A	2.67	2.67	0.04		0.1	92.4		26.0	0.349							
BH-262	27.40-27.70	A	2.63	2.63	0.09		0.1	98.6		28.8	0.268							
BH-262	29.30-29.40	A	2.62	2.61	0.13		0.4		*1)									

Key:

Lithology	A-calcisiltite, B-argillaceous calcisiltite, C-calcareous shale, FG-fault gouge material
UCS	UCS...uniaxial compressive strength
*1)	scheduled test not performed, because sample to weak, unsufficient or broken during preparation
✓	performed, for results refer to test report sheets

Notes:

1. Non-bold density values are calculated from dry density and porosity
2. Bold density values were determined as part of UCS tests
3. (UCS) and (E) determined from samples with diameter/height=1

APPENDIX–D

ABAQUS INPUT FILE

```
*Heading
** Job name: Job-1 Model name: Model-1
*Preprint, echo=NO, model=NO, history=NO, contact=NO
**
** PARTS
**
*Part, name=Part-1
*Node
      1,          56.,          8.5,          30.
      2,          0.,           8.5,          30.
      3,          0.,           8.5,          20.
      4,          56.,          8.5,          20.
      5,          56.,          0.,           20.
      6,          56.,          0.,           30.
      7,          0.,           0.,           30.
      8,          0.,           0.,           20.
      9,          0.,           8.5,          10.
     10,          56.,          8.5,          10.
     11,          0.,           0.,           10.
     12,          56.,          0.,           10.
     13,          -56.,         8.5,          20.
     14,          -56.,         8.5,          10.
     15,          -56.,         0.,           20.
     16,          -56.,         0.,           10.
     17,          -56.,         8.5,          30.
     18,          -56.,         0.,           30.
     19,          -56.,         8.5,          8.5
     20,          -56.,         0.,           0.
     21,          -56.,         10.,          0.
     22,          -56.,         10.,          8.5
     23,          0.,           8.5,          8.5
     24,          0.,           0.,           0.
     25,          0.,           10.,          0.
     26,          0.,           10.,          8.5
     27,          56.,          8.5,          8.5
     28,          56.,          0.,           0.
     29,          56.,          10.,          8.5
     30,          56.,          10.,          0.
     31,          57.5,         10.,          10.
     32,          57.5,         10.,          20.
     33,          66.,          10.,          20.
     34,          66.,          10.,          10.
     35,          57.5,         8.5,          20.
     36,          66.,          0.,           20.
     37,          66.,          0.,           10.
```

38, 57.5, 8.5, 10.
39, 66., 0., 30.
40, 57.5, 8.5, 30.
41, 57.5, 10., 30.
42, 66., 10., 30.
43, 56., 8.5, 31.5
44, 56., 0., 40.
45, 56., 10., 40.
46, 56., 10., 31.5
47, 0., 0., 40.
48, 0., 10., 40.
49, 0., 10., 31.5
50, 0., 8.5, 31.5
51, -56., 0., 40.
52, -56., 8.5, 31.5
53, -56., 10., 31.5
54, -56., 10., 40.
55, -57.5, 10., 20.
56, -57.5, 10., 10.
57, -66., 10., 10.
58, -66., 10., 20.
59, -57.5, 8.5, 10.
60, -66., 0., 10.
61, -66., 0., 20.
62, -57.5, 8.5, 20.
63, -57.5, 8.5, 30.
64, -66., 0., 30.
65, -66., 10., 30.
66, -57.5, 10., 30.
67, 56., 10., 10.
68, 57.5, 10., 8.5
69, 57.5, 8.5, 8.5
70, 56., 10., 20.
71, 56., 10., 30.
72, 57.5, 8.5, 31.5
73, 57.5, 10., 31.5
74, 0., 10., 30.
75, -56., 10., 30.
76, -57.5, 8.5, 31.5
77, -57.5, 10., 31.5
78, -57.5, 26., 31.5
79, -57.5, 26., 30.
80, -56., 26., 31.5
81, -56., 26., 30.
82, -57.5, 26., 20.
83, -56., 10., 20.
84, -56., 26., 20.
85, -66., 10., 40.
86, -66., 26., 40.
87, -66., 26., 30.

88, -56., 26., 40.
89, -56., 36.5, 31.5
90, -57.5, 36.5, 31.5
91, -57.5, 36.5, 30.
92, -56., 36.5, 30.
93, -66., 36.5, 40.
94, -66., 36.5, 30.
95, -56., 36.5, 40.
96, -57.5, 36.5, 20.
97, -56., 36.5, 20.
98, -56., 10., 10.
99, -56., 26., 10.
100, -57.5, 26., 10.
101, -57.5, 36.5, 10.
102, -56., 36.5, 10.
103, -6., 26., 30.
104, 0., 20., 30.
105, 0., 20., 20.
106, -6., 26., 20.
107, 0., 10., 20.
108, 0., 10., 10.
109, 56., 26., 30.
110, 56., 26., 20.
111, 6., 26., 20.
112, 6., 26., 30.
113, -56., 47.5, 31.5
114, -57.5, 47.5, 31.5
115, -57.5, 47.5, 30.
116, -56., 47.5, 30.
117, 0., 47.5, 31.5
118, 0., 36.5, 31.5
119, 0., 36.5, 30.
120, 0., 47.5, 30.
121, -57.5, 47.5, 20.
122, -56., 47.5, 20.
123, -66., 47.5, 40.
124, -66., 47.5, 30.
125, -56., 47.5, 40.
126, 0., 32., 30.
127, 0., 36.5, 20.
128, 0., 32., 20.
129, -57.5, 47.5, 10.
130, -56., 47.5, 10.
131, 56., 36.5, 31.5
132, 56., 36.5, 30.
133, 56., 47.5, 30.
134, 56., 47.5, 31.5
135, 56., 36.5, 20.
136, -56., 26., 8.5
137, -57.5, 10., 8.5

138, -57.5, 26., 8.5
139, -66., 10., 0.
140, -66., 26., 10.
141, -66., 26., 0.
142, -57.5, 36.5, 8.5
143, -56., 36.5, 8.5
144, -66., 36.5, 0.
145, -66., 36.5, 10.
146, -57.5, 8.5, 8.5
147, 57.5, 26., 31.5
148, 56., 26., 31.5
149, 57.5, 26., 30.
150, 66., 10., 40.
151, 66., 26., 40.
152, 56., 26., 40.
153, 57.5, 26., 20.
154, 57.5, 26., 10.
155, 56., 26., 10.
156, -57.5, 50., 31.5
157, -56., 50., 31.5
158, -56., 50., 30.
159, -57.5, 50., 30.
160, -66., 50., 40.
161, -56., 50., 40.
162, 0., 50., 31.5
163, 0., 50., 30.
164, -57.5, 50., 20.
165, -56., 50., 20.
166, -66., 50., 30.
167, 0., 47.5, 20.
168, 56., 50., 31.5
169, 56., 50., 30.
170, 56., 47.5, 20.
171, 0., 36.5, 10.
172, 0., 47.5, 10.
173, -57.5, 50., 10.
174, -56., 50., 10.
175, 56., 47.5, 10.
176, 56., 36.5, 10.
177, -57.5, 47.5, 8.5
178, -56., 47.5, 8.5
179, 0., 36.5, 8.5
180, 0., 47.5, 8.5
181, -66., 47.5, 0.
182, -66., 47.5, 10.
183, 57.5, 36.5, 30.
184, 57.5, 36.5, 31.5
185, 57.5, 47.5, 30.
186, 57.5, 47.5, 31.5
187, 57.5, 36.5, 20.

188, 57.5, 47.5, 20.
189, 56., 36.5, 40.
190, 56., 47.5, 40.
191, 66., 36.5, 40.
192, 66., 47.5, 40.
193, 57.5, 36.5, 10.
194, -56., 26., 0.
195, -56., 36.5, 0.
196, -56., 47.5, 0.
197, 56., 47.5, 8.5
198, 56., 36.5, 8.5
199, 57.5, 26., 8.5
200, 56., 26., 8.5
201, 66., 10., 0.
202, 66., 26., 0.
203, 56., 26., 0.
204, 66., 26., 30.
205, 66., 36.5, 30.
206, 66., 26., 10.
207, 0., 50., 20.
208, 56., 50., 20.
209, 0., 50., 10.
210, 57.5, 50., 31.5
211, 57.5, 50., 30.
212, 66., 50., 40.
213, 56., 50., 40.
214, 57.5, 50., 20.
215, 56., 50., 10.
216, 57.5, 47.5, 10.
217, -56., 50., 8.5
218, -57.5, 50., 8.5
219, 0., 50., 8.5
220, -66., 50., 10.
221, -66., 50., 0.
222, 57.5, 36.5, 8.5
223, 66., 36.5, 0.
224, 56., 36.5, 0.
225, -56., 50., 0.
226, 56., 50., 8.5
227, 66., 47.5, 30.
228, 66., 50., 30.
229, 57.5, 50., 10.
230, 66., 36.5, 10.
231, 57.5, 47.5, 8.5
232, 66., 47.5, 0.
233, 56., 47.5, 0.
234, 66., 47.5, 10.
235, 57.5, 50., 8.5
236, 56., 50., 0.
237, 66., 50., 0.

238, 66., 50., 10.
239, -6., 26., 31.5
240, 0., 20., 31.5
241, 0., 20., 40.
242, -6., 26., 40.
243, -66., 26., 20.
244, 0., 32., 31.5
245, 0., 32., 40.
246, 0., 36.5, 40.
247, 0., 26., 20.
248, 0., 26., 10.
249, 0., 26., 8.5
250, 0., 26., 0.
251, -66., 36.5, 20.
252, 6., 26., 31.5
253, 6., 26., 40.
254, -66., 47.5, 20.
255, 0., 47.5, 40.
256, 0., 36.5, 0.
257, 0., 50., 40.
258, -66., 50., 20.
259, 66., 26., 20.
260, 66., 36.5, 20.
261, 0., 47.5, 0.
262, 66., 47.5, 20.
263, 66., 50., 20.
264, 0., 50., 0.
265, 1.51351357, 8.5, 30.
266, 3.02702713, 8.5, 30.
267, 4.5405407, 8.5, 30.
268, 6.05405426, 8.5, 30.
269, 7.56756735, 8.5, 30.
270, 9.08108139, 8.5, 30.
271, 10.594595, 8.5, 30.
272, 12.1081085, 8.5, 30.
273, 13.6216221, 8.5, 30.
274, 15.1351347, 8.5, 30.
275, 16.6486492, 8.5, 30.
276, 18.1621628, 8.5, 30.
277, 19.6756763, 8.5, 30.
278, 21.1891899, 8.5, 30.
279, 22.7027035, 8.5, 30.
280, 24.216217, 8.5, 30.
281, 25.7297306, 8.5, 30.
282, 27.2432442, 8.5, 30.
283, 28.7567558, 8.5, 30.
284, 30.2702694, 8.5, 30.
285, 31.783783, 8.5, 30.
286, 33.2972984, 8.5, 30.
287, 34.8108101, 8.5, 30.

288, 36.3243256, 8.5, 30.
289, 37.8378372, 8.5, 30.
290, 39.3513527, 8.5, 30.
291, 40.8648643, 8.5, 30.
292, 42.3783798, 8.5, 30.
293, 43.8918915, 8.5, 30.
294, 45.405407, 8.5, 30.
295, 46.9189186, 8.5, 30.
296, 48.4324341, 8.5, 30.
297, 49.9459457, 8.5, 30.
298, 51.4594612, 8.5, 30.
299, 52.9729729, 8.5, 30.
300, 54.4864883, 8.5, 30.
301, 0., 8.5, 28.5714283
302, 0., 8.5, 27.1428566
303, 0., 8.5, 25.7142849
304, 0., 8.5, 24.2857151
305, 0., 8.5, 22.8571434
306, 0., 8.5, 21.4285717
307, 54.4864883, 8.5, 20.
308, 52.9729729, 8.5, 20.
309, 51.4594612, 8.5, 20.
310, 49.9459457, 8.5, 20.
311, 48.4324341, 8.5, 20.
312, 46.9189186, 8.5, 20.
313, 45.405407, 8.5, 20.
314, 43.8918915, 8.5, 20.
315, 42.3783798, 8.5, 20.
316, 40.8648643, 8.5, 20.
317, 39.3513527, 8.5, 20.
318, 37.8378372, 8.5, 20.
319, 36.3243256, 8.5, 20.
320, 34.8108101, 8.5, 20.
321, 33.2972984, 8.5, 20.
322, 31.783783, 8.5, 20.
323, 30.2702694, 8.5, 20.
324, 28.7567558, 8.5, 20.
325, 27.2432442, 8.5, 20.
326, 25.7297306, 8.5, 20.
327, 24.216217, 8.5, 20.
328, 22.7027035, 8.5, 20.
329, 21.1891899, 8.5, 20.
330, 19.6756763, 8.5, 20.
331, 18.1621628, 8.5, 20.
332, 16.6486492, 8.5, 20.
333, 15.1351347, 8.5, 20.
334, 13.6216221, 8.5, 20.
335, 12.1081085, 8.5, 20.
336, 10.594595, 8.5, 20.
337, 9.08108139, 8.5, 20.

338, 7.56756735, 8.5, 20.
339, 6.05405426, 8.5, 20.
340, 4.5405407, 8.5, 20.
341, 3.02702713, 8.5, 20.
342, 1.51351357, 8.5, 20.
343, 56., 8.5, 21.4285717
344, 56., 8.5, 22.8571434
345, 56., 8.5, 24.2857151
346, 56., 8.5, 25.7142849
347, 56., 8.5, 27.1428566
348, 56., 8.5, 28.5714283
349, 56., 0., 21.4285717
350, 56., 0., 22.8571434
351, 56., 0., 24.2857151
352, 56., 0., 25.7142849
353, 56., 0., 27.1428566
354, 56., 0., 28.5714283
355, 54.4864883, 0., 30.
356, 52.9729729, 0., 30.
357, 51.4594612, 0., 30.
358, 49.9459457, 0., 30.
359, 48.4324341, 0., 30.
360, 46.9189186, 0., 30.
361, 45.405407, 0., 30.
362, 43.8918915, 0., 30.
363, 42.3783798, 0., 30.
364, 40.8648643, 0., 30.
365, 39.3513527, 0., 30.
366, 37.8378372, 0., 30.
367, 36.3243256, 0., 30.
368, 34.8108101, 0., 30.
369, 33.2972984, 0., 30.
370, 31.783783, 0., 30.
371, 30.2702694, 0., 30.
372, 28.7567558, 0., 30.
373, 27.2432442, 0., 30.
374, 25.7297306, 0., 30.
375, 24.216217, 0., 30.
376, 22.7027035, 0., 30.
377, 21.1891899, 0., 30.
378, 19.6756763, 0., 30.
379, 18.1621628, 0., 30.
380, 16.6486492, 0., 30.
381, 15.1351347, 0., 30.
382, 13.6216221, 0., 30.
383, 12.1081085, 0., 30.
384, 10.594595, 0., 30.
385, 9.08108139, 0., 30.
386, 7.56756735, 0., 30.
387, 6.05405426, 0., 30.

388, 4.5405407, 0., 30.
389, 3.02702713, 0., 30.
390, 1.51351357, 0., 30.
391, 0., 0., 28.5714283
392, 0., 0., 27.1428566
393, 0., 0., 25.7142849
394, 0., 0., 24.2857151
395, 0., 0., 22.8571434
396, 0., 0., 21.4285717
397, 1.51351357, 0., 20.
398, 3.02702713, 0., 20.
399, 4.5405407, 0., 20.
400, 6.05405426, 0., 20.
401, 7.56756735, 0., 20.
402, 9.08108139, 0., 20.
403, 10.594595, 0., 20.
404, 12.1081085, 0., 20.
405, 13.6216221, 0., 20.
406, 15.1351347, 0., 20.
407, 16.6486492, 0., 20.
408, 18.1621628, 0., 20.
409, 19.6756763, 0., 20.
410, 21.1891899, 0., 20.
411, 22.7027035, 0., 20.
412, 24.216217, 0., 20.
413, 25.7297306, 0., 20.
414, 27.2432442, 0., 20.
415, 28.7567558, 0., 20.
416, 30.2702694, 0., 20.
417, 31.783783, 0., 20.
418, 33.2972984, 0., 20.
419, 34.8108101, 0., 20.
420, 36.3243256, 0., 20.
421, 37.8378372, 0., 20.
422, 39.3513527, 0., 20.
423, 40.8648643, 0., 20.
424, 42.3783798, 0., 20.
425, 43.8918915, 0., 20.
426, 45.405407, 0., 20.
427, 46.9189186, 0., 20.
428, 48.4324341, 0., 20.
429, 49.9459457, 0., 20.
430, 51.4594612, 0., 20.
431, 52.9729729, 0., 20.
432, 54.4864883, 0., 20.
433, 0., 8.5, 18.5714283
434, 0., 8.5, 17.1428566
435, 0., 8.5, 15.7142859
436, 0., 8.5, 14.2857141
437, 0., 8.5, 12.8571424

438, 0., 8.5, 11.4285717
439, 1.51351357, 8.5, 10.
440, 3.02702713, 8.5, 10.
441, 4.5405407, 8.5, 10.
442, 6.05405426, 8.5, 10.
443, 7.56756735, 8.5, 10.
444, 9.08108139, 8.5, 10.
445, 10.594595, 8.5, 10.
446, 12.1081085, 8.5, 10.
447, 13.6216221, 8.5, 10.
448, 15.1351347, 8.5, 10.
449, 16.6486492, 8.5, 10.
450, 18.1621628, 8.5, 10.
451, 19.6756763, 8.5, 10.
452, 21.1891899, 8.5, 10.
453, 22.7027035, 8.5, 10.
454, 24.216217, 8.5, 10.
455, 25.7297306, 8.5, 10.
456, 27.2432442, 8.5, 10.
457, 28.7567558, 8.5, 10.
458, 30.2702694, 8.5, 10.
459, 31.783783, 8.5, 10.
460, 33.2972984, 8.5, 10.
461, 34.8108101, 8.5, 10.
462, 36.3243256, 8.5, 10.
463, 37.8378372, 8.5, 10.
464, 39.3513527, 8.5, 10.
465, 40.8648643, 8.5, 10.
466, 42.3783798, 8.5, 10.
467, 43.8918915, 8.5, 10.
468, 45.405407, 8.5, 10.
469, 46.9189186, 8.5, 10.
470, 48.4324341, 8.5, 10.
471, 49.9459457, 8.5, 10.
472, 51.4594612, 8.5, 10.
473, 52.9729729, 8.5, 10.
474, 54.4864883, 8.5, 10.
475, 56., 8.5, 11.4285717
476, 56., 8.5, 12.8571424
477, 56., 8.5, 14.2857141
478, 56., 8.5, 15.7142859
479, 56., 8.5, 17.1428566
480, 56., 8.5, 18.5714283
481, 1.51351357, 0., 10.
482, 3.02702713, 0., 10.
483, 4.5405407, 0., 10.
484, 6.05405426, 0., 10.
485, 7.56756735, 0., 10.
486, 9.08108139, 0., 10.
487, 10.594595, 0., 10.

488, 12.1081085, 0., 10.
489, 13.6216221, 0., 10.
490, 15.1351347, 0., 10.
491, 16.6486492, 0., 10.
492, 18.1621628, 0., 10.
493, 19.6756763, 0., 10.
494, 21.1891899, 0., 10.
495, 22.7027035, 0., 10.
496, 24.216217, 0., 10.
497, 25.7297306, 0., 10.
498, 27.2432442, 0., 10.
499, 28.7567558, 0., 10.
500, 30.2702694, 0., 10.
501, 31.783783, 0., 10.
502, 33.2972984, 0., 10.
503, 34.8108101, 0., 10.
504, 36.3243256, 0., 10.
505, 37.8378372, 0., 10.
506, 39.3513527, 0., 10.
507, 40.8648643, 0., 10.
508, 42.3783798, 0., 10.
509, 43.8918915, 0., 10.
510, 45.405407, 0., 10.
511, 46.9189186, 0., 10.
512, 48.4324341, 0., 10.
513, 49.9459457, 0., 10.
514, 51.4594612, 0., 10.
515, 52.9729729, 0., 10.
516, 54.4864883, 0., 10.
517, 56., 0., 11.4285717
518, 56., 0., 12.8571424
519, 56., 0., 14.2857141
520, 56., 0., 15.7142859
521, 56., 0., 17.1428566
522, 56., 0., 18.5714283
523, 0., 0., 18.5714283
524, 0., 0., 17.1428566
525, 0., 0., 15.7142859
526, 0., 0., 14.2857141
527, 0., 0., 12.8571424
528, 0., 0., 11.4285717
529, -1.51351357, 8.5, 20.
530, -3.02702713, 8.5, 20.
531, -4.5405407, 8.5, 20.
532, -6.05405426, 8.5, 20.
533, -7.56756735, 8.5, 20.
534, -9.08108139, 8.5, 20.
535, -10.594595, 8.5, 20.
536, -12.1081085, 8.5, 20.
537, -13.6216221, 8.5, 20.

538, -15.1351347, 8.5, 20.
539, -16.6486492, 8.5, 20.
540, -18.1621628, 8.5, 20.
541, -19.6756763, 8.5, 20.
542, -21.1891899, 8.5, 20.
543, -22.7027035, 8.5, 20.
544, -24.216217, 8.5, 20.
545, -25.7297306, 8.5, 20.
546, -27.2432442, 8.5, 20.
547, -28.7567558, 8.5, 20.
548, -30.2702694, 8.5, 20.
549, -31.783783, 8.5, 20.
550, -33.2972984, 8.5, 20.
551, -34.8108101, 8.5, 20.
552, -36.3243256, 8.5, 20.
553, -37.8378372, 8.5, 20.
554, -39.3513527, 8.5, 20.
555, -40.8648643, 8.5, 20.
556, -42.3783798, 8.5, 20.
557, -43.8918915, 8.5, 20.
558, -45.405407, 8.5, 20.
559, -46.9189186, 8.5, 20.
560, -48.4324341, 8.5, 20.
561, -49.9459457, 8.5, 20.
562, -51.4594612, 8.5, 20.
563, -52.9729729, 8.5, 20.
564, -54.4864883, 8.5, 20.
565, -56., 8.5, 11.4285717
566, -56., 8.5, 12.8571424
567, -56., 8.5, 14.2857141
568, -56., 8.5, 15.7142859
569, -56., 8.5, 17.1428566
570, -56., 8.5, 18.5714283
571, -54.4864883, 8.5, 10.
572, -52.9729729, 8.5, 10.
573, -51.4594612, 8.5, 10.
574, -49.9459457, 8.5, 10.
575, -48.4324341, 8.5, 10.
576, -46.9189186, 8.5, 10.
577, -45.405407, 8.5, 10.
578, -43.8918915, 8.5, 10.
579, -42.3783798, 8.5, 10.
580, -40.8648643, 8.5, 10.
581, -39.3513527, 8.5, 10.
582, -37.8378372, 8.5, 10.
583, -36.3243256, 8.5, 10.
584, -34.8108101, 8.5, 10.
585, -33.2972984, 8.5, 10.
586, -31.783783, 8.5, 10.
587, -30.2702694, 8.5, 10.

588, -28.7567558, 8.5, 10.
589, -27.2432442, 8.5, 10.
590, -25.7297306, 8.5, 10.
591, -24.216217, 8.5, 10.
592, -22.7027035, 8.5, 10.
593, -21.1891899, 8.5, 10.
594, -19.6756763, 8.5, 10.
595, -18.1621628, 8.5, 10.
596, -16.6486492, 8.5, 10.
597, -15.1351347, 8.5, 10.
598, -13.6216221, 8.5, 10.
599, -12.1081085, 8.5, 10.
600, -10.594595, 8.5, 10.
601, -9.08108139, 8.5, 10.
602, -7.56756735, 8.5, 10.
603, -6.05405426, 8.5, 10.
604, -4.5405407, 8.5, 10.
605, -3.02702713, 8.5, 10.
606, -1.51351357, 8.5, 10.
607, -56., 0., 18.5714283
608, -56., 0., 17.1428566
609, -56., 0., 15.7142859
610, -56., 0., 14.2857141
611, -56., 0., 12.8571424
612, -56., 0., 11.4285717
613, -54.4864883, 0., 10.
614, -52.9729729, 0., 10.
615, -51.4594612, 0., 10.
616, -49.9459457, 0., 10.
617, -48.4324341, 0., 10.
618, -46.9189186, 0., 10.
619, -45.405407, 0., 10.
620, -43.8918915, 0., 10.
621, -42.3783798, 0., 10.
622, -40.8648643, 0., 10.
623, -39.3513527, 0., 10.
624, -37.8378372, 0., 10.
625, -36.3243256, 0., 10.
626, -34.8108101, 0., 10.
627, -33.2972984, 0., 10.
628, -31.783783, 0., 10.
629, -30.2702694, 0., 10.
630, -28.7567558, 0., 10.
631, -27.2432442, 0., 10.
632, -25.7297306, 0., 10.
633, -24.216217, 0., 10.
634, -22.7027035, 0., 10.
635, -21.1891899, 0., 10.
636, -19.6756763, 0., 10.
637, -18.1621628, 0., 10.

638, -16.6486492, 0., 10.
639, -15.1351347, 0., 10.
640, -13.6216221, 0., 10.
641, -12.1081085, 0., 10.
642, -10.594595, 0., 10.
643, -9.08108139, 0., 10.
644, -7.56756735, 0., 10.
645, -6.05405426, 0., 10.
646, -4.5405407, 0., 10.
647, -3.02702713, 0., 10.
648, -1.51351357, 0., 10.
649, -1.51351357, 0., 20.
650, -3.02702713, 0., 20.
651, -4.5405407, 0., 20.
652, -6.05405426, 0., 20.
653, -7.56756735, 0., 20.
654, -9.08108139, 0., 20.
655, -10.594595, 0., 20.
656, -12.1081085, 0., 20.
657, -13.6216221, 0., 20.
658, -15.1351347, 0., 20.
659, -16.6486492, 0., 20.
660, -18.1621628, 0., 20.
661, -19.6756763, 0., 20.
662, -21.1891899, 0., 20.
663, -22.7027035, 0., 20.
664, -24.216217, 0., 20.
665, -25.7297306, 0., 20.
666, -27.2432442, 0., 20.
667, -28.7567558, 0., 20.
668, -30.2702694, 0., 20.
669, -31.783783, 0., 20.
670, -33.2972984, 0., 20.
671, -34.8108101, 0., 20.
672, -36.3243256, 0., 20.
673, -37.8378372, 0., 20.
674, -39.3513527, 0., 20.
675, -40.8648643, 0., 20.
676, -42.3783798, 0., 20.
677, -43.8918915, 0., 20.
678, -45.405407, 0., 20.
679, -46.9189186, 0., 20.
680, -48.4324341, 0., 20.
681, -49.9459457, 0., 20.
682, -51.4594612, 0., 20.
683, -52.9729729, 0., 20.
684, -54.4864883, 0., 20.
685, -54.4864883, 8.5, 30.
686, -52.9729729, 8.5, 30.
687, -51.4594612, 8.5, 30.

688, -49.9459457, 8.5, 30.
689, -48.4324341, 8.5, 30.
690, -46.9189186, 8.5, 30.
691, -45.405407, 8.5, 30.
692, -43.8918915, 8.5, 30.
693, -42.3783798, 8.5, 30.
694, -40.8648643, 8.5, 30.
695, -39.3513527, 8.5, 30.
696, -37.8378372, 8.5, 30.
697, -36.3243256, 8.5, 30.
698, -34.8108101, 8.5, 30.
699, -33.2972984, 8.5, 30.
700, -31.783783, 8.5, 30.
701, -30.2702694, 8.5, 30.
702, -28.7567558, 8.5, 30.
703, -27.2432442, 8.5, 30.
704, -25.7297306, 8.5, 30.
705, -24.216217, 8.5, 30.
706, -22.7027035, 8.5, 30.
707, -21.1891899, 8.5, 30.
708, -19.6756763, 8.5, 30.
709, -18.1621628, 8.5, 30.
710, -16.6486492, 8.5, 30.
711, -15.1351347, 8.5, 30.
712, -13.6216221, 8.5, 30.
713, -12.1081085, 8.5, 30.
714, -10.594595, 8.5, 30.
715, -9.08108139, 8.5, 30.
716, -7.56756735, 8.5, 30.
717, -6.05405426, 8.5, 30.
718, -4.5405407, 8.5, 30.
719, -3.02702713, 8.5, 30.
720, -1.51351357, 8.5, 30.
721, -56., 8.5, 21.4285717
722, -56., 8.5, 22.8571434
723, -56., 8.5, 24.2857151
724, -56., 8.5, 25.7142849
725, -56., 8.5, 27.1428566
726, -56., 8.5, 28.5714283
727, -56., 0., 28.5714283
728, -56., 0., 27.1428566
729, -56., 0., 25.7142849
730, -56., 0., 24.2857151
731, -56., 0., 22.8571434
732, -56., 0., 21.4285717
733, -1.51351357, 0., 30.
734, -3.02702713, 0., 30.
735, -4.5405407, 0., 30.
736, -6.05405426, 0., 30.
737, -7.56756735, 0., 30.

738, -9.08108139, 0., 30.
739, -10.594595, 0., 30.
740, -12.1081085, 0., 30.
741, -13.6216221, 0., 30.
742, -15.1351347, 0., 30.
743, -16.6486492, 0., 30.
744, -18.1621628, 0., 30.
745, -19.6756763, 0., 30.
746, -21.1891899, 0., 30.
747, -22.7027035, 0., 30.
748, -24.216217, 0., 30.
749, -25.7297306, 0., 30.
750, -27.2432442, 0., 30.
751, -28.7567558, 0., 30.
752, -30.2702694, 0., 30.
753, -31.783783, 0., 30.
754, -33.2972984, 0., 30.
755, -34.8108101, 0., 30.
756, -36.3243256, 0., 30.
757, -37.8378372, 0., 30.
758, -39.3513527, 0., 30.
759, -40.8648643, 0., 30.
760, -42.3783798, 0., 30.
761, -43.8918915, 0., 30.
762, -45.405407, 0., 30.
763, -46.9189186, 0., 30.
764, -48.4324341, 0., 30.
765, -49.9459457, 0., 30.
766, -51.4594612, 0., 30.
767, -52.9729729, 0., 30.
768, -54.4864883, 0., 30.
769, -54.4864883, 10., 8.5
770, -52.9729729, 10., 8.5
771, -51.4594612, 10., 8.5
772, -49.9459457, 10., 8.5
773, -48.4324341, 10., 8.5
774, -46.9189186, 10., 8.5
775, -45.405407, 10., 8.5
776, -43.8918915, 10., 8.5
777, -42.3783798, 10., 8.5
778, -40.8648643, 10., 8.5
779, -39.3513527, 10., 8.5
780, -37.8378372, 10., 8.5
781, -36.3243256, 10., 8.5
782, -34.8108101, 10., 8.5
783, -33.2972984, 10., 8.5
784, -31.783783, 10., 8.5
785, -30.2702694, 10., 8.5
786, -28.7567558, 10., 8.5
787, -27.2432442, 10., 8.5

788, -25.7297306, 10., 8.5
789, -24.216217, 10., 8.5
790, -22.7027035, 10., 8.5
791, -21.1891899, 10., 8.5
792, -19.6756763, 10., 8.5
793, -18.1621628, 10., 8.5
794, -16.6486492, 10., 8.5
795, -15.1351347, 10., 8.5
796, -13.6216221, 10., 8.5
797, -12.1081085, 10., 8.5
798, -10.594595, 10., 8.5
799, -9.08108139, 10., 8.5
800, -7.56756735, 10., 8.5
801, -6.05405426, 10., 8.5
802, -4.5405407, 10., 8.5
803, -3.02702713, 10., 8.5
804, -1.51351357, 10., 8.5
805, -1.51351357, 8.5, 8.5
806, -3.02702713, 8.5, 8.5
807, -4.5405407, 8.5, 8.5
808, -6.05405426, 8.5, 8.5
809, -7.56756735, 8.5, 8.5
810, -9.08108139, 8.5, 8.5
811, -10.594595, 8.5, 8.5
812, -12.1081085, 8.5, 8.5
813, -13.6216221, 8.5, 8.5
814, -15.1351347, 8.5, 8.5
815, -16.6486492, 8.5, 8.5
816, -18.1621628, 8.5, 8.5
817, -19.6756763, 8.5, 8.5
818, -21.1891899, 8.5, 8.5
819, -22.7027035, 8.5, 8.5
820, -24.216217, 8.5, 8.5
821, -25.7297306, 8.5, 8.5
822, -27.2432442, 8.5, 8.5
823, -28.7567558, 8.5, 8.5
824, -30.2702694, 8.5, 8.5
825, -31.783783, 8.5, 8.5
826, -33.2972984, 8.5, 8.5
827, -34.8108101, 8.5, 8.5
828, -36.3243256, 8.5, 8.5
829, -37.8378372, 8.5, 8.5
830, -39.3513527, 8.5, 8.5
831, -40.8648643, 8.5, 8.5
832, -42.3783798, 8.5, 8.5
833, -43.8918915, 8.5, 8.5
834, -45.405407, 8.5, 8.5
835, -46.9189186, 8.5, 8.5
836, -48.4324341, 8.5, 8.5
837, -49.9459457, 8.5, 8.5

838, -51.4594612, 8.5, 8.5
839, -52.9729729, 8.5, 8.5
840, -54.4864883, 8.5, 8.5
841, -54.4864883, 10., 0.
842, -52.9729729, 10., 0.
843, -51.4594612, 10., 0.
844, -49.9459457, 10., 0.
845, -48.4324341, 10., 0.
846, -46.9189186, 10., 0.
847, -45.405407, 10., 0.
848, -43.8918915, 10., 0.
849, -42.3783798, 10., 0.
850, -40.8648643, 10., 0.
851, -39.3513527, 10., 0.
852, -37.8378372, 10., 0.
853, -36.3243256, 10., 0.
854, -34.8108101, 10., 0.
855, -33.2972984, 10., 0.
856, -31.783783, 10., 0.
857, -30.2702694, 10., 0.
858, -28.7567558, 10., 0.
859, -27.2432442, 10., 0.
860, -25.7297306, 10., 0.
861, -24.216217, 10., 0.
862, -22.7027035, 10., 0.
863, -21.1891899, 10., 0.
864, -19.6756763, 10., 0.
865, -18.1621628, 10., 0.
866, -16.6486492, 10., 0.
867, -15.1351347, 10., 0.
868, -13.6216221, 10., 0.
869, -12.1081085, 10., 0.
870, -10.594595, 10., 0.
871, -9.08108139, 10., 0.
872, -7.56756735, 10., 0.
873, -6.05405426, 10., 0.
874, -4.5405407, 10., 0.
875, -3.02702713, 10., 0.
876, -1.51351357, 10., 0.
877, -1.51351357, 0., 0.
878, -3.02702713, 0., 0.
879, -4.5405407, 0., 0.
880, -6.05405426, 0., 0.
881, -7.56756735, 0., 0.
882, -9.08108139, 0., 0.
883, -10.594595, 0., 0.
884, -12.1081085, 0., 0.
885, -13.6216221, 0., 0.
886, -15.1351347, 0., 0.
887, -16.6486492, 0., 0.

888, -18.1621628, 0., 0.
889, -19.6756763, 0., 0.
890, -21.1891899, 0., 0.
891, -22.7027035, 0., 0.
892, -24.216217, 0., 0.
893, -25.7297306, 0., 0.
894, -27.2432442, 0., 0.
895, -28.7567558, 0., 0.
896, -30.2702694, 0., 0.
897, -31.783783, 0., 0.
898, -33.2972984, 0., 0.
899, -34.8108101, 0., 0.
900, -36.3243256, 0., 0.
901, -37.8378372, 0., 0.
902, -39.3513527, 0., 0.
903, -40.8648643, 0., 0.
904, -42.3783798, 0., 0.
905, -43.8918915, 0., 0.
906, -45.405407, 0., 0.
907, -46.9189186, 0., 0.
908, -48.4324341, 0., 0.
909, -49.9459457, 0., 0.
910, -51.4594612, 0., 0.
911, -52.9729729, 0., 0.
912, -54.4864883, 0., 0.
913, 54.4864883, 0., 0.
914, 52.9729729, 0., 0.
915, 51.4594612, 0., 0.
916, 49.9459457, 0., 0.
917, 48.4324341, 0., 0.
918, 46.9189186, 0., 0.
919, 45.405407, 0., 0.
920, 43.8918915, 0., 0.
921, 42.3783798, 0., 0.
922, 40.8648643, 0., 0.
923, 39.3513527, 0., 0.
924, 37.8378372, 0., 0.
925, 36.3243256, 0., 0.
926, 34.8108101, 0., 0.
927, 33.2972984, 0., 0.
928, 31.783783, 0., 0.
929, 30.2702694, 0., 0.
930, 28.7567558, 0., 0.
931, 27.2432442, 0., 0.
932, 25.7297306, 0., 0.
933, 24.216217, 0., 0.
934, 22.7027035, 0., 0.
935, 21.1891899, 0., 0.
936, 19.6756763, 0., 0.
937, 18.1621628, 0., 0.

938, 16.6486492, 0., 0.
939, 15.1351347, 0., 0.
940, 13.6216221, 0., 0.
941, 12.1081085, 0., 0.
942, 10.594595, 0., 0.
943, 9.08108139, 0., 0.
944, 7.56756735, 0., 0.
945, 6.05405426, 0., 0.
946, 4.5405407, 0., 0.
947, 3.02702713, 0., 0.
948, 1.51351357, 0., 0.
949, 1.51351357, 8.5, 8.5
950, 3.02702713, 8.5, 8.5
951, 4.5405407, 8.5, 8.5
952, 6.05405426, 8.5, 8.5
953, 7.56756735, 8.5, 8.5
954, 9.08108139, 8.5, 8.5
955, 10.594595, 8.5, 8.5
956, 12.1081085, 8.5, 8.5
957, 13.6216221, 8.5, 8.5
958, 15.1351347, 8.5, 8.5
959, 16.6486492, 8.5, 8.5
960, 18.1621628, 8.5, 8.5
961, 19.6756763, 8.5, 8.5
962, 21.1891899, 8.5, 8.5
963, 22.7027035, 8.5, 8.5
964, 24.216217, 8.5, 8.5
965, 25.7297306, 8.5, 8.5
966, 27.2432442, 8.5, 8.5
967, 28.7567558, 8.5, 8.5
968, 30.2702694, 8.5, 8.5
969, 31.783783, 8.5, 8.5
970, 33.2972984, 8.5, 8.5
971, 34.8108101, 8.5, 8.5
972, 36.3243256, 8.5, 8.5
973, 37.8378372, 8.5, 8.5
974, 39.3513527, 8.5, 8.5
975, 40.8648643, 8.5, 8.5
976, 42.3783798, 8.5, 8.5
977, 43.8918915, 8.5, 8.5
978, 45.405407, 8.5, 8.5
979, 46.9189186, 8.5, 8.5
980, 48.4324341, 8.5, 8.5
981, 49.9459457, 8.5, 8.5
982, 51.4594612, 8.5, 8.5
983, 52.9729729, 8.5, 8.5
984, 54.4864883, 8.5, 8.5
985, 54.4864883, 10., 0.
986, 52.9729729, 10., 0.
987, 51.4594612, 10., 0.

988, 49.9459457, 10., 0.
989, 48.4324341, 10., 0.
990, 46.9189186, 10., 0.
991, 45.405407, 10., 0.
992, 43.8918915, 10., 0.
993, 42.3783798, 10., 0.
994, 40.8648643, 10., 0.
995, 39.3513527, 10., 0.
996, 37.8378372, 10., 0.
997, 36.3243256, 10., 0.
998, 34.8108101, 10., 0.
999, 33.2972984, 10., 0.
1000, 31.783783, 10., 0.
1001, 30.2702694, 10., 0.
1002, 28.7567558, 10., 0.
1003, 27.2432442, 10., 0.
1004, 25.7297306, 10., 0.
1005, 24.216217, 10., 0.
1006, 22.7027035, 10., 0.
1007, 21.1891899, 10., 0.
1008, 19.6756763, 10., 0.
1009, 18.1621628, 10., 0.
1010, 16.6486492, 10., 0.
1011, 15.1351347, 10., 0.
1012, 13.6216221, 10., 0.
1013, 12.1081085, 10., 0.
1014, 10.594595, 10., 0.
1015, 9.08108139, 10., 0.
1016, 7.56756735, 10., 0.
1017, 6.05405426, 10., 0.
1018, 4.5405407, 10., 0.
1019, 3.02702713, 10., 0.
1020, 1.51351357, 10., 0.
1021, 1.51351357, 10., 8.5
1022, 3.02702713, 10., 8.5
1023, 4.5405407, 10., 8.5
1024, 6.05405426, 10., 8.5
1025, 7.56756735, 10., 8.5
1026, 9.08108139, 10., 8.5
1027, 10.594595, 10., 8.5
1028, 12.1081085, 10., 8.5
1029, 13.6216221, 10., 8.5
1030, 15.1351347, 10., 8.5
1031, 16.6486492, 10., 8.5
1032, 18.1621628, 10., 8.5
1033, 19.6756763, 10., 8.5
1034, 21.1891899, 10., 8.5
1035, 22.7027035, 10., 8.5
1036, 24.216217, 10., 8.5
1037, 25.7297306, 10., 8.5

1038, 27.2432442, 10., 8.5
1039, 28.7567558, 10., 8.5
1040, 30.2702694, 10., 8.5
1041, 31.783783, 10., 8.5
1042, 33.2972984, 10., 8.5
1043, 34.8108101, 10., 8.5
1044, 36.3243256, 10., 8.5
1045, 37.8378372, 10., 8.5
1046, 39.3513527, 10., 8.5
1047, 40.8648643, 10., 8.5
1048, 42.3783798, 10., 8.5
1049, 43.8918915, 10., 8.5
1050, 45.405407, 10., 8.5
1051, 46.9189186, 10., 8.5
1052, 48.4324341, 10., 8.5
1053, 49.9459457, 10., 8.5
1054, 51.4594612, 10., 8.5
1055, 52.9729729, 10., 8.5
1056, 54.4864883, 10., 8.5
1057, 57.5, 10., 11.4285717
1058, 57.5, 10., 12.8571424
1059, 57.5, 10., 14.2857141
1060, 57.5, 10., 15.7142859
1061, 57.5, 10., 17.1428566
1062, 57.5, 10., 18.5714283
1063, 66., 10., 18.5714283
1064, 66., 10., 17.1428566
1065, 66., 10., 15.7142859
1066, 66., 10., 14.2857141
1067, 66., 10., 12.8571424
1068, 66., 10., 11.4285717
1069, 57.5, 8.5, 18.5714283
1070, 57.5, 8.5, 17.1428566
1071, 57.5, 8.5, 15.7142859
1072, 57.5, 8.5, 14.2857141
1073, 57.5, 8.5, 12.8571424
1074, 57.5, 8.5, 11.4285717
1075, 66., 0., 11.4285717
1076, 66., 0., 12.8571424
1077, 66., 0., 14.2857141
1078, 66., 0., 15.7142859
1079, 66., 0., 17.1428566
1080, 66., 0., 18.5714283
1081, 66., 10., 21.4285717
1082, 66., 10., 22.8571434
1083, 66., 10., 24.2857151
1084, 66., 10., 25.7142849
1085, 66., 10., 27.1428566
1086, 66., 10., 28.5714283
1087, 66., 0., 28.5714283

1088, 66., 0., 27.1428566
1089, 66., 0., 25.7142849
1090, 66., 0., 24.2857151
1091, 66., 0., 22.8571434
1092, 66., 0., 21.4285717
1093, 57.5, 10., 21.4285717
1094, 57.5, 10., 22.8571434
1095, 57.5, 10., 24.2857151
1096, 57.5, 10., 25.7142849
1097, 57.5, 10., 27.1428566
1098, 57.5, 10., 28.5714283
1099, 57.5, 8.5, 28.5714283
1100, 57.5, 8.5, 27.1428566
1101, 57.5, 8.5, 25.7142849
1102, 57.5, 8.5, 24.2857151
1103, 57.5, 8.5, 22.8571434
1104, 57.5, 8.5, 21.4285717
1105, 54.4864883, 10., 31.5
1106, 52.9729729, 10., 31.5
1107, 51.4594612, 10., 31.5
1108, 49.9459457, 10., 31.5
1109, 48.4324341, 10., 31.5
1110, 46.9189186, 10., 31.5
1111, 45.405407, 10., 31.5
1112, 43.8918915, 10., 31.5
1113, 42.3783798, 10., 31.5
1114, 40.8648643, 10., 31.5
1115, 39.3513527, 10., 31.5
1116, 37.8378372, 10., 31.5
1117, 36.3243256, 10., 31.5
1118, 34.8108101, 10., 31.5
1119, 33.2972984, 10., 31.5
1120, 31.783783, 10., 31.5
1121, 30.2702694, 10., 31.5
1122, 28.7567558, 10., 31.5
1123, 27.2432442, 10., 31.5
1124, 25.7297306, 10., 31.5
1125, 24.216217, 10., 31.5
1126, 22.7027035, 10., 31.5
1127, 21.1891899, 10., 31.5
1128, 19.6756763, 10., 31.5
1129, 18.1621628, 10., 31.5
1130, 16.6486492, 10., 31.5
1131, 15.1351347, 10., 31.5
1132, 13.6216221, 10., 31.5
1133, 12.1081085, 10., 31.5
1134, 10.594595, 10., 31.5
1135, 9.08108139, 10., 31.5
1136, 7.56756735, 10., 31.5
1137, 6.05405426, 10., 31.5

1138, 4.5405407, 10., 31.5
1139, 3.02702713, 10., 31.5
1140, 1.51351357, 10., 31.5
1141, 1.51351357, 8.5, 31.5
1142, 3.02702713, 8.5, 31.5
1143, 4.5405407, 8.5, 31.5
1144, 6.05405426, 8.5, 31.5
1145, 7.56756735, 8.5, 31.5
1146, 9.08108139, 8.5, 31.5
1147, 10.594595, 8.5, 31.5
1148, 12.1081085, 8.5, 31.5
1149, 13.6216221, 8.5, 31.5
1150, 15.1351347, 8.5, 31.5
1151, 16.6486492, 8.5, 31.5
1152, 18.1621628, 8.5, 31.5
1153, 19.6756763, 8.5, 31.5
1154, 21.1891899, 8.5, 31.5
1155, 22.7027035, 8.5, 31.5
1156, 24.216217, 8.5, 31.5
1157, 25.7297306, 8.5, 31.5
1158, 27.2432442, 8.5, 31.5
1159, 28.7567558, 8.5, 31.5
1160, 30.2702694, 8.5, 31.5
1161, 31.783783, 8.5, 31.5
1162, 33.2972984, 8.5, 31.5
1163, 34.8108101, 8.5, 31.5
1164, 36.3243256, 8.5, 31.5
1165, 37.8378372, 8.5, 31.5
1166, 39.3513527, 8.5, 31.5
1167, 40.8648643, 8.5, 31.5
1168, 42.3783798, 8.5, 31.5
1169, 43.8918915, 8.5, 31.5
1170, 45.405407, 8.5, 31.5
1171, 46.9189186, 8.5, 31.5
1172, 48.4324341, 8.5, 31.5
1173, 49.9459457, 8.5, 31.5
1174, 51.4594612, 8.5, 31.5
1175, 52.9729729, 8.5, 31.5
1176, 54.4864883, 8.5, 31.5
1177, 54.4864883, 10., 40.
1178, 52.9729729, 10., 40.
1179, 51.4594612, 10., 40.
1180, 49.9459457, 10., 40.
1181, 48.4324341, 10., 40.
1182, 46.9189186, 10., 40.
1183, 45.405407, 10., 40.
1184, 43.8918915, 10., 40.
1185, 42.3783798, 10., 40.
1186, 40.8648643, 10., 40.
1187, 39.3513527, 10., 40.

1188, 37.8378372, 10., 40.
1189, 36.3243256, 10., 40.
1190, 34.8108101, 10., 40.
1191, 33.2972984, 10., 40.
1192, 31.783783, 10., 40.
1193, 30.2702694, 10., 40.
1194, 28.7567558, 10., 40.
1195, 27.2432442, 10., 40.
1196, 25.7297306, 10., 40.
1197, 24.216217, 10., 40.
1198, 22.7027035, 10., 40.
1199, 21.1891899, 10., 40.
1200, 19.6756763, 10., 40.
1201, 18.1621628, 10., 40.
1202, 16.6486492, 10., 40.
1203, 15.1351347, 10., 40.
1204, 13.6216221, 10., 40.
1205, 12.1081085, 10., 40.
1206, 10.594595, 10., 40.
1207, 9.08108139, 10., 40.
1208, 7.56756735, 10., 40.
1209, 6.05405426, 10., 40.
1210, 4.5405407, 10., 40.
1211, 3.02702713, 10., 40.
1212, 1.51351357, 10., 40.
1213, 1.51351357, 0., 40.
1214, 3.02702713, 0., 40.
1215, 4.5405407, 0., 40.
1216, 6.05405426, 0., 40.
1217, 7.56756735, 0., 40.
1218, 9.08108139, 0., 40.
1219, 10.594595, 0., 40.
1220, 12.1081085, 0., 40.
1221, 13.6216221, 0., 40.
1222, 15.1351347, 0., 40.
1223, 16.6486492, 0., 40.
1224, 18.1621628, 0., 40.
1225, 19.6756763, 0., 40.
1226, 21.1891899, 0., 40.
1227, 22.7027035, 0., 40.
1228, 24.216217, 0., 40.
1229, 25.7297306, 0., 40.
1230, 27.2432442, 0., 40.
1231, 28.7567558, 0., 40.
1232, 30.2702694, 0., 40.
1233, 31.783783, 0., 40.
1234, 33.2972984, 0., 40.
1235, 34.8108101, 0., 40.
1236, 36.3243256, 0., 40.
1237, 37.8378372, 0., 40.

1238, 39.3513527, 0., 40.
1239, 40.8648643, 0., 40.
1240, 42.3783798, 0., 40.
1241, 43.8918915, 0., 40.
1242, 45.405407, 0., 40.
1243, 46.9189186, 0., 40.
1244, 48.4324341, 0., 40.
1245, 49.9459457, 0., 40.
1246, 51.4594612, 0., 40.
1247, 52.9729729, 0., 40.
1248, 54.4864883, 0., 40.
1249, -1.51351357, 10., 40.
1250, -3.02702713, 10., 40.
1251, -4.5405407, 10., 40.
1252, -6.05405426, 10., 40.
1253, -7.56756735, 10., 40.
1254, -9.08108139, 10., 40.
1255, -10.594595, 10., 40.
1256, -12.1081085, 10., 40.
1257, -13.6216221, 10., 40.
1258, -15.1351347, 10., 40.
1259, -16.6486492, 10., 40.
1260, -18.1621628, 10., 40.
1261, -19.6756763, 10., 40.
1262, -21.1891899, 10., 40.
1263, -22.7027035, 10., 40.
1264, -24.216217, 10., 40.
1265, -25.7297306, 10., 40.
1266, -27.2432442, 10., 40.
1267, -28.7567558, 10., 40.
1268, -30.2702694, 10., 40.
1269, -31.783783, 10., 40.
1270, -33.2972984, 10., 40.
1271, -34.8108101, 10., 40.
1272, -36.3243256, 10., 40.
1273, -37.8378372, 10., 40.
1274, -39.3513527, 10., 40.
1275, -40.8648643, 10., 40.
1276, -42.3783798, 10., 40.
1277, -43.8918915, 10., 40.
1278, -45.405407, 10., 40.
1279, -46.9189186, 10., 40.
1280, -48.4324341, 10., 40.
1281, -49.9459457, 10., 40.
1282, -51.4594612, 10., 40.
1283, -52.9729729, 10., 40.
1284, -54.4864883, 10., 40.
1285, -54.4864883, 0., 40.
1286, -52.9729729, 0., 40.
1287, -51.4594612, 0., 40.

1288, -49.9459457, 0., 40.
1289, -48.4324341, 0., 40.
1290, -46.9189186, 0., 40.
1291, -45.405407, 0., 40.
1292, -43.8918915, 0., 40.
1293, -42.3783798, 0., 40.
1294, -40.8648643, 0., 40.
1295, -39.3513527, 0., 40.
1296, -37.8378372, 0., 40.
1297, -36.3243256, 0., 40.
1298, -34.8108101, 0., 40.
1299, -33.2972984, 0., 40.
1300, -31.783783, 0., 40.
1301, -30.2702694, 0., 40.
1302, -28.7567558, 0., 40.
1303, -27.2432442, 0., 40.
1304, -25.7297306, 0., 40.
1305, -24.216217, 0., 40.
1306, -22.7027035, 0., 40.
1307, -21.1891899, 0., 40.
1308, -19.6756763, 0., 40.
1309, -18.1621628, 0., 40.
1310, -16.6486492, 0., 40.
1311, -15.1351347, 0., 40.
1312, -13.6216221, 0., 40.
1313, -12.1081085, 0., 40.
1314, -10.594595, 0., 40.
1315, -9.08108139, 0., 40.
1316, -7.56756735, 0., 40.
1317, -6.05405426, 0., 40.
1318, -4.5405407, 0., 40.
1319, -3.02702713, 0., 40.
1320, -1.51351357, 0., 40.
1321, -1.51351357, 10., 31.5
1322, -3.02702713, 10., 31.5
1323, -4.5405407, 10., 31.5
1324, -6.05405426, 10., 31.5
1325, -7.56756735, 10., 31.5
1326, -9.08108139, 10., 31.5
1327, -10.594595, 10., 31.5
1328, -12.1081085, 10., 31.5
1329, -13.6216221, 10., 31.5
1330, -15.1351347, 10., 31.5
1331, -16.6486492, 10., 31.5
1332, -18.1621628, 10., 31.5
1333, -19.6756763, 10., 31.5
1334, -21.1891899, 10., 31.5
1335, -22.7027035, 10., 31.5
1336, -24.216217, 10., 31.5
1337, -25.7297306, 10., 31.5

1338, -27.2432442, 10., 31.5
1339, -28.7567558, 10., 31.5
1340, -30.2702694, 10., 31.5
1341, -31.783783, 10., 31.5
1342, -33.2972984, 10., 31.5
1343, -34.8108101, 10., 31.5
1344, -36.3243256, 10., 31.5
1345, -37.8378372, 10., 31.5
1346, -39.3513527, 10., 31.5
1347, -40.8648643, 10., 31.5
1348, -42.3783798, 10., 31.5
1349, -43.8918915, 10., 31.5
1350, -45.405407, 10., 31.5
1351, -46.9189186, 10., 31.5
1352, -48.4324341, 10., 31.5
1353, -49.9459457, 10., 31.5
1354, -51.4594612, 10., 31.5
1355, -52.9729729, 10., 31.5
1356, -54.4864883, 10., 31.5
1357, -54.4864883, 8.5, 31.5
1358, -52.9729729, 8.5, 31.5
1359, -51.4594612, 8.5, 31.5
1360, -49.9459457, 8.5, 31.5
1361, -48.4324341, 8.5, 31.5
1362, -46.9189186, 8.5, 31.5
1363, -45.405407, 8.5, 31.5
1364, -43.8918915, 8.5, 31.5
1365, -42.3783798, 8.5, 31.5
1366, -40.8648643, 8.5, 31.5
1367, -39.3513527, 8.5, 31.5
1368, -37.8378372, 8.5, 31.5
1369, -36.3243256, 8.5, 31.5
1370, -34.8108101, 8.5, 31.5
1371, -33.2972984, 8.5, 31.5
1372, -31.783783, 8.5, 31.5
1373, -30.2702694, 8.5, 31.5
1374, -28.7567558, 8.5, 31.5
1375, -27.2432442, 8.5, 31.5
1376, -25.7297306, 8.5, 31.5
1377, -24.216217, 8.5, 31.5
1378, -22.7027035, 8.5, 31.5
1379, -21.1891899, 8.5, 31.5
1380, -19.6756763, 8.5, 31.5
1381, -18.1621628, 8.5, 31.5
1382, -16.6486492, 8.5, 31.5
1383, -15.1351347, 8.5, 31.5
1384, -13.6216221, 8.5, 31.5
1385, -12.1081085, 8.5, 31.5
1386, -10.594595, 8.5, 31.5
1387, -9.08108139, 8.5, 31.5

1388, -7.56756735, 8.5, 31.5
1389, -6.05405426, 8.5, 31.5
1390, -4.5405407, 8.5, 31.5
1391, -3.02702713, 8.5, 31.5
1392, -1.51351357, 8.5, 31.5
1393, -57.5, 10., 18.5714283
1394, -57.5, 10., 17.1428566
1395, -57.5, 10., 15.7142859
1396, -57.5, 10., 14.2857141
1397, -57.5, 10., 12.8571424
1398, -57.5, 10., 11.4285717
1399, -66., 10., 11.4285717
1400, -66., 10., 12.8571424
1401, -66., 10., 14.2857141
1402, -66., 10., 15.7142859
1403, -66., 10., 17.1428566
1404, -66., 10., 18.5714283
1405, -57.5, 8.5, 11.4285717
1406, -57.5, 8.5, 12.8571424
1407, -57.5, 8.5, 14.2857141
1408, -57.5, 8.5, 15.7142859
1409, -57.5, 8.5, 17.1428566
1410, -57.5, 8.5, 18.5714283
1411, -66., 0., 18.5714283
1412, -66., 0., 17.1428566
1413, -66., 0., 15.7142859
1414, -66., 0., 14.2857141
1415, -66., 0., 12.8571424
1416, -66., 0., 11.4285717
1417, -57.5, 10., 28.5714283
1418, -57.5, 10., 27.1428566
1419, -57.5, 10., 25.7142849
1420, -57.5, 10., 24.2857151
1421, -57.5, 10., 22.8571434
1422, -57.5, 10., 21.4285717
1423, -57.5, 8.5, 21.4285717
1424, -57.5, 8.5, 22.8571434
1425, -57.5, 8.5, 24.2857151
1426, -57.5, 8.5, 25.7142849
1427, -57.5, 8.5, 27.1428566
1428, -57.5, 8.5, 28.5714283
1429, -66., 10., 28.5714283
1430, -66., 10., 27.1428566
1431, -66., 10., 25.7142849
1432, -66., 10., 24.2857151
1433, -66., 10., 22.8571434
1434, -66., 10., 21.4285717
1435, -66., 0., 21.4285717
1436, -66., 0., 22.8571434
1437, -66., 0., 24.2857151

1438, -66., 0., 25.7142849
1439, -66., 0., 27.1428566
1440, -66., 0., 28.5714283
1441, 56., 10., 11.4285717
1442, 56., 10., 12.8571424
1443, 56., 10., 14.2857141
1444, 56., 10., 15.7142859
1445, 56., 10., 17.1428566
1446, 56., 10., 18.5714283
1447, 56., 10., 28.5714283
1448, 56., 10., 27.1428566
1449, 56., 10., 25.7142849
1450, 56., 10., 24.2857151
1451, 56., 10., 22.8571434
1452, 56., 10., 21.4285717
1453, 54.4864883, 10., 30.
1454, 52.9729729, 10., 30.
1455, 51.4594612, 10., 30.
1456, 49.9459457, 10., 30.
1457, 48.4324341, 10., 30.
1458, 46.9189186, 10., 30.
1459, 45.405407, 10., 30.
1460, 43.8918915, 10., 30.
1461, 42.3783798, 10., 30.
1462, 40.8648643, 10., 30.
1463, 39.3513527, 10., 30.
1464, 37.8378372, 10., 30.
1465, 36.3243256, 10., 30.
1466, 34.8108101, 10., 30.
1467, 33.2972984, 10., 30.
1468, 31.783783, 10., 30.
1469, 30.2702694, 10., 30.
1470, 28.7567558, 10., 30.
1471, 27.2432442, 10., 30.
1472, 25.7297306, 10., 30.
1473, 24.216217, 10., 30.
1474, 22.7027035, 10., 30.
1475, 21.1891899, 10., 30.
1476, 19.6756763, 10., 30.
1477, 18.1621628, 10., 30.
1478, 16.6486492, 10., 30.
1479, 15.1351347, 10., 30.
1480, 13.6216221, 10., 30.
1481, 12.1081085, 10., 30.
1482, 10.594595, 10., 30.
1483, 9.08108139, 10., 30.
1484, 7.56756735, 10., 30.
1485, 6.05405426, 10., 30.
1486, 4.5405407, 10., 30.
1487, 3.02702713, 10., 30.

1488, 1.51351357, 10., 30.
1489, -1.51351357, 10., 30.
1490, -3.02702713, 10., 30.
1491, -4.5405407, 10., 30.
1492, -6.05405426, 10., 30.
1493, -7.56756735, 10., 30.
1494, -9.08108139, 10., 30.
1495, -10.594595, 10., 30.
1496, -12.1081085, 10., 30.
1497, -13.6216221, 10., 30.
1498, -15.1351347, 10., 30.
1499, -16.6486492, 10., 30.
1500, -18.1621628, 10., 30.
1501, -19.6756763, 10., 30.
1502, -21.1891899, 10., 30.
1503, -22.7027035, 10., 30.
1504, -24.216217, 10., 30.
1505, -25.7297306, 10., 30.
1506, -27.2432442, 10., 30.
1507, -28.7567558, 10., 30.
1508, -30.2702694, 10., 30.
1509, -31.783783, 10., 30.
1510, -33.2972984, 10., 30.
1511, -34.8108101, 10., 30.
1512, -36.3243256, 10., 30.
1513, -37.8378372, 10., 30.
1514, -39.3513527, 10., 30.
1515, -40.8648643, 10., 30.
1516, -42.3783798, 10., 30.
1517, -43.8918915, 10., 30.
1518, -45.405407, 10., 30.
1519, -46.9189186, 10., 30.
1520, -48.4324341, 10., 30.
1521, -49.9459457, 10., 30.
1522, -51.4594612, 10., 30.
1523, -52.9729729, 10., 30.
1524, -54.4864883, 10., 30.
1525, -57.5, 11.6000004, 31.5
1526, -57.5, 13.1999998, 31.5
1527, -57.5, 14.8000002, 31.5
1528, -57.5, 16.3999996, 31.5
1529, -57.5, 18., 31.5
1530, -57.5, 19.6000004, 31.5
1531, -57.5, 21.2000008, 31.5
1532, -57.5, 22.7999992, 31.5
1533, -57.5, 24.3999996, 31.5
1534, -57.5, 24.3999996, 30.
1535, -57.5, 22.7999992, 30.
1536, -57.5, 21.2000008, 30.
1537, -57.5, 19.6000004, 30.

1538, -57.5, 18., 30.
1539, -57.5, 16.3999996, 30.
1540, -57.5, 14.8000002, 30.
1541, -57.5, 13.1999998, 30.
1542, -57.5, 11.6000004, 30.
1543, -56., 24.3999996, 31.5
1544, -56., 22.7999992, 31.5
1545, -56., 21.2000008, 31.5
1546, -56., 19.6000004, 31.5
1547, -56., 18., 31.5
1548, -56., 16.3999996, 31.5
1549, -56., 14.8000002, 31.5
1550, -56., 13.1999998, 31.5
1551, -56., 11.6000004, 31.5
1552, -56., 11.6000004, 30.
1553, -56., 13.1999998, 30.
1554, -56., 14.8000002, 30.
1555, -56., 16.3999996, 30.
1556, -56., 18., 30.
1557, -56., 19.6000004, 30.
1558, -56., 21.2000008, 30.
1559, -56., 22.7999992, 30.
1560, -56., 24.3999996, 30.
1561, -57.5, 11.6000004, 20.
1562, -57.5, 13.1999998, 20.
1563, -57.5, 14.8000002, 20.
1564, -57.5, 16.3999996, 20.
1565, -57.5, 18., 20.
1566, -57.5, 19.6000004, 20.
1567, -57.5, 21.2000008, 20.
1568, -57.5, 22.7999992, 20.
1569, -57.5, 24.3999996, 20.
1570, -57.5, 26., 21.4285717
1571, -57.5, 26., 22.8571434
1572, -57.5, 26., 24.2857151
1573, -57.5, 26., 25.7142849
1574, -57.5, 26., 27.1428566
1575, -57.5, 26., 28.5714283
1576, -56., 10., 21.4285717
1577, -56., 10., 22.8571434
1578, -56., 10., 24.2857151
1579, -56., 10., 25.7142849
1580, -56., 10., 27.1428566
1581, -56., 10., 28.5714283
1582, -56., 24.3999996, 20.
1583, -56., 22.7999992, 20.
1584, -56., 21.2000008, 20.
1585, -56., 19.6000004, 20.
1586, -56., 18., 20.
1587, -56., 16.3999996, 20.

1588, -56., 14.8000002, 20.
1589, -56., 13.1999998, 20.
1590, -56., 11.6000004, 20.
1591, -56., 26., 28.5714283
1592, -56., 26., 27.1428566
1593, -56., 26., 25.7142849
1594, -56., 26., 24.2857151
1595, -56., 26., 22.8571434
1596, -56., 26., 21.4285717
1597, -66., 11.6000004, 40.
1598, -66., 13.1999998, 40.
1599, -66., 14.8000002, 40.
1600, -66., 16.3999996, 40.
1601, -66., 18., 40.
1602, -66., 19.6000004, 40.
1603, -66., 21.2000008, 40.
1604, -66., 22.7999992, 40.
1605, -66., 24.3999996, 40.
1606, -66., 24.3999996, 30.
1607, -66., 22.7999992, 30.
1608, -66., 21.2000008, 30.
1609, -66., 19.6000004, 30.
1610, -66., 18., 30.
1611, -66., 16.3999996, 30.
1612, -66., 14.8000002, 30.
1613, -66., 13.1999998, 30.
1614, -66., 11.6000004, 30.
1615, -56., 24.3999996, 40.
1616, -56., 22.7999992, 40.
1617, -56., 21.2000008, 40.
1618, -56., 19.6000004, 40.
1619, -56., 18., 40.
1620, -56., 16.3999996, 40.
1621, -56., 14.8000002, 40.
1622, -56., 13.1999998, 40.
1623, -56., 11.6000004, 40.
1624, -56., 27.5, 30.
1625, -56., 29., 30.
1626, -56., 30.5, 30.
1627, -56., 32., 30.
1628, -56., 33.5, 30.
1629, -56., 35., 30.
1630, -56., 35., 31.5
1631, -56., 33.5, 31.5
1632, -56., 32., 31.5
1633, -56., 30.5, 31.5
1634, -56., 29., 31.5
1635, -56., 27.5, 31.5
1636, -57.5, 35., 30.
1637, -57.5, 33.5, 30.

1638, -57.5, 32., 30.
1639, -57.5, 30.5, 30.
1640, -57.5, 29., 30.
1641, -57.5, 27.5, 30.
1642, -57.5, 27.5, 31.5
1643, -57.5, 29., 31.5
1644, -57.5, 30.5, 31.5
1645, -57.5, 32., 31.5
1646, -57.5, 33.5, 31.5
1647, -57.5, 35., 31.5
1648, -66., 35., 30.
1649, -66., 33.5, 30.
1650, -66., 32., 30.
1651, -66., 30.5, 30.
1652, -66., 29., 30.
1653, -66., 27.5, 30.
1654, -66., 27.5, 40.
1655, -66., 29., 40.
1656, -66., 30.5, 40.
1657, -66., 32., 40.
1658, -66., 33.5, 40.
1659, -66., 35., 40.
1660, -56., 27.5, 40.
1661, -56., 29., 40.
1662, -56., 30.5, 40.
1663, -56., 32., 40.
1664, -56., 33.5, 40.
1665, -56., 35., 40.
1666, -57.5, 36.5, 28.5714283
1667, -57.5, 36.5, 27.1428566
1668, -57.5, 36.5, 25.7142849
1669, -57.5, 36.5, 24.2857151
1670, -57.5, 36.5, 22.8571434
1671, -57.5, 36.5, 21.4285717
1672, -56., 36.5, 21.4285717
1673, -56., 36.5, 22.8571434
1674, -56., 36.5, 24.2857151
1675, -56., 36.5, 25.7142849
1676, -56., 36.5, 27.1428566
1677, -56., 36.5, 28.5714283
1678, -56., 35., 20.
1679, -56., 33.5, 20.
1680, -56., 32., 20.
1681, -56., 30.5, 20.
1682, -56., 29., 20.
1683, -56., 27.5, 20.
1684, -57.5, 27.5, 20.
1685, -57.5, 29., 20.
1686, -57.5, 30.5, 20.
1687, -57.5, 32., 20.

1688, -57.5, 33.5, 20.
1689, -57.5, 35., 20.
1690, -56., 10., 18.5714283
1691, -56., 10., 17.1428566
1692, -56., 10., 15.7142859
1693, -56., 10., 14.2857141
1694, -56., 10., 12.8571424
1695, -56., 10., 11.4285717
1696, -57.5, 26., 18.5714283
1697, -57.5, 26., 17.1428566
1698, -57.5, 26., 15.7142859
1699, -57.5, 26., 14.2857141
1700, -57.5, 26., 12.8571424
1701, -57.5, 26., 11.4285717
1702, -56., 26., 11.4285717
1703, -56., 26., 12.8571424
1704, -56., 26., 14.2857141
1705, -56., 26., 15.7142859
1706, -56., 26., 17.1428566
1707, -56., 26., 18.5714283
1708, -56., 11.6000004, 10.
1709, -56., 13.1999998, 10.
1710, -56., 14.8000002, 10.
1711, -56., 16.3999996, 10.
1712, -56., 18., 10.
1713, -56., 19.6000004, 10.
1714, -56., 21.2000008, 10.
1715, -56., 22.7999992, 10.
1716, -56., 24.3999996, 10.
1717, -57.5, 24.3999996, 10.
1718, -57.5, 22.7999992, 10.
1719, -57.5, 21.2000008, 10.
1720, -57.5, 19.6000004, 10.
1721, -57.5, 18., 10.
1722, -57.5, 16.3999996, 10.
1723, -57.5, 14.8000002, 10.
1724, -57.5, 13.1999998, 10.
1725, -57.5, 11.6000004, 10.
1726, -57.5, 36.5, 18.5714283
1727, -57.5, 36.5, 17.1428566
1728, -57.5, 36.5, 15.7142859
1729, -57.5, 36.5, 14.2857141
1730, -57.5, 36.5, 12.8571424
1731, -57.5, 36.5, 11.4285717
1732, -56., 36.5, 11.4285717
1733, -56., 36.5, 12.8571424
1734, -56., 36.5, 14.2857141
1735, -56., 36.5, 15.7142859
1736, -56., 36.5, 17.1428566
1737, -56., 36.5, 18.5714283

1738, -56., 27.5, 10.
1739, -56., 29., 10.
1740, -56., 30.5, 10.
1741, -56., 32., 10.
1742, -56., 33.5, 10.
1743, -56., 35., 10.
1744, -57.5, 35., 10.
1745, -57.5, 33.5, 10.
1746, -57.5, 32., 10.
1747, -57.5, 30.5, 10.
1748, -57.5, 29., 10.
1749, -57.5, 27.5, 10.
1750, -6., 26., 21.4285717
1751, -6., 26., 22.8571434
1752, -6., 26., 24.2857151
1753, -6., 26., 25.7142849
1754, -6., 26., 27.1428566
1755, -6., 26., 28.5714283
1756, -5.79555511, 24.4470863, 30.
1757, -5.19615221, 23., 30.
1758, -4.2426405, 21.7573586, 30.
1759, -3., 20.8038483, 30.
1760, -1.55291426, 20.2044449, 30.
1761, -7.5151515, 26., 30.
1762, -9.030303, 26., 30.
1763, -10.545455, 26., 30.
1764, -12.060606, 26., 30.
1765, -13.575758, 26., 30.
1766, -15.090909, 26., 30.
1767, -16.60606, 26., 30.
1768, -18.121212, 26., 30.
1769, -19.636364, 26., 30.
1770, -21.151516, 26., 30.
1771, -22.666666, 26., 30.
1772, -24.181818, 26., 30.
1773, -25.69697, 26., 30.
1774, -27.212122, 26., 30.
1775, -28.727272, 26., 30.
1776, -30.242424, 26., 30.
1777, -31.757576, 26., 30.
1778, -33.272728, 26., 30.
1779, -34.7878799, 26., 30.
1780, -36.3030319, 26., 30.
1781, -37.8181801, 26., 30.
1782, -39.3333321, 26., 30.
1783, -40.848484, 26., 30.
1784, -42.363636, 26., 30.
1785, -43.878788, 26., 30.
1786, -45.39394, 26., 30.
1787, -46.9090919, 26., 30.

1788, -48.4242439, 26., 30.
1789, -49.9393921, 26., 30.
1790, -51.4545441, 26., 30.
1791, -52.969696, 26., 30.
1792, -54.484848, 26., 30.
1793, 0., 20., 28.5714283
1794, 0., 20., 27.1428566
1795, 0., 20., 25.7142849
1796, 0., 20., 24.2857151
1797, 0., 20., 22.8571434
1798, 0., 20., 21.4285717
1799, 0., 19., 30.
1800, 0., 18., 30.
1801, 0., 17., 30.
1802, 0., 16., 30.
1803, 0., 15., 30.
1804, 0., 14., 30.
1805, 0., 13., 30.
1806, 0., 12., 30.
1807, 0., 11., 30.
1808, -1.56184399, 20.2068443, 20.
1809, -3.00747848, 20.8081722, 20.
1810, -4.24039602, 21.7551155, 20.
1811, -5.18896198, 22.9875793, 20.
1812, -5.79228783, 24.4349442, 20.
1813, 0., 19., 20.
1814, 0., 18., 20.
1815, 0., 17., 20.
1816, 0., 16., 20.
1817, 0., 15., 20.
1818, 0., 14., 20.
1819, 0., 13., 20.
1820, 0., 12., 20.
1821, 0., 11., 20.
1822, -54.484848, 26., 20.
1823, -52.969696, 26., 20.
1824, -51.4545441, 26., 20.
1825, -49.9393921, 26., 20.
1826, -48.4242439, 26., 20.
1827, -46.9090919, 26., 20.
1828, -45.39394, 26., 20.
1829, -43.878788, 26., 20.
1830, -42.363636, 26., 20.
1831, -40.848484, 26., 20.
1832, -39.3333321, 26., 20.
1833, -37.8181801, 26., 20.
1834, -36.3030319, 26., 20.
1835, -34.7878799, 26., 20.
1836, -33.272728, 26., 20.
1837, -31.757576, 26., 20.

1838, -30.242424, 26., 20.
1839, -28.727272, 26., 20.
1840, -27.212122, 26., 20.
1841, -25.69697, 26., 20.
1842, -24.181818, 26., 20.
1843, -22.666666, 26., 20.
1844, -21.151516, 26., 20.
1845, -19.636364, 26., 20.
1846, -18.121212, 26., 20.
1847, -16.60606, 26., 20.
1848, -15.090909, 26., 20.
1849, -13.575758, 26., 20.
1850, -12.060606, 26., 20.
1851, -10.545455, 26., 20.
1852, -9.030303, 26., 20.
1853, -7.5151515, 26., 20.
1854, 0., 10., 28.5714283
1855, 0., 10., 27.1428566
1856, 0., 10., 25.7142849
1857, 0., 10., 24.2857151
1858, 0., 10., 22.8571434
1859, 0., 10., 21.4285717
1860, -1.51351357, 10., 20.
1861, -3.02702713, 10., 20.
1862, -4.5405407, 10., 20.
1863, -6.05405426, 10., 20.
1864, -7.56756735, 10., 20.
1865, -9.08108139, 10., 20.
1866, -10.594595, 10., 20.
1867, -12.1081085, 10., 20.
1868, -13.6216221, 10., 20.
1869, -15.1351347, 10., 20.
1870, -16.6486492, 10., 20.
1871, -18.1621628, 10., 20.
1872, -19.6756763, 10., 20.
1873, -21.1891899, 10., 20.
1874, -22.7027035, 10., 20.
1875, -24.216217, 10., 20.
1876, -25.7297306, 10., 20.
1877, -27.2432442, 10., 20.
1878, -28.7567558, 10., 20.
1879, -30.2702694, 10., 20.
1880, -31.783783, 10., 20.
1881, -33.2972984, 10., 20.
1882, -34.8108101, 10., 20.
1883, -36.3243256, 10., 20.
1884, -37.8378372, 10., 20.
1885, -39.3513527, 10., 20.
1886, -40.8648643, 10., 20.
1887, -42.3783798, 10., 20.

1888, -43.8918915, 10., 20.
1889, -45.405407, 10., 20.
1890, -46.9189186, 10., 20.
1891, -48.4324341, 10., 20.
1892, -49.9459457, 10., 20.
1893, -51.4594612, 10., 20.
1894, -52.9729729, 10., 20.
1895, -54.4864883, 10., 20.
1896, 0., 10., 11.4285717
1897, 0., 10., 12.8571424
1898, 0., 10., 14.2857141
1899, 0., 10., 15.7142859
1900, 0., 10., 17.1428566
1901, 0., 10., 18.5714283
1902, -1.51351357, 10., 10.
1903, -3.02702713, 10., 10.
1904, -4.5405407, 10., 10.
1905, -6.05405426, 10., 10.
1906, -7.56756735, 10., 10.
1907, -9.08108139, 10., 10.
1908, -10.594595, 10., 10.
1909, -12.1081085, 10., 10.
1910, -13.6216221, 10., 10.
1911, -15.1351347, 10., 10.
1912, -16.6486492, 10., 10.
1913, -18.1621628, 10., 10.
1914, -19.6756763, 10., 10.
1915, -21.1891899, 10., 10.
1916, -22.7027035, 10., 10.
1917, -24.216217, 10., 10.
1918, -25.7297306, 10., 10.
1919, -27.2432442, 10., 10.
1920, -28.7567558, 10., 10.
1921, -30.2702694, 10., 10.
1922, -31.783783, 10., 10.
1923, -33.2972984, 10., 10.
1924, -34.8108101, 10., 10.
1925, -36.3243256, 10., 10.
1926, -37.8378372, 10., 10.
1927, -39.3513527, 10., 10.
1928, -40.8648643, 10., 10.
1929, -42.3783798, 10., 10.
1930, -43.8918915, 10., 10.
1931, -45.405407, 10., 10.
1932, -46.9189186, 10., 10.
1933, -48.4324341, 10., 10.
1934, -49.9459457, 10., 10.
1935, -51.4594612, 10., 10.
1936, -52.9729729, 10., 10.
1937, -54.4864883, 10., 10.

1938, 56., 24.3999996, 20.
1939, 56., 22.7999992, 20.
1940, 56., 21.2000008, 20.
1941, 56., 19.6000004, 20.
1942, 56., 18., 20.
1943, 56., 16.3999996, 20.
1944, 56., 14.8000002, 20.
1945, 56., 13.1999998, 20.
1946, 56., 11.6000004, 20.
1947, 54.4864883, 10., 20.
1948, 52.9729729, 10., 20.
1949, 51.4594612, 10., 20.
1950, 49.9459457, 10., 20.
1951, 48.4324341, 10., 20.
1952, 46.9189186, 10., 20.
1953, 45.405407, 10., 20.
1954, 43.8918915, 10., 20.
1955, 42.3783798, 10., 20.
1956, 40.8648643, 10., 20.
1957, 39.3513527, 10., 20.
1958, 37.8378372, 10., 20.
1959, 36.3243256, 10., 20.
1960, 34.8108101, 10., 20.
1961, 33.2972984, 10., 20.
1962, 31.783783, 10., 20.
1963, 30.2702694, 10., 20.
1964, 28.7567558, 10., 20.
1965, 27.2432442, 10., 20.
1966, 25.7297306, 10., 20.
1967, 24.216217, 10., 20.
1968, 22.7027035, 10., 20.
1969, 21.1891899, 10., 20.
1970, 19.6756763, 10., 20.
1971, 18.1621628, 10., 20.
1972, 16.6486492, 10., 20.
1973, 15.1351347, 10., 20.
1974, 13.6216221, 10., 20.
1975, 12.1081085, 10., 20.
1976, 10.594595, 10., 20.
1977, 9.08108139, 10., 20.
1978, 7.56756735, 10., 20.
1979, 6.05405426, 10., 20.
1980, 4.5405407, 10., 20.
1981, 3.02702713, 10., 20.
1982, 1.51351357, 10., 20.
1983, 56., 11.6000004, 30.
1984, 56., 13.1999998, 30.
1985, 56., 14.8000002, 30.
1986, 56., 16.3999996, 30.
1987, 56., 18., 30.

1988, 56., 19.6000004, 30.
1989, 56., 21.2000008, 30.
1990, 56., 22.7999992, 30.
1991, 56., 24.3999996, 30.
1992, 56., 26., 28.5714283
1993, 56., 26., 27.1428566
1994, 56., 26., 25.7142849
1995, 56., 26., 24.2857151
1996, 56., 26., 22.8571434
1997, 56., 26., 21.4285717
1998, 54.484848, 26., 30.
1999, 52.969696, 26., 30.
2000, 51.4545441, 26., 30.
2001, 49.9393921, 26., 30.
2002, 48.4242439, 26., 30.
2003, 46.9090919, 26., 30.
2004, 45.39394, 26., 30.
2005, 43.878788, 26., 30.
2006, 42.363636, 26., 30.
2007, 40.848484, 26., 30.
2008, 39.3333321, 26., 30.
2009, 37.8181801, 26., 30.
2010, 36.3030319, 26., 30.
2011, 34.7878799, 26., 30.
2012, 33.272728, 26., 30.
2013, 31.757576, 26., 30.
2014, 30.242424, 26., 30.
2015, 28.727272, 26., 30.
2016, 27.212122, 26., 30.
2017, 25.69697, 26., 30.
2018, 24.181818, 26., 30.
2019, 22.666666, 26., 30.
2020, 21.151516, 26., 30.
2021, 19.636364, 26., 30.
2022, 18.121212, 26., 30.
2023, 16.60606, 26., 30.
2024, 15.090909, 26., 30.
2025, 13.575758, 26., 30.
2026, 12.060606, 26., 30.
2027, 10.545455, 26., 30.
2028, 9.030303, 26., 30.
2029, 7.5151515, 26., 30.
2030, 7.5151515, 26., 20.
2031, 9.030303, 26., 20.
2032, 10.545455, 26., 20.
2033, 12.060606, 26., 20.
2034, 13.575758, 26., 20.
2035, 15.090909, 26., 20.
2036, 16.60606, 26., 20.
2037, 18.121212, 26., 20.

```
 7588, -51.4545441,        26.,  27.1428566
 7589,  -52.969696,        26.,  27.1428566
 7590,  -54.484848,        26.,  27.1428566
 7591,   -9.030303,        26.,  25.7142849
 7592,  -10.545455,        26.,  25.7142849
 7593,  -12.060606,        26.,  25.7142849
19588,  25.5652523,  22.7341595,       31.5
19589,  27.0870094,  22.7374763,       31.5
19590,  28.6087685,  22.7407837,       31.5
19591,  30.1305275,  22.7440872,       31.5
19592,  31.6522865,  22.7473907,       31.5
19593,  33.1740456,  22.7506905,       31.5
10036, 29901, 30379, 30030, 29809, 29896, 30364, 30027, 29810
10037, 30379, 30380, 30031, 30030, 30364, 30365, 30028, 30027 17261, 17262, 17263,
17264, 17265, 17266, 17267, 17268, 17269, 17270, 17271
 17272, 17273, 17274, 17275, 17276, 17277, 17278, 17279, 17280, 17281, 17282, 17283,
17284, 17285, 17286, 17287
 17288, 17289, 17290, 17291, 17292, 17293, 17294, 17295, 17296, 17297, 17298, 17299,
17300, 17301, 17302, 17303
 17304, 17305, 17306, 17307, 17308, 17309, 17310, 17311, 17312, 17313, 17314, 17315,
17316, 17317, 17318, 17319
 17320, 17321, 17322, 17323, 17324, 17325, 17326, 17597, 17598, 17599, 17600, 17601,
17602, 17603, 17604, 17605
 17606, 17607, 17608, 17609, 17610, 17611, 17612, 17613, 17614, 17615, 17616, 17617,
17618, 17619, 17620, 17621
 17622, 17623, 17624, 17625, 17626, 17627, 17628, 17629, 17630, 17631, 17632, 17633,
17634, 17635, 17636, 17637
 17638, 17639, 17640, 17641, 17642, 17643, 17644, 17645, 17646, 17647, 17648, 17649,
17650, 17651, 17652, 17653
 17654, 17655, 17656, 17657, 17658, 17659, 17660, 17661, 17662, 17663, 17664, 17665,
17666, 17667, 17668, 17669
 17670, 17671, 17672, 17673, 17674, 17675, 17676, 17677, 17678, 17679, 17680, 17681,
17682, 17683, 17684, 176,0.97375  ,       0
0.975  ,       0      ,0.97625      ,       0      ,0.9775       ,       0      ,0.97875
       ,       0
0.98   ,       0      ,0.98125      ,       0      ,0.9825       ,       0      ,0.98375
       ,       0
0.985  ,       0      ,0.98625      ,       0      ,0.9875       ,       0      ,0.98875
       ,       0
0.99   ,       0      ,0.99125      ,       0      ,0.9925       ,       0      ,0.99375
       ,       0
0.995  ,       0      ,0.99625      ,       0      ,0.9975       ,       0      ,0.99875
       ,       0
1      ,       0      ,1.00125      ,       0      ,1.005  ,       0      ,1.00625 ,       0
** STEP: Step-1
**
*Step, name=Step-1, nlgeom=NO
*Dynamic, Explicit
, 1.
*Bulk Viscosity
```

```
0.06, 1.2
**
** BOUNDARY CONDITIONS
**
** Name: BC-4 Type: Velocity/Angular velocity
*Boundary, type=VELOCITY, amplitude=pulse
_PickedSet185, 3, 3, -1.
**
** INTERACTIONS
**
** Interaction: Int-1
*Contact, op=NEW
*Contact Inclusions, ALL ELEMENT BASED
*Contact property assignment
 ,  , IntProp-1
**
** OUTPUT REQUESTS
**
*Restart, write, number interval=1, time marks=NO
**
** FIELD OUTPUT: F-Output-1
**
*Output, field, number intervals=800
*Node Output
V,
**
** HISTORY OUTPUT: H-Output-1
**
*Output, history, time interval=0.00125
*Node Output, nset=topnode
V1, V2, V3
*End Step
```

Appendix E

Publications

ICSV13 - Vienna
The Thirteenth International Congress on Sound and Vibration
Vienna, Austria, July 2-6, 2006

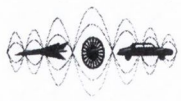

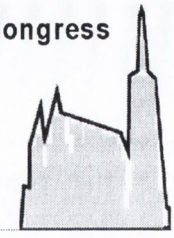

A PARAMETRIC STUDY OF BACKFILLED TRENCH FOR REDUCTION OF TBM INDUCED GROUND VIBRATIONS

Muhammad E. Rahman* and Trevor L. L. Orr

Department of Civil Engineering, University of Dublin, Trinity College
Dublin-2, Ireland
rahmanme@tcd.ie

Abstract

Wave barriers in the form of backfilled trenches are often installed in the ground to reduce the ground vibrations induced by man-made sources, such as traffic and machine foundations. This type of ground vibration and ground vibrations due to tunnel boring machines (TBMs) can be a major problem in densely populated urban areas and for structures housing sensitive equipment. No previously published research has been found in the literature on the use of backfilled trenches to provide a screen to the vibrations due to TBMs. In this paper the results of a numerical study, using a 3-D finite element model with infinite elements, to investigate the effectiveness of backfilled trenches in reducing the ground surface vibration due to tunnelling activities are presented. The ABAQUS V6.4 finite element software has been used to construct the model and three-dimensional eight-noded linear brick and reduced integration elements are employed for the ground and the tunnel lining. The effects of variations in the geometrical and material properties of the backfilled trench on reducing the ground vibrations have been studied. The findings of this study are that only a thin trench is required to provide an effective wave barrier giving a significant reduction in the vibration velocity, the percentage reduction in the vibration velocity increases with increasing depth of the wave barriers, and softer backfill material yields a better screening effect than stiffer material.

INTRODUCTION

Wave barriers in the form of backfilled trenches are often installed in the ground to reduce the ground vibrations induced by man-made sources such as traffic and machine foundations [1]. Such ground vibrations and ground vibrations due to a tunnel-boring machines (TBMs) can be a major problem in densely populated urban areas and for structures which house sensitive equipment. The environmental effects of vibrations have received considerable attention in recent years owing to the damage they can cause both to buildings and people and in many countries new rules

Eds.: J. Eberhardsteiner, H.A. Mang, H. Waubke

and regulations have been introduced to control vibrations [2]. Therefore, screening of vibrations induced by traffic and construction activities has become an important issue in recent times and it has been shown that it is possible to reduce the ground vibration significantly by placing a suitable wave barrier in the ground [3].

The methods of vibration isolation for soil-structure interaction systems may be classified into two families: active isolation and passive isolation. Active isolation, also known as source isolation, refers to the installation of barriers so close to the wave source that energy transmitted from it can be directly cut off, or to the installation of barriers surrounding the vibration source [4]. Passive isolation, also known as receiver isolation, involves the placing of suitable barriers in the ground before the structure or surrounding the structure [3]. An active isolation barrier can effectively isolate stationary sources of vibration, whereas a passive isolation barrier is effective for a wide variety of wave generating sources, including moving sources. Different kinds of wave barriers, among them open and backfilled trenches are the most common in practical applications as they are most effective and their installation cost is low [5], [6].

In the past few decades, the boundary element method (BEM) has emerged as a very efficient numerical technique for solving a wide class of engineering problems. This method is especially well suited for wave propagation problems in soils involving a semi-infinite domain. A number of researchers have carried out 2-D and 3-D numerical analyses using the BEM to investigate the screening of vibrations by means of open and backfilled trenches and the use of different types of foundations to screen the vibration due to machines [1], [3], [7], [8], [9]. However, the BEM is not well suited for the modelling of irregular geometries. To overcome this problem, several procedures for coupling finite elements with boundary elements or finite elements with infinite elements have been proposed by a number of researchers [6].

It can be observed from the above literature review that a number of researchers have carried out a lot of work on systems to provide isolation from machine foundation or high-speed train induced vibrations. To the best knowledge of the author, no work has been reported in the published geotechnical literature on the screening by backfilled trenches of the ground vibrations due to a TBM. Therefore, an investigation of the performance of backfilled trenches in reducing the ground vibrations due to a TBM is timely. In this paper, numerical studies, using 3-D finite element model coupling with infinite element, are presented which investigate the effectiveness of backfilled trenches, in reducing the ground surface vibrations due to tunnelling activities.

NUMERICAL MODELLING

Initially 3-D FE analyses were carried out to simulate the magnitudes of the ground vibrations at the surface due to TBM. The accuracy of the model was verified by comparing the measured and predicted vibrations and good agreement was found between these. In this paper, the effectiveness of backfilled trenches as wave barriers for isolating TBM induced ground vibrations has been examined. The FE model is

shown in Figure 1. The geometry was idealised by a finite region (Zone I) and by a semi-infinite far field region (Zone II). The ABAQUS V6.4 finite element software was used to construct the model and three-dimensional eight-noded linear brick and reduced integration elements, C3D8R, were employed for the ground and the tunnel lining in Zone I. Reduced-integration elements use fewer integration points in each direction than the fully integrated elements. These reduce the running time, especially in 3-D finite element model analyses. In Zone II, the soils and tunnel lining in the far field that extends to infinity, were modelled by the infinite elements, CIN3D8. In the model, the top layer is brown clay, the middle layer is Dublin boulder clay and the bottom layer is limestone. The dimensions of the finite element model are 132.0m in the transverse direction, 50.0m in the vertical direction and 40m in the direction of the tunnel. The top layer is 2.5m thick, the middle layer is 11m thick and the bottom layer is 36.5m thick. The diameter of the tunnel is 12.0m. The material properties that were used for the different soil layer in the finite element analyses are given in Table 1.

The geometric dimensions of the trench barrier and the properties of the backfill material are shown in Table 2 and Table 3, respectively. As all the dimensions are assumed and the properties of the backfill material have been taken from reference [6]. A series of parametric studies to examine the sensitivity of the vibration predictions to variations in the input parameters of the trench dimensions and the properties of the backfill material have been carried out. Note that when a certain parameter is investigated, the other parameters are kept constant.

By advancing in the ground, the tunnel-boring machine is a vibrating source from which vibrations are transmitted into the ground. Therefore, the vibrations in the ground due to the TBM during boring have been modelled by a dynamic loading system. The finite elements representing the TBM cutter have been loaded by a short triangular pulse. Due to this pulse, waves propagate through the soil and the response at the surface has been predicted. The analyses have been carried out in the time domain. The isolation effects have been calculated using the percentage velocity reduction defined as,

$$\text{Percentage velocity reduction} = \left(1 - \frac{\text{vibration velocity with barrier}}{\text{vibration velocity without barrier}}\right) * 100 \quad (1)$$

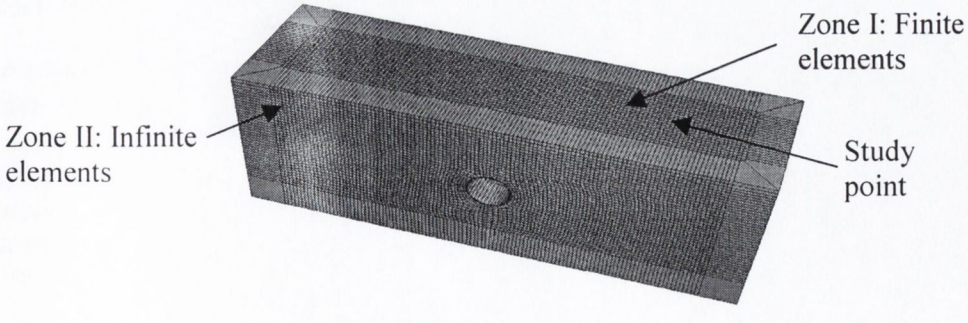

Figure 1– Three-Dimensional FE model

Table 1– Values of soil parameters used in models

Parameter	Top layer, (brown clay)	Dublin boulder clay	Limestone	Concrete	Steel
Density, kg/m^3	2000	2300	2710	2400	7800
Young's modulus, GPa	0.2	1	60	40	200
Poisson's ratio	0.495	0.495	0.25	0.2	0.3
Damping, %	2.85	1.75	1	1	0.5

Table 2– Geometric parameters of the trench barrier

Parameter	Assumed values (m)
Depth of trench below ground surface (D)	2.5, 5.0, 10, 13.5, 18, 24 and 30
Location of trench from the study zone (L)	0.0, 3.0, 6.0, 9.0, 12, and 15
Width of the backfilled trench (W)	1.5, 3.0 and 4.5

Table 3– Material properties of the backfill

Material	Density, kg/m^3	Shear wave velocity, m/s	Poisson's ratio
Backfill	1200, 1600 and 2000	30, 60, and 90	0.25, 0.33 and 0.45

PARAMETRIC STUDIES OF BACK FILLED TRENCH

In this study, the analyses have been performed assuming that the trench barrier is filled with a bentonite-soil mixture, which is softer than the natural soil. The advantage of a backfilled trench is that one can achieve larger trench depths with no need for permanent lateral supports of the vertical sides [6].

The analyses were carried out for trenches with different depths D and widths W, for different distances, L, of the trenches from the study point and for different damping ratios (ξ), densities (ρ), Poisson's ratios (υ) and impedance ratios (IR) of the backfill material.

Effect of the Normalized Depth and Location of the Trench

The effects on the amplitude of the vibration velocity of the depth D of the backfilled trench and the horizontal distance L of the backfilled trench from study point have been investigated. Figures 2 and 3 show the influence of D and L, normalised with respect to the maximum values of 30m and 15m respectively, on the % reduction in vibration velocity in the case of a trench backfilled with a bentonite-soil mixture with a density, ρ_b = 1200 kg/m^3 and shear wave velocity, v_b = 30 m/s and in soil having ρ_s = 2000 kg/m^3 and v_s = 180 m/s. Using these values in Equation 2, the impedance ratio is calculated as IR = 0.1, which indicates a very soft backfill material.

Examining the graphs in Figures 2 and 3, it is evident that the depth of the trench D and the distance of the trench from the study point, L both have important

effects on the reduction in vibration velocity. It can be observed that the achieved reduction in vibration velocity increases with increasing depth of the trench D, while it decreases with increasing L.

Based on these findings, it can state that the depth of the backfilled trench and the location of backfilled trench with respect to the study zone are important parameters with regard to the reduction of vibration velocity.

Effect of the Width of the Trench

For the purpose of the investigation, it was assumed that the width of the backfilled trench varies between 1.5m and 4.5m. In Figure 4, the reduction in the vibration velocity for different values of the trench width, normalised with respect to the 4.5m, is shown. It can be observed that, for all vibration velocities, the width of the trench has very little effect on the percentage reduction in the vibration velocity. The reductions of the vibration velocity are 40%, 41% and 44.2% for trench widths of 1.5m, 3.0m and 4.5m respectively. This implies that only a thin trench is required to provide a wave barrier giving a significant reduction in the vibration velocity.

Effect of the Poisson's Ratio of the Backfill Material

The effect of the values of the Poisson's ratio of the backfill material in the trench on the reduction in vibration velocity has been examined using the same model. The depth of the trench was 10.0m. The results obtained from numerical analyses when varying the Poisson's ratio are shown in Figure 5. Reductions in the vibration velocity of 40%, 40% and 39% were obtained for Poisson's ratios of 0.25, 0.33 and 0.45 respectively. It is concluded, therefore, that variations in Poisson's ratio have virtually no influence on the vibrations.

Effect of the Damping Ratio of the Backfill Material

Damping is the property of material to absorb vibration energy. The ratio between the damping of the material to the critical damping is called damping ratio, ξ, where critical damping is the smallest amount of damping required to prevent any oscillation occurring in the vibration system. To investigate the effects of the damping ratio of the backfill material on the effectiveness of the backfilled trench for vibration screening, it has been assumed that the damping ratio varies between 2% and 8%. The depth of the trench was 5.0m. Figure 6 shows the computed vibration reduction at the study point when changing the damping ratio of the backfill material. As can be seen, the percentage velocity reduction remains nearly constant at the measuring point as the damping ratio is changed. The reduction in the vibration velocity is 13.68% for damping ratios of 2%, 5% and 8%. Since the velocity reduction is unaffected by the damping ratio, the effect of damping can be neglected.

Effect of the Density of the Backfill Material

The effect of variations in the density of the backfill material on the effectiveness of

the backfilled trench on vibration screening has also been investigated. The effects of changing the density of the backfill material, plotted as the ratio of the density of the backfill material, ρ_b, to the top layer soil density, ρ_s, are shown in Figure 7. While the density of the backfill can be adjusted by controlling the consistency of the bentonite-soil mixture, the margin for varying the mass density is rather narrow in practice; therefore, the value of ratio only ranges from 0.6 to 1.0 in the present analysis. The depth of the trench was 10.0m. As can be seen from the results plotted in Figure 7, variations in the density of the backfill material have very little effect on the vibration reduction, as the percentage velocity reduction is approximately constant with changes in the density ratio.

Effect of the Shear Modulus Ratio (G_b/G_s) of the Backfill Material

G_b and G_s are the shear moduli of the backfill material in the trench and the top layer soil, respectively. In order to relate the shear modulus ratio G_b/G_s to a more practical parameter, the impedance ratio (IR), used by geotechnical engineers for determining whether a barrier is soft or hard has been adopted. The impedance ratio is the ratio between the mass density times the shear wave velocity of the backfill material and the original soil [4], [6] and is expressed as follows:

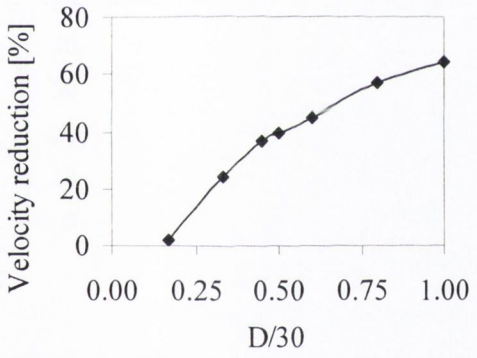

Figure 2 – Effect of normalised trench depth

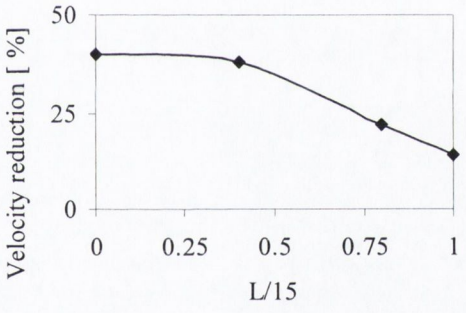

Figure 3 – Effect of normalised distance

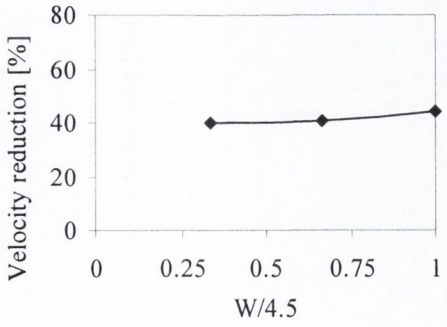

Figure 4 – Effect of normalised trench width

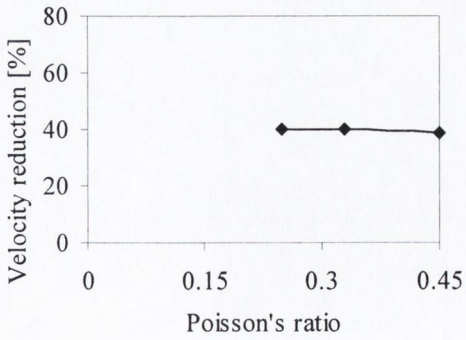

Figure 5 – Effect of the Poisson's ratio (v)

$$IR = \rho_b v_b / \rho_s v_s \quad (2)$$

where ρ_b and ρ_s denote the mass densities of the backfill material and the soil, respectively and v_b and v_s are the shear wave velocities of the two materials. Values of IR<1 mean that the trench barrier is softer than the surrounding soil and visa versa.

When investigating the effect of the shear modulus ratio, the Young's modulus was used instead of the shear modulus. The Young's modulus of the backfill material was considered to be variable while the Young's modulus of the different soil layers was kept constant of the values shown in Table 1. The density and shear wave velocity values given in Table 3 were used to calculate the Young's modulus using Equation (3) and the IR values using Equation (2). The IR values were found to be between 0.1 and 0.3. The depth of the trench was 10m. The percentage velocity reduction verses the impedance ratio IR is presented in Figure 8. It can be observed from Figure 8 that the percentage velocity reduction decreased with increasing IR, indicating that the softer backfill material, which has a lower IR value, is more effective in reducing TBM induced ground vibrations.

$$E_b = 2\rho_b v_b^2(1+\nu_b) \quad (3)$$

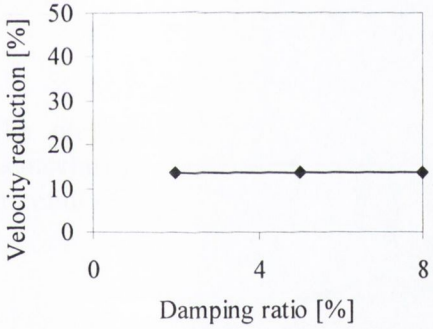

Figure 6 – Effect of damping ratio (ξ)

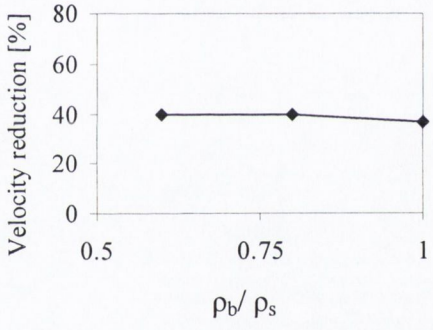

Figure 7 – Effect of normalised density

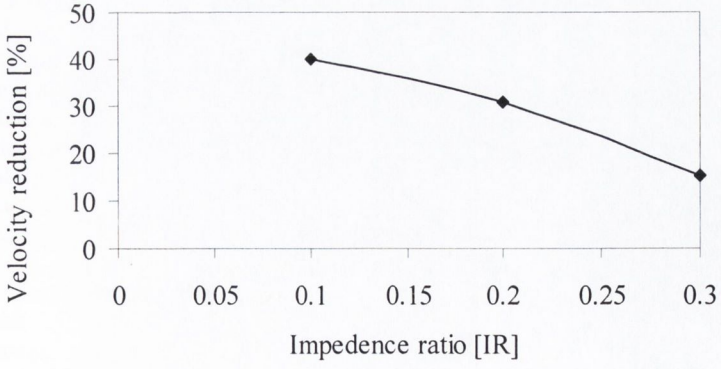

Figure 8 – Effect of the impedance ratio

CONCLUSIONS

The screening of TBM induced ground vibrations by means of a backfilled trench in layered soil between the TBM and the point of interest has been studied using 3-D finite elements coupled with infinite elements. The influences of various parameters such as the trench depth, width, location, Poisson's ratio, density, damping ratio and impedance ratio of the backfill material in the barrier have been investigated. The important observations may be summarized as follows:

- TBM induced ground vibrations can be reduced significantly by means of even thin backfilled trenches.
- Increasing the distance between a trench and the study point decreases its reduction effect due to the propagation of waves below the trench, making the screening effect less significant.
- The width of the backfilled trench, and the damping ratio, density and Poisson's ratio of the backfill material has no any significant effects on the reduction of the ground vibrations.
- Increasing the impedance ratio IR of the backfill material decreases its reduction effects; i.e. a backfill material that is soft with respect to the surrounding soil, generally performs better than a stiffer material.

ACKNOWLEDGEMENTS

The project was supported by the Nishimatsu Construction Co., Ltd and the Geotechnical Trust Fund of the Institution of Engineers of Ireland. This support is gratefully acknowledged.

REFERENCES

[1] T. M. Al-Hussaini and S. Ahmad, "Design of wave barriers for reduction of horizontal ground vibration", ASCE Journal of Geotechnical Engineering, 117, 616-636, (1991).
[2] L. Hall, "Simulations and analyses of train-induced ground vibrations in finite element models", International Journal of Soil Dynamics and Earthquake Engineering, 23, 403-413 (2003).
[3] S. Ahmad and T. M. Al-Hussaini, "Simplified design for vibration screening by open and in-filled trenches", Journal of Geotechnical Engineering ASCE, 117, 67-88 (1991).
[4] Y. B. Yang and H. H. Hung, "A parametric study of wave barriers for reduction of train-induced vibrations", International Journal for Numerical Methods in Engineering, 40, 3729-3747 (1997).
[5] H. H. Hung and Y. Yang, "A review of researches on ground-borne vibrations with emphasis on those induced by trains", Proc. National Science Council, 25, 1-16 (2001).
[6] M. Adam and O. V. Estorff, "Reduction of train-induced building vibrations by using open and filled trenches", Computers and Structures, 83, 11-24 (2005).
[7] R. Klein, H. Antes and D. L. Houedec, "Efficient 3-D modelling of vibration isolation by open trenches", Computers & Structures, 64, 809-817 (1997).
[8] S. Ahmad, T. M. Al-Hussaini and K.L. Fisherman, "An Investigation on active isolation of machine foundation by open trenches", ASCE Journal of Geotechnical Engineering, 122, 454-464 (1996).
[9] S. E. Kattis, D. Polyzos and D. E. Beskos, "Modelling of pile wave barriers by effective trenches and their screening effectiveness", Soil Dynamics and Earthquake Engineering, 18, 1-10 (1999).

ICSV13 - Vienna
The Thirteenth International Congress on Sound and Vibration
Vienna, Austria, July 2-6, 2006

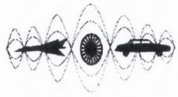

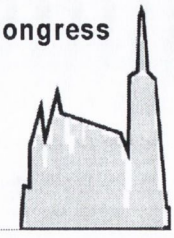

A REVIEW OF STRATEGIES TO CONTROL MANMADE INDUCED GROUND VIBRATIONS

Muhammad E. Rahman*, and Trevor L. L. Orr

Department of Civil Engineering, University of Dublin, Trinity College
Dublin-2, Ireland
rahmanme@tcd.ie

Abstract

Ground-transmitted waves generated by machine foundation, traffic, or blasting may result in ground vibrations, causing distress to adjacent structures and disruption to the operation of nearby sensitive machinery. Most of the vibratory energy affecting nearby structures is carried by surface waves that propagate in a zone close to the ground surface. Therefore, it is possible to reduce the ground vibration significantly by placing a suitable isolation system beneath the surface of the ground. This paper presents the findings of an investigation of different vibration isolation systems including floating slab tracks (FST), wave impending barriers (WIB) and trenches, which have been used to reduce the effects of machine foundation and traffic induced vibrations on nearby structures.

INTRODUCTION

Railway trains have been a major form of public transportation in the world for more than one and half centuries [1]. A wide variety of railway systems exists in the world, ranging from traditional weight freight and express passenger lines to modern metropolitan subways and high-speed railways. Different types of railway system should meet different safety and environmental requirements. Even though advanced transportation systems, such as airlines, have made rapid progress in the last half-century, the status of railways as a key transportation vehicle remains the same [1].

Unbalanced forces developed in machinery may result in significant foundation vibrations. Waves generated by trains and machine foundations may cause distress to adjacent structures and sensitive machinery. The disturbance introduced into residential and sleeping accommodation by an underground railway. Trains can be more intolerable than that caused by others forms of transport because it is often unexpected and has arisen from an unseen source [2]. One is prepared to tolerate

Eds.: J. Eberhardsteiner, H.A. Mang, H. Waubke

some disturbance from road traffic as one has very likely travelled by road to the residential accommodation and this is remembered. The noise from aircraft is tolerated, except perhaps by those living close to a major airport, because there is something inevitable about it and the aircraft is rather remote. When an underground railway creates sufficient ground vibrations that the occupants in an adjacent building can hear the trains and possibly feel the vibrations, however short the duration may be, an element of the unexpected is introduced. The source of such a disturbance is somewhere below the building, near its foundations and thus close by, not remote as with an aircraft. There is sometimes an element of fear involved in that it is thought the vibrations may cause structural damage. The trend towards lightweight and framed structures with continuous floor slabs means that buildings are becoming dynamically more "alive" and hence there is a greater possibility of a resonant response.

Vibrations can be amplified by the passage of trains due to the surface irregularities of wheels and rails, by the rise and fall of axles on rails resting on sleepers and by the propagation of deformation patterns in the track and ground. Such vibrations are transmitted through the track structure, including the rails, sleepers, ballast and sub-layers, and propagate as wave through the soil medium, after which they can be sensed by the people living alongside the railway or over a tunnel through which a railway passes. Four phases in the process of the transmission of vibrations are: generation, transmission, reception and interception. During each phase, various factors can affect the final vibration levels to different degrees. The main factors involved include the train type, train speed, embankment design, ground condition, building foundation, building type, and the distance between the railway and buildings [1].

ISOLATION OF VIBRATION

To isolate ground vibrations a number of methods have been developed during the past few decades. The most common methods include floating slab tracks for railway vibrations, wave impeding barriers and the installation of trenches. Other possible methods include in the case of tunnels, increasing the tunnel depth and, in the case of railway, using ballast layers and resilient wheels.

Floating Slab Track

Floating slabs, which consist of concrete slab tracks supported on resilient elements, have been widely used in modern rail transit systems [3]. It is well known that greater effectiveness can be achieved in reducing ground vibrations when the vibration frequency exceed 1.414 times the resonance frequency of the floating slab system. Resilient pads support the floating slab system. However, when the frequency is equal or close to the resonant frequency, vibrations will be greatly amplified. Designs which employ floating slab tracks assume the existence of a single-degree-of-freedom system, in which the lumped mass includes that of the floating slab and the unsprung

mass of the train, and in which the spring stiffness is determined by the supporting resilient pads. In order to increase the effectiveness of the floating slab track, that is, to lower the resonant frequency, the mass of the floating slab should be made as large as possible, as the resilient pads have to maintain a minimum level of rigidity to ensure rail stability under full axle loads [1].

Many devices can be used as resilient elements. These can be: a rubber or steel spring under the rail, the ballast, a resilient element under the sleepers or the plates that support the rail, or a foam rubber under the ballast. The best results are obtained when the resilient elements are made as soft as safety considerations allow them to be, and when the mass between the rail and the resilient element is made as large as space [4].

In the high frequency range, a floating slab track system behaves as an effective vibration isolator [5]. A floating slab track system is also effective for cut-and-cover type of construction. A design approach has also been proposed for a floating slab track inside a bored tunnel without the need to increase the tunnel diameter [2].

High vibration attenuation levels can be reliably achieved with well designed, low-tuned floating track beds, supported on steel springs. Long slabs or troughs provide advantages in terms of construction, installation and performance. The springs are generally accessible. They allow fast and easy re-adjustment of deviated track levels. Being fatigue-proof and provided with a durable anti-corrosion system, the springs are designed for a long lifetime [6].

Floating slabs were effective in isolating train induced ground vibrations in the frequency range above 20 Hz, although floating slabs can be designed to extend the effectiveness to lower frequencies [3].

Wave Isolation Using a Wave Impeding Block

A wave-impeding block (WIB) is an artificial stiff plate installed at a certain depth below a vibration source that acts as artificial bedrock. A WIB can effectively reduce ground vibrations due to trains but wave propagation into the surrounding area cannot be much impeded because the artificial bedrock also vibrates. The effectiveness of the artificial bedrock can be improved by increasing its stiffness. Shielding a building from soil vibrations can also be achieved by installing artificial bedrock directly beneath the building [1], [7], [8].

Wave Isolation by Trenches

Ground vibrations due to man-made sources, such as traffic and machine foundations, and ground vibrations due to TBMs can be a major problem in densely populated urban areas and for structures which are housing sensitive equipment. The environmental effects of vibrations have received considerable attention in recent years owing to the damage they can cause, both to buildings and people. In many countries new rules and regulations have been introduced to control vibrations [9] for example BS 7385 in the UK and DIN 4150 in Germany. Therefore, screening of vibrations induced by traffic and construction activities has become an important

issue in recent times and it has been shown that it is possible to reduce the ground vibration significantly by placing a suitable wave barrier in the ground. Wave barriers are often installed in the ground to reduce ground vibrations induced by man-made sources such as traffic and machine foundations [10].

The methods of vibration isolation for soil-structure interaction systems may be classified into two families: active isolation and passive isolation. Active isolation, also known as source isolation, refers to the installation of barriers at a distance so close to the wave source that energy transmitted from it can be directly cut off or to the installation of barriers surrounding the vibration source [11]. Passive isolation, also known as receiver isolation, involves placing suitable barriers in the ground between the source and the structure or surrounding the structure [12]. An active isolation barrier can effectively isolate stationary sources of vibration, whereas a passive isolation barrier is effective for a wide variety of wave generating sources, including moving sources. Different kinds of wave barriers, among them open and backfilled trenches, are the most common in practical applications as they are most effective and their installation cost is low. The ratio of the shear wave velocities of the barrier and the soil is one of the important parameters that govern the screening efficiency of a backfilled trench barrier and a backfill material that is soft with respect to the surrounding soil, generally performs better than a stiffer material [13], [14].

Much research, both experimental and numerical, has been carried out in the past few decades to study the effectiveness of wave barriers for reducing ground vibrations. An analytical approach has rarely been used because closed-form solutions are extremely difficult to obtain, except for very simple geometries and boundary conditions that rarely exist in practice. While full-scale experimentation is expensive to carry out, small-scale model test results can be difficult to extrapolate to prototype situations. An efficient numerical technique, on the other hand, can be an effective alternative method for conducting a thorough investigation into the vibration isolation phenomena [12], [15], [16].

Using field tests, Barkan [17] investigated the screening of waves by means of a trench and found that the amplitude of the waves decreased the depth of the trench was increased. Woods [18] also carried out a series of field test on vibration isolation by installing open trenches from very close to the wave source to the far field and found that reduction in the amplitude of ground vibrations of up to 75% could be achieved.

In the previous few decades, many researchers have used several numerical techniques to study the vibration isolation problem. Ju [19] used three-dimensional finite element analyses with absorbing boundary conditions to investigate the isolation of structures from train-induced vibrations by means of soil improvement and open and infilled trenches. As a result of this research it was found that soil improvements near bridges did not significantly reduce low-frequency vibrations. Open and backfilled trenches could reduce vertical vibrations but their efficiency seemed disproportionate to their cost. Yang and Hung [11] carried out a parametric study of the use of open and backfilled trenches and elastic foundations for the reduction of train–induced vibrations and found that all three-wave barriers are suitable for screening vibrations associated with waves of higher frequencies. Segol et

al. [20] used the FEM along with special non-reflecting boundaries to study vibration isolation by means of open and backfilled trenches in layered soils. They concluded that the width of the trench is insignificant. Lysmer and Wass [21] applied the lumped mass method to investigate layered soil systems as a means of reducing vibrations. Aboudi [22] carried out a combined perturbation-finite difference method analysis of the screening effect due to a thin barrier in a half space and suggested that an open trench barrier will yield the best results for screening purposes. Ju [23] applied the 3-D finite element method to simulate soil vibrations due to a high-speed train moving across bridges and investigated the screening of vibrations by means of open and backfilled trenches. Ju found that these trenches could not provide a barrier against low-frequency waves. Yang and Hung [24] proposed a 2.5D finite/infinite element procedure to model ground vibrations induced by moving loads. Besides the two in-plane degrees of freedom per node conventionally used for plane strain elements, an extra degree of freedom is introduced to account for out-of-plane wave transmission. The profile of the half-space was divided into a near field and a semi-infinite far field. The near field, containing loads and irregular structures, was modelled by the finite elements, while the far field, covering the soils extending to infinity, was modelled by the infinite elements, with due account taken of the radiation effects produced by the moving loads.

In recent decades, the boundary element method (BEM) has emerged as a very efficient numerical technique for solving a wide class of engineering problems. This method is especially well suited for wave propagation problems in soils involving a semi-infinite domain. A number of researchers have carried out 2-D and 3-D numerical analyses using the BEM to investigate the screening of vibrations by means of open and backfilled trenches and the use of different types of foundations to screen the vibration due to machines [12], [14], [15], [16], [25]. However, the BEM is not well suited for the modelling of irregular geometries. To overcome this problem, several procedures for coupling finite elements with boundary elements or finite elements with infinite elements have been proposed by a number of researchers [13].

CONCLUSIONS

A review has been carried out of different techniques to impede the vibrations due to trains and machines. The disturbance due to vibrations caused by a railway running through a residential area can be eliminated by boxing the railway in and by providing a floating track slab. However, care has to be taken to avoid slab resonance.

An open trench or a backfilled trench barrier are most effective for providing active isolation from vibrations due to a machine foundation. The reduction in the amplitude of ground vibrations depends not only on the depth of the trench, but also on the size of the foundation and the distance of the barrier from the source. The ratio of the shear wave velocities of the barrier and the soil is one of the important parameters that govern the screening efficiency of a backfilled trench barrier. Softer backfill materials yield a better screening effect than stiffer materials.

ACNOWLEDGEMENTS

The work was carried out at the Department of Civil Engineering, University of Dublin, Trinity College. The project was supported by the Nishimatsu Construction Co., Ltd and the Geotechnical Trust Fund of the Institution of Engineers of Ireland. This support is gratefully acknowledged.

REFERENCES

[1] H. H. Hung and Y. Yang, "A review of researches on ground-borne vibrations with emphasis on those induced by trains", Proc. National Science Council, **25**, 1-16 (2001).
[2] P. Grootenhuis, "Floating track slab isolation for railways", Journal of Sound and Vibration, **51**, 443-448 (1977).
[3] G. P. Wilson, H. J. Saurenman and J. T. Nelson, "Control of ground-borne noise and vibration", Journal of Sound and Vibration, **87**, 339-350 (1983).
[4] M. Heckl and G. Hauck, Wettschureck, "Structure-borne sound and vibration from rail traffic", Journal of Sound and Vibration, **193**, 175-184 (1996).
[5] T. Balendra, K. H. Chua, K. W. Lo and S. L. Lee, "Steady-state vibration of subway-soil-building system", ASCE Journal of Engineering Mechanics, **115**, 145-162 (1989).
[6] H. G. Wagner, "Attenuation of transmission of vibrations and ground-borne noise by means of steel spring supported low-tuned floating track beds", World Metro Symposium and Exhibition, Taipei, (2002).
[7] H. Antes and O. V. Estorff, "Dynamic response of 2D and 3D block foundations on a half space with inclusions", International Journal of Soil Dynamics and Earthquake Engineering, **13,** 305-311 (2000).
[8] H. Takemiva and A. Fujiwara, "Wave propagation/impediment in a stratum and wave impeding block (WIB) measured for SSI response reduction, "International Journal of Soil Dynamics and Earthquake Engineering, **13**, 49-61 (1994).
[9] L. Hall, "Simulations and analyses of train-induced ground vibrations in finite element models", International Journal of Soil Dynamics and Earthquake Engineering, **23**, 403-413 (2003).
[10] T. M. Al-Hussaini and S. Ahmad, "Design of wave barriers for reduction of horizontal ground vibration", ASCE Journal of Geotechnical Engineering, **117**, 616-636 (1991).
[11] Y. B. Yang and H. H. Hung, "A parametric study of wave barriers for reduction of train-induced vibrations", International Journal for Numerical Methods in Engineering, **40**, 3729-3747 (1997).
[12] S. Ahmad and T. M. Al-Hussaini, "Simplified design for vibration screening by open and in-filled trenches", Journal of Geotechnical Engineering ASCE, **117**, 67-88 (1991).
[13] M. Adam and O. V. Estorff, "Reduction of train-induced building vibrations by using open and filled trenches", Computers and Structures, **83**, 11-24 (2005).

[14] R. Klein, H. Antes and D. L. Houedec, "Efficient 3D modelling of vibration isolation by open trenches", Computers & Structures, **64**, 809-817 (1997).
[15] S. Ahmad, T. M. Al-Hussaini and K.L. Fisherman, "An Investigation on active isolation of machine foundation by open trenches", ASCE Journal of Geotechnical Engineering, **122**, 454-464 (1996).
[16] T. M. Al-Hussaini and S. Ahmad, "Active isolation of machine foundations by in-filled trench barriers", ASCE Journal of Geotechnical Engineering, **122**, 288-294 (1996).
[17] D. D. Barkan, *Dynamics of bases and foundations.* (McGraw-Hill, New York, 1962).
[18] R. D. Woods, "Screening of surface waves in soils", ASCE Journal of Soil Mechanics Foundation Division, **SM4**, 951-979 (1968).
[19] S. H. Ju, "Three-dimensional analyses of wave barriers for reduction of train-induced vibrations", Journal of Geotechnical and Geoenvironmental Engineering", **130**, 740-748 (2004).
[20] G. Segol, P. C. Lee and J. F. Abel, (1978), "Amplitude reduction of surface waves by trenches", ASCE Journal of Engineering Mechanics, **104**, 621-638 (1978).
[21] J. Lysmer and G. Wass, "Shear waves in plane infinite structures", ASCE Journal of Engineering Mechanics, **98**, 85-105 (1972).
[22] J. Aboudi, "Elastic waves in half-space with thin barrier", ASCE Journal of Engineering Mechanics, **99**, 69-83 (1973).
[23] S. H. Ju, "Finite element analyses of wave propagations due to high-speed train across bridges", International Journal for Numerical Methods in Engineering, **54,** 1391-1408 (2002).
[24] Y. B. Yang and H. H. Hung, "A 2.5-D finite/infinite element approach for modelling viscoelastic bodies subjected to moving loads", International Journal for Numerical Methods in Engineering, **51**, 1317-1336 (2001).
[25] S. E. Kattis, D. Polyzos and D. E. Beskos, "Modelling of pile wave barriers by effective trenches and their screening effectiveness", Soil Dynamics and Earthquake Engineering, **18**, 1-10 (1999).